Technical University of Denmark

DTU

Operational stability of large scale OPV modules: interfaces, materials selection and stack design

Roth, Bérenger; Krebs, Frederik C; Søndergaard, Roar R.

Publication date:
2016

Document Version
Publisher's PDF, also known as Version of record

[Link back to DTU Orbit](#)

DTU Library
Technical Information Center of Denmark

Technical University of Denmark

Operational stability of large scale OPV modules:
interfaces, materials selection and stack design

Ph.D. thesis - Bérenger Roth

March 2016

Preface

This Ph.D. thesis is the compilation of three years of work at the Technical University of Denmark (DTU) from April 2013 to March 2016. My scientific endeavors were supervised by Prof. Frederik C. Krebs and by Dr. Roar R. Søndergaard and funded by the Eurotech Universities alliance project: Interface Science for Photovoltaics (ISPV). Most of my work was carried out at the Solar Energy Section of the Department of Energy Conversion and Storage (DTU) in Roskilde, Denmark. As part of my Ph.D. study, I also did a 6 months stay abroad in The Lipomi Research Group at University of California, San Diego, USA. During my time at DTU, I had also the opportunity to collaborate with multiple other institutions in Europe and in the United States.

Through my work, I contributed to 13 peer reviewed publications. To keep the core of this thesis consistent, only 10 among these publications were used for the redaction of this manuscript.

Denne Ph.d. er resultatet af tre års arbejde ved Danmarks Tekniske Universitet (DTU) fra april 2013 til marts 2016. Mit videnskabelige arbejde har været superviseret af Prof. Frederik C. Krebs samt af seniorforsker Roar R. Søndergaard og er støttet af "The Eurotech Universities Alliance Project: Interface Science for Photovoltaics (ISPV)"Det meste af mit arbejde blev udført ved sektionen for Solenergi under Institut for Energikonvertering og –lagring (DTU) i Roskilde, Danmark. Som del af mit Ph.D. studie tilbragte jeg 6 måneder ved Darren Lipomis forskningsgruppe ved University of California, San Diego, USA. Derudover havde jeg i min tid på DTU muligheden for at samarbejde med flere forskningsinstitutioner i Europa og i USA.

Gennem mit arbejde har jeg bidraget til 13 peer-reviewed publikationer. For at bibeholde en tematisk konsistens er kun 10 af disse brugt til udarbejdelsen af denne afhandling.

Acknowledgments

First and foremost, I would like to express my special appreciation and thanks to my principal supervisor Prof. Frederik C. Krebs for his support and for sharing his expertise with me. I also would like to thank my co-supervisor Dr. Roar R. Søndergaard for his help and for always be available for discussions. None of the work presented in this thesis would have been possible without their contagious passion and energy. Thank you both for encouraging me in my research and leaving me the freedom to grow as a scientist.

I would like to express my gratitude to Dr. Suren Gevorgyan for his help and guidance during all my lifetime studies.

I wish to thank the entire SOL group at DTU for their help and contributions. Working together has been great.

My sincere thanks to Prof. Darren J. Lipomi for inviting me to stay 6 months in his research group at UCSD. To the all group, thanks for the warm welcome, the help and the fun times.

A Special thanks to my friend Michael Corazza for his countless help at work and the fun times outside! And a big thank you to my office mate Francesco Livi even though he disappeared along the way!

Finally, I want to thank my family and friends from here in Denmark or elsewhere around the world, for their support and understanding during these three years of my life.

Abstract

The work presented in this thesis centers on the third generation of photovoltaics technology: Organic Photovoltaics (OPV). So far the efficiency has been the main focus of OPV research and small lab scale devices have now reached performances above 10%. One major caveat on the road to commercialization is the intrinsic low stability of OPV cells. This dissertation will focus on some aspects of OPV stability from materials to large scale modules.

This thesis starts with an introduction of the energy challenges the world faces and on how solar energy can help fix them. Followed by a quick introduction to the OPV field. The roll-to-roll techniques available for OPV manufacturing are introduced. Many of these techniques were used for sample preparation as part of the work presented here.

The ISOS testing standards which are at the base of most stability studies in this thesis are introduced. The photochemical stability and lifetime of poly(3-hexylthiophene) modified with cyano groups by random co-polymerization is studied. The results show that improvement in photochemical stability of the pristine polymer does not necessary lead to a higher stability of the final solar cell. An extended meta analysis of published stability data identified some key issues for OPV stability.

A rational approach derived from the pharmaceutical industry to screen high efficiency polymers for their suitability with roll-to-roll manufacturing is then presented. During that study, only 13% of the 104 screened polymers outperformed the common P3HT based on a merit factor. The same library of polymers was later screened for mechanical properties to identify trends linking the molecular structure and the mechanical properties of the pristine polymer film. Another merit factor was used in order to find guidelines to co-optimize electronic and mechanical performances.

Finally, multiple indoor and outdoor lifetime tests of large scale ITO-free OPV modules were conducted. These studies focused particularly on the impact of PEDOT:PSS for long-term stability. The first study looked into the effect of the PEDOT:PSS ink formulation, in particular the high boiling additives. The results showed that both the initial performances and the long-term stability are affected noticeably by those additives. The lifetime outdoor of the full modules could potentially be extended by 2-3 times if dimethylsufoxide (DMSO) is replaced by ethylene glycol (EG). The next study showed that the lifetime outdoor can be further

extended by one order of magnitude by removing the front PEDOT:PSS using a hybrid zinc oxide/silver nanowires electrode.

Resumé

Da verdens energiforbrug bliver ved med at stige vil mange energiressourcer, som olie og gas, være opbrugt ved udgangen af dette århundrede. Set i forhold til de andre alternative energiformer som findes, har udnyttelsen solenergi gode fremtidsmuligheder for at kunne erstatte disse begrænsede ressourcer.

Arbejdet præsenteret i denne afhandling er centreret om den tredje generation af solcelleteknologier: organiske solceller (OS). Entusiastmen for OS kommer af deres mulighed for billig fremstilling ved hjælp af hurtige printe/coate-teknikker.

Ind til videre har hovedfokus inden for OS-forskning været at øge sol-til-strøm konverterings effektiviteten af små laboratorieskala solceller, som nu har opnået ydeevner på over 10%. Tilbage står en af hovedudfordringerne på vejen mod kommercialisering af OS, deres lave operationelle stabilitet.

Denne afhandling ser på flere aspekter af OS stabilitet, heriblandt stabilitet af materialer samt stabilitet af færdige storskala moduler. Afhandlingen giver først en introduktion til de energiudfordringer verden står over for, hvordan solenergi kan afhjælpe nogle af disse samt en hurtig introduktion til OS som forskningsfelt. Dette efterfølges af en kort introduktion til nogle af de rulle-til-rulle printe/coate-teknikker som kan bruges til fremstilling af OS. Mange af disse teknikker har været brugt til fremstillingen af de OS, som er brugt i denne afhandling.

Også ISOS-test-standarderne som ligger til grund for de fleste af stabilitetsstudierne udført i denne afhandling introduceres.

Den fotokemiske stabilitet og levetid af poly(3-hexylthiophen) modificeret med cyanogrupper ved tilfældig co-polymerisering studeres. Resultaterne viser, at selvom der er en fotokemisk stabilitetsforøgelse af den rene polymer ved at introducere cyanogrupper, så leder en sådan introduktion ikke nødvendigvis til en højere stabilitet i den færdige solcelle.

En udvidet meta-analyse af publicerede stabilitetsdata identificerede nogle nøglepunkter for OS stabilitet. En systematisk tilgangsvinkel, analogt til hvad man bruger i medicinalindustrien, hvor højeffektivitets OS polymerer screenes for deres egnethed i rulle-til-rulle OS produktion bliver præsenteret. Baseret på en, til studiet defineret, merit-faktor viste det sig at kun 10% af de 104 screenede polymerer var bedre end den almindeligt anvendte polymer P3HT. Den samme gruppe af polymerer blev senere screenet for deres mekaniske egenskaber, for

derved at identificere tendenser mellem de molekylære strukturer og de mekaniske egenskaber i tynde film af de rene polymerer. En anden merit-faktor blev derpå defineret, for slutteligt at finde frem til et sæt retningslinjer til co-optimering af både den elektroniske og mekaniske ydelse.

Endeligt blev flere indendørs og udendørs levetids-studier af storskala ITO-frie OS moduler udført. Disse studier fokuserede hovedsagligt på indvirkningen af PEDOT:PSS på den langsigtede stabilitet af modulerne. Resultaterne viste at ved at fjerne PEDOT:PSS kunne modulernes levetid udvides med flere år.

Contents

List of abbreviations

Ag	Silver	EROI	Energy return on investment
AgNW	Silver nanowire		
Al	Aluminium	ETL	Electron transport layer
a-Si	Amorphous silicon	FF	Fill factor
Au	Gold	GaAs	Gallium arsenide
AZO	Aluminium doped zinc oxide	HOMO	Highest occupied molecular orbital
BHJ	Bulk-heterojunction	HTL	Hole transport layer
Ca	Calcium	I_{SC}	Short circuit current
CB	Chlorobenzene	ISOS	International Summit on OPV Stability
CF	Chloroform		
CdS	Cadmium sulfide	ITO	Indium tin oxide
Cd-Te	Cadmium telluride	LiF	Lithium fluoride
CIGS	Copper indium-gallium diselenide	LUMO	Lowest unoccupied molecular orbital
CN-P3HT	poly(3-hexylthiophene -co-cyanothiophene)	MoO_X	Molybdenum oxide
		MPP	Maximum power point
CO_2	Carbon dioxide	NiO_X	Nickel oxide
CoS	crack-onset strain	ODCB	*Ortho*-dichlorobenzene
CVD	Chemical vapor deposition	OPV	Organic photovoltaics
		P3AT	Poly(3-alkylthiophene)
CZTSSe	Copper zinc tin sulfide selenide	P3HT	Poly(3-hexylthiphene)
		PAL	Photoactive layer
D/A	Donor/acceptor	PbS	Lead-sulfur
DMSO	Dimethyl sulfoxide	PCBM	[6,6]-phenyl-C_{61}-butyric acid methyl ester
DOD	Drop on demand		
DSSC	Dye sensitized solar cells	PCE	Power conversion efficiency
E_G	Band gap	PDMS	Polydimethylsiloxane
EG	Ethylene glycol	PEDOT:PSS	Poly(3,4-ethylene dioxythiophene): poly(styrenesulfonate)
E_F	Tensile modulus		
EPBT	Energy payback time		

PET	Polyethylene terephthalate	T_{S80}	Time to reach 80% of T_S
PSA	Pressure sensitive adhesive	TiO_2	Titanium oxide
		TWy	Terawatt-year
PSC	Polymer solar cells	UV	Ultraviolet
PV	Photovoltaics	UV-vis	Ultraviolet-visible spectroscopy
R2R	Roll-to-roll		
SC	Semiconductor	V_2O_5	Vanadium oxide
T_{80}	Time to reach 80% of initial value	VB	Valence band
		V_{OC}	Open circuit voltage
T_S	Time when the degradation stabilizes	WO_3	Tungsten oxide
		ZnO	Zinc oxide

List of publications

First author publications

- <u>B. Roth</u>, R. R. Søndergaard, F. C. Krebs, "Roll-to-roll printing and coating techniques for manufacturing large-area flexible organic electronics", *Handbook of Flexible Organic Electronics: Materials, Manufacturing and Applications,* (ed. Logothetidis, S.) pp 171-192 (2014)

- <u>B. Roth</u>, A. E. Rudenko, B. C. Thompson, F. C. Krebs, "Photochemical stability of random poly(3-hexylthiophene-co-3-cyanothiophene) and its use in roll coated ITO-free organic photovoltaics. *J. Photonics Energy* **5**, 057205 (2014)

- <u>B. Roth</u>, G. A. dos Reis Benatto, M. Corazza, R. R. Søndergaard, S. A. Gevorgyan, M. Jørgensen, F. C. Krebs, "The Critical Choice of PEDOT:PSS Additives for Long Term Stability of Roll-to-Roll Processed OPVs", *Adv. Energy Mater.* **5**, (2015)

- <u>B. Roth</u>, G. A dos Reis Benatto, M. Corazza, J. E. Carlé, M. Helgesen, S. A. Gevorgyan, M. Jørgensen, R. R Søndergaard, F. C Krebs, "Improving the Operational Stability of PBDTTTz-4 Polymer Solar Cells Modules by Electrode Modification", *Adv. Eng. Mater.* **18**, 511-517, (2015).

- <u>B. Roth</u>, S. Savagatrup, N. V. De Los Santos, O. Hagemann, J. E. Carlé, M. Helgesen, F. Livi, E. Bundgaard, R. R. Søndergaard, F. C. Krebs, D. J. Lipomi, "Molecular Design Rules for Mechanical Stability of Organic Solar Cells Derived from a Library of Low-Bandgap Polymers", *Chem. Mater.* **28**, 7, 2363-2373 (2016).

Co-author publications

- F. C. Krebs, M. Hösel, M. Corazza, <u>B. Roth</u>, M. V. Madsen, S. A. Gevorgyan, R. R. Søndergaard, D. Karg, M. Jørgensen*,* "Freely available OPV-The fast way to progress", *Energy Technol.* **1,** 378–381 (2013)

- G. A. dos Reis Benatto, <u>B. Roth</u>, M. V. Madsen, M. Hösel, R. R. Søndergaard, M. Jørgensen, F. C. Krebs, "Carbon: The Ultimate Electrode Choice for Widely Distributed Polymer Solar Cells", *Adv. Energy Mater.* **4**, (2014).

- F. Livi, R. R Søndergaard, T. R. Andersen, <u>B. Roth</u>, S. Gevorgyan, H. F. Dam, J. E. Carlé, M. Helgesen, G. D. Spyropoulos, J. Adams, T. Ameri, C. J. Brabec, M. Legros, N. Lemaitre, S. Berny, O. R. Lozman, S. Schumann, A. Scheel, P. Apilo, M. Vilkman, E. Bundgaard, F. C. Krebs*, "Round-Robin Studies on Roll-Processed ITO-free Organic Tandem Solar Cells Combined with Inter-Laboratory Stability Studies", *Energy Technol.* **3**, 423–427 (2015).

- E. Bundgaard, F. Livi, O. Hagemann, J. E. Carlé, M. Helgesen, I. M. Heckler, N. K. Zawacka, D. Angmo, T. T. Larsen-Olsen, G. A. dos Reis Benatto, <u>B. Roth</u>, M. V. Madsen, M. R. Andersson, M. Jørgensen, R. R. Søndergaard, F. C. Krebs, "Matrix Organization and Merit Factor Evaluation as a Method to Address the Challenge of Finding a Polymer Material for Roll Coated Polymer Solar Cells", *Adv. Energy Mater.* **5**, (2015). doi: 10.1002/aenm.201402186

- S. A. Gevorgyan, M. V. Madsen, <u>B. Roth</u>, M. Corazza, M. Hösel, R. R. Søndergaard, M. Jørgensen, F. C. Krebs, "Lifetime of Organic Photovoltaics: Status and Predictions", *Adv. Energy Mater.* **6**, (2016). doi: 10.1002/aenm.201501208

- G. A. dos Reis Benatto, <u>B. Roth</u>, M. Corazza, R. R. Søndergaard, S. A. Gevorgyan, M.l Jørgensen, F. C. Krebs, "Roll-to-roll printed silver nanowires for increased stability of flexible ITO-free organic solar cell modules", *Nanoscale* **8**, 318–326 (2016)

- F. A. S. Lima, M. J. Beliatis, <u>B. Roth</u>, T. R. Andersen, A. Bortoti, Y. Reyna, E. Castro, I. F. Vasconcelos, S. A. Gevorgyan, F. C. Krebs, M. Lira-Cantu, "Flexible ITO-free organic solar cells applying aqueous solution-processed V2O5 hole transport layer: An outdoor stability study", *APL Mater.* **4**, 026104 (2016)

- M. J. Beliatis, M. Helgesen, R. García-Valverde, <u>B. Roth</u>, J. E. Carlé, M. Corazza, M. Jørgensen, F. C. Krebs, S. A. Gevorgyan, "Slot-Die-Coated V_2O_5 as Hole Transport Layer for Flexible Organic Solar Cells and Optoelectronic Devices." Adv. Eng. Mater., doi: 10.1002/adem.201600119

Chapter 1 - Introduction

1.1. Background: the energy challenge

The worldwide energy demand rises continuously year after year. The global energy consumption increased by 38 % throughout the twenty-first century to reach 16,8 TWy* in 2014.[1] The yearly energy demand is expected to reach 27 TWy by 2050 due to the growing world population, the United Nation projects the world population to be above 9 billion in 2050, and to the continuous technological development.[2,3] The increasing need for energy puts enormous pressure on the limited earth's resources. Each year since 1970, we consume more natural resources than Earth biocapacity (*i.e.*: how much natural resources the Earth can generate in one year).[4] In 2015, the Earth Overshoot day, meaning the day humanity's resources consumption exceeds the Earth biocapacity, was August 13.[4] At this rate, there are only 109 years of coal, 54 years of natural gas and 53 years of crude oil left.[1] Today most of the energy consumed comes from fossil fuels which are not renewable at the human lifetime scale (see Fig 1.1). To sustain the current technological development of the human society new sustainable energy sources are needed. In 2014, according to the US Energy Information Agency (IEA), the share of renewable energy sources in the total electricity installed capacity was 26,2%.[5] However, this is mostly based on hydroelectricity and biomass, wind and solar energy are still under exploited. Another effect of the current unsustainable human development is the global warming due to the extreme emissions of greenhouse gases particularly CO_2. The CO_2 emissions have dramatically risen since the beginning of the twentieth century (Fig 1.2). One impact is the increase of the global earth's surface temperature, especially since the 1950s which menaces the fragile ecological balance of our planet. To keep the current technological and economic development and ensure a sustainable future it is required to substitute finite fossil fuels resources with renewable energy sources.

---

*Terawatt-year (TWy) is unit of power but is here used as energy unit. 1 TWy = 8766 TWh

Primary Energy Consumption 2014
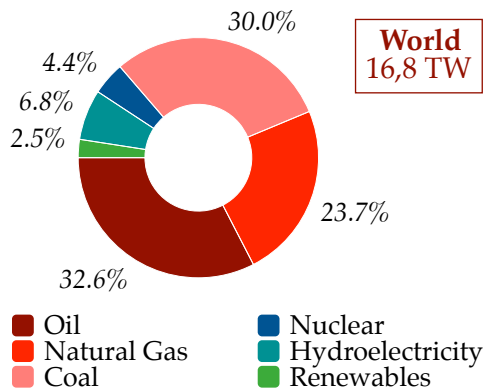
Installed Electricity Capacity 2012
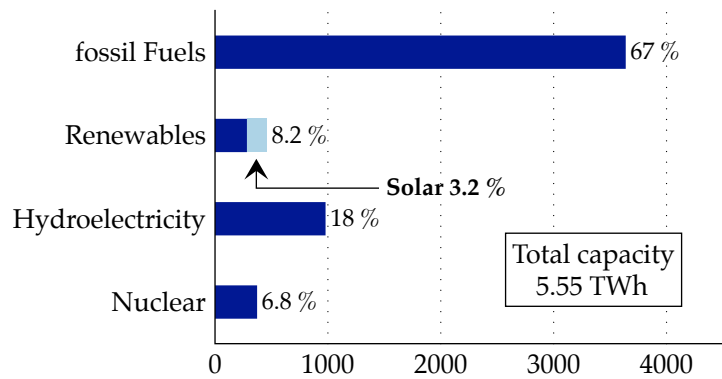
Fig 1.1 – Worldwide energy consumption in 2014 (left).[1] Electricity production capacity in 2012 (right).[6]
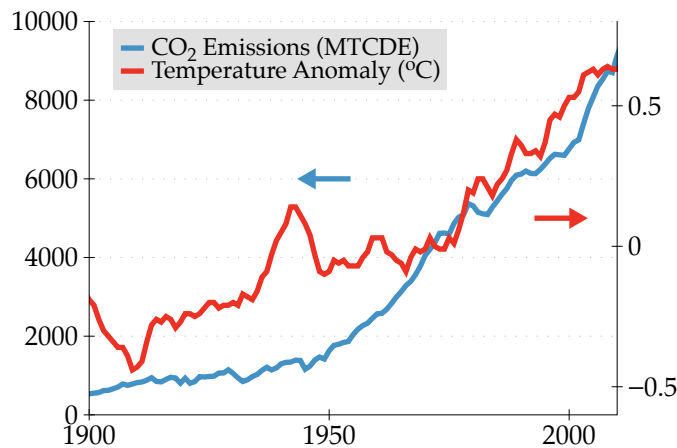
Fig 1.2 – Worldwide CO2 emissions since 1900 and Annual temperature anomaly compared to the average temperature between 1951 and 1980.[7,8]

1.2. Why solar energy?

As mentioned in the previous section the scarcity of fossil fuels which today dominate our energy mix, challenges us to find alternative energy sources. Currently most renewable installed capacity is biomass (burned for heating) or hydropower based. [5] However a quick look at the available energy sources in Fig 1.3 is sufficient to determine that one source outshine all the others with respect to potential: Solar Power. Electromagnetic radiations emanate constantly from the Sun toward the Earth. The actual irradiance at the Earth's surface varies depending on location, season and time of the day. Nevertheless, it amounts to about 23000 TWy of

energy that could potentially be harvested over a year.[2] It is also important to notice that most dynamic processes on Earth are driven by solar radiation and consequently all renewable energy sources except geothermal also are. Temperatures fluctuations induce wind, wave and precipitations, which are harvested for hydropower, wind power and wave power. As for biomass and biofuels, they originate from photosynthesis induced by solar radiations. Among all these energy sources only solar power is a one-step conversion of solar radiation into energy without CO_2 emissions. Others sources are inefficient multi-steps processes which means that the amount of energy available for harvesting is a few orders of magnitude lower than for solar power (Fig 1.3). The result is that solar power is the only energy source that can cover the world's demand by itself. It is important to note that the 23000 TWy is the potential energy received by the entire land mass on earth. However estimations based on 2% land used for PV deployment and 12% efficiency show that about 67 TWy can be harvested every year.[9] This amount is well above the predicted 27 TWy energy consumption for 2050.[2]

Solar 23000 TWy/y

Other Renewables 156,3 TWy/y

- **Tidal** 0.3 TWy/y
- **Waves** 0.2 - 2 TWy/y
- **Hydro** 3 - 4 TWy/y
- **Biomass** 2 - 6 TWy/y
- **OTEC** 3 - 11 TWy/y
- **Wind** 75 - 130 TWy/y

2015 Energy Consumption 18,5 TWy/y

Finite resources 1570 TWy

- **Coal** 830 TWy
- **Pretrolum** 335 TWy
- **Natural Gas** 220 TWy
- **Uranium** 185 TWy

Fig 1.3 – Earth available resources in 2015.[2]

There are two types of solar power: solar heating and photovoltaics. Solar heating transforms the solar energy into thermal energy by heating water or air for residential or commercial used as well as in some cases for electrical power generation. Photovoltaics convert the solar energy

directly into electric power. Since the beginning of the twenty-first century the photovoltaic cumulative capacity has increased exponentially. The installed photovoltaic capacity was 177 GW in 2014 and is projected to be about 233 GW by end of 2015.[10] 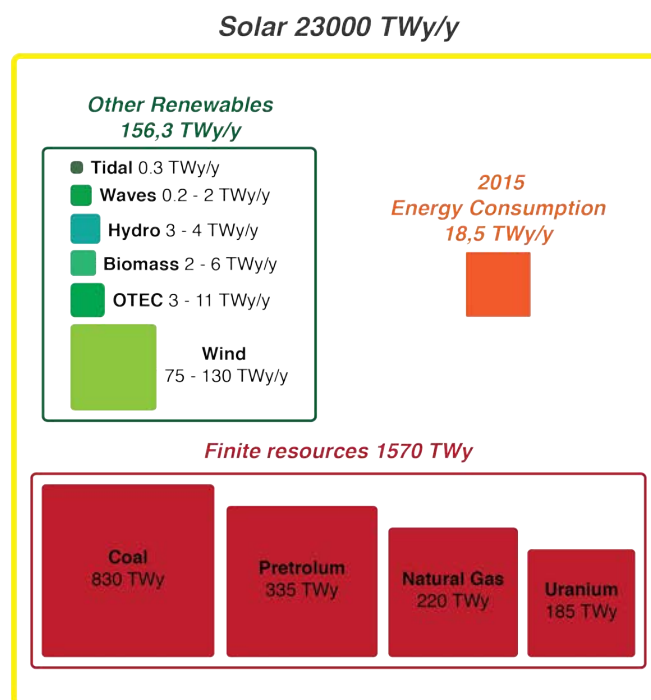One main advantage of solar power is that it can be scaled to answer the local needs, for example small off-grid installations in remote areas are possible. The main disadvantage of solar power is that it is a fluctuating energy source because it depends on the sun irradiance. It requires therefore low cost and efficient storage technologies. Consequently, a solar dominated mix of renewable energies is the favored approach to answer energy demand sustainably in the future.

1.3. Photovoltaic technologies

All the photovoltaic technologies are based on a phenomenon called: the photovoltaic effect. This phenomenon was first introduced by A.E. Becquerel in 1839 in "Comptes rendu de l'Académie des sciences" (*i.e.*: Proceedings of the Academy of Sciences). Becquerel generated voltage and current by illuminating an acidic solution of silver chloride connected to platinum electrodes. Briefly explained, the photovoltaic effect is the creation of voltage and electric current that occurs when some semiconductor materials are exposed to light. The first silicon solar cell was presented in 1954 by the Bell Laboratories. Today the market is still dominated by crystalline silicon cells which accounted for 92 % of the solar cell production in 2014.[11]

1.3.1. The three photovoltaic generations

The first generation solar cells

First introduced in the 1950s, this solar cells use bulk mono or poly crystalline silicon doped with boron or phosphorus as semiconducting material. In the lab, the record efficiencies are 25,6 % for mono-crystalline silicon cells and 20,8% for poly-crystalline cells.[11] However, the average efficiency for commercial modules is about 16 % with a lifetime of roughly 20 years. The main drawback is that these cells require high grade silicon wafers which are produced with costly high energy processes. The high energy uses for manufacturing also means that the energy payback time (EPBT) for a first generation photovoltaic system ranges from 1.5 to a few years depending on the type of module and on geographical location.[11,12] This means that the energy return on energy invested (EROI) is only about 10.

The second generation solar cells

Thin film solar cells were developed to answer the high manufacturing cost of the first generation photovoltaics. In 2014 they represented only 9 % of produced photovoltaic modules.[11] The cost reduction is obtained mainly because of the reduction of material use. The active layer is about 100 times thinner in thin film solar cells (a few μm or below) than for crystalline silicon cells that employ a silicon wafer ~ 200 μm thick. In most cases, the manufacturing of thin film solar cells is done with low temperatures processes such as chemical vapor deposition (CVD), which also lowers the embodied energy. However, in order not to compromise the efficiency, the active materials need to be stronger absorbers. Thin film solar cells are typically made with amorphous silicon (a-Si), copper indium gallium selenide (CIGS), cadmium telluride (Cd-Te) or gallium arsenide (GaAs). GaAs cells are expensive but hold the record efficiency for a single junction cells (28.8 %).[13] For lab scale devices, the record for both CIGS and Cd-Te cells is 21 %.[13] The efficiency of commercial thin film solar cells ranges from 7 % (a-Si) to 16.3 % (CdTe).[10] The lifetime of thin film solar cells is well above 20 years.[12] Life cycle analyses show that thin fil solar cells have an EPBT between 1 and 2 years and an EROI of from 14.5 for a-Si up to 34.2 for Cd-Te.[12,14] The drawbacks of the 2nd generation photovoltaics is the toxicity and the scarcity of the active materials except a-Si which presents lower performances.

The third generation solar cells: emerging technologies

This last generation groups all the photovoltaic technologies still in the developing stage with little to no commercial applications. The development of these new technologies is still driven by the search for lower cost and for higher efficiencies.

Copper zinc tin sulfide selenide (CZTSSe) solar cells:

These thin film solar cells employ an inorganic material (CZTSSe) with similar absorbing properties than CiGS and Cd-Te. CZTSSe is only made with abundant and non-toxic materials a clear plus compared to the 2nd generation thin film solar cells. However, the efficiency of CZTSSe solar cells remains low. The maximum reported efficiency is 12.6 %.[13]

Dye-sensitized solar cells (DSSC):

Introduced in 1991, DSSC are a novel photoelectrochemical photovoltaic system using an organic dye. The dye is deposited on a titanium oxide (TiO_2) network of nanoparticles dipped in an electrolyte. When the dye absorbs photons, it is oxidized. The excited electrons are injected in the TiO_2 network and the dye is reduced by the ion in the electrolyte. The maximum efficiency reported for DSSC is 11.9%.[13] Many issues such as stability, toxicity of the dye and handling of the liquid electrolyte have slowed down commercialization of DSSC.

Quantum dots solar cells:

In these solar cell the absorbing layer is replace by quantum dots typically lead-sulfur (PbS) dots. The band gap of a bulk material is fixed but in the case of quantum dots it can be tuned by modifying the size of the dots. This characteristic is particularly attractive for multi-junction cells where the band gap of each sub-cell can be tuned to harvest a wider range of the sunlight. Efficiencies for single junction cells remain low with a record efficiency of 10.6%.[13]

Perovskite solar cell:

Research in the field of perovskite solar cells is recent (first report in 2009 by Kojima *et al.*) but the efficiencies have risen dramatically from 3.8 % to 21 %.[13,15] At first these cells used a DSSC architecture where the absorber material has a perovskite crystallographic structure. The liquid electrolyte and the TiO2 nanoparticles have since then been replaced to improve efficiency and stability. Stability still remains an issue especially in humid conditions. Another major issue is that most active materials in perovskite solar cells are lead based, a highly toxic compound. Lead can be replaced by tin but the efficiency of the overall device drops significantly.

Polymer/organic solar cells:

These solar cells are the focus of this thesis and will be introduced in depth in the next paragraph.

1.4. Organic Photovoltaics (OPV)

Organic solar cells are made with organic semiconductors as light absorber. Anthracene was the first organic compound reported to exhibit photoconductivity in the beginning of the 20th century.[16,17] Later in the 1960s, the interest in such compound as photoreceptors for imaging system led to the discovery that many common dyes were semiconductors.

Forwarding to today, OPV are made with either conjugated polymers or small organic molecules. These materials have many advantages over silicon for photovoltaic applications. They are cheap, non-toxic (even if the synthesis can be toxic) and require only earth abundant materials for synthesis.[14] Furthermore organic semiconductors are strong absorbers meaning only a thin film is needed, which reduces the material need and so the cost of manufacturing.[18] The extreme thinness of OPV gives them superior mechanical properties compared to silicon based cells. For example, Kaltenbrunner *et al.* have reported an ultra-flexible OPV cell than can be rolled up around a hair.[19] They can be processed from solution using low cost and low temperature roll-to-roll (R2R) manufacturing processes.[20] Flexibility and low cost R2R manufacturing are the key properties driving the development of OPV.

Even though, polymer solar cells (PSC) are the topic of this thesis, the operating principle of small molecules and polymer solar cells is similar and is described in the rest of this section.

If OPV are struggling to penetrate the market, it is because they also suffer from critical issues such has low efficiency and poor stability. In order to compete with others photovoltaic technologies, OPV need to fulfill the three criteria illustrated in Fig 1.4: efficiency, cost and stability.[21] As of today no OPV cell architecture fulfills all three criteria at the same time. An estimation based on current technologies and processes, is that a cell efficiency > 10 % is required for market penetration.[22] Even though the highest reported efficiency for a single junction OPV cell is as high as 11%, most cells have an active area below 1 cm^2 and are prepared on glass substrates with processing methods (spin coating, vacuum deposition) and scarce materials such as indium tin oxide (ITO) which are not compatible with the low cost R2R manufacturing approach.[23,24] For the lifetime, between 3 and 5 years of operational stability are needed. The longest lifetime reported for large scale OPV modules under outdoor operation is about 2 years.[25] The recent drop of crystalline silicon cells cost (0.3 $/W) is another challenge for OPV commercialization.[26] To achieve a production cost below 1 $/W upscaling to high speed R2R manufacturing is needed. Recent reports show that the levelised cost of electricity

for OPV would be competitive with current photovoltaic technologies for a module efficiency around 2 % and a lifetime of 3 years.[27]
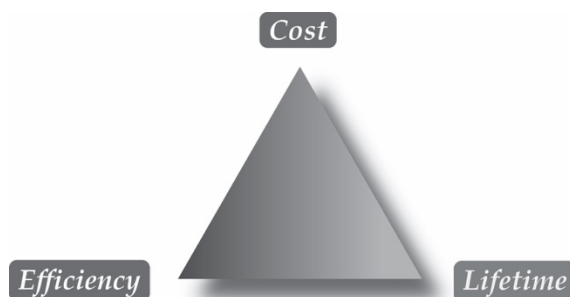
Fig 1.4 – the critical triangle of OPV.

1.4.1. Organic semiconductors

Organic semiconductors (SC) are π-conjugated molecules (alternating single and multiple bounds). The delocalization of π-electrons across the overlapping P-orbitals creates a polarizable structure. The properties of organic SC are different from the ones of inorganic SC. The reason being that inorganic SC crystallize into a 3 dimensional crystal lattice when the crystallization is at best partial in organic SC. The high order of organization in inorganic SC results in the interaction of the discrete energy levels and into their degeneration in valence band (VB) and conduction band (CB). The disorder in organic semiconductors is due to the low inter-molecular forces and high conformational freedom, meaning that molecular orbitals in organic semiconductors do not interact enough to create a CB and a VB.[28,29] What is referred as band gap (E_G) in organic semiconductor is therefore not the difference between the VB and the CB but the difference between the highest occupied molecular orbital (HOMO) and the lowest unoccupied molecular orbital (LUMO). Charge transport occurs by hopping in conjugated materials (the charges jump from a localized state to another) so the charge mobility is low in organic SC. In organic SC the dielectric constant is also low (2-4).[30] This is not without consequence for the use of organic SC for photovoltaic application. When photons are absorbed in organic materials free carriers (electrons and holes) are not created as in inorganic SC. A neutral localized excited state called frenkel exciton (strongly bonded electron hole pair ~ 1eV) is generated.[31] The exciton binding energy is well above the thermal energy at 300 K (k_BT ~ 2.6×10^{-2} eV) meaning that dissociation is unlikely. For charge dissociation to occur in

OPV cells a high free energy difference is required. This usually occurs when an exciton reaches an interface across which the chemical potential of electrons decreases.

1.4.2. Principle of OPV[18,29,31]

The first OPV cells developed were single layer cells using an organic dye sandwiched between two electrodes with dissimilar workfunctions (see Fig 1.5 left).[32] In cells with that architecture, the primary site for exciton dissociation is the electrodes interfaces. Only the excitons generated close enough to reach the interfaces before recombination (~ 10 nm) contribute to charges generation. Therefore, the actual light harvesting thickness is only a few nm, which is not optically dense. This is why the efficiency of the first OPV cells was low.

To improve the exciton separation and consequently the efficiency, a new architecture with a double layer was proposed (Fig 1.5 middle).[33] One layer has a high electron affinity (Acceptor material) and the other has a high ionization energy (Donor material). The interface between the acceptor (A) and the donor (D) becomes the primary site for exciton dissociation because of the free energy difference. The D/A interface is referred as heterojunction. However, generated excitons still need to reach the heterojunction to dissociate. The efficiency of the cell is still low because the harvesting thickness is limited to a few nm around the D/A interface and most organic SC need a thickness of about 100 nm to absorb most of the light.[29]

This issue was solved with the introduction of bulk heterojunction cells (Fig 1.5 right) in 1995 by Yu *et al.*.[34] The idea is simple: all the excitons need to be photogenerated in the proximity of a D/A interface in order to be dissociated. In a bulk heterojunction cell, an interpenetrating nanoscale network of D/A junctions is formed through the bulk harvesting layer. This has a few advantages:

- A large D/A interface area ensuring an efficient charge separation
- Continuous path to both electrodes for efficient charge collection
- The harvesting thickness is optically dense

A bulk heterojunction is prepared by deposition of a mixed solution of a donor and an acceptor in an organic solvent. After solvent evaporation and in some case a thermal treatment the bulk heterojunction is formed.
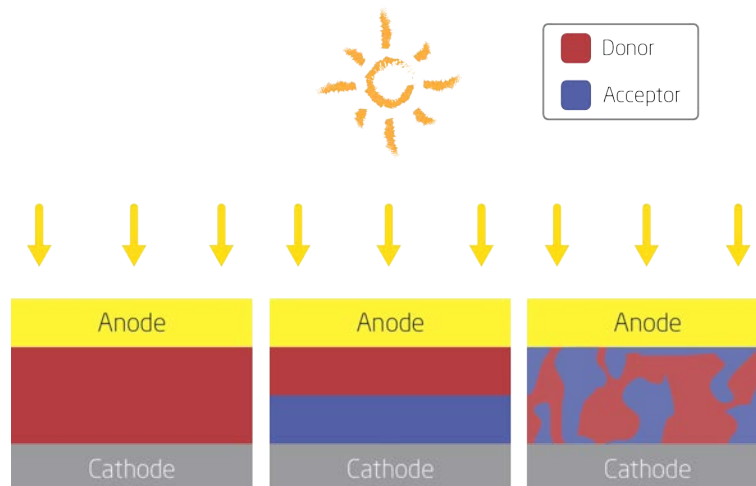
Fig 1.5 – OPV cells structures: (left) single layer cell; (middle) double layer cell; (right) Bulk heterojunction cell.

Bulk heterojunctions are now used in most OPV devices with a wide range of donor and acceptor materials. The most common donor is Poly(3-hexylthiophene-2,5-diyl) (P3HT) and the most common acceptor is [6,6]-Phenyl C61 butyric acid methyl ester (PCBM) (Fig 1.6).
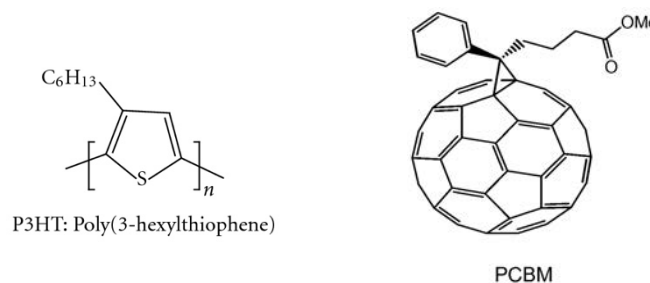
Fig 1.6 – Chemical structure of P3HT (left) and PCBM (right).

The working principle of a bulk heterojunction (BHJ) is a four step process (Fig 1.7).[31]

Absorption of light & exciton generation

Under illumination of the BHJ, a photoexcited state is created by the absorption of a photon by the donor if the energy of the incident photon (E_{photon}) is equal or superior to the optical band gap (E_g). An electron is transferred from the HOMO to the LUMO of the donor. The associated positive charge carrier (hole) remains in the HOMO of the donor. The two charge carriers are bound together by Coulomb forces and form an exciton.
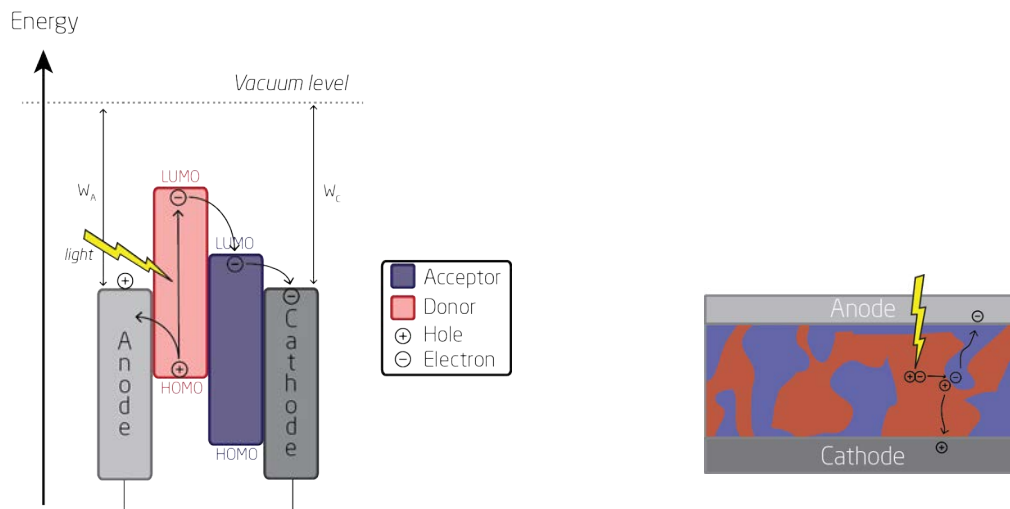
Fig 1.7 – (left) Band diagram of the heterojunction in an organic solar cell. The electrodes are short circuited so their workfunction are aligned. (right) Schematic illustration of charges photogeneration in a bulk heterojunction.

Exciton diffusion

The exciton diffuses through the donor phase toward a D/A interface. Excitons diffusion length is about 10 nm meaning that the dimension of the heterojunction network needs to be in the same range or smaller.[31] When excitons are generated too far from a D/A interface recombination may occur.

Exciton dissociation

When the exciton reaches the D/A interface the electron is attracted by the higher electron affinity of the acceptor. The electron is transferred to the LUMO of the acceptor and the charges are separated. The dissociation will only happen if the energy difference between the LUMO of the donor and the LUMO of the acceptor is at least equal to the bonding energy. Otherwise the exciton recombines and no charges are created. In such case, energy is lost as heat or reemitted at longer wavelength.

Charge transport and collection

The internal electric field created by the difference in workfunction of the electrodes, separates the free charges. The free charges diffuse through the donor and acceptor network and are

collected at the cathode for the electrons and at the anode for the holes. The generation of photocurrent is achieved through short circuiting or by applying an external load.

1.4.3. Electrical characterization

Typically, OPV cells are characterized by current – voltage (I-V) measurement. Common I-V curves for OPV are shown in Fig 1.8 both in the dark and under illumination. The illumination is standardized at 1000 W/m^2 with a spectral intensity distribution matching that of the sun on the earth's surface at an incident angle of 48.2°.[35]
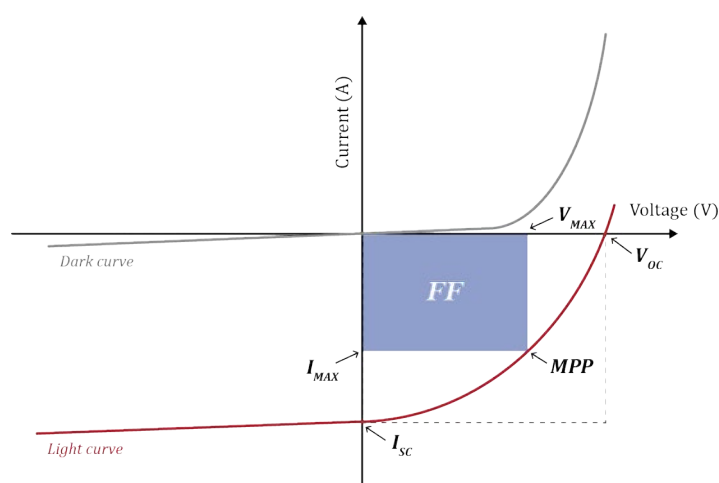
Fig 1.8 – I-V curves of an OPV cell in dark and under illumination

In the dark, an OPV cell acts as a simple diode (Fig 1.8) where almost no current flows until a forward voltage bias above the open circuit voltage (V_{OC}) is applied.[35] Under illumination the I-V curve is shifted down. The short circuit current (I_{SC}) is the maximum current that can flow through the cell under standard (1000 W/m^2) illumination. For most OPV, the short circuit current density (J_{SC}) is in the 0.2 – 80 mA/cm^2 range.[29] Another important parameter is the V_{OC} which is the maximum voltage difference achievable between the two electrodes. V_{OC} is usually around 0.5 – 1.5 V.[29] In general, in a metal-insulator-metal (MIM) device, V_{OC} is fixed by the difference between the metal electrode workfunctions. But in a D/A heterojunction, V_{OC} is determined by the difference of the quasi Fermi levels of the two charge carriers (equation 1.1).[35] For OPV, V_{OC} is directly dependent on the HOMO of the donor (p-type SC quasi Fermi level) and on the LUMO of the acceptor (n-type SC quasi Fermi level). This linear correlation

was shown by Brabec *et al.* for the LUMO of fullerene acceptors and by Scharber *et al.* for the HOMO of conjugated polymer donors.[36,37] The actual V_{OC} is lowered by energetic disorder.[38]

$$(1.1) \quad V_{OC} \sim {}^1\!/_q \, (E_{HOMO,D} - E_{LUMO,A})$$

q is the elementary charge, $E_{HOMO,D}$ the energy level of the donor HOMO and $E_{LUMO,A}$ the energy level of the acceptor LUMO.

The I-V curve under illumination allows for determination of the maximum power point (MPP). The MPP is the maximum power the cell can produce under illumination. V_{MAX} and I_{MAX} are the voltage and the current at MPP. The fill factor (FF) is defined by the ratio between the power at MPP and the theoretical maximum power output ($I_{SC}V_{OC}$) (equation 2). A high FF is warranted to be as close as possible to the theoretical maximum output. But the FF usually ranges from 0.4 to 0.6.[29] The FF is directly related to series resistance (R_S) and to the shunt resistance (R_{SH}) of the cell. R_S depends on the layers interfaces resistances and on the conductivity of the semiconductors and of the electrodes. Defects due to the manufacturing processes can created shorts which lowers R_{SH}.

$$(1.2) \quad FF = \frac{I_{MAX}V_{MAX}}{I_{SC}V_{OC}}$$

The last important parameter is the power conversion efficiency (PCE). The PCE is the ratio of the power output and the power of the incident light (P_{IN}) (equation 1.3).[19] P_{IN} is the solar irradiance (I_{IN}) received by the active area of the cell (A).

$$(1.3) \quad PCE = \frac{P_{MPP}}{P_{IN}} = \frac{I_{MAX}V_{MAX}}{I_{IN}A} = \frac{I_{SC}V_{OC}FF}{I_{IN}A} = \frac{J_{SC}V_{OC}FF}{I_{IN}}$$

1.5. OPV devices structures

Even tough flexibility is the goal of OPV, the majority of the cells prepared in the laboratories are deposited on glass substrates.[25] For flexible substrate polyethylene terephthalate (PET) is

the most common. OPV cells have a planar structure where the organic active layer is sandwiched between two electrodes with different workfunctions. At least one electrode needs to be transparent so the light can reach the active layer. Indium tin oxide (ITO) is widely used as such. However, ITO is expensive, scarce, brittle and is deposited through a vacuum step. ITO has therefore a high embodied energy and is not compatible with the low cost R2R approach and should be replaced.[38] One way to do so is to use a fine metal grid such as silver covered with a layer of PEDOT:PSS.[39] Opaque electrodes are usually metallic: Calcium (Ca), Aluminum (Al), Silver (Ag), Gold (Au). For the active layer a D/A BHJ is nowadays favored. The most studied system is by far Poly(3-hexylthiophene-2,5-diyl) (P3HT) as a donor and [6,6]-Phenyl C61 butyric acid methyl ester (PCBM) as acceptor (Fig 1.6). P3HT:PCBM cells have reached efficiencies up to 5 % which pushes the development of new high efficiency polymer.[25,40] Charges selective layers are inserted between the BHJ and the electrodes for better contact and charges extraction. The hole transport layer (HTL) between the BHJ and the anode can be a semiconducting polymer or an oxide (NiO, WO_3, MoO_3, V_2O_5).[31] Poly(3,4-ethylenedioxythiophene)-poly(styrenesulfonate) (PEDOT:PSS) is used as HTL in most OPV devices. Finally the electron transport layer (ETL) can be ZnO, LiF, TiOx.[31,41]

Shown in Fig 1.9 are the two types of organic solar cells architecture: normal and inverted. The normal or regular architecture was the first one used for OPV cells but is mostly limited to lab scale cells to test new material. The reasons being that regular cells suffer from a poor stability and require vacuum steps to deposit the top layers.[26,41] The inverted architecture is favored for large scale R2R manufacturing because it allows for full solution processing.[42] And also high workfunction metal such as silver are used for the back electrode which sensibly increases the stability of the cell.[26]

1) Normal geometry   *2) Inverted geometry*
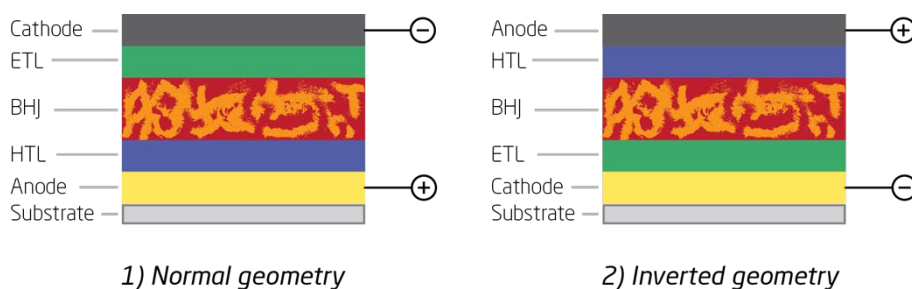
Fig 1.9 – (left) regular architecture OPV with substrate: glass, Anode: ITO, HTL: PEDOT:PSS, ETL: LiF, Cathode: Al; (right) Inverted architecture OPV with Cathode: ITO, ETL: ZnO, HTL:PEDOT:PSS, Anode: Ag.

1.6. Thesis Outline

Among the three keys parameters (efficiency, lifetime and cost) to OPV development into a commercial technology, this thesis focuses solely on lifetime. The devices studied are all ITO-free and prepared by roll coating/printing from solution.

Chapter 2 introduces in details the R2R coating and printing techniques. This was deemed necessary even though no study was done on these already available techniques, because most samples in this work were prepared using these techniques.

Chapter 3 presents stability studies of OPV cells as well as a meta-analysis of thousands of reports on the stability of organic solar cells.

Chapter 4 focuses on the selection of high efficiency donor material suitable for R2R upscaling. The mechanical properties of these materials are also studied in function of their molecular structure.

Chapter 5 is a collection of indoor and outdoor lifetime studies of large scale OPV modules focusing on electrode design and PEDOT:PSS as intermediate layer.

1.7. References

(1)   BP Statistical Review of World Energy June 2015
        https://www.bp.com/content/dam/bp/pdf/energy-economics/statistical-review-2015/bp-statistical-
        review-of-world-energy-2015-full-report.pdf (accessed Dec 8, 2015).

(2)   Perez, R.; Perez, M. A Fundamental Look At Supply Side Energy Reserves For The Planet. *Int. energy
        Agency SHC Program. Sol. Updat.* **2015**, 4–6.

(3)   World Population Prospects - Population Division - United Nations http://esa.un.org/unpd/wpp/
        (accessed Dec 8, 2015).

(4)   Earth Overshoot Day http://www.overshootday.org/newsroom/media-backgrounder/#8 (accessed
        Dec 8, 2015).

(5)   U.S. Energy Information Administration. Annual Energy Outlook 2015. **2015**, 154.

(6)   EIA. International Energy Statistics
        https://www.eia.gov/cfapps/ipdbproject/iedindex3.cfm?tid=2&pid=29&aid=7&cid=ww,&syid=2008
        &eyid=2012&unit=MK (accessed Mar 16, 2016).

(7)   CO2 emissions per year
        http://cdiac.ornl.gov/images/global_fossil_carbon_emissions_google_chart.jpg (accessed Dec 8,
        2015).

(8)   Climate Change: Vital Signs of the Planet: Global Temperature http://climate.nasa.gov/vital-
        signs/global-temperature/ (accessed Dec 8, 2015).

(9)   Darling, S. B.; You, F. The Case for Organic Photovoltaics. *RSC Adv.* **2013**, *3* (39), 17633–17648.

(10)   International Energy Agency Photovoltaic Power System Program. *Trends 2015 in Photovoltaic
        Applications*; 2015.

(11)   Fraunhofer Institute for Solar Energy Systems. *Photovoltaics Report*; 2015.

(12)   Price Quotes_EnergyTrend PV http://pv.energytrend.com/pricequotes.html (accessed Dec 10,
        2015).

(13)   Bhandari, K. P.; Collier, J. M.; Ellingson, R. J.; Apul, D. S. Energy Payback Time (EPBT) and Energy
        Return on Energy Invested (EROI) of Solar Photovoltaic Systems: A Systematic Review and Meta-
        Analysis. *Renew. Sustain. Energy Rev.* **2015**, *47*, 133–141.

(14)   Green, M. A.; Emery, K.; Hishikawa, Y.; Warta, W.; Dunlop, E. D. Solar Cell Efficiency Tables (version
        46). *Prog. Photovoltaics Res. Appl.* **2015**, *23*, 805–812.

(15)   Espinosa, N.; Hösel, M.; Angmo, D.; Krebs, F. C. Solar Cells with One-Day Energy Payback for the
        Factories of the Future. *Energy Environ. Sci.* **2012**, *5* (1), 5117–5132.

(16)   Kojima, A.; Teshima, K.; Shirai, Y.; Miyasaka, T. Organometal Halide Perovskites as Visible-Light
        Sensitizers for Photovoltaic Cells. *J. Am. Chem. Soc.* **2009**, *131* (17), 6050–6051.

(17)   Pochettino, A. *Acad. Lincei Rend.* **1906**, *15*, 355.

(18)   Volmer, M. *Ann. Phys.* **1913**, *40* (775).

(19)   Hoppe, H.; Sariciftci, N. S. Organic Solar Cells: An Overview. *J. Mater. Res.* **2004**, *19* (07), 1924–
        1945.

(20)   Kaltenbrunner, M.; White, M. S.; Głowacki, E. D.; Sekitani, T.; Someya, T.; Sariciftci, N. S.; Bauer, S.
        Ultrathin and Lightweight Organic Solar Cells with High Flexibility. *Nat. Commun.* **2012**, *3*, 1–7.

(21)   Roth, B.; Søndergaard, R. R.; Krebs, F. C. Roll-to-Roll Printing and Coating Techniques for

Manufacturing Large-Area Flexible Organic. In *Handbook of Flexible Organic Electronics: Materials, Manufacturing and Applications*; Logothetidis, S., Ed.; Elsevier, 2014; pp 171–197.

(22) Brabec, C. J. Organic Photovoltaics: Technology and Market. *Sol. Energy Mater. Sol. Cells* **2004**, *83* (2-3), 273–292.

(23) Brabec, C. J.; Hauch, J. A.; Schilinsky, P.; Waldauf, C. Production Aspects of Organic Photovoltaics and Commercialization of Devices. *MRS Bull.* **2005**, *30*, 50–52.

(24) NREL Best Research cell efficiencies. Best Research-Cell Efficiencies - NREL http://www.nrel.gov/ncpv/images/efficiency_chart.jpg (accessed Jun 9, 2015).

(25) Jørgensen, M.; Carlé, J. E.; Søndergaard, R. R.; Lauritzen, M.; Dagnæs-Hansen, N. A.; Byskov, S. L.; Andersen, T. R.; Larsen-Olsen, T. T.; Böttiger, A. P. L.; Andreasen, B.; Fu, L.; Zuo, L.; Liu, Y.; Bundgaard, E.; Zhan, X.; Chen, H.; Krebs, F. C. The State of Organic Solar cells—A Meta Analysis. *Sol. Energy Mater. Sol. Cells* **2013**, *119*, 84–93.

(26) Gevorgyan, S. A.; Madsen, M. V.; Roth, B.; Corazza, M.; Hösel, M.; Søndergaard, R. R.; Jørgensen, M.; Krebs, F. C. Lifetime of Organic Photovoltaics: Status and Predictions. *Adv. Energy Mater.* **2016**, *6* (2), 1501208.

(27) Mulligan, C. J.; Bilen, C.; Zhou, X.; Belcher, W. J.; Dastoor, P. C. Levelised Cost of Electricity for Organic Photovoltaics. *Sol. Energy Mater. Sol. Cells* **2015**, *133*, 26–31.

(28) Noriega, R.; Rivnay, J.; Vandewal, K.; Koch, F. P. V.; Stingelin, N.; Smith, P.; Toney, M. F.; Salleo, A. A General Relationship between Disorder, Aggregation and Charge Transport in Conjugated Polymers. *Nat. Mater.* **2013**, *12* (11), 1038–1044.

(29) Spanggaard, H.; Krebs, F. C. A Brief History of the Development of Organic and Polymeric Photovoltaics. *Sol. Energy Mater. Sol. Cells* **2004**, *83* (2-3), 125–146.

(30) Torabi, S.; Jahani, F.; Van Severen, I.; Kanimozhi, C.; Patil, S.; Havenith, R. W. A.; Chiechi, R. C.; Lutsen, L.; Vanderzande, D. J. M.; Cleij, T. J.; Hummelen, J. C.; Koster, L. J. A. Strategy for Enhancing the Dielectric Constant of Organic Semiconductors Without Sacrificing Charge Carrier Mobility and Solubility. *Adv. Funct. Mater.* **2015**, *25* (1), 150–157.

(31) Nelson, J. Polymer:fullerene Bulk Heterojunction Solar Cells. *Mater. Today* **2011**, *14* (10), 462–470.

(32) Chamberlain, G. A. Organic Solar Cells: A Review. *Sol. Cells* **1983**, *8* (1), 47–83.

(33) Tang, C. W. Two-Layer Organic Photovoltaic Cell. *Appl. Phys. Lett.* **1986**, *48* (2), 183–185.

(34) Yu, G.; Gao, J.; Hummelen, J. C.; Wudl, F.; Heeger, A. J. Polymer Photovoltaic Cells: Enhanced Efficiencies via a Network of Internal Donor-Acceptor Heterojunctions. *Science (80-.).* **1995**, *270* (5243), 1789–1791.

(35) Günes, S.; Neugebauer, H.; Sariciftci, N. S. Conjugated Polymer-Based Organic Solar Cells. *Chem. Rev.* **2007**, *107* (4), 1324–1338.

(36) Brabec, C. J.; Cravino, A.; Meissner, D.; Sariciftci, N. S.; Fromherz, T.; Rispens, M. T.; Sanchez, L.; Hummelen, J. C. Origin of the Open Circuit Voltage of Plastic Solar Cells. *Adv. Funct. Mater.* **2001**, *11* (5), 374–380.

(37) Scharber, M. C.; Mühlbacher, D.; Koppe, M.; Denk, P.; Waldauf, C.; Heeger, A. J.; Brabec, C. J. Design Rules for Donors in Bulk-Heterojunction Solar Cells—Towards 10 % Energy-Conversion Efficiency. *Adv. Mater.* **2006**, *18* (6), 789–794.

(38) Espinosa, N.; García-Valverde, R.; Urbina, A.; Krebs, F. C. A Life Cycle Analysis of Polymer Solar Cell Modules Prepared Using Roll-to-Roll Methods under Ambient Conditions. *Sol. Energy Mater. Sol. Cells* **2011**, *95* (5), 1293–1302.

(39) Krebs, F. C.; Espinosa, N.; Hösel, M.; Søndergaard, R. R.; Jørgensen, M. 25th Anniversary Article:

Rise to Power - OPV-Based Solar Parks. *Adv. Mater.* **2014**, *26* (1), 29–39.

(40)   Bundgaard, E.; Hagemann, O.; Manceau, M.; Jørgensen, M.; Krebs, F. C. Low Band Gap Polymers for Roll-to-Roll Coated Polymer Solar Cells. *Macromolecules* **2010**, *43* (19), 8115–8120.

(41)   Hau, S. K.; Yip, H.-L.; Jen, A. K.-Y. A Review on the Development of the Inverted Polymer Solar Cell Architecture. *Polym. Rev.* **2010**, *50* (4), 474–510.

(42)   Krebs, F. C.; Gevorgyan, S. A.; Alstrup, J. A Roll-to-Roll Process to Flexible Polymer Solar Cells: Model Studies, Manufacture and Operational Stability Studies. *J. Mater. Chem.* **2009**, *19* (30), 5442–5451.

Chapter 2 - Roll-to-Roll manufacturing of Organic Solar Cells

2.1. Introduction

One of the ideas spearheading the development of organic photovoltaics (OPV) is the potential manufacturing of these cells at low cost and at very high speeds by Roll-to-Roll (R2R) manufacturing. Therefore, the final goal of the development of OPV was always the full manufacturing of modules by R2R on flexible substrates, which is the perfect combination for high processing speeds and cheap substrates. After two decades of intense research the OPV technology is now mature at the laboratory level and upscaling is the natural next step. However, the upscaling from small glass substrate cells to large area R2R modules is extremely challenging. One reason being that many common techniques used to prepare OPV cells in the lab (spin-coating, metal evaporation…) are not compatible with high throughput R2R manufacturing. A study of all reports on OPV up to 2012 showed that 99%, of the OPV cells are prepared with glass and required vacuum processing such as evaporation of metal electrode.[1] Even though R2R metal evaporation is possible and used many industry, it is challenging to keep the registration for multilayers structures and requires high capital investments. The consequence is that until now examples of true full R2R manufacturing of OPV are limited. The focus of this chapter is solely on R2R deposition techniques without vacuum and with solution processing. Most of the methods have been commonly used in the printing industry for many years and have just been transferred to the manufacturing of OPV. The following chapter is based on a non-exhaustive review of scientific reports and more recent reports where R2R printing and coating techniques were used to deposit at least one layer in OPV devices.[2] These deposition methods can be divided in two categories: printing techniques (contact techniques) and non-contact coating techniques.

2.2. Printing techniques

All Roll-to-Roll printing techniques are contact methods except for inkjet printing. The ink is transferred through contact, from a solid printing form to a substrate to print a two dimensional pattern. Extensive ranges of thickness, resolution and printing speeds are available. Inkjet printing is not really a printing technique because it employs neither contact nor a solid master carrier but owes its name to the fact that it is employed in many home printers.

2.2.1. Screen printing

Two types of screen printing (illustrated in Fig 2.1) are compatible with R2R processing: Flatbed screen printing and rotary screen printing.
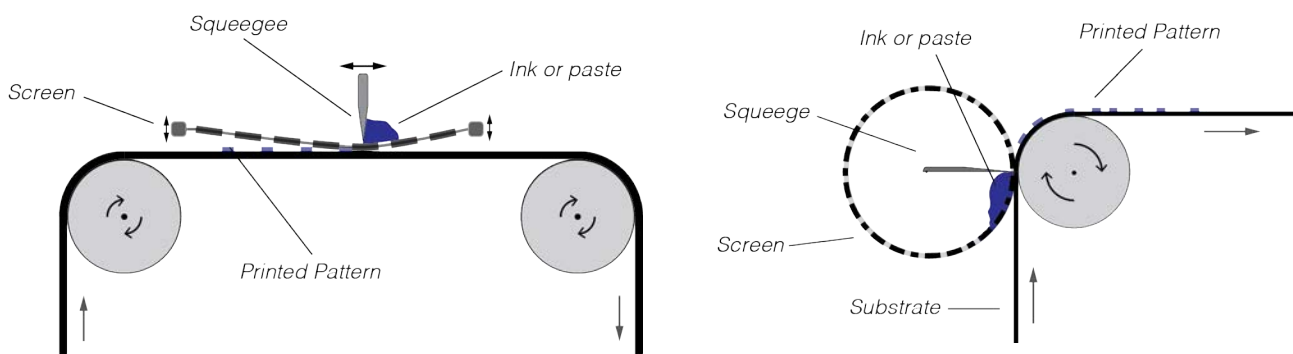
Fig 2.1 – Schematic illustration of flat bead (left) and rotary (right) screen printing. Adapted with permission from reference 2.

The operating principle of both techniques is similar. Only the screen's shape changes. A squeegee pushes the ink through the open area of an otherwise solid mesh. The open area, the thickness of the screen and the ink viscosity determine the printed pattern. Typical wet layer thickness is high (10-500 μm). The ink's viscosity is a key parameter because low viscosity inks would run through the screen by gravity. Therefore, high viscosity inks with thixotropic (shear thinning) properties are needed.

Flatbed screen printing is intrinsically a stepwise process but it has been fitted to R2R. Areas as large as 10 m^2 can be printed at once. During the first step, the screen is pressed into contact with the substrate. Then the pattern is transferred onto the web by sweeping the squeegee across the screen to force the ink through the mesh's open area. Finally, the

screen is raised while the web moves forward. One drawback of flatbed screen printing is that the ink is standing on top of the screen in contact with the ambient atmosphere, meaning that external factors such as solvent evaporation can potentially impact the printing process.

On the other hand, rotary screen printing is fully compatible with R2R because the screen has a cylinder shape. The squeegee is fixed inside the screen and pushes the ink through the mesh as the screen rotates resulting in a continuous printing of the pattern at each cylinder rotation. The screen rotates at the same rate as the web which allows for printing speeds over 100 m/min compared to only 0-35 m/min in the case of flatbed screen printing. Another advantage of rotary screen printing is that the ink is held inside the cylindrical screen and is consequently more protected from the ambient. Rotary screen printing has a few disadvantages, for example the screen is more expensive than for flatbed screen printing. Cleaning the screen is also an issue because of the limited access inside it. Finally, a multilayer screen printing process is also more difficult to set up with a rotary printer but once working it is more reliable. For these reasons rotary screen printing is more suitable for large scale processes when flatbed screen printing is the preferred technique for small scale lab experiments.

For OPV, screen printing has so far mainly been used to print silver electrodes because it gives a high conductive thick silver layer.[3–16] Reports where poly(3,4-ethylenedioxythiophene) polystyrene sulfonate (PEDOT:PSS) is screen printed can also be found.[16–24] Ink formulation for the active layer is particularly challenging because it needs to meet both the criteria for printing (high viscosity, thixotropic) and for obtaining the right active layer morphology. Therefore, there are only a few reports where the active layer is screen printed.[18,25–27] And only one report where the whole OPV stack is screen printed.[18]

2.2.2. Flexoprinting

The operating principle of flexoprinting is similar to the one of a stamp. The printing pattern stands in relief on a soft printing cylinder typically made of rubber or a photopolymer. To transfer the ink, the soft printing cylinder is put into contact with the substrate. The cylindrical shape of the printing plate makes flexoprinting fully R2R compatible. The ink is transferred onto the printing cylinder with a ceramic anilox roller. The anilox cylinder is covered of micro

cavities filled with ink. The ink is transferred onto the printing cylinder simply by surface tension forces when the anilox roll and the printing cylinder are touching. Therefore, the wet thickness of the printed pattern is directly linked to the volume of the anilox's micro cavities (mL/m^2). To fill up the anilox cylinder a fountain roll is used. This fountain roll is partially dipped into an ink bath and a doctor blade removes any excess of ink (see Fig 2.2). It is possible to avoid solvent evaporation by using a chambered doctor blade system.

So far there are only a few reports of flexography implement for OPV and most of them are limited to the printing of fine silver grids for electrodes as a replacement of ITO.[14,28–30] Flexoprinting was also used in some instances to print a PEDOT:PSS layer, a wetting agent on the active layer, Vanadium oxide as HTL or a UV curable adhesive before encapsulation.[9,19,31,32]
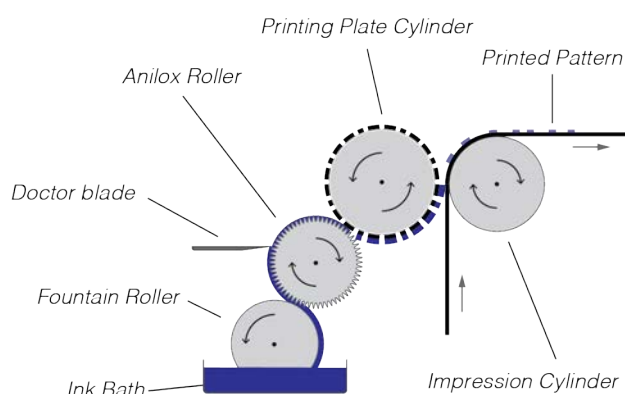
Fig 2.2 – Schematic illustration of flexoprinting. Adapted with permission from reference 2.

2.2.3. Gravure printing

Gravure printing is the last true printing technique used for OPV preparation. This technique is quite common and widely used in the industry for high volume printing (magazines, catalogues, newspapers…). Gravure printing is the opposite process to flexoprinting meaning that the printing pattern is not in relief but rather designed by micro cavities carved into the printing cylinder. The printing cylinder is made of steel with a thin layer of copper that comprises the engraved cells forming the printing pattern. A final top layer of chromium is added to ensure resistance to wear. When a second soft cylinder pushes the web into contact with the primary printing cylinder, the ink is transferred from the micro cavities onto the substrate through matching surface energies of the ink and web. Similarly, to

flexoprinting, the printing cylinder is partially dipped in an ink bath and a doctor blade is used to remove any excess of ink (see Fig 2.3). Gravure printing is compatible with low viscosity ink and speeds up to 15 m/s can be achieved. However, the operating conditions need to be carefully chosen because ink viscosity, substrate speed and the pressure applied by the secondary printing cylinder all influence the printing.

Gravure printing is attractive for OPV manufacturing because of the possibility to print thin and homogeneous layers. Several reports where PEDOT:PSS and the active layer are gravure printed can be found.[31,33–37] For example, Kopola *et al.* have used a desktop gravure printability tester (single sheets, not R2R) to deposit PEDOT:PSS and Poly(3-hexylthiophene-2,5-diyl) (P3HT) : Phenyl-C61-butyric acid methyl ester (PCBM) for single cells (PCE: 2.8%, 0.19 cm2) and small modules of 5 cells in series (PCE: 1.9%, 9.6 cm^2).[35,36] Many other materials have been reported to be gravure printed such as zinc oxide (ZnO), titanium oxide (TiOx), silver electrodes or PTB7:PCBM.[38–42]
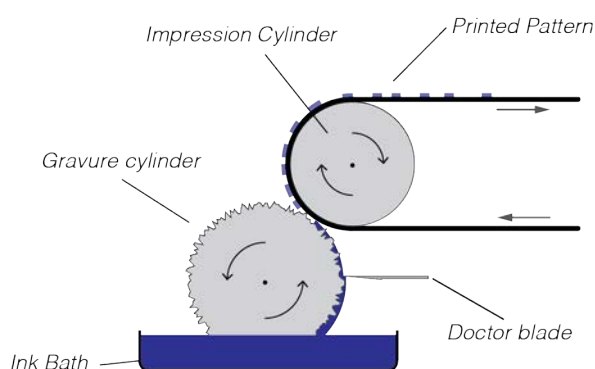
Fig 2.3 – Illustration of gravure printing adapted with permission from reference 2.

2.2.4. Inkjet printing

As stated at the beginning of this section, inkjet printing (IJP) does not require contact to transfer the printing pattern contrary to traditional printing techniques. This is actually one of the advantages of inkjet because it can be used to print on sensitive substrates or delicate three dimensional structures. IJP is also a fully digital method meaning that the two dimensional printing pattern is based on a pixelated drawing where each pixel is either left blank or receives an ink drop. This is another advantage of inkjet because it makes it very easy to change the printing pattern with just a computer compared to other printing method

where a new screen or a new printing cylinder is needed for each pattern. Ink formulation is the main issue for inkjet printing: density, surface tension, viscosity, boiling point are all factors that need to be tailored in order to fit the nozzle size, the printing surface, the material. There are two common types of inkjet printers: drop on demand and continuous. In continuous inkjet printing the jet of droplets is continuous and is then electrostatically deviated to print on the desired pixels. This method requires only one nozzle which makes it very fast, but limits the printing area. Drop on demand (DOD) inkjet printing is classified in 3 types: Piezoelectric, thermal and electrostatic. Electrostatic inkjet is limited because the ink needs to be charged. An electrostatic field is applied between the nozzle and an electrode drawing the free charges contained in the ink to the surface. Droplets are formed when the electrostatic forces exceed the surface tension. Thermal inkjet is less demanding than electrostatic but it does require the ink to have a low boiling point compound. When the ink is heated, this compound vaporizes which ejects a droplet. Finally, piezoelectric inkjet printing (illustrated in Fig 2.4) is suitable for most materials. A piezoelectric element is placed in the channel on top of the nozzle and when a voltage waveform is applied to this element, it expands and ejects a droplet through the nozzle.
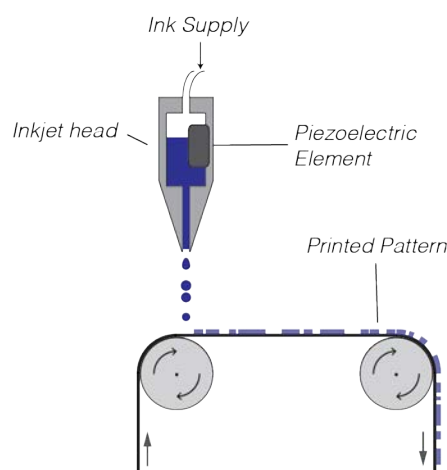
Fig 2.4 – Schematic illustration of drop on demand piezoelectric inkjet printing. Adapted with permission from reference 2.

There are many reports using inkjet to prepare OPV because of the versatility of DOD inkjet and the ease to change printing forms. However most of them are still limited to small glass substrate (0.03-1 cm^2). Inkjet printing has been reported to deposit PEDOT:PSS,

P3HT:PCBM or other active materials, as well as ZnO.[43–50] Reports where multiple layers of the OPV stack were inkjet printed can be found.[43,51,52] Recently, Eggenhuisen *et al.* reported the fabrication of fully inkjet printed OPV cells with an industrial printer.[53,54] In true R2R processing of OPV most examples using inkjet are limited to the deposition of silver electrodes.[14,20,55]

2.3. Coating techniques

Contrary to printing techniques, coating techniques are non-contact methods. However, they are in most cases one dimensional and limited to the coating of a homogeneous layer along the substrate length. One advantage of coating techniques is the possibility to control precisely the coated layer thickness from nanometers to millimeters. The ink formulation is also less challenging because the ink is poured on the substrate. Consequently, a wide range of viscosities and surface tension can be employed.

2.3.1. Knife coating
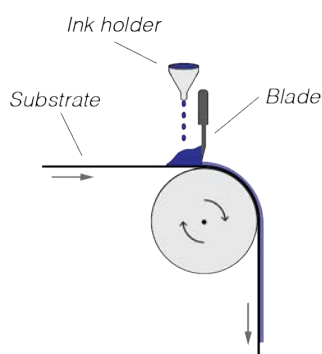
Fig 2.5 – Illustration of knife coating adapted with permission from reference 2.

Knife or blade coating is the R2R equivalent to the lab's doctor-blading. A fixed knife stands on top of the moving substrate. A meniscus is created between the knife and the substrate and is fed by an ink reservoir placed in front of the knife as shown in Fig 2.5. The layer is coated as the substrate moves and the wet thickness is related to the gap size as well as to the substrate speed. An empirical estimation is that the wet thickness is roughly half of the gap size. Knife coating mostly allows to deposit homogeneous layers over large area at high speeds (> 10 m/s) on rigid or flexible substrates.

Blade coating is easy to set up on the lab scale and there are therefore many reports on OPV where one or more layers are blade coated. P3HT and other active materials have been extensively studied.[56–60] This is also the case for PEDOT:PSS.[61–64] Finally there a few example where ZnO and aluminum doped zinc oxide (AZO) layers are blade coated.[17,62,63,65]

2.3.2. Slot-die coating

In slot-die coating a meniscus is formed between the moving substrate and a stationary coating head. The meniscus is continuously fed with ink through a slot inside the coating head (see Fig 2.6). Once again it is the substrate's movement that leads to the deposition of a very homogeneous layer along the web. A wide range of viscosities and speeds (1 – 600 m/min) are compatible with slot-die coating. The wet thickness is tightly controlled by the pumping rate, the web speed and the width of the coating. It is also possible to deposit stripes by using a meniscus guide. Another advantage of slot-die coating is that the ink is kept in a close system and is therefore protected from the environment. slot-die coating is by far the most used R2R processing technique and has been used to deposit most layers: the active layer, PEDOT:PSS, HTL such as vanadium oxide (V_2O_5), molybdenum oxide (MoO_x) or ZnO.[28,66–70] There are also many instances where multiple layers are slot-die coated.[17,28,29,71–74]
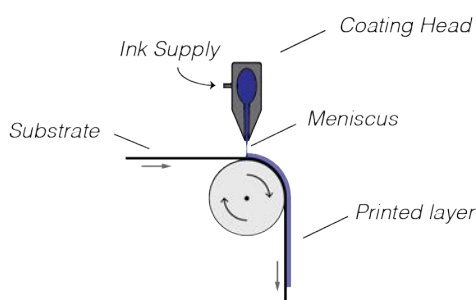
Fig 2.6 – Schematic illustration of Slot-die coating adapted with permission from reference 2.

2.4. Encapsulation

Roll-to-roll encapsulation is needed in order to protect the final device from the surrounding environment during operation. After R2R deposition of the OPV stack, the last step, namely lamination, is done to ensure stability of the OPV modules over time. The substrate bearing the modules is joined with a second protective foil with low permeability of oxygen and

humidity to prevent chemical degradation. In some cases, the substrate is laminated on both sides to further improve the stability. There are three types of lamination which are commonly used to encapsulate OPV modules: pressure sensitive adhesive (PSA), hot and UV laminations. The laminations techniques mostly differ by the type of adhesive used to join the foil together and are shown in Fig 2.7.

PSA lamination is achieved through a pressure sensitive adhesive. A liner is used to put this pressure sensitive adhesive on the laminate and it needs to be removed right before the two foils meet. The substrate and the laminate are pressed together through a nip. Even though this process is simple and fast (> 20 m/min), it suffers from the thick adhesive (50 μm or more) and the tricky handling of the sticky laminate.

Hot lamination is performed similarly to cold lamination but the adhesive is easier to use because it is heat activated. When the substrate and the laminate join, they are pressed together by two heated rolls. The heat makes the adhesive melt ensuring a tight seal upon cooling.
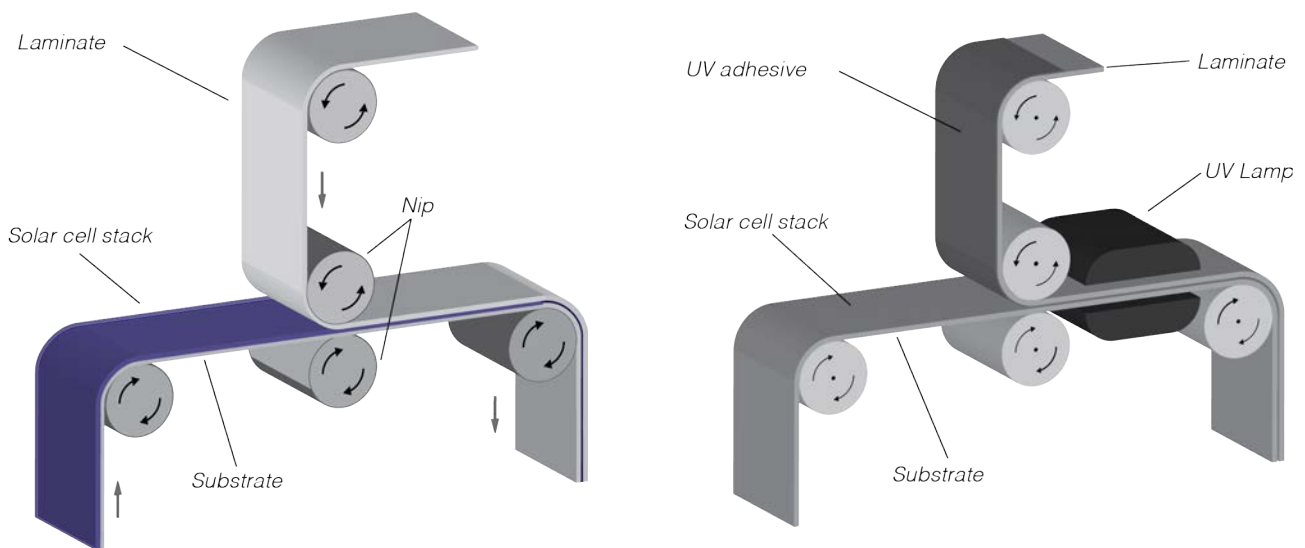
Fig 2.7 – Schematic illustration of Cold/Hot lamination (left) and UV lamination (right). Reproduced with permission from reference 2.

UV lamination is the last technique used for encapsulation of OPV. In this case the laminate foil does not carry the adhesive. The UV curing adhesive is added onto the laminate before it joins the substrate in a nib where the foils are pressed together. Finally, the adhesive is

activated by UV light in order to seal the foils together. The deposition of the adhesive adds an extra step and complexity to the process.

2.5. Outlook

Even tough implementing R2R manufacturing was not part of this thesis introducing R2R processing of OPV was deemed necessary because all cells and modules studied were prepared by Roll coating or printing. Either with a mini roll-coater described in using slot-die coating and flexoprinting or with a large scale R2R equipment (see Fig 2.8).[6,22–24,29,75,76]

Fig 2.8 – Photograph of the R2R machine used for coating and printing of large scale OPV modules.

2.6. References

(1)   Jørgensen, M.; Carlé, J. E.; Søndergaard, R. R.; Lauritzen, M.; Dagnæs-Hansen, N. A.; Byskov, S. L.; Andersen, T. R.; Larsen-Olsen, T. T.; Böttiger, A. P. L.; Andreasen, B.; Fu, L.; Zuo, L.; Liu, Y.; Bundgaard, E.; Zhan, X.; Chen, H.; Krebs, F. C. The State of Organic Solar cells—A Meta Analysis. *Sol. Energy Mater. Sol. Cells* **2013**, *119*, 84–93.

(2)   Roth, B.; Søndergaard, R. R.; Krebs, F. C. Roll-to-Roll Printing and Coating Techniques for Manufacturing Large-Area Flexible Organic. In *Handbook of Flexible Organic Electronics: Materials, Manufacturing and Applications*; Logothetidis, S., Ed.; Elsevier, 2014; pp 171–197.

(3)   Amb, C. M.; Craig, M. R.; Koldemir, U.; Subbiah, J.; Choudhury, K. R.; Gevorgyan, S. A.; Jørgensen, M.; Krebs, F. C.; So, F.; Reynolds, J. R. Aesthetically Pleasing Conjugated Polymer: Fullerene Blends for Blue-Green Solar Cells Via Roll-to-Roll Processing. *ACS Appl. Mater. Interfaces* **2012**, *4* (3), 1847–1853.

(4)   Angmo, D.; Hösel, M.; Krebs, F. C. All Solution Processing of ITO-Free Organic Solar Cell Modules Directly on Barrier Foil. *Sol. Energy Mater. Sol. Cells* **2012**, *107*, 329–336.

(5)   Bundgaard, E.; Hagemann, O.; Manceau, M.; Jørgensen, M.; Krebs, F. C. Low Band Gap Polymers for Roll-to-Roll Coated Polymer Solar Cells. *Macromolecules* **2010**, *43* (19), 8115–8120.

(6)   Dam, H. F.; Krebs, F. C. Simple Roll Coater with Variable Coating and Temperature Control for Printed Polymer Solar Cells. *Sol. Energy Mater. Sol. Cells* **2012**, *97*, 191–196.

(7)   Galagan, Y.; Rubingh, J. J.; Andriessen, R.; Fan, C.-C.; Blom, P. W. M.; Veenstra, S. C.; Kroon, J. M. ITO-Free Flexible Organic Solar Cells with Printed Current Collecting Grids. *Sol. Energy Mater. Sol. Cells* **2011**, *95* (5), 1339–1343.

(8)   Helgesen, M.; Carlé, J. E.; Andreasen, B.; Hösel, M.; Norrman, K.; Søndergaard, R.; Krebs, F. C. Rapid Flash Annealing of Thermally Reactive Copolymers in a Roll-to-Roll Process for Polymer Solar Cells. *Polym. Chem.* **2012**, *3* (9), 2649–2655.

(9)   Krebs, F. C.; Fyenbo, J.; Jørgensen, M. Product Integration of Compact Roll-to-Roll Processed Polymer Solar Cell Modules: Methods and Manufacture Using Flexographic Printing, Slot-Die Coating and Rotary. *J. Mater. Chem.* **2010**, *20* (41), 8994–9001.

(10)   Krebs, F. C.; Gevorgyan, S. A.; Alstrup, J. A Roll-to-Roll Process to Flexible Polymer Solar Cells: Model Studies, Manufacture and Operational Stability Studies. *J. Mater. Chem.* **2009**, *19* (30), 5442–5451.

(11)   Krebs, F. C.; Tromholt, T.; Jørgensen, M. Upscaling of Polymer Solar Cell Fabrication Using Full Roll-to-Roll Processing. *Nanoscale* **2010**, *2* (6), 873–886.

(12)   Krebs, F. C.; Fyenbo, J.; Tanenbaum, D. M.; Gevorgyan, S. A.; Andriessen, R.; van Remoortere, B.; Galagan, Y.; Jørgensen, M. The OE-A OPV Demonstrator Anno Domini 2011. *Energy Environ. Sci.* **2011**, *4* (10), 4116–4123.

(13)   Manceau, M.; Angmo, D.; Jørgensen, M.; Krebs, F. C. ITO-Free Flexible Polymer Solar Cells: From Small Model Devices to Roll-to-Roll Processed Large Modules. *Org. Electron.* **2011**, *12* (4), 566–574.

(14)   Yu, J.-S.; Kim, I.; Kim, J.-S.; Jo, J.; Larsen-Olsen, T. T.; Søndergaard, R. R.; Hösel, M.; Angmo, D.; Jørgensen, M.; Krebs, F. C. Silver Front Electrode Grids for ITO-Free All Printed Polymer Solar Cells with Embedded and Raised Topographies, Prepared by Thermal Imprint, Flexographic and Inkjet Roll-to-Roll Processes. *Nanoscale* **2012**, *4* (19), 6032–6040.

(15)   Yan, F.; Noble, J.; Peltola, J.; Wicks, S.; Balasubramanian, S. Semitransparent OPV Modules Pass Environmental Chamber Test Requirements. *Sol. Energy Mater. Sol. Cells* **2013**, *114* (June 2012),

214–218.

(16)   Välimäki, M.; Apilo, P.; Po, R.; Jansson, E.; Bernardi, A.; Ylikunnari, M.; Vilkman, M.; Corso, G.; Puustinen, J.; Tuominen, J.; Hast, J.; Po, R.; Bernardi, A.; Corso, G.; Ylikunnari, M.; Vilkman, M.; Tuominen, J.; Puustinen, J.; Hast, J. R2R-Printed Inverted OPV Modules – towards Arbitrary Patterned Designs. *Nanoscale* **2015**, *7* (21), 9570–9580.

(17)   Krebs, F. C. Polymer Solar Cell Modules Prepared Using Roll-to-Roll Methods: Knife-over-Edge Coating, Slot-Die Coating and Screen Printing. *Sol. Energy Mater. Sol. Cells* **2009**, *93* (4), 465–475.

(18)   Krebs, F. C.; Jørgensen, M.; Norrman, K.; Hagemann, O.; Alstrup, J.; Nielsen, T. D.; Fyenbo, J.; Larsen, K.; Kristensen, J. A Complete Process for Production of Flexible Large Area Polymer Solar Cells Entirely Using Screen Printing—first Public Demonstration. *Sol. Energy Mater. Sol. Cells* **2009**, *93* (4), 422–441.

(19)   Hösel, M.; Søndergaard, R. R.; Jørgensen, M.; Krebs, F. C. Comparison of UV-Curing, Hotmelt, and Pressure Sensitive Adhesive as Roll-to-Roll Encapsulation Methods for Polymer Solar Cells. *Adv. Eng. Mater.* **2013**, *15* (11), 1068–1075.

(20)   Espinosa, N.; Lenzmann, F. O.; Ryley, S.; Angmo, D.; Hösel, M.; Søndergaard, R. R.; Huss, D.; Dafinger, S.; Gritsch, S.; Kroon, J. M.; Jørgensen, M.; Krebs, F. C. OPV for Mobile Applications: An Evaluation of Roll-to-Roll Processed Indium and Silver Free Polymer Solar Cells through Analysis of Life Cycle, Cost and Layer Quality Using Inline Optical and Functional Inspection Tools. *J. Mater. Chem. A* **2013**, *1* (24), 7037–7049.

(21)   Sommer-Larsen, P.; Jørgensen, M.; Søndergaard, R. R.; Hösel, M.; Krebs, F. C. It Is All in the Pattern-High-Efficiency Power Extraction from Polymer Solar Cells through High-Voltage Serial Connection. *Energy Technol.* **2013**, *1* (1), 15–19.

(22)   dos Reis Benatto, G. A.; Roth, B.; Madsen, M. V.; Hösel, M.; Søndergaard, R. R.; Jørgensen, M.; Krebs, F. C. Carbon: The Ultimate Electrode Choice for Widely Distributed Polymer Solar Cells. *Adv. Energy Mater.* **2014**, *4* (15), 1400732.

(23)   Roth, B.; A. dos Reis Benatto, G.; Corazza, M.; Carlé, J. E.; Helgesen, M.; Gevorgyan, S. a.; Jørgensen, M.; Søndergaard, R. R.; Krebs, F. C. Improving the Operational Stability of PBDTTTz-4 Polymer Solar Cells Modules by Electrode Modification. *Adv. Eng. Mater.* **2015**, 1–7.

(24)   Roth, B.; dos Reis Benatto, G. a.; Corazza, M.; Søndergaard, R. R.; Gevorgyan, S. a.; Jørgensen, M.; Krebs, F. C. The Critical Choice of PEDOT:PSS Additives for Long Term Stability of Roll-to-Roll Processed OPVs. *Adv. Energy Mater.* **2015**, *5* (9).

(25)   Zhang, B.; Chae, H.; Cho, S. M. Screen-Printed Polymer:Fullerene Bulk-Heterojunction Solar Cells. *Jpn. J. Appl. Phys.* **2009**, *48* (2), 020208.

(26)   Aernouts, T.; Vanlaeke, P.; Poortmans, J.; Heremans, P. Polymer Solar Cells: Screen-Printing as a Novel Deposition Technique. *MRS Proc.* **2004**, *836* (0), L3.9.

(27)   Shaheen, S. E.; Radspinner, R.; Peyghambarian, N.; Jabbour, G. E. Fabrication of Bulk Heterojunction Plastic Solar Cells by Screen Printing. *Appl. Phys. Lett.* **2001**, *79* (18), 2996–2999.

(28)   Krebs, F. C.; Espinosa, N.; Hösel, M.; Søndergaard, R. R.; Jørgensen, M. 25th Anniversary Article: Rise to Power - OPV-Based Solar Parks. *Adv. Mater.* **2014**, *26* (1), 29–39.

(29)   Krebs, F. C.; Hösel, M.; Corazza, M.; Roth, B.; Madsen, M. V.; Gevorgyan, S. A.; Søndergaard, R. R.; Karg, D.; Jørgensen, M. Freely Available OPV-The Fast Way to Progress. *Energy Technol.* **2013**, *1* (7), 378–381.

(30)   Andersen, T. R.; Dam, H. F.; Andreasen, B.; Hösel, M.; Madsen, M. V.; Gevorgyan, S. A.; Søndergaard, R. R.; Jørgensen, M.; Krebs, F. C. A Rational Method for Developing and Testing Stable Flexible Indium- and Vacuum-Free Multilayer Tandem Polymer Solar Cells Comprising up to

Twelve Roll Processed Layers. *Sol. Energy Mater. Sol. Cells* **2014**, *120*, 735–743.

(31)   Hübler, A. C.; Trnovec, B.; Zillger, T.; Ali, M.; Wetzold, N.; Mingebach, M.; Wagenpfahl, A.; Deibel, C.; Dyakonov, V. Printed Paper Photovoltaic Cells. *Adv. Energy Mater.* **2011**, *1* (6), 1018–1022.

(32)   Kololuoma, T.; Lu, J.; Alem, S.; Graddage, N.; Movileanu, R.; Moisa, S.; Tao, Y. Flexo Printed Sol-Gel Derived Vanadium Oxide Films as an Interfacial Hole-Transporting Layer for Organic Solar Cells. In *Spie Opto*; Teherani, F. H., Look, D. C., Rogers, D. J., Eds.; 2015; Vol. 9364, p 93640K.

(33)   Koidis, C.; Logothetidis, S.; Ioakeimidis, A.; Laskarakis, A.; Kapnopoulos, C. Key Factors to Improve the Efficiency of Roll-to-Roll Printed Organic Photovoltaics. *Org. Electron.* **2013**, *14* (7), 1744–1748.

(34)   Koidis, C.; Logothetidis, S.; Kassavetis, S.; Kapnopoulos, C.; Karagiannidis, P. G.; Georgiou, D.; Laskarakis, a. Effect of Process Parameters on the Morphology and Nanostructure of Roll-to-Roll Printed P3HT:PCBM Thin Films for Organic Photovoltaics. *Sol. Energy Mater. Sol. Cells* **2013**, *112*, 36–46.

(35)   Kopola, P.; Aernouts, T.; Guillerez, S.; Jin, H.; Tuomikoski, M.; Maaninen, A.; Hast, J. High Efficient Plastic Solar Cells Fabricated with a High-Throughput Gravure Printing Method. *Sol. Energy Mater. Sol. Cells* **2010**, *94* (10), 1673–1680.

(36)   Kopola, P.; Aernouts, T.; Sliz, R.; Guillerez, S.; Ylikunnari, M.; Cheyns, D.; Välimäki, M.; Tuomikoski, M.; Hast, J.; Jabbour, G.; Myllylä, R.; Maaninen, A. Gravure Printed Flexible Organic Photovoltaic Modules. *Sol. Energy Mater. Sol. Cells* **2011**, *95* (5), 1344–1347.

(37)   Apilo, P.; Hiltunen, J.; Välimäki, M.; Heinilehto, S.; Sliz, R.; Hast, J. Roll-to-Roll Gravure Printing of Organic Photovoltaic Modules-Insulation of Processing Defects by an Interfacial Layer. *Prog. Photovoltaics Res. Appl.* **2015**, *23* (7), 918–928.

(38)   Schneider, a.; Traut, N.; Hamburger, M. Analysis and Optimization of Relevant Parameters of Blade Coating and Gravure Printing Processes for the Fabrication of Highly Efficient Organic Solar Cells. *Sol. Energy Mater. Sol. Cells* **2014**, *126*, 149–154.

(39)   Yang, J.; Vak, D.; Clark, N.; Subbiah, J.; Wong, W. W. H.; Jones, D. J.; Watkins, S. E.; Wilson, G. Organic Photovoltaic Modules Fabricated by an Industrial Gravure Printing Proofer. *Sol. Energy Mater. Sol. Cells* **2013**, *109*, 47–55.

(40)   Vilkman, M.; Apilo, P.; Välimäki, M.; Ylikunnari, M.; Bernardi, A.; Po, R.; Corso, G.; Hast, J. Gravure-Printed ZnO in Fully Roll-to-Roll Printed Inverted Organic Solar Cells: Optimization of Adhesion and Performance. *Energy Technol.* **2015**, *3* (4), 407–413.

(41)   Park, J.; Nguyen, H. A. D.; Park, S.; Lee, J.; Kim, B.; Lee, D. Roll-to-Roll Gravure Printed Silver Patterns to Guarantee Printability and Functionality for Mass Production. *Curr. Appl. Phys.* **2015**, *15* (3), 367–376.

(42)   Voigt, M. M.; Mackenzie, R. C. I.; King, S. P.; Yau, C. P.; Atienzar, P.; Dane, J.; Keivanidis, P. E.; Zadrazil, I.; Bradley, D. D. C.; Nelson, J. Gravure Printing Inverted Organic Solar Cells: The Influence of Ink Properties on Film Quality and Device Performance. *Sol. Energy Mater. Sol. Cells* **2012**, *105*, 77–85.

(43)   Eggenhuisen, T. M.; Galagan, Y.; Coenen, E. W. C.; Voorthuijzen, W. P.; Slaats, M. W. L.; Kommeren, S. a.; Shanmuganam, S.; Coenen, M. J. J.; Andriessen, R.; Groen, W. a. Digital Fabrication of Organic Solar Cells by Inkjet Printing Using Non-Halogenated Solvents. *Sol. Energy Mater. Sol. Cells* **2015**, *134*, 364–372.

(44)   Hermerschmidt, F.; Papagiorgis, P.; Savva, A.; Christodoulou, C.; Itskos, G.; Choulis, S. A. Inkjet Printing Processing Conditions for Bulk-Heterojunction Solar Cells Using Two High-Performing Conjugated Polymer Donors. *Sol. Energy Mater. Sol. Cells* **2014**, *130*, 474–480.

(45) Lange, A.; Schindler, W.; Wegener, M.; Fostiropoulos, K.; Janietz, S. Inkjet Printed Solar Cell Active Layers Based on a Novel, Amorphous Polymer. *J. Nanosci. Nanotechnol.* **2013**, *13* (7), 5209–5214.

(46) Aernouts, T.; Aleksandrov, T.; Girotto, C.; Genoe, J.; Poortmans, J. Polymer Based Organic Solar Cells Using Ink-Jet Printed Active Layers. *Appl. Phys. Lett.* **2008**, *92* (3), 033306.

(47) Hoth, C. N.; Choulis, S. A.; Schilinsky, P.; Brabec, C. J. High Photovoltaic Performance of Inkjet Printed Polymer:Fullerene Blends. *Adv. Mater.* **2007**, *19* (22), 3973–3978.

(48) Hoth, C.; Schilinsky, P.; Choulis, S.; Brabec, C. J. Printing Highly Efficient Organic Solar Cells. *Nano Lett.* **2008**, 8 (9), 2806–2813

(49) Eom, S. H.; Senthilarasu, S.; Uthirakumar, P.; Yoon, S. C.; Lim, J.; Lee, C.; Lim, H. S.; Lee, J.; Lee, S.-H. Polymer Solar Cells Based on Inkjet-Printed PEDOT:PSS Layer. *Org. Electron.* **2009**, *10* (3), 536–542.

(50) De Girolamo Del Mauro, A.; Diana, R.; Grimaldi, I. A.; Loffredo, F.; Morvillo, P.; Villani, F.; Minarini, C. Polymer Solar Cells with Inkjet-Printed Doped-PEDOT: PSS Anode. *Polym. Compos.* **2013**, *34* (9), 1493–1499.

(51) Eom, S. H.; Park, H.; Mujawar, S. H.; Yoon, S. C.; Kim, S.-S.; Na, S.-I.; Kang, S.-J.; Khim, D.; Kim, D.-Y.; Lee, S.-H. High Efficiency Polymer Solar Cells via Sequential Inkjet-Printing of PEDOT:PSS and P3HT:PCBM Inks with Additives. *Org. Electron.* **2010**, *11* (9), 1516–1522.

(52) Lange, A.; Wegener, M.; Boeffel, C.; Fischer, B.; Wedel, A.; Neher, D. A New Approach to the Solvent System for Inkjet-Printed P3HT:PCBM Solar Cells and Its Use in Devices with Printed Passive and Active Layers. *Sol. Energy Mater. Sol. Cells* **2010**, *94* (10), 1816–1821.

(53) Eggenhuisen, T. M.; Galagan, Y.; Biezemans, A.; Coenen, M.; Gilot, J.; Groen, P.; Andriessen, R. Organic Photovoltaic Cells with All Inkjet Printed Layers and Freedom of Form. **2014**, *2*, 2842–2845.

(54) Eggenhuisen, T. M.; Galagan, Y.; Biezemans, a. F. K. V.; Slaats, T. M. W. L.; Voorthuijzen, W. P.; Kommeren, S.; Shanmugam, S.; Teunissen, J. P.; Hadipour, a.; Verhees, W. J. H.; Veenstra, S. C.; Coenen, M. J. J.; Gilot, J.; Andriessen, R.; Groen, W. a. High Efficiency, Fully Inkjet Printed Organic Solar Cells with Freedom of Design. *J. Mater. Chem. A* **2015**, *3* (14), 7255–7262.

(55) Hösel, M.; Søndergaard, R. R.; Angmo, D.; Krebs, F. C. Comparison of Fast Roll-to-Roll Flexographic, Inkjet, Flatbed, and Rotary Screen Printing of Metal Back Electrodes for Polymer Solar Cells. *Adv. Eng. Mater.* **2013**, *15* (10), 995–1001.

(56) Tsai, P.-T.; Yu, K.-C.; Chang, C.-Y. C.-J.; Horng, S.-F.; Meng, H.-F. Large-Area Organic Solar Cells by Accelerated Blade Coating. *Org. Electron.* **2015**, *22* (March), 1–7.

(57) Tait, J. G.; Merckx, T.; Li, W.; Wong, C.; Gehlhaar, R.; Cheyns, D.; Turbiez, M.; Heremans, P. Determination of Solvent Systems for Blade Coating Thin Film Photovoltaics. *Adv. Funct. Mater.* **2015**, *25* (22), 3393–3398.

(58) Chang, J.-H.; Chen, Y.-H.; Lin, H.-W.; Lin, Y.-T.; Meng, H.-F.; Chen, E.-C. Highly Efficient Inverted Rapid-Drying Blade-Coated Organic Solar Cells. *Org. Electron.* **2012**, *13* (4), 705–709.

(59) Schmidt-Hansberg, B.; Do, H.; Colsmann, A.; Lemmer, U.; Schabel, W. Drying of Thin Film Polymer Solar Cells. *Eur. Phys. J. Spec. Top.* **2009**, *166* (1), 49–53.

(60) Lim, S.-L.; Chen, E.-C.; Chen, C.-Y.; Ong, K.-H.; Chen, Z.-K.; Meng, H.-F. High Performance Organic Photovoltaic Cells with Blade-Coated Active Layers. *Sol. Energy Mater. Sol. Cells* **2012**, *107*, 292–297.

(61) Hoth, C.; Steim, R.; Schilinsky, P.; Choulis, S. A.; Tedde, S. F.; Hayden, O.; Brabec, C. J. Topographical and Morphological Aspects of Spray Coated Organic Photovoltaics. *Org. Electron.* **2009**, *10* (4), 587–593.

(62)   Li, N.; Baran, D.; Forberich, K.; Turbiez, M.; Ameri, T.; Krebs, F. C.; Brabec, C. J. An Efficient Solution-Processed Intermediate Layer for Facilitating Fabrication of Organic Multi-Junction Solar Cells. *Adv. Energy Mater.* **2013**, *3* (12), 1597–1605.

(63)   Guo, F.; Zhu, X.; Forberich, K.; Krantz, J.; Stubhan, T.; Salinas, M.; Halik, M.; Spallek, S.; Butz, B.; Spiecker, E.; Ameri, T.; Li, N.; Kubis, P.; Guldi, D. M.; Matt, G. J.; Brabec, C. J. ITO-Free and Fully Solution-Processed Semitransparent Organic Solar Cells with High Fill Factors. *Adv. Energy Mater.* **2013**, *3* (8), 1062–1067.

(64)   Stubhan, T.; Litzov, I.; Li, N.; Salinas, M.; Steidl, M.; Sauer, G.; Forberich, K.; Matt, G. J.; Halik, M.; Brabec, C. J. Overcoming Interface Losses in Organic Solar Cells by Applying Low Temperature, Solution Processed Aluminum-Doped Zinc Oxide Electron Extraction Layers. *J. Mater. Chem. A* **2013**, *1* (19), 6004–6009.

(65)   Ameri, T.; Min, J.; Li, N.; Machui, F.; Baran, D.; Forster, M.; Schottler, K. J.; Dolfen, D.; Scherf, U.; Brabec, C. J. Performance Enhancement of the P3HT/PCBM Solar Cells through NIR Sensitization Using a Small-Bandgap Polymer. *Adv. Energy Mater.* **2012**, *2* (10), 1198–1202.

(66)   Carlé, J. E.; Helgesen, M.; Madsen, M. V.; Bundgaard, E.; Krebs, F. C.; Carle, J. E.; Helgesen, M.; Madsen, M. V.; Bundgaard, E.; Krebs, F. C. Upscaling from Single Cells to Modules – Fabrication of Vacuum- and ITO-Free Polymer Solar Cells on Flexible Substrates with Long Lifetime. *J. Mater. Chem. C* **2014**, *2* (7), 1290–1297.

(67)   Liu, F.; Ferdous, S.; Schaible, E.; Hexemer, A.; Church, M.; Ding, X.; Wang, C.; Russell, T. P. Fast Printing and In Situ Morphology Observation of Organic Photovoltaics Using Slot-Die Coating. *Adv. Mater.* **2015**, *27* (5), 886–891.

(68)   Machui, F.; Lucera, L.; Spyropoulos, G. D.; Cordero, J.; Ali, A. S.; Kubis, P.; Ameri, T.; Voigt, M. M.; Brabec, C. J. Large Area Slot-Die Coated Organic Solar Cells on Flexible Substrates with Non-Halogenated Solution Formulations. *Sol. Energy Mater. Sol. Cells* **2014**, *128*, 441–446.

(69)   Hong, S.; Lee, J.; Kang, H.; Lee, K. Slot-Die Coating Parameters of the Low-Viscosity Bulk-Heterojunction Materials Used for Polymer Solarcells. *Sol. Energy Mater. Sol. Cells* **2013**, *112*, 27–35.

(70)   Larsen-Olsen, T. T.; Machui, F.; Lechene, B.; Berny, S.; Angmo, D.; Søndergaard, R. R.; Blouin, N.; Mitchell, W.; Tierney, S.; Cull, T.; Tiwana, P.; Meyer, F.; Carrasco-Orozco, M.; Scheel, A.; Lövenich, W.; de Bettignies, R.; Brabec, C. J.; Krebs, F. C. Round-Robin Studies as a Method for Testing and Validating High-Efficiency ITO-Free Polymer Solar Cells Based on Roll-to-Roll-Coated Highly Conductive and Transparent Flexible Substrates. *Adv. Energy Mater.* **2012**, *2* (9), 1091–1094.

(71)   Espinosa, N.; García-Valverde, R.; Urbina, A.; Lenzmann, F.; Manceau, M.; Angmo, D.; Krebs, F. C. Life Cycle Assessment of ITO-Free Flexible Polymer Solar Cells Prepared by Roll-to-Roll Coating and Printing. *Sol. Energy Mater. Sol. Cells* **2012**, *97*, 3–13.

(72)   Hösel, M.; Søndergaard, R. R.; Jørgensen, M.; Krebs, F. C. Fast Inline Roll-to-Roll Printing for Indium-Tin-Oxide-Free Polymer Solar Cells Using Automatic Registration. *Energy Technol.* **2013**, *1* (1), 102–107.

(73)   Espinosa, N.; García-Valverde, R.; Urbina, A.; Krebs, F. C. A Life Cycle Analysis of Polymer Solar Cell Modules Prepared Using Roll-to-Roll Methods under Ambient Conditions. *Sol. Energy Mater. Sol. Cells* **2011**, *95* (5), 1293–1302.

(74)   Galagan, Y.; Fledderus, H.; Gorter, H.; 't Mannetje, H. H.; Shanmugam, S.; Mandamparambil, R.; Bosman, J.; Rubingh, J.-E. J. M.; Teunissen, J.-P.; Salem, A.; de Vries, I. G.; Andriessen, R.; Groen, W. a. Roll-to-Roll Slot-Die Coated Organic Photovoltaic (OPV) Modules with High Geometrical Fill Factors. *Energy Technol.* **2015**, *3* (8), 834–842.

(75)   Bundgaard, E.; Livi, F.; Hagemann, O.; Carlé, J. E.; Helgesen, M.; Heckler, I. M.; Zawacka, N. K.;

Angmo, D.; Larsen-Olsen, T. T.; dos Reis Benatto, G. a.; Roth, B.; Madsen, M. V.; Andersson, M. R.; Jørgensen, M.; Søndergaard, R. R.; Krebs, F. C. Matrix Organization and Merit Factor Evaluation as a Method to Address the Challenge of Finding a Polymer Material for Roll Coated Polymer Solar Cells. *Adv. Energy Mater.* **2015**, *5* (10).

(76)   Roth, B.; Rudenko, A. E.; Thompson, B. C.; Krebs, F. C. Photochemical Stability of Random poly(3-Hexylthiophene-Co-3-Cyanothiophene) and Its Use in Roll Coated ITO-Free Organic Photovoltaics. *J. Photonics Energy* **2014**, *5* (1), 057205.

Chapter 3 – Stability of OPV modules

3.1. Introduction

The commercial viability of organic photovoltaics (OPV) hinges on reducing their degradation during operation. Current predictions expect that a lifetime of at least 5 years outdoor is needed to compete against other photovoltaic technologies.[1] This chapter is not a review on the stability of OPV but simply introduces concepts necessary to comprehend the work presented in this thesis. Publications focusing on stability and authored during the span of this PhD are also presented.

The intense research on improving the power conversion efficiency (PCE) of OPV cells has led to efficiencies above 10 % which is competitive with other photovoltaic technologies.[2] However, OPV device lifetime is inherently limited by the stability of the organic materials. Improving the intrinsic stability of the active materials is therefore required to reach the stability milestone. The active materials used in OPV are organic materials which tend to photo-oxidized under light. This phenomena is also called photo-bleaching because the organic semiconductor loses its color during photo-oxidation.[3] The photochemical behavior of organic semiconductors can be studied with a simple UV-vis setup.[4]

In this work, the photochemical stability of random poly(3-hexylthiophene-co-cyanothiophene) (CN-P3HT) copolymer both as the pure polymer and as a blend with Phenyl-C61-butyric acid methyl ester (PCBM) was examined with such a UV-vis system.[5,6] The stability of OPV cells with CN-P3HT was compared to cells prepared with pristine P3HT under various stability tests.

Improving the photochemical stability of organic materials for OPV is critical but many other factors need to be controlled due to the wide diversity of degradation phenomena occurring in OPV.[7] To identify the multiple degradation mechanisms, functional OPV devices need to undergo controlled and repeated studies. Such standard tests have been established by the International Summit on OPV Stability (ISOS).[8] The standard ISOS tests allow for comparing stability results from laboratories all over the world.

Finally, the number of publications presenting stability data has increased dramatically in recent years.[9] This large pool of data if analyzed can yield large statistics on OPV stability. In order to learn from others, a meta-analysis of stability reports was conducted.[9]

3.2. Measuring and characterizing OPV stability

The degradation of OPV devices is so complex that a yearly conference is dedicated to the subject: The International Summit on OPV Stability (ISOS). The first three editions were necessary to establish guidelines for stability testing and reporting of OPV cells and modules.[8] This consensus allows for a better comparison of stability results between laboratories as well as increases the reliability of the studies.

3.2.1. ISOS standards
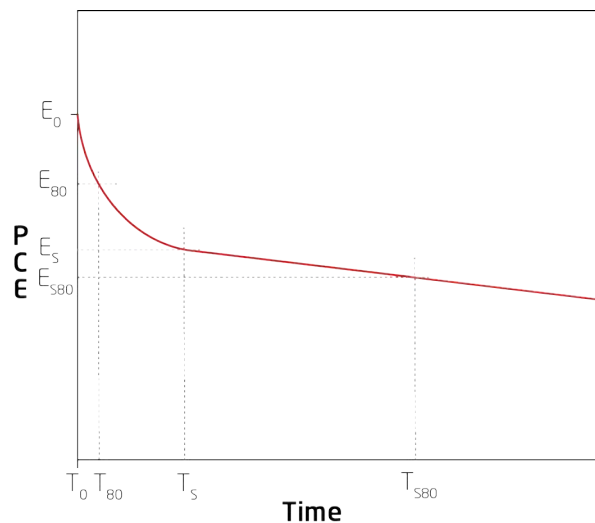
Fig 3.1 - Typical degradation curve of an OPV device. The four data pairs (E_0,T_0; E_{80},T_{80}; E_S,T_S; E_{S80},T_{S80}) are described in the text.

To report stability data, a degradation curve is plotted. Usually, the evolution of efficiency throughout the stability study is reported (a typical curve is shown in Fig 3.1). Other parameters such as the open circuit voltage (V_{OC}), the short circuit current (I_{SC}) and the fill factor (FF) are often reported. The degradation curve is characterized by four pairs of data points:

(E_0, T_0): E_0 is the initial measurement of an OPV device at T_0: the start of the study.

(E_{80}, T_{80}): E_{80} is the measurement when the OPV device has reached 80 % of E_0. T_{80} is the time it took the device to decay to E_{80}.

(E_S, T_S): Data point defined arbitrary, usually when the degradation stabilizes.

(E_{S80}, T_{S80}): E_{S80} is the measurement when the OPV device has reached 80 % of E_S. T_{S80} is the time it took the device to decay to E_S.

Many different categories of tests were defined: dark, outdoor, simulated light, temp cycling. For each test the main parameters are specified: temperature, light intensity, electric load, humidity, environment, testing equipment. Table 3.1 gives an overview of the ISOS tests used for the work reported in this thesis.

Dark storage

Three dark tests were applied to OPV cells or modules. ISOS-D-1 is a simple shelf storage study where the cell is left in a drawer or a shelf in the lab and characterized at regular time intervals. ISOS-D-2 introduces temperature control and requires an oven or a hot plate. Finally, in ISOS-D-3 both the temperature and the humidity are controlled. In order to do so a weathering chamber is needed. In our case, a Damp heat chamber from Thermotron was used.
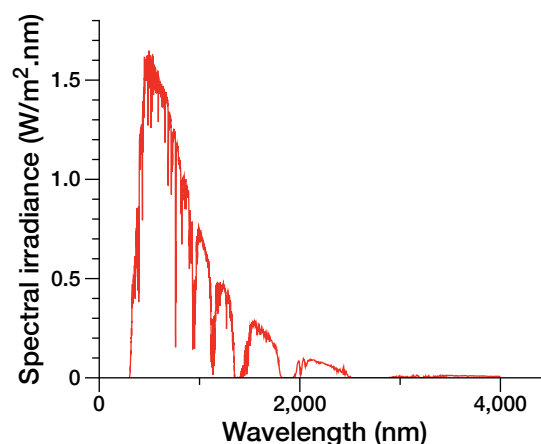
Fig 3.2 – AM1.5G spectrum.[10]

Light tests

For indoor tests under continuous illumination the choice of the light source is critical.[8] Each type of light has a different spectrum. OPV Cells are especially sensitive to the UV dose they receive which depends of the spectrum of the light source. For both tests used during this work, ISOS-L-2 and ISOS-L-3, the light source spectrum must be as close as possible to the real sun spectrum. The solar irradiance depends on the time of the day and the location. To enable comparison a standard is needed. For OPV, this reference spectrum is AM1.5G, which stands for Air Mass 1.5 global spectrum. This spectrum is measured at sea level, with 1000 W/m^2 irradiance and the sun shining at a 48.2° angle (1.5 atmosphere thickness) (Fig 3.2).[10] For both tests, the cells/modules are characterized continuously *in situ*. For ISOS-L-2, the modules are simply left under a sun simulator. The heat emanating from the light source is sufficient to raise the temperature of the modules to 65 °C. A thermoelectric component is taped onto the back of the cell/module and is used to monitor the temperature of the samples. For ISOS-L-3, both the temperature and the humidity need to be controlled. Therefore, a weathering chamber is needed, in our case a weathering chamber from Q-lab.

Table 3.1 – Overview ISOS tests protocols[8]

	ISOS-D-1	ISOS-D-2	ISOS-D-3	ISOS-L-2	ISOS-L-3	ISOS-O-1	ISOS-O-2
Light source	None	None	None	Constant light source (AM1.5G)	Constant light source (AM1.5G)	Sunlight	Sunlight
Temperature (°C)	Ambient	65/85 ± 2	65/85 ± 2	65/85	65/85	Ambient	Ambient
Humidity (%)	Ambient	Ambient (low)	85 ± 3	Ambient (low)	50	Ambient	Ambient
Electrical load	Open circuit	Open circuit	Open circuit	MPP* tracking or open circuit	MPP* tracking or open circuit	MPP* tracking or open circuit	MPP* tracking or open circuit
Characterization light source	Solar simulator or sunlight	Sun simulator AM1.5G	Sun simulator AM1.5G	*In situ*	*In situ*	Inside - Sun simulator AM1.5G	Outside under sunlight

* *MPP: maximum power point*

Outdoor tests

Putting the cells/modules outdoor is a straightforward way to tests them under real operating conditions. Depending on the test the samples are either characterized indoor with a sun simulator (ISOS-O-1) or *in situ* outdoor (ISOS-O-2). In the case of ISOS-O-2, a

continuous monitoring of the irradiance is necessary in order to normalize the degradation data and to measure the accumulated irradiance the samples received during the tests.

3.3. Photochemical stability of organic material for OPV

In the last decades, the intense research into developing high efficiency materials for OPV lead numerous π-conjugated materials with   better absorption characteristics.[11,12]   For example, a strong absorbance and a smaller band gap help to better harvest the photons in the solar spectrum. But all these improvements in efficiency are meaningless if the solar cell is not stable. And the device lifetime is intrinsically limited by the stability of the organic materials used for light harvesting. Finding materials combining good efficiencies and good stability is primordial. One critical issue of organic materials is that they often are sensitive to irradiation especially UV radiations and short wavelengths in the visible range. Under irradiation many photochemical processes can occur (chains-scission, crosslinking reaction…), which cause losses in the original properties of the organic material (electrical, optical, mechanical…). One example for OPV is the polyphenylenevinylene (PPV) derivatives. This family of polymers was popular to prepare OPV cells at the beginning but is now totally abandoned because of poor photochemical stability. Under 1 sun illumination, a PPV derivative Poly[2-methoxy-5-(2-ethylhexyloxy)-1,4-phenylenevinylene] (MEH-PPV) has a degradation rate of 0,96 %/min compared to 0,0082 %/min for P3HT.[13]

3.3.1. How to measure photochemical stability

Ultraviolet-visible spectroscopy (UV-vis) is a widely spread technique to measure the absorption spectrum of a conjugated material. UV-vis is a non-destructive technique that gives information on conjugation length, crystallinity and optical band gap. UV-vis spectroscopy is also a simple and easy way to monitor conjugated materials photochemical behavior. It is possible to characterize the relative stability of a material under light exposure by measuring its absorbance at regular intervals. The loss in absorption is directly correlated to the photo oxidation of the conjugated material.

In this work, an automatized system was used to monitor the photochemical stability of polymer films through losses in absorbance.[4] The polymer films were placed under a

Steuernagel solar simulator with an Osram 1200W metal halide arc lamp giving a AM1.5G spectrum of 1000 W/m^2 intensity. No UV filter was used yielding a UV-rich spectrum with a cut-off at 280 nm. The films were studied at room temperature (~23 °C) and ambient humidity (~20%). To monitor the degradation of multiple samples at the same time an automated sample exchanger was used. For each polymer film, the absorbance was monitored in multiple points at regular intervals using a UV-vis spectroscopic probe set up with an optical fiber-based CCD spectrometer (Avantes AvaSpec 1024) and a halogen/deuterium light source (Avantes AvaLight-DHc). Finally, the degradation rates were obtained by calculating the decrease of the number of absorbed photons over time.[13]

3.3.2. CN-P3HT[*]

The chemistry of active materials in OPV is critical for photochemical stability.[4,14–16] The constitution and the morphology of the film impact as well as the photochemical stability in a OPV cell.[17] Modifying the chemistry of the active material is one way to stabilize the morphology and thus stabilize the performances of the cells over time.[18,19] However, the morphology of the active blends also influences the electronic properties of the cells, and often an improvement in morphological stability leads to lower PCE. The challenge is therefore to enhance the photochemical stability while maintaining the electronic properties. In order to do so, the chemical modification needs to be subtle.

Among the reported ways to do it are random and semi random co-polymerizations.[5,20–22] During such polymerization the backbone of the pristine polymer is only slightly modified. By adding a small amount of a carefully selected monomer (5-15% in weight), the original properties of the pristine polymer such as morphology and structural order can be maintained while the optical properties like the band gap can be significantly modified leading for example to better light harvesting and higher efficiency.[23]

The most commonly used donor material in OPV is P3HT (Fig 3.3 center). On top of being widely available and easy to deposit, it also has relatively good performances stability wise. P3HT has a good photochemical stability compared to other common donor materials such as PPVs. It also yields stable blend morphologies. Studies of random and semi-random

---

[*] Section based on reference 6.

copolymerization of functional units showed that the bulk properties of P3HT are not modified for comonomer amounts between 5 and 15 % in weight.[20]
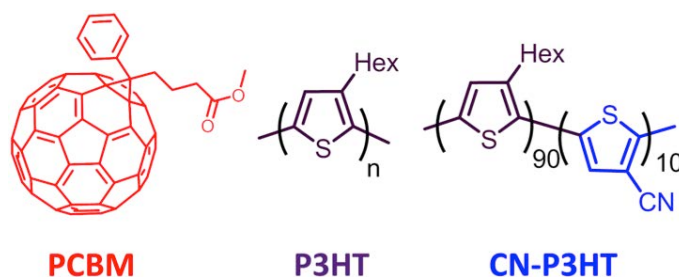
Fig 3.3 – chemical structures of PCBM (left), pristine P3HT (middle) and CN-P3HT (right). Reprinted with permission from 6.

The following work sprouted from these conclusions. A previous report by Khlyabich *et al.* showed that incorporating electron withdrawing cyano group (CN) (Fig 3.3) in the backbone through random copolymerization improved noticeably the V_{OC} compared to pure P3HT spin coated cells.[6] The aim of this study is to if the incorporation CN groups influences as well the photochemical stability of the polymer. The photochemical stability of the pure poly(3-hexylthiophene-co-3-cyanothiophene) (CN-P3HT) and its blend with PCBM was measured and compared to the one of pristine P3HT. CN-P3HT was then incorporated in ITO-free R2R coated cells. These cells were finally tested according to the ISOS-L-2 protocol.

Previous reports showed that the incorporation of 10 % cyano group only slightly affects the optical behavior compared to pristine P3HT.[5,24] The CN-P3HT was synthesized at USC by Thompson and coworker.[5]

Photochemical Stability

The photochemical stability of random copolymer CN-P3HT was compared to pristine P3HT and their blend. The following solutions were prepared in Chlorobenzene:

- P3HT (15 mg/mL)
- P3HT:PCBM (15 mg/mL:15 mg/mL)
- CN-P3HT (15 mg/mL)
- CN-P3HT:PCBM (15 mg/mL : 15 mg/mL)

- CN-P3HT:P3HT (7.5 mg∕mL：7.5 mg∕mL)

- CN-P3HT:P3HT:PCBM(7.5 mg∕mL：7.5 mg∕mL：15 mg∕mL)

P3HT was purchased from BASF (Sepiolid P-200), PCBM was obtained from Merck. CN-P3HT was synthesized as previously reported (Mn: 12 kDa, dispersity: 2.4).[5] The solutions were stirred at 70 °C overnight, filtered with a 0.45 micron Teflon filter before being spin coated on 25 x 50 mm^2 glass slides (cut-off 315nm) at 850 rpm for 30 s. The films were then studied as is with the photochemical setup described above.

As expected the optical properties are not noticeably changed by the incorporation of cyano groups. The initial absorbance spectra of the films are similar for P3HT, CN-P3HT and their blend (Fig 3.4 left). The shoulder at 680 nm in the pristine P3HT film spectra was attributed to contamination of the sample. When mixed with PCBM, the spectra are also similar (Fig 3.4 right) but there is a red shift from 480 nm for P3Ht to 520 nm for CN-P3HT. This could be due to the presence of cyano groups leading to a different solid state packing structure.
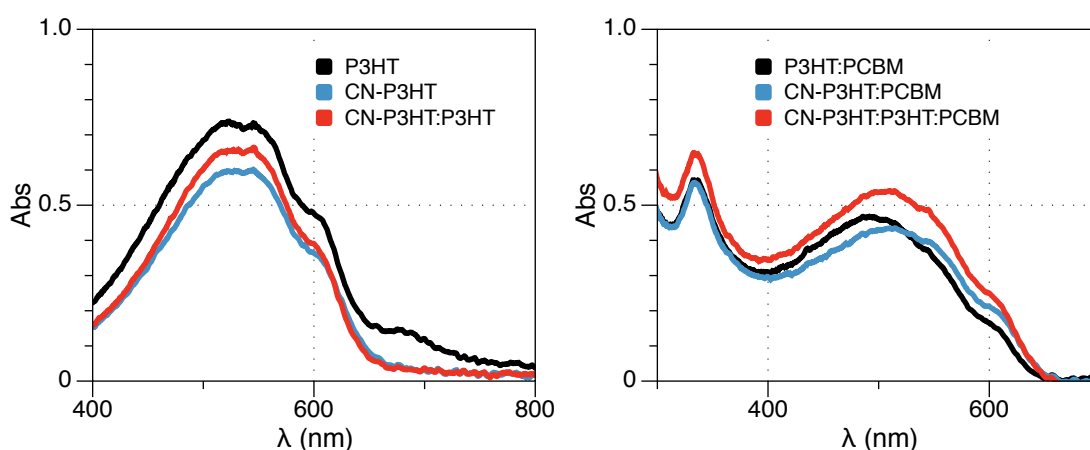
Fig 3.4 – Initial absorbance of the six polymers films. Adapted with permission from 6.

The decrease in absorbance under continuous light exposure is shown in Fig 3.5. For all the films the initial absorbance was comprised between 0.4 and 1 (Table 3.2). Madsen *et al.* have shown that the impact of the film thickness on the degradation rate is negligible when the absorbance is in this range.[17]

The introduction of cyano groups in the co-polymer CN-P3HT has a clear impact on the photochemical stability. The degradation rate of CN-P3HT is a factor 2 lower than the degradation rate of pristine P3HT. Another interesting result is that CN-P3HT and the blend

CN-P3HT:P3HT have a similar degradation rate (Table 3.2). By simply mixing CN-P3HT to P3HT the stability of the latter is improved.
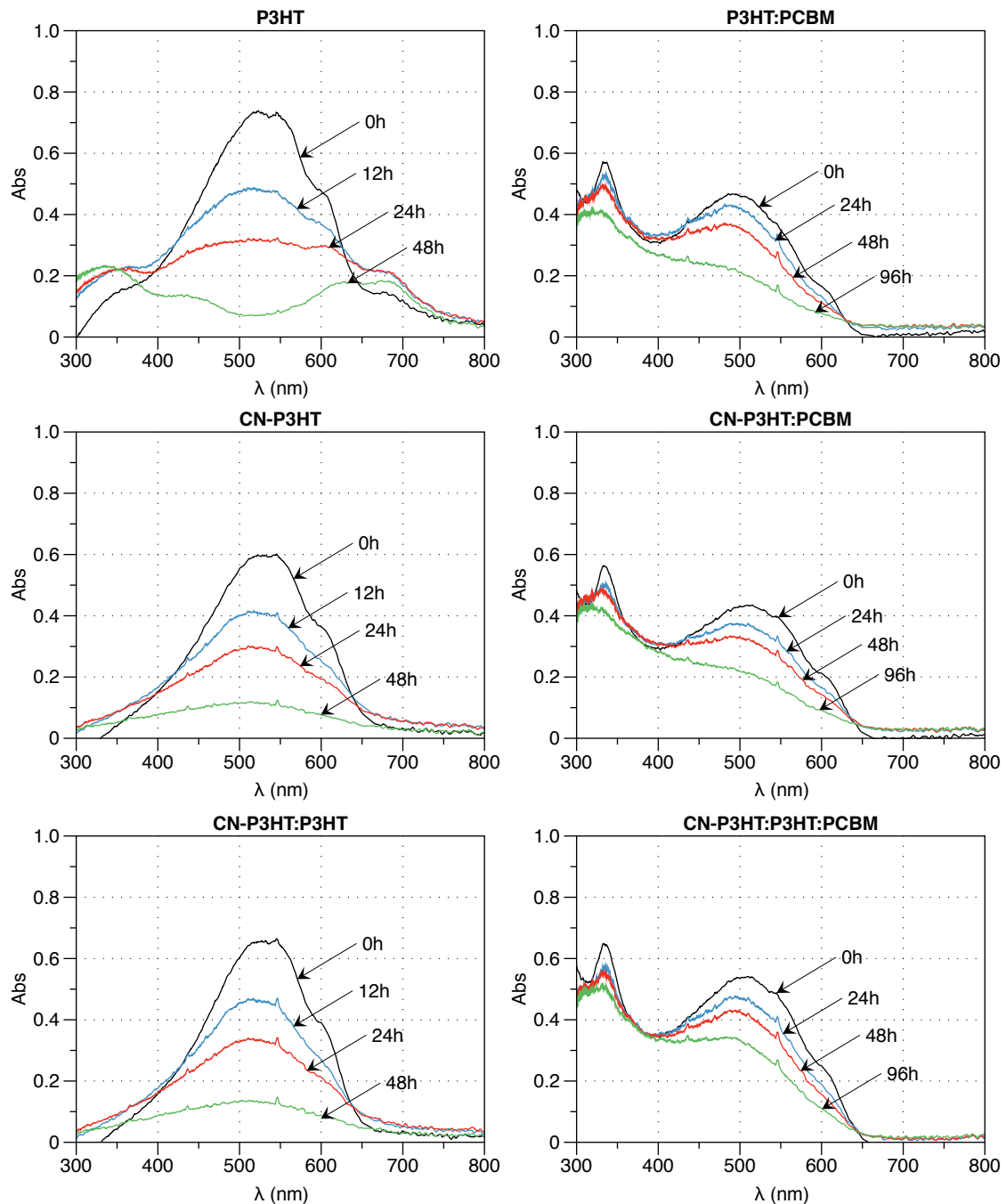
Fig 3.5 – Evolution of absorbance under continuous light exposure of P3HT (top left), CN-P3HT (middle left), CN-P3HT:P3HT (bottom left), P3HT:PCBM (top right), CN-P3HT:PCBM (middle right) and CN-P3HT:P3HT:PCBM (bottom right). Reprinted with permission from 6.

However, all films containing PCBM have the same degradation rate which is lower than without PCBM. Therefore, PCBM is the dominant stabilizer in this case.

The conclusion of this photochemical study is that the incorporation of cyano group in the backbone noticeably improves the photochemical stability of pristine P3HT. The simple mixing of both CN-P3HT and P3HT has the same effect. However, PCBM is still a better stabilizer.

Table 3.2 – Starting absorbance and degradation rates of the six films

Film	Starting Absorbance	Degradation rate (%/h)
P3HT	0,60 ± 0,05	2,3 ± 0,4
CN-P3HT	0,61 ± 0,04	1,48 ± 0,04
CN-P3HT:P3HT	0,66 ± 0,03	1,4 ± 0,2
P3HT:PCBM	0,46 ± 0,06	0,46 ± 0,04
CN-P3HT:PCBM	0,44 ± 0,03	0,40 ± 0,02
CN-P3HT:P3HT:PCBM	0,47 ± 0,02	0,38 ± 0,03

Lifetime study

Even though the impact of CN-P3HT on stability appears limited compared to PCBM, the next natural steps was to study its impact on full devices stability. Three type of cells were prepared with different active layers: P3HT:PCBM, CN-P3HT:PCBM and CN-P3HT:P3HT:PCBM. All the cells were ITO-free and prepared by roll coating. P3HT:PCBM (15 mg/mL:15 mg/mL), CN-P3HT:PCBM (15 mg/mL:15 mg/mL) and CN-P3HT:P3HT:PCBM (7.5 mg/mL:7.5 mg/mL:15 mg/mL) were dissolved in a mixture of chlorobenzene (100 parts), chloroform (10 parts) and chloronaphtalene (3 parts) and stirred at 70 °C overnight. The cells were then coated with a mini roll-coater.[25] The active layer was slot-die coated using a 10 mm meniscus guide (flow rate: 0.15 mL/ min; speed: 1 m/ min; temperature: 70 °C) on a 1 m stretch of Flextrode.[26] Next, two type of PEDOT:PSS were slot-die coated on top of the active layer, PEDOT:PSS Agfa 5010 (1.2 mL/ min; 0.8 m/ min) or a three layer PEDOT:PSS structure:

    - PEDOT:PSS F10 (diluted in isopropanol (IPA) (1:4 in volume); 0.11 mL/min; 1.3 m/min),

    - PEDOT:PSS Al 4083 (diluted in IPA (1:2 in volume); 0.3 mL/min; 1.3 m/min),

- PEDOT:PSS F10 (diluted in IPA (1:2 in volume); 0.5 mL⁄min; 1.3 m⁄min).

The three PEDOT:PSS layers structure has been found to be useful in some cases, for example in tandem cells.[27] In order to find which back PEDOT:PSS is optimal for CN-P3HT, cells with both type were measured (Table 3.3). In the case of CN-P3HT there is no clear difference between the two back PEDOT:PSS. The top silver grid electrode was flexoprinted using a silver ink (Dupont 5025). The cells were encapsulated with glass slides (15 x 15 mm^2) and UV-curing epoxy (DELO LP655). Finally, the cells were annealed at 120°C for 2 min. The active area of the cells was 0.8 cm^2.

Table 3.3 – Initial IV characteristics averaged over three cells for each type.

		P3HT:PCBM	CN-P3HT:PCBM	CN-P3HT:P3HT:PCBM
PCE (%)	*Agfa 5010*	1,23 ± 0,07	0,52 ± 0,07	0,71 ± 0,04
	3 layers	0,94 ± 0,05	0,6 ± 0,09	0,5 ± 0,01
VOC (V)	*Agfa 5010*	0,53 ± 0,01	0,66 ± 0,01	0,57 ± 0,01
	3 layers	0,51 ± 0,01	0,62 ± 0,04	0,57 ± 0,01
ISC (mA)	*Agfa 5010*	3,7 ± 0,3	2,1 ± 0,2	3,2 ± 0,3
	3 layers	3,9 ± 0,2	2,3 ± 0,2	2,2 ± 0,6
FF (%)	*Agfa 5010*	51 ± 2	29 ± 2	31 ± 1
	3 layers	37,8 ± 0,2	34,7 ± 0,3	29 ± 4
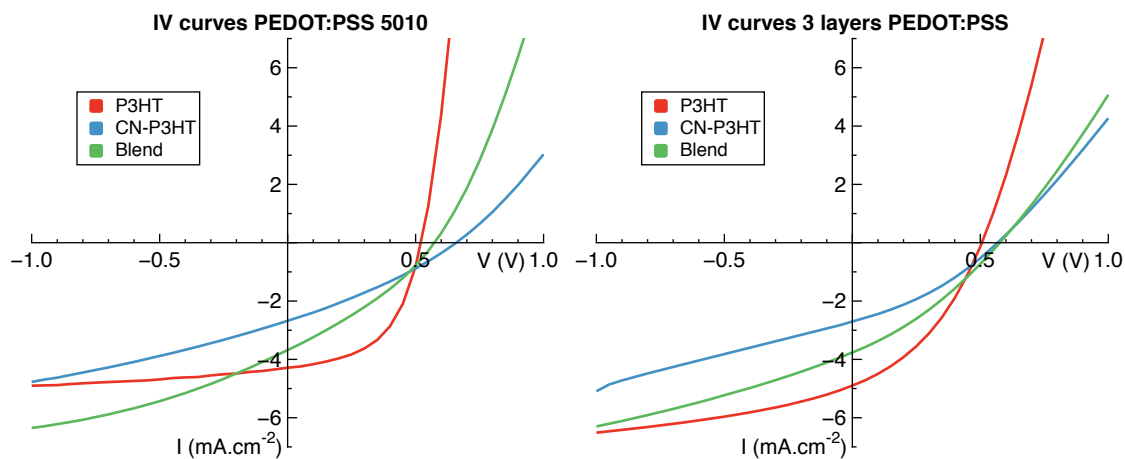
Fig 3.6 – typical IV curves with PEDOT:PSS 5010 (left) and with 3 layers PEDOT:PSS structure (right). Reprinted with permission 6.

The initial IV characteristics averaged over three cells for each type are gathered in Table 3.3. Even though, the introduction of cyano groups should not noticeably modify the electronic properties of P3HT, the cells' architecture was optimized for P3HT not CN-P3HT. It means

that the processing conditions and the polymer:fullerene ratio are optimal for the P3HT but might not be for CN-P3HT. Differences in synthesis method and in size distribution could explain the apparent lower performances of CN-P3HT and the blend CN-P3HT:P3HT cells (Fig 3.6).

For both back PEDOT:PSS, the P3HT cells have an efficiency about two times higher than the cells with CN-P3HT. As for the cells with the CN-P3HT:P3HT blend, they have efficiencies in between. The decrease in efficiency (in that particular cell architecture) is an unwanted effect of the introduction of cyano groups in the P3HT backbone. This observation contradict previous reports where the incorporation of cyano groups increased the PCE mainly through the enhancement of V_{oc} for solar cells spin-coated on ITO.[5,28] Even though, a similar improvement of the V_{oc} is also observed in this study (Table 3.3), the drop in performance for CN-P3HT roll coated cells is due to a decrease in I_{SC} and FF. The differences in this study could come from the inherently different active layer morphologies or from the fact that the polymer:PCBM ratio was optimized for P3HT and not for CN-P3HT.
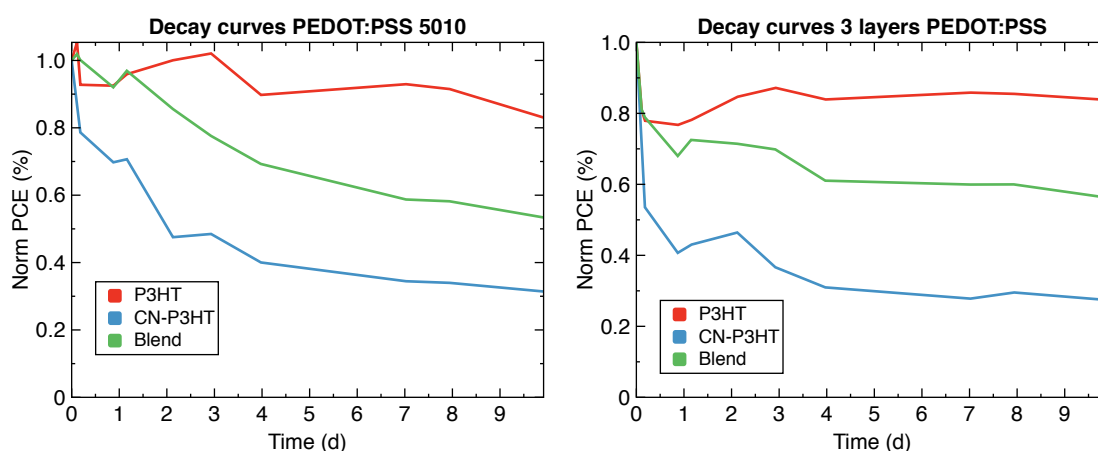
Fig 3.7 – Typical decay curves of cells with PEDOT:PSS Agfa 5010 (left) and with the three PEDOT:PSS layers (right). Adapted with permission 6.

The cells were tested under continuous light exposure according to the ISOS-L-2 standard described earlier in this chapter. For each kind of cell, a typical decay curve is plotted in Fig 3.7. The degradation parameters are given in Table 3.4. These parameters are described in the ISOS section. For CN-P3HT:P3HT with the triple PEDOT:PSS back electrode, the values are given for a single cell because the two other cells failed during the experiment.

For both back PEDOT:PSS, the P3HT cells were the most stable and retained an efficiency stabilized around 80% of their initial value (Fig 3.7). Only one cell with P3HT degraded by more than 20% during the study. The cells with CN-P3HT were the least stable and decayed much faster (Fig 3.7). The CN-P3HT cells decayed by 20% in only a few hours (Table 3.4). The CN-P3HT cells with PEDOT:PSS 5010 stabilized at a lower value (E_S) than the cells with the three PEDOT:PSS. However, they were then more stable with a T_{S80} of about 2 days compared to one day for the cells with the triple layer PEDOT:PSS.

Table 3.4 – Stability Data under ISOS-L-2 testing. The data is averaged over three cells.

		P3HT:PCBM	CN-P3HT:PCBM	CN-P3HT:P3HT:PCBM
E_0 (%)	Agfa 5010	1,23 ± 0,07	0,52 ± 0,07	0,71 ± 0,04
	3 layers	0,94 ± 0,05	0,6 ± 0,09	0,56[b]
E_S (%)	Agfa 5010	1,16 ± 0,04	0,24 ± 0,03	0,40 ± 0,02
	3 layers	0,89 ± 0,05	0,37 ± 0,01	0,51[b]
T_{80} (h)	Agfa 5010	235 ± 4	5 ± 3	53 ± 7
	3 layers	237,6[a]	1,88 ± 0,07	3,5[b]
T_S (h)	Agfa 5010	88 ± 5	40 ± 16	150 ± 40
	3 layers	78 ± 7	3,6 ± 0,8	20,9[b]
T_{S80} (h)	Agfa 5010	237,6[a]	58 ± 10	237,6[a]
	3 layers	237,6[a]	20 ± 30	237,6[a]

[a]The final time (T_f) is given when the cells did not decay by 20% from E_0 or E_S.
[b]Two cells failed during the experiment. The values for only one cell are given.

The cells prepared with the blend have a stability in between pristine P3HT and CN-P3HT. The cells with PEDOT:PSS 5010 were more stable than the cells with three layers. They have a T_{80} one order of magnitude higher. Even better they remained above 80% of ES for the whole study. For the cells with the triple PEDOT:PSS layer as back PEDOT:PSS two cells failed early during the study. The data is given as indication but is not statically relevant. Even though CN-P3HT has a better photochemical stability than pristine P3HT, this did not translate in a higher stability of the full devices. It actually yielded cells with poorer stability.

3.3.3. Conclusion

The CN-P3HT study showed that one can improve the photochemical stability of P3HT while retaining the optical properties. However, PCBM was still a better stabilizer and the higher stability of CN-P3HT did not lead to OPV cells with better stability. On the contrary these cells

decayed faster than the ones with pristine P3HT. This indicates that even if photochemical stability is critical for OPV devices stability others parameters need to be optimized to improve the lifetime.

3.4. Meta-Analysis of OPV cells[†]

Despite the rising number of scientific publications reporting on OPV stability, it is still difficult to ascertain exactly where OPV stand in term of lifetime.[7,29–31] This is mainly due to the complex architecture of OPV cells[32], and to the multiple aging mechanisms occurring in OPV devices at the same time.[31,32] The consequence is that aging curves often have complex shapes for OPVs and they are therefore complex to model.[33] Another issue is that up until the recent introduction of testing standards by the ISOS, all stability tests were conducted with homemade apparatus making comparison impossible between laboratories.[33,34] The aim of the work presented in this section was to define a generic marker to be applied to any degradation curve. So, one would be able to determine the lifetime from aging curves of diverse shapes and to compare the stability of different architectures and materials. Once this marker was found the next step was to develop a tool to predict OPV lifetime based on accelerated tests and to implement more stable technologies.

The methodology was to compile and analyze a large volume of scientific reports on OPV stability. This meta-analysis was done as follow. A "Sciencedirect" search conducted in March 2013 with the key words: polymer, plastic, organic, solar cells, photovoltaics, stability, lifetime; yielded 2500 articles. Other more recent and relevant publications were added throughout the study. The publications were then classified as either relevant, irrelevant or with no data. The papers of the last two categories were discarded, leaving 303 articles to be compiled. Device specifications and stability data were extracted and analyzed. The results allowed identifying the bottlenecks (configuration, packaging…) for stability of OPV cells, as well as the current level of OPV lifetimes reported under different aging conditions.

This section will only present results that are relevant for this thesis: PEDOT:PSS and photoactive layer (PAL) studies. For more information, on the methodology, the generic lifetime marker, lifetime prediction refer to reference [9].

[†] This section is based on the reference 9.

3.4.1. PEDOT:PSS studies

The impact of PEDOT:PSS on aging in OPV device is commonly discussed.[7,30,31] It is well known that PEDOT:PSS does play a significant role in OPV degradation but how it is unclear. PEDOT:PSS is still widely used because it has many advantages. PEDOT:PSS has a tunable work function, which make it easy to align the highest occupied molecular orbital (HOMO) of the donor material in the PAL with the work function of the electrode - either Indium tin oxide (ITO) in regular architecture cells or the top metal electrode (Ag or Au) in inverted cells.

The aging mechanisms due to PEDOT:PSS have been linked to its hygroscopic nature.[35–37] This has consequences in a humid environment: the conductivity of PEDOT:PSS diminishes because of water uptake; PEDOT:PSS accelerates the corrosion of the metal electrodes even for high work function electrodes in inverted structures; and the acidity of the PEDOT:PSS layer increases, resulting in the etching of ITO. [35,36,38–40] UV light also lowers the conductivity of PEDOT:PSS.[41] However, in some cases PEDOT:PSS was reported to not affect the aging rate of the devices or even to improve the stability when replacing metal oxides.[42,43] To better apprehend the impact of PEDOT:PSS on OPV lifetime, the data was separated and plotted (Fig 3.8) according to the cells' architecture and packaging as well as test conditions. The position of PEDOT:PSS was classified as follow:

- Normal geometry: PEDOT:PSS is between the transparent anode and the PAL (PEDOT-n).
- Inverted geometry: PEDOT:PSS is between the back electrode and the PAL (PEDOT-i).
- PEDOT:PSS-free (PEDOT-free).

The data was further classified into unencapsulated (a, b) and encapsulated (c, d) cells tested in dark conditions (left) or under illumination (right).

For the non-encapsulated devices in the dark, the cells with a normal geometry have the shortest lifetime. This is as expected since in a humid environment PEDOT:PSS will absorb water and react as explain earlier. Inverted cells, where the PEDOT:PSS is between the PAL and the top electrode, have a good stability in dark. It has been claimed that PEDOT:PSS by itself is stable under dark and ambient conditions, and is only detrimental to the device stability when in contact with ITO or Al.[40] Under light tests, the unprotected devices with an inverted structure are less stable. This is linked to the low barrier properties of the top

electrode against oxygen diffusion and to the fact that PEDOT:PSS is vulnerable to UV light.[44] Finally, unencapsulated PEDOT:PSS-free samples appear to be stable in the dark and under illumination for both normal and inverted geometry. Removing PEDOT:PSS from the OPV architecture could improve dramatically the stability.
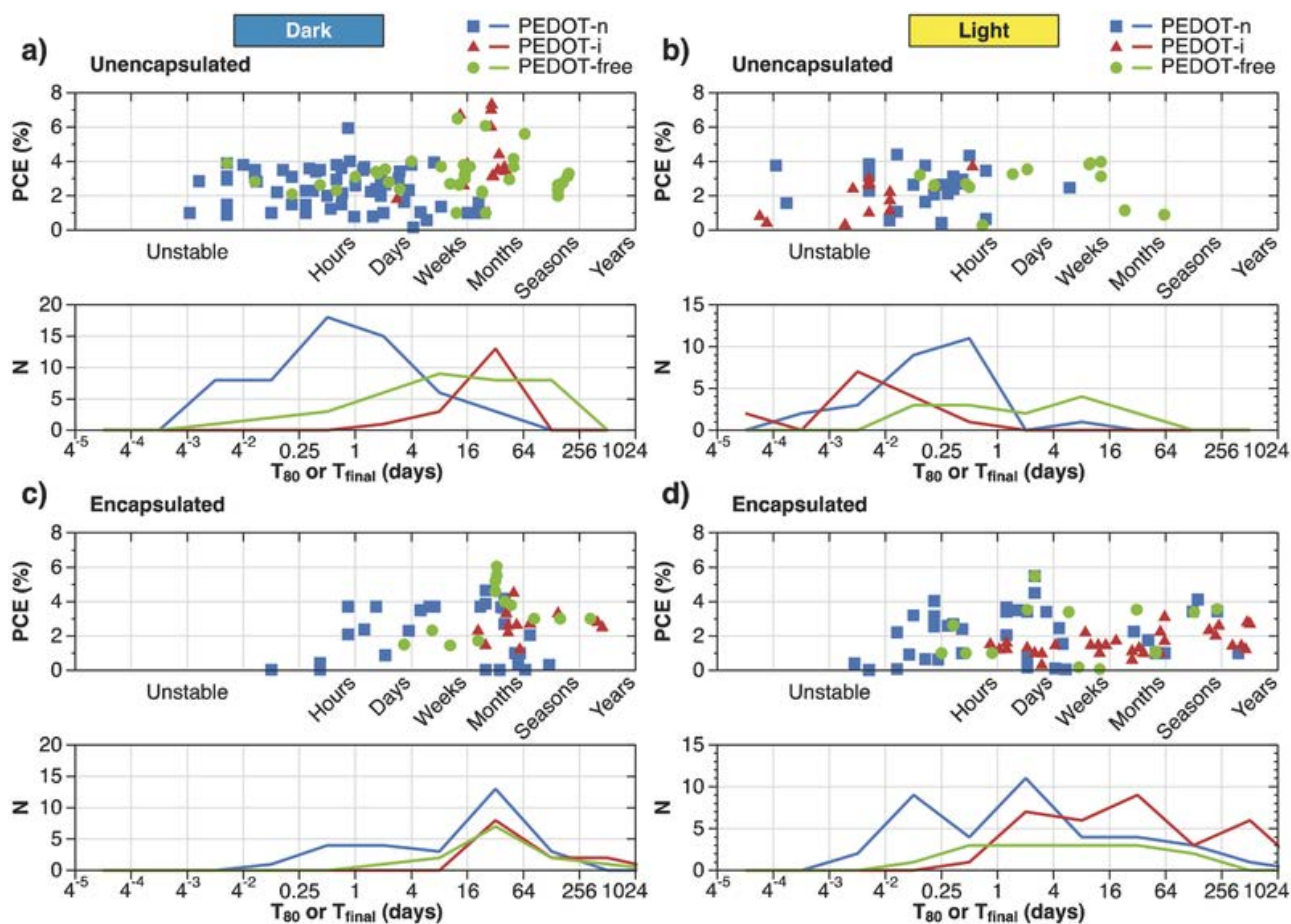
Fig 3.8 – Distribution of lifetimes for unencapsulated (a,b) and encapsulated (c,d) samples grouped into three categories: PEDOT-n (blue squares), PEDOT-i (red triangles) and PEDOT-free (green circles). Plots are grouped according to dark (a,c) and illumination (b,d) tests. Each data point corresponds to one aged sample reported in the literature. The bottom plots show the distribution of the data in a histogram format, where the y-axis represents the number of the reported data points. Reprinted with permission from reference 9.

For the encapsulated devices, there is little difference between the three cell architectures. The reason could be that the encapsulation significantly lowers the diffusion of water and oxygen in the cell. In addition, common encapsulating material protects the cells from UV

radiations. Glass reduces transmission in the UV range and plastic foils are furnished with UV-filter. Therefore, the aging induced by PEDOT:PSS in encapsulated devices is negligible. However, it is likely that aging mechanisms associated with PEDOT:PSS will appear over longer time scales in encapsulated samples. Thus, removing PEDOT:PSS completely from the OPV stack is the best course of action to improve stability.

3.4.2. Photoactive layer studies

The PAL as it degrades has a direct impact on the light absorption and the charge generation processes. For this reason, it has a critical role in OPV devices stability. Most often the PAL is made of a mixture of a conjugated polymer (donor material) and of a fullerene derivative (acceptor material). When exposed to external factors such as oxygen, water, light, elevated temperature both the PAL materials degrade quickly.[7,30,31] The following are common degradation mechanisms associated to the PAL: Exposure to UV and oxygen leads to the photochemical scission of the conjugated polymer chain; Generation of traps in the PAL by oxygen doping in presence of oxygen. [3,45] This process is speeded up by exposure to light; The metal electrodes diffuse into the PAL and when exposed to light react with the polymer in presence of humidity and oxygen.[46–49] The morphology of the polymer/fullerene mixture is modified mostly by temperature and light, but also possibly by oxygen and humidity.[50,51]

Similarly to the previous PEDOT:PSS study, the stability data gathered during the meta-analysis was plotted in (Fig 3.9) against the PAL materials. The PAL was classified as following:

- P3HT
- High PCE (h-PCE): see Table 3.5 these materials are mostly mixed with phenyl-C71-butyric acid ([70]PCBM).
- Small Molecules: typically phthalocyanine-based materials (Copper phthalocyanine (CuPc), zinc phthalocyanine (ZnPc), subphthalocyanine (SubPc), chloroaluminum phthalocyanine (ClAlPc)) or Pentacene, combined with either C60 or PCBM.[48]
- Others

Plots a and c in Fig 3.9 correspond to the tests conducted in the dark and the b and d to tests under illumination. The top plots are for unencapsulated devices (Fig 3.9 a,b) and bottom plots for encapsulated samples (Fig 3.9 c,d).
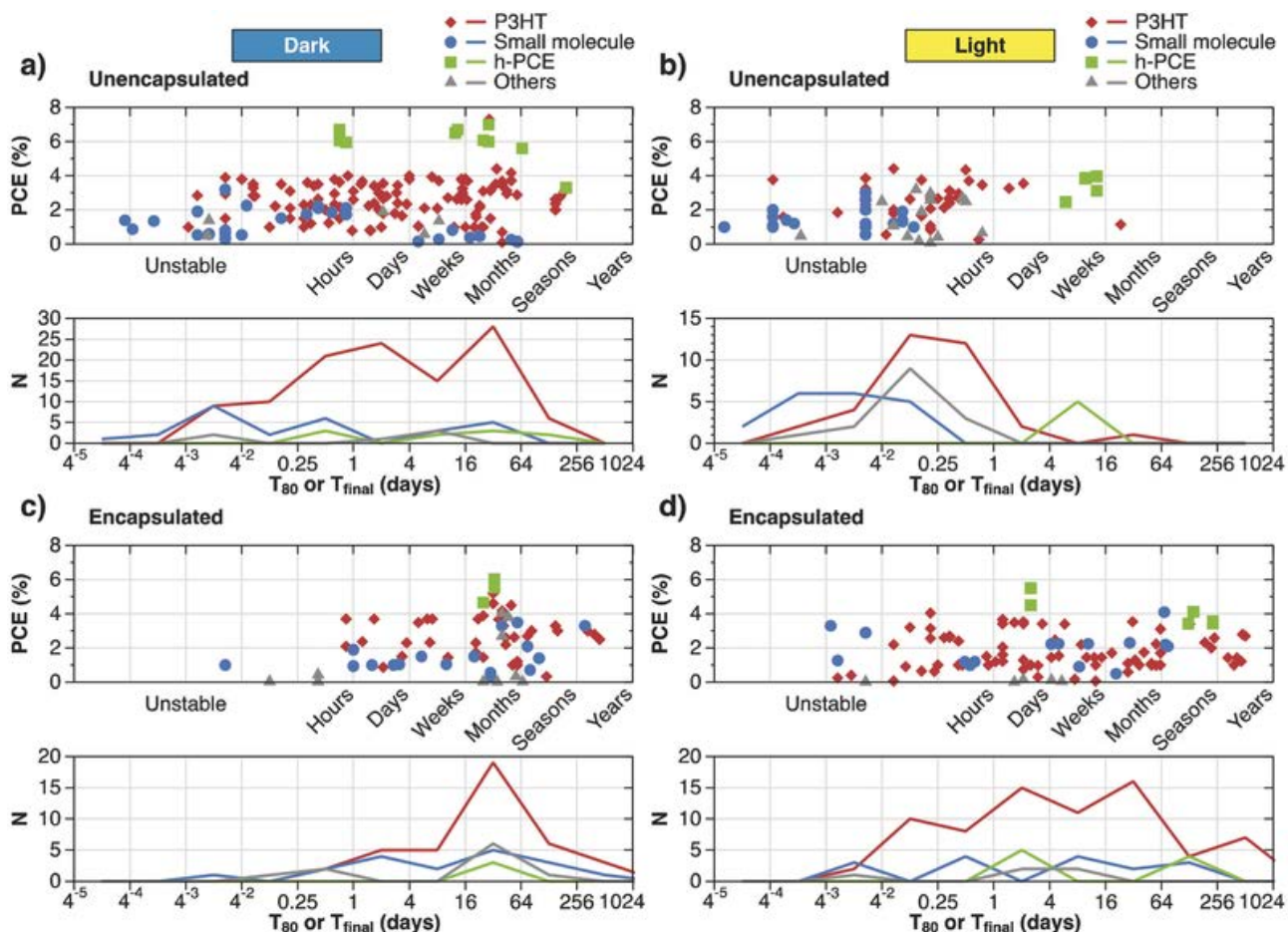
Fig 3.9 - Distribution of lifetime for samples grouped according to the PAL: P3HT (red diamonds), small molecule based (blue circles), h-PCE (green squares) and others (grey triangles). a) Dark test of unencapsulated samples, b) light tests of unencapsulated samples, c) dark tests of encapsulated samples, and d) light tests of encapsulated samples. The data is presented as scatter plots with the corresponding histogram showing the distribution below. Reprinted with permission from 9.

For unencapsulated devices, under illumination (Fig 3.9 b) h-PCE devices have the best stability. The three other categories have a poor stability, especially the small molecules. In dark, there is not much differences between the four categories showing that light is a key factor in PAL degradation.

Table 3.5 – High efficiency polymers tested either in dark or light conditions. Among all the compounds PCDTBT is the most frequently reported polymer. Extracted with permission from reference 9.

Name	Description
PCDTBT	poly[N-9″-hepta-decanyl-2,7-carbazole-alt-5,5-(4′,7′-di-2-thienyl-2′,1′,3′-benzothiadiazole)
PCPDTBT	poly[(4,4-bis(2-ethylhexyl)-4H-cyclopenta[2,1-b;3,4-b]dithiophene-2,6-diyl-alt-2,1,3-benzothiadiazole-4,7-diyl]
BTI-BDT	bithiophene imide and benzodithiophene based copolymer
PDTSTPD	poly(4,4-bis(2-ethylhexyl)-dithieno[3,2-b:2′,3′-d]silole and N-octyl-thieno[3,4-c]pyrrole-4,6-dione)
PBDTTPD	poly({4,8-di (2-ethylhexyloxyl) benzo[1,2-b:4,5-b′] dithiophene – 2,6-diyl) – alt – ({5-octylthieno[3,4-c] pyrrole – 4,6-dione-1,3-diyl)
PFDCTBT-C8	poly(fluorenedicyclopentathiophene-alt-benzothiadiazole) with octyl side chains
a-PTPTBT	Poly(thiophene-phenylene-thiophene – 2,1,3-benzothia-diazole)

In the case of encapsulated devices (Fig 3.9 c,d), there is no differences between the various devices both in the dark and under light. The diffusion of oxygen and water into the devices is slowed down by the encapsulation. The PAL degradation still happens but the difference between the four categories is negligible.

When focusing on P3HT devices, the large stability range (Fig 3.9 d), from a few minutes to years shows that in encapsulated devices, the decay of encapsulated devices is not mainly determined by the PAL. This means that to extend the lifetime of OPV devices, all the other parts of the device need to be studied. This will allow identifying the key components for stability in order to develop a stable technology.

3.4.3. Conclusion

The analysis of hundreds of scientific reports on OPV stability showed how the lifetime of OPV progressed in recent years. At the beginning, the reported stability of OPV devices was of barely minutes. However, now lifetimes ranging from weeks to month are reported. This analysis also pointed out the critical factors in devices structure for stability. For example, the PAL material was showed to not matter much in encapsulated devices. However, PEDOT:PSS clearly lowers the stability of OPV devices and should be removed or replaced.

3.5. Summary and Outlook

In this chapter, the ISOS standards were presented as a metric to test and report the lifetime of OPV devices. This chapter highlighted the relative importance of the PAL photochemical stability to the intrinsic stability of OPV devices and described an easy UV-vis technique to do it. Random and semi-random copolymerizations were introduced as an elegant way to modify the photochemical properties of a polymer while retaining its original optical properties. The study of CN-P3HT, obtained by such copolymerization showed an increased photochemical stability compared to pristine P3HT. However, lifetime studies pointed out for encapsulated devices, that an improved photochemical stability does not necessarily means an improved stability of the full device. Finally, the results of an analysis of hundreds of scientific reports on OPV stability were presented. The negligible impact of the PAL stability on the full encapsulated device lifetime was highlighted. The other noticeable result concerned the clear impact of PEDOT:PSS on OPV degradation. The need to replace PEDOT:PSS was emphasized by the results of the meta-analysis.

To successfully improve the stability of OPV cells, it is necessary to find or develop new absorbing materials for the PAL that combine both high performance and high intrinsic stability and to replace PEDOT:PSS. The screening of multiple high efficiency polymers will be the focus of the next chapter. The issue of replacing PEDOT:PSS will be tackled in the chapter 5 of this thesis.

3.6. References

(1)   Brabec, C. J.; Hauch, J. A.; Schilinsky, P.; Waldauf, C. Production Aspects of Organic Photovoltaics and Commercialization of Devices. *MRS Bull.* **2005**, *30*, 50–52.

(2)   Green, M. A.; Emery, K.; Hishikawa, Y.; Warta, W.; Dunlop, E. D. Solar Cell Efficiency Tables (version 46). *Prog. Photovoltaics Res. Appl.* **2015**, *23*, 805–812.

(3)   Manceau, M.; Rivaton, A.; Gardette, J.-L. Involvement of Singlet Oxygen in the Solid-State Photochemistry of P3HT. *Macromol. Rapid Commun.* **2008**, *29* (22), 1823–1827.

(4)   Tromholt, T.; Madsen, M. V.; Carlé, J. E.; Helgesen, M.; Krebs, F. C. Photochemical Stability of Conjugated Polymers, Electron Acceptors and Blends for Polymer Solar Cells Resolved in Terms of Film Thickness and Absorbance. *J. Mater. Chem.* **2012**, *22* (15), 7592-7601.

(5)   Khlyabich, P. P.; Rudenko, A. E.; Thompson, B. C. Random poly(3-Hexylthiophene- Co -3-Cyanothiophene) Copolymers with High Open-Circuit Voltage in Organic Solar Cells. *J. Polym. Sci. Part A Polym. Chem.* **2014**, *52* (8), 1055–1058.

(6)   Roth, B.; Rudenko, A. E.; Thompson, B. C.; Krebs, F. C. Photochemical Stability of Random poly(3-Hexylthiophene-Co-3-Cyanothiophene) and Its Use in Roll Coated ITO-Free Organic Photovoltaics. *J. Photonics Energy* **2014**, *5* (1), 057205.

(7)   Jørgensen, M.; Norrman, K.; Krebs, F. C. Stability/degradation of Polymer Solar Cells. *Sol. Energy Mater. Sol. Cells* **2008**, *92* (7), 686–714.

(8)   Reese, M. O.; Gevorgyan, S. a.; Jørgensen, M.; Bundgaard, E.; Kurtz, S. R.; Ginley, D. S.; Olson, D. C.; Lloyd, M. T.; Morvillo, P.; Katz, E. a.; Elschner, A.; Haillant, O.; Currier, T. R.; Shrotriya, V.; Hermenau, M.; Riede, M.; R. Kirov, K.; Trimmel, G.; Rath, T.; Inganäs, O.; Zhang, F.; Andersson, M.; Tvingstedt, K.; Lira-Cantu, M.; Laird, D.; McGuiness, C.; Gowrisanker, S. (Jimmy); Pannone, M.; Xiao, M.; Hauch, J.; Steim, R.; DeLongchamp, D. M.; Rösch, R.; Hoppe, H.; Espinosa, N.; Urbina, A.; Yaman-Uzunoglu, G.; Bonekamp, J.-B.; van Breemen, A. J. J. M.; Girotto, C.; Voroshazi, E.; Krebs, F. C. Consensus Stability Testing Protocols for Organic Photovoltaic Materials and Devices. *Sol. Energy Mater. Sol. Cells* **2011**, *95* (5), 1253–1267.

(9)   Gevorgyan, S. A.; Madsen, M. V.; Roth, B.; Corazza, M.; Hösel, M.; Søndergaard, R. R.; Jørgensen, M.; Krebs, F. C. Lifetime of Organic Photovoltaics: Status and Predictions. *Adv. Energy Mater.* **2016**, *6* (2), 1501208.

(10)   Solar Spectral Irradiance: Air Mass 1.5 http://rredc.nrel.gov/solar/spectra/am1.5/ (accessed Feb 1, 2016).

(11)   Scharber, M. C. On the Efficiency Limit of Conjugated Polymer:Fullerene-Based Bulk Heterojunction Solar Cells. *Adv. Mater.* **2016**, 28 (10), 1994-2001.

(12)   Facchetti, A. π-Conjugated Polymers for Organic Electronics and Photovoltaic Cell Applications †. *Chem. Mater.* **2011**, *23* (3), 733–758.

(13)   Tromholt, T.; Manceau, M.; Helgesen, M.; Carlé, J. E.; Krebs, F. C. Degradation of Semiconducting Polymers by Concentrated Sunlight. *Sol. Energy Mater. Sol. Cells* **2011**, *95* (5), 1308–1314.

(14)   Manceau, M.; Bundgaard, E.; Carlé, J. E.; Hagemann, O.; Helgesen, M.; Søndergaard, R.; Jørgensen, M.; Krebs, F. C. Photochemical Stability of π-Conjugated Polymers for Polymer Solar Cells: A Rule of Thumb. *J. Mater. Chem.* **2011**, *21* (12), 4132-4141.

(15)   Burrows, H. D.; Narwark, O.; Peetz, R.; Thorn-Csányi, E.; Monkman, A. P.; Hamblett, I.; Navaratnam, S. Mechanistic Studies on the Photodegradation of 2,5-Dialkyloxyl-Substituted Para-Phenylenevinylene Oligomers by Singlet Oxygen. *Photochem. Photobiol. Sci.* **2010**, *9* (7), 942–948.

(16)   Soon, Y. W.; Cho, H.; Low, J.; Bronstein, H.; McCulloch, I.; Durrant, J. R. Correlating Triplet Yield,

Singlet Oxygen Generation and Photochemical Stability in Polymer/fullerene Blend Films. *Chem. Commun. (Camb).* **2013**, *49* (13), 1291–1293.

(17)   Madsen, M. V; Tromholt, T.; Böttiger, A.; Andreasen, J. W.; Norrman, K.; Krebs, F. C. Influence of Processing and Intrinsic Polymer Parameters on Photochemical Stability of Polythiophene Thin Films. *Polym. Degrad. Stab.* **2012**, *97* (11), 2412–2417.

(18)   Derue, L.; Dautel, O.; Tournebize, A.; Drees, M.; Pan, H.; Berthumeyrie, S.; Pavageau, B.; Cloutet, E.; Chambon, S.; Hirsch, L.; Rivaton, A.; Hudhomme, P.; Facchetti, A.; Wantz, G. Thermal Stabilisation of Polymer-Fullerene Bulk Heterojunction Morphology for Efficient Photovoltaic Solar Cells. *Adv. Mater.* **2014**, n/a – n/a.

(19)   Wong, H. C.; Li, Z.; Tan, C. H.; Zhong, H.; Huang, Z.; Bronstein, H.; McCulloch, I.; Cabral, J. T.; Durrant, J. R. Morphological Stability and Performance of Polymer-Fullerene Solar Cells under Thermal Stress: The Impact of Photoinduced PC60BM Oligomerization. *ACS Nano* **2014**, *8* (2), 1297–1308.

(20)   Burkhart, B.; Khlyabich, P. P.; Thompson, B. C. Influence of the Ethylhexyl Side-Chain Content on the Open-Circuit Voltage in Rr-Poly(3-Hexylthiophene- Co -3-(2-Ethylhexyl)thiophene) Copolymers. *Macromolecules* **2012**, *45* (9), 3740–3748.

(21)   Khlyabich, P. P.; Burkhart, B.; Ng, C. F.; Thompson, B. C. Efficient Solar Cells from Semi-Random P3HT Analogues Incorporating Diketopyrrolopyrrole. *Macromolecules* **2011**, *44* (13), 5079–5084.

(22)   Burkhart, B.; Khlyabich, P. P.; Cakir Canak, T.; LaJoie, T. W.; Thompson, B. C. "Semi-Random" Multichromophoric Rr-P3HT Analogues for Solar Photon Harvesting. *Macromolecules* **2011**, *44* (6), 1242–1246.

(23)   Khlyabich, P. P.; Burkhart, B.; Rudenko, A. E.; Thompson, B. C. Optimization and Simplification of Polymer–fullerene Solar Cells through Polymer and Active Layer Design. *Polymer (Guildf).* **2013**, *54* (20), 5267–5298.

(24)   Greve, D. R.; Apperloo, J. J.; Janssen, R. A. J. Synthesis and and Characterisation of Novel Regioregular Polythiophenes – Tuning the Redox Properties. *European J. Org. Chem.* **2001**, *2001* (18), 3437–3443.

(25)   Dam, H. F.; Krebs, F. C. Simple Roll Coater with Variable Coating and Temperature Control for Printed Polymer Solar Cells. *Sol. Energy Mater. Sol. Cells* **2012**, *97*, 191–196.

(26)   Hösel, M.; Søndergaard, R. R.; Jørgensen, M.; Krebs, F. C. Fast Inline Roll-to-Roll Printing for Indium-Tin-Oxide-Free Polymer Solar Cells Using Automatic Registration. *Energy Technol.* **2013**, *1* (1), 102–107.

(27)   Andersen, T. R.; Dam, H. F.; Andreasen, B.; Hösel, M.; Madsen, M. V.; Gevorgyan, S. A.; Søndergaard, R. R.; Jørgensen, M.; Krebs, F. C. A Rational Method for Developing and Testing Stable Flexible Indium- and Vacuum-Free Multilayer Tandem Polymer Solar Cells Comprising up to Twelve Roll Processed Layers. *Sol. Energy Mater. Sol. Cells* **2014**, *120*, 735–743.

(28)   Rudenko, A. E.; Khlyabich, P. P.; Thompson, B. C. Random Poly(3-Hexylthiophene- Co -3-Cyanothiophene) Copolymers via Direct Arylation Polymerization (DArP) for Organic Solar Cells with High Open-Circuit Voltage. *ACS Macro Lett.* **2014**, *3* (4), 387–392.

(29)   Cao, H.; He, W.; Mao, Y.; Lin, X.; Ishikawa, K.; Dickerson, J. H.; Hess, W. P. Recent Progress in Degradation and Stabilization of Organic Solar Cells. *Journal of Power Sources*. Elsevier B.V 2014, pp 168–183.

(30)   Grossiord, N.; Kroon, J. M.; Andriessen, R.; Blom, P. W. M. Degradation Mechanisms in Organic Photovoltaic Devices. *Org. Electron.* **2012**, *13* (3), 432–456.

(31)   Giannouli, M.; Drakonakis, V. M.; Savva, A.; Eleftheriou, P.; Florides, G.; Choulis, S. a. Methods for

Improving the Lifetime Performance of Organic Photovoltaics with Low-Costing Encapsulation. *ChemPhysChem* **2015**, *16* (6), 1134–1154.

(32)   Angmo, D.; Gonzalez-Valls, I.; Veenstra, S.; Verhees, W.; Sapkota, S.; Schiefer, S.; Zimmermann, B.; Galagan, Y.; Sweelssen, J.; Lira-Cantu, M.; Andriessen, R.; Kroon, J. M.; Krebs, F. C. Low-Cost Upscaling Compatibility of Five Different ITO-Free Architectures for Polymer Solar Cells. *J. Appl. Polym. Sci.* **2013**, *130* (2), 944–954.

(33)   Gevorgyan, S. A.; Medford, A. J.; Bundgaard, E.; Sapkota, S. B.; Schleiermacher, H.-F.; Zimmermann, B.; Würfel, U.; Chafiq, A.; Lira-Cantu, M.; Swonke, T.; Wagner, M.; Brabec, C. J.; Haillant, O.; Voroshazi, E.; Aernouts, T.; Steim, R.; Hauch, J. A.; Elschner, A.; Pannone, M.; Xiao, M.; Langzettel, A.; Laird, D.; Lloyd, M. T.; Rath, T.; Maierm, E.; Trimmel, G.; Hermenau, M.; Menke, T.; Leo, K.; Rösch, R.; Seeland, M.; Hoppe, H.; Nagle, T. J.; Burke, K. B.; Fell, C. J.; Vak, D.; Singh, T. B.; Watkins, S. E.; Galagan, Y.; Manor, A.; Katz, E. A.; Kim, T.; Kim, K.; Sommeling, P. M.; Verhees, W. J. H.; Veenstra, S. C.; Riede, M.; Christoforo, M. G.; Currier, T.; Shrotriya, V.; Schwartz, G.; Krebs, F. C. An Inter-Laboratory Stability Study of Roll-to-Roll Coated Flexible Polymer Solar Modules. *Sol. Energy Mater. Sol. Cells* **2011**, *95* (5), 1398–1416.

(34)   Gevorgyan, S. a.; Madsen, M. V.; Dam, H. F.; Jørgensen, M.; Fell, C. J.; Anderson, K. F.; Duck, B. C.; Mescheloff, A.; Katz, E. a.; Elschner, A.; Roesch, R.; Hoppe, H.; Hermenau, M.; Riede, M.; Krebs, F. C. Interlaboratory Outdoor Stability Studies of Flexible Roll-to-Roll Coated Organic Photovoltaic Modules: Stability over 10,000h. *Sol. Energy Mater. Sol. Cells* **2013**, *116*, 187–196.

(35)   Bulle-Lieuwma, C. W. T.; Van Gennip, W. J. H.; Van Duren, J. K. J.; Jonkheijm, P.; Janssen, R. A. J.; Niemantsverdriet, J. W. Characterization of Polymer Solar Cells by TOF-SIMS Depth Profiling. In *Applied Surface Science*; 2003; Vol. 203-204, pp 547–550.

(36)   Kawano, K.; Pacios, R.; Poplavskyy, D.; Nelson, J.; Bradley, D. D. C. C.; Durrant, J. R. Degradation of Organic Solar Cells due to Air Exposure. *Sol. Energy Mater. Sol. Cells* **2006**, *90* (20), 3520–3530.

(37)   Nardes, a. M.; Kemerink, M.; de Kok, M. M.; Vinken, E.; Maturova, K.; Janssen, R. a J. Conductivity, Work Function, and Environmental Stability of PEDOT:PSS Thin Films Treated with Sorbitol. *Org. Electron. physics, Mater. Appl.* **2008**, *9* (5), 727–734.

(38)   Drakonakis, V. M.; Savva, A.; Kokonou, M.; Choulis, S. A. Investigating Electrodes Degradation in Organic Photovoltaics through Reverse Engineering under Accelerated Humidity Lifetime Conditions. *Sol. Energy Mater. Sol. Cells* **2014**, *130*, 544–550.

(39)   Lloyd, M. T.; Peters, C. H.; Garcia, A.; Kauvar, I. V.; Berry, J. J.; Reese, M. O.; McGehee, M. D.; Ginley, D. S.; Olson, D. C. Influence of the Hole-Transport Layer on the Initial Behavior and Lifetime of Inverted Organic Photovoltaics. *Sol. Energy Mater. Sol. Cells* **2011**, *95* (5), 1382–1388.

(40)   Voroshazi, E.; Verreet, B.; Buri, A.; Müller, R.; Di Nuzzo, D.; Heremans, P. Influence of Cathode Oxidation via the Hole Extraction Layer in Polymer:fullerene Solar Cells. *Org. Electron.* **2011**, *12* (5), 736–744.

(41)   Sapkota, S. B.; Fischer, M.; Zimmermann, B.; Würfel, U. Analysis of the Degradation Mechanism of ITO-Free Organic Solar Cells under UV Radiation. *Sol. Energy Mater. Sol. Cells* **2014**, *121*, 43–48.

(42)   Bovill, E.; Scarratt, N.; Griffin, J.; Yi, H.; Iraqi, A.; Buckley, A. R.; Kingsley, J. W.; Lidzey, D. G. The Role of the Hole-Extraction Layer in Determining the Operational Stability of a Polycarbazole:fullerene Bulk-Heterojunction Photovoltaic Device. *Appl. Phys. Lett.* **2015**, *106* (7), 073301.

(43)   Lloyd, M. T.; Olson, D. C.; Lu, P.; Fang, E.; Moore, D. L.; White, M. S.; Reese, M. O.; Ginley, D. S.; Hsu, J. W. P. Impact of Contact Evolution on the Shelf Life of Organic Solar Cells. *J. Mater. Chem.* **2009**, *19* (41), 7638-7642.

(44)   Krebs, F. C.; Gevorgyan, S. A.; Alstrup, J. A Roll-to-Roll Process to Flexible Polymer Solar Cells:

Model Studies, Manufacture and Operational Stability Studies. *J. Mater. Chem.* **2009**, *19* (30), 5442–5451.

(45) Hintz, H.; Egelhaaf, H.-J.; Lüer, L.; Hauch, J.; Peisert, H.; Chassé, T. Photodegradation of P3HT–A Systematic Study of Environmental Factors. *Chem. Mater.* **2011**, *23* (2), 145–154.

(46) Hermenau, M.; Riede, M.; Leo, K.; Gevorgyan, S. A.; Krebs, F. C.; Norrman, K. Water and Oxygen Induced Degradation of Small Molecule Organic Solar Cells. *Sol. Energy Mater. Sol. Cells* **2011**, *95* (5), 1268–1277.

(47) Norrman, K.; Krebs, F. C. Lifetimes of Organic Photovoltaics: Using TOF-SIMS and 18O2 Isotopic Labelling to Characterise Chemical Degradation Mechanisms. *Sol. Energy Mater. Sol. Cells* **2006**, *90* (2), 213–227.

(48) Reese, M. O.; Nardes, A. M.; Rupert, B. L.; Larsen, R. E.; Olson, D. C.; Lloyd, M. T.; Shaheen, S. E.; Ginley, D. S.; Rumbles, G.; Kopidakis, N. Photoinduced Degradation of Polymer and Polymer-Fullerene Active Layers: Experiment and Theory. *Adv. Funct. Mater.* **2010**, *20* (20), 3476–3483.

(49) Schafferhans, J.; Baumann, A.; Wagenpfahl, A.; Deibel, C.; Dyakonov, V. Oxygen Doping of P3HT:PCBM Blends: Influence on Trap States, Charge Carrier Mobility and Solar Cell Performance. *Org. Electron.* **2010**, *11* (10), 1693–1700.

(50) Rivaton, A.; Chambon, S.; Manceau, M.; Gardette, J.-L.; Lemaître, N.; Guillerez, S. Light-Induced Degradation of the Active Layer of Polymer-Based Solar Cells. *Polym. Degrad. Stab.* **2010**, *95* (3), 278–284.

(51) Zhao, J.; Swinnen, A.; Van Assche, G.; Manca, J.; Vanderzande, D.; Mele, B. Van. Phase Diagram of P3HT/PCBM Blends and Its Implication for the Stability of Morphology. *J. Phys. Chem. B* **2009**, *113* (6), 1587–1591.

Chapter 4 – Evaluation of low band-gap polymers for roll-to-roll organic photovoltaics
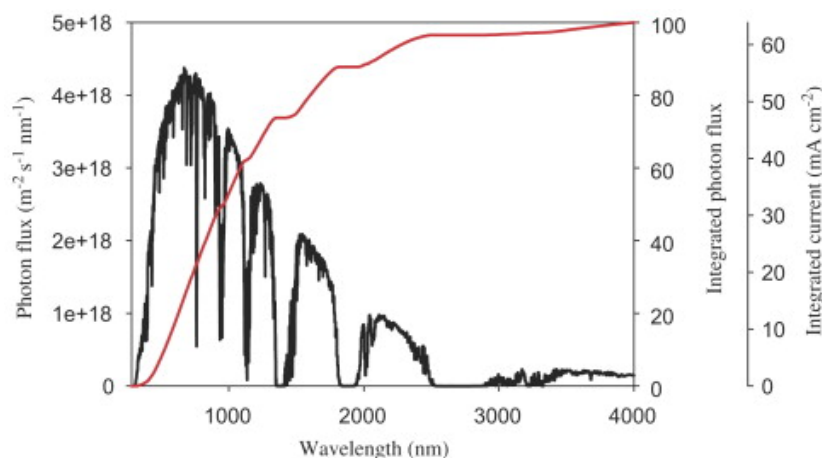
Fig 4.1 – Photon flux from the sun spectrum AM1.5G (black). Integral curve (red) of the total number of photons and theoretical obtainable current density. Reprinted with permission from 1.

The power conversion efficiency (PCE) is commonly used as a yardstick to gauge the advancement of the organic photovoltaics (OPV) technology. This race to increase the PCE has led to the synthesis of multiple absorbing materials and their use in OPV cells. The result is now that top reported efficiencies are above 10%.[2] Many of these high efficiency materials are low band gap polymers. Low band gap polymers are synthesized to absorb light at wavelengths above 600 nm.[1] This means that the band gap of the absorbing material is below 2 eV (which correspond to wavelength of 620 nm). Why do low band gap polymers yield higher efficiencies in OPV cells? When looking at AM1.5G spectrum described in chapter 3, most of the intensity is below 2000 nm even though it extends to 4000 nm (Fig 4.1). However, instead of plotting this spectrum in function of irradiance (Fig 4.1), it is more relevant to plot it in function of the photons flux (Fig 4.1). The current density of an OPV cell is directly linked to the number of absorbed photons.[3] Ideally one absorbed photon yields one electron. Integral of the photon flux and the theoretical current density ensuing from it are plotted in Fig 4.1. In reality, that current density is lowered by the fraction of charges

recombining before reaching the electrode.[3] The maximum of the AM1.5G for photons flux is towards the near infra-red. Therefore, to potentially harvest more photons, the absorbing material needed to absorb at higher wavelengths.[1] By extending absorption above 600 nm, low band gap polymers have a better overlap with the solar spectrum. For example, the common P3HT has a band gap of 1.9 eV (650nm) which means that at best only 22.4% of photons available can be collected.[1] But if the band gap is extended to 1000 nm then over 50 % of photons could be harvested (Fig 4.1).

The high efficiencies reported for low band gap polymers are misleading, because most OPV cells still have an active area < 1 mm^2 and are prepared with techniques (spin coating, evaporation…) and architectures (ITO, glass substrates…) not compatible with expected applications for OPV.[1,4] A common agreement is that in order to succeed OPV need to be produced by roll-to-roll (R2R) on flexible substrate using cheap materials. There is therefore a need to identify and develop high efficiency materials which are compatible with such R2R approach. This chapter reports on the screening of a large library of low band gap polymers.[5] The proceedings of the first publication reported below were inspired by common practices in the pharmaceutical industry. A library containing a large number of low band gap polymers was screened using simple techniques in order to identify the best candidates for further development. A weighted merit factor based on the measured properties allowed finding 13 potential candidates that outperformed P3HT for R2R application.

The second report focuses on the analysis of the same library of material from a mechanical point of view. Guidelines to develop mechanical compliant absorbing materials were given.

4.1. The SOLAR 100 project[*]

A common approach to synthesize low band gap polymers is to use two monomers: one electron donating unit and one electron accepting unit.[6] The following report presents the screening of an acceptor/donor library of low band gap polymer.[5] 8 donor units and 13 acceptor units were combined to yield a total of 104 polymers (Fig 4.2).

First, the following properties were measured for each polymer using simple and available techniques: molecular weight, electrochemical energy levels, band gap, photochemical

---

[*] This section is based on reference 5.

stability, and charges carrier mobility. Then, the photovoltaic properties were measured. The OPV cells were prepared by roll coating using a mini roll coater on an ITO-free flexible substrate (Flextrode).[7,8]
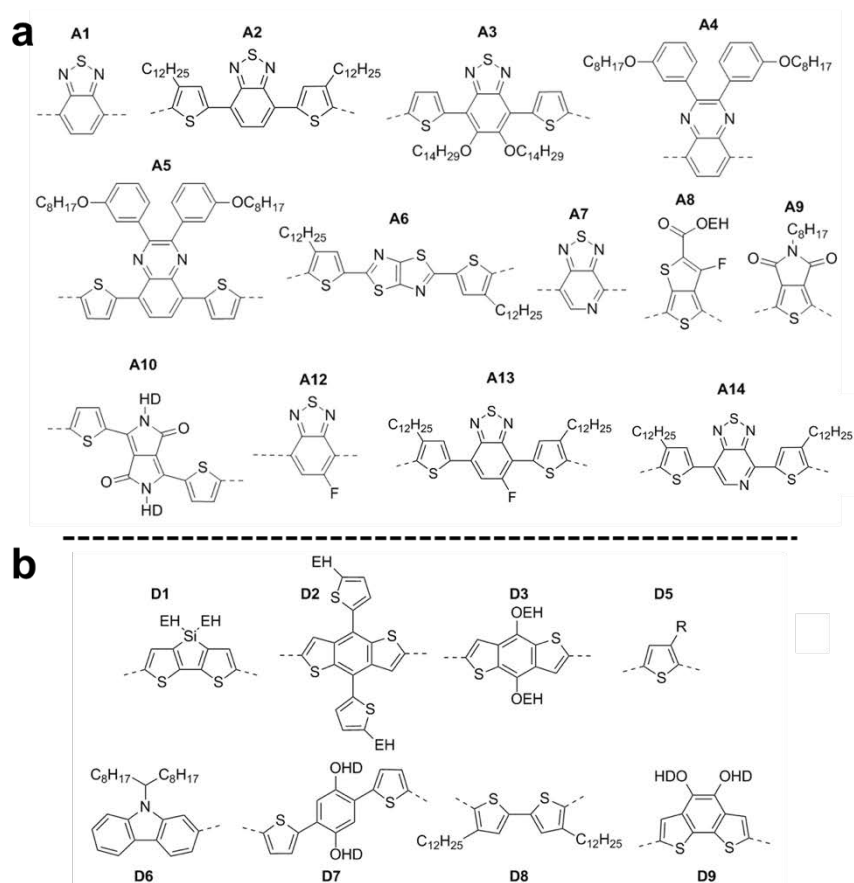
Fig 4.2 – Chemical structures of acceptor (a) and donor (b) units. The abbreviation EH stands for 2-ethylhexyl, and HD stands for 2-hexyldecyl. Extracted with permission from reference 9.

Then, using a weighted merit factor the best candidates for R2R upscaling were identified. The amount of work necessary for this project was enormous and required the equivalent of 26 month of manpower. The author of this thesis was part of a 15 person team. Therefore, only the results related to the author's contribution will be further highlighted. This includes the UV-vis measurement of polymers solutions and films, the photochemical stability of such films as well as the preparation and testing of OPV cells. The acceptor and donor units were chosen for their reported high efficiency. However, some of these units could not be purchased (A11) or synthesized in sufficient quantities (D4) and were dropped from the study

(Fig 4.3). The synthesis of some of the 104 polymers was not possible because of low reactivity or steric hindrance. For these reasons, there is no data for these polymers. The rest of the data can be found in [5].
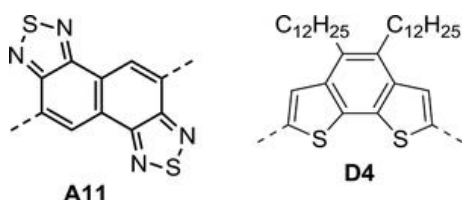
Fig 4.3 – Chemical structures of dropped units. Reproduced with permission.5

4.1.1. UV-vis

A Schimatzu UV-3600 Spectrophotometer was used to measure two spectra per polymer: one for the film and one for the solution. The polymers were dissolved in chlorobenzene (CB) (20 mg/L) and stirred overnight at 70 °C. A5D3, A9D8, A13D3 were difficult to dissolve in CB so they were instead dissolved in dichlorobenzene (ODCB) (10 mg/mL). The solutions were then spin coated as is on glass substrates (Fig 4.4). After spin coating the films, the solutions were diluted to 0.02 mg/mL. A6D5, A10D1, A10D2 and A10D3 were diluted at 0.01 mg/mL to keep the absorption below 1.

The band gap was then estimated from the onset of the UV-vis spectra. A tangent was fitted to the UV curve; the intersection gave the cut-off wavelength ($\lambda_{cut\text{-}off}$). The band gap (E_G) is given by the following equation.

$$(4.1) \quad E_G = \frac{hC}{\lambda_{cut-off}}$$

Where h is Planck's constant and C the speed of light.[10]
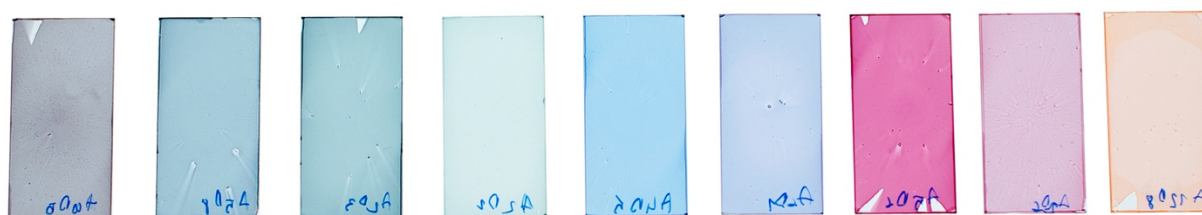
Fig 4.4 – Picture of some of the polymer films showing the wide range of colors obtained.

All the band gap values are plotted in Fig 4.5 for both the solutions and the films. For the films, the band gaps range from 2.09 to 1.27 eV. Only four polymers have a band gap above 2 eV for the films. This validates the acceptor/donor synthesis approach to make low band gap polymers. Acceptors 8 and 10 have the lowest band gaps for the polymers films.
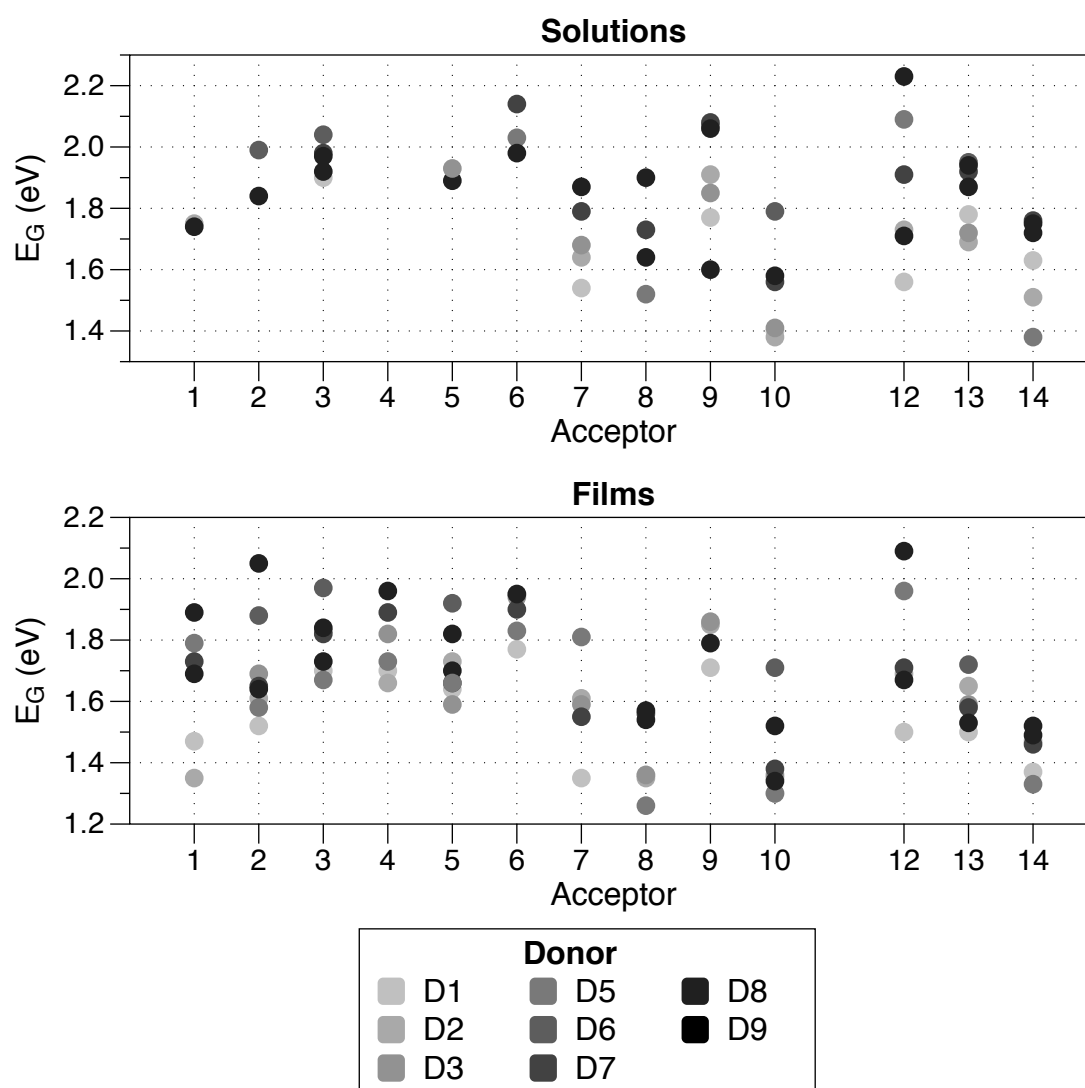
Fig 4.5 – Band gap values for the polymers solutions and films.

4.1.2. Photochemical stability

The photochemical stability of the polymer was measured on the same films used to obtain the UV-vis spectra. The stability measurements were performed using the setup described in chapter 3.[11] After acquisition, the data was normalized to the P3HT degradation rate to be

later integrated into the merit factor. The degradation rates are plotted in Fig 4.6. The lower the rate the higher is the stability of the polymer. P3HT has a degradation rate of 4%/h. In agreement with the literature, the photochemical stability is higher for the combinations of benzothiadiazole-like acceptor units (A1, A2, A5, A7, A12, A13 and A14) and the thiophene (D5, D8), the dithienosilole (D1) and the thiophene/benzene (D3, D7) donor units.[12]
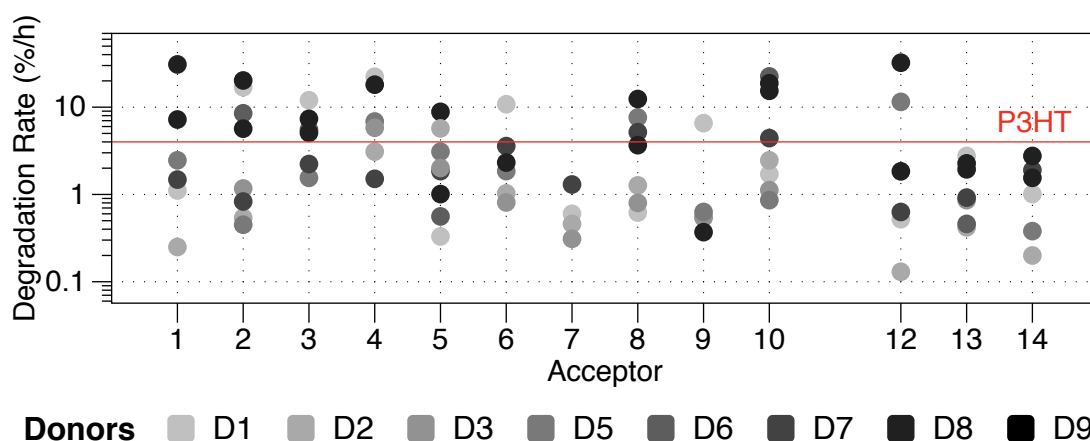
Fig 4.6 – Photochemical degradation rates averaged over multiple points of the film.

4.1.3. Roll coating and testing

The polymer and PCBM (40 mg/mL in total) were dissolved in chloroform (CF) or in o-dichlorobenzene (ODCB) and stirred at 50 ℃ overnight. The cells were prepared as reported earlier on a ITO-free flexible substrate (PET/Ag grid/PEDOT:PSS/ZnO).[7,8] To obtain the best possible cell, many parameters need to be optimized: solvent, polymer:PCBM ratio, coating speed and temperature, annealing. Because of the large number of polymers in this study it was impossible to explore all these parameters. The study was limited to the following variations:

- Two polymer:PCBM ratio 1.1 or 1.2 in weight.
- Two solvents: Chloroform (CF) or ortho-dichlorobenzene (ODCB)
- Three coated thickness: Wet thicknesses 10, 12 and 15 μm (estimated dry thicknesses 315, 400, and 475 nm).

These conditions add up to 12 different cell types for each polymer. Even with these different conditions, multiple polymers failed to generate working devices because of the dewetting of the active layer on top of the Flextrode or of the top PEDOT:PSS layer on the active layer,

poor dissolution in the selected solvents or burned devices during switching.[13] Switching is a post-processing step, were a short electrical pulse is applied to the cell to render it functional. The OPV cells were characterized under a solar simulator (1000 W/m^2 and AM1.5G) using a Keithley (2400 SMU) and a mask (0.526 cm^2). For each polymer, a minimum of 5 cells were measured. The average data is given in table 4.1.

Table 4.1 – Average PCE values of the 10 best devices for each polymer. NA indicates that no data could be acquired.

		Donors							
		D1	D2	D3	D5	D6	D7	D8	D9
Acceptors	A1	1.3	0.37	NA	0.02	NA	2.0	NA	0.03
	A2	0.44	1.02	0.5	0.07	NA	1.24	NA	NA
	A3	0.21	NA	0.55	0.49	0.19	0.35	0.22	0.23
	A4	0.05	0.17	0.03	0.49	NA	NA	NA	NA
	A5	0.29	1.37	1.09	0.18	0.1	0.57	0.06	NA
	A6	1.03	0.85	0.61	NA	NA	0.3	NA	0.71
	A7	0.02	NA	NA	NA	NA	0.03	NA	NA
	A8	0.2	0.57	0.12	0.04	NA	0.04	NA	0.01
	A9	0.23	0.67	0.47	NA	NA	NA	NA	NA
	A10	NA	0.04	NA	NA	NA	NA	NA	NA
	A12	1.22	0.16	NA	NA	NA	0.85	0.01	0.25
	A13	0.53	NA	NA	NA	0.01	NA	NA	NA
	A14	0.21	0.35	NA	0.02	NA	0.19	0.02	0.06

4.1.4. Overview

The difficulty to obtain working roll coated cells shows that when developing high efficiency polymers for OPV it is important to take into account all the parameters and not only the PCE. For this reason, we implemented a merit factor (χ) to compare the polymers to P3HT for R2R suitability (Equation 4.2).

$$(4.2) \quad \chi = \frac{PCE \times Stability \times V_{OC} \times band\ gap}{number\ synthetic\ steps}$$

The merit factor encompasses the efficiency (PCE), the photochemical degradation rate of the polymer normalized to P3HT degradation rate (Stability), the open circuit voltage (V_{OC}), the band gap in nm and the number of synthetic steps. These factors have been selected because high PCE, V_{OC} and stability values are wanted. The band gap correlates with how much of the solar spectrum can be harvested as well as the theoretical maximum current

density. V_{OC} is already included in the PCE but a high V_{OC} is important for successful R2R upscaling and is given a higher weight in the merit factor. The synthesis steps should be low to reduce the cost. A merit factor relative (χ_{rel}) to P3HT was calculated for simpler comparison (Equation 4.3).

$$(4.3) \quad \chi_{rel} = \frac{\chi}{\chi_{P3HT:PCBM}}$$

The relative merit factors are given in Table 4.2. Out of the 104 polymer the study began with only 13 polymers have a (χ_{rel}) better than P3HT and warrant further development (Fig 4.7). The low success rate (12.5%) illustrates the difficulty to find suitable high efficiency materials for R2R manufacturing of OPV.

Table 4.2 – Relative merit factor for each polymer. NA indicates failure.

		D1	D2	D3	D5	D6	D7	D8	D9
					Donors				
	A1	1.4	0.3	NA	NA	NA	2.7	NA	0.03
	A2	NA	13.1	0.6	1	NA	1.2	NA	NA
	A3	NA	NA	0.2	NA	NA	0.1	NA	NA
	A4	NA	NA	NA	1	NA	NA	NA	NA
	A5	NA	2.9	0.4	0.2	NA	0.7	NA	NA
Acceptors	A6	0.2	0.8	0.5	NA	NA	0.1	NA	0.4
	A7	0.1	NA	NA	NA	NA	0.1	NA	NA
	A8	0.1	0.5	0.2	NA	NA	NA	NA	NA
	A9	NA	1.9	0.9	NA	NA	NA	NA	NA
	A10	NA	NA	NA	NA	NA	NA	NA	NA
	A12	1.8	2.6	NA	NA	NA	2.7	NA	NA
	A13	0.2	NA	NA	NA	NA	NA	NA	NA
	A14	0.3	1.6	NA	0.1	NA	0.1	NA	NA

The polymers can fail at any steps from material selection to cells characterization:

1) Material design
2) Material synthesis
3) Material characterization
4) Ink formulation

28 Polymers

5) Ink coating

20 Polymers

6) Working device

46 Polymers

7) Low PCE

8 Polymers

8) Higher PCE than P3HT

1 Polymer
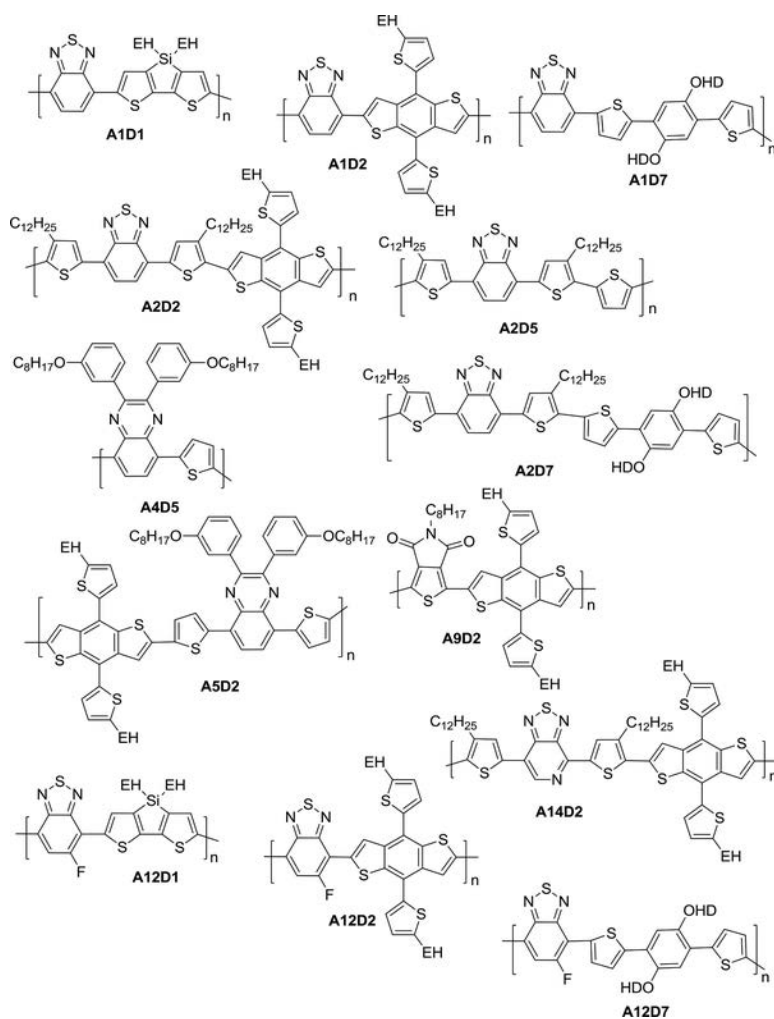
Fig 4.7 – 13 polymers with a relative merit factor above 1. Reprinted with permission from 5.

Many of the issues could be fixed by using different solvents, substrates, architectures… However, to improve the chance of success, a linear approach similar to this one is encouraged to identify the best candidates for further development and optimization.

4.1.5. Conclusion

The results of this study show the extreme difficulty to identify and foster high efficiency materials for "real life" OPV devices. Still 13 low band gap polymers were identified as suitable for further development for R2R manufacturing of OPV cells. However, an important parameter was left out of this study: Stability of the cells under operation. As demonstrated in the previous chapter, stability of the performances depends not only on the material but also

on the cell architecture and encapsulation. Therefore, relevant studies cannot be conducted as long as the coating and architecture parameters have not been optimized. The next section will look into the thermomechanical stability of this library of low band gap polymers.

4.2. Mechanical stability of solar cells[†]

If the path of all R2R manufactured OPV on flexible substrate is to be followed, thermomechanical stability cannot be neglected. The solar cells need to handle the mechanical and thermal stresses endured during both manufacturing and operation outdoor. R2R coating and printing means bending, stretching and many other types of thermomechanical deformations.[14] Furthermore, superior mechanical performances combined with high efficiencies would allow the integration of OPV in many applications (clothing, portable electronics, biomedical applications…) unsuitable for conventional PV.[14]

Despite the potentially attractive mechanical properties of OPV, studies of these properties have been limited. One reason is that most OPV cells are still prepared on glass.[4] Therefore, thermomechanical behavior does not limit the lifetime of such devices. So far most studies on mechanical properties of OPV focus on the poly(3-alkylthiophenes) (P3ATs) family.[14,15] P3ATs and especially P3HT have been a good system to study and to model but their maximum efficiency is limited.[16] State of the art high efficiency OPV cells use low band-gap D/A polymer. The Solar 100 study provided the opportunity to study a large number of D/A low band gap polymers at once.[5] From this study we know that the reported efficiencies above 10% for laboratory scale cells on ITO coated glass substrates do not transfer easily to roll coated devices.[17] Moreover, a rigid substrate like glass hides the mechanical properties of the D/A polymers and polymer:fullerene blends which are potentially determining for the mechanical stability of flexible devices.[14]

For this reason, the mechanical data available for D/A polymers is scarce. Still a few studies have shown how the chemical structure of D/A polymers influences their mechanical properties.[18–21] A study of two structurally similar D/A polymers (PDPP-2TTT: repeating units: diketopyrrolopyrrole (DPP), thiophene (T) and thienothiophene (TT), and PDPP-4T: the fused TT unit was replaced with bithiophene, which comprises two isolated thiophene rings),

---

[†] Section based on reference 9.

showed that the polymer with the fused ring has a higher tensile modulus.[18] The tensile modulus of a material describes its stiffness or how much force is needed to deform it. A low tensile modulus is considered best for mechanical stability. A material that requires a low energy density to deform in the elastic regime will accommodate better the interfacial stresses in the final device.
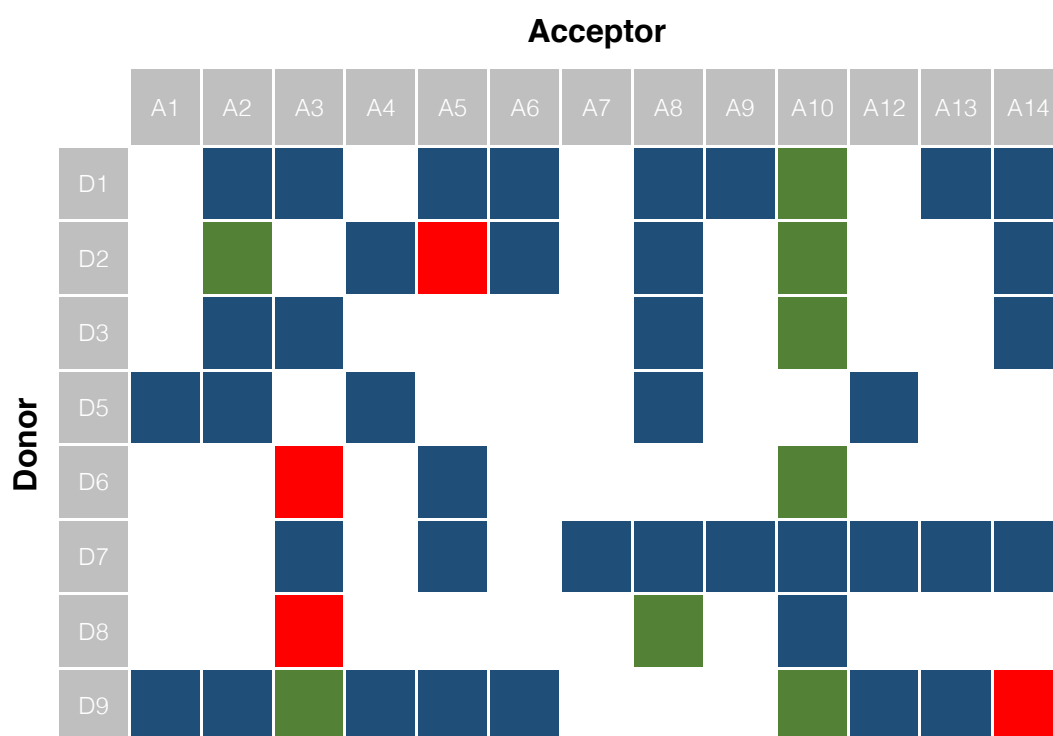
Fig 4.8 – Combinations of D/A polymers measured during this study: Tensile modulus (red), Crack-Onset (green) or both (blue).

Another study showed that the random incorporation of bithiophene units into the structure of PDPP-2FT (where F = furan) led to a decreased of the tensile modulus from 2.17 ± 0.35 GPa to 0.93 ± 0.16 GPa.[19] A study by Wu *et al*. suggested as well that the brittleness of polymers is higher when they have rigid fused rings in their backbone.[20] Organic thin film transistors prepared with a DPP-based polymer with four fused thiophene rings showed significant cracking at low crack-onset strains (the strain when the film start cracking). Finally, Kim *et al.* studied a D/A polymers with the same structure as A9D2, called PBDTTTPD (not available for this study).[21] This study focused mainly on the impact of the acceptor material in the BHJ on the mechanical properties. The tensile modulus of the composite of PBDTTTPD

and a non-fullerene electron acceptor (1:1 ratio) is much lower (0.43 GPa) than when PBDTTTPD is combined with PCBM (1.76 GPa for a 1:1.5 ratio).[21]

Using the large library of compounds synthesized for the Solar 100 study (Fig 4.2), we aimed at acquiring a deeper understanding of how structural components determine the mechanical properties of D/A polymers. Fig 4.8 shows the 51 D/A polymers available for this study. The stiffness (tensile modulus) or ductility (crack onset) or both were measured using previously reported methods.[22–24] The driving idea behind the study was to draw up rules of molecular design to develop polymers for R2R application that combine high efficiency and mechanical robustness. The initial hypothesis was that the mechanical properties would be affected by two main features of the chemical structures:

     (1) fused vs. isolated rings and

     (2) branched vs. linear side chains

The units with fused rings are the following: A6, A10, D1, D2, D3, D6, and D9. Only the structures with fused rings aligned along the backbone like in diketopyrrolopyrrole (DPP) (A10) were classified as "with fused rings". Units like benzothiadiazole (BT) (A1) where the fused rings are not in the direction of the backbone were not classified as structures with fused rings. The solubilizing side chains were classified from short alkyl side chains with eight carbons (C_8H_{17}) to long alkyl side chains with fourteen carbons ($C_{14}H_{29}$) or as branching side chains of 2-ethylhexyl (EH) and 2-hexyldecyl (HD). Last, the impact of the molecular weight and the dispersity on the mechanical properties of the polymers were studied as well.

4.2.1. Limitations of the study

The large number of polymers tested during this study was expected to give meaningful trends for molecular design of low band gap polymers. However, some limitations were identified. For one, the mechanical properties do not only depend on the molecular structure but also on the solid state microstructure. The microstructure of the dried film is dependent of the solvent, the film-casting method, the drying, and the *post*-processing steps.[25,26] Optimizing all these steps and measuring the microstructure was not possible because of the large library of compounds. Another limitation was that for for step-growth polymerizations controlling the molecular weight and the dispersity (*Đ*) is difficult. Even though, the stiffness of

D/A polymers might prevent a highly entangled microstructure, even at high molecular weights.[27] Lastly, the mechanical properties of a bulk heterojunction are also dependent of the acceptor material.[14] For example, the tensile moduli of polythiophene:[60]PCBM blends was found to be linearly correlated to the tensile moduli of the pure polymers.[28] However, this behavior cannot be assumed to be true for all polymers. It cannot also be presumed that methanofullerenes will be used in the future. For this reason, the properties of the pure polymers were measured.

4.2.2. Mechanical studies

Tensile moduli

The tensile moduli of the D/A polymers were measured with a film-on-elastomer technique called the "buckling instability" developed by Stafford *et al.*.[22] Later, Tahk *et al*. applied this technique to conjugated polymers.[23] The buckling instability has since then been used in many occasion for such materials.[14,18,29,30] Briefly, Polydimethylsiloxane (PDMS) substrates were made following the manufacturer instructions with a ratio of 10:1 (base:crosslinker) and then left curing in ambient condition for 48-72 h. A razor blade was used to cut PDMS strips (1 cm × 8 cm × 0.3 cm). Using a computer-controlled stage (Newmark model ET-100-11) the PDMS strips were stretched to strains of 4% and clipped onto a glass substrate with binder clips. For the film deposition, glass substrates (2.5 cm x 2.5 cm) were cleaned by sonication in four baths (Alconox solution, deionized water, acetone, and isopropanol), then dried with compressed air and plasma-treated (3 min, 30 W, 200 mtorr ambient air). Polymer solutions were prepared by dissolving in chloroform at a 20 mg mL^{-1} concentration. The solutions were then stirred on a hotplate at 50 $^{\circ}$C with a magnetic stirrer for 2 h. Before spin-coating the solutions were cooled down to ambient temperature and filtered through a 1 μm glass microfiber filter. For each polymer, three different thicknesses were prepared by spin coating the solution on top of the plasma treated glass substrates at 500, 1000, and 2000 rpm for 2.5 min. The transfer of the polymer film onto the PDMS strip was operated as follow: the spin coated polymer film was pressed onto the pre-stretched PDMS strip. Then the sample was dipped into a deionized (DI) water bath for a time ranging from 30 s up to 20 min depending of the polymer. Using tweezers, the sample was removed from the water bath and then the glass substrate bearing the polymer was stripped of the PDMS leaving the

polymer layer on top of the PDMS. To remove the water, the sample was put in a desiccator to dry under dynamic vacuum for 30 min. The final step was to release the prestrained PDMS to form buckles and to observe the buckles with an optical microscope. Optical micrographs of the buckled films were acquired and analyzed using an in-house MATLAB code. The tensile modulus of each batch of PDMS was measured using a conventional pull-tester. The thickness of each polymer film was measured using a Veeco Dektak stylus profilometer. The tensile modulus of the polymers (E_f) was calculated using equation (4.4). First, the buckling wavelength λb was plotted as a function of the film thickness df. The slope λb/df obtained by linear fit was then substituted in Equation (4.4) where Es is the PDMS substrate modulus, the Poisson ratios of the film (vf) and the PDMS substrate (vs) were assumed to be 0.35 and 0.5 respectively.[23]

$$(4.4) \quad E_f = 3E_s \left(\frac{1 - v_f^2}{1 - v_s^2} \right) \left(\frac{\lambda_b}{2\pi d_f} \right)^3$$

For mechanical stability, a low tensile modulus is considered better. A low modulus means that the polymer film needs a low energy density to elongate in the elastic regime. Therefore, the interfacial stresses in the solar cell will be minimized and prevent delamination.[14,31] The calculated tensile moduli are collected in Table 4.3. The standard deviation values are based on the propagation of standard errors of the line fits (buckling wavelength vs. film thickness) and on the standard deviation of the tensile moduli of the PDMS substrates. There are two reasons for polymers to be marked as not applicable (NA) in Table 4.3 either the samples had standard errors of the line fit too high (R^2 < 0.95) or the characteristic buckling wavelengths could not be obtained. These failures mostly come from the difficulty to handle some of the polymer films:

- Strong adhesion of the polymer film to the glass substrate would lead to partial transfer of the film onto the PDMS substrate or to damages to the films.
- Delamination or crackling of the films due to either the strain induced by handling the transferred film on PDMS or the compressive strain induced to generate buckles or both.[32]

Table 4.3 – Overview of the tensile moduli and crack-onset strain data obtained by film-on-elastomer techniques for all the D/A polymers. Averaged molecular weights and the dispersity are extracted the Solar 100 study.[5]

Polymer	Mn (Da)	Đ	Tensile Modulus (GPa)	Crack-onset Strain (%)	Crack Behavior
A1D5	9 300	2.2	0.24 ± 0.08	7.3 ± 2	Ductile
A1D9	6 900	1.4	0.44 ± 0.18	0 [†]	Brittle
A2D1	9 500	2.0	3.79 ± 0.80	0.5 [‡]	Brittle
A2D2	12 400	11.4	NA*	0 [†]	Brittle
A2D3	90 000	4.5	1.45 ± 0.47	1 [‡]	Brittle
A2D5	540 000	4.2	0.32 ± 0.02	1.5 [‡]	Brittle
A2D9	9 400	1.8	0.33 ± 0.12	2.7 ± 1.5	Brittle
A3D1	50 000	10.8	1.23 ± 0.52	18 ± 5	Ductile
A3D3	16 000	3.5	2.91 ± 1.30	2.75 [‡]	Brittle
A3D6	3 800	3.1	0.17 ± 0.02	NA*	NA
A3D7	24 000	2.7	0.32 ± 0.03	68 ± 14	Ductile
A3D8	2 200	3.1	0.68 ± 0.14	NA*	NA
A3D9	19 000	2.1	NA*	5.2 ± 2	Ductile
A4D2	22 000	9.1	1.35 ± 0.76	5.0 ± 1.3	Brittle
A4D5	29 000	9.2	0.92 ± 0.19	2.7 ± 0.6	Brittle
A4D9	7 000	1.5	0.34 ± 0.18	19.7 ± 1.5	Ductile
A5D1	18 000	3.0	0.87 ± 0.11	3.5 ± 0.5	Brittle
A5D2	100 700	3.1	0.75 ± 0.23	NA*	NA
A5D6	11 000	26.7	1.24 ± 0.29	4.2 ± 1.3	Brittle
A5D7	34 000	3.4	0.15 ± 0.04	56.8 ± 9.9	Ductile
A5D9	138 000	8.0	0.44 ± 0.15	10 ± 3.6	Ductile
A6D1	9 600	2.0	0.27 ± 0.02	6.5 ± 2.0	Brittle
A6D2	11 000	2.2	1.61 ± 0.51	0 [†]	Brittle
A6D9	21 600	2.7	0.17 ± 0.05	2.2 ± 0.8	Brittle
A7D7	1 200	3.3	0.49 ± 0.18	0 [†]	Brittle
A8D1	16 000	2.0	3.00 ± 0.56	7.8 ± 0.8	Brittle
A8D2	14 000	2.4	0.88 ± 0.40	10 ± 2	Ductile
A8D3	14 000	2.2	1.58 ± 0.64	2.2 ± 0.8	Brittle
A8D5	5 000	1.4	0.85 ± 0.21	0 [†]	Brittle
A8D7	6 100	2.6	0.37 ± 0.10	7.8 ± 1.6	Ductile
A8D8	3 700	2.2	NA*	2.5 ± 1.5	Brittle
A9D1	9 500	2.8	0.62 ± 0.20	1.2 ± 0.6	Brittle
A9D7	7 200	1.7	0.45 ± 0.17	NA*	NA
A10D1	21 000	2.5	NA*	2.2 ± 0.8	Brittle
A10D2	103 000	3.3	NA*	1.8 ± 0.6	Brittle
A10D3	68 000	3.3	NA*	4 ± 1	Brittle
A10D6	6 700	3.5	NA*	4.3 ± 1.3	Brittle
A10D7	34 000	4.2	0.32 ± 0.06	9.3 ± 1.5	Ductile
A10D8	1 200	2.8	0.41 ± 0.22	6.7 ± 0.8	Ductile
A10D9	2 300	5.4	NA*	3 ± 1.7	Brittle
A12D5	13 000	3.1	0.56 ± 0.25	5.2 ± 2.4	Brittle
A12D7	5 600	2.1	0.54 ± 0.24	2.2 ± 0.8	Brittle
A12D9	37 000	2.3	0.32 ± 0.05	0.8 ± 0.6	Brittle
A13D1	12 000	7.5	0.54 ± 0.25	3.8 ± 2.4	Brittle
A13D7	10 000	2.1	0.60 ± 0.16	4.8 ± 0.3	Brittle
A13D9	12 000	76.7	0.48 ± 0.13	0 [†]	Brittle
A14D1	9 800	1.7	0.43 ± 0.26	3.3 ± 0.8	Brittle
A14D2	4 600	4.1	0.26 ± 0.05	1.75 [‡]	Brittle
A14D3	-	-	0.42 ± 0.14	2.2 ± 1.0	Brittle
A14D7	19 000	2.6	0.55 ± 0.09	13.7 ± 1.5	Ductile

| A14D9 | 1 600 | 1.9 | 0.25 ± 0.12 | NA* | NA |

NA: not applicable. *No data available for these polymers: (1) insufficient material available, (2) failure to obtain smooth films, or (3) too large of propagated error. †The polymer samples cracked upon the start of the test under the strain of less than the minimum step of 0.5% strain. ‡The polymer samples exhibited inconsistent cracking behaviors and the values of the crack-onset strains reported are the lowest measured crack-onset strains.

The tensile modulus of the polymer films ranged from 200 MPa to 4 GPa (Table 4.3), which is in the same range as previous reports of other D/A conjugated polymers moduli measured with the same method of measurement.[14] A2D1 had the highest measured modulus (3.79 ± 0.80 GPa). The hypothesis that fused rings increase the modulus seems to be correlated by the qualitative trend observed. Polymers with donor units including fused rings have a relatively high stiffness (larger values of tensile moduli). The polymers with D1, D2 and D3 units had an average tensile modulus of about 1 GPa. However, polymers with D5, D7 and D8 units (which have isolated rings) had a lower averaged modulus (around 500 MPa). The results were not fully conclusive because polymers including D6 and D9 (also with fused rings) had a much lower averaged modulus (~ 400 MPa). The lower stiffness of these polymers was attributed to the side-chains. Both D6 and D9 have long and branched side chains. This correlate with the second hypothesis that the solubilizing side-chains have an effect on the modulus.[24] In the case of P3ATs, an increase of the alkyl side-chains' length from 4 (P3BT) to 8 (P3OT) resulted in a decrease of the tensile modulus by a factor of ten. The lowering of the tensile modulus was attributed to the decrease in glass transition temperature with longer side chains as well as the reduction of the volume fraction of the load-bearing main chain.[24] Long and branching side-chains have also been reported to affect the microstructure of polymers such as increasing the separation between main chains.[25] The reduction of the tensile modulus for polymers with D6 and D9 could be linked to the reduction of the intermolecular packing of the polymer chains.

Crack-Onset

In the case of polythiophenes, low tensile modulus is also strongly correlated to high crack-onset strain. P3ATs films with higher moduli tend to crack at lower applied strains.[24,30] To test if such dependency of ductility on molecular structure exist for the low band gap polymers

library, their crack-onset strains were measured. The polymer films were transferred onto unstrained PDMS strips. The samples were then stretched using a computer-controlled linear actuator with a step size of 0.5% strain. Each step was imaged using an optical microscope. The level of strain at which the first crack was observed, was recorded as crack-onset strain. The qualitative nature of the cracks was also recorded: brittle cracks (which propagated the entire length of the film perpendicular to the stretched axis) or ductile cracks (whose propagation was limited). Examples of both types of propagation are shown in Figure 4.9. Both brittle and ductile fractures are detrimental to the films mechanical stability and possibly to the performance of the full OPV device. However, ductile cracks would have a lower tendency to propagate and to cause failure such as short circuits in solar cells.
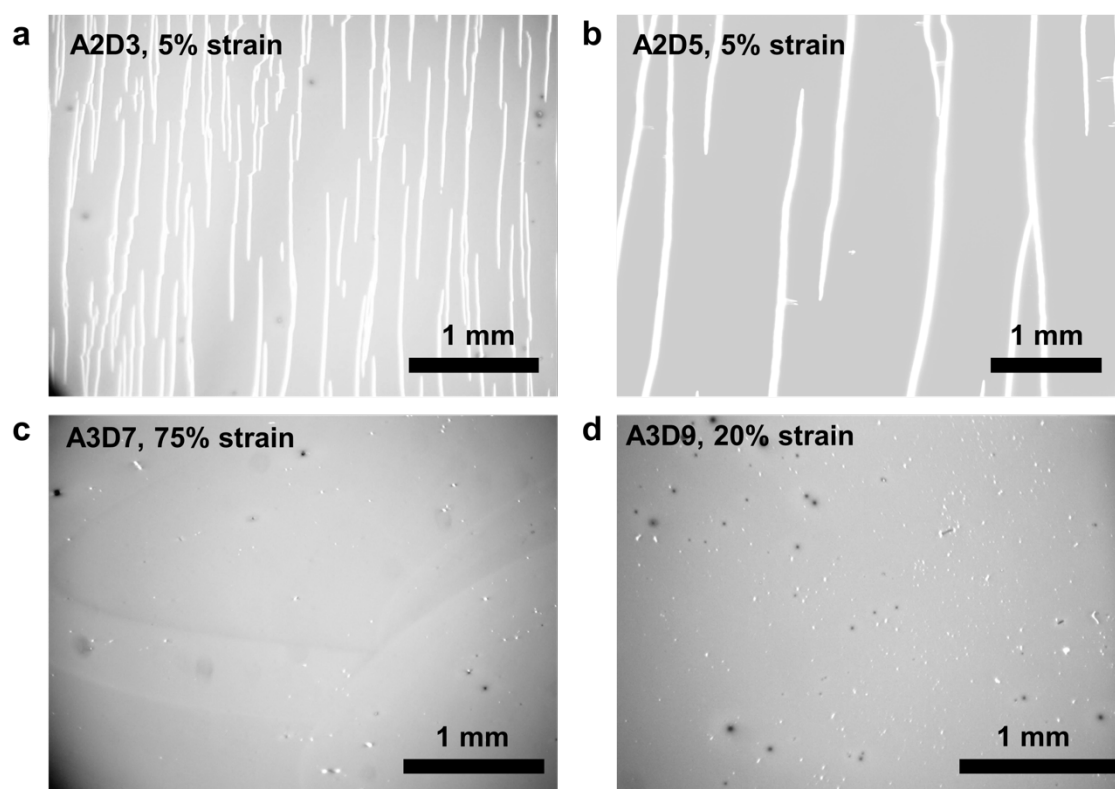
Fig 4.9 - Optical micrographs of the two different natures of cracking behavior: brittle fracture perpendicular to the starching direction (a, b) and ductile fracture as pinholes (c, d). Extracted with permission from reference 9.

The average crack-onset strains values are reported in Table 4.3 with their standard deviations from measurements of 3 or more samples. Even though the strain applied during preparation of the samples was minimized, some finite tensile strains were induced during the

preparation steps (estimated to be lower than 0.5%). Six polymers cracked during sample preparation and their crack-onset strains were reported as 0% (Table 4.3). The majority of D/A polymers has low crack-onset strains and presented cracking at tensile strains lower than 5% (Table 4.3). The films with a crack-onset below 5% exhibited brittle cracks. A few D/A polymers were found to have higher crack-onset strains (Table 4.3). They are combinations of the monomer units A3, A8, D1, D5, D7, and D9. One explanation for the higher crack-onset strains of these polymers could be the ductile nature of the fractures in these films. In these films, "ductile" cracks appeared as pinholes and showed less tendency to propagate with increased in strain.

Fig 4.10 - Plot of crack-onset strains vs. tensile moduli of the polymers tested in this study. Data points are distinguished in color by the nature of the fracture: red (brittle) and blue (ductile). Extracted with permission from reference 9.

Previous studies on conjugated polymers, especially on P3ATs have shown that there is a correlation between the tensile modulus and the ductility of the polymer films.[24,30] Low ductility was linked to high tensile modulus. However, the same correlation was not found during his study of D/A polymers. The crack-onset was plotted as a function of tensile modulus (Fig 4.10) for the 39 polymers which were measured for both. It is true that polymers with a high crack-onset strain, all have a relatively low tensile modulus (≤1 GPa) and exhibited

a ductile crack behavior (Fig 4.10 blue). However among the "brittle" polymers (Fig 4.10 red) many presented a low stiffness.

Out of the 47 D/A polymers tested for crack-onset, only 16 of them resisted to 5% strain or above before cracking. The brittleness of the D/A polymers correlates with previous reports on D/A polymers.[20,21] Using the pseudo free-standing tensile test, Kim *et al.* measured the mechanical properties of composites of PBDTTTPD (A9D2) and PCBM or P(NDI2HD-T), a non-PCBM electron acceptor.[21] The composite with PCBM cracked below 0.30% strain and the composite with P(NDI2HD-T) cracked around 7% strain.[21] In another study, Wu et al. compared P3HT and PTDPPTFT4 (a DPP-based polymer with four fused thiophene rings in the backbone).[20] The D/A polymer film could only withstand tensile strains below 5% compared to over 100% for P3HT.

4.2.3. Design rules for mechanical deformability

The purpose of this study was to identify the molecular structural determinants that influence the mechanical properties of D/A polymers so one could optimize the mechanical and electrical performance, and scalability for OPV R2R manufacturing. The general trends followed the hypotheses on the influence of side-chains length and of fused rings. However, several exceptions were also found. The origins of these exceptions could be multiple: the differences in molecular weight and dispersity, or possibly effects of certain combinations of donor and acceptor monomers which are difficult to predict. As stated before, both the molecular structure and the solid-state microstructure needed to be understood to predict trends in mechanical properties.[14] Some combinations of acceptor and donor monomers could lead to drastically different solid-state packing structure which have been shown to to impact the mechanical properties.[19,29]

Fused rings

Polymers with fused rings in the backbone structures (units D1, D2, and D3) had average tensile moduli of about 1 GPa (Table 4.3). The hypothesis is that the fused rings reduce the flexibility and increase the length of conjugation of the backbone. The polymers with donor units with isolated rings D5, D7, and D8, had respectively an averaged tensile modulus of 0.58, 0.42, and 0.55 GPa, which correlates with the hypothesis. However, there were

exceptions to this trend. Especially for the polymers with the donor unit D9 (fused ring in the backbone), which had tensile moduli around 0.5 GPa. The lower tensile moduli for D9 are attributed to the long and branching solubilizing side chains (2-hexyldecyl), this will be discussed in depth in the next section. As for the acceptor units with fused rings (A6 and A10), the effect on the tensile modulus was small (Table 4.3). For example, A6D1 that contained fused ring structures in both the donor and acceptor monomers has a tensile modulus of only 0.27 ± 0.02 GPa.

For ductility no obvious trend could be found regarding fused rings. Polymers with D3 had low crack-onset values (<5% crack-onset strain) and were brittle, which is consistent with the hypothesis that fused rings in the backbone produced brittle polymer films. But for the donor units D1 and D2 which also have fused rings, some polymer combinations yielded ductile films. Namely A3D1 and A8D2 had a ductile behavior and crack-onset strains above 10%. Once again, this deviation in the trend is believed to issue from the side chains on the acceptors and will be discussed in the next section. For the acceptor unit DPP (A10) with fused rings, the polymer combinations with donor units with fused rings (D1, D2, D3, D6, and D9) yielded brittle films with low crack-onset strain. However, the polymers combining A10 and the non-fused donor monomers (D7 and D8) produced ductile films with higher crack-onset strains. The higher ductility was attributed to a possible change in solid-state morphologies and packing when the DPP (A10) acceptors were combined with dialkoxybenzene (D7) and bithiophene (D8).

 Influence of long and branching solubilizing side-chains.

From the previous section, it is clear that long and branching solubilizing side-chains can dominate the mechanical properties of a polymer film. For example, the polymers with donor units D6, D7 and D9, which have branching side-chains, had a lower tensile modulus than for donor monomers with linear side chains. The same goes for monomers with either 2-hexyldecyl or 2-ethylhexyl side-chains. 14 polymers out of the 16 with a crack-onset strain above 5% have either HD or EH side-chains. For example, three of the polymers with high crack-onset strains values are combination with D7 (HD side-chains with ether linkages): A3D7 (crack-onset strain of 68%), A5D7 (57%), and A14D7 (14%).

Acceptors A2 and A3, have similar structures: benzothiadiazole with two flanking thiophenes. All polymers with A3, Except A3D3, have a lower tensile modulus and a higher crack-onset strain than polymers with A2 (Table 4.3). The difference in mechanical behavior was attributed to the locations of the alkyl side chains. For the A2 monomer, the alkyl side chains ($C_{12}H_{25}$) are on the two flanking thiophenes. But for the acceptor A3, the alkyl side chains ($C_{14}H_{29}$) are connected onto the benzothiadiazole with ether linkages.

The effect of side-chains structures on the mechanical properties could be explained by the solid-state molecular packing.[33] Some previous reports suggested that introducing branched side-chains reduces the packing efficiency and lowers the crystallinity which could increase the deformability of the polymer.[34,35] A report by Yiu *et al.* showed that for a DPP-based polymer branched side-chains led to more steric hindrance between polymer chains and to lower crystalline coherence length than linear side-chains.[35] Ho *et al.* replaced the hexyl side-chains in P3HT by 2-ethylhexyl side chains (P3EHT). P3EHT had lower melting temperature and crystallization kinetics.[34]

Notes and unresolved questions.

The limitations of this methodology to identify molecular design rules for optimizing mechanical properties were discussed earlier in section 4.2.1. These limitations when focusing on a single aspect of the molecular structure are illustrated in Fig 4.11. The tensile moduli and the crack-onset strains of the D/A polymers are ranked and separated in three groups in Fig 4.11 a & b: (1) fused-rings in both donor and acceptor, (2) fused-rings in the donor or in the acceptor, and (3) all isolated rings. In Fig 4.11 c & d, the D/A polymers are separated according to side-chains: (1) only linear chains, (2) branching chains in either the donor or the acceptor, and (3) all branching side chains.

The initial hypotheses were that the polymers with all isolated rings and with all branching chains would be the most mechanically robust. However, even if the general trends follow the hypotheses, the tensile modulus and the crack-onset strain measured for each group (Fig 4.11 a, b, c & d) occupied a wide range of values and overlap substantially. For example, polymers with isolated rings and branching side chains had poor mechanical performances (fig 4.11 a, b, c & d). The outliers were attributed to the unknown stiffness of the chains, film morphology and the solid state packing structures of the polymers.
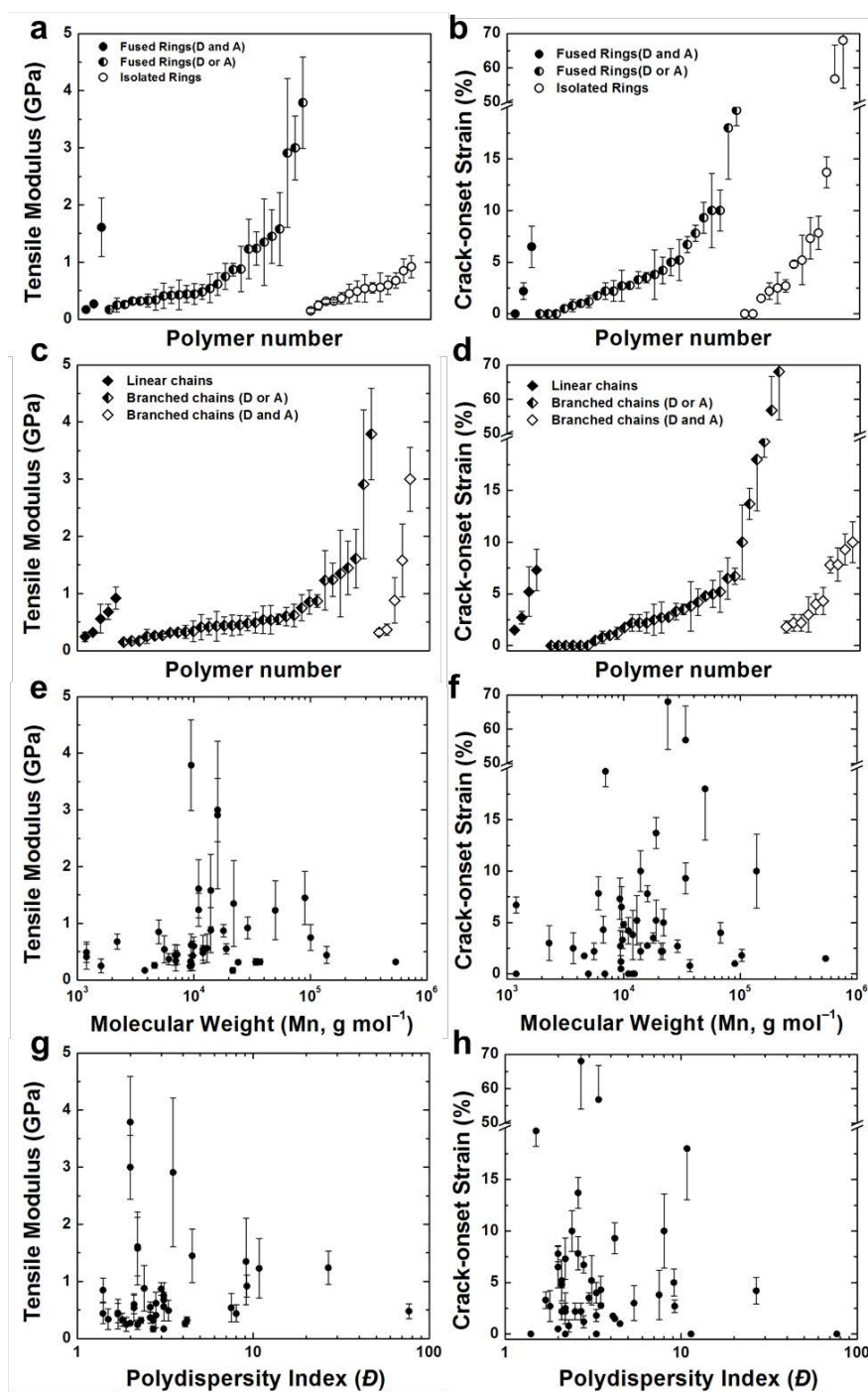
Fig 4.11 - The range of tensile modulus and crack-onset strains for all the polymer samples. (a, b) Ranking of the polymer samples separated by the presence of fused rings in both donor and acceptor (filled circles), either fused ring in donor or acceptor (half-filled circles), and all isolated rings (open circles). (c, d) Plot in which the polymer samples are separated by the nature of the solubilizing side chains: all linear chains (filled diamonds), branched chain on either the donor or acceptor monomers (half-filled diamonds), and all branched side chains (open diamonds). Plots of tensile moduli and crack-onset strains as

a function of number average molecular weight (e and f) and Đ (g and h); values of Mn and Đ are reproduced from Solar 100 study.[5] Reproduced with permission from reference 9.

Other properties need to be taken into account such as the dispersity and molecular weight of the D/A polymers to predict the mechanical properties. Previous reports on P3ATs showed the dependence of the solid state packing structure on molecular weight and regioregularity.[36–39] In such experiments, the synthesis needs to be carefully controlled to be able to isolate polymers with precise molecular weight, dispersity, and regioregularity. This can be achieved for only a few polymers like P3ATs.[40,41] Because most D/A polymer are synthesized by Stille polycondensation, the control over the molecular weight and the dispersity of the finished product is usually low.[40,42] Beside in this study, the size-exclusion chromatography (SEC) system used to measure the values of Đ operates at low temperatures and employs chloroform as the solvent. Under these conditions, aggregation of some polymers could potentially lead to unrealistic Đ values.

Nevertheless, tensile moduli and crack-onset strains were plotted as a function of molecular weight (Fig 4.11 e & f) and of dispersity (Fig 4.11 g & h). No clear trends could be identified. One reason could be that while it could be meaningful to compare the molecular weight and dispersity of a single polymer, these two factor cannot by themselves explain the difference in mechanical properties between multiple polymers.

Electronic-mechanical merit factor.

The aim of this study was to establish molecular design rules to co-optimize electrical and mechanical properties in polymers for R2R manufacturing of OPV. The challenge to do so is illustrated by the fact that many D/A polymers with a low stiffness still had a brittle behavior. To identify promising candidates with favorable electronic and mechanical properties, we used a merit factor. This merit factor (Ψ) combined the power conversion efficiency (reported in the Solar 100 study for roll-fabricated solar cells), the tensile modulus and the crack-onset strain (Equation 4.5).

$$(4.5) \quad \Psi = PCE \times \frac{1}{E_\mathrm{f}} \times CoS$$

where E_f is the tensile modulus and the CoS is the crack-onset strain.

For easier comparison with P3HT, the most used polymer for large scale R2R OPV modules, a relative merit factor (Ψ_{rel}) was defined (Equation 4.6).

$$(4.6) \quad \Psi_{rel} = \Psi / \Psi_{P3HT}$$

where Ψ_{P3HT} is the merit factor associate to P3HT with data from previous reports.[5,24]

Relative Merit Factor

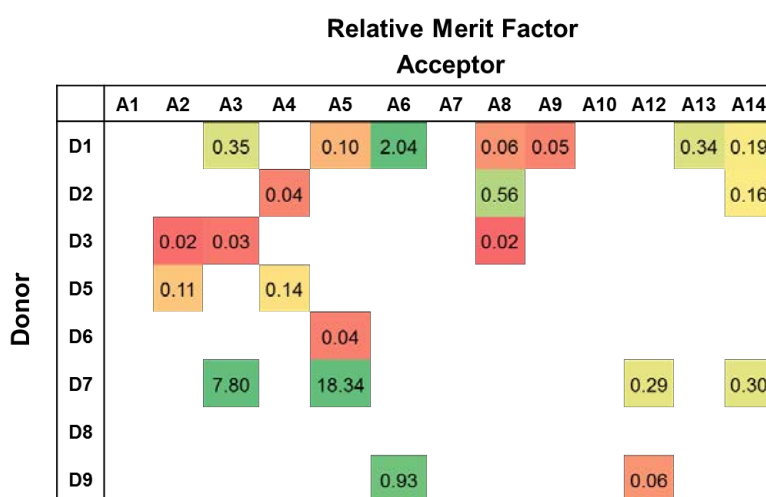|		A1	A2	A3	A4	A5	A6	A7	A8	A9	A10	A12	A13	A14
	D1			0.35		0.10	2.04		0.06	0.05			0.34	0.19
	D2				0.04				0.56					0.16
	D3	0.02	0.03						0.02					
	D5	0.11			0.14									
	D6					0.04								
	D7			7.80		18.34						0.29		0.30
	D8													
	D9						0.93					0.06		

Fig 4.12 - The relative merit factor incorporating the power conversion efficiency (PCE) as reported for the Roll coated solar cells,[5] the tensile modulus, and crack-onset strains in relationship to those of P3HT. Blank cells indicate missing information where at least one quantity was missing. The tensile modulus of P3HT and crack-onset strain were 1.09 ± 0.15 GPa and 9 ± 1.2%.[24] Extracted with permission from reference 9.

The relative merit factor (Ψ_{rel}) of the polymers tested during this study is given in Fig 4.12. When at least one quantity was missing to calculate the merit factor the cell was left blank. The merit factor highlighted nine potential candidates (marked in green in Fig 4.12, with similar performances than P3HT or higher. It is important to keep in mind that this merit factor is based on the mechanical properties of the donor material of a bulk heterojunction alone. The mechanical properties of the blend with the acceptor are expected to have a different mechanical behavior. For example, the addition of fullerene-based electron acceptors (especially [60]PCBM) has been reported to lower the mechanical robustness of the blend compared to the single polymer.[23,24] One hope is to use non-fullerene electron acceptors to avoid such problems.[21] Another limitation of this merit factor is its simplicity, especially the equal contributions of the PCE, the E_f and the CoS. A full characterization of the electronic

and mechanical properties goes through an in-depth analysis of the effect of the addition of the electron acceptor, the film thickness and deposition technique as well as the electronic and mechanical properties of the full device.

4.2.4. Conclusion

The tensile modulus and the crack-onset strains of a large library of D/A polymers were successfully measured. For most D/A polymers, the tensile modulus was of the same order of magnitude as P3HT or lower (ranging from 200 MPa to 1 GPa). However, most polymers were brittle and had low crack-onset strains (<5%). We were able to identify some trends linking the molecular structure and the mechanical properties as well as plausible reasons for the exceptions. The polymers with donor monomers having fused rings had in average a higher stiffness and a higher tendency to fracture. The polymers with branching solubilizing side chains showed higher ductility. These two trends are good guidelines to keep in mind when designing highly mechanically robust materials for R2R fabrication.

Furthermore, we identified the best candidates from the D/A polymer library for R2R upscaling using a simple merit factor including the PCE, the tensile modulus and the crack-onset strain. Finally, from the results of this study, it is clear that the molecular structures of the D/A polymers alone do not dictate the mechanical properties of the dried polymer film. A full investigation of the solid state packing structure by computation and microstructural analysis, is needed to fully understand the relationship between mechanical and electronic behaviors of D/A polymers.

4.3. Summary and outlook

This chapter illustrated the difficulty to find and develop high efficiency low band gap polymers suitable for large scale OPV modules. Only 13 polymers out of a library of 104 low band gap polymers were identified as suitable for upscaling to R2R manufacturing. High efficiencies in lab scale devices do not guarantee a successful implementation for upscaling, especially when prepared with materials and techniques not suitable for R2R manufacturing. A novel high efficiency material needs to pass many thresholds to replace P3HT in large scale

modules from synthesis to actual devices operation and can fail at any given step. A majority of the polymers tested failed to yield a working OPV cell when roll-coated.

We also looked at the thermomechanical stability of the library of low band gap polymers. Mechanical stability is important for R2R manufacturing implementation as well as for integration of OPV in high form factor application such as clothing. The measured tensile moduli were of the same order of P3HT or lower (ranging from 200 MPa to 1 GPa). However, the majority of the D/A polymer had low crack-onset strains (below 5%) and had a brittle behavior. Nevertheless, we identify trends between the molecular structures and the mechanical properties. Fused rings in the backbone of the polymers tend to increase the stiffness and lower the ductility of the polymers. Oppositely, branched side-chains improve the ductility of the material. Using a merit factor combining efficiencies and mechanical properties, nine polymers were identified for further development. Among these nine polymers, only one (A12D7) was also identified in the best candidates of the Solar 100 study.

The two studies reported in this chapter, have the ambition to draw a roadmap to find high efficiency polymers to bridge the gap with common photovoltaic technologies. The idea was to identify potential candidates combining all the required properties for successful up and to introduce a more efficient way to screen materials. Only 10% of the polymers selected made the cut, highlighting the tremendous task ahead.

4.4. References

(1)   Bundgaard, E.; Krebs, F. C. Low Band Gap Polymers for Organic Photovoltaics. *Sol. Energy Mater. Sol. Cells* **2007**, *91* (11), 954–985.

(2)   Green, M. A.; Emery, K.; Hishikawa, Y.; Warta, W.; Dunlop, E. D. Solar Cell Efficiency Tables (version 46). *Prog. Photovoltaics Res. Appl.* **2015**, *23*, 805–812.

(3)   Hoppe, H.; Sariciftci, N. S. Organic Solar Cells: An Overview. *J. Mater. Res.* **2004**, *19* (07), 1924–1945.

(4)   Jørgensen, M.; Carlé, J. E.; Søndergaard, R. R.; Lauritzen, M.; Dagnæs-Hansen, N. A.; Byskov, S. L.; Andersen, T. R.; Larsen-Olsen, T. T.; Böttiger, A. P. L.; Andreasen, B.; Fu, L.; Zuo, L.; Liu, Y.; Bundgaard, E.; Zhan, X.; Chen, H.; Krebs, F. C. The State of Organic Solar cells—A Meta Analysis. *Sol. Energy Mater. Sol. Cells* **2013**, *119*, 84–93.

(5)   Bundgaard, E.; Livi, F.; Hagemann, O.; Carlé, J. E.; Helgesen, M.; Heckler, I. M.; Zawacka, N. K.; Angmo, D.; Larsen-Olsen, T. T.; dos Reis Benatto, G. a.; Roth, B.; Madsen, M. V.; Andersson, M. R.; Jørgensen, M.; Søndergaard, R. R.; Krebs, F. C. Matrix Organization and Merit Factor Evaluation as a Method to Address the Challenge of Finding a Polymer Material for Roll Coated Polymer Solar Cells. *Adv. Energy Mater.* **2015**, *5* (10).

(6)   Ajayaghosh, A. Donor–acceptor Type Low Band Gap Polymers: Polysquaraines and Related Systems. *Chem. Soc. Rev.* **2003**, *32* (4), 181–191.

(7)   Hösel, M.; Søndergaard, R. R.; Jørgensen, M.; Krebs, F. C. Fast Inline Roll-to-Roll Printing for Indium-Tin-Oxide-Free Polymer Solar Cells Using Automatic Registration. *Energy Technol.* **2013**, *1* (1), 102–107.

(8)   Dam, H. F.; Krebs, F. C. Simple Roll Coater with Variable Coating and Temperature Control for Printed Polymer Solar Cells. *Sol. Energy Mater. Sol. Cells* **2012**, *97*, 191–196.

(9)   Roth, B.; Savagatrup, S.; V. de los Santos, N.; Hagemann, O.; Carlé, J. E.; Helgesen, M.; Livi, F.; Bundgaard, E.; Søndergaard, R. R.; Krebs, F. C.; Lipomi, D. J. Mechanical Properties of a Library of Low-Band-Gap Polymers. *Chem. Mater.* **2016**, doi: 10.1021/acs.chemmater.6b00525

(10)   Bundgaard, E.; Krebs, F. C. Low-Band-Gap Conjugated Polymers Based on Thiophene, Benzothiadiazole, and Benzobis(thiadiazole). *Macromolecules* **2006**, *39* (8), 2823–2831.

(11)   Tromholt, T.; Madsen, M. V.; Carlé, J. E.; Helgesen, M.; Krebs, F. C. Photochemical Stability of Conjugated Polymers, Electron Acceptors and Blends for Polymer Solar Cells Resolved in Terms of Film Thickness and Absorbance. *J. Mater. Chem.* **2012**, *22* (15), 7592-7601.

(12)   Manceau, M.; Bundgaard, E.; Carlé, J. E.; Hagemann, O.; Helgesen, M.; Søndergaard, R.; Jørgensen, M.; Krebs, F. C. Photochemical Stability of π-Conjugated Polymers for Polymer Solar Cells: A Rule of Thumb. *J. Mater. Chem.* **2011**, *21* (12), 4132–4141.

(13)   Larsen-Olsen, T. T.; Søndergaard, R. R.; Norrman, K.; Jørgensen, M.; Krebs, F. C. All Printed Transparent Electrodes through an Electrical Switching Mechanism: A Convincing Alternative to Indium-Tin-Oxide, Silver and Vacuum. *Energy Environ. Sci.* **2012**, *5* (11), 9467–9471.

(14)   Savagatrup, S.; Printz, A. D.; O'Connor, T. F.; Zaretski, A. V.; Rodriquez, D.; Sawyer, E. J.; Rajan, K. M.; Acosta, R. I.; Root, S. E.; Lipomi, D. J. Mechanical Degradation and Stability of Organic Solar Cells: Molecular and Microstructural Determinants. *Energy Environ. Sci.* **2015**, *8* (1), 55–80.

(15)   Printz, A. D.; Zaretski, A. V.; Savagatrup, S.; Chiang, A. S. C.; Lipomi, D. J. Yield Point of Semiconducting Polymer Films on Stretchable Substrates Determined by Onset of Buckling. *ACS Appl. Mater. Interfaces* **2015**, *7* (41), 23257–23264.

(16)   Dang, M. T.; Hirsch, L.; Wantz, G. P3HT:PCBM, Best Seller in Polymer Photovoltaic Research. *Adv.*

Mater. **2011**, *23* (31), 3597–3602.

(17)   Liu, Y.; Zhao, J.; Li, Z.; Mu, C.; Ma, W.; Hu, H.; Jiang, K.; Lin, H.; Ade, H.; Yan, H. Aggregation and Morphology Control Enables Multiple Cases of High-Efficiency Polymer Solar Cells. *Nat. Commun.* **2014**, *5* (9), 5293–5301.

(18)   Lipomi, D. J.; Chong, H.; Vosgueritchian, M.; Mei, J.; Bao, Z. Toward Mechanically Robust and Intrinsically Stretchable Organic Solar Cells: Evolution of Photovoltaic Properties with Tensile Strain. *Sol. Energy Mater. Sol. Cells* **2012**, *107*, 355–365.

(19)   Printz, A.; Savagatrup, S.; Burke, D.; Purdy, T.; Lipomi, D. Increased Elasticity of a Low-Bandgap Conjugated Copolymer by Random Segmentation for Mechanically Robust Solar Cells. *RSC Adv.* **2014**, *4*, 13635.

(20)   Wu, H.-C.; Benight, S. J.; Chortos, A.; Lee, W.-Y.; Mei, J.; To, J. W. F.; Lu, C.; He, M.; Tok, J. B.-H.; Chen, W.-C.; Bao, Z. A Rapid and Facile Soft Contact Lamination Method: Evaluation of Polymer Semiconductors for Stretchable Transistors. *Chem. Mater.* **2014**, *26* (15), 4544–4551.

(21)   Kim, T.; Kim, J.-H.; Kang, T. E.; Lee, C.; Kang, H.; Shin, M.; Wang, C.; Ma, B.; Jeong, U.; Kim, T.-S.; Kim, B. J. Flexible, Highly Efficient All-Polymer Solar Cells. *Nat. Commun.* **2015**, *6* (May), 1–7.

(22)   Stafford, C. M.; Harrison, C.; Beers, K. L.; Karim, A.; Amis, E. J.; VanLandingham, M. R.; Kim, H.-C.; Volksen, W.; Miller, R. D.; Simonyi, E. E. A Buckling-Based Metrology for Measuring the Elastic Moduli of Polymeric Thin Films. *Nat. Mater.* **2004**, *3* (8), 545-550.

(23)   Tahk, D.; Lee, H. H.; Khang, D.-Y. Elastic Moduli of Organic Electronic Materials by the Buckling Method. *Macromolecules* **2009**, *42* (18), 7079–7083.

(24)   Savagatrup, S.; Makaram, A. S.; Burke, D. J.; Lipomi, D. J. Mechanical Properties of Conjugated Polymers and Polymer-Fullerene Composites as a Function of Molecular Structure. *Adv. Funct. Mater.* **2014**, *24* (8), 1169–1181.

(25)   Duan, C.; Huang, F.; Cao, Y. Recent Development of Push–pull Conjugated Polymers for Bulk-Heterojunction Photovoltaics: Rational Design and Fine Tailoring of Molecular Structures. *J. Mater. Chem.* **2012**, *22* (21), 10416.

(26)   Guo, X.; Baumgarten, M.; Müllen, K. Designing π-Conjugated Polymers for Organic Electronics. *Prog. Polym. Sci.* **2013**, *38* (12), 1832–1908.

(27)   Takacs, C. J.; Brady, M. A.; Treat, N. D.; Kramer, E. J.; Chabinyc, M. L. Quadrites and Crossed-Chain Crystal Structures in Polymer Semiconductors. *Nano Lett.* **2014**, *14* (6), 3096–3101.

(28)   Printz, A. D.; Savagatrup, S.; Rodriquez, D.; Lipomi, D. J. Role of Molecular Mixing on the Stiffness of Polymer:fullerene Bulk Heterojunction Films. *Sol. Energy Mater. Sol. Cells* **2015**, *134*, 64–72.

(29)   O'Connor, B.; Chan, E. P.; Chan, C.; Conrad, B. R.; Richter, L. J.; Kline, R. J.; Heeney, M.; McCulloch, I.; Soles, C. L.; DeLongchamp, D. M. Correlations between Mechanical and Electrical Properties of Polythiophenes. *ACS Nano* **2010**, *4* (12), 7538–7544.

(30)   Awartani, O.; Lemanski, B. I.; Ro, H. W.; Richter, L. J.; DeLongchamp, D. M.; O'Connor, B. T. Correlating Stiffness, Ductility, and Morphology of Polymer:Fullerene Films for Solar Cell Applications. *Adv. Energy Mater.* **2013**, *3* (3), 399–406.

(31)   Dupont, S. R.; Oliver, M.; Krebs, F. C.; Dauskardt, R. H. Interlayer Adhesion in Roll-to-Roll Processed Flexible Inverted Polymer Solar Cells. *Sol. Energy Mater. Sol. Cells* **2012**, *97*, 171–175.

(32)   Lee, J.-B.; Yoon, S.-S.; Khang, D.-Y. The Importance of Interfacial Adhesion in the Buckling-Based Mechanical Characterization of Materials. *RSC Adv.* **2013**, *3* (38), 17364.

(33)   Mei, J.; Bao, Z. Side Chain Engineering in Solution-Processable Conjugated Polymers. *Chem. Mater.* **2014**, *26* (1), 604–615.

(34) Ho, V.; Boudouris, B. W.; Segalman, R. A. Tuning Polythiophene Crystallization through Systematic Side Chain Functionalization. *Macromolecules* **2010**, *43* (19), 7895–7899.

(35) Yiu, A. T.; Beaujuge, P. M.; Lee, O. P.; Woo, C. H.; Toney, M. F.; Fréchet, J. M. J. Side-Chain Tunability of Furan-Containing Low-Band-Gap Polymers Provides Control of Structural Order in Efficient Solar Cells. *J. Am. Chem. Soc.* **2012**, *134* (4), 2180–2185.

(36) Meille, S. V.; Romita, V.; Caronna, T.; Lovinger, A. J.; Catellani, M.; Belobrzeckaja, L. Influence of Molecular Weight and Regioregularity on the Polymorphic Behavior of Poly (3-Decylthiophenes). *Macromolecules* **1997**, *30* (25), 7898–7905.

(37) Goh, C.; Kline, R. J.; McGehee, M. D.; Kadnikova, E. N.; Fréchet, J. M. J. Molecular-Weight-Dependent Mobilities in Regioregular poly(3-Hexyl-Thiophene) Diodes. *Appl. Phys. Lett.* **2005**, *86* (12), 122110.

(38) Wu, Z.; Petzold, A.; Henze, T.; Thurn-Albrecht, T.; Lohwasser, R. H.; Sommer, M.; Thelakkat, M. Temperature and Molecular Weight Dependent Hierarchical Equilibrium Structures in Semiconducting Poly(3-Hexylthiophene). *Macromolecules* **2010**, *43* (10), 4646–4653.

(39) Kline, R. J.; McGehee, M. D.; Kadnikova, E. N.; Liu, J.; Fréchet, J. M. J.; Toney, M. F. Dependence of Regioregular Poly(3-Hexylthiophene) Film Morphology and Field-Effect Mobility on Molecular Weight. *Macromolecules* **2005**, *38* (8), 3312–3319.

(40) Burke, D. J.; Lipomi, D. J. Green Chemistry for Organic Solar Cells. *Energy Environ. Sci.* **2013**, *6* (7), 2053–2066.

(41) Kim, J.-S.; Kim, J.-H.; Lee, W.; Yu, H.; Kim, H. J.; Song, I.; Shin, M.; Oh, J. H.; Jeong, U.; Kim, T.-S.; Kim, B. J. Tuning Mechanical and Optoelectrical Properties of Poly(3-Hexylthiophene) through Systematic Regioregularity Control. *Macromolecules* **2015**, *48* (13), 4339–4346.

(42) Brouwer, F.; Alma, J.; Valkenier, H.; Voortman, T. P.; Hillebrand, J.; Chiechi, R. C.; Hummelen, J. C. Using Bis(pinacolato)diboron to Improve the Quality of Regioregular Conjugated Co-Polymers. *J. Mater. Chem.* **2011**, *21* (5), 1582–1592.

Chapter 5 – Lifetime of large scale OPV module: the case of PEDOT:PSS

5.1. Introduction

This last chapter is a compilation of indoor and outdoor lifetime tests of large scale organic photovoltaic (OPV) modules. All the modules are fully processed from solution by roll-to roll (R2R) on flexible plastic substrates. Moreover, these modules are indium tin oxide (ITO) free and do not require any vacuum steps. Therefore, these so called "freeOPV" modules are fully consistent with the low cost R2R approach to upscale OPV manufacturing.

Starting assessments are based on studies conducted on an outdoor solar park installed here at DTU.[1] This solar park comprises tilted wood panels upon which six 100 m stretch of OPV rolls are rolled out (Fig 5.1).

Fig 5.1 – Picture of the solar park at DTU. Reprinted with permission from 1.

The OPV rolls used for the solar park were manufactured according the infinity concept.[2] The infinity structure is shown in Fig 5.2. One roll was left outdoor under operating conditions (plugged into the Danish grid) for two years.[3] After two years outdoor, the roll was still operational and retained 60 % of its initial performance (Fig 5.3). Even tough, two years is among the longest reported lifetimes for OPV outdoor this not enough as five years are needed to make OPV marketable as a photovoltaic product.[4]

The necessity to improve the lifetime of these large scale modules is clear but why is it necessary to do large scale studies? As one can imagine such studies are costly in resources

compared to lifetime testing of lab scale cells. Lifetime studies of large scale OPV modules require more time and more man power from the manufacturing to the actual lifetime study. The manufacturing demands for costly equipment and more materials. Finally, the lifetime studies themselves require specific chambers, sun simulators and platforms that can accommodate large size OPV modules. This last point appeared clearly during the first study presented in this chapter.[5] The size of the climatic chambers and of the outdoor sun tracking platform limited the number of samples. Another concern was the homogeneity of the degradation conditions in the climatic chamber especially the temperature.
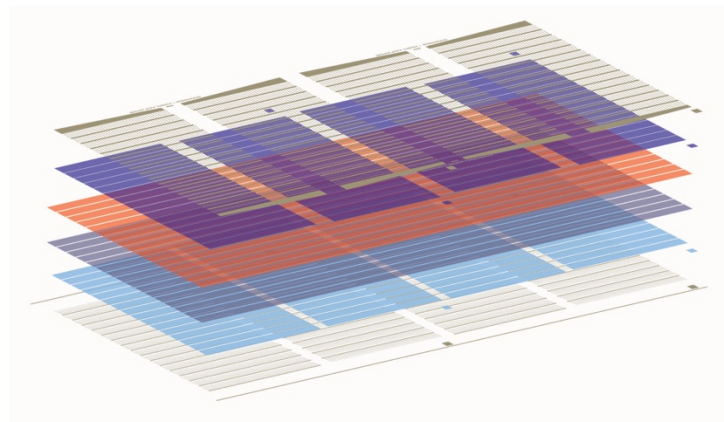

Fig 5.2 – Illustration of the infinity OPV stack. From bottom to top: flexoprinted silver grid, screen printed PEDOT:PSS, slot-die coated ZnO, slot die-coated active layer (P3HT:PCBM), screen printed PEDOT:PSS and screen printed silver grid.
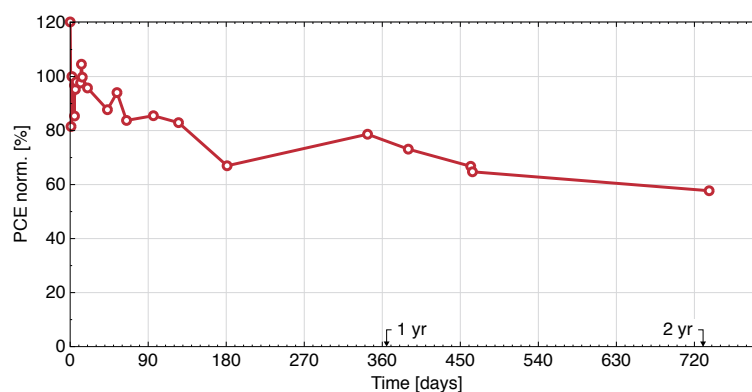

Fig 5.3 – Lifetime solar park: the efficiency of one 100 m stretch is measured through 2 years under sunlight.

For all the reasons above sticking with small lab size OPV cells (< 1 cm^2) would be easier. However, what is true for lab scale cells is not necessary true for commercial size

cells/modules.[3] So far predicting the lifetime of a large scale OPV module based on how well a small cell with the same structure did under lifetime testing is challenging.[6] Moreover, when dealing with OPV modules in real life conditions new failures modes appear (Fig 5.4).[7] These failures come from the outdoor conditions (rain, thunderstorm, animals...), the mechanical stress during manufacturing, handling and installation of the modules and the high voltage ensuing from the series design of the modules. For OPV to be commercially viable, all these issues should be anticipated and resolved.

The motivations to undertake lifetime studies of large size OPV modules are clear. But it is obviously impossible to work with 100 m stretch of OPV foils. Therefore, for this study, it was necessary to redesign the modules to accommodate our facilities. The new modules, called freeOPV, had the size of a postcard. These modules were manufactured in the exact same conditions as the infinity architecture but the electrodes pattern was modified so these modules could be laser cut after manufacturing.[8]

Fig 5.4 – pictures of failures in the solar park. Reprinted with permission from 7.

5.2. First generation freeOPV[*]

At the beginning of this work, the state of the art architecture of the freeOPV modules was the same than the infinity concept (Fig 5.5 left).[8] Many known factors of degradation for lab scale devices are absent from the infinity/freeOPV architecture. This lead to an already remarkable lifetime outdoor (2 years) for the solar park at DTU. FreeOPV modules have an inverted structure which is more stable than the regular one.[3] There is no ITO or other highly sensitive metal electrodes (calcium, aluminum).[9] Plus the modules are encapsulated in a flexible barrier foil with low diffusion rates for oxygen and water (oxygen transmission rate 1×10^{-2} $cm^3.m^{-2}.day^{-1}$ and water vapor transmission rate 4×10^{-2} $g.m^{-2}.day^{-1}$) and a UV filter.[10,11] Among the

---

[*] Section based on reference 5.

remaining known factors of degradation are the photoactive layer (PAL) and PEDOT:PSS. For the active layer, there are many reports on improving the photochemical stability of the polymers for OPV.[12,13] Even though this is a highly interesting line of inquiry, it was not pursued because it is difficult to synthesize or acquire such novel polymers in sufficient quantity for large scale R2R manufacturing. This chapter will focus on Poly(3,4-ethylenedioxythiophene) polystyrene sulfonate (PEDOT:PSS) (Fig 5.6). There are actually two layers of PEDOT:PSS in the freeOPV stack and it is a known decay factor.[3,9,14–17] PEDOT:PSS is still widely used because it is easy to deposit (soluble in water) and it has a tunable work function.
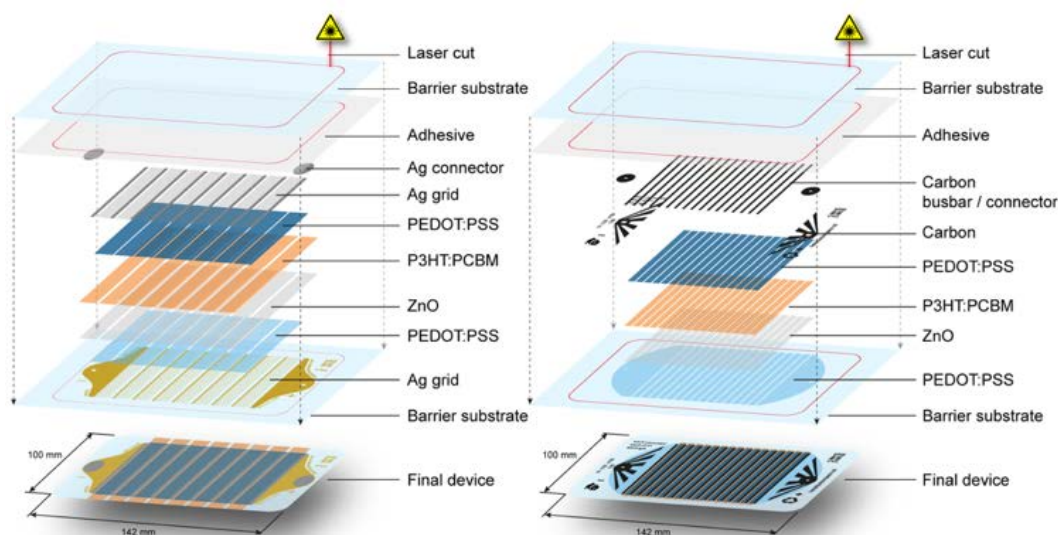

Fig 5.5 – Illustration of the freeOPV architecture with silver grid electrodes (left) and with carbon electrodes (right). Reprinted with permission from references 8,11.

But PEDOT:PSS is highly hygroscopic which is damaging for the stability of the OPV cell.[14,15] In humid environment its conductivity decreases, its acidity increases (which corrodes electrodes).[14,16,18,19] In lab scale cells, the ageing mechanisms associated with PEDOT:PSS are negligible for encapsulated devices, but are they still negligible during long-term operation?[3]

5.2.1. PEDOT:PSS additives

Tens of inks are available commercially so one question is: does the PEDOT:PSS ink formulation impact the overall lifetime of the OPV module? Many different additives are used

(dimethylsulfoxide, Ethylene Glycol, polyethylene glycol, meso-erythritol , 2-nitroenthanol, sorbitol) to help with deposition, wetting, to tune the workfunction, conductivity.[16,20–22] One class of additives that could potentially impact the lifetime of the OPV module is the high boiling additives. These additives are used to tune the conductivity of the PEDOT:PSS layer.[16,21] Traces of these additives are expected to remain in the dried layer because of their high boiling point.
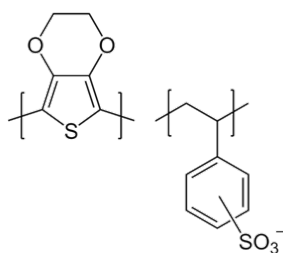

Fig 5.6 – chemical structure PEDOT:PSS.

Table 5.1 – Composition commercial PEDOT:PSS inks

Ink	PEDOT:PSS	High boiling additive	Solid content (% w/w)	Additive content (% w/w)
P5010	Agfa 5010	Unknown (alcohol)	3	5
*PDMSO-1**	PH1000	DMSO	2.2	5
*PDMSO-2**	PH1000	DMSO	2.2	5
PEG	PH1000	EG	2.2	5

*According to the supplier: PDMSO-2 has a surfactant and a crosslinker which PDMSO-1 does not have.*

The following study focuses on various commercially available types of PEDOT:PSS, which are compatible with the freeOPV manufacturing (both PEDOT:PSS layers are rotary screen printed).[8] Four inks from two suppliers (Agfa and Heraeus) were selected, their composition is shown in Table 5.1. The different high boiling additives are dimethylsulfoxide (DMSO), ethylene glycol (EG) and an unknown alcohol for the Agfa ink. The four inks are not all suitable to be used for both front and back PEDOT:PSS layer. The front layer needs to be thin and highly conductive so the light can pass through. The back layer needs to be thick enough to handle the printing of the top silver grid by avoiding shorts. Five combinations of PEDOT:PSS were selected for an initial prescreening. These combinations are shown in table 5.2 with their initial performances. As R2R manufacturing and the testing of a large number of samples is time consuming, a quick prescreening stability study was done on a few samples of each combination to eliminate any low performing combination.

Table 5.2 – The different PEDOT:PSS combinations and the initial performances of freeOPV modules. Data extracted from[5].

Combination		C1	C2	C3	C4	C5
Front PEDOT:PSS		PDMSO-1	PDMSO-1	PEG	PDMSO-1	PEG-1
Back PEDOT:PSS		P5010	PEG	PEG	PDMSO-2	PDMSO-2
	PCE (%)	1.75 ± 0.06	1.1 ± 0.2	1.3 ± 0.1	1.14 ± 0.08	0.81 ± 0.07
Initial	I_{SC} (mA)	4.1 ± 0.3	3.9 ± 0.2	3.9 ± 0.2	3.9 v0.1	3.1 ± 0.3
performances[*]	V_{OC} (V)	40 ± 2	35 ± 4	39 ± 2	38 ± 2	40 ± 2
	FF (%)	60 ± 4	47 ± 3	50 ± 2	44 ± 1	37 ± 2

[*] *Values average over 8 modules.*

The C1 combination is the one used for the solar park OPV meaning that it is the benchmark of this study.[1,8] Four indoor ISOS test were done with two freeOPV of each type per test: ISOS-L-2; ISOS-L-3; ISOS-D-2; ISOS-D-3 (these tests are described in chapter 3). As stated above C1 was the state of the art freeOPV structure at the beginning of this experiment and was therefore thoroughly studied.[6] The results of this previous study are compared with the ones of the others combinations. This is possible because all the tests followed the ISOS standard.[23]
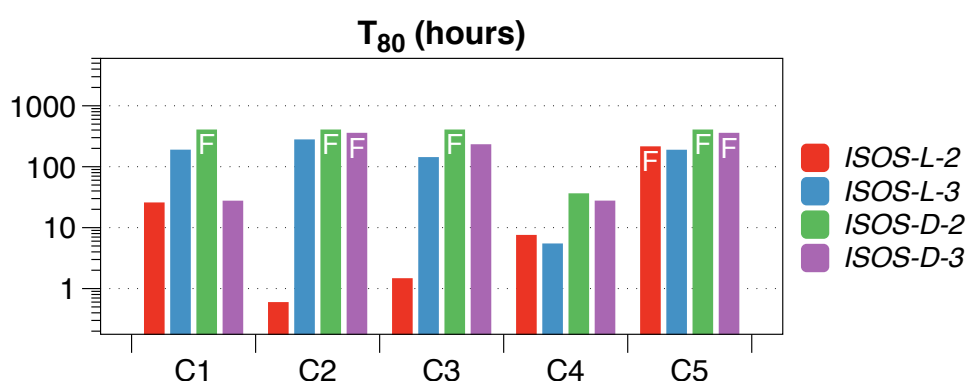
Fig 5.7 – T_{80} in hours for each PEDOT:PSS combinations under four different ISOS tests. F signal when the final time was plotted instead of T_{80}.

First when looking at the initial performance of the freeOPV modules with different combinations (Table 5.2), the combination C5 modules had a poor initial efficiency. This combination was to be kept only in case of extreme stability. Fig 5.7 shows the T_{80} values for each combination modules under the four ISOS tests. When the performance of the modules did not degrade by 20 % or more during the experiment timeframe, the final time was plotted. The modules with the combination C4 performed poorly in all tests except for the light test (ISOS-L-2) where they were in the middle of the pack. Consequently, the C4 combination was discarded for the main

study. All four other combinations performed well but none stand out. The combination C5 was also discarded because of its low initial performances.

Combinations C1, C2 and C3 were used for the main study. Another combination referred as C6 (see table 5.3) was deemed necessary because of the good stability of modules with PEG as front PEDOT:PSS.

Table 5.3 – Initial performances of freeOPV modules with combination C6 averaged over 35 modules.

Combination		C6
Front PEDOT:PSS		PEG
Back PEDOT:PSS		P5010
Initial performances	PCE (%)	1.57 ± 0.08
	I_{SC} (mA)	8.3 ± 0.2
	V_{OC} (V)	12.2 ± 0.8
	FF (%)	40 ± 1

The long-term stability study was done with a new freeOPV design (fig 5.5 right) with carbon electrodes.[11] The stack architecture is the same as the first generation freeOPV except that the front electrode is only one layer of PEDOT:PSS and the back electrode is a layer of PEDOT:PSS with carbon busbars on top. Carbon freeOPV modules were manufactured with the four selected combinations (C1, C2, C3 and C6). In total 140 modules were tested:

- ISOS-D-1: 10 modules of each combination
- ISOS-D-3: 10 modules of each combination
- ISOS-L-3: 5 modules of each combination
- ISOS-O-1: 10 modules of each combination.

The number of samples was limited for ISOS-L-3 because of the limited size of the weathering chamber (Q-sun chamber) used for the test. There were also concerns about the homogeneity of the degradation conditions in the chamber used for ISOS-L-3. A non-uniform light exposure of the samples could lead to temperatures differences during ageing which would result into different ageing rates for the modules. This phenomenon was easily identified with the freeOPV modules subjected to ISOS-L-3 testing during this study. The encapsulating foil (Fig 5.8) is sensitive to temperature and degrades by forming bubbles when subjected to too much heat. The bubble formation impacts the stability significantly as it leads to delamination of the solar cell stack (Fig 5.8). The foil is a superposition of multiple 10 μm layers. By using a scanning

electron microscope (SEM) bubbles between these layers could be observed (Fig 5.8). After a few days in the chamber, some of the modules exhibited more bubbles than others. This was attributed to slight temperature differences within the chamber.
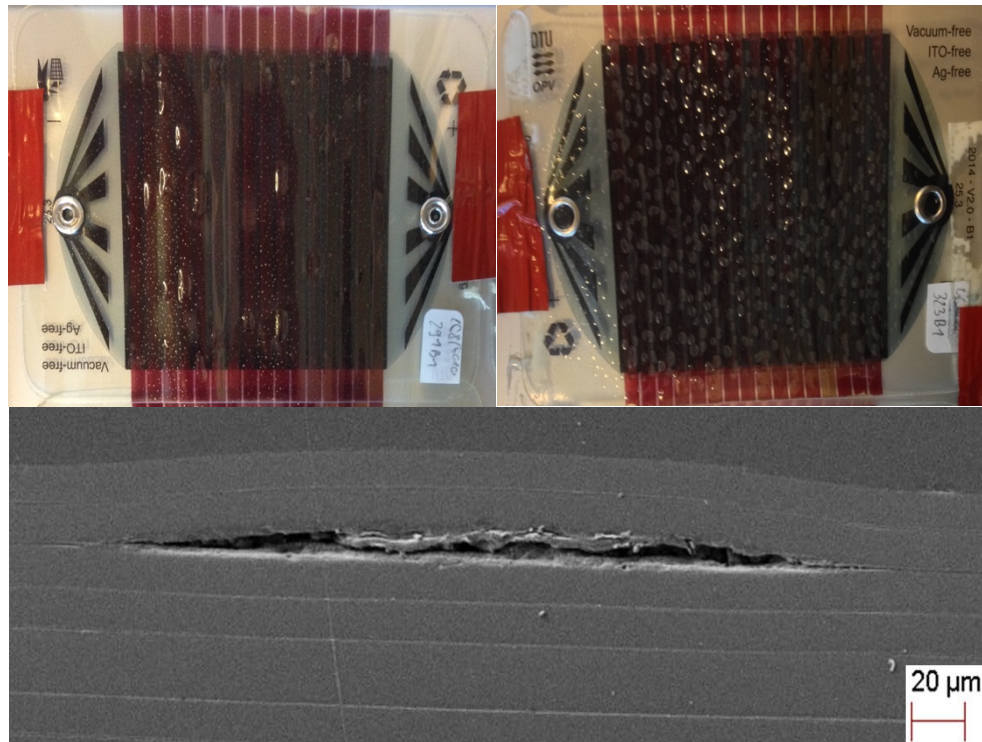

Fig 5.8 – (top) Pictures of carbon freeOPV modules after 3 days in the Q-sun chamber. The modules have different degrees of bubbling because of slight temperatures differences. (bottom) A bubble observed by SEM of a cross section of the barrier foil. Reprinted with permission from 5.

Fig 5.9 shows the degradation curve of two freeOPV modules placed on the left side (#291B1) and on the right side (#290B1) of the chamber. These two modules were in adjacent motifs on the manufactured OPV foil and exhibited similar initial performance. The module on the right side of the chamber degraded twice as fast. To avoid this problem, the modules were cycled around after each measurement.

The reproducibility of the manufacturing process is illustrated in Fig 5.10 (bottom right). The initial performances of the modules for all four combinations are tightly grouped.
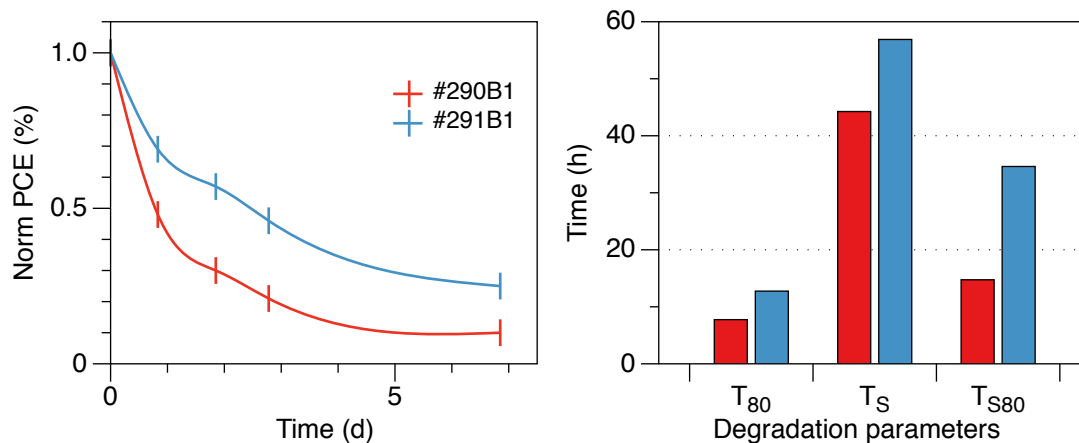
Fig 5.9 – Degradation curves for two carbon freeOPV modules placed on both side of the ISOS-L-3 chamber. Reprinted with permission from reference 5.

For the dark storage at room temperature (ISOS-D-1) test, all the combinations were stable and remained above 80 % of their initial efficiency for the whole experiment (see Fig 5.11). After 3 months (126 days total), the modules with the C1 and C6 combinations lost about 10 % of efficiency. Because the two other combinations retained their initial efficiency, we can conclude that in the ISOS-D-1 conditions, PEG is superior to P5010 for back PEDOT:PSS.

For the second dark test (ISOS-D-3), where the modules were subjected to high humidity and high temperature. All modules degraded fast regardless of the PEDOT:PSS combination (Fig 5.11). The combinations C1 and C2 performed better. They degraded respectively by 56 % and 70 % in 2 weeks. The modules with C3 and C6 combinations respectively lost 90 % and 75 %. The same trend is observed when looking at the degradation parameters (Fig 5.10). T_{80} and T_{S80} are higher for modules with C1 and C2 combinations. C1 and C2 have PDMSO-1 as front PEDOT:PSS. This means that in the conditions of ISOS-D-3 PDMSO-1 is better than PEG as front PEDOT:PSS. For the back PEDOT:PSS, C1 and C6 modules are respectively slightly better than C2 and C3 modules. So P5010 is somewhat better.

The last indoor test (ISOS-L-3) combines high temperature, high humidity and light. In these harsh conditions, all combinations degraded by more than 80 % (Fig 5.11). This was expected because there was no UV filter on the modules tested. Not using UV filter was made on purpose to shorten the study time especially outdoor. The modules with C2 and C3 have T_{80} and T_{S80} higher than the two other combinations. Therefore in these conditions modules with PEG as back PEDOT:PSS are more stable.
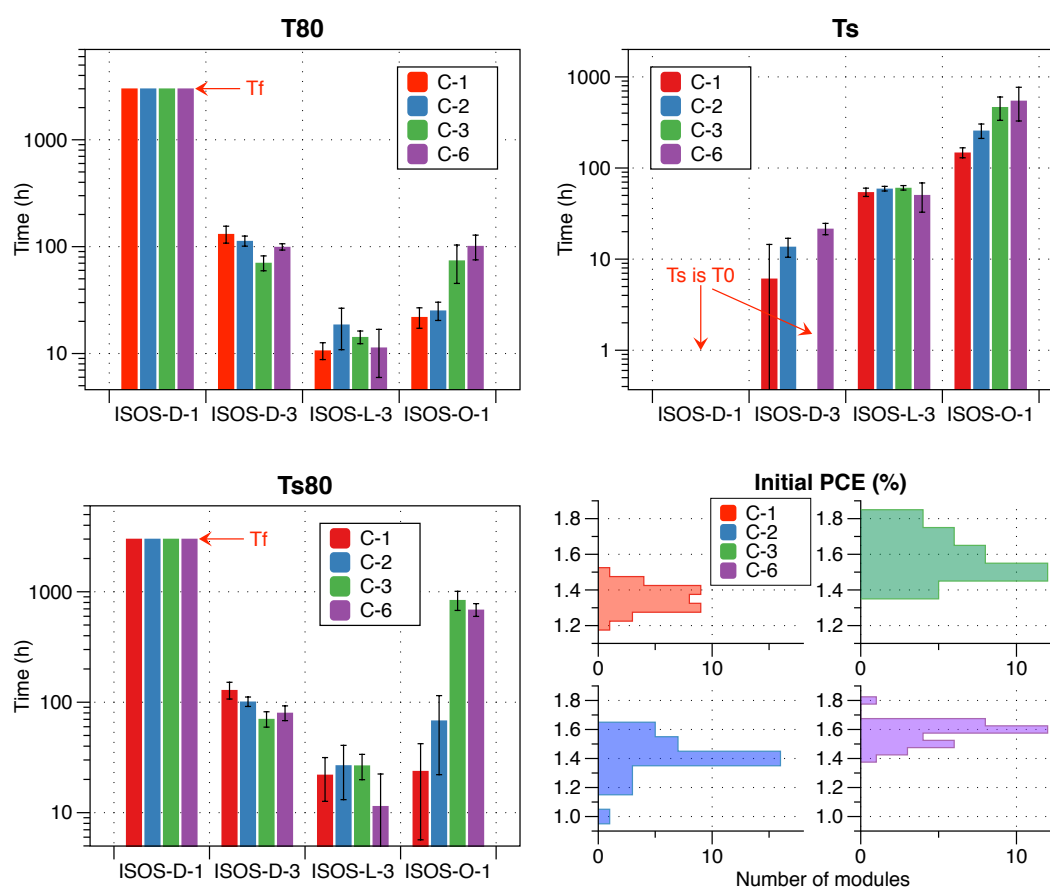
Fig 5.10 – Initial performances carbon freeOPV modules (bottom right); Degradation parameters: T_{80} (top left), T_S (top right), T_{S80} (bottom left). The final time (Tf) was plotted when T80 was not reached for the testing time (3000 h). Reprinted with permission from reference 5.

The final test was run outdoor (ISOS-O-1) from May to September 2014. The modules were mounted on a sun tracking platform to maximized light exposure (Fig 5.12 left). The degradation curves in Fig 5.11 clearly show that modules with C3 and C6 PEDOT:PSS combination are more stable. C3 and C6 modules retained over 50 % of their initial performances after 50 days outdoor. The C1 and C2 combination degraded by 80 % in 2 weeks. The same trend is found in the degradation parameters (Fig 5.10). Modules with C3 and C6 PEDOT:PSS combination have T_{80} and T_{S80} about ten times higher. For outdoor operation PEG is superior to PDMSO-1 for front PEDOT:PSS. This is a decisive result as outdoor use is ultimately the goal for the OPV technology.

The apparent lower stability of the freeOPV modules outdoor compared to the solar park modules with similar architecture is due to:

- The absence of UV filter on the modules used for this study.

- The smaller edge size which lead to faster diffusion of water and oxygen.

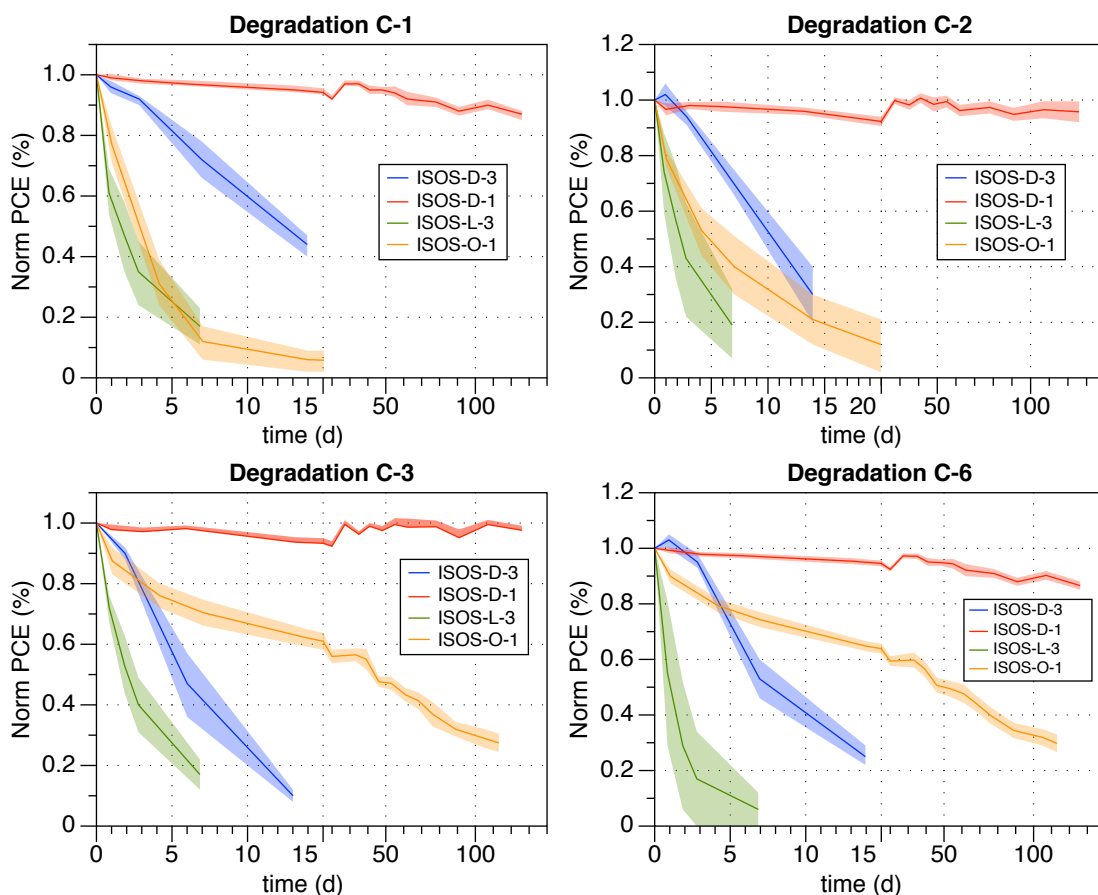- The buttons used for connecting the modules

Fig 5.11 – Average degradation curves for each four PEDOT:PSS combination under different ISOS tests. Reprinted with permission from reference 5.

Another observation from the ISOS-O-1 test is that the modules with the combination C1 and C2 degraded faster outdoor than during ISOS-D3 and ISOS-L-3 tests. But the conditions in these two indoor tests are harsher than outdoor so one would expect the modules to degrade faster during ISOS-L-3 and ISOS-D-3 than outdoor (which is the case for the two other combinations). This accelerated degradation of the C1 and C2 modules outdoor is attributed to the installation set up outdoor. The freeOPV modules are taped onto a plastic plate (Fig 5.12 left) which allows for the condensation of the rain and of the morning dew between the plate and the modules. The contact buttons are snapped through the barrier foil, creating a direct

path for water to diffuse inside the modules. PDMSO-1 appears to be much more hydrophilic than PEG. The water ingress in modules with PDMSO-1 as front PEDOT:PSS (C1 and C2) was considerable. Actual "bubbles" of water could be seen inside the module (Fig 5.12 right).

Fig 5.12 – (left) the freeOPV mounted on the sun tracking platform are circled in blue. (right) picture of a freeOPV module with water ingress (blue circle). Reprint with permission from 5.

The difference in hygroscopic behavior of PDMSO and PEG is attributed to the different high boiling additive. However, because the PEDOT:PSS inks are commercial products it is difficult to obtain information on the other additives used in the inks. To be sure that the different hydrophilic behavior is due to the high boiling additives and not to any other additive, PDMSO-2 and PEG were compared by contact angle measurement. According to the supplier these two inks are identical except for the high boiling additive.

The higher hydrophilic behavior of PDMSO-2 was confirmed by contact angle measurements (see fig 5.13). Water droplets were dropped on printed layer of both PEDOT:PSS. From the pictures in Fig 5.13, it is clear that both surfaces are hydrophilic but PEG less than PDMSO-2. The contact angle of water on PDMSO-2 is about 15° compared to 75° on PEG.

DMSO is a highly polar aprotic (ε_r 48) solvent. On the other hand, EG is a protic slightly less polar (ε_r 41) solvent. To explain what occurs during the fast drying of the PEDOT:PSS layer in R2R printing, we propose that the liquid phase of the PEDOT:PSS layer is constituted in majority of water at the beginning of the drying process. However, towards the end of the drying, one would expect that mostly the high boiling additive remains. In the case of DMSO, we believe that exposure of the ionic parts of PEDOT:PSS gel particles are more favored, which

consequently leads to a more hydrophilic surface of the dry layer. Oppositely, we believe that for EG, the more apolar part of PEDOT:PSS are exposed.

Fig 5.13 – contact angle measurements reprinted with permission from reference 5.

The overall conclusions from this study are compiled in Table 5.4. For the front PEDOT:PSS, there is no apparent winner. Modules with PDMSO-1 performed better under ISOS-L-3 and ISOS-D-3 conditions. However, modules with PEG outperformed the others outdoors. Outdoor operation is of course the ultimate aim for OPV modules. For this reason, EG should be favored as additive compared to DMSO. For the back PEDOT:PSS, modules with PEG were more stable during ISOS-D-1 and ISOS-L-3 tests. For the two other tests, there is no difference. Here again, EG is better than DMSO for stability.

Table 5.4 – Comparative stability of the different freeOPV modules under ISOS tests. Under the conditions the PEDOT:PSS seems to = not impact stability;+ improve stability; - lower stability.

ISOS test		D-1	D-3	L-3	O-1
Front PEDOT:PSS	*PDMSO-1*	=	+	+	-
	PEG	=	-	-	+
Back PEDOT:PSS	*P5010*	-	=	-	=
	PEG	+	=	+	=

5.2.2. Conclusion

The impact on OPV modules stability of the high boiling additives used in PEDOT:PSS ink has been clearly showed. One should keep this in mind when optimizing a device architecture as the PEDOT:PSS ink formulation yielding the best initial efficiency might not be the best one for ensuring long term stability. In our case, the initial performances will suffer but replacing DMSO by EG will extend the lifetime of the OPV modules outdoor by two or three times, preventing any other new failure occurs. It is possible to work around the lower lifetime of large scale OPV

modules due to PEDOT:PSS with for example a good encapsulation but finding some suitable replacement is the best course of action.

5.3. Silver Nanowire based freeOPV[†]

Replacing PEDOT:PSS means modifying the electrodes to accommodate new materials while retaining similar efficiency. The requirement for such novel electrodes are:

- No ITO
- No vacuum steps
- Compatible with R2R manufacturing
- No PEDOT:PSS
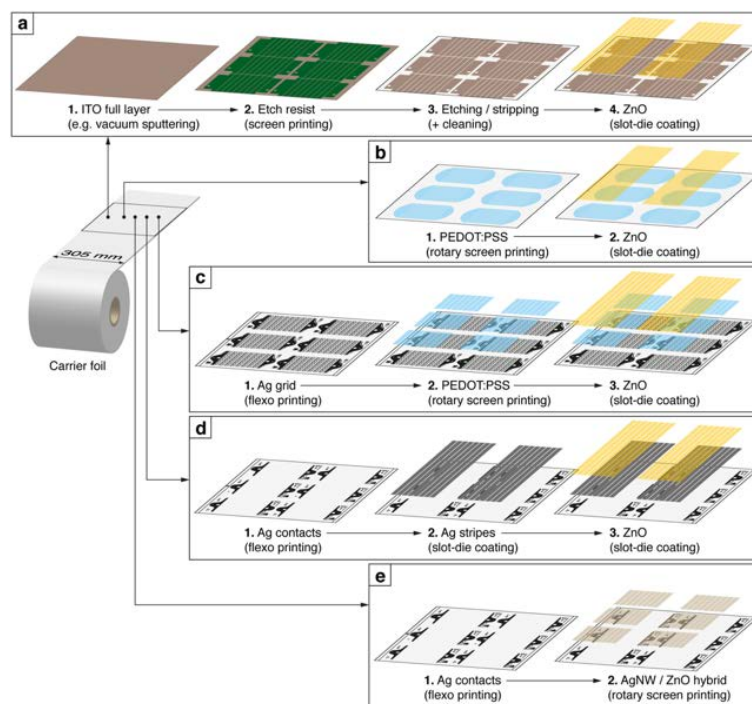- Good transmittance in the absorbing range of the active material.

Fig 5.14 – Illustration R2R substrates and superstrates for OPV. Reprinted with permission from 24.

For the front electrode, the state of the art for R2R electrodes was reported by Hösel *et al.* listing five substrates and superstrates (Fig 5.14).[24] Among these potential electrodes, one uses ITO (Fig 5.14 a) and is eliminated. Another electrode (Fig 5.14 d), is not transparent and is compatible only with a regular architecture and is therefore discarded as well because the freeOPV modules have an inverted architecture. Among the three remaining electrode design, two include a PEDOT:PSS layer (Fig 5.14 b & c) and are actually used in the first generation and the carbon freeOPV. Only one design remains (Fig 5.14 e) with a hybrid silver nanowires (AgNW)/Zinc oxide (ZnO) layer. On top of removing PEDOT:PSS this electrode requires the printing of only one layer compared to three for the previous generations of freeOPV. This has no impact on stability but lowers the manufacturing cost which is also critical for commercialization. The compatibility of AgNW electrodes with R2R manufacturing has been proven.[24] AgNW electrodes also have a good conductivity/transmittance ratio.[25] Last but not least AgNW need to be stable over time. The nanowire structure means that the ratio surface/volume is high for the silver particles which could potentially be detrimental for stability. Mayousse *et al.* reported on the stability of unencapsulated pristine AgNW over two years.[26] The AgNW were exposed to light, high humidity, high temperatures. The only case where the conductivity of the AgNW decreased was when exposed to high temperature due to the breaking down of some Ag wires. One interesting result was that under light the AgNW sintered leading to an increase in conductivity of the AgNW network.
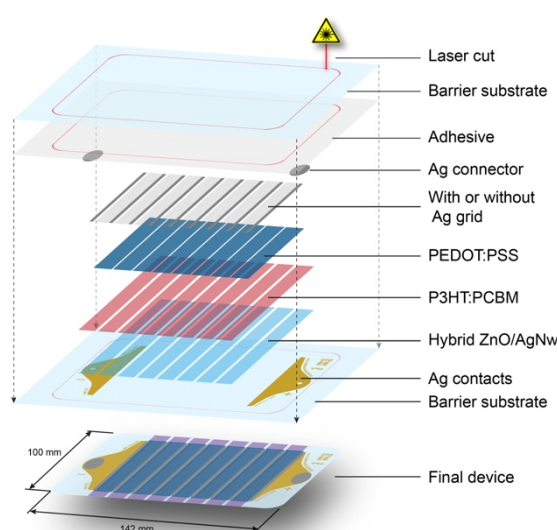

Fig 5.15 – Illustration of the AgNw freeOPV stack. Extracted with permission from 27.

The new freeOPV architecture including the AgNw front electrode is illustred in Fig 5.15. For the back electrode, two designs were selected: a single PEDOT:PSS layer or a PEDOT:PSS layer topped by a silver grid. The AgNW freeOPV were produced in the same R2R conditions than for the earlier study.[27] The stability of the AgNW freeOPV modules was then tested under different ISOS conditions. The results of this study were finally compared to the stability of previous freeOPV designs. Depending of the infrastructure available two to five modules were tested for each ISOS tests (D-2, D-3, L-2, L-3, O-1, O-2).
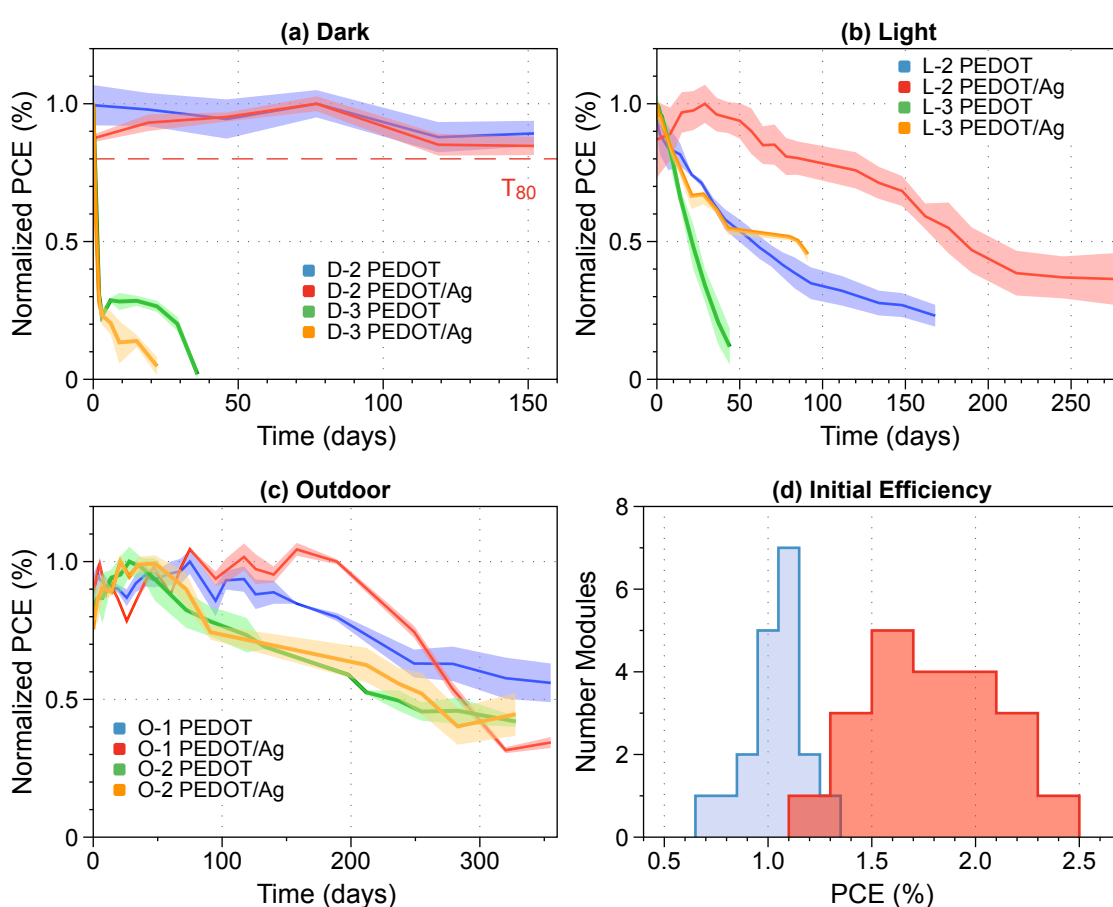
Fig 5.16 – Degradation curves AgNW modules during (a) dark tests, (b) light tests and (c) outdoor tests. Initial performances AgNW modules (d). Data extracted from reference 27.

5.3.1. Lifetime studies

The initial efficiencies of both types of AgNW modules are given in Fig 5.16 d. The higher efficiency of modules with the PEDOT:PSS/Ag grid back electrode is due to the higher conductivity of this electrode compared to a single layer of PEDOT:PSS.[24]

Dark tests

In ISOS-D-2, the modules are expected to remain stable for months or even years. After 80 days of testing both module types are still above 80 % of their initial efficiency (Fig 5.16 a). T_{80} is estimated by linear interpolation to be around 200 days for both module types. Under ISOS-D-3 conditions the modules degraded fast to below 20 % of their starting efficiency in a few days (Fig 5.16 a). After a couple weeks both module types were inoperative. The degradation is linked to diffusion of humidity through the edges of the module and the button contacts.[28] Modules with only PEDOT:PSS as back electrode were slightly more stable. This is ascribed to the fact that in humid environment the PEDOT:PSS sees its acidity rise which would speed up corrosion of the Ag grid.[18]

Light tests

The two tests (ISOS-L-2 and L-3) confirmed that humidity is the main cause for degradation of the studied OPV modules. Under ISOS-L-2 the humidity is low due to the heat diffused by the strong 1 sun simulator. In that test the AgNW freeOPV modules were extremely stable (Fig 5.16 b). After 6 month under continuous light exposure the modules with a single PEDOT:PSS layer as back electrode retained 30% of their initial efficiency. For the other modules with PEDOT:PSS/Ag a back electrode, the sintering of the AgNW network yields an increase in performances for the first 40 days.[26] These modules still performed at 60 % of their starting efficiency after 6 months. This is an impressive result as most cells and modules tested under ISOS-L-2 decay in hours.[3] However, under ISOS-L-3 conditions, the modules degraded faster due to the high humidity (Fig 5.16 b). The back PEDOT:PSS modules degraded linearly to 0% in 50 days. The other modules with Ag grid decayed by only 50 % after 100 days in the ISOS-L-3 chamber. This is a surprising result because usually modules decay as fast or faster under ISOS-L-3 than under ISOS-D-3 conditions.[3] The improved stability is attributed to the sintering of the AgNW electrode and to the back Ag grid compensating for PEDOT:PSS decreased conductivity.

Outdoor tests

The outdoor tests were conducted for a one year period starting July 2014. The number of channels available for the acquisition system was limited so only two modules of each type

were tested. For comparison the data from the ISOS-O-2 test was normalized to 1000 W/m^2. The results from both tests are in agreement as expected (Fig 5.16 c). The modules were stable for about 5 months and then started to decay. After a year outdoor, all modules are still above 30% of their initial efficiency.

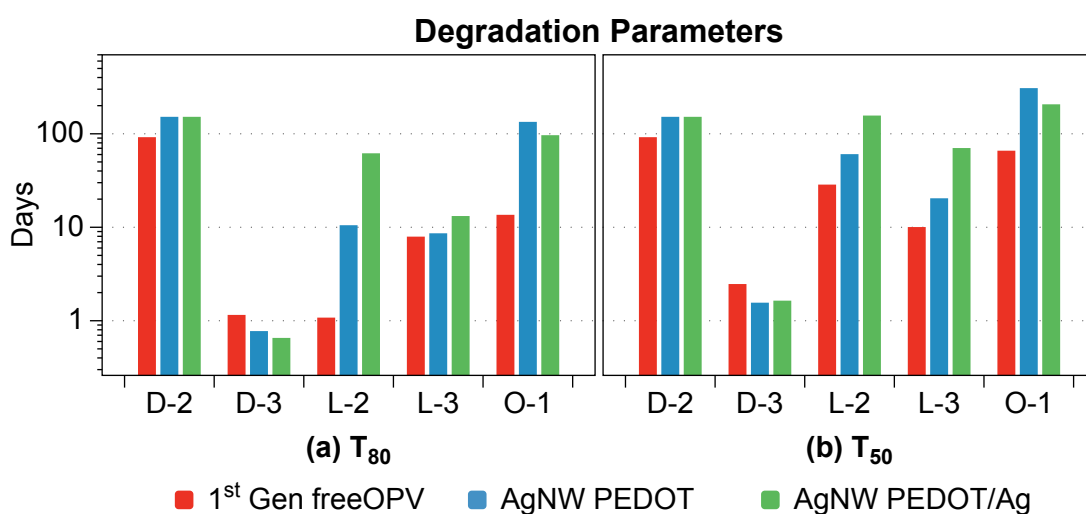### 5.3.2. freeOPV generations comparison

Fig 5.17 – Degradation parameters for first generation and AgNw freeOPV. Data from 27.

The lifetime results obtained for AgNW freeOPV modules are compared with the ones of the first generation freeOPV.[5,6] The main difference being the front electrode. The first generation has the following electrode: Ag grid/PEDOT:PSS/ZnO compared to just one layer (AgNW:ZnO) for the AgNW modules. The usual degradation parameters are T_{80}, T_S, T_{S80}, but here many of the degradation curves do not stabilize. So T_{S80} was therefore replaced by T_{50}, the time it takes to reach 50 % of the initial efficiency (Fig 5.17 b). As expected, all modules are stable under ISOS-D-2 conditions, so the final time (T_F) was plotted instead of T_{80} and T_{50} (Fig 5.17 a&b). The estimated T_{80} values are about 200 days or more. For ISOS-D-3, there is not much difference between the three type of modules (Fig 5.17). The fast decay is attributed to diffusion from the edges and the contacts.[28] The packaging is identical for all modules which explains the similar degradation timescale. The stabilities of both types of AgNW modules are significantly higher compared to the first generation freeOPV during ISOS-L-2. T_{80} is about one

day for the first generation modules but ranges from weeks for AgNW modules with back PEDOT:PSS electrode to months for the AgNW modules with a Ag grid back electrode (Fig 5.17 a). Similarly, T_{50} is one order of magnitude higher for AgNW modules compare to first generation modules (Fig 5.17 b). Under ISOS-L-3 condition, the stability of AgNW modules is also better (Fig 5.17). Especially for the Ag grid back electrode modules which have a T_{50} around 100 days (Fig 5.17 b). Finally, for the outdoor test ISOS-O-1, the same increase in stability for the AgNW modules is seen (Fig 5.17) for both T_{80} and T_{50}. Even though all modules were tested outdoor following the ISOS-O-1 parameters, the first generation freeOPV modules were not tested at the same time than the AgNW modules. Because of the disparity in the weather conditions one would expect differences in the degradation factors ref. However both tests were started at the same time of the year (July 2013 for first generation modules and July 2014 for AgNW modules) which limits the difference in temperatures and precipitations. Finally the difference in T_{80} and T_{50} (one order of magnitude) is sufficient to conclude that AgNW are much more stable.

5.3.3. Conclusion

The implement of the AgNW/ZnO hybrid layer for front electrode in the design of freeOPV modules yielded a significant improvement in stability. Especially outdoor, where the degradation factors indicate a lifetime increased by one order of magnitude. The longer lifetime is attributed to the removal of the PEDOT:PSS layer in the front electrode as well as the sintering of the AgNW network under light. For the back electrode, as long as the PEDOT:PSS is kept, a top Ag grid is necessary to maintain the conductivity of the electrode during operation.

5.4. High efficiency low band gap polymer[‡]

P3HT is by far the most common donor material used to make OPV.[29] It is available in large quantities and easy to coat/print but the maximum efficiency is limited to 4-5 % for small scale devices and 2-3 % for R2R devices.[29,30] To be successfully commercialized OPV modules need higher efficiency.[4] This is why all recent developments in high efficiency low band gap polymers are critical.[31,32] From the work presented in this chapter, it is clear that PEDOT:PSS is lowering

---

[‡] Section based on reference 34.

the operational stability of OPV modules noticeably when prepared with P3HT especially outdoor. But does it has the same impact on modules manufactured with low band gap materials?

One example of such low band gap polymer is PBDTTTz-4 (Fig 5.18). PBDTTTz-4 was recently reported by Carlé *et al.* to keep its efficiency when used in large scale roll-coated ITO-free OPV modules.[33]
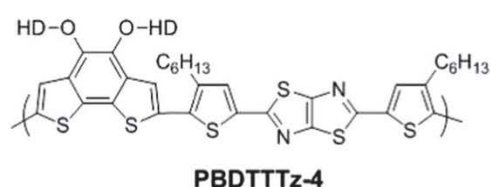

Fig 5.18 – chemical structure PBDTTTz-4

The initial efficiency of PBDTTTz-4 modules is higher than for P3HT but their lifetime is much lower (Table 5.5). At the current level of stability, P3HT is still the best option for large scale module. To benefit fully from the higher efficiency of PBDTTTz-4, the stability of modules prepared with it needs to be extended. The hope is that electrode substitution will extend the lifetime for PBDTTTz-4 modules like it did for P3HT modules. Three type of PBDTTTz-4 modules were manufactured (Fig 5.19) with the exact same architectures than before except that P3HT was swapped for PBDTTTz-4 in carbon electrodes modules (Fig 5.5 right) and in AgNW modules with or without Ag grid as back electrode (Fig 5.15). No first generation freeOPV were manufactured with PBDTTTz-4 but when first reported, mini roll coated modules (8 cm^2) with the same architecture were studied. [33] The different architectures and their initial performances are given in Table 5.5.

The comparison of the data from the previous report on PBDTTTz-4 with the data acquired during this study (Table 5.5), shows that there is only a small drop in performances when upscaling PBDTTTz-4 modules from 8 to 30 and 57 cm^2.[33] The apparent lower efficiency of AgNW modules is attributed to the challenging coating of the active layer (PBDTTTz-4:PCBM) on top of the hybrid AgNW/ZnO layer. Once again the AgNW modules with only PEDOT:PSS as back electrode underperform the ones with PEDOT:PSS/Ag grid because of the lower conductivity of the back electrode. The PBDTTTz-4 modules were studied under ISOS

conditions like for P3HT in dark (ISOS-D-2, ISOS-D-3), in light (ISOS-L-2, ISOS-L-3) and outdoor (ISOS-O-1 ISOS-O-2).
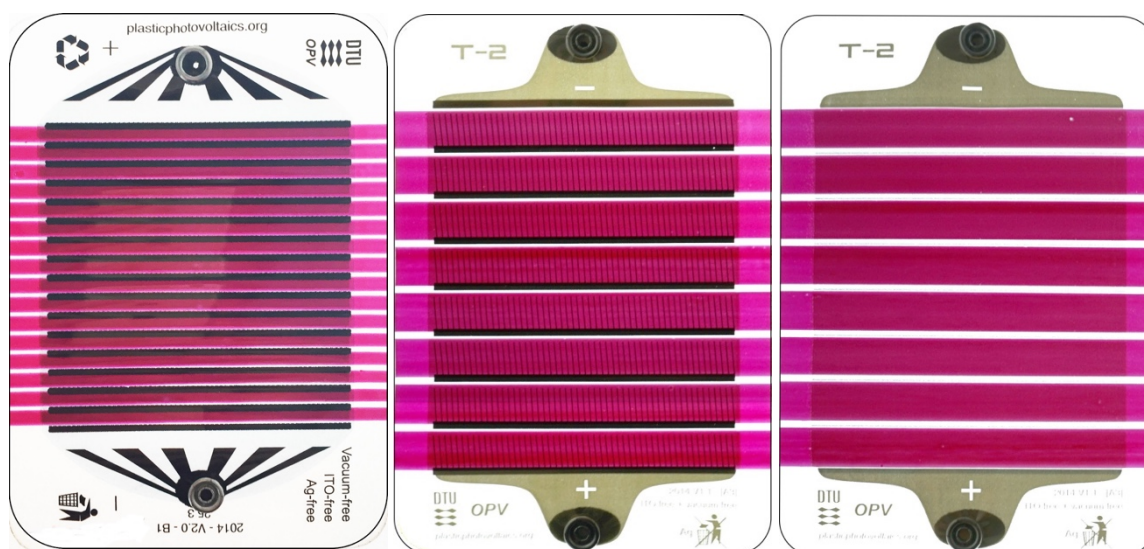

Fig 5.19 – Picture of the three PBDTTTz-4 freeOPV modules: carbon electrode (left), AgNW modules with PEDOT:PSS back electrode (middle) and with PEDOT:PSS back electrode (right). reprinted with permission from reference 34.

Table 5.5 –PBDTTTz-4 modules architecture and their initial performances.

	1st Generation FreeOPV[a]	Carbon FreeOPV	AgNW – back PEDOT:PSS	AgNW – back AG grid	Mini roll coater Ag grid[b]
Front electrode	Flextrode	PEDOT:PSS/ ZnO	AgNW/ZnO	AgNW/ZnO	Flextrode
Active layer	P3HT:PCBM	PBDTTTz-4:PCBM	PBDTTTz-4:PCBM	PBDTTTz-4:PCBM	PBDTTTz-4:PCBM
Back electrode	PEDOT:PSS/Ag grid	PEDOT:PSS/ carbon	PEDOT:PSS	PEDOT:PSS/AG grid	PEDOT:PSS/Ag grid
Active area (cm)	57	30	57	57	8
Voc (V)	4,1 ± 0,3	12,54 ± 0,08	4,89 ± 0,14	6,3 ± 0,3	3,22 ± 0,03
Isc (mA)	40 ± 2	16,4 ± 0,5	37,8 ± 1,6	41 ± 2,2	14,4 ± 0,8
FF (%)	60 ± 4	45 ± 1	31 ± 1,5	42 ± 3,2	50,4 ± 1,45
PCE (%)	1,75 ± 0,06	3,07 ± 0,06	1,01 ± 0,06	1,9 ± 0,2	2,9 ± 0,2

[a] *data extracted with permission from* 6.
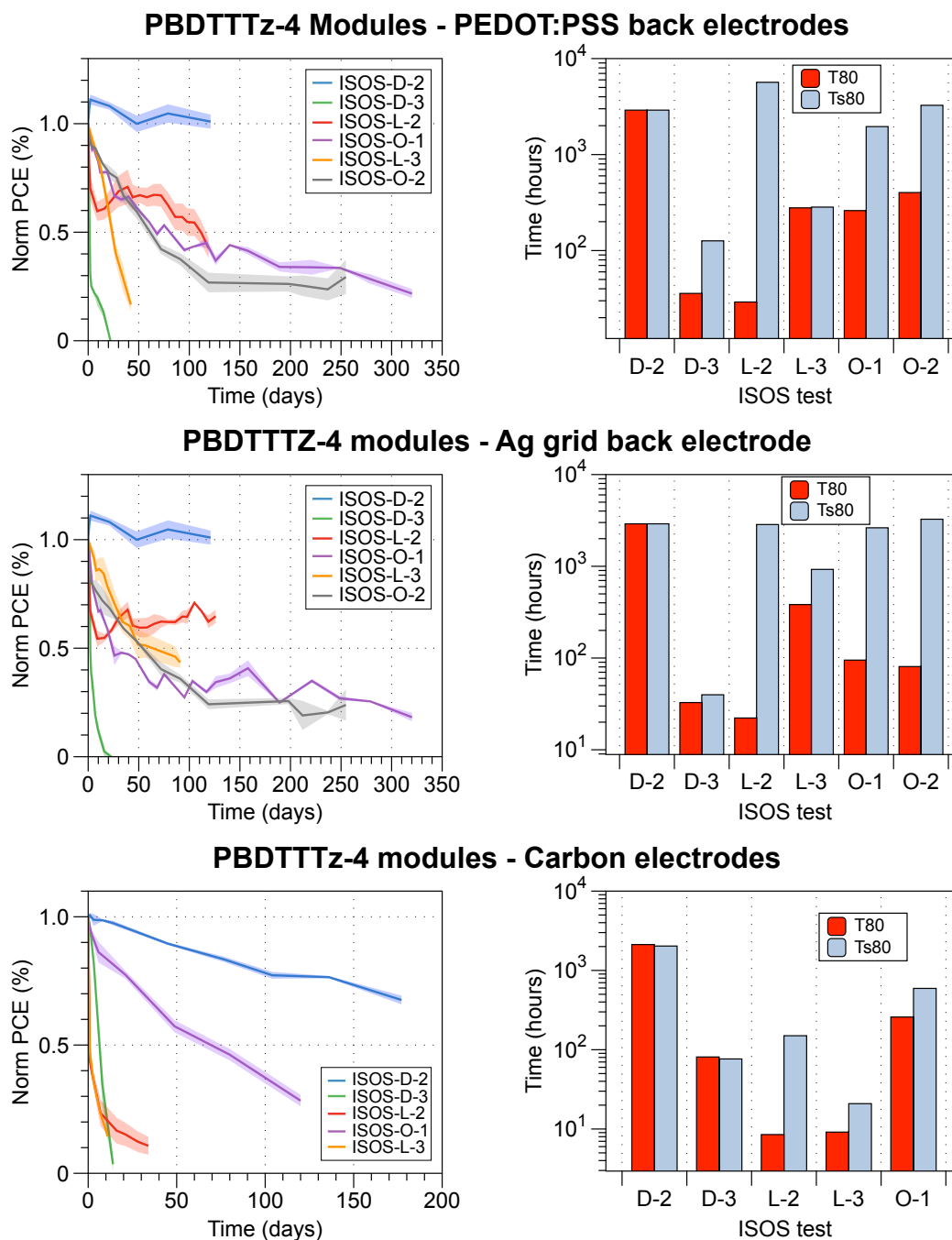[b] *data extracted with permission from* 33.

5.4.1. Lifetime studies

Fig 5.20 – Degradation curves and parameters: (top) AgNW modules with PEDOT:PSS back electrode, (middle) AgNW modules with PEDOT:PSS/Ag grid back electrode, (bottom) Carbon modules. Reprinted with permission from 34.

Dark tests

As expected, under ISOS-D-2 all architectures are stable because of the absence of significant degradation factors. After 3 months, all three module types were above 80% (Fig 5.20) of their initial efficiency. However, the carbon modules degraded linearly to about 70 % of their initial efficiency after 6 months. The AgNW modules did not degrade and retained 100 % of performances during four months of testing. The introduction of humidity in ISOS-D-3 causes fast degradation like for P3HT modules. Surprisingly the carbon modules with two layers of PEDOT:PSS performed better than AgNW modules with a single layer of PEDOT:PSS. The AgNW modules have a T_{80} of 1 day (Fig 5.20) and were fully degraded in 2 weeks of testing. The carbon modules fared better at the beginning with a T_{80} of 3 days (Fig 5.20) but were as well fully degraded after 2 weeks.

Light tests

During ISOS-L-2, the carbon modules were the least stable (Fig 5.20). They degraded by 20% in one week and the degradation continued with no sign of stabilization. After 10 days the carbon modules performances are below 20% of their initial performances. Even though, the AgNW degraded as fast as the carbon modules, they later stabilized around 50 % of their initial efficiency and remained stable for three months. Actually their performances even started going up for a while (Fig 5.20). This effect is attributed to the sintering of the AgNW network.[26] In the later stages of the test, the AgNW modules with PEDOT:PSS back electrode started to slowly decrease but the ones with PEDOT:PSS/Ag grid were stable until the end of the test.

During the other light test, ISOS-L-3, there was a large difference in degradation between the three types of modules (Fig 5.20). The carbon modules degraded the fastest. They reached T_{80} in a few hours and were fully degraded in two weeks. Next, the AgNW modules with only PEDOT:PSS as back electrode degraded to T_{80} in one day and then all the way in 6 weeks. Finally the AgNW modules with the PEDOT:PSS/Ag grid back electrode were the most stable with a T80 of 10 days. Even more, they were still above 50 % of performances after three months.

Outdoor tests

No carbon modules were tested under ISOS-O-2 because no channel was available for monitoring. For the AgNW modules, the degradation curves match for ISOS-O-1 and ISOS-O-2 as expected (Fig 5.20). Both tests were run from July 11th 2014. During ISOS-O-1, the carbon modules degraded at the same rate as AgNW modules (similar T_{80}) but never stabilized compared to the AgNW modules (T_{S80} is one order of magnitude lower for carbon modules). After 3 months outside, the carbon modules had degraded to 30 % of their initial performance. On the other hand, both AgNW module types stabilized around 60 % of their initial performances for six months (Fig 5.20) before degrading slowly.

5.4.2. Bubble degradation

During the light tests, the high temperature generated a new degradation mechanism regardless of the active material (P3HT or PBDTTTz-4). For ISOS-L-3, only the AgNW modules with a Ag grid in the back and the carbon modules presented this degradation. However during ISOS-L-2 the AgNW modules with PEDOT:PSS as back electrode presented the same degradation as well. After some time, bubbles appeared inside the modules (Fig 5.21 left). Contrary to the bubbles reported in the first study of this chapter, these bubbles do not come from the barrier foil but are inside the solar cell stack. The hypothesis is that these bubbles are due to trapped gas in the porous layers of the solar cell. For example, Dam *et al.* reported on the Ag electrode which has a 60% porosity in its volume.[35] The carbon electrode is expected to have a similar porosity. Finally, in the case where there is neither silver nor carbon electrode, the bubbles are linked to trapped gas during encapsulation of the solar cells. When the trapped gas expands upon exposure to elevated temperature, it creates delamination of the solar cell stack. The LBIC picture in Fig 5.21 right shows the absence of contact where the bubbles are present. Preventing this phenomenon would extend the lifetime of the modules under high temperature tests (ISOS-L-2 and L-3). However, this degradation mechanism was not observed during the outdoor tests, meaning that this degradation might not matter much for "real life" applications.
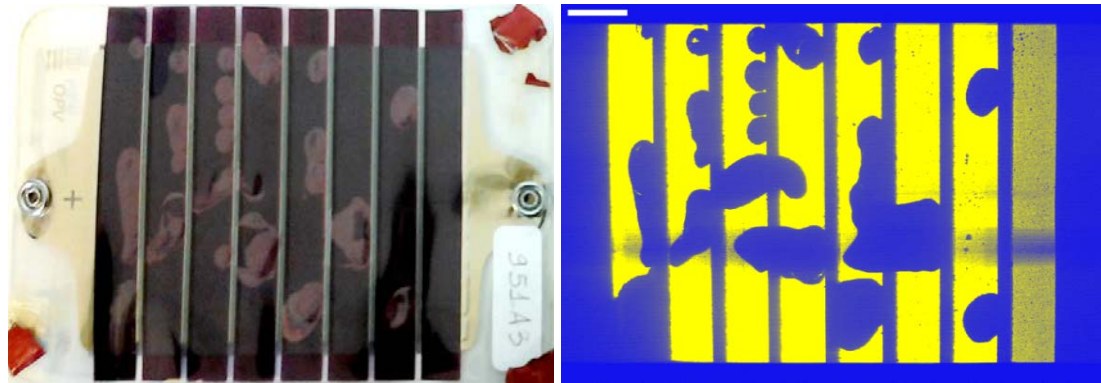
Fig 5.21 – Picture of a AgNW module with PEDOT:PSS/Ag grid back electrode after ISOS-L-3 testing (left). LBIC image of the same module showing delamination where the bubbles appeared (right). Reprinted with permission from reference 34.

5.4.3. Conclusion

Similarly as for P3HT modules, the stability of the PBDTTTz-4 modules under both indoor and outdoor tests, was improved when the front PEDOT:PSS was removed. With the exception of the ISOS-D-3 test where the carbon modules with two layers of PEDOT:PSS were more stable. The reasons for the higher stability of carbon modules in these conditions require further study. Even though the stability of the PBDTTTz-4 modules is improved by removing the front PEDOT:PSS layer, one major issue remains: the stability of these modules is still than for P3HT modules. This means that there is a need to develop a module architecture optimized for PBDTTTz-4 to fully take advantage of the higher initial efficiency.

5.5. Summary & Outlook

The importance of conducting lifetime studies of large scale modules has been demonstrated. Each component of the OPV stack needs to be carefully selected and tailored to ensure long term stability. The use of PEDOT:PSS as charge selective layer is inhibiting lifetimes in the multi years range. The removal of PEDOT:PSS as electron transport layer with a hybrid AgNW/ZnO electrode successfully increased the stability of modules by one order of magnitude. The natural next step is to replace PEDOT:PSS as hole transport layer. Many alternative materials to PEDOT:PSS have been reported (V_2O_5, MoOx, WO_3, NiO….).[36–40] A recent study by Lima *et*

al., showed that roll coated ITO free cells with V2O5 instead of PEDOT:PSS were two times more stable outdoor (ISOS-O-2).[40]

5.6. References

(1)   Krebs, F. C.; Espinosa, N.; Hösel, M.; Søndergaard, R. R.; Jørgensen, M. 25th Anniversary Article: Rise to Power - OPV-Based Solar Parks. *Adv. Mater.* **2014**, *26* (1), 29–39.

(2)   Sommer-Larsen, P.; Jørgensen, M.; Søndergaard, R. R.; Hösel, M.; Krebs, F. C. It Is All in the Pattern-High-Efficiency Power Extraction from Polymer Solar Cells through High-Voltage Serial Connection. *Energy Technol.* **2013**, *1* (1), 15–19.

(3)   Gevorgyan, S. A.; Madsen, M. V.; Roth, B.; Corazza, M.; Hösel, M.; Søndergaard, R. R.; Jørgensen, M.; Krebs, F. C. Lifetime of Organic Photovoltaics: Status and Predictions. *Adv. Energy Mater.* **2016**, *6* (2), 1501208.

(4)   Brabec, C. J.; Hauch, J. A.; Schilinsky, P.; Waldauf, C. Production Aspects of Organic Photovoltaics and Commercialization of Devices. *MRS Bull.* **2005**, *30*, 50–52.

(5)   Roth, B.; dos Reis Benatto, G. A.; Corazza, M.; Søndergaard, R. R.; Gevorgyan, S. a.; Jørgensen, M.; Krebs, F. C. The Critical Choice of PEDOT:PSS Additives for Long Term Stability of Roll-to-Roll Processed OPVs. *Adv. Energy Mater.* **2015**, *5* (9).

(6)   Corazza, M.; Krebs, F. C.; Gevorgyan, S. a. Predicting, Categorizing and Intercomparing the Lifetime of OPVs for Different Ageing Tests. *Sol. Energy Mater. Sol. Cells* **2014**, *130*, 99–106.

(7)   Hösel, M.; Søndergaard, R. R.; Jørgensen, M.; Krebs, F. C. Failure Modes and Fast Repair Procedures in High Voltage Organic Solar Cell Installations. *Adv. Energy Mater.* **2014**, *4* (7), 1301625.

(8)   Krebs, F. C.; Hösel, M.; Corazza, M.; Roth, B.; Madsen, M. V.; Gevorgyan, S. A.; Søndergaard, R. R.; Karg, D.; Jørgensen, M. Freely Available OPV-The Fast Way to Progress. *Energy Technol.* **2013**, *1* (7), 378–381.

(9)   Jørgensen, M.; Norrman, K.; Krebs, F. C. Stability/degradation of Polymer Solar Cells. *Sol. Energy Mater. Sol. Cells* **2008**, *92* (7), 686–714.

(10)   Cros, S.; de Bettignies, R.; Berson, S.; Bailly, S.; Maisse, P.; Lemaitre, N.; Guillerez, S. Definition of Encapsulation Barrier Requirements: A Method Applied to Organic Solar Cells. *Sol. Energy Mater. Sol. Cells* **2011**, *95*, S65–S69.

(11)   dos Reis Benatto, G. A.; Roth, B.; Madsen, M. V.; Hösel, M.; Søndergaard, R. R.; Jørgensen, M.; Krebs, F. C. Carbon: The Ultimate Electrode Choice for Widely Distributed Polymer Solar Cells. *Adv. Energy Mater.* **2014**, *4* (15), 1400732.

(12)   Tromholt, T.; Madsen, M. V.; Carlé, J. E.; Helgesen, M.; Krebs, F. C. Photochemical Stability of Conjugated Polymers, Electron Acceptors and Blends for Polymer Solar Cells Resolved in Terms of Film Thickness and Absorbance. *J. Mater. Chem.* **2012**, *22* (15), 7592–7601.

(13)   Manceau, M.; Bundgaard, E.; Carlé, J. E.; Hagemann, O.; Helgesen, M.; Søndergaard, R.; Jørgensen, M.; Krebs, F. C. Photochemical Stability of π-Conjugated Polymers for Polymer Solar Cells: A Rule of Thumb. *J. Mater. Chem.* **2011**, *21* (12), 4132–4141.

(14)   Kawano, K.; Pacios, R.; Poplavskyy, D.; Nelson, J.; Bradley, D. D. C. C.; Durrant, J. R. Degradation of Organic Solar Cells due to Air Exposure. *Sol. Energy Mater. Sol. Cells* **2006**, *90* (20), 3520–3530.

(15)   Cao, H.; He, W.; Mao, Y.; Lin, X.; Ishikawa, K.; Dickerson, J. H.; Hess, W. P. Recent Progress in Degradation and Stabilization of Organic Solar Cells. *Journal of Power Sources*. Elsevier B.V 2014, pp 168–183.

(16)   Nardes, a. M.; Kemerink, M.; de Kok, M. M.; Vinken, E.; Maturova, K.; Janssen, R. a J. Conductivity, Work Function, and Environmental Stability of PEDOT:PSS Thin Films Treated with Sorbitol. *Org. Electron. physics, Mater. Appl.* **2008**, *9* (5), 727–734.

(17) Grossiord, N.; Kroon, J. M.; Andriessen, R.; Blom, P. W. M. Degradation Mechanisms in Organic Photovoltaic Devices. *Org. Electron.* **2012**, *13* (3), 432–456.

(18) Voroshazi, E.; Verreet, B.; Buri, A.; Müller, R.; Di Nuzzo, D.; Heremans, P. Influence of Cathode Oxidation via the Hole Extraction Layer in Polymer:fullerene Solar Cells. *Org. Electron.* **2011**, *12* (5), 736–744.

(19) Groenendaal, L.; Jonas, F.; Freitag, D.; Pielartzik, H.; Reynolds, J. R. Poly(3,4-Ethylenedioxythiophene) and Its Derivatives: Past, Present, and Future. *Adv. Mater.* **2000**, *12* (7), 481–494.

(20) Ouyang, J.; Chu, C.-W.; Chen, F.-C.; Xu, Q.; Yang, Y. High-Conductivity Poly(3,4-ethylenedioxythiophene):Poly(styrene Sulfonate) Film and Its Application in Polymer Optoelectronic Devices. *Adv. Funct. Mater.* **2005**, *15* (2), 203–208.

(21) Dimitriev, O. P.; Grinko, D. A.; Noskov, Y. V.; Ogurtsov, N. A.; Pud, A. A. PEDOT:PSS films—Effect of Organic Solvent Additives and Annealing on the Film Conductivity. *Synth. Met.* **2009**, *159* (21-22), 2237–2239.

(22) Alemu Mengistie, D.; Wang, P.-C.; Chu, C.-W. Effect of Molecular Weight of Additives on the Conductivity of PEDOT:PSS and Efficiency for ITO-Free Organic Solar Cells. *J. Mater. Chem. A* **2013**, *1* (34), 9907–9915.

(23) Reese, M. O.; Gevorgyan, S. a.; Jørgensen, M.; Bundgaard, E.; Kurtz, S. R.; Ginley, D. S.; Olson, D. C.; Lloyd, M. T.; Morvillo, P.; Katz, E. a.; Elschner, A.; Haillant, O.; Currier, T. R.; Shrotriya, V.; Hermenau, M.; Riede, M.; R. Kirov, K.; Trimmel, G.; Rath, T.; Inganäs, O.; Zhang, F.; Andersson, M.; Tvingstedt, K.; Lira-Cantu, M.; Laird, D.; McGuiness, C.; Gowrisanker, S. (Jimmy); Pannone, M.; Xiao, M.; Hauch, J.; Steim, R.; DeLongchamp, D. M.; Rösch, R.; Hoppe, H.; Espinosa, N.; Urbina, A.; Yaman-Uzunoglu, G.; Bonekamp, J.-B.; van Breemen, A. J. J. M.; Girotto, C.; Voroshazi, E.; Krebs, F. C. Consensus Stability Testing Protocols for Organic Photovoltaic Materials and Devices. *Sol. Energy Mater. Sol. Cells* **2011**, *95* (5), 1253–1267.

(24) Hösel, M.; Angmo, D.; Søndergaard, R. R.; dos Reis Benatto, G. a.; Carlé, J. E.; Jørgensen, M.; Krebs, F. C. High-Volume Processed, ITO-Free Superstrates and Substrates for Roll-to-Roll Development of Organic Electronics. *Adv. Sci.* **2014**, *1* (1).

(25) Nam, S.; Song, M.; Kim, D.-H.; Cho, B.; Lee, H. M.; Kwon, J.-D.; Park, S.-G.; Nam, K.-S.; Jeong, Y.; Kwon, S.-H.; Park, Y. C.; Jin, S.-H.; Kang, J.-W.; Jo, S.; Kim, C. S. Ultrasmooth, Extremely Deformable and Shape Recoverable Ag Nanowire Embedded Transparent Electrode. *Sci. Rep.* **2014**, *4*, 1–7.

(26) Mayousse, C.; Celle, C.; Fraczkiewicz, A.; Simonato, J.-P. Stability of Silver Nanowire Based Electrodes under Environmental and Electrical Stresses. *Nanoscale* **2015**, *7* (5), 2107–2115.

(27) dos Reis Benatto, G. A.; Roth, B.; Corazza, M.; Søndergaard, R. R.; Gevorgyan, S. A.; Jørgensen, M.; Krebs, F. C. Roll-to-Roll Printed Silver Nanowires for Increased Stability of Flexible ITO-Free Organic Solar Cell Modules. *Nanoscale* **2016**, *8* (1), 318–326.

(28) Gevorgyan, S. a.; Madsen, M. V.; Dam, H. F.; Jørgensen, M.; Fell, C. J.; Anderson, K. F.; Duck, B. C.; Mescheloff, A.; Katz, E. a.; Elschner, A.; Roesch, R.; Hoppe, H.; Hermenau, M.; Riede, M.; Krebs, F. C. Interlaboratory Outdoor Stability Studies of Flexible Roll-to-Roll Coated Organic Photovoltaic Modules: Stability over 10,000h. *Sol. Energy Mater. Sol. Cells* **2013**, *116*, 187–196.

(29) Jørgensen, M.; Carlé, J. E.; Søndergaard, R. R.; Lauritzen, M.; Dagnæs-Hansen, N. A.; Byskov, S. L.; Andersen, T. R.; Larsen-Olsen, T. T.; Böttiger, A. P. L.; Andreasen, B.; Fu, L.; Zuo, L.; Liu, Y.; Bundgaard, E.; Zhan, X.; Chen, H.; Krebs, F. C. The State of Organic Solar cells—A Meta Analysis. *Sol. Energy Mater. Sol. Cells* **2013**, *119*, 84–93.

(30) Dang, M. T.; Hirsch, L.; Wantz, G. P3HT:PCBM, Best Seller in Polymer Photovoltaic Research. *Adv.*

Mater. **2011**, *23* (31), 3597–3602.

(31)   Bundgaard, E.; Hagemann, O.; Manceau, M.; Jørgensen, M.; Krebs, F. C. Low Band Gap Polymers for Roll-to-Roll Coated Polymer Solar Cells. *Macromolecules* **2010**, *43* (19), 8115–8120.

(32)   Bundgaard, E.; Krebs, F. C. Low Band Gap Polymers for Organic Photovoltaics. *Sol. Energy Mater. Sol. Cells* **2007**, *91* (11), 954–985.

(33)   Carlé, J. E.; Helgesen, M.; Madsen, M. V.; Bundgaard, E.; Krebs, F. C.; Carle, J. E.; Helgesen, M.; Madsen, M. V.; Bundgaard, E.; Krebs, F. C. Upscaling from Single Cells to Modules – Fabrication of Vacuum- and ITO-Free Polymer Solar Cells on Flexible Substrates with Long Lifetime. *J. Mater. Chem. C* **2014**, *2* (7), 1290–1297.

(34)   Roth, B.; A. dos Reis Benatto, G.; Corazza, M.; Carlé, J. E.; Helgesen, M.; Gevorgyan, S. a.; Jørgensen, M.; Søndergaard, R. R.; Krebs, F. C. Improving the Operational Stability of PBDTTTz-4 Polymer Solar Cells Modules by Electrode Modification. *Adv. Eng. Mater.* **2015**, 1–7.

(35)   Dam, H. F.; Andersen, T. R.; Pedersen, E. B. L.; Thydén, K. T. S.; Helgesen, M.; Carlé, J. E.; Jørgensen, P. S.; Reinhardt, J.; Søndergaard, R. R.; Jørgensen, M.; Bundgaard, E.; Krebs, F. C.; Andreasen, J. W. Enabling Flexible Polymer Tandem Solar Cells by 3D Ptychographic Imaging. *Adv. Energy Mater.* **2015**, *5* (1).

(36)   Manders, J. R.; Tsang, S.-W.; Hartel, M. J.; Lai, T.-H.; Chen, S.; Amb, C. M.; Reynolds, J. R.; So, F. Solution-Processed Nickel Oxide Hole Transport Layers in High Efficiency Polymer Photovoltaic Cells. *Adv. Funct. Mater.* **2013**, *23* (23), 2993–3001.

(37)   Lu, L.; Xu, T.; Jung, I. H.; Yu, L. Match the Interfacial Energy Levels between Hole Transport Layer and Donor Polymer To Achieve High Solar Cell Performance. *J. Phys. Chem. C* **2014**, *118* (40), 22834–22839.

(38)   Tan, Z.; Li, L.; Cui, C.; Ding, Y.; Xu, Q.; Li, S.; Qian, D.; Li, Y. Solution-Processed Tungsten Oxide as an Effective Anode Buffer Layer for High-Performance Polymer Solar Cells. *J. Phys. Chem. C* **2012**, *116* (35), 18626–18632.

(39)   Lee, Y.-J.; Yi, J.; Gao, G. F.; Koerner, H.; Park, K.; Wang, J.; Luo, K.; Vaia, R. A.; Hsu, J. W. P. Low-Temperature Solution-Processed Molybdenum Oxide Nanoparticle Hole Transport Layers for Organic Photovoltaic Devices. *Adv. Energy Mater.* **2012**, *2* (10), 1193–1197.

(40)   Lima, F. A. S.; Beliatis, M. J.; Roth, B.; Andersen, T. R.; Bortoti, A.; Reyna, Y.; Castro, E.; Vasconcelos, I. F.; Gevorgyan, S. A.; Krebs, F. C.; Lira-Cantu, M. Flexible ITO-Free Organic Solar Cells Applying Aqueous Solution-Processed V2O5 Hole Transport Layer: An Outdoor Stability Study. *APL Mater.* **2016**, *4* (2), 026104.

Conclusion

All along the work presented in this thesis, the complexity of OPV degradation is apparent. Despite the many scientific reports on the subject, the multiple factors and mechanisms of degradation are still not fully apprehended. The meta-analysis of hundreds of reports on OPV stability presented in chapter 3 had as ambition to acquire a better understanding of the field. This analysis yielded some meaningful trends. The stability of the photoactive layer is less critical when the final devices is encapsulated. This observation was confirmed during the study of CN-P3HT. Even thought the photochemical stability of P3HT is improved by incorporation of cyano group in the polymer backbone, cells with pristine P3HT are still more stable.

Another observation from the meta-analysis is the detrimental effect of PEDOT:PSS on long-term stability of OPV cells. Lifetime studies of freeOPV modules showed that even the formulation of the PEDOT:PSS, in this case the high boiling additives, can have a significant impact on stability. Replacing DMSO by ethylene glycol could extend the lifetime outdoor of OPV modules by a few years. A first step to replace PEDOT:PSS was made by using a new transparent electrode made of a single hybrid AgNW/ZnO to manufacture freeOPV modules without PEDOT:PSS as electron transport layer. The lifetime of these modules outdoor was extended 10 fold confirming that replacing PEDOT:PSS is necessary for long-term stability.

The next step to continue the lifetime studies presented in this thesis would be to replace the PEDOT:PSS as hole transport layer. Many alternative materials have already been used to prepare small lab scale cells (V2O5, MoOx, WO3, NiO....).

Most of the large scale modules studied for the work presented in this thesis were prepared with P3HT as donor material which efficiency is limited to 3%. Replacing P3HT by the high efficiency polymer PBDTTTz-4 did not yield the expected results. The freeOPV modules with PBDTTTz-4 had an efficiency around 2% (compared to 3.4% for small scale devices) and were less stable than P3HT modules.

This perfectly illustrates the extreme difficulty to find and develop high efficiency polymers compatible with large scale OPV modules prepared by roll-to-roll (R2R). To undertake this

challenge a library of 104 low band-gap polymer was screened toward their suitability for R2R manufacturing. Thirteen polymers were found to outperform P3HT and should be further developed for R2R OPV modules.

Finally, the thermomechanical stability of the same library of low band gap polymers was studied. Most polymers were found to have a stiffness equivalent to P3HT but suffered from a brittle behavior. During the study two trends were identified. Fused rings in the backbone of the polymers tend to increase the stiffness and lower the ductility of the pristine polymer films. Long and branched side-chains in the molecular structure have the opposite effect. They improve the ductility and lower the stiffness of the material. A merit factor was suggested to identify polymers combining high electrical performances and good mechanical properties. The hope behind this study was to lay the ground work for a better understanding and how the molecular structure of one polymer determines its thermomechanical behavior and to generate interest in computational and microstructure studies to link molecular structure and mechanical performances. Future work in this field could provide a deeper understanding of the relationship between mechanical and electronic properties which would speed up the development of promising polymers for large scale R2R manufacturing.

Appendix

The work presented in this thesis is based on the following publications:

Appendix A. <u>B. Roth</u>, R. R. Søndergaard, F. C. Krebs, "Roll-to-roll printing and coating techniques for manufacturing large-area flexible organic electronics", *Handbook of Flexible Organic Electronics: Materials, Manufacturing and Applications,* (ed. Logothetidis, S.) pp 171-192 (2014)

Appendix B. <u>B. Roth</u>, A. E. Rudenko, B. C. Thompson, F. C. Krebs, "Photochemical stability of random poly(3-hexylthiophene-co-3-cyanothiophene) and its use in roll coated ITO-free organic photovoltaics. *J. Photonics Energy* **5**, 057205 (2014)

Appendix C. <u>B. Roth</u>, G. A. dos Reis Benatto, M. Corazza, R. R. Søndergaard, S. A. Gevorgyan, M. Jørgensen, F. C. Krebs, "The Critical Choice of PEDOT:PSS Additives for Long Term Stability of Roll-to-Roll Processed OPVs", *Adv. Energy Mater.* **5**, (2015)

Appendix D. <u>B. Roth</u>, G. A dos Reis Benatto, M. Corazza, J. E. Carlé, M. Helgesen, S. A. Gevorgyan, M. Jørgensen, R. R Søndergaard, F. C Krebs, "Improving the Operational Stability of PBDTTTz-4 Polymer Solar Cells Modules by Electrode Modification", *Adv. Eng. Mater.* (2015). doi:10.1002/adem.201500361

Appendix E. <u>B. Roth</u>, S. Savagatrup, N. V. De Los Santos, O. Hagemann, J. E. Carlé, M. Helgesen, F. Livi, E. Bundgaard, R. R. Søndergaard, F. C. Krebs, D. J. Lipomi, "Molecular Design Rules for Mechanical Stability of Organic Solar Cells Derived from a Library of Low-Bandgap Polymers", *Chem. Mater.* (2016) doi:10.1021/acs.chemmater.6b00525

Appendix F. F. C. Krebs, M. Hösel, M. Corazza, <u>B. Roth</u>, M. V. Madsen, S. A. Gevorgyan, R. R. Søndergaard, D. Karg, M. Jørgensen, "Freely available OPV-The fast way to progress", *Energy Technol.* **1,** 378–381 (2013).

Appendix G. G. A. dos Reis Benatto, <u>B. Roth</u>, M. V. Madsen, M. Hösel, R. R. Søndergaard, M. Jørgensen, F. C. Krebs, "Carbon: The Ultimate Electrode Choice for Widely Distributed Polymer Solar Cells", *Adv. Energy Mater.* **4**, (2014).

Appendix H. E. Bundgaard, F. Livi, O. Hagemann, J. E. Carlé, M. Helgesen, I. M. Heckler, N. K. Zawacka, D. Angmo, T. T. Larsen-Olsen, G. A. dos Reis Benatto, <u>B. Roth</u>, M. V. Madsen, M. R. Andersson, M. Jørgensen, R. R. Søndergaard, F. C. Krebs, "Matrix Organization and Merit Factor Evaluation as a Method to Address the Challenge of Finding a Polymer Material for Roll Coated Polymer Solar Cells", *Adv. Energy Mater.* **5**, (2015).

Appendix I. S. A. Gevorgyan, M. V. Madsen, <u>B. Roth</u>, M. Corazza, M. Hösel, R. R. Søndergaard, M. Jørgensen, F. C. Krebs, "Lifetime of Organic Photovoltaics: Status and Predictions", *Adv. Energy Mater.* **6**, (2016).

Appendix J. G. A. dos Reis Benatto, <u>B. Roth</u>, M. Corazza, R. R. Søndergaard, S. A. Gevorgyan, M.I Jørgensen, F. C. Krebs, "Roll-to-roll printed silver nanowires for increased stability of flexible ITO-free organic solar cell modules", *Nanoscale* **8**, 318–326 (2016)

The following publications were authored during my Ph.D but not used in the redaction of this thesis:

Appendix K. F. Livi, R. R Søndergaard, T. R. Andersen, <u>B. Roth</u>, S. Gevorgyan, H. F. Dam, J. E. Carlé, M. Helgesen, G. D. Spyropoulos, J. Adams, T. Ameri, C. J. Brabec, M. Legros, N. Lemaitre, S. Berny, O. R. Lozman, S. Schumann, A. Scheel, P. Apilo, M. Vilkman, E. Bundgaard, F. C. Krebs, "Round-Robin Studies on Roll-Processed ITO-free

Organic Tandem Solar Cells Combined with Inter-Laboratory Stability Studies", *Energy Technol.* **3**, 423–427 (2015).

Appendix L. F. A. S. Lima, M. J. Beliatis, <u>B. Roth</u>, T. R. Andersen, A. Bortoti, Y. Reyna, E. Castro, I. F. Vasconcelos, S. A. Gevorgyan, F. C. Krebs, M. Lira-Cantu, "Flexible ITO-free organic solar cells applying aqueous solution-processed V2O5 hole transport layer: An outdoor stability study", *APL Mater.* **4**, 026104 (2016)

Roll-to-roll printing and coating techniques for manufacturing large-area flexible organic electronics

7

B. Roth, R.R. Søndergaard, F.C. Krebs
Technical University of Denmark, Roskilde, Denmark

7.1 Introduction

The need for electronics that can be processed at low cost and very high speeds has created the potential for new technologies based on organic materials to emerge, as they can be developed using solution processing. Organic photovoltaics (OPVs), organic thin film transistors (OTFTs), organic light-emitting diodes (OLEDs) and electrochromic devices (ECs) are all examples of such technologies. Most of them have now reached a maturity stage at the laboratory level, where upscaling and faster processing becomes the next development phase. In that context, roll-to-roll (R2R) processing on flexible substrates has always been the final goal for such upscaling, as it represents the ultimate combination of fast processing and cheap substrates. So far, only a few examples of actual transfer to R2R processing have been carried out, and this chapter aims at introducing some of the different R2R printing and coating techniques that have so far been employed for the preparation of organic electronics.

Going from small glass substrates to large-area R2R processing is not as straightforward as one would think. Some of the most common techniques used in the preparation of organic electronics on a laboratory scale, such as spin-coating and metal evaporation, are not compatible with high-throughput R2R production. R2R metal evaporation can be carried out in principle, but it requires a vacuum, which is time-consuming and comes with a high cost that does not comply with the philosophy of low-cost technologies. Consequently, silver is presently the only real candidate for metal electrode deposition by R2R, as silver inks are uniquely available commercially in forms that can be both coated and printed. Another issue that needs consideration in the long term upscaling process is the environmental impact of production of large volumes. In that respect the solvents generally used for processing of small-scale electronics constitutes a serious problem in the transfer, as they are generally toxic, carcinogenic or otherwise harmful. It is of course possible to perform R2R processing from such solvents. However, when envisaging for example the OPV technology in relation to energy production and the sheer volumes of solvents needed for such, it is evident that only water or other benign solvents can be used.

Doing otherwise will simply be too expensive if precautions has to be taken towards ensuring a healthy working environment and avoiding damage to the surrounding ecosystems.

Such changes in processing methods, materials and processing solvents evidently have their consequences and transfer to large area basically requires re-optimization of every parameter taken into account in preparation of a device — parameters that took years to refine in the laboratory. Compared to small-scale devices, little focus has been put on actual large-scale processing of organic electronics, and experience with, and understanding of, R2R processing in this context is limited to very few people — especially when processing at high speeds. A clear indication of the difficulty of such a transfer is observed from the current status of large-area OPV technology, probably the most mature of the technologies mentioned in this chapter with respect to R2R progress: among all the high-performing low-band-gap polymers that have proven their worth in small-scale devices, only a tiny fraction have outperformed the old P3HT polymer when it comes to larger areas - but it is not for lack of trying.

Because organic electronics can be processed from solution, there are a number of existing R2R methods suitable for processing them on a larger scale. Roughly two kinds of deposition methods have proven useful in the preparation of organic electronics, noncontact coating techniques and contact printing techniques (except for ink-jet printing). Printing allows two-dimensional patterning, whereas coating at best allows for one-dimensional patterning and is mostly used for layer deposition over large areas.

The following chapter is a nonexhaustive review of roll-to-roll deposition techniques that are of interest for high-throughput, cheap preparation of flexible electronics. The chapter will also include references to R2R-compatible reports on organic electronics in order to broaden the perspective.

7.2   Printing techniques

Roll-to-roll printing techniques are all contact methods, with the exception of ink-jet printing where the name may be misleading, as it is not a 'true' printing technique. Generally, printing techniques involve a pattern transfer from a solid carrier onto a substrate by physical contact resulting in a two-dimensional motif.

7.2.1   Screen printing

In screen printing the ink is pushed through the open area of an otherwise solid mesh with the help of a squeegee. high-viscosity inks with thixotropic (shear thinning) properties are required for this kind of printing, as low-viscosity inks will simply run through the screen by gravity. The printed pattern is defined by the screen's open area and thickness as well as ink viscosity. The wet-layer thickness is therefore usually high (10–500 μm). Two existing screen-printing methods are suitable for R2R: flatbed screen printing and rotary screen printing. Illustrations of the two techniques are shown in Figure 7.1 and Figure 7.2.
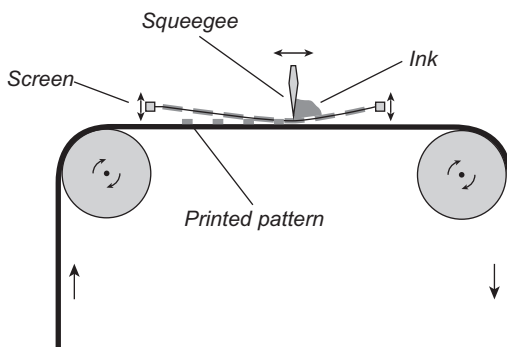
Flat bed screen printing

Figure 7.1 Illustration of the flatbed screen-printing principle.
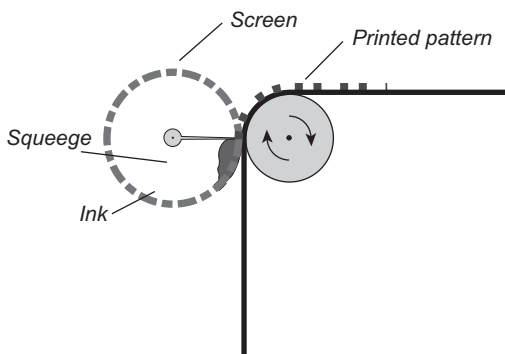
Rotary screen printing

Figure 7.2 Illustration of the rotary screen-printing principle.

Albeit flatbed screen printing is a stepwise process, it has been successfully adapted to R2R. First, the mesh is pressed into contact with the web. Then a squeegee is swept across the screen, forcing the ink through the mesh's open area and transferring the printing pattern on to the substrate. Finally, the screen is raised and the web is moved forward — and so on. This method allows the printing on large areas up to 10 m². However, the ink is left in contact with the ambient and factors such as solvent evaporation can affect the printing process.

In the case of rotary screen printing, the screen is bent into a cylinder shape. This cylinder is rotating at the same rate as the web, making rotary screen printing a fully R2R process that allows speeds over 100 m/min opposed to 0—35 m/min for flatbed screen printing. The ink is situated inside the cylinder and is therefore less exposed to the surroundings. The squeegee (also inside the screen) is placed in a stationary

position and forces the ink through the mesh as the screen rotates, resulting in a continuous printing of the pattern at each cylinder rotation.

Although rotary screen printing gives better edge definition/resolution, the screen is significantly more expensive than the flatbed analogue and more difficult to clean because of its limited access. Setting up and starting a multilayer screen print process is also more challenging in the rotary case, but more reliable once running, making rotary screen printing more suitable for large-scale processes. Flatbed screen printing, on the other hand, is the go-to technique for small-scale lab experiments.

For OPVs, screen printing has so far mainly been used to print electrodes (Amb et al., 2012; Angmo, Hösel, & Krebs, 2012; Bundgaard, Hagemann, Manceau, Jørgensen, & Krebs, 2010; Dam & Krebs, 2012; Galagan, Rubingh, et al., 2011; Helgesen et al., 2012; Krebs, Fyenbo, & Jørgensen, 2010; Krebs et al., 2011; Krebs, Gevorgyan, & Alstrup, 2009; Krebs, Tromholt, & Jørgensen, 2010; Manceau, Angmo, Jørgensen, & Krebs, 2011; Yu et al., 2012) because it gives a thick silver layer ensuring high conductivity (Figure 7.3 shows an example of flatbed-screen-printed silver back electrodes). Some cases where PEDOT:PSS (Espinosa et al., 2013; Hösel, Søndergaard, Jørgensen, & Krebs, 2013; Krebs, 2009; Krebs, Jørgensen, et al., 2009; Sommer-Larsen, Jørgensen, Søndergaard, Hösel, & Krebs, 2013) (see rotary screen printing of PEDOT:PSS in Figure 7.4) and/or the active layer (Krebs, Jørgensen, et al., 2009; Zhang, Chae, & Cho, 2009) were printed using screen printing, have also been reported.

Screen printing has also been used to print electrodes for OLEDs and OTFTs. Ryu et al. have prepared an active matrix organic light-emitting diode (AMOLED) using screen printing (Ryu, Kim, Jeong, & Song, 2013). In the AMOLED, they prepared the OTFT's silver gate electrodes, as well as the scan bus lines of the panel, by screen printing silver nanoparticle ink on the full surface of the device followed by photolithography and etching to obtain the desired pattern.

The technology has also been used to print the emitting layer in OLEDs. Lee et al. screen-printed a green-emitting layer (Lee, Choi, Chae, Chung, & Cho, 2008) based on

Figure 7.3 Flatbed screen-printing of silver top electrodes: The squeegee is sweeping across the screen. The printed electrodes can be observed in the lower left part of the picture.
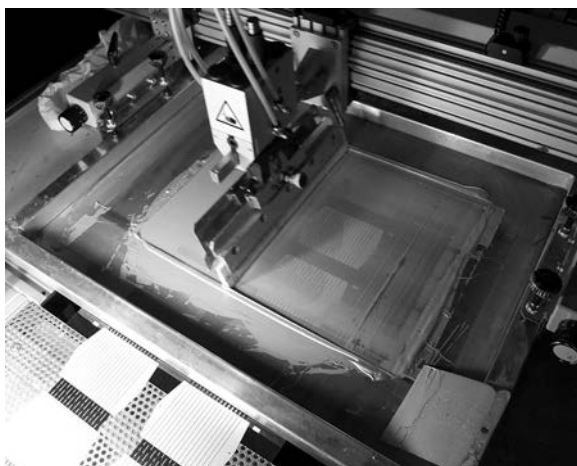
Figure 7.4 Rotary screen-printing of PEDOT:PSS, the printing pattern is visible on the screen (top of the picture).

Ir(ppy)$_3$ (a widely used green emitter) mixed with poly(N-vinyl carbazole) (PVK) as polymer host, 2-(4-biphenylyl)-5-(4-*tert*-butylphenyl)-1,3,4-oxadiazole (PBD) as electron-transporting materials and N,N-Di(naphthalene-1-yl)-N,N-diphenyl-benzidine (α-NPD) as hole-transporting material. The screen-printed layers on indium tin oxide (ITO) glass substrate are shown in Figure 7.5.

Finally, Verilhac et al. have screen-printed a polytriarylamine as the P-channel semiconductor of OTFTs (Verilhac et al., 2010).

7.2.2   Flexoprinting

In flexoprinting, the contact and transfer of the ink is made between a soft printing-plate cylinder and the substrate. The cylinder is usually made of rubber or a photo-polymer, where the printing pattern stands in relief like a stamp (an example of a
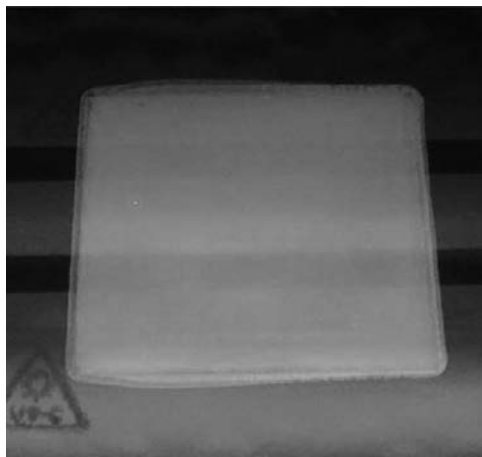

Figure 7.5 Photograph showing the screen-printed green-emissive layer (the bright square − colours are not shown) on patterned ITO substrate for OLED preparation.
Reproduced from Lee et al. (2008) with the permission from Elsevier.

Figure 7.6 The printing cylinder with the relief carrying the ink (in this case a silver paste) during printing. The final printed pattern on the web can be observed in the bottom part of the picture.

patterned printing plate cylinder can be seen in the upper part of the picture in Figure 7.6). The cylinder shape ensures R2R compatibility. A ceramic anilox cylinder provides the inking of the printing cylinder through micro cavities embedded in its surface. The printed-layer thickness is directly linked to the volume of the cavities in the anilox roll in a process where ink is transferred through simple surface tension forces when the printing plate and the anilox are touching. The anilox cylinder itself is often supplied with ink by a fountain roller partially dipped in an ink bath. A doctor blade is used to doff off any excess ink on the anilox roll ensuring that only the cavities are filled with ink. It is also possible to use a chambered-doctor-blade system to avoid solvent evaporation. The process is illustrated in Figure 7.7.

Flexoprinting is quite new to the field of organic electronics, and only a few examples have been reported (Hübler et al., 2011; Krebs, Fyenbo, et al., 2010; Søndergaard, Hösel, Jørgensen, & Krebs, 2013; Yu et al., 2012). Søndergaard et al. have made ITO-free ECs by using flexoprinting to print a hexagonal silver grid on a flexible

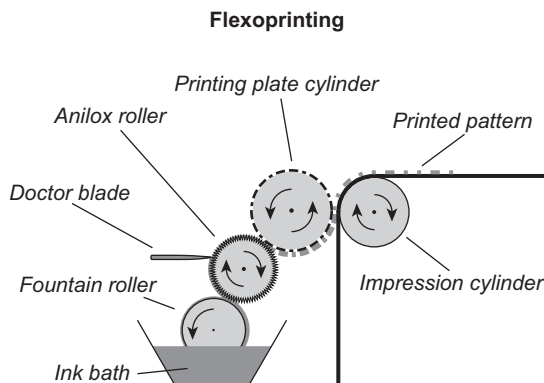**Flexoprinting**

Figure 7.7 Illustration of the flexoprinting principle.

substrate (Søndergaard et al., 2013) and flexoprinted fine silver grids (<50 μm) has also proven suitable for replacement of ITO in OPVs (Yu et al., 2012). For OPVs, flexo-printing has furthermore been used to print PEDOT:PSS (Hübler et al., 2011) as well as to deposit a wetting agent on the active layer (Krebs, Fyenbo, et al., 2010) and for OTFTs it has been used to print an insulator and the gates (Huebler et al., 2007).

7.2.3   Gravure printing

Gravure printing is a widely used processing method often used to print large volumes of magazines and catalogues. Opposed to flexoprinting, the ink in gravure printing is transferred from carved micro cavities and not from a relief. These cavities, embedded in the printing cylinder, form the printing pattern. A second softer impression cylinder pushes the web against the primary printing cylinder and the ink is transferred from the cavities to the web through matching surface energies of the ink and substrate. The printing cylinder is partially immersed in an ink bath and similar to the anilox in flexo-printing a doctor blade is used to remove any excess ink from the printing cylinder leaving ink only in the cavities (operating principle is shown in Figure 7.8). As for flexoprinting it is also possible to use a chambered doctor blade. Gravure printing is highly dependent of ink viscosity, substrate speeds as well as the pressure applied by the impression roller and great care is therefore required in the choosing of process-ing conditions and ink formulation. However, the process is suitable for low-viscosity ink and high printing rates up to 15 m/s can be achieved.

Gravure printing has been used on several occasions to prepare OTFTs. Hambsch et al. printed 50.000 transistors using only gravure printing with a yield of 75% (Hambsch et al., 2010). Other reports include printing of the semiconductor layer of OTFTs (Huebler et al., 2007; Verilhac et al., 2010; Voigt et al., 2010; Vornbrock, Sung, Kang, Kitsomboonloha, & Subramanian, 2010), as well as silver gate electrodes (Voigt et al., 2010; Vornbrock et al., 2010) and insulators (Huebler et al., 2007; Voigt et al., 2010; Vornbrock et al., 2010). Use of gravure printing for OLEDs was also re-ported recently by Kopola, Tuomikoski, Suhonen, and Maaninen (2009) who prepared 30 cm^2 OLEDs on glass substrates using gravure to process both PEDOT:PSS and a
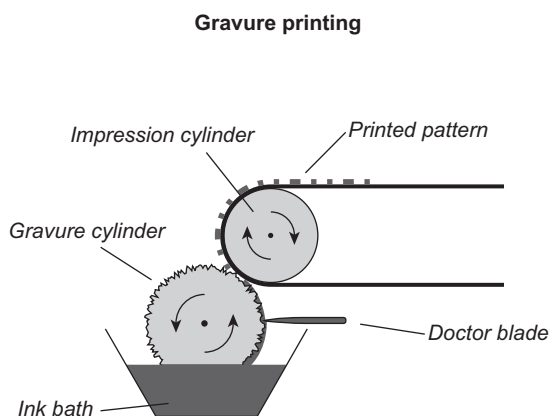
Gravure printing

Figure 7.8 Illustration of the gravure-printing principle.

Figure 7.9 Gravure-printed large-area OLED (active area 30 cm^2) with two printed organic layers (PEDOT and a blue-emitting layer − colour does not show).
Reproduced from Kopola et al. (2009) with the permission from Elsevier.

blue-emitting layer. In the final device (see Figure 7.9), these were sandwiched between ITO and a metallic cathode.

Until now, only a few cases employing gravure printing to prepare OPVs have been reported. Kopola et al. have on two occasions used gravure printing to prepare regular architecture devices. A desktop gravure printability tester (single sheets, not R2R) was used to deposit PEDOT:PSS and P3HT:PCBM for single cells (PCE: 2.8%, 0.19 cm^2) (Kopola et al., 2010) and the same printer was used for processing small modules of five cells in series (PCE: 1.9%, 9.6 cm^2) (Kopola et al., 2011). Other noteworthy examples are the printing of an OPV on paper reported by Hübler et al. (2011) and the use of an industrial gravure printer for OPV preparation by Yang et al. (2013). In the latter case, the top silver electrode was evaporated, whereas the hole-transporting layer (PEDOT:PSS), the electron-transporting layer (ZnO) and the active layer (P3HT: PCBM) were all printed with the gravure printer using ITO-coated polyethylene terephthalate (PET) as substrate. The modules composed of five cells in series (45 cm^2) yielded a PCE in the range 0.22−0.86%.

7.2.4 Ink-jet printing

As stated previously, contrary to traditional printing techniques, ink-jet printing does not transfer the printing pattern through contact. Ink-jet printing is a fully digital nonimpact method. The two-dimensional pattern is based on a pixelated drawing where each pixel is either left blank or receives an ink drop, and in special cases it is possible to work in 3D by printing multiple layers.

Ink-jet printing is advantageous because it is easy to change the printing pattern by computer, and no physical adjustment of the printing apparatus is required. Furthermore, as it is a noncontact technique it can be used to print on sensitive substrates or 3D structures. The main drawback lies within the ink formulation (density, surface tension, viscosity, boiling point, etc.), which needs to be adjusted to fit a number of parameters including nozzle size, printing surface and materials − such parameters make it more difficult to formulate an ink with only benign solvents. However, Lange, Schindler, Wegener, Fostiropoulos, and Janietz (2013) used ink jets to print a blend of

poly[9,9-dioctylfluorenyl-2,7-dyil-co-10,12-bis(thiophen-2-y)-3,6-dioxooctyl-11-thia-9,13-diaza-cyclopenta[b]triphenylene] (PFDTBTP) and PCBM as active layer in a solar cell using only nonchlorinated solvents.

Two kinds of ink-jet printing are commonly used: drop-on-demand and continuous.

In continuous ink-jet printing, a continuous jet of droplets is formed and is then electrostatically deviated to print on the desired pixels. Because only one nozzle is required, this type of ink-jet printing is very fast. However, the printing area is limited.

Three types of drop-on-demand ink-jet printing are generally available: piezoelectric, thermal and electrostatic. Piezoelectric ink-jet printing (illustrated in Figure 7.10) is the most commonly used, as it is suitable for the printing of most materials. A piezoelectric element is placed in the channel on top of the nozzle, and when a voltage is applied to this element it expands and ejects a droplet through the nozzle. Thermal ink-jet printing requires one of the ink compounds to have a low boiling point and the ejection of a droplet is carried out by momentarily heating the ink inside the nozzle. For electrostatic ink-jet printing, an electrostatic field is applied between the nozzle and an electrode drawing the free charges contained in the ink to the surface. Droplets are formed when the electrostatic forces exceed the surface tension. In order to comply with this technology the ink needs to be charged.

Commercially available ink-jet printers allow resolutions up to 600 DPI and speeds up to 75 m/min.

Ink-jet printing of silver gates and source/drain in OTFTs has been reported on several occasions (Chung, Kim, Kwon, Lee, & Hong, 2011; Lee, Lim, Park, Kim, & Kim, 2013; Tobjörk, Kaihovirta, Mäkelä, Pettersson, & Österbacka, 2008; Vornbrock et al., 2010), as has the printing of PEDOT:PSS as gate (Tobjörk et al., 2008). Chung et al. (2011) have shown that ink-jet printing is a promising technology
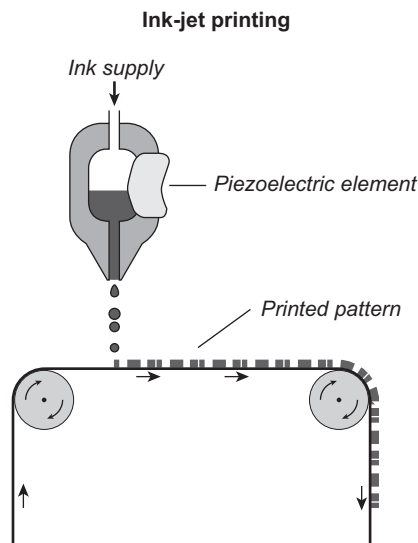
Ink-jet printing

Figure 7.10 Schematic illustration of piezo-based drop-on-demand ink-jet printing.

for OTFT preparation, by making a fully ink-jet-printed inverter on a flexible polyarylate substrate. This inverter is made of two p-type OTFTs with silver gate, source/drain electrodes, poly-4-vinylphenol (PVP) as gate-dielectric layer and 6,13-bis (triisopropylsilylethynyl) (TIPS) pentacene as active semiconductor layer. The OTFTs yielded a mobility of 10.02 cm^2/(V·s), an on/off ratio of 10^4 and a threshold voltage of -1.2 V.

For OPVs, ink-jet printing has mostly been used to prepare small-scale devices on glass (0.03−1 cm^2) as well as to deposit PEDOT:PSS (Eom et al., 2009), P3HT: PCBM (Aernouts, Aleksandrov, Girotto, Genoe, & Poortmans, 2008; Hoth, Choulis, Schilinsky, & Brabec, 2007; Hoth, Schilinsky, Choulis, & Brabec, 2008) or both (Eom et al., 2010; Lange et al., 2010). In true R2R processing of OPVs, ink jets have also been used to deposit patterned silver front grid lines (Yu et al., 2012) as shown in Figure 7.11.

For OLEDs, ink jets have also been used to print the emissive layer (Kwon et al., 2012; Teichler et al., 2013), and recently Gorter et al. (2013) prepared small-molecule OLEDs on ITO-coated glass substrate (30 × 30 mm^2) using ink jets to print the emissive layer (Tris-(8-hydroxyquinoline)aluminium) (Alq3)), the hole-injection layer (PEDOT:PSS) and the hole transport layer (α-NPD).

7.2.5   Spray coating

Similar to ink-jet printing, spray coating is also a noncontact technique where the layer is deposited through a spurt of ink droplets. However, in this case the spray is random and there is no digital control of the deposited pattern. Spray coating is consequently by definition a zero-dimensional coating method. Masking can be used to deposit a two-dimensional pattern, but the edge definition is low, and recovery of the ink deposited on the mask can be tricky. Another option is to use a laser after spray coating to etch the desired pattern.

Figure 7.11 Example of a R2R ink-jet-printed silver grid.
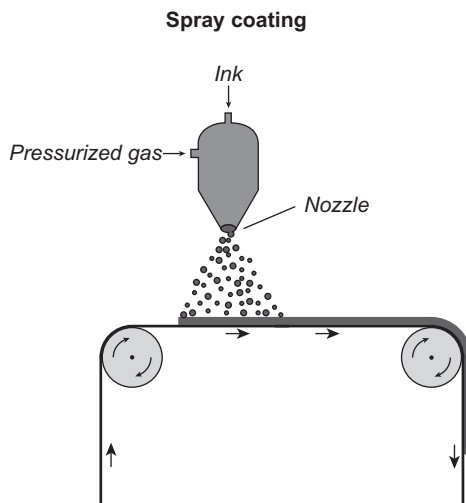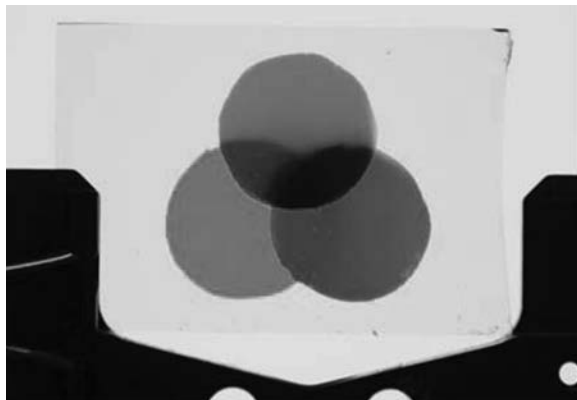
Spray coating

Figure 7.12 Illustration of spray coating.

In most spray coating apparatus the ink is atomized with a pressurized gas such as nitrogen (Yu et al., 2010) (this principle is illustrated in Figure 7.12), but ultra-sonication (Steirer et al., 2009) with a directed carried gas, or electrospraying (Kim et al., 2012), is also possible. The droplet size is related to the ink viscosity, surface tension, density as well as the gas pressure and the nozzle shape. The droplets kinetic energy influence how they will spread upon impact on the substrate, and the deposited layer quality depends on numerous factors such as the length between the nozzle and the web's surface, coating speed, how many layers are coated, ink and surface energy of the ink and of the substrate.

Although spray coating is a fully R2R-compatible technique, it has not been used much because of the risk of contamination of the equipment by the ink mist. However, small lab-scale roll coaters have been developed (Dam & Krebs, 2012) and used successfully to spray-coat polymeric layers in ECs (Jensen, Dam, Reynolds, Dyer, & Krebs, 2012). Several reports using spray coating for the processing of ECs with a large range of colours can be found (Amb, Beaujuge, & Reynolds, 2010; Beaujuge et al., 2012; Beaujuge, Ellinger, & Reynolds, 2008; Mortimer, Graham, Grenier, & Reynolds, 2009; Reeves et al., 2004), but all are limited to small ITO-coated glass substrates (Figure 7.13). The use of spray coating to prepare small-scale OPVs has been reported for the active layer (Chen et al., 2010; Girotto, Rand, Genoe, & Heremans, 2009; Park et al., 2011), silver back electrodes (Girotto, Rand, Steudel, Genoe, & Heremans, 2009; Hau, Yip, Leong, & Jen, 2009), hole-transport layer and active layer (Girotto, Moia, Rand, & Heremans, 2011; Kang et al., 2012) and electron-transport, active and hole-transport layers (Lewis, Lafalce, Toglia, & Jiang, 2011). Some of the prepared OPVs yield similar performances to spin-coated devices, demonstrating the potential of this technique (Kang et al., 2012). The use of spray coating for OLED preparation is so far limited. One noticeable application was replacement of ITO as

Figure 7.13 Thin films of blue, red, and yellow polymers (colours do not show) ECs spray-cast onto ITO slides through circular shadow masks. Reproduced from Amb, Kerszulis, Thompson, Dyer, and Reynolds (2011) with permission from The Royal Society of Chemistry.

anode in a flexible OLEDs by a double-layer graphene/PEDOT:PSS where the PEDOT:PSS was spray coated (Wu, Li, Wu, & Guo, 2014).

7.3 Coating techniques

Coating techniques are generally noncontact techniques and are in most cases limited to deposition of a homogenous layer following the web length. Accordingly most coating techniques are one-dimensional. However, compared to printing techniques the layer thickness can in most cases be tightly controlled. Coating methods are also suitable for a broad range of viscosities and are less sensible with respect to surface wetting, as the ink is 'poured' onto the substrate compared to the surface-energy-dependent transfer involved in many printing techniques. Briefly, coating is achieved through a meniscus standing between the coating head and the substrate that is continuously fed with ink as the web moves.

7.3.1 Knife coating

Knife coating as a R2R technique is similar to doctor-blading on a laboratory scale. The layer is deposited at a stationary knife, in front of which an ink reservoir is continuously supplying the meniscus standing between the web and the blade, as shown in Figure 7.14. The web movement ensures the layer deposition as it passes the knife. The wet thickness is related to the gap size between the knife and the substrate and to some extent also to the web speed. As a rule of thumb the wet thickness is roughly half the gap size. Knife coating is suitable for deposition of homogeneous layers on large areas and can be carried out at high speed (>10 m/min). For OPVs, deposition of ZnO as a hole-blocking layer (Krebs, 2009), and PEDOT:PSS as an electron-blocking layer (Hoth et al., 2009) and active layer (Wengeler, Schmidt-Hansberg, Peters, Scharfer, & Schabel, 2011) have been reported. Knife coating has also been used on a small scale (4×4 cm^2) to coat organic layers (hole-transport
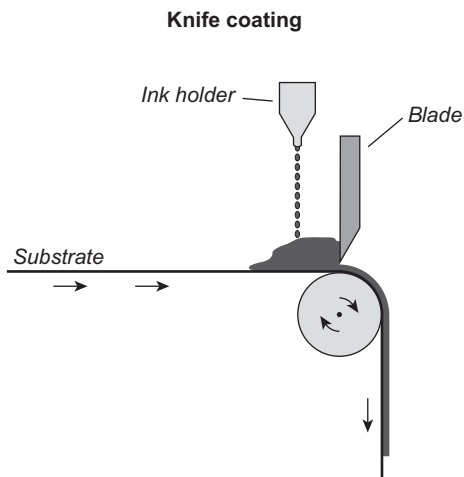
Knife coating

Figure 7.14 Illustration of Knife coating operating principle.

layer, emissive layer, electron-transport layer) in OLEDs (Chang et al., 2012). Chen et al. developed a multilayer blade-coating method that can be used for both polymers and small-molecule OLEDs (Chen et al., 2011) (see Figure 7.15).

7.3.2   Slot-die coating

In slot-die coating, the ink is pumped through a slot inside the coating head mounted close to the web. After formation of a meniscus, which is maintained by continuous pumping, the moving substrate leads to the deposition of a homogeneous layer along the web (illustrated in Figure 7.16). When fitted with a meniscus guide the coating
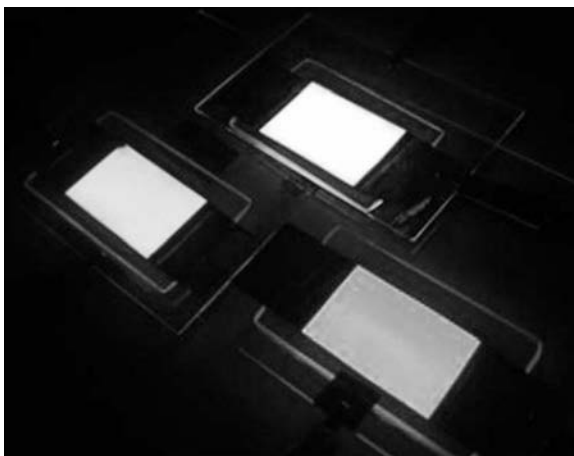
Figure 7.15 Large-area OLED made by the blade-only method. The active area is $2 \times 3 \ cm^2$. Reproduced from Chen et al. (2011) with permission from AIP Publishing LLC.
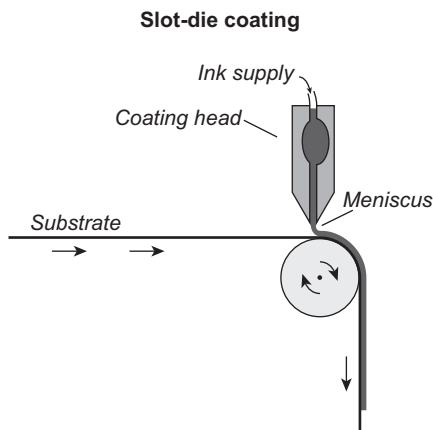
Slot-die coating

Figure 7.16 Illustration of slot-die coating.

head allows deposition of stripes. It is possible to regulate the wet-layer thickness precisely, as this is defined directly by the pumping rate, the web speed and the width of the coat. Slot-die coating is a powerful technique that allows for the simultaneous deposition of tightly grouped homogeneous stripes at speeds up to 100 m/min.

Wu, Kerk, and Wong (2013) used slot-die to coat an aqueous solution of PEDOT: PSS and silver nanowires on PET substrates, as a substitute for ITO as a transparent electrode. Within ECs, slot-die coating has also been used to deposit the active-polymer layer and the counter-polymer layer in ITO- and vacuum-free ECs (Søndergaard et al., 2013). As for OPVs, slot-die coating is by far the most widely used R2R processing technique and it has been used on numerous occasions to deposit hole-blocking layers, active layers and electron-blocking layers (Amb et al., 2012; Angmo et al., 2012; Blankenburg, Schultheis, Schache, Sensfuss, & Schrödner, 2009; Bundgaard et al., 2010; Dam & Krebs, 2012; Galagan, Vries, et al., 2011; Helgesen et al., 2012; Krebs, 2009; Krebs, Fyenbo, et al., 2010; Krebs et al., 2011; Krebs, Gevorgyan, et al., 2009; Krebs, Tromholt, et al., 2010; Larsen-Olsen, Machui, et al., 2012; Manceau et al., 2011; Søndergaard, Manceau, Jørgensen, & Krebs, 2012; Wengeler et al., 2011; Yu et al., 2012; Zimmermann, Schleiermacher, Niggemann, & Würfel, 2011). Similarly to knife coating, slot-die coating has been used to prepare OLEDs mainly through deposition of PEDOT:PSS, the emissive layer (see Figure 7.17) (Youn, Jeon, Shin, & Yang, 2012) and ZnO (Sandström, Dam, Krebs, & Edman, 2012).

7.4 Specialist coating techniques

7.4.1 Brush painting

As a layer-forming process, brush painting is probably the oldest; it is also one of the toughest to model, as brush painting is a blend of multiple techniques. The brush is soaked in the ink, which is then retained in the brush hairs by surface tension.
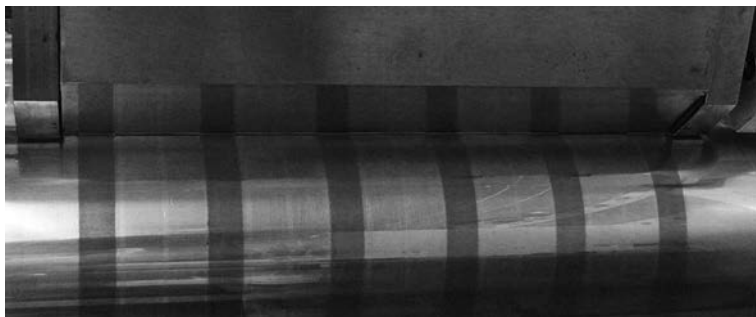
Figure 7.17 Slot die coating of the emissive layer 'Super Yellow' on a flexible ITO substrate for OLEDs.

When the brush is put in contact with the substrate a meniscus is formed, and the subsequent brushing movement pulls the ink from the brush and on to the web. Depending on the brush size, two-dimensional patterning is possible.

Only a few examples of brush painting have been published within organic electronics. For small-scale OPVs, one or more layers have been reported deposited by this technique (Heo, Lee, Song, Ku, & Moon, 2011; Kim, Na, Jo, Tae, & Kim, 2007; Kim, Na, Kang, & Kim, 2010), and recently Lee, Shin, Noh, Na, and Kim (2013) prepared an electrode that is an interesting alternative to ITO by brush painting on a flexible substrate (in this case, PET). Once integrated in OPV devices, this electrode made of PEDOT:PSS and silver nanowires yields efficiencies similar to devices with ITO. The use of brush painting on a R2R scale is fully conceivable, but so far no attempts have been reported.

7.4.2 Double slot-die coating

Double slot-die coating is a recent evolution in R2R processing of organic electronics and so far has only been used in the preparation of OPVs. During this particular process, two inks are deposited at the same time with a single coating head (see Figure 7.18) reducing production time as well as cost. Ideally the technique should allow for coating of numerous layers in one step. However, the deposition of just two layers at the same time has proven quite challenging. Recently, Larsen-Olsen et al. used this technique in order to coat an aqueous suspension of P3HT:PCBM and PEDOT:PSS simultaneously at a rate of 1 m/min (Larsen-Olsen, Andreasen, et al., 2012).

7.4.3 Differentially pumped slot-die coating

This technique was developed by Alstrup, Jørgensen, Medford, and Krebs (2010) as a fast and easy way to investigate acceptor/donor ratio in the active layer of an organic solar cell. The two compounds are pumped simultaneously into the coating head (where they are mixed), but with dissimilar pumping rates (see Figure 7.19). By varying the

Double slot-die coating
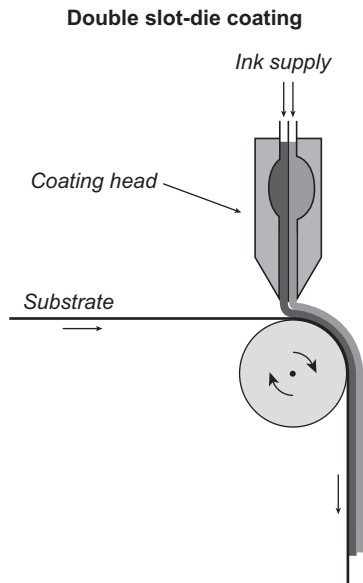
Figure 7.18 Illustration of double slot-die coating.

Differentialy pumped slot die
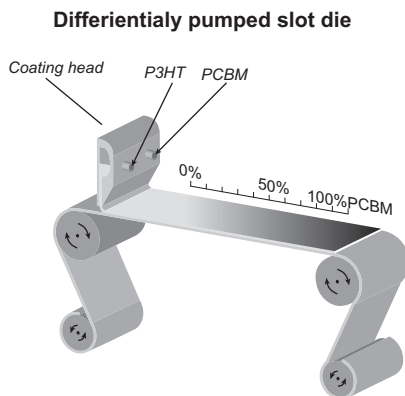
Figure 7.19 Differentially pumped slot-die coating. Screening P3HT:PCBM ratio from 0 : 1 to 1 : 0.

relative pumping rates gradually, while maintaining a constant combined pumping rate, a film with a gradient composition is produced. Subsequent analysis of device performance along this gradient allows determining the optimal ratio of a specific pair of donor and acceptor materials. This method is a powerful tool in OPV research that reduces the time for donor/acceptor ratio screening from days/weeks to a matter of hours (Amb et al., 2012; Bundgaard et al., 2010; Søndergaard et al., 2012). Although the method is developed for OPVs, in principle it should be directly transferrable to any other two-component system where an optimized ratio is desired.

7.5   Encapsulation techniques

Protection of the finished device from the surrounding environment is often needed when organic materials and especially conducting polymers are involved. Roll-to-roll encapsulation has so far only been applied to organic solar cells and the following section is thus exclusively about solar cell encapsulation. Though the principles described are general, they might serve as fruitful inspiration for other organic electronic technologies.

   Once a solar cell is processed onto the substrate encapsulation is required. Lamination is performed mainly to ensure device stability over time, but it also protects the sensitive device stack from mechanical stress. The lamination principle basically consists of joining a second foil, called a laminate, with the one on which the cells have been deposited. In order to ensure chemical stability of the device, a barrier foil is normally used to ensure minimum permeability of oxygen and water. The foil carrying the devices can be laminated on both sides to improve the stability.

7.5.1   Cold lamination

Cold lamination is carried out with a pressure sensitive adhesive. This adhesive is put onto the laminate with the help of a liner, which is removed (Krebs, Tromholt, et al., 2010) right before the laminate is put into contact with the substrate carrying the devices. The two foils meet in a nip where they are pressed together between two rolls in order to ensure good adhesion as shown in Figure 7.20. This lamination process is simple and fast (>20 m/min). The principal issue is that a relatively thick adhesive layer (around 50 μm or more) is needed compared to adhesives used in different lamination processes. Handling the sticky laminate can also prove challenging. A comparative OPV stability study performed by Hösel et al. (2013) analysed the different lamination
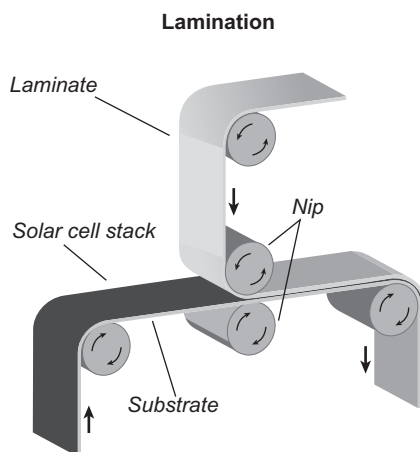
Lamination

Figure 7.20 Illustration of Cold and Hot lamination. The laminate holds the adhesive. Nip rolls can be heated for hot lamination.

techniques described in this section. The study showed that for cold lamination the active layer experiences bleaching around the edges when laminated on only one side. Long-term stability requires lamination on both sides.

7.5.2   Hot lamination

Hot lamination is a process similar to cold lamination (see Figure 7.20). However, in this case the adhesive can be handled on the laminate surface without a liner and because this adhesive is heat activated handling the laminate is much easier. The laminate is joined with the substrate carrying solar cells as the foils are pressed together between two heated rolls. This causes the adhesive to melt momentarily and upon cooling it forms a tight seal. Figure 7.21 shows the hot lamination of OPV modules. Besides being easier to handle this lamination process also allows use of thinner adhesive layers (down to 20 μm). Stability-wise, only slight bleaching is observed around the edges of the active layer when single laminated by hot-melt (Hösel et al., 2013).

7.5.3   UV lamination

In UV lamination the adhesive is UV sensitive. The UV curable adhesive is added to the laminate foil and after joining with the OPV carrying substrate in a nib the combined foils are exposed to UV light, ensuring the formation of a tight seal (Figure 7.22). Stability wise no bleaching is observed making UV-curable resin the best fit for single lamination (Hösel et al., 2013). This lamination technique is by far the more complex, as it requires an extra step to deposit the UV adhesive onto the laminate. This deposition is usually done through flexoprinting. Although complicated the technique allows for precise tuning of the adhesive thickness (1−100 μm).

Figure 7.21 Hot lamination of organic solar cells modules.
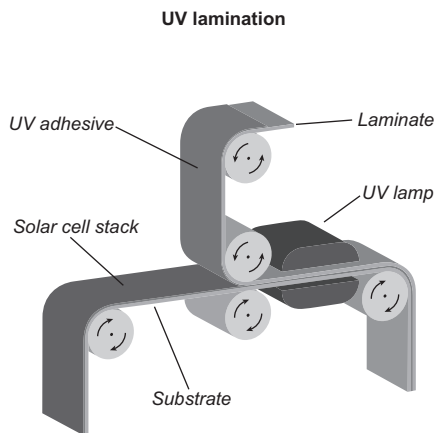
UV lamination

Figure 7.22 Illustration of UV lamination. The UV reactive adhesive is applied on the laminate by flexoprinting.

7.6   Applications

The ultimate goal of preparation by R2R processing is of course to have a product that can be integrated and commercialized.

As previously mentioned, OPV is probably the most mature technology with respect to R2R processing, but so far the commercialisation process has not really shown its potential. The Konarka solar bag, which allows the user to recharge small devices such as mobile phones, is the only real product so far. Several noncommercial demonstrations of integrating the technology have been reported though. One of the earliest examples is the 'solar hat' that can be used to power a small radio. More than 2000 130 cm^2 modules were produced for this campaign using only screen printing (Krebs, Jørgensen, et al., 2009). Another example was carried out as part of the 'Lighting Africa Project', where solar cell modules (20 × 25 cm^2) were used to charge a small reading light equipped with a rechargeable battery (Krebs, Nielsen, Fyenbo, Wadstrøm, & Pedersen, 2010). The same concept was later used to make 10,000 credit card sized OE-A flashlight demonstrators (Krebs et al., 2011). Recently, Espinosa et al. prepared small laser pointers similar in size to the OE-A flashlight to show the current progresses in OPV technology. These laser pointers use ITO-free OPV modules to charge a lithium-ion polymer battery (Espinosa et al., 2013). Although OPVs have been greatly studied, only a few examples have been publicly available (most of them are listed above). As a platform for researchers as well as a means to educate the public on 'what is an organic solar cell', Krebs, Hösel, et al. (2013) prepared tens of thousands of 'freeOPV' modules available for free to anyone who asks. These entirely R2R-processed modules are ITO-free and yield a PCE in the range of 1.5−2% (10.0 × 14.2 cm^2).

All of the examples above are good illustrations of OPV technology's potential, but in order to prosper as a renewable energy source, the OPV technology needs to be connected to the electrical grid. By introducing the infinity concept where interconnected

single cells are R2R processed continuously along the web Sommer-Larsen et al. showed that in order to effectively integrate R2R processed OPV the whole solar cell roll needs to be handled uncut (Sommer-Larsen et al., 2013), as the cutting and wiring of small discrete units is time- and cost-consuming. Using the uncut roll of solar cells is quite challenging because it does not allow for reconfiguration of the cells after R2R coating. The thin film structure of OPVs makes them unable to carry high current, meaning that all the cells along the roll must be connected in series. Such configuration delivers much higher voltages (around 10 kV for a roll of 0.305×100 m) than typical silicon modules and is much less sensible to individual cell performances than the silicon analogue. Pushing the use of the uncut OPV roll further, Krebs, Espinosa, Hösel, Søndergaard, and Jørgensen (2013) constructed a 1000 m^2 solar park. This solar park is connected to the electrical grid and consists of four tilted wood platforms (100 m long and 2.5 m high) that can be fitted with six rows of one-foot-wide foils (see Figure 7.23). The solar cells employed are based on the infinity process described earlier (Sommer-Larsen et al., 2013). As of now infinity stretches up to $1.5-2.2$ km long have been prepared constituting over 300,000 single cells connected in series. To be efficiently used, these rolls are only cut once and then laid onto the platform. Krebs et al. developed a simple process to install and remove the foil at the same time at a rate over 100 m/min. At this rate with the current technology it is possible to install over 200 W_{peak} per minute, far beyond the rate of other solar cell technologies.

Albeit not as mature as OPVs in R2R development, OLEDs are present in many commercial products. Lamps were the first commercially available products to use OLEDs and nowadays a large range of colours are available. OLEDs have also been used for displays in MP3 players, digital cameras, smartphones and TVs. However, none of these OLEDs devices reportedly have been prepared by R2R processing.

Similarly, EC technology has yielded several interesting applications spreading from light control, switching between clear and frosted glass, small EC displays that can be used for postcards and even a moisture sensor that lets you know when to water your plants — but again, none of these reports the use of R2R processing.

Figure 7.23 Solar park based on OPV, 250-square-metre wood panel with six solar-cell foils and an active area of 88 square metres.

Figure 7.24 Photograph of printed paper loudspeaker demonstrating its flexibility. Reproduced from Hübler et al. (2012) with permission from Elsevier.

Of the more surprising but notable applications, the printing of loudspeakers on paper by Hübler et al. should be mentioned (Hübler et al., 2012). These speakers, shown in Figure 7.24, were made by sandwiching the active piezoelectric layer between two PEDOT:PSS layers that act as electrodes and yield a sound pressure up to 80 dB.

7.7 Future trends

Roll-to-roll processing certainly has a bright future for fast and low-cost large-area organic electronics production. However, several challenges lie ahead for most of the technologies that are at the verge of transferring from the laboratory to the larger R2R processing scale. Many of the methodologies have to be adapted to new R2R-compatible processing methods, which is often not a straightforward process. Other challenges, such as finding functionally reliable substitutes for ITO as the transparent electrode on flexible substrates, will be crucial to keeping costs down. On the technical level, the registration used to align the multilayer structures during processing must still be improved — especially at high speeds. Particularly, OTFT and high-resolution OLEDs require precise multilayer structures.

In the long run environmental factors also have to be considered and development of new materials that can be processed from benign solvents will be required. In a large-scale production the toxic solvents currently used simply have too many complications and hazards with respect to both the working environment and the surrounding ecosystems and using such will affect the cost negatively. Life cycle and financial analyses of R2R-processed large-area organic electronics are powerful tools to guide the research

toward large-scale production. Such analysis have so far mostly been applied in relation to OPVs (Azzopardi et al., 2011; Espinosa, García-Valverde, & Krebs, 2011; Espinosa, García-Valverde, Urbina, & Krebs, 2011; Espinosa, García-Valverde, et al., 2012; García-Valverde, Cherni, & Urbina, 2010; Kalowekamo & Baker, 2009; Nielsen, Cruickshank, Foged, Thorsen, & Krebs, 2010; Powell, Bender, & Lawryshyn, 2009), and recent studies on OPV production have shown that if avoiding scarce elements and vacuum steps, and if using only solar heat and solar energy during processing, energy payback times can be brought down to a few days (Espinosa, Hösel, Angmo, & Krebs, 2012). The use of such tools will be essential to the success of all the technologies described in this chapter in order to navigate around the pitfalls that can negatively affect the insurance of fast production of low-cost organic electronics.

References

Aernouts, T., Aleksandrov, T., Girotto, C., Genoe, J., & Poortmans, J. (2008). Polymer based organic solar cells using ink-jet printed active layers. *Applied Physics Letter, 92*, 033306.

Alstrup, J., Jørgensen, M., Medford, A. J., & Krebs, F. C. (2010). Ultra fast and parsimonious materials screening for polymer solar cells using differentially pumped slot-die coating. *ACS Applied Materials and Interfaces, 2*, 2819−2827.

Amb, C. M., Beaujuge, P. M., & Reynolds, J. R. (2010). Spray-Processable Blue-to-Highly transmissive switching polymer Electrochromes via the Donor−Acceptor approach. *Advanced Materials, 22*, 724−728.

Amb, C. M., Craig, M. R., Koldemir, U., Subbiah, J., Choudhury, K. R., Gevorgyan, S. A., et al. (2012). Aesthetically pleasing conjugated polymer: fullerene blends for blue-green solar cells via roll-to-roll processing. *ACS Applied Materials & Interfaces, 4*, 1847−1853.

Amb, C. M., Kerszulis, J. A., Thompson, E. J., Dyer, A. L., & Reynolds, J. R. (2011). Propylenedioxythiophene (ProDOT)−phenylene copolymers allow a yellow-to-transmissive electrochrome. *Polymer Chemistry, 2*, 812.

Angmo, D., Hösel, M., & Krebs, F. C. (2012). All solution processing of ITO-free organic solar cell modules directly on barrier foil. *Solar Energy Materials and Solar Cells, 107*, 329−336.

Azzopardi, B., Emmott, C. J. M., Urbina, A., Krebs, F. C., Mutale, J., & Nelson, J. (2011). Economic assessment of solar electricity production from organic-based photovoltaic modules in a domestic environment. *Energy and Environmental Science, 4*, 3741.

Beaujuge, P. M., Ellinger, S., & Reynolds, J. R. (2008). Spray processable green to highly transmissive electrochromics via chemically polymerizable donor−acceptor heterocyclic pentamers. *Advanced Materials, 20*, 2772−2776.

Beaujuge, P. M., Vasilyeva, S. V., Liu, D. Y., Ellinger, S., McCarley, T. D., & Reynolds, J. R. (2012). Structure-performance correlations in spray-processable green dioxythiophene-benzothiadiazole donor−acceptor polymer Electrochromes. *Chemistry of Materials, 24*, 255−268.

Blankenburg, L., Schultheis, K., Schache, H., Sensfuss, S., & Schrödner, M. (2009). Reel-to-reel wet coating as an efficient up-scaling technique for the production of bulk-heterojunction polymer solar cells. *Solar Energy Materials and Solar Cells, 93*, 476−483.

Bundgaard, E., Hagemann, O., Manceau, M., Jørgensen, M., & Krebs, F. C. (2010). Low band gap polymers for roll-to-roll coated polymer solar cells. *Macromolecules, 43*, 8115−8120.

Chang, Y.-F., Chiu, Y.-C., Yeh, H.-C., Chang, H.-W., Chen, C.-Y., Meng, H.-F., et al. (2012). Unmodified small-molecule organic light-emitting diodes by blade coating. *Organic Electronics, 13*, 2149−2155.

Chen, C.-Y., Chang, H.-W., Chang, Y.-F., Chang, B.-J., Lin, Y.-S., Jian, P.-S., et al. (2011). Continuous blade coating for multi-layer large-area organic light-emitting diode and solar cell. *Journal of Applied Physics, 110*, 094501.

Chen, L., Hong, Z., Kwan, W., Lu, C.-H., Lai, Y., Lei, B., et al. (2010). Multi-source/component spray coating for polymer solar cells. *ACS Nano, 4*, 4744−4752.

Chung, S., Kim, S. O., Kwon, S.-K., Lee, C., & Hong, Y. (2011). All-inkjet-printed organic thin-film transistor inverter on flexible plastic substrate. *IEEE Electron Device Letters, 32*, 1134−1136.

Dam, H. F., & Krebs, F. C. (2012). Simple roll coater with variable coating and temperature control for printed polymer solar cells. *Solar Energy Materials and Solar Cells, 97*, 191−196.

Eom, S., Park, H., Mujawar, S. H., Yoon, S., Kim, S.-S., Na, S.-I., et al. (2010). High efficiency polymer solar cells via sequential inkjet-printing of PEDOT: PSS and P3HT: PCBM inks with additives. *Organic Electronics, 11*, 1516−1522.

Eom, S. H., Senthilarasu, S., Uthirakumar, P., Yoon, S. C., Lim, J., Lee, C., et al. (2009). Polymer solar cells based on inkjet-printed PEDOT: PSS layer. *Organic Electronics, 10*, 536−542.

Espinosa, N., García-Valverde, R., & Krebs, F. C. (2011). Life-cycle analysis of product integrated polymer solar cells. *Energy & Environmental Science, 4*, 1547.

Espinosa, N., García-Valverde, R., Urbina, A., & Krebs, F. C. (2011). A life cycle analysis of polymer solar cell modules prepared using roll-to-roll methods under ambient conditions. *Solar Energy Materials and Solar Cells, 95*, 1293−1302.

Espinosa, N., García-Valverde, R., Urbina, A., Lenzmann, F., Manceau, M., Angmo, D., et al. (2012). Life cycle assessment of ITO-free flexible polymer solar cells prepared by roll-to-roll coating and printing. *Solar Energy Materials and Solar Cells, 97*, 3−13.

Espinosa, N., Hösel, M., Angmo, D., & Krebs, F. C. (2012). Solar cells with one-day energy payback for the factories of the future. *Energy & Environmental Science, 5*, 5117.

Espinosa, N., Lenzmann, F. O., Ryley, S., Angmo, D., Hösel, M., Søndergaard, R. R., et al. (2013). OPV for mobile applications: an evaluation of roll-to-roll processed indium and silver free polymer solar cells through analysis of life cycle, cost and layer quality using inline optical and functional inspection tools. *Journal of Materials Chemistry A, 1*, 7037.

Galagan, Y., Rubingh, J. J., Andriessen, R., Fan, C.-C., Blom, P. W. M., Veenstra, S. C., et al. (2011). ITO-free flexible organic solar cells with printed current collecting grids. *Solar Energy Materials and Solar Cells, 95*, 1339−1343.

Galagan, Y., Vries, I. G. de, Langen, A. P., Andriessen, R., Verhees, W. J. H., Veenstra, S. C., et al. (2011). Technology development for roll-to-roll production of organic photovoltaics. *Chemical Engineering and Processing: Process Intensification, 50*, 454−461.

García-Valverde, R., Cherni, J. A., & Urbina, A. (2010). Life cycle analysis of organic photovoltaic technologies. *Progress in Photovoltaics: Research and Application, 18*, 535−558.

Girotto, C., Moia, D., Rand, B., & Heremans, P. (2011). High-performance organic solar cells with spray-coated hole-transport and active layers. *Advanced Functional Materials, 21*, 64−72.

Girotto, C., Rand, B., Genoe, J., & Heremans, P. (2009). Exploring spray coating as a deposition technique for the fabrication of solution-processed solar cells. *Solar Energy Materials and Solar Cells, 93*, 454−458.

Girotto, C., Rand, B., Steudel, S., Genoe, J., & Heremans, P. (2009). Nanoparticle-based, spray-coated silver top contacts for efficient polymer solar cells. *Organic Electronics, 10*, 735−740.

Gorter, H., Coenen, M. J. J., Slaats, M. W. L., Ren, M., Lu, W., Kuijpers, C. J., et al. (2013). Toward inkjet printing of small molecule organic light emitting diodes. *Thin Solid Films, 532*, 11−15.

Hambsch, M., Reuter, K., Stanel, M., Schmidt, G., Kempa, H., Fügmann, U., et al. (2010). Uniformity of fully gravure printed organic field-effect transistors. *Materials Science and Engineering: B, 170*, 93−98.

Hau, S. K., Yip, H.-L., Leong, K., & Jen, A. K.-Y. (2009). Spraycoating of silver nanoparticle electrodes for inverted polymer solar cells. *Organic Electronics, 10*, 719−723.

Helgesen, M., Carlé, J. E., Andreasen, B., Hösel, M., Norrman, K., Søndergaard, R. R., et al. (2012). Rapid flash annealing of thermally reactive copolymers in a roll-to-roll process for polymer solar cells. *Polymer Chemistry, 3*, 2649−2655.

Heo, S., Lee, J., Song, H., Ku, J., & Moon, D. (2011). Patternable brush painting process for fabrication of flexible polymer solar cells. *Solar Energy Materials and Solar Cells, 95*, 3041−3046.

Hösel, M., Søndergaard, R. R., Jørgensen, M., & Krebs, F. C. (2013). Comparison of UV-Curing, hotmelt, and pressure sensitive adhesive as roll-to-roll encapsulation methods for polymer solar cells. *Advanced Engineering Materials, 15*, 1068−1075.

Hoth, C., Choulis, S., Schilinsky, P., & Brabec, C. J. (2007). High photovoltaic performance of inkjet printed polymer: fullerene blends. *Advanced Materials, 19*, 3973−3978.

Hoth, C., Schilinsky, P., Choulis, S., & Brabec, C. J. (2008). Printing highly efficient organic solar cells. *Nano Letters, 8*(9), 2806−2813.

Hoth, C., Steim, R., Schilinsky, P., Choulis, S. A., Tedde, S. F., Hayden, O., et al. (2009). Topographical and morphological aspects of spray coated organic photovoltaics. *Organic Electronics, 10*, 587−593.

Hübler, A. C., Bellmann, M., Schmidt, G. C., Zimmermann, S., Gerlach, A., & Haentjes, C. (2012). Fully mass printed loudspeakers on paper. *Organic Electronics, 13*, 2290−2295.

Hübler, A. C., Trnovec, B., Zillger, T., Ali, M., Wetzold, N., Mingebach, M., et al. (2011). Printed paper photovoltaic cells. *Advanced Energy Materials, 1*, 1018−1022.

Huebler, A. C., Doetz, F., Kempa, H., Katz, H. E., Bartzsch, M., Brandt, N., et al. (2007). Ring oscillator fabricated completely by means of mass-printing technologies. *Organic Electronics, 8*, 480−486.

Jensen, J., Dam, H. F., Reynolds, J. R., Dyer, A. L., & Krebs, F. C. (2012). Manufacture and demonstration of organic photovoltaic-powered electrochromic displays using roll coating methods and printable electrolytes. *Journal of Polymer Science Part B: Polymer Physics, 50*, 536−545.

Kalowekamo, J., & Baker, E. (2009). Estimating the manufacturing cost of purely organic solar cells. *Solar Energy, 83*, 1224−1231.

Kang, J., Kang, Y., Jung, S., Song, M., Kim, D.-G., Kim, C.-S., et al. (2012). Fully spray-coated inverted organic solar cells. *Solar Energy Materials and Solar Cells, 103*, 76−79.

Kim, Y., Lee, J., Kang, H., Kim, G., Kim, N., & Lee, K. (2012). Controlled electro-spray deposition of highly conductive PEDOT: PSS films. *Solar Energy Materials and Solar Cells, 98*, 39−45.

Kim, S., Na, S.-I., Jo, J., Tae, G., & Kim, D.-Y. (2007). Efficient polymer solar cells fabricated by simple brush painting. *Advanced Materials, 19*, 4410−4415.

Kim, S., Na, S., Kang, S., & Kim, D. (2010). Annealing-free fabrication of P3HT: PCBM solar cells via simple brush painting. *Solar Energy Materials and Solar Cells, 94*, 171−175.

Kopola, P., Aernouts, T., Guillerez, S., Jin, H., Tuomikoski, M., Maaninen, A., et al. (2010). High efficient plastic solar cells fabricated with a high-throughput gravure printing method. *Solar Energy Materials and Solar Cells, 94*, 1673−1680.

Kopola, P., Aernouts, T., Sliz, R., Guillerez, S., Ylikunnari, M., Cheyns, D., et al. (2011). Gravure printed flexible organic photovoltaic modules. *Solar Energy Materials and Solar Cells, 95*, 1344−1347.

Kopola, P., Tuomikoski, M., Suhonen, R., & Maaninen, A. (2009). Gravure printed organic light emitting diodes for lighting applications. *Thin Solid Films, 517*, 5757−5762.

Krebs, F. C. (2009). Polymer solar cell modules prepared using roll-to-roll methods: knife-over-edge coating, slot-die coating and screen printing. *Solar Energy Materials and Solar Cells, 93*, 465−475.

Krebs, F. C., Espinosa, N., Hösel, M., Søndergaard, R. R., & Jørgensen, M. (2013). Rise to power − OPV-based solar Parks. *Advanced Materials, 26*, 29−39.

Krebs, F. C., Fyenbo, J., & Jørgensen, M. (2010). Product integration of compact roll-to-roll processed polymer solar cell modules: methods and manufacture using flexographic printing, slot-die coating and rotary. *Journal of Materials Chemistry, 20*, 8994.

Krebs, F. C., Fyenbo, J., Tanenbaum, D. M., Gevorgyan, S. A., Andriessen, R., Remoortere, B. van, et al. (2011). The OE-A OPV demonstrator anno domini 2011. *Energy & Environmental Science, 4*, 4116−4123.

Krebs, F. C., Gevorgyan, S. A., & Alstrup, J. (2009). A roll-to-roll process to flexible polymer solar cells: model studies, manufacture and operational stability studies. *Journal of Materials Chemistry, 19*, 5442.

Krebs, F. C., Hösel, M., Corazza, M., Roth, B., Madsen, M. V., Gevorgyan, S. A., et al. (2013). Freely available OPV—the fast way to progress. *Energy Technology, 1*, 378−381.

Krebs, F. C., Jørgensen, M., Norrman, K., Hagemann, O., Alstrup, J., Nielsen, T. D., et al. (2009). A complete process for production of flexible large area polymer solar cells entirely using screen printing—first public demonstration. *Solar Energy Materials and Solar Cells, 93*, 422−441.

Krebs, F. C., Nielsen, T. D., Fyenbo, J., Wadstrøm, M., & Pedersen, M. S. (2010). Manufacture, integration and demonstration of polymer solar cells in a lamp for the "Lighting Africa" initiative. *Energy & Environmental Science, 3*, 512.

Krebs, F. C., Tromholt, T., & Jørgensen, M. (2010). Upscaling of polymer solar cell fabrication using full roll-to-roll processing. *Nanoscale, 2*, 873−886.

Kwon, J., Eom, S. H., Moon, B. S., Shin, J., Kim, K.-S., Lee, S.-H., et al. (2012). Studies on printing inks containing poly [2-methoxy-5-(2-ethylhexyl-oxyl)-1,4-phenylenevinylene] as an emissive material for the fabrication of polymer light-emitting diodes by inkjet printing. *Bulletin of the Korean Chemical Society, 33*, 464−468.

Lange, A., Schindler, W., Wegener, M., Fostiropoulos, K., & Janietz, S. (2013). Inkjet printed solar cell active layers prepared from chlorine-free solvent systems. *Solar Energy Materials and Solar Cells, 109*, 104−110.

Lange, A., Wegener, M., Boeffel, C., Fischer, B., Wedel, A., & Neher, D. (2010). A new approach to the solvent system for inkjet-printed P3HT: PCBM solar cells and its use in devices with printed passive and active layers. *Solar Energy Materials and Solar Cells, 94*, 1816−1821.

Larsen-Olsen, T. T., Andreasen, B., Andersen, T. R., Böttiger, A. P. L., Bundgaard, E., Norrman, K., et al. (2012). Simultaneous multilayer formation of the polymer solar cell stack using roll-to-roll double slot-die coating from water. *Solar Energy Materials and Solar Cells, 97*, 22−27.

Larsen-Olsen, T. T., Machui, F., Lechene, B., Berny, S., Angmo, D., Søndergaard, R. R., et al. (2012). Round-robin studies as a method for testing and validating high-efficiency ITO-free polymer solar cells based on roll-to-roll-coated highly conductive and transparent flexible substrates. *Advanced Energy Materials, 2*, 1091−1094.

Lee, D.-H., Choi, J. S., Chae, H., Chung, C.-H., & Cho, S. M. (2008). Highly efficient phosphorescent polymer OLEDs fabricated by screen printing. *Displays, 29*, 436−439.

Lee, D.-H., Lim, K.-T., Park, E.-K., Kim, J.-M., & Kim, Y.-S. (2013). Optimized ink-jet printing condition for stable and reproducible performance of organic thin film transistor. *Microelectronic Engineering, 111*, 242−246.

Lee, J.-H., Shin, H.-S., Noh, Y.-J., Na, S.-I., & Kim, H.-K. (2013). Brush painting of transparent PEDOT/Ag nanowire/PEDOT multilayer electrodes for flexible organic solar cells. *Solar Energy Materials and Solar Cells, 114*, 15−23.

Lewis, J. E., Lafalce, E., Toglia, P., & Jiang, X. (2011). Over 30% transparency large area inverted organic solar array by spray. *Solar Energy Materials and Solar Cells, 95*, 2816−2822.

Manceau, M., Angmo, D., Jørgensen, M., & Krebs, F. C. (2011). ITO-free flexible polymer solar cells: from small model devices to roll-to-roll processed large modules. *Organic Electronics, 12*, 566−574.

Mortimer, R. J., Graham, K. R., Grenier, C. R. G., & Reynolds, J. R. (2009). Influence of the film thickness and morphology on the colorimetric properties of spray-coated electrochromic disubstituted 3,4-propylenedioxythiophene polymers. *ACS Applied Materials & Interfaces, 1*, 2269−2276.

Nielsen, T. D., Cruickshank, C., Foged, S., Thorsen, J., & Krebs, F. C. (2010). Business, market and intellectual property analysis of polymer solar cells. *Solar Energy Materials and Solar Cells, 94*, 1553−1571.

Park, S.-Y., Kang, Y.-J., Lee, S., Kim, D.-G., Kim, J.-K., Kim, J. H., et al. (2011). Spray-coated organic solar cells with large-area of 12.25 cm^2. *Solar Energy Materials and Solar Cells, 95*, 852−855.

Powell, C., Bender, T., & Lawryshyn, Y. (2009). A model to determine financial indicators for organic solar cells. *Solar Energy, 83*, 1977−1984.

Reeves, B. D., Grenier, C. R. G., Argun, A. A., Cirpan, A., McCarley, T. D., & Reynolds, J. R. (2004). Spray coatable electrochromic dioxythiophene polymers with high coloration efficiencies. *Macromolecules, 37*, 7559−7569.

Ryu, G. S., Kim, J. S., Jeong, S. H., & Song, C. K. (2013). A printed OTFT-backplane for AMOLED display. *Organic Electronics, 14*, 1218−1224.

Sandström, A., Dam, H. F., Krebs, F. C., & Edman, L. (2012). Ambient fabrication of flexible and large-area organic light-emitting devices using slot-die coating. *Nature Communications, 3*, 1002.

Sommer-Larsen, P., Jørgensen, M., Søndergaard, R. R., Hösel, M., & Krebs, F. C. (2013). It is all in the pattern-high-efficiency power extraction from polymer solar cells through high-voltage serial connection. *Energy Technology, 1*, 15−19.

Søndergaard, R. R., Hösel, M., Jørgensen, M., & Krebs, F. C. (2013). Fast printing of thin, large area, ITO free electrochromics on flexible barrier foil. *Journal of Polymer Science Part B: Polymer Physics, 51*, 132−136.

Søndergaard, R. R., Manceau, M., Jørgensen, M., & Krebs, F. C. (2012). New low-bandgap materials with good stabilities and efficiencies comparable to P3HT in R2R-coated solar cells. *Advanced Energy Materials, 2*, 415−418.

Steirer, K. X., Reese, M. O., Rupert, B. L., Kopidakis, N., Olson, D. C., Collins, R. T., et al. (2009). Ultrasonic spray deposition for production of organic solar cells. *Solar Energy Materials and Solar Cells, 93*, 447−453.

Teichler, A., Shu, Z., Wild, A., Bader, C., Nowotny, J., Kirchner, G., et al. (2013). Inkjet printing of chemically tailored light-emitting polymers. *European Polymer Journal, 49*, 2186−2195.

Tobjörk, D., Kaihovirta, N. J., Mäkelä, T., Pettersson, F. S., & Österbacka, R. (2008). All-printed low-voltage organic transistors. *Organic Electronics, 9*, 931−935.

Verilhac, J.-M., Benwadih, M., Seiler, A.-L., Jacob, S., Bory, C., Bablet, J., et al. (2010). Step toward robust and reliable amorphous polymer field-effect transistors and logic functions made by the use of roll to roll compatible printing processes. *Organic Electronics, 11*, 456−462.

Voigt, M. M., Guite, A., Chung, D.-Y., Khan, R. U. A., Campbell, A. J., Bradley, D. D. C., et al. (2010). Polymer field-effect transistors fabricated by the sequential gravure printing of polythiophene, two insulator layers, and a metal ink gate. *Advanced Functional Materials, 20*, 239−246.

Vornbrock, A. de la F., Sung, D., Kang, H., Kitsomboonloha, R., & Subramanian, V. (2010). Fully gravure and ink-jet printed high speed pBTTT organic thin film transistors. *Organic Electronics, 11*, 2037−2044.

Wengeler, L., Schmidt-Hansberg, B., Peters, K., Scharfer, P., & Schabel, W. (2011). Investigations on knife and slot die coating and processing of polymer nanoparticle films for hybrid polymer solar cells. *Chemical Engineering and Processing: Process Intensification, 50*, 478−482.

Wu, L. Y. L., Kerk, W. T., & Wong, C. C. (2013). Transparent conductive film by large area roll-to-roll processing. *Thin Solid Films, 544*, 427−432.

Wu, X., Li, F., Wu, W., & Guo, T. (2014). Flexible organic light emitting diodes based on double-layered graphene/PEDOT: PSS conductive film formed by spray-coating. *Vacuum, 101*, 53−56.

Yang, J., Vak, D., Clark, N., Subbiah, J., Wong, W. W. H., Jones, D. J., et al. (2013). Organic photovoltaic modules fabricated by an industrial gravure printing proofer. *Solar Energy Materials and Solar Cells, 109*, 47−55.

Youn, H., Jeon, K., Shin, S., & Yang, M. (2012). All-solution blade−slit coated polymer light-emitting diodes. *Organic Electronics, 13*, 1470−1478.

Yu, J.-S., Kim, I., Kim, J.-S., Jo, J., Larsen-Olsen, T. T., Søndergaard, R. R., et al. (2012). Silver front electrode grids for ITO-free all printed polymer solar cells with embedded and raised topographies, prepared by thermal imprint, flexographic and inkjet roll-to-roll processes. *Nanoscale, 4*, 6032−6040.

Yu, B., Vak, D., Jo, J., Na, S., Kim, S.-S., Kim, M.-K., et al. (2010). Factors to be considered in bulk heterojunction polymer solar cells fabricated by the spray process. *IEEE Journal of Selected Topics in Quantum Electronics, 16*, 1838−1846.

Zhang, B., Chae, H., & Cho, S. M. (2009). Screen-printed polymer: fullerene bulk-heterojunction solar cells. *Japanese Journal of Applied Physics, 48*, 020208.

Zimmermann, B., Schleiermacher, H.-F., Niggemann, M., & Würfel, U. (2011). ITO-free flexible inverted organic solar cell modules with high fill factor prepared by slot die coating. *Solar Energy Materials and Solar Cells, 95*, 1587−1589.

Photochemical stability of random poly(3-hexylthiophene-co-3-cyanothiophene) and its use in roll coated ITO-free organic photovoltaics

Bérenger Roth
Andrey E. Rudenko
Barry C. Thompson
Frederik C. Krebs

SPIE.

Photochemical stability of random poly(3-hexylthiophene-co-3-cyanothiophene) and its use in roll coated ITO-free organic photovoltaics

Bérenger Roth,[a] Andrey E. Rudenko,[b] Barry C. Thompson,[b,]* and Frederik C. Krebs[a,]*

[a]Technical University of Denmark, Department of Energy Conversion and Storage, Frederiksborgvej 399, 4000 Roskilde, Denmark
[b]University of Southern California, Department of Chemistry and Loker Hydrocarbon Research Institute, 837 Bloom Walk, Los Angeles, California 90089-1661, United States

Abstract. The photochemical stability of the active layer blend for organic solar cells was explored by introducing electron withdrawing cyano groups into the backbone of poly-3-hexylthiophene (P3HT). Random copolymerization of 2-bromo-3-hexyl-5-trimethylstannylthiophene and 2-bromo-3-cyano-5-trimethylstannylthiophene enabled introduction of the cyanogroups along the polythiophene backbone. The percentage of the cyano groups was 10%. The photochemical stability of poly(3-hexylthiophene-co-3-cyanothiophene) (CN-P3HT) was shown to be significantly better than pristine P3HT and the addition of CN-P3HT to P3HT also increased the photochemical stability of the blend. The photochemical stability of bulk heterojunction mixtures of the polymers and their blends with the fullerene phenyl-C61-butyric acid methyl ester ([60]PCBM) were then studied and it was found that [60]PCBM had a significantly more stabilizing effect on P3HT than CN-P3HT and that the stabilization of the bulk heterojunction mixture was dominated by the fullerene. The mixture comprising both fullerene and CN-P3HT, however, demonstrated the highest degree of photochemical stability supporting earlier observations that the stabilizing effects are additive. Finally, the blends were explored in fully printed flexible ITO-free roll coated inverted devices (with an active area of 0.8 cm^2) using two different back PEDOT:PSS electrode compositions and the operational stability of the devices was studied under ISOS-L-2 conditions. The pure P3HT:PCBM devices were found to be the most stable in operation demonstrating that photochemical stability alone is not necessarily the dominant factor for overall device stability. © *2015 Society of Photo-Optical Instrumentation Engineers (SPIE)* [DOI: 10.1117/1.JPE.5.057205]

Keywords: organic photovoltaic; roll-to-roll; photochemical stability; active blend stabilization; random copolymers.

Paper 14056SS received Aug. 26, 2014; accepted for publication Nov. 21, 2014; published online Dec. 22, 2014.

1 Introduction

The organic solar cell can, when in operation, degrade following a myriad of different paths.[1] Most often one degradation mechanism is dominant but in most cases several processes are in play simultaneously. The device failure is a macroscopic observable which is most often established through measuring the electrical performance of the solar cell over time under a given set of experimental conditions with certain environmental stimuli such as temperature, humidity, UV-light, etc. The electrical data can give some information on how the device fails but because it is limited to a measurement of an electrical current, a voltage, and a fill factor, there is generally little that can be said about the many mechanisms that are in play and especially the extent to

---

*Address all correspondence to: Barry C. Thompson, E-mail: barrycth@usc.edu or Frederik C. Krebs, E-mail: frkr@dtu.dk

which they are present. One of the known failure modes is the photochemical reaction of the organic constituents especially with oxygen from the atmosphere. The combination of light and oxygen will bleach the materials and destroy the electronic properties needed for solar cell operation. For some materials, such as the polyphenylenevinylenes, this mechanism can be the dominant failure path when the device is operated in dry air. The extent of degradation as a consequence of photochemical oxidation is most often eliminated by packaging the device or testing it under inert conditions to significantly reduce the effect of oxygen. It will, however, still be in operation with the amount of oxygen available and, in a practical device, there is always some oxygen present. Efforts made to counteract the failure of organic solar cells are thus sought through reduction of all the known failure modes and in the case of photochemical stability, it has been shown that the chemistry of the conjugated materials used for the solar cells plays a decisive role.[2–6] In addition to the chemistry, the constitution of the film and its morphology are also important.[7] It is, for instance, important that photochemical stability studies are carried out on a number of different film thicknesses before data between the materials can be compared. Another factor that influences the performance and stability of organic solar cell devices is the morphology of the active blend.[8] A number of reports have demonstrated how morphology can be stabilized and used to improve device performance over time.[9,10] Most importantly, it was demonstrated that the chemistry also plays a central role not only on morphological stabilization, but also on the morphology that can be achieved.[11] Successful attempts to improve photochemical stability through chemical modification thus lead to unintended changes in the morphological behavior that most often imply lower power conversion efficiency and perhaps even a poorer morphological stability. The same observations can be made in the opposite case where attempts to improve the morphological stability adversely affect photochemical stability. It has to be borne in mind that morphological stability and photochemical stability are just two important factors and that there are a large number of additional parameters that intertwine, thus making the art of improving the operational stability of the organic solar cell highly challenging.

In this work, we study the effect of enhancing the photochemical stability of the conjugated polymer through chemical modification with electron withdrawing groups and we further establish the effect this has on the operational stability of devices.

2 Experimental Methods

2.1 CN-Poly-3-Hexylthiophene Synthesis

Synthesis of CN-P3HT was performed according to the literature report without any modifications.[12] 2-Bromo-3-hexyl-5-trimethylstannylthiophene and 2-bromo-3-cyano-5-trimethylstannylthiophene were dissolved in dry DMF in a 90:10 molar ratio to yield a 0.04 M (overall) solution. This solution was degassed with nitrogen gas flow for 10 min. Then 4 mol % of $Pd(PPh_3)_4$ was added and the reaction mixture was degassed for 20 more minutes. The reaction mixture was then immersed into a preheated to 95°C oil bath and stirred at that temperature under nitrogen atmosphere for 48 h. Then the reaction mixture was cooled, precipitated into methanol, filtered, and purified via Soxhlet extraction with methanol, hexanes and finally chloroform. The chloroform fraction was concentrated *in vacuo* and precipitated into methanol. The polymer was filtered and dried in high vacuum overnight to yield CN-poly-3-hexylthiophene (P3HT) in 50% yield (M_n = 12 kDa, polydispersity index = 2.4). ^{1}H NMR (600 MHz, $C_2D_2Cl_4$): δ 7.41 to 6.95 (m, 1.00 H), 2.77 to 2.55 (m, 1.80 H), 1.68 (m, 1.81 H), 1.44 to 1.32 (m, 5.44 H), 0.88 (m, 2.51 H) ppm.

2.2 Photochemical Stability

The following six solutions were prepared: P3HT (15 mg/mL); P3HT:PCBM (15 mg/mL: 15 mg/mL); CN-P3HT (15 mg/mL); CN-P3HT:PCBM (15 mg/mL: 15 mg/mL); CN-P3HT: P3HT (7.5 mg/mL : 7.5 mg/mL); CN-P3HT:P3HT:PCBM (7.5 mg/mL : 7.5 mg/mL : 15 mg/mL). P3HT was obtained from BASF (Sepiolid P-200), PCBM was obtained from Merck and CN-P3HT was synthesized following the procedure described above (Sec. 2.1). All the solutions were made

with Chlorobenzene (from Aldrich) and left stirring overnight at 70°C. The solutions were then filtered with a 0.45 micron Teflon filter before being spin coated on 25×50 mm^2 glass slides at 850 rpm for 30 s. These films were then put in an automatized system described previously[3] to study their photochemical stability. Briefly, the film is placed under a Steuernagel solar simulator with an Osram 1200 W metal halide arc lamp giving a AM1.5G spectrum of 1000 W/m^2 intensity. The absorbance of the sample is monitored in multiple points at regular intervals with a UV-vis spectroscopic probe set up with an optical fiber-based CCD spectrometer (Avantes AvaSpec 1024) and a halogen/deuterium light source (Avantes AvaLight-DHc). Degradation rates are obtained by calculating the decrease of the number of absorbed photons over time.

2.3 Solar Cell Preparation

Three solutions were prepared P3HT:PCBM (15 mg/mL : 15 mg/mL); CN-P3HT:PCBM (15 mg/mL : 15 mg/mL); CN-P3HT:P3HT:PCBM (7.5 mg/mL : 7.5 mg/mL : 15 mg/mL) with a mixture of chlorobenzene (100 parts), chloroform (10 parts) and chloronaphtalene (3 parts). All the solutions were left stirring overnight at 70°C before being filtered with a 0.45 micron Teflon filter. The organic solar cells were prepared using the roll-to-roll coater described in Ref. 13. The process was the same for all three solutions. The solution was slot-die coated using a 10 mm meniscus guide (flow rate: 0.15 mL/ min; speed: 1 m/ min) on a 1 m stretch of Flextrode[14] heated up to 70°C. Then also using a 10-mm wide meniscus guide two different types of PEDOT:PSS were slot-die coated on top of the active layer. PEDOT:PSS 5010 was slot-die coated on half of the stripes (1.2 mL/ min; 0.8 m/ min). On the other half, a three layer PEDOT: PSS structure[15] was slot-die coated. First, PEDOT:PSS F10 diluted with isopropanol (IPA) (1:4 in volume) was coated (0.11 mL/ min : 1.3 m/ min), then PEDOT:PSS Al 4083 diluted with IPA (1:2 in volume) (0.3 mL/ min; 1.3 m/ min), and PEDOT:PSS F10 diluted with IPA (1:2 in volume (0.5 mL/ min; 1.3 m/ min). Finally, the back silver grid and the silver contact with the front electrode were flexoprinted using a mask and silver ink (Dupont 5025). The prepared cells had an active area of 0.8 cm^2 and were encapsulated with 15×15 mm^2 glass slides using UV-curing epoxy (DELO LP655) and annealed at 120°C for 2 min.

2.4 Lifetime Measurements

The cells were tested according to the ISOS-L-2 standard describe in Ref. 16. The cells were mounted under a solar simulator and cooled down to about 60°C to 65°C with a fan (unregulated). The IV characteristics were monitored using a Keithley 2400 SMU.

3 Results and Discussion

3.1 Photochemical Stability

One of the most successful conjugated donor materials for polymer solar cells is P3HT that performs very well over most of the parameter space that affects the operational stability of devices. It enables stable morphologies and presents a significant photochemical stability compared to, for instance, the polyphenylenevinylenes. In addition, it is a mechanically robust material which is central to the operation of, for instance, flexible devices.[17,18] Several reports describe attempts to improve the performance of P3HT through chemical modification and the general conclusion is that the modifications that can be made to the chemical structure of a material while maintaining the properties must be slight and this has presented some difficulty. The most elegant approaches to this are random[12,19] and semirandom copolymerization,[20,21] where the backbone of the polymer is only changed slightly such that the general properties (i.e., morphology, structural order) can be maintained while optical properties such as the band gap can be changed very significantly such that a higher degree of optical absorption is achieved and better light harvesting and a higher power conversion efficiency are realized.[22] In careful studies, it was shown that copolymerization by the random or semirandom incorporation of a functional unit with the desired properties

Fig. 1 Chemical structures of PCBM, P3HT, and CN-P3HT.

can take place without changing the bulk properties of i.e., P3HT, when 5% to 15% of a comonomer is incorporated.[22] In this work, we sought to improve the photochemical stability of P3HT by incorporation of cyano groups in the backbone without changing the other parameters of the traditional P3HT material. We incorporated 10% cyano groups (as seen in Fig. 1) and found that it only marginally affects the optical behavior as compared to native P3HT, which is consistent with previous literature reports.[12,23]

The absorbance spectra of the polymer films before degradation are shown in Fig. 2 and the photochemical degradation curves of P3HT, CN-P3HT, and the CN-P3HT:P3HT mixtures as well as their blends with PCBM are shown in Fig. 3. The spectra shown in Fig. 2 are similar for P3HT, CN-P3HT, and the blend showing that the incorporation of cyano groups did not significantly modify the optical properties of P3HT. As explained above, the photochemical degradation was monitored by measuring the absorbance of the different layers at regular intervals. The decrease in absorbance under continuous light exposure is shown in Fig. 3.

The effect of incorporating cyano groups into the backbone has a clear effect on the photochemical stability of the pristine polymer and the cyanopolymer presents an improvement in photochemical stability by a factor of 2. Interestingly, CN-P3HT can also be used to improve the photochemical stability of native P3HT by simple mixing the two materials together. As shown in Table 1, the CN-P3HT:P3HT blend degrades at the same rate as CN-P3HT.

As shown in Table 1, all the films have a starting absorbance between 0.4 and 1 meaning that the influence of film thickness on the observed degradation rates can be neglected.[7] The degradation rates that are compiled in Table 1 are averaged over all the points where the absorbance of the film was monitored. This is achieved using an automated robotic system that enables UV-vis measurement on a very large number of independent samples over time during the photochemical degradation. All films containing PCBM have a similar degradation rate, showing that PCBM is the dominant stabilizer in these cases. However, the PCBM-free films have different degradation rates. This clearly shows that the inclusion of CN groups in the polymer chain increases the photochemical stability of the pristine polymer, whereas PCBM is a significantly better stabilizer.
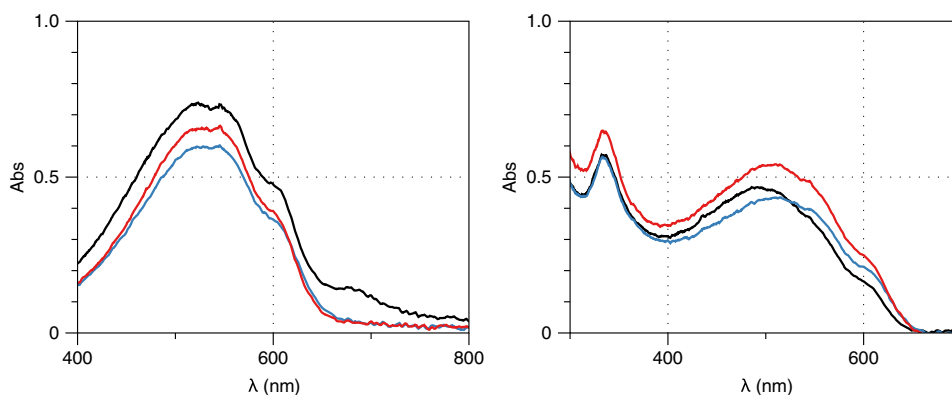
Fig. 2 The UV-spectra are shown for the two polymers (P3HT in black, CN-P3HT in blue) explored and their blend (red) pure (left) or mixed with PCBM (right).
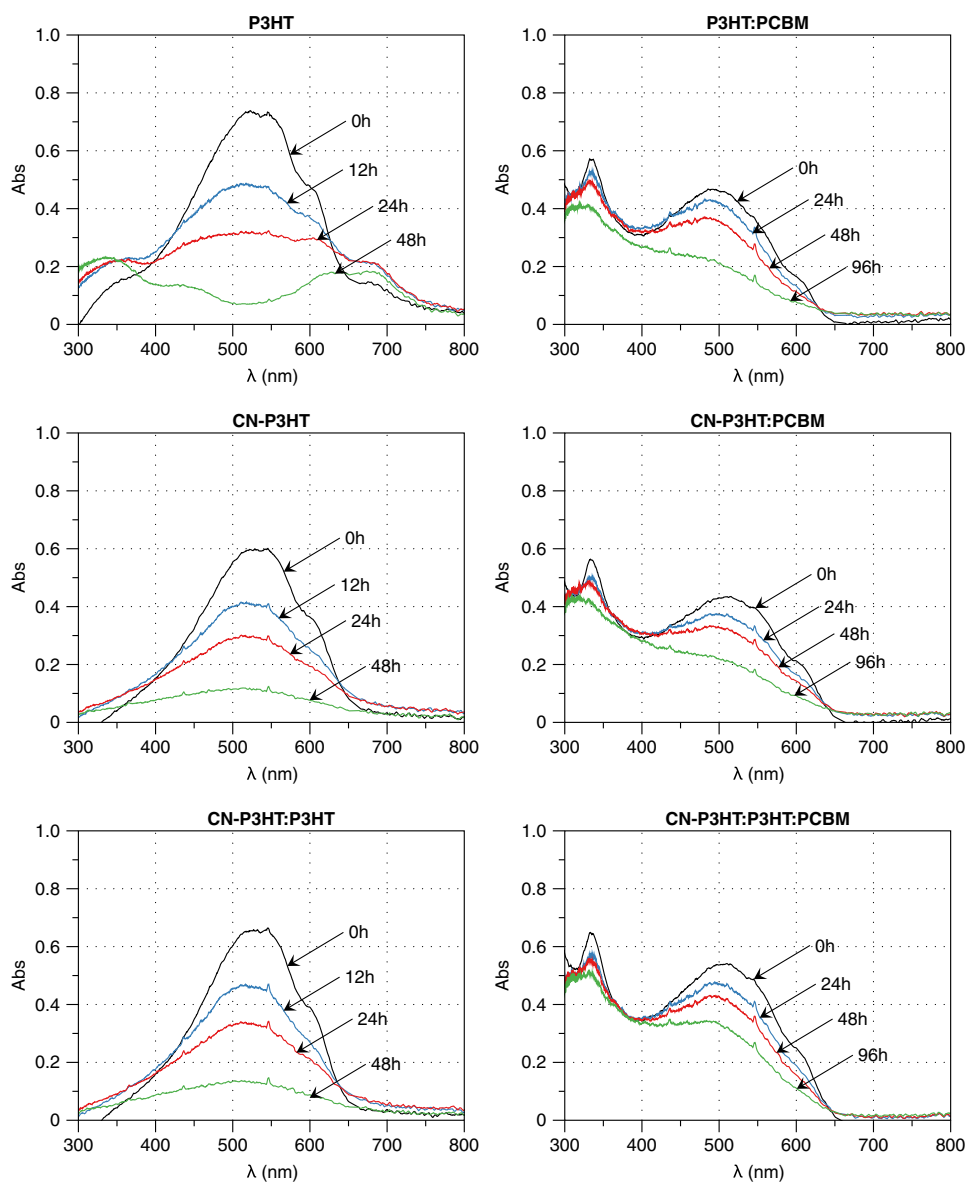
Fig. 3 Evolution of absorbance of P3HT (top left), CN-P3HT (middle left), CN-P3HT:P3HT (bottom left), P3HT:PCBM (top right), CN-P3HT:PCBM (middle right) and CN-P3HT:P3HT:PCBM (bottom right) under light exposure.

Table 1 The initial film absorbances and degradation rates of the six different different materials combinations.

Film	Starting absorbance	Degradation rate (%/h)
P3HT	0.60 ± 0.05	2.3 ± 0.4
CN-P3HT	0.61 ± 0.04	1.48 ± 0.04
CN-P3HT:P3HT	0.66 ± 0.03	1.4 ± 0.2
P3HT:PCBM	0.46 ± 0.06	0.46 ± 0.04
CN-P3HT:PCBM	0.44 ± 0.03	0.40 ± 0.02
CN-P3HT:P3HT:PCBM	0.47 ± 0.02	0.38 ± 0.03

3.2 *IV Characteristics*

The solar cell preparation process used in this study was optimized for regular P3HT cells and not CN-P3HT. In some devices, a three PEDOT:PSS layers' structure has shown to perform better than the commonly used Agfa 5010 PEDOT:PSS. For this reason, two types of back PEDOT:PSS were tested in order to find which one works better with CN-P3HT. IV-curves for each type of cells are shown in Fig. 4. Just by looking at these curves, the P3HT cells appear to perform better, which may in part be due to utilization of the solar cell processing conditions as well as the polymer:fullerene ratio optimal for P3HT rather than CN-P3HT.

Three cells of each type were used for this study. Their characteristics are given in Table 2.

For the cells with PEDOT:PSS 5010 as back PEDOT:PSS, the P3HT cells have an efficiency about twice higher than the cells with CN-P3HT. The cells with the mix of P3HT and CN-P3HT as an active layer have efficiencies in between. The same pattern is observed for the cells with the three layers back PEDOT:PSS. It shows that the addition of the CN group on the P3HT backbone decreases the photovoltaic properties of the active layer. This result differs from previous literature reports, which demonstrate that introduction of 10% CN groups into P3HT backbone leads to an increase of PCE mainly through the enhancement of V_{oc} for solar cells spin-coated on ITO.[12,24] Enhancement of the V_{oc} is also observed for the ITO-free cells prepared for this study, but the differences may originate from inherently different active layer morphologies as well as from the fact that the utilized polymer:PCBM ratio was optimized for P3HT rather than CN-P3HT in the current case printed ITO-free devices.

3.3 *Lifetime Measurements*

Typical decay curves for each type of cells are plotted in Fig. 5. For both back PEDOT:PSS, the P3HT cell has an efficiency stabilized around 80% of its initial value. The cells with CN-P3HT
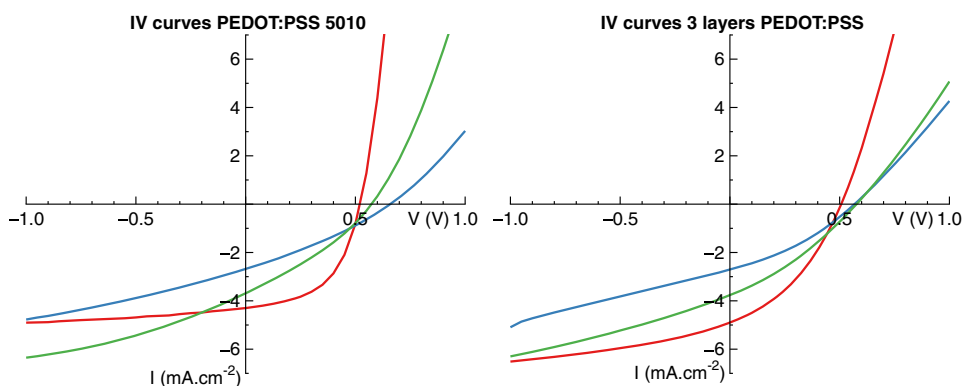
Fig. 4 Typical IV curves of P3HT cell (red), CN-P3HT (blue), CN-P3HT:P3HT (green) with back PEDOT:PSS 5010 (left) or three layered PEDOT:PSS structure (right).

Table 2 IV-characteristics.

Cell type	Back PEDOT:PSS	PCE (%)	V_{oc} (V)	I_{sc} (mA)	FF (%)
P3HT	5010	1.23 ± 0.07	0.53 ± 0.01	3.7 ± 0.3	51 ± 2
	three layers	0.94 ± 0.05	0.51 ± 0.01	3.9 ± 0.2	37.8 ± 0.2
CN-P3HT	5010	0.52 ± 0.07	0.66 ± 0.01	2.1 ± 0.2	29 ± 2
	three layers	0.6 ± 0.09	0.62 ± 0.04	2.3 ± 0.2	34.7 ± 0.3
CN-P3HT:P3HT	5010	0.71 ± 0.04	0.57 ± 0.01	3.2 ± 0.3	31 ± 1
	three layers	0.5 ± 0.1	0.57 ± 0.01	2.2 ± 0.6	29 ± 4
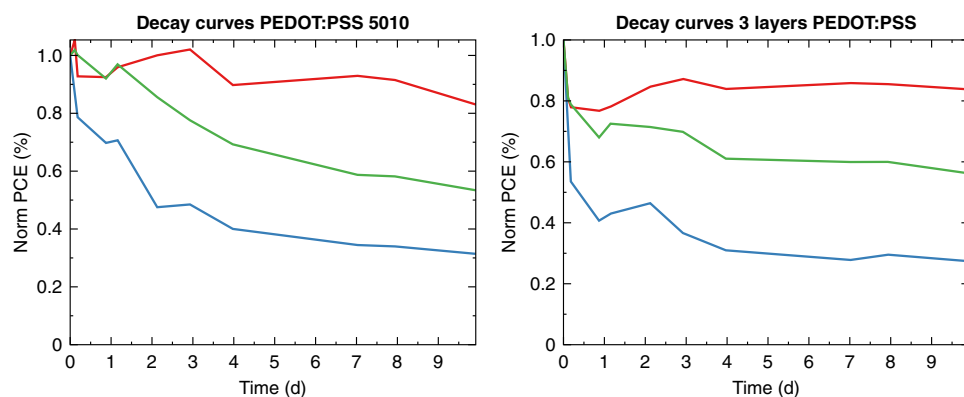
Fig. 5 The decay curves for one cell of each type is shown, (red) P3HT, (blue) CN-P3HT, (green) CN-P3HT:P3HT.

and CN-P3HT:P3HT as the active layer, decay much faster and are only stabilized after reaching about 50% of their starting value. The cells with only CN-P3HT as the active layer, clearly decay much faster with both back PEDOT:PSS. All the stability indicators are given in Table 3, where T80 is the time it takes the cells to reach an efficiency of 80% of their starting value (E_0), T_S and E_S are the time and the efficiency when the degradation stabilizes after the initial burn-in and T_{S80} is the time it takes starting from T_S to reach 80% of E_S. For CN-P3HT:P3HT with the triple PEDOT:PSS back electrode, the values are given for only one cell. Cells with only CN-P3HT degrade by 20% in a few hours. After stabilizing, the cells with PEDOT:PSS 5010 are more stable; it takes them about 2 days to reach 80% of E_S compared to about a day for the ones with the three-layered PEDOT:PSS structure. For the cells with the mix as the active layer, the cells with PEDOT:PSS 5010 are more stable than the cells with only CN-P3HT and take about 10 times longer to degrade by 20%. These cells also did not reach 80% of E_S during the length of the study. For the cells with triple PEDOT:PSS layer as back PEDOT:PSS and CN-P3HT:P3HT as the active layer, two cells failed early during the study. The remaining cell degrades as fast as the ones with only CN-P3HT at the beginning and has a T_{80} of 3.5 h. However, once stabilized, the degradation is faint. Finally, the P3HT cells are much more stable than all the others as illustrated by the plots in Fig. 5. Only one cell degrades by 20% during the study, the other five are still above 80% of their starting value at the end of the test. This study shows that even though CN-P3HT has by itself a better photochemical stability than P3HT once used in a full device it does not perform as well and degrades much faster than devices with regular P3HT.

Table 3 Stability data (in hours) for the PCE (in %) averaged over three cells for each type of cell during ISOS-L2 testing.

Active layer	Back PEDOT:PSS	E_0 (%)	E_S (%)	T_{80} (h)	T_S (h)	T_{S80} (h)
P3HT	5010	1.23 ± 0.07	1.16 ± 0.04	235 ± 4	88 ± 5	237.6[a]
P3HT	three layers	0.94 ± 0.05	0.89 ± 0.05	237.6[a]	78 ± 7	237.6[a]
CN-P3HT	5010	0.52 ± 0.07	0.24 ± 0.03	5 ± 3	40 ± 16	58 ± 10
CN-P3HT	three layers	0.6 ± 0.09	0.37 ± 0.01	1.88 ± 0.07	3.6 ± 0.8	20 ± 30
CN-P3HT:P3HT	5010	0.71 ± 0.04	0.40 ± 0.02	53 ± 7	150 ± 40	237.6[a]
CN-P3HT:P3HT	three layers[b]	0.56	0.51	3.5	20.9	237.6[a]

[a]T_f (the duration of the experiment) is given in these cases, meaning that the cells did not reach 80% of E_0 or E_S. The values for T_{80} are expected to be significantly higher.
[b]The values for only one cell are given because two cells failed during the experiment.

4 Conclusion

We have demonstrated that incorporation of cyano groups into the backbone of P3HT improves the photochemical stability by a factor of 2. Simple mixing of native P3HT with CN-P3HT also leads to a similar improvement in the photochemical stability of the blend. Mixtures with PCBM were also studied to establish the effect on blends relevant to functional solar cells and PCBM was found to present a more stabilizing effect than CN-P3HT. The studies on devices showed that the operational stability of devices was not significantly increased by the improved photochemical stability and traditional P3HT:PCBM bulk heterojunction devices presented the most stable behavior under operation. While our efforts clearly showed that photochemical stability of a polymer can be improved with minimum perturbation of the optical properties, we also found that a photochemically stable material is not the only parameter that must be optimized on the path to stable and high performing materials for polymer solar cells.

References

1. M. Jørgensen, K. Norrman, and F. C. Krebs, "Stability/degradation of polymer solar cells," *Sol. Energy Mater. Sol. Cells* **92**, 686–714 (2008).
2. M. Manceau et al., "Photochemical stability of π-conjugated polymers for polymer solar cells: a rule of thumb," *J. Mater. Chem.* **21**, 4132–4141 (2011).
3. T. Tromholt et al., "Photochemical stability of conjugated polymers, electron acceptors and blends for polymer solar cells resolved in terms of film thickness and absorbance," *J. Mater. Chem.* **22**, 7592–7601 (2012).
4. H. D. Burrows et al., "Mechanistic studies on the photodegradation of 2,5-dialkyloxyl-substituted para-phenylenevinylene oligomers by singlet oxygen," *Photochem. Photobiol. Sci.* **9**, 942–948 (2010).
5. Y. Soon et al., "Correlating triplet yield, singlet oxygen generation and photochemical stability in polymer/fullerene blend films," *Chem. Commun. (Camb).* **49**, 1291–1293 (2013).
6. E. T. Hoke et al., "The role of electron affinity in determining whether fullerenes catalyze or inhibit photooxidation of polymers for solar cells," *Adv. Energy Mater.* **2**, 1351–1357 (2012).
7. M. V. Madsen et al., "Influence of processing and intrinsic polymer parameters on photochemical stability of polythiophene thin films," *Polym. Degrad. Stab.* **97**, 2412–2417 (2012).
8. J. V. Loos, "Volume morphology of printable solar cells," *Mater. Today* **13**, 14–20 (2010).
9. L. Derue et al., "Thermal stabilisation of polymer-fullerene bulk heterojunction morphology for efficient photovoltaic solar cells," *Adv. Mater.* **26**, 5831–5838 (2014).
10. H. C. Wong et al., "Morphological stability and performance of polymer-fullerene solar cells under thermal stress: the impact of photoinduced PC60BM oligomerization," *ACS Nano* **8**, 1297–308 (2014).
11. J. U. Lee et al., "Degradation and stability of polymer-based solar cells," *J. Mater. Chem.* **22**, 24265–24283 (2012).
12. P. P. Khlyabich, A. E. Rudenko, and B. C. Thompson, "Random poly(3-hexylthiophene-co -3-cyanothiophene) copolymers with high open-circuit voltage in organic solar cells," *J. Polym. Sci. A* **52**, 1055–1058 (2014).
13. H. F. Dam and F. C. Krebs, "Simple roll coater with variable coating and temperature control for printed polymer solar cells," *Sol. Energy Mater. Sol. Cells* **97**, 191–196 (2012).

14. M. Hösel et al., "Fast inline roll-to-roll printing for indium-tin-oxide-free polymer solar cells using automatic registration," *Energy Technol.* **1**, 102–107 (2013).

15. T. R. Andersen et al., "A rational method for developing and testing stable flexible indium- and vacuum-free multilayer tandem polymer solar cells comprising up to twelve roll processed layers," *Sol. Energy Mater. Sol. Cells* **120**, 735–743 (2014).

16. M. O. Reese et al., "Consensus stability testing protocols for organic photovoltaic materials and devices," *Sol. Energy Mater. Sol. Cells* **95**, 1253–1267 (2011).

17. D. J. Lipomi et al., "Toward mechanically robust and intrinsically stretchable organic solar cells: evolution of photovoltaic properties with tensile strain," *Sol. Energy Mater. Sol. Cells* **107**, 355–365 (2012).

18. S. Savagatrup et al., "Mechanical properties of conjugated polymers and polymer-fullerene composites as a function of molecular structure," *Adv. Funct. Mater.* **24**, 1169–1181 (2014).

19. B. Burkhart, P. P. Khlyabich, and B. C. Thompson, "Influence of the ethylhexyl side-chain content on the open-circuit voltage in rr-poly(3-hexylthiophene- co -3-(2-ethylhexyl)thiophene) copolymers," *Macromolecules* **45**, 3740–3748 (2012).

20. P. P. Khlyabich et al., "Efficient solar cells from semi-random P3HT analogues incorporating diketopyrrolopyrrole," *Macromolecules* **44**, 5079–5084 (2011).

21. B. Burkhart et al., "Semi-random" multichromophoric rr-P3HT analogues for solar photon harvesting," *Macromolecules* **44**, 1242–1246 (2011).

22. P. P. Khlyabich et al., "Optimization and simplification of polymer–fullerene solar cells through polymer and active layer design," *Polymer (Guildf)* **54**, 5267–5298 (2013).

23. D. R. Greve, J. J. Apperloo, and R. A. J. Janssen, "Synthesis and characterisation of novel regioregular polythiophenes—tuning the redox properties," *Eur. J. Org. Chem.* **2001**, 3437–3443 (2001).

24. A. E. Rudenko, P. P. Khlyabich, and B. C. Thompson, "Random poly(3-hexylthiophene- co -3-cyanothiophene) copolymers via direct arylation polymerization (DArP) for organic solar cells with high open-circuit voltage," *ACS Macro Lett.* **3**, 387–392 (2014).

Biographies of the authors are not available.

The Critical Choice of PEDOT:PSS Additives for Long Term Stability of Roll-to-Roll Processed OPVs

Bérenger Roth, Gisele A. dos Reis Benatto, Michael Corazza, Roar R. Søndergaard, Suren A. Gevorgyan, Mikkel Jørgensen, and Frederik C. Krebs*

The impact of additives mixed with poly(3,4-ethylenedioxythiophene):polystyrenesulfonate (PEDOT:PSS) on the stability of organic photovoltaic modules is investigated for fully ambient roll-to-roll (R2R) processed indium tin oxide free modules. Four different PEDOT:PSS inks from two different suppliers are used. The modules are manufactured directly on barrier foil without a UV filter to accelerate degradation and enable completion of the study in a reasonable time span. The modules are subjected to stability testing following well-established protocols developed by the international summit on organic photovoltaic stability (ISOS). For the harsh indoor test (ISOS-L-3) only a slight difference in stability is observed between the different modules. During both ISOS-L-3 and ISOS-D-3 one new failure mode is observed as a result of tiny air inclusions in the barrier foil and a R2R method is developed to detect and quantify these. During outdoor operation (ISOS-O-1) the use of ethylene glycol (EG) as an additive is found to drastically increase the operational stability of the modules as compared to dimethylsulfoxide (DMSO) and a new failure mode specific to modules with DMSO as the additive is identified. The data are extended in an ongoing experiment where DMSO is used as additive for long-term outdoor testing in a solar park.

1. Introduction

The promise of organic solar cells being a low cost alternative to current photovoltaic technologies has long been supported by the prospect of low cost and fast roll-to-roll (R2R) manufacturing. This forecast ensues from the organic photovoltaics (OPVs) having the ability to be coated and/or printed at high speed and low temperature on flexible substrates such as polyethyleneterephtalate. Recently, a study demonstrated the manufacture and deployment of a large solar park connected to the grid with an energy payback time lower than any other PV technology.[1] This shows that if given the possibility to cover very large areas at low cost the demand for very high efficiency becomes less crucial.

However, in addition to low cost OPV must also provide a high operational stability as this is also an essential requirement for commercial viability. In order to yield similar energy return factors, compared to first and second generation photovoltaics, a few years of operational stability are needed with the current materials and efficiencies.[2–6] Because of the complex multilayer structure, which contains not only several different materials but also a multitude of interfaces, OPVs can degrade through multiple pathways[2] and it can be very difficult to determine which materials combinations will provide the most stable cell. In addition to the materials, also the solvents used in the processing can have an influence on morphology and through that on the performance and operational stability of a device. Poly(3,4-ethylenedioxythiophene): polystyrenesulfonate (PEDOT:PSS) is an example of a material which is extensively used in OPVs as both hole-conductor and as a transparent conducting electrode. It comes in a multitude of formulations from different commercial suppliers (e.g., Agfa and Heraeus) with the properties (especially the conductivity) of PEDOT:PSS being tuned by doping or addition of high boiling solvents.[7–10] It is well known that PEDOT:PSS plays a major role in OPV stability[11–14] but the role of the high boiling additives on stability has not yet been examined. Because of their high boiling points, trace amounts of these additives are very likely to remain after coating/printing of the PEDOT:PSS and it is very plausible that such compounds could influence the long term operational lifetime of the OPV.

Here we present an extensive study on the stability of indium tin oxide-free OPV modules based on the previously reported freeOPV architecture (**Figure 1**) that is manufactured using full R2R processing for all steps under ambient conditions.[15,16] The initial prescreening was conducted on first generation freeOPV modules which has silver electrodes. The main study was then carried out with a second generation of freeOPV modules in which the silver electrodes have been replaced by printed carbon. The stability of these modules, where different types of PEDOT:PSS have been used at the front and the back of the cell, is studied in order to select the best PEDOT:PSS for long term stability of OPVs for large scale production.

B. Roth, G. A. dos Reis Benatto, M. Corazza,
Dr. R. R. Søndergaard, Dr. S. A. Gevorgyan,
Dr. M. Jørgensen, Prof. F. C. Krebs
Department of Energy Conversion and Storage
Technical University of Denmark
Frederiksborgvej 399, DK-4000 Roskilde, Denmark
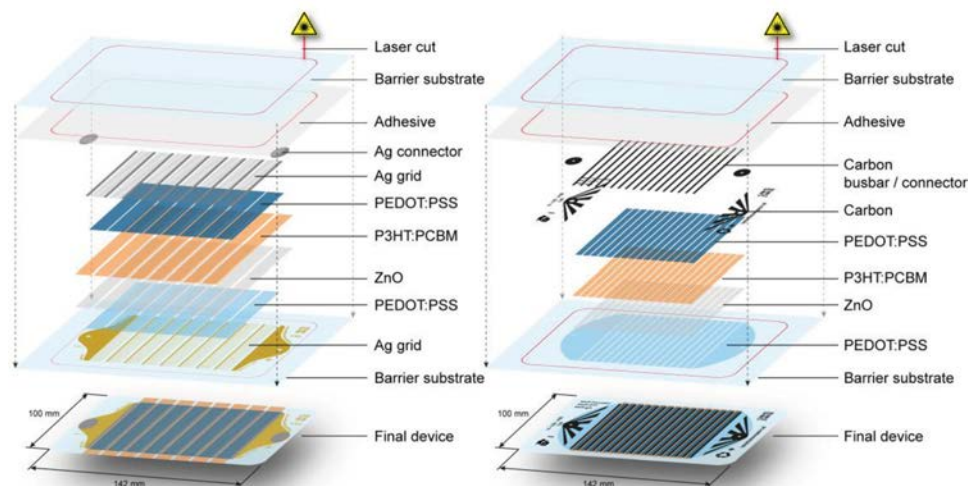E-mail: frkr@dtu.dk

Figure 1. Illustration of the multilayer stack of the silver freeOPV (left) and of the carbon freeOPV (right). The left illustration is reproduced with permission.[15]

2. Results and Discussion

Four types of highly conductive PEDOT:PSS inks typically used in R2R manufacturing of OPVs were selected for this study. The preparation of these is described in the Experimental Section. The commercial name of the PEDOT:PSS and the high boiling additives associated with each of these are given in **Table 1**.

The architecture of the first generation of freeOPV (shown in Figure 1) comprises two PEDOT:PSS layers, one between the bottom silver grid and the zinc oxide (ZnO) layer and a second one on top of the active layers. These are in the following referred to as front PEDOT and back PEDOT, respectively.

The freeOPV process was developed using rotary screen printed PEDOT:PSS layers and this study therefore focuses only on the four PEDOT:PSS inks which we have found to be compatible with this type of screen printing process. Furthermore, the four inks are not all suitable for both the front and back PEDOT layer. The front PEDOT needs to be thin and highly conducting in order to let light through while maintaining good conductivity whereas the back PEDOT has no requirement for transparency but it should generally be thicker in order to comply with the silver or carbon printing. The state of the art stack at the beginning of this study used PEDOT:PSS with DMSO as high boiling additive (hereafter called PDMSO-1) as front PEDOT:PSS and P5010 as back

PEDOT:PSS. Devices with this architecture have previously been shipped all around the world through the freeOPV initiative.[15] Five different combinations (C-1–C-5) of the four PEDOT types were selected for the prescreening as shown in **Table 2** together with their initial photovoltaic parameters: power conversion efficiency (PCE), open circuit voltage (V_{oc}), short circuit current (I_{sc}) and fill factor (FF). In addition to using DMSO as the high boiling solvent we also employed PEDOT:PSS mixed with ethylene glycol (hereafter called PEG). A sixth combination (C-6) which was later used in the main study is also shown in Table 2 which differs in that it employed carbon electrodes instead of silver and was chosen based on the outcome of the prescreening study.

The manufacture of modules using full R2R processing is time consuming and ensuing stability testing of a large number of those is necessary to obtain good statistics. The most rational approach is to make a shorter initial screening to get an indication of the spread and parameters followed by the main stability test. The ageing experiments were carried out for the most stable combinations under different conditions defined by the international summit on OPV stability (ISOS)[19] shown in **Table 3**. The initial test involved ten modules of each type for each condition.

2.1. Initial Screening

During this primary screening, modules of each combination underwent lifetime studies according to ISOS-L-2, ISOS-L-3, ISOS-D-3, and ISOS-D-2. As stated above, C-1 was the first one used in freeOPV and was therefore extensively studied at the time of its release.[17] The results from that study are compared with the four other combinations studied here. Comparing the results of both studies is only possible because both are following the ISOS standards and a sufficient number of modules were lifetime tested to ensure that data were representative and not dominated by singular defects from the manufacturing process.

Table 1. Composition of the commercially available PEDOT:PSS formulations.

	P5010	PDMSO-1[a]	PEG-1	PDMSO-2[a]
PEDOT:PSS	Agfa 5010	PH1000	PH1000	PH1000
High boiling additive	Unknown	DMSO	EG	DMSO
Solid content [% w/w]	3%	2.2	2.2	2.2
Additive content [% w/w]	Unknown	5	5	5

[a]According to the manufacturer PDMSO-2 contains a surfactant and a cross-linking agent which do not enter in the composition of PDMSO-1.

www.MaterialsViews.com

ADVANCED
ENERGY
MATERIALS
www.advenergymat.de

FULL PAPER

Table 2. Initial performances of the PEDOT:PSS combinations on freeOPV modules comprising eight serially connected cells and silver grid electrodes. No UV-filter was employed in the barrier stack that accelerates degradation. The last column shows data for the C-6 PEDOT:PSS combination that was not a part of the initial screening study. C-6 was chosen as an additional PEDOT:PSS combination based on the outcome of the screening study (C-1–C-5).

Combination		C-1[a]	C-2	C-3	C-4	C-5	C-6
Front PEDOT:PSS		PDMSO-1	PDMSO-1	PEG-1	PDMSO-1	PEG-1	PEG-1
Back PEDOT		P5010	PEG-1	PEG-1	PDMSO-2	PDMSO-2	P5010
Initial performances[b]	PCE [%]	1.75 ± 0.06	1.1 ± 0.2	1.3 ± 0.1	1.14 ± 0.08	0.81 ± 0.07	1.57 ± 0.08
	V_{OC} [V]	4.1 ± 0.3	3.9 ± 0.2	3.9 ± 0.2	3.9 ± 0.1	3.1 ± 0.3	8.3 ± 0.2
	I_{SC} [mA]	40 ± 2	35 ± 4	39 ± 2	38 ± 2	40 ± 2	12.2 ± 0.8
	FF [%]	60 ± 4	47 ± 3	50 ± 2	44 ± 1	37 ± 2	47 ± 1

[a]Data extracted from ref. [17,18]; [b]Mean values of eight modules for C-1–C-5 and 35 modules for C-6.

Figure 2 shows the radar plot of the lifetime performance for the modules with different combinations expressed via T_{80} values (the time it takes for the module to reach the 80% of the initial performance). In the case where the efficiency had not decreased by 20% at the end of the study the final time (T_f) was used instead of T_{80}. In addition to T_{80} the other relevant degradation parameters are the performance value when the degradation pattern switches into a more stabilized mode (E_S) and the time it takes to reach 80% of the value calculated from that point (T_{S80}).

The results shown in Figure 2 show that C-4 underperforms in all the ISOS tests compared to the four other combinations. Therefore C-4 was discarded for the main study. All the other combinations perform relatively well in most tests especially C-2, C-3, and C-5. However modules manufactured with C-5 have a poor initial efficiency, and adding that the poor stability of C-4 seems to indicate that PDMSO-2 used as back PEDOT can lower the stability of the module, we chose to discard C-5 as well for the main study. Finally, the good stability of C-3 based modules indicates that PEG-1 is a promising candidate as front PEDOT. So in addition to the three that performed well in the prescreening we decided to add a new combination C-6 with PEG-1 as front PEDOT and P5010 as back PEDOT to the main study.

2.2. Main Stability Study

By the time the main stability study was started the design of the freeOPV had evolved[16] to a completely silver free architecture. The front electrode here consists solely of the high conducting front PEDOT:PSS and the back electrode of a combination of PEDOT:PSS and carbon layers. An illustration of the structure of such a module is shown in Figure 1. The modules with the combinations C-1, C-2, C-3, and C-6 used in the main stability study were manufactured using this architecture.

A total of 35 modules were tested for each combination: five modules for ISOS-L-3 and ten for the other tests. For a given combination all the modules had a similar initial efficiency. The grouping of the initial efficiencies is illustrated on the lower right in **Figure 3**. This illustrates the high reproducibility of the manufacturing process. The results of the collected stability studies are compiled in **Figures** 3 and 4.

For ISOS-D-1, all the modules were kept in dark storage at room temperature. Under these conditions all the combinations were extremely stable and remained above 80% of their initial efficiency after 126 days as expected. At the end of the test C-1 and C-6 had degraded by roughly 10% while C-2 and C-3 retained efficiencies close to their initial values. The main conclusion from this study is that, when stored in the dark, PEG-1 gives a slightly better stability than P5010 as back PEDOT.

Under high humidity/high temperature conditions in the main stability test (ISOS-D-3 conditions) all the combinations degrade fast and almost no stabilization is seen for either combination (Figure 4). A small difference can be observed between those that have PDMSO-1 as front PEDOT (C-1 and C-2) and those that have PEG-1 (C-3 and C-6). After 14 days under the ISOS-D-3 conditions the C-1 modules have degraded by 56% and the C-2's by 70% whereas the degradation for C-3 and C-6 is 90% and 75%, respectively. The same trend is observed when looking at the degradation parameters (Figure 3). C-1 and C-2 have higher T_{80} and T_{S80} than C-3 and C-6. Therefore under ISOS-D-3 conditions modules with PDMSO-1 as front PEDOT perform more stable than modules with PEG-1. In addition under the hot and humid conditions P5010 seems to be slightly more stable as back PEDOT compared to PEG-1.

Table 3. ISOS conditions[19] employed in this study.

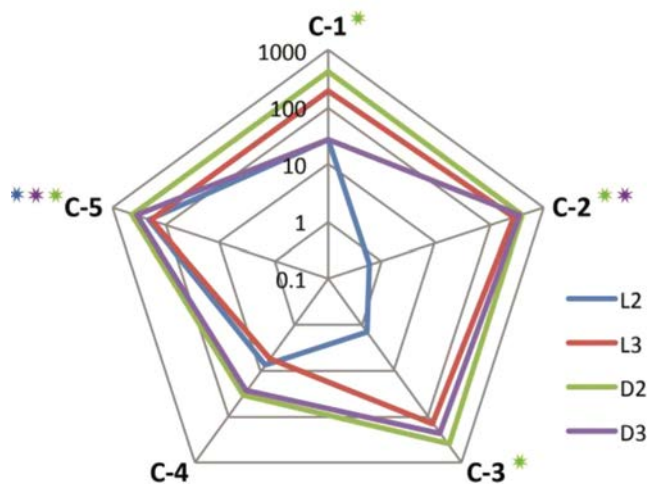| Test	ISOS-D-1	ISOS-D-2	ISOS-D-3	ISOS-L-2	ISOS-L-3	ISOS-O-1
Type	Dark	Dark	Dark	Light	Light	Outdoor
Temperature [°C]	Ambient	65	65	65	85	Ambient
Relative humidity [%]	Ambient	Ambient	85	Ambient	≈50%	Ambient

Figure 2. T_{80} in hours for each combination under different ISOS standards averaged over two samples for each structure. The colored star indicates when T_f was used.

Under ISOS-L-3 conditions, the last indoor test, all the combinations degraded by more than 80% during the first 7 days. This can be expected due to the absence of a UV-protective filter in the modules. The hard UV from the Q-sun rapidly degrades the performance in addition to the high humidity/temperature. The degradation curves in Figure 4 show that C-1, C-2, and C-3 behaved very similarly under these conditions with the C-6 modules degrading slightly faster. It is very difficult to draw any final conclusions from those results although the T_{80} values indicate that PEG-1 as back PEDOT (C-2 and C-3) yields slightly more stable modules than P5010.

The final test was conducted outdoor on a tracking platform which ensures that the plane of the modules is always perpendicular to the sun (maximum light exposure) when the sky is clear (see **Figure 5**). The study was performed in the period from May to September 2014. The degradation curves clearly show that C-3 and C-6 are much more stable outdoor than C-1 and C-2. C-3 and C-6 retained more than 50% of their starting efficiency after 50 days while C-1 and C-2 had degraded by more than 80% in 15 days. Similarly C-3 and C-6 had about ten times higher T_{80} and T_{S80}. These results show that outdoor modules with PEG-1 as front PEDOT are more stable.

The conditions of ISOS-L-3 and ISOS-D-3 are much harsher than the outdoor testing (ISOS-O-1). Therefore one would expect OPV modules to degrade much faster under these two tests than outdoor, which was the case for C-3 and C-6. However C-1 and C-2 modules degraded faster outdoor than during
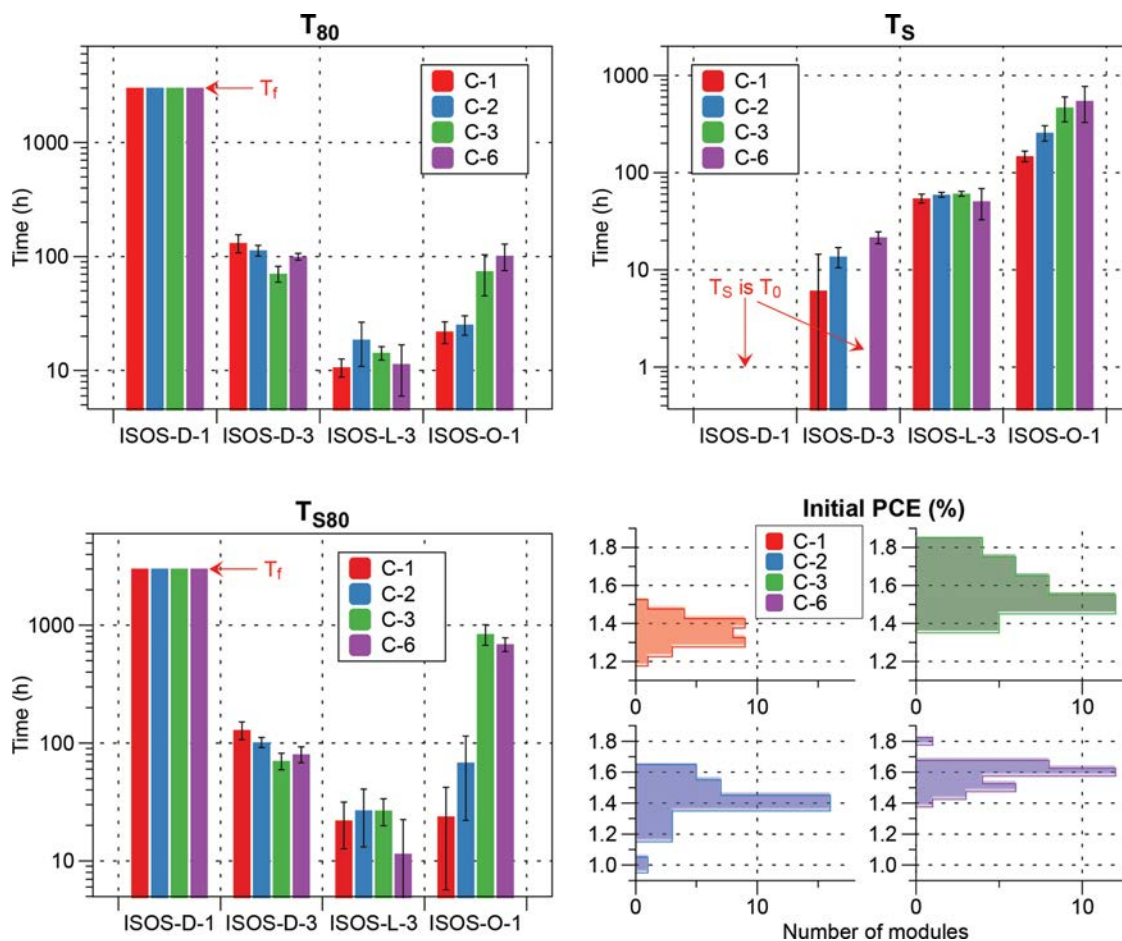

Figure 3. Degradation statistics T_{80} (top left), T_S (top right), T_{S80} (bottom left), and initial performances (bottom right) of the carbon freeOPV modules. The experiment was run for 3000 h.
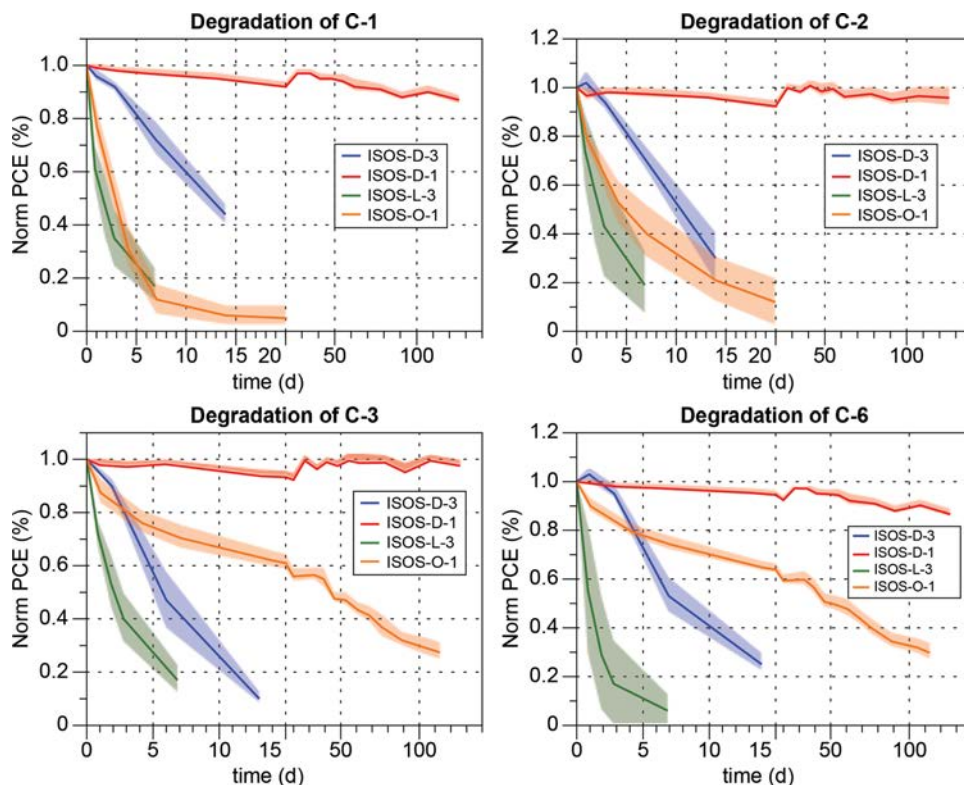
Figure 4. Degradation curves for each ISOS condition for the four chosen PEDOT:PSS combinations.

ISOS-D-3 testing and about as fast as the modules kept in the ISOS-L-3 chamber. The reason for this faster degradation should probably be ascribed to the fact that the modules were taped onto a plastic plate as shown in **Figure 6**. Such a setup allows for water to condensate between the module and the plastic plate when it rains or simply from the morning dew. The snap buttons used for contacting the module are punched through the barrier and are thus in direct contact with the PEDOT:PSS|carbon electrode. This creates a path for the water diffusion into the device where it is absorbed by PDMSO-1 which appears to be much more hydrophilic than its PEG-1

counterpart. This was confirmed by contact angle experiments with liquid water droplets on the surface of PEG-1, PDMSO-1, and PDMSO-2. This clearly shows that the printed PEDOT:PSS with DMSO as additive is much more hydrophilic than printed PEDOT:PSS with ethylene glycol (EG) as additive (Figure 6).

Figure 6. C-1 module carbon based freeOPV mounted outdoor. The water ingress is circled in blue (top). Below water droplets on surfaces of PEG-1 (left) and PDMSO-1 (right) show a much lower contact angle for PEDOT:PSS surfaces printed when using DMSO as high boiling additives.

Figure 5. Carbon freeOPV modules mounted outside on a sun-tracking platform during ISOS-O-1 testing (the modules circled in blue are fixed in groups with red tape).

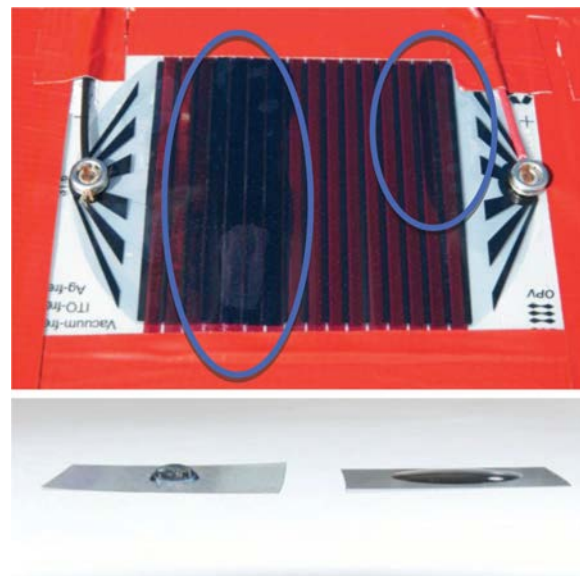While both types of surfaces are hydrophilic, printed surfaces of PEDOT:PSS with DMSO have a much lower contact angle (≈15°) compared to the surfaces of PEDOT:PSS printed with EG (75°). Little detail is available on commercial PEDOT:PSS formulations beyond the nature of the high boiling additives that we explore here. But we have tested the effect of the unknown additives indirectly through the PEG-1 and PDMSO-2 that are identical in formulation (except for the high boiling additive) and both contain the same cross linking agent and surfactant so we rule out that the effect is due to the presence/absence of those materials. In order to try and explain a mechanism that could account for this when considering the R2R based drying method which is fast (compared to, i.e., spin coating) we can view DMSO as being a highly polar ($\varepsilon_r = 48$) aprotic high boiling solvent and EG as a protic and less polar ($\varepsilon_r = 41$) high boiling solvent. During the drying process we propose that the liquid phase of the (initially) water based PEDOT:PSS dispersion to a large extent comprises only the high boiling solvent towards the end of the drying process. In the case of DMSO we believe that exposure of the ionic parts of the PEDOT:PSS gel particles are more favored thus yielding a more hydrophilic surface whereas in the case of EG the more apolar parts of the PEDOT:PSS gel particles are exposed. This is then reflected in the interaction between liquid water and the finally dried surface. The increased hydrophilicity of PEDOT:PSS films dried with DMSO as high boiling solvent is thus also a likely cause for the observed decrease in operational stability for these devices even in the absence of liquid water when used as a back electrode where electronic contact at the interface is critical for proper function. This is observed as rapid failure in C-4 devices and poor performance of C-5 devices. The use of DMSO as a high boiling additive for PEDOT:PSS back electrodes is thus not meaningful. When used as front electrode only the bulk electrical properties and optical transparency is needed and the critical interface with the active layer is buffered by ZnO thus rendering the device operation less reliant on the water content in PEDOT:PSS during operation and this makes the use of DMSO as high boiling additive for PEDOT:PSS front electrodes possible even though the operational stability is increased when using ethyleneglycol as high boiling additive.

The water ingress in the modules with PDMSO-1 was so significant that liquid water was accumulated inside the module in some cases (the black areas circled in blue in Figure 6). This failure mode of course resulted in significant acceleration of the ageing under outdoor conditions making the ageing rate of the modules comparable to the indoor harsh tests (ISOS-L-3 and ISOS-D-3). The failure mechanism is however not the same since liquid water was not observed under either ISOS-D-3 or ISOS-L-3. This underlines the fact that there is only so much, one can conclude from a degradation curve and comparison is only valid when the mode of degradation is confirmed to be the same. In the case of ISOS-O-1 the new failure mode with ingress of liquid water made the direct comparison with failure modes operating in ISOS-D-3 and ISOS-L-3 impossible (or at least very difficult). It is likely that the degradation of C-1 and C-2 devices would have exhibited similar degradation behavior to C-3 and C-6 devices in the case where liquid water was prevented from entering the device. It would of course be impractical to carry out extra sealing and the experiments simply show

Table 4. Stability comparison of the different PEDOT:PSS combinations under different ISOS testing conditions.

		ISOS-D-1[a]	ISOS-D-3	ISOS-L-3	ISOS-O-1
Front PEDOT:PSS	PDMSO-1	=	+	+	−
	PEG-1	=	−	−	+
Back PEDOT:PSS	P5010	−	=	−	=
	PEG-1	+	=	+	=

[a] +, Under the given ISOS condition the PEDOT:PSS seems to relatively improve stability; −, seems to relatively lower stability; =, no apparent difference in stability.

that the C-3 and C-6 devices are better technologies when operating under ISOS-O-1 conditions.

The overall conclusions from the different stability tests are compiled in **Table 4**. For the back PEDOT experiments PEG-1 performs better than P5010 in ISOS-D-1 and ISOS-L-3. For the two other tests (ISOS-L-3 and ISOS-O-1) there are no significant differences. This shows that EG is better suited as high boiling additive for PEDOT:PSS printed on the anode side. For the front PEDOT there is no clear winner. PDMSO-1 performs better under the harsh indoor tests (ISOS-L-3 and ISOS-D-3) but PEG-1 is by far more stable when the modules are put outside. Assuming that outdoor operation is the ultimate goal for most photovoltaic technologies EG should in such cases also be favored as the conductivity inducing high boiling solvent in PEDOT:PSS for the cathode side of the device.

2.3. Upscaling Lifetime Testing

Recent developments of OPV manufacturing[1,20] have demonstrated the fast coating/printing of thousands of large area modules with a high yield (100% yield over 700 m of foil). The high reproducibility of such manufacturing allows for the preparation of a large number of similar OPV modules which when used for lifetime testing gives a high number of statistics. For example, for the study described in this work 180 modules were selected.

Ideally all the samples should be tested at the same time under the same conditions even though the implementation of ISOS standards does allow for comparing modules tested at different times. Obviously most research laboratories have a limited testing capacity (size of the climatic chambers or of the available "one sun" simulators) which will therefore limit the number of large area samples that can be tested (see **Figure 7**). For this reason there is a need to develop an optimal routine to allow obtaining good statistics with limited equipment.

Another concern is the homogeneity of the degradation conditions. For example during our tests we have encountered issues related to temperatures of the samples that were exposed to illuminated tests. Often the light exposure may not be 100% uniform, resulting in temperature differences among the samples, which may then create differences in the ageing rates (this can be the case even for the commercial weathering chambers). An example is shown in **Figure 8**. The foil used to encapsulate the carbon freeOPV is sensitive to temperature cycling and degrades by formation of bubbles or blisters when heated too much. Those lead to local delamination in the solar cell stack

Figure 7. A photograph of the carbon-based freeOPV modules in the Thermotron chamber for ISOS-D-3 testing.

directly under the bubble defect. Through visual examination it was difficult to establish whether the bubbles derived from the solar cell stack itself or from the barrier and we subjected it to further analysis using electron microscopy (as shown in Figure 8). The scanning electron microscopy (SEM) image shows that the encapsulation foil is composed of barrier layers

with a layer repeat of ≈10 µm. The image shows in particular the formation of a bubble between these barrier layers.

In addition we found that high temperature cycling leads to growth of these bubbles (both in number and size) depending on the source and batch of the barrier foil. As this has severe implications because of the delamination and eventually failure of the
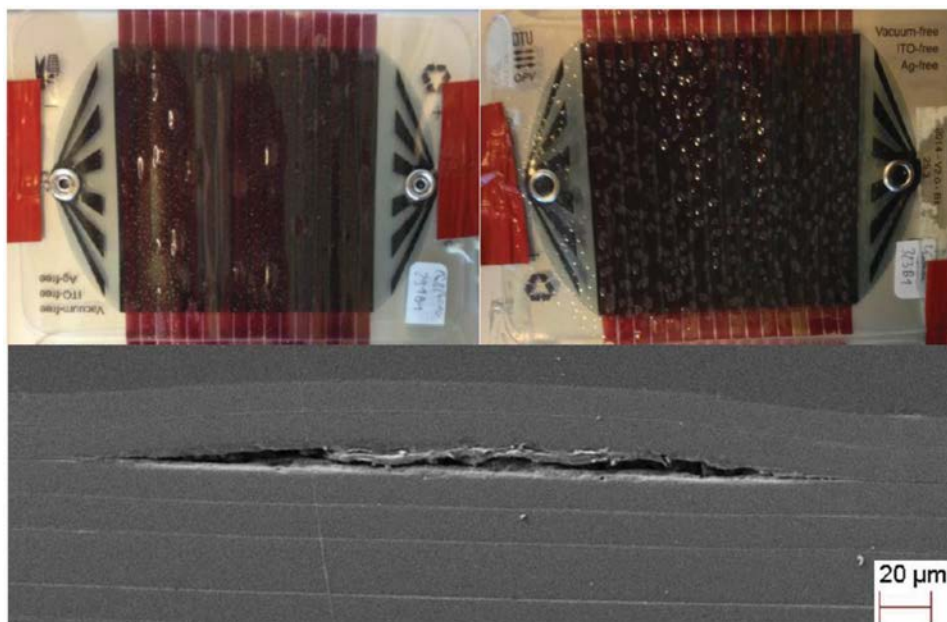

Figure 8. Photographs of carbon based freeOPV after 3 days in the ISOS-L-3 chamber exhibiting different degrees of bubbling due to slight differences in temperature (above). A SEM cross section of an area identified as a bubble was found between some of the layers in the barrier stack (below).

ADVANCED
ENERGY
MATERIALS
www.advenergymat.de

www.MaterialsViews.com

FULL PAPER

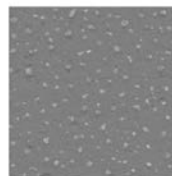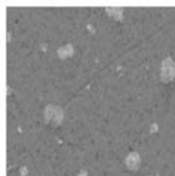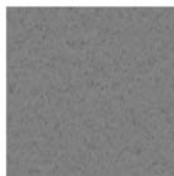| #Bubbles/m²	0	>190.000	>300.000
Image			

Figure 9. A photograph (above) of the Solar Inspect system with the R2R based line scanning cameras (in the red square). To the right of the photograph the operating system is shown where the defects are characterized. In the table (below) small images from the line scanning camera are shown highlighting the bubble count for different barrier foils.

device we had an interest in developing an efficient R2R based method to detect these microbubbles prior to use of the barrier foil and found an enormous range of bubbles present depending on the source and batch of the foil as shown in **Figure 9**.

The degradation of the foil also impacts the performances of the module by delamination and by allowing water and oxygen to penetrate faster. This was proven by comparing the degradation of two C-1 modules placed on each side of the weathering chamber for ISOS-L-3 test. The ageing curves of the two modules are compared in **Figure 10**. The module (#290B1) placed on the extreme right of the chamber degraded two times faster than the module (#291B1) placed on the other side of the chamber. To minimize effects stemming from such inhomogeneity, it is highly recommended both to check the temperature of all samples under test but also to periodically swap the sample positions to assure a more uniform ageing condition for all the samples. Ideally the sample stage should be rotating mechanically to ensure that all samples experience the same conditions during the test.

3. Future and Outlook

In terms of testing, the ISOS standards and methods have undoubtedly been established as a very important tool for developing stable OPV. However, one issue that arises is the dealing with the large amounts of samples and testing over long periods of time and the handling of the large amount of data generated by each study. For example during the full study presented here more than 1500 data points were taken (IV curves). And for each of them efficiency, V_{OC}, I_{SC}, and FF were extracted and analyzed. Ideally the data extraction and its analysis should be automated.[17] In this study the data were extracted and analyzed with a Microsoft Excel macro previously developed[17] but was then manually analyzed. Now, that fast R2R manufacturing of OPV has been demonstrated,[21] ISOS testing platforms and analysis tools having a throughput compatible with R2R manufacture need to be developed. A secondary aspect is of course how to project operational lifetime from the data, established using an approach as described here where a number of ISOS
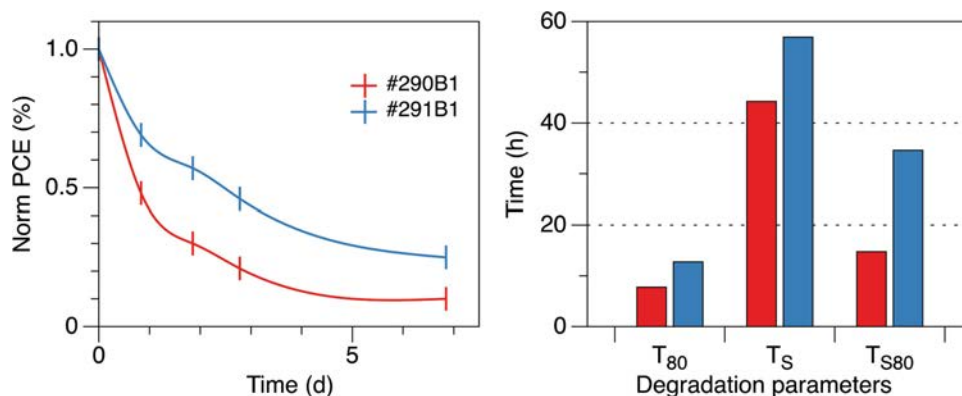
Figure 10. Evolution of the efficiency with time (left) and degradation parameters (right) for modules 290B1 and 291B1 that were adjacent in manufacture and near identical in performance at the start of the experiment.

test conditions are employed to chart the degradation behavior. In the case of OPV prepared using the C-1 PEDOT:PSS combinations an ongoing test on a large scale under ISOS-O-1 conditions have shown operational stabilities well in excess of 1 year (see **Figure 11**). The stability increase that is potentially offered by using PEDOT:PSS combinations of the C-2 or C-3 type is thus significant and a conservative estimate is that the increase is a factor of 3 but it could be significantly higher when considering the decay curves in Figure 4.

4. Conclusion

We have successfully demonstrated that the choice of the high boiling point additive used to prepare highly conductive PEDOT:PSS can significantly impact the stability of R2R processed OPV modules. The freeOPV modules prepared with a PEDOT:PSS mixed with EG are more stable outdoor than their counterpart manufactured with a PEDOT:PSS mixed with DMSO. However, it was found that for some indoor tests (ISOS-D-3 and ISOS-L-3) modules with PEDOT:PSS mixed with DMSO were slightly more stable. The undeniable impact of additives in PEDOT:PSS on the long term stability should always be kept in mind when optimizing an OPV device, since
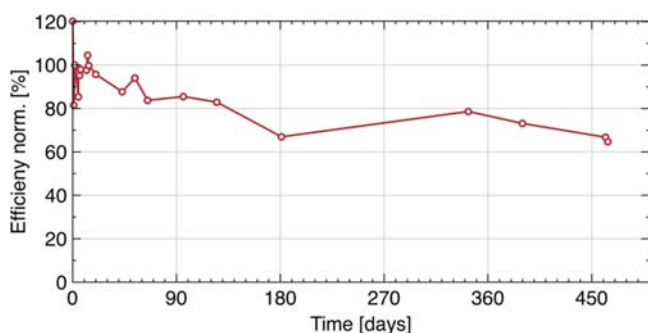
the PEDOT:PSS composition giving the best efficiency might include additives that reduce significantly the stability over extended periods of time. We observed a significant improvement in operational stability for devices where EG was used as a high boiling additive for PEDOT:PSS and ascribe this to a higher degree of hydrophilicity observed for PEDOT:PSS formulations where DMSO is used as a high boiling additive. This is most critical for the PEDOT:PSS used in the back where there is intimate contact with the active layer. While the use of DMSO in the PEDOT:PSS for the front electrode was found more tolerable since there is no direct contact between the PEDOT:PSS. A higher hydrophilicity for the PEDOT:PSS layers was found to be undesired. We finally also observed additional failure modes linked to the ISOS testing of the modules. The competing causes of death were linked both to the packaging method and to the packaging material and we developed a R2R method to quality check barrier foil before use.

5. Experimental Section

Materials and Inks: PEDOT:PSS P5010 was purchased from Agfa (Orgacon EL-P-5010) and diluted with isopropanol 10:5 w/w and a had a viscosity of 270 mPa s. PEDOT:PSS PDMSO-1 had a solid content of 2.2% containing 5% w/w DMSO and a viscosity of 250 mPa s was purchased from Heraeus (Clevios FE T DK which is a PH1000 without cross linker and surfactant) and diluted with isopropanol 10:3 w/w. PDMSO-2 had a solid content of 2.2% containing 5% w/w DMSO and a viscosity of 230 mPa s was purchased from Heraeus (as PH1000) and diluted with isopropanol 10:3 w/w. PEG-1 having a solid content of 2.2% containing 5% w/w ethyleneglycol and a viscosity of 290 mPa s was purchased from Heraeus (Clevios F HC Solar 2) and diluted with isopropanol 10:3 w/w. All PEDOT:PSS from Heraeus are formulated using the same PH1000 base PEDOT:PSS material and only differ in the high boiling additive and in the case of PDMSO-1 also the absence of cross linker and surfactant. The barrier material employed was a 40 µm thick four-ply material from Amcor without UV-filter.

R2R Processing: The OPVs modules were manufactured as described in ref.[15] for the ones with silver electrodes and in ref.[16] for the ones with carbon electrodes. Briefly, the OPVs modules were manufactured with an inline coating/printing machine on a web of 305 mm width. This R2R module is equipped in order with an unwinder, an edge guide, a corona unit, a flexo printing unit, a first slot-die coating unit, a hot air oven (2 m length), a rotary screen printer, a second slot-die unit, three 1.5 kW IR driers, a second hot air oven (2 m length), an ink jet printer (for barcodes),

Figure 11. Operational stability over 1.5 years of large scale modules prepared using the C-1 PEDOT:PSS combination with UV-filtering. The module was prepared according to the Infinity concept[1] and had a nominal output of 215 W (100%). The efficiency has not been corrected for irradiance and the lower performance at 180 days and 570 days was lower due to the season (late autumn 2013 and 2014, respectively).

FULL PAPER

barcode readers and finally, a rewinder. All the PEDOT:PSS formulations were rotary screen printed at a web speed of 8 m min^{-1} with a nominal wet thickness of 20 µm. The oven had a temperature of 140 °C and 3×1.5 kW infrared heaters were used. The lamination employed a R2R machine as described in the literature with DELO LP655 as adhesive.[22] Finally, the foil was cut into discrete OPV modules with a R2R laser-cutter (90 W CO_2) before snap buttons were added for contacts.

Testing: The modules were tested according to the ISOS standards described in the literature.[19] For outdoor testing, the modules were attached to the solar tracking platform. A damp heat chamber (from Thermotron) was used for ISOS-D-3 and a xenon lamp based weathering chamber (from Q-Lab) was used for ISOS-L-3. The IV characteristics were measured under a solar simulator with an AM1.5G spectrum of 1000 W m^{-2} in conjunction with a Keithley 2400 SMU. For ISOS-L-2 the modules were put under a sun simulator and IV characteristics were continuously monitored with a Keithley 2400 source measure unit.

SEM: A freeOPV module was cut and embedded in epoxy, in order to allow imaging of a cross section. The sample was then mechanically polished in order to achieve a flat specimen, followed by a thin carbon coating to limit charging effects. Details on the sample preparation can be found in the literature.[23] The image was finally acquired with a SEM model Zeiss Cross Beam XB1540 using a secondary electron detector.

[1] F. C. Krebs, N. Espinosa, M. Hösel, R. R. Søndergaard, M. Jørgensen, *Adv. Mater.* **2014**, *26*, 29.

[2] M. Jørgensen, K. Norrman, F. C. Krebs, *Sol. Energy Mater. Sol. Cells* **2008**, *92*, 686.

[3] C. J. Brabec, *Sol. Energy Mater. Sol. Cells* **2004**, *83*, 273.

[4] C. J. Brabec, J. A. Hauch, P. Schilinsky, C. Waldauf, *MRS Bull.* **2005**, *30*, 50.

[5] N. Espinosa, R. García-Valverde, A. Urbina, F. Lenzmann, M. Manceau, D. Angmo, F. C. Krebs, *Sol. Energy Mater. Sol. Cells* **2012**, *97*, 3.

[6] N. Espinosa, M. Hösel, M. Jørgensen, F. C. Krebs, *Energy Environ. Sci.* **2014**, *7*, 855.

[7] J.-S. Yeo, J.-M. Yun, D.-Y. Kim, S.-S. Kim, S.-I. Na, *Sol. Energy Mater. Sol. Cells* **2013**, *114*, 104.

[8] V. Singh, S. Arora, M. Arora, V. Sharma, R. P. Tandon, *Semicond. Sci. Technol.* **2014**, *29*, 045020.

[9] C. M. Palumbiny, C. Heller, C. J. Schaffer, V. Körstgens, G. Santoro, S. V Roth, P. Müller-Buschbaum, *J. Phys. Chem. C* **2014**, *118*, 13598.

[10] A. Keawprajak, W. Koetniyom, P. Piyakulawat, K. Jiramitmongkon, S. Pratontep, U. Asawapirom, *Org. Electron.* **2013**, *14*, 402.

[11] D. Angmo, P. M. Sommeling, R. Gupta, M. Hösel, S. A. Gevorgyan, J. M. Kroon, G. U. Kulkarni, F. C. Krebs, *Adv. Eng. Mater.* **2014**, *16*, 976.

[12] E. Voroshazi, B. Verreet, A. Buri, R. Müller, D. Di Nuzzo, P. Heremans, *Org. Electron.* **2011**, *12*, 736.

[13] C. Girotto, E. Voroshazi, D. Cheyns, P. Heremans, B. P. Rand, *ACS Appl. Mater. Interfaces* **2011**, *3*, 3244.

[14] V. M. Drakonakis, A. Savva, M. Kokonou, S. A. Choulis, *Sol. Energy Mater. Sol. Cells* **2014**, *130*, 544.

[15] F. C. Krebs, M. Hösel, M. Corazza, B. Roth, M. V. Madsen, S. A. Gevorgyan, R. R. Søndergaard, D. Karg, M. Jørgensen, *Energy Technol.* **2013**, *1*, 378.

[16] G. A. dos Reis Benatto, B. Roth, M. V. Madsen, M. Hösel, R. R. Søndergaard, M. Jørgensen, F. C. Krebs, *Adv. Energy Mater.* **2014**, *4*, 1400732.

[17] M. Corazza, F. C. Krebs, S. A. Gevorgyan, *Sol. Energy Mater. Sol. Cells* **2014**, *130*, 99.

[18] S. A. Gevorgyan, M. Corazza, M. V. Madsen, G. Bardizza, A. Pozza, H. Müllejans, J. C. Blakesley, G. F. A. Dibb, F. A. Castro, J. F. Trigo, C. M. Guillén, J. R. Herrero, P. Morvillo, M. G. Maglione, C. Minarini, F. Roca, S. Cros, C. Seraine, C. H. Law, P. S. Tuladhar, J. R. Durrant, F. C. Krebs, *Polym. Degrad. Stab.* **2014**, *109*, 162.

[19] M. O. Reese, S. A. Gevorgyan, M. Jørgensen, E. Bundgaard, S. R. Kurtz, D. S. Ginley, D. C. Olson, M. T. Lloyd, P. Morvillo, E. A. Katz, A. Elschner, O. Haillant, T. R. Currier, V. Shrotriya, M. Hermenau, M. Riede, K. R. Kirov, G. Trimmel, T. Rath, O. Inganäs, F. Zhang, M. Andersson, K. Tvingstedt, M. Lira-Cantu, D. Laird, C. McGuiness, S. (Jimmy) Gowrisanker, M. Pannone, M. Xiao, J. Hauch, R. Steim, D. M. DeLongchamp, R. Rösch, H. Hoppe, N. Espinosa, A. Urbina, G. Yaman-Uzunoglu, J.-B. Bonekamp, A. J. M. van Breemen, C. Girotto, E. Voroshazi, F. C. Krebs, *Sol. Energy Mater. Sol. Cells* **2011**, *95*, 1253.

[20] P. Sommer-Larsen, M. Jørgensen, R. R. Søndergaard, M. Hösel, F. C. Krebs, *Energy Technol.* **2013**, *1*, 15.

[21] M. Hösel, R. R. Søndergaard, M. Jørgensen, F. C. Krebs, *Energy Technol.* **2013**, *1*, 102.

[22] M. Hösel, R. R. Søndergaard, M. Jørgensen, F. C. Krebs, *Adv. Eng. Mater.* **2013**, *15*, 1068.

[23] K. Kjellsen, A. Monsøy, K. Isachsen, R. Detwiler, *Cem. Concr. Res.* **2003**, *33*, 611.

Improving the Operational Stability of PBDTTTz-4 Polymer Solar Cells Modules by Electrode Modification**

By *Bérenger Roth, Gisele A. dos Reis Benatto, Michael Corazza, Jon E. Carlé, Martin Helgesen, Suren A. Gevorgyan, Mikkel Jørgensen, Roar R. Søndergaard* and *Frederik C. Krebs**

PBDTTTz-4 is employed in the ambient manufacturing of fully Roll-to-Roll organic solar cell modules. Modules are manufactured using a novel silver nanowire electrode or a previously reported carbon electrode. The average PCE of carbon modules (3.07%) and AgNW modules (1.46%) shows that PBDTTTz-4 is a good candidate for upscaling. Stability measurements following the ISOS standards are used to compare the lifetime of the different modules. In all tests but one, the carbon modules are less stable. The higher stability of AgNW is attributed to the removal of the PEDOT:PSS in the front electrode. Finally during indoor light tests, a new degradation phenomenon is observed where bubbles are formed inside the modules contrary to previous reports of bubble formation by thermal expansion of trapped gas inside the barrier.

1. Introduction

Among the sustainable sources of energy, polymer solar cells (PSCs) have attracted a large interest, because they can be processed from solution which allows for high throughput R2R manufacturing.[1–4] Meaning that their manufacturing can be scaled up under ambient conditions at high speed. Consequently large-area organic photovoltaics (OPVs) would become an energy source with a high power to weight ratio and a short energy payback time.[5–9]

In order to compete with current photovoltaic technologies, however, low cost by itself is not enough and therefore the efficiency as well as the lifetime of PSCs need to be improved.[10,11] Through extensive research, the efficiency has steadily increased for both single and tandem devices and has now been reported to exceed a power conversion efficiency (PCE) of 10% for laboratory size cells ($\approx$mm^2).[12] Such PSCs are prepared with materials (glass, indium tin oxide...) and processing techniques (spin-coating, evaporation...), which are incompatible with the intended fast R2R processing and low cost manufacturing philosophy. Bridging

the gap from lab-to-fab is technologically extremely challenging and real large-scale fully R2R processed PSCs have at best efficiencies in the range of 2–3%.[13–16]

Recently, high-performance polymers compatible with upscaling have been developed,[17–20] some of which show great potential. Particularly PBDTTTz-4 (Figure 1) has been reported by Carlé *et al.* to retain its efficiency,[17] when upscaled in ITO-free and fully R2R processed PSCs, at about 3% for both single cells (1 cm^2) and modules (8 and 29 cm^2). Initial efficiencies of PBDTTTz-4 cells are higher than typical large-area PSCs prepared with P3HT. However, their operational stability (another critical parameter) is much lower than the P3HT PSCs.[17] This probably relates to the fact that the current design of ITO-free, R2R processed PSCs has been optimized for P3HT and therefore needs to be modified to better fit PBDTTTz-4.

In this work, we present three different architectures of freeOPV modules with PBDTTTz-4:PCBM as the active layer (Figure 2) and various previously reported front and back electrodes.[21–23] The lifetimes of these modules are tested according to the standards defined by the International Summit on OPV stability (ISOS).

2. Results and Discussion

2.1. Modules Manufacturing and Characterization

In order to study PBDTTTz-4 as the absorber material in R2R processed large-area PSCs, the blend PBDTTTz-4:PCBM was integrated in three different freeOPV designs with similar stack architecture but with different front and back electrodes. A graphical representation of the architecture of these

[*] B. Roth, G. A. dos Reis Benatto, M. Corazza, Dr. J. E. Carlé,
Dr. M. Helgesen, Dr. S. A. Gevorgyan, Dr. M. Jørgensen, Dr.
R. R. Søndergaard, Prof. F. C. Krebs
Department of Energy Conversion and Storage, Technical
University of Denmark, Frederiksborgvej 399 DK-4000,
Roskilde, Denmark
E-mail: frkr@dtu.dk
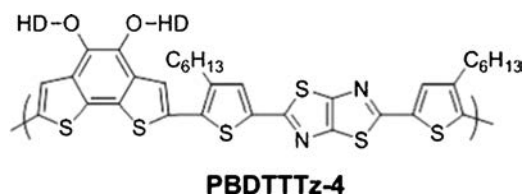
Fig. 1. Chemical structure of PBDTTTz-4.

modules is given in Figure 3 along with a "classical freeOPV" with P3HT:PCBM (Figure 3 left). The silver-free architecture (Figure 3 center) referred to as Carbon freeOPV has previously been extensively described and studied with P3HT:PCBM as the active layer.[22,24] The two final architectures, both included in the illustration to the right in Figure 2, represent the use of a novel front electrode made of silver nanowires (AgNW) and ZnO previously reported by Hösel et al.[23] and later integrated in R2R manufactured PSCs with P3HT:PCBM as active layer and subjected to stability studies as a function of PEDOT:PSS electrodes.[24] The two AgNW architectures differ in their back electrodes made with either a PEDOT:PSS layer in combination with a silver grid (similar to the first freeOPV generation) or only with a PEDOT:PSS layer. At the time of this study, the first generation of freeOPV[21] (Figure 2 left) was not manufactured anymore and therefore no modules with this architecture were made with PBDTTTz-4. However, when first reported, PBDTTTz-4 was extensively studied in PSC modules, prepared with a mini-roll coater,[17] having a stack architecture identical to the first-generation freeOPV with the exception of the active layer. The detailed compositions of each architecture are given in Table 1 along with their initial photovoltaic performance parameters: the power conversion efficiency (PCE), the open circuit voltage (V_{oc}), the short circuit current (I_{sc}), and the fill factor (FF).
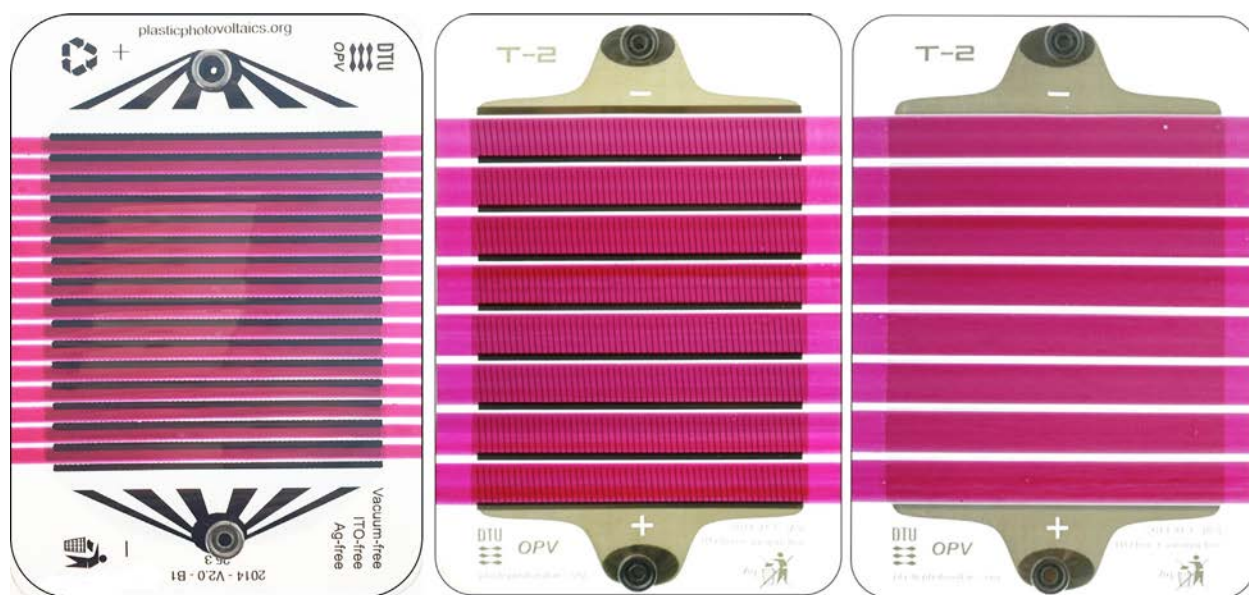
Fig. 2. Front photographs of the freeOPV PBDTTTz-4 devices manufactured respectively with a carbon back electrode (left), a silver back grid (center), and without a silver grid (right).
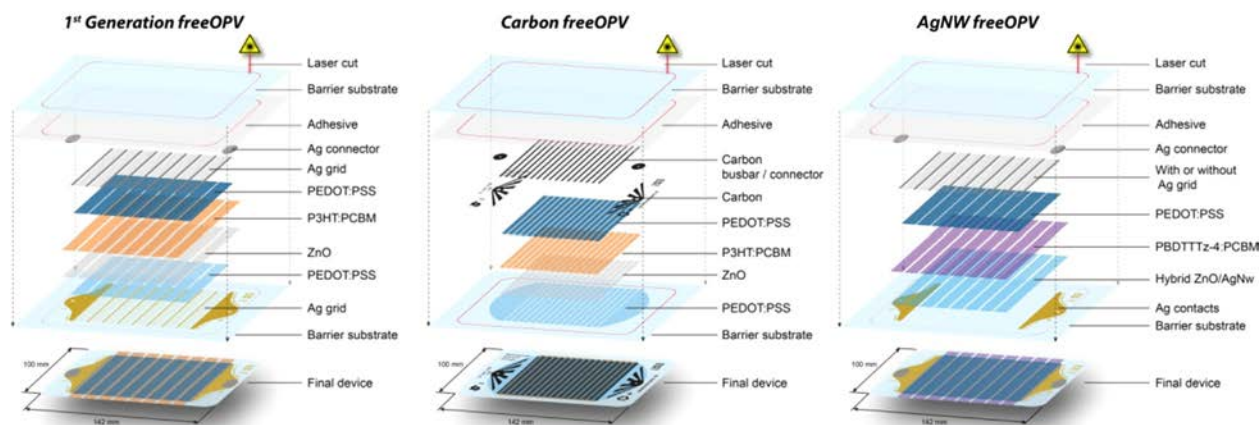
Fig. 3. The different freeOPV architectures: first generation (left), carbon (center), and AgNW (right).

Table 1. FreeOPV architectures and initial photovoltaic performances averaged over 19 modules for each architecture.

	1st Generation freeOPV[a]	Carbon freeOPV	AgNW–back PEDOT:PSS	AgNW–back Ag grid	Mini roll coated Ag grid[b]
Front electrode	Flextrode[34]	PEDOT:PSS/ZnO	AgNW/ZnO	AgNW/ZnO	Flextrode
Active layer	P3HT:PCBM	PBDTTTz-4:PCBM	PBDTTTz-4:PCBM	PBDTTTz-4:PCBM	PBDTTTz-4:PCBM
Back electrode	PEDOT:PSS/Ag grid	PEDOT:PSS/carbon	PEDOT:PSS	PEDOT:PSS/AG grid	PEDOT:PSS/Ag grid
Active area [cm^2]	57	30	57	57	8
Voc [V]	$4.1 \pm 0{,}3$	12.54 ± 0.08	4.89 ± 0.14	6.3 ± 0.3	3.22 ± 0.03
Isc [mA]	40 ± 2	16.4 ± 0.5	$37.\,8 \pm 1.6$	41 ± 2.2	14.4 ± 0.8
FF [%]	60 ± 4	45 ± 1	31 ± 1.5	42 ± 3.2	50.4 ± 1.45
PCE [%]	1.75 ± 0.06	3.07 ± 0.06	1.01 ± 0.06	1.9 ± 0.2	2.9 ± 0.2

[a] Data extracted with permission from ref.[26]
[b] Data extracted with permission from ref.[17]

The upscaling from the smaller modules (8 cm^2) to the freeOPV modules (30 or 57 cm^2) only results in a small drop in PCE for PBDTTTz-4 where most common polymers used in OPVs drastically lose performance when upscaled.[2] This illustrates that PBDTTTz-4 is a promising candidate for manufacture of large-scale R2R processed PSCs. However, the AgNW modules do have a lower starting efficiency which is attributed to a more challenging coating of the active layer on top of the AgNW/ZnO layer. Finally, the difference in performance between the two AgNW architectures is attributed to the lower conductivity of the back electrode when there is no Ag grid.

2.2. Polymer Solar Cell Stability Study

The different modules previously described underwent both indoor and outdoor stability tests which are described in the experimental part. The conditions of these tests followed the standards established by the "International Summit on OPV Stability" known as ISOS and are given in Table 2.[25] Following these guidelines, allows us to accurately compare the present results between the different architectures as well as with previous studies that used the same standards. A recent study by Corazza et al.[26] tackled the issue of comparing different PSCs architectures giving guidelines to compare PSCs uncoupled from processing methods and locations. From that study, it was observed that freeOPV modules are about twice as stable as the cells prepared with a mini roll-coater (for the same stack architecture). This allows

comparison of results obtained from PSCs prepared by mini roll coating with the freeOPV modules used in this study.[17]

During this study, the PBDTTTz-4 modules underwent four indoor tests as well as two outdoor tests. For the indoor test, ISOS-D-2 and ISOS-D-3 are dark tests and the modules are only exposed to light when measured. During ISOS-L-2 and ISOS-L-3, the modules are continuously exposed to light from a solar simulator. While the ISOS-L-2 is carried out in the ambient atmosphere (resulting in a relatively low humidity because of the elevated temperature), the ISOS-L-3 is carried out in a humidity-controlled chamber. The three indoor tests ISOS-D-3, ISOS-L-2, and ISOS-L-3 are referred to as accelerated because of their harsh testing conditions, which result in faster degradation of the modules. For the two outdoor tests, the only difference is the light source used to characterize the modules. For the ISOS-O-1 test, the modules are dismounted from the sun tracking platform and measured under a sun simulator as described in the experimental section. In the case of ISOS-O-2, the photovoltaic performances are measured outdoor using natural sunlight which can yield day-to-day variation depending on the weather conditions. In order to get reliable statistics, four modules were used for each test except for ISOS-D-2 where only three modules were used, because of the general high stability of PSCs modules in this test (no light and low humidity) which rarely leads to extreme failure.[2] As for ISOS-O-2, only the two AgNW architectures were tested (two modules each). The reason here is purely technical; there were not enough free channels available to connect to

Table 2. ISOS tests conditions.

	ISOS-D-2	ISOS-D-3	ISOS-L-2	ISOS-L-3	ISOS-O-1	ISOS-O-2
Light source	None	None	Simulator AM1.5G	Simulator AM1.5G	The sun, outdoor	The sun, outdoor
Temperature	65 °C (oven)	65 °C	65 °C	85 °C	Ambient outdoor	Ambient outdoor
Relative humidity	Ambient	85% (Environment chamber)	Ambient	Controlled (50%)	Ambient outdoor	Ambient outdoor
Characterization light source	Solar simulator	Solar simulator	Solar simulator	Solar simulator	Solar simulator	Sunlight

the keithley 2400 SMU used to monitor the outdoor PSCs modules. Because of limited space availability for the different stability tests not all of these were started at the same time leading to variation in the testing times for ISOS-D-2, ISOS-L-2, and ISOS-O-1. All the stability data obtained from these tests have been grouped in Figure 4. For the three freeOPV module architectures, the evolution of the efficiency over time is plotted for all the ISOS tests. The main degradation parameters are also given: T_{80} (the time it takes for the module to reach the 80% of its initial performance), and T_{S80} the time it takes to degrade by 20% after stabilization.

2.3. Analysis

In the ISOS-D-2 test, the absence of two major factors that significantly accelerate the ageing mechanisms, the light, and the humidity (the latter is due to the elevated temperatures that create a dry environment around the sample) produce very moderate test condition for the samples.[27] Thus, as

expected all the freeOPV modules tested under ISOS-D-2 in this study, regardless of their architecture, are stable and remained above 80% of their initial performances for the 3 months of testing. The carbon module efficiencies show an almost linear decrease during the whole study reaching 80% after approximately 3 months, whereas both types of AgNW modules still performed above 80% of their initial performances at the time this work was submitted. The tests of the modules are still ongoing and are expected to be stable for many more months.

The second dark test ISOS-D-3 introduces a high level of humidity. Water is a well-known degradation source for PSCs[4] and as expected all the freeOPV modules tested under the ISOS-D-3 conditions degraded extremely quickly. Both types of AgNW modules reached T80 in about a day and were fully degraded in about 2 weeks. Under ISOS-D-3, the carbon modules performed slightly better and only reached 80% of their initial efficiency after 3 days. However, the degradation
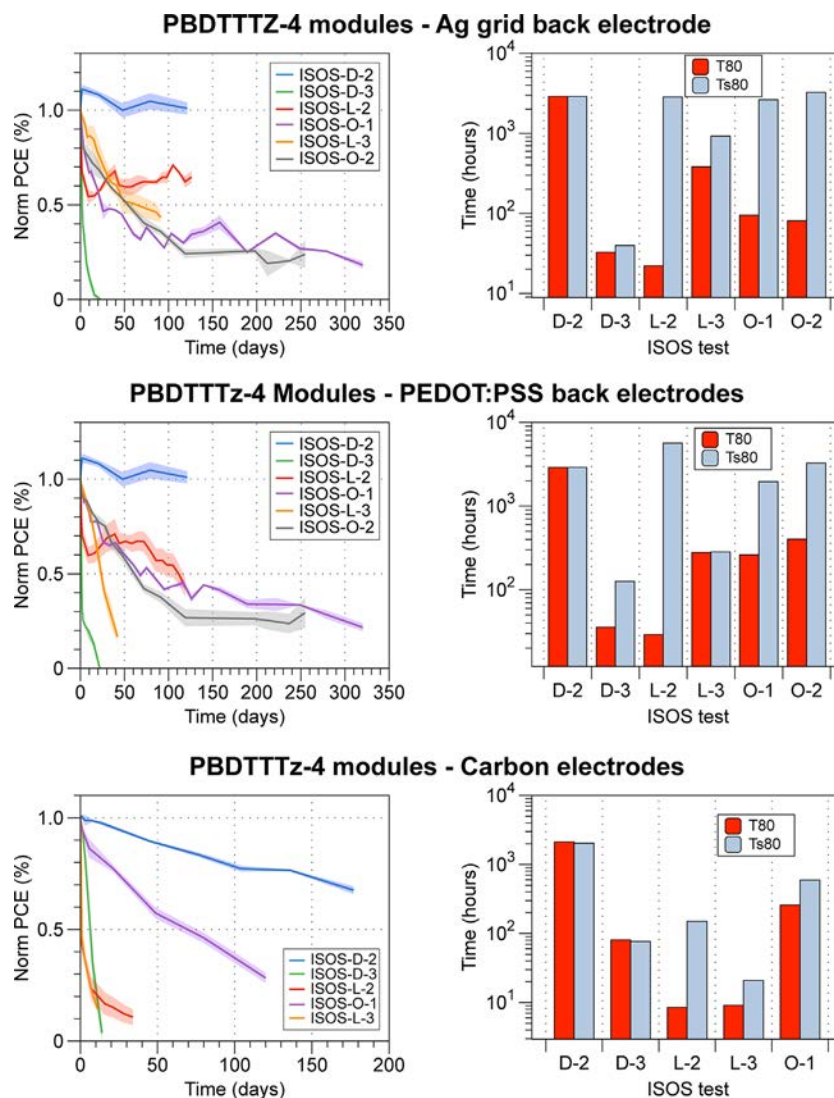
Fig. 4. Degradation curves and lifetime factors for PBDTTTz-4 freeOPV modules with silver grid back electrode (top), PEDOT:PSS back electrode (middle), and carbon electrodes (bottom). For ISOS-D-2, the final time (TF) is plotted instead of T_{80} and T_{S80} for both type of AgNW architectures as all modules retained more than 80% of their starting efficiency. For ISOS-L-2, in the case of the modules with AgNW front electrode (top and middle) T_F is plotted instead of T_{S80} as the modules are stable after the burn in phase.

never slowed down on the carbon modules that were completely degraded after 2 weeks.

The first indoor test with light (ISOS-L-2) has an intrinsically low humidity level because of the higher ambient temperature generated by the sun simulator. Under these conditions, the carbon modules proved to be the least stable and their performances dropped by 80% in a week. In contrast both types of AgNW modules stabilized at around half of their starting efficiency after a few days and remained stable for 3 months. However, the modules with only PEDOT:PSS in the back started slowly to degrade again toward the last weeks of the study while the modules with PEDOT:PSS/Ag grid as back electrode remained stable.

During the last indoor test (ISOS-L-3), which combines both light and humidity, the three different architectures showed drastic differences in degradation. The carbon modules reached T80 in a few hours and were fully degraded in 2 weeks. The modules with AgNW in the front and only PEDOT:PSS in the back degraded much slower than the carbon modules. These modules reached T80 in about a day and were fully degraded after 6 weeks. The last set of modules with AgNW as front electrode and PEDOT:PSS/Ag grid as back electrode degraded even slower with a T80 of 10 days. And after almost 2 months, their efficiency stabilized around 50% of their initial value.

Finally, for the outdoor tests, as mentioned earlier, no carbon modules underwent ISOS-O-2 due to lack of space. Only two AgNW modules of each architecture were tested. It is noticeable that as expected, the modules under ISOS-O-2 appear to degrade according to the same pattern as the modules under ISOS-O-1. The lower performance is due to the fact that the modules were measured outside in Denmark where the light intensity tends to be low especially during the winter. The study started on July 11th, 2014 so the dip in the degradation curve (Figure 4 top and middle) corresponds to the winter season.

Although the carbon modules do not degrade faster than the other two sets of modules with AgNW under ISOS-O-1 conditions, they do not stabilize and have lost 70% in efficiency after 4 months. The behavior of both types of AgNW modules is similar; they degraded to about 40–50% of their starting efficiency in a little over a month and after that their efficiency is stable for roughly 6 months before starting to slowly diminish again.

An overview of the results is given below in Table 3 with a ranking of the tested architectures in the different tests. All the ISOS tests except ISOS-D-3 show that the modules with

AgNW as front electrode are more stable than the modules with carbon electrodes. This effect is attributed to the removal of PEDOT:PSS in the front electrode of the AgNW modules. In fact, PEDOT:PSS is known to impact OPV stability negatively because it is hygroscopic.[28–30] Increase of the water content in the PEDOT:PSS layer leads to a decrease in the conductivity of PEDOT:PSS[29,30] and corrosion of metal layers in contact with PEDOT:PSS can be observed[31] as well as an increase in the acidity of PSS.[32]

Between the two type of AgNW modules, the superiority of the ones with a silver grid on the back electrodes is also linked to PEDOT:PSS. As stated above, the absorption of water by PEDOT:PSS reduces its conductivity. The resulting higher sheet resistance has a less pronounced effect in the presence of Ag grid and the back electrode retains a good conductivity[23] compared to the modules with only PEDOT:PSS as the back electrode.

2.4. Elevated Temperature Degradation

During ISOS-L-2 and ISOS-L-3, a new type of degradation mechanism was observed. Bubbles appeared inside the module (Figure 5 left) contrary to a previously reported degradation mechanism where the bubbles formed inside the barrier laminate used for encapsulation.[24] In the case of ISOS-L-3, only the carbon modules and the AgNW modules with a silver grid exhibited this phenomena. However, during ISOS-L-2 all three types of freeOPV modules displayed bubbles. The initiations of the bubbles are probably due to trapped gas and/or solvents in the porous layers of the modules. Such trapped substances would be expected to expand under the high temperatures of both tests which could explain the bubbles. The porosity of the printed silver grid electrode has previously been identified by Dam et al.[33] to be above 60% of its volume and a similar porosity could be expected to be present in the carbon electrode. The phenomena is also observed during ISOS-L-2 for the modules with only PEDOT:PSS as back electrodes (without any porous layer). In that case, the hypothesis is that during encapsulation of the modules a small amount of gas is trapped. By light beam-induced current (LBIC), it is observed that the modules have delaminated at the locations of the bubbles (see Figure 5 right) and they are thus an additional source of degradation of the modules.

2.5. Conclusion

The study described in this work successfully identifies factors impacting the long-term stability of large-area R2R

Table 3. Ranking of the device architectures in the different lifetime studies.

Module type	ISOS-D-2	ISOS-D-3	ISOS-L-2	ISOS-L-3	ISOS-O-1
Carbon	–	+	–	–	–
AgNW/PEDOT:PSS	+	–	+	+	+
AgNW/PEDOT:PSS + Ag grid	+	–	++	++	++

FULL PAPER

Fig. 5. (Left) front picture of a degraded AgNW module with Ag grid in the back after ISOS-L-3. (Right) LBIC of the same module where the light yellow areas correspond to photovoltaic function and the blue areas to non-active or destroyed areas.

processed PSC modules prepared with the high-efficiency polymer PBDTTTz-4. Both indoor and outdoor stability measurements show that modules without a PEDOT:PSS layer in the front electrodes are more stable. One exception to that conclusion is the high humidity dark test (ISOS-D-3) were the carbon modules (with both a front and a back PEDOT:PSS layer) performed better. However, even with the improvement yielded by the use of AgNW front electrodes the lifetime of the best large-area PBDTTTz-4 modules still remains low compared to large-area P3HT modules with reported outdoor lifetimes above 1.5 years.[24] This clearly indicates the need to develop new electrode combinations tailored to PBDTTTz-4 and other high-performance polymers in order to improve their lifetimes. This study shows that PEDOT:PSS dramatically lowers the lifetimes and that the replacement of this component in both front and back electrodes should be a priority. Finally, for the fully R2R processed PSC modules a new type of degradation was identified during the high-temperature indoor tests. The thermal expansion of trapped gas/solvent leads to the formation of bubbles inside the solar cells which causes the cells to delaminate.

3. Experimental Section

3.1. Materials and Inks

The modules were manufactured on a polyethylene terephthalate (PET) flexible substrate (OTR $= 0.01$ cm^3 m^{-2} day^{-1} and WVTR $= 0l04$ g m^{-2} day^{-1}) without UV-filter obtained from Amcor. The substrate was also employed for the back encapsulation of the modules. The silver nanowire substrates were prepared as described previously.[23] The ZnO ink employed for manufacturing was prepared by dispersing nanoparticles in acetone with a concentration of 56 mg mL^{-1}. For the active layer, PBDTTTz-4 was synthesized as described previously.[17] Inks comprising PBDTTz-4 and[60] PCBM (from Nano-C) were prepared as described previously.[17] For the back electrodes of the AgNW modules, PEDOT:PSS purchased from Heraeus (Clevios PH1000) was used. For the carbon modules, both front and back PEDOT:PSS was obtained from Heraeus (Clevios PH1000). The carbon paste (Electrodag PF-407C from Acheson) was used as purchased. For the silver grid, back electrode Dupont 5025 was employed and used as

received. Finally, the adhesive used for encapsulation (LP655) was purchased from DELO.

3.2. Polymer Solar Cells Preparation

The manufacturing of freeOPV modules was carried out as previously described.[21,22] The modules were prepared on a 305 mm wide substrate moving through an inline R2R manufacturing unit equipped with: an unwinder, an edge guide, a corona treater, a flexo printer, two slot-die coating units, two hot air ovens (2 m length), a rotary screen-printer, 3 IR drier (1.5 kW), an ink-jet printer, a barcode reader, and a rewinder. The modules were then laminated with a second R2R unit. Finally, the freeOPV modules were cut with a laser (90 W CO2) and contacted with snap buttons.

3.3. Device Characterization

All stability measurements were carried out following the ISOS standards[25] (shown in Table 2). Except for the ISOS-O-2 test, all the photovoltaic performances were acquired using a solar simulator with an AM1.5G spectrum of 1 000 W m^{-2} with a Keithley 2400 SMU. For the ISOS-O-2 studies, the performances were measured outdoor under natural sunlight illumination and ambient conditions using a Keithley 2400 SMU. A bolometer from Eppley Laboratories was employed to record the irradiance. For both outdoor tests (ISOS-O-1 and ISOS-O-2), the modules were placed on a solar tracking platform. A damp heat chamber (from Thermotron) was used for ISOS-D-3 and a xenon lamp-based weathering chamber (from Q-Lab) was used for ISOS-L-3. Finally, in the case of ISOS-L-2, the modules were placed under a solar simulator and IV-characteristics were continuously recorded with a Keithley 2400 SMU.

[1] K. A. Mazzio, C. K. Luscombe, *Chem. Soc. Rev.* **2015**, *44*, 78.

[2] M. Jørgensen, J. E. Carlé, R. R. Søndergaard, M. Lauritzen, N. A. Dagnæs-Hansen, S. L. Byskov, T. R. Andersen, T. T. Larsen-Olsen, A. P. L. Böttiger, B. Andreasen, L. Fu, L. Zuo, Y. Liu, E. Bundgaard,

X. Zhan, H. Chen, F. C. Krebs, *Sol. Energy Mater. Sol. Cells* **2013**, *119*, 84.

[3] C. J. Brabec, J. A. Hauch, P. Schilinsky, C. Waldauf, *MRS Bull.* **2005**, *30*, 50.

[4] M. Giannouli, V. M. Drakonakis, A. Savva, P. Eleftheriou, G. Florides, S. A. Choulis, *Chem. Phys. Chem.* **2015**, *16*, 1134.

[5] N. Espinosa, M. Hösel, D. Angmo, F. C. Krebs, *Energy Environ. Sci.* **2012**, *5*, 5117.

[6] N. Espinosa, F. O. Lenzmann, S. Ryley, D. Angmo, M. Hösel, R. R. Søndergaard, D. Huss, S. Dafinger, S. Gritsch, J. M. Kroon, M. Jørgensen, F. C. Krebs, *J. Mater. Chem. A* **2013**, *1*, 7037.

[7] C. Powell, Y. Lawryshyn, T. Bender, *Sol. Energy Mater. Sol. Cells* **2012**, *107*, 236.

[8] C. J. Mulligan, M. Wilson, G. Bryant, B. Vaughan, X. Zhou, W. J. Belcher, P. C. Dastoor, *Sol. Energy Mater. Sol. Cells* **2014**, *120*, 9.

[9] C. J. Mulligan, C. Bilen, X. Zhou, W. J. Belcher, P. C. Dastoor, *Sol. Energy Mater. Sol. Cells* **2015**, *133*, 26.

[10] O. Haillant, *Sol. Energy Mater. Sol. Cells* **2011**, *95*, 1284.

[11] C. J. Brabec, *Sol. Energy Mater. Sol. Cells* **2004**, *83*, 273.

[12] M. A. Green, efficiency tables.

[13] F. C. Krebs, N. Espinosa, M. Hösel, R. R. Søndergaard, M. Jørgensen, *Adv. Mater.* **2014**, *26*, 29.

[14] P.-T. Tsai, K.-C. Yu, C.-Y. Chang, S.-F. Horng, H.-F. Meng, *Org. Electron.* **2015**, 1.

[15] F. Guo, P. Kubis, T. Przybilla, E. Spiecker, A. Hollmann, S. Langner, K. Forberich, C. J. Brabec, *Adv. Energy Mater.* **2015**, *5*, 1401779.

[16] M. Hösel, H. F. Dam, F. C. Krebs, *Energy Technol.* **2015**, *3*, 293.

[17] J. E. Carlé, M. Helgesen, M. V. Madsen, E. Bundgaard, F. C. Krebs, *J. Mater. Chem. C* **2014**, *2*, 1290.

[18] M. Helgesen, J. E. Carlé, G. A. dos Reis Benatto, R. R. Søndergaard, M. Jørgensen, E. Bundgaard, F. C. Krebs, *Adv. Energy Mater.* **2015**, *5*, 1401996.

[19] R. G. Brandt, W. Yue, T. R. Andersen, T. T. Larsen-Olsen, M. Hinge, E. Bundgaard, F. C. Krebs, D. Yu, *J. Mater. Chem. C* **2015**, *3*, 1633.

[20] W. Liu, S. Liu, N. K. Zawacka, T. R. Andersen, P. Cheng, L. Fu, M. Chen, W. Fu, E. Bundgaard, M. Jørgensen, X. Zhan, F. C. Krebs, H. Chen, *J. Mater. Chem. A* **2014**, *2*, 19809.

[21] F. C. Krebs, M. Hösel, M. Corazza, B. Roth, M. V. Madsen, S. A. Gevorgyan, R. R. Søndergaard, D. Karg, M. Jørgensen, *Energy Technol.* **2013**, *1*, 378.

[22] G. A. dos Reis Benatto, B. Roth, M. V. Madsen, M. Hösel, R. R. Søndergaard, M. Jørgensen, F. C. Krebs, *Adv. Energy Mater.* **2014**, *4*, 1400732.

[23] M. Hösel, D. Angmo, R. R. Søndergaard, G. A. dos Reis Benatto, J. E. Carlé, M. Jørgensen, F. C. Krebs, *Adv. Sci.* **2014**, *1*, 1400002.

[24] B. Roth, G. A. dos Reis Benatto, M. Corazza, R. R. Søndergaard, S. A. Gevorgyan, M. Jørgensen, F. C. Krebs, *Adv. Energy Mater.* **2015**, *5*, 1401912.

[25] M. O. Reese, S. A. Gevorgyan, M. Jørgensen, E. Bundgaard, S. R. Kurtz, D. S. Ginley, D. C. Olson, M. T. Lloyd, P. Morvillo, E. A. Katz, A. Elschner, O. Haillant, T. R. Currier, V. Shrotriya, M. Hermenau, M. Riede, K. R. Kirov, G. Trimmel, T. Rath, O. Inganäs, F. Zhang, M. Andersson, K. Tvingstedt, M. Lira-Cantu, D. Laird, C. McGuiness, S. (Jimmy) Gowrisanker, M. Pannone, M. Xiao, J. Hauch, R. Steim, D. M. DeLongchamp, R. Rösch, H. Hoppe, N. Espinosa, A. Urbina, G. Yaman-Uzunoglu, J.-B. Bonekamp, A. J. J. M. van Breemen, C. Girotto, E. Voroshazi, F. C. Krebs, *Sol. Energy Mater. Sol. Cells* **2011**, *95*, 1253.

[26] M. Corazza, F. C. Krebs, S. A. Gevorgyan, *Sol. Energy Mater. Sol. Cells* **2014**, *130*, 99.

[27] M. Jørgensen, K. Norrman, F. C. Krebs, *Sol. Energy Mater. Sol. Cells* **2008**, *92*, 686.

[28] H. Cao, W. He, Y. Mao, X. Lin, K. Ishikawa, J. H. Dickerson, W. P. Hess, *J. Power Sources* **2014**, *264*, 168.

[29] K. Kawano, R. Pacios, D. Poplavskyy, J. Nelson, D. D. C. Bradley, J. R. Durrant, *Sol. Energy Mater. Sol. Cells* **2006**, *90*, 3520.

[30] A. M. Nardes, M. Kemerink, M. M. de Kok, E. Vinken, K. Maturova, R. A. J. Janssen, *Org. Electron. Physics, Mater. Appl.* **2008**, *9*, 727.

[31] E. Voroshazi, B. Verreet, A. Buri, R. Müller, D. Di Nuzzo, P. Heremans, *Org. Electron.* **2011**, *12*, 736.

[32] L. Groenendaal, F. Jonas, D. Freitag, H. Pielartzik, J. R. Reynolds, *Adv. Mater.* **2000**, *12*, 481.

[33] H. F. Dam, T. R. Andersen, E. B. L. Pedersen, K. T. S. Thydén, M. Helgesen, J. E. Carlé, P. S. Jørgensen, J. Reinhardt, R. R. Søndergaard, M. Jørgensen, E. Bundgaard, F. C. Krebs, J. W. Andreasen, *Adv. Energy Mater.* **2015**, *5*, 1400736.

[34] M. Hösel, R. R. Søndergaard, M. Jørgensen, F. C. Krebs, *Energy Technol.* **2013**, *1*, 102.

FULL PAPER

# Mechanical Properties of a Library of Low-Band-Gap Polymers

Bérenger Roth,[†,‡] Suchol Savagatrup,[§,‡] Nathaniel V. de los Santos,[§] Ole Hagemann,[†] Jon E. Carlé,[†] Martin Helgesen,[†] Francesco Livi,[†] Eva Bundgaard,[†] Roar R. Søndergaard,[†] Frederik C. Krebs,[†] and Darren J. Lipomi*,[§]

[†]Department of Energy Conversion and Storage, Technical University of Denmark, Frederiksborgvej 399, DK-4000 Roskilde, Denmark

[§]Department of NanoEngineering, University of California San Diego, 9500 Gilman Drive, Mail Code 0448, La Jolla, California 92093−0448, United States

ⓢ *Supporting Information*

ABSTRACT: The mechanical properties of low-band-gap polymers are important for the long-term survivability of roll-to-roll processed organic electronic devices. Such devices, e.g., solar cells, displays, and thin-film transistors, must survive the rigors of roll-to-roll coating and also thermal and mechanical forces in the outdoor environment and in stretchable and ultraflexible form factors. This paper measures the stiffness (tensile modulus), ductility (crack-onset strain), or both of a combinatorial library of 51 low-band-gap polymers. The purpose of this study is to systematically screen a library of low-band-gap polymers to better understand the connection between molecular structures and mechanical properties in order to design conjugated polymers that permit mechanical robustness and even extreme deformability. While one of the principal conclusions of these experiments is that the structure of an isolated molecule only partially determines the mechanical properties—another important codeterminant is the packing structure—some general trends can be identified. (1) Fused rings tend to increase the modulus and decrease the ductility. (2) Branched side chains have the opposite effect. Despite the rigidity of the molecular structure, the most deformable films can be surprisingly compliant (modulus ≥ 150 MPa) and ductile (crack-onset strain ≤ 68%). This paper concludes by proposing a new composite merit factor that combines the power conversion efficiency in a fully solution processed device obtained via roll and roll-to-roll coating and printing (as measured in an earlier paper) and the mechanical deformability toward the goal of producing modules that are both efficient and mechanically stable.
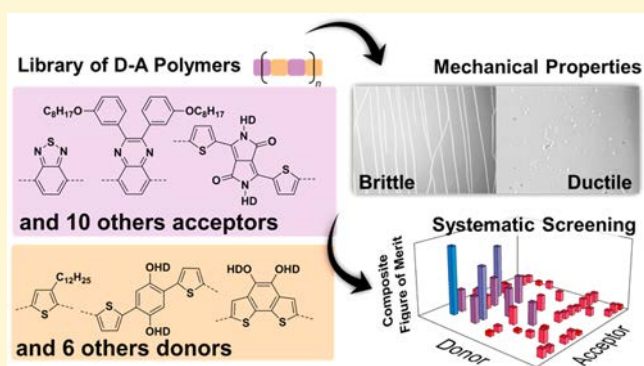
■ INTRODUCTION

The conventional rationale for research on organic photovoltaic (OPV) materials and devices is the promise of inexpensive, lightweight, flexible solar modules that can be fabricated by roll-to-roll (R2R) processing in ambient atmosphere on flexible substrates.[1] These defining advantages are thus contingent on stability against bending and other thermomechanical modes of deformation.[2] The work of Dauskardt et al. has shown, however, that the cohesive and adhesive fracture energies encountered within and between layers in organic solar cells occupy a typical range of 1−5 J m^{-2}, which is significantly lower than the values that characterize devices based on conventional semiconducting materials (though these values are dependent on the thickness of the active layer, polymer:fullerene blend, processing conditions, composition, molecular weight, and relative humidity).[3] Despite an increase in interest in the mechanical properties of nominally flexible electronic materials,[4,5] almost all previous work has focused on the properties of poly(3-alkylthiophenes) (P3ATs, for which we have previously shown that structural features such as the length of the alkyl

side chain play critical roles in determining the stiffness, yield point, and ductility of conjugated polymers[2,6]). While the P3ATs (particularly where A = hexyl) have been a useful model system,[7] and also appears to have significant advantages in R2R production,[8] the best power conversion efficiencies are achieved with low-band-gap polymers comprising an alternating arrangement of donor and acceptor (D−A) units.[9]

This paper describes a large-scale investigation of the mechanical properties of D−A polymers by measuring the tensile modulus, cracking behavior, or both of a combinatorial library of 51 compounds, which represent combinations of acceptors A1−10 and A12−14 and donors D1−D3 and D5−D9, shown in Figure 1. The purpose of this study was to take the first steps toward developing guidelines for the rational design of conjugated polymers for increased mechanical stability and deformability. Combined with an earlier report
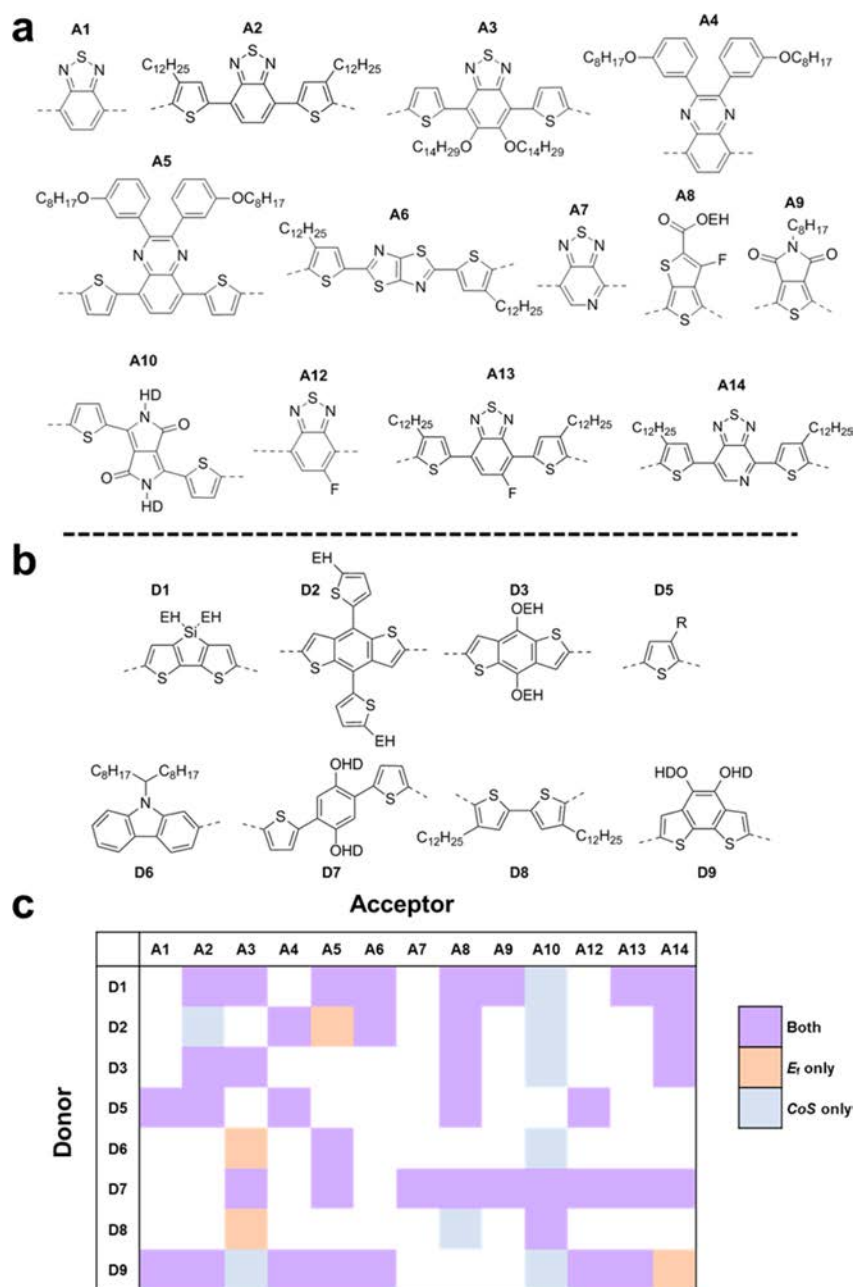
Figure 1. Chemical structures of the 13 acceptor monomers (a) and 8 donor monomers (b) as synthesized and described in a previous paper.[8] (c) Table of the combination of D−A polymers measured in this work. Tensile moduli (E_f) were measured for a total of 43 polymers, the crack-onset strains (*CoS*) were measured for 47 polymers, and both quantities were measured for 39 polymers. The "missing" combinations are the result of failure to obtain the material by synthesis, failure to create devices via roll coating, or insufficient material available after the initial studies performed in ref 8. For D5, R is H for A2 and A4 and $C_{12}H_{25}$ for A1, A8, and A12. The abbreviation EH stands for 2-ethylhexyl, and HD stands for 2-hexyldecyl.

from Bundgaard et al.[8] on the photovoltaic performance of a library of which the materials studied here is a subset, the ultimate goal of this work is thus to permit the co-optimization of electronic and mechanical performance. A favorable outcome would not only improve the stability of R2R-processed organic solar modules but also allow the integration of OPVs—or any organic electronic devices—in many form factors inaccessible by conventional devices, such as in clothing, portable electronics, biomedical applications, and extremely flexible and stretchable devices.[2]

■ **BACKGROUND**

The mechanical stability of conjugated polymers, specifically D−A polymers, has until now received little attention in the literature. The absence of emphasis on this topic has been due to the focus on improving the power conversion efficiency (*PCE*) on a small-scale laboratory device on glass where thermomechanical properties rarely present a limitation to observations of device performance. However, for flexible devices that require flexibility during manufacturing, in the actual application/integration, and in the operation of the device, the thermomechanical properties become a dominant boundary condition that if not met will prevent success

(regardless of device PCE).[1] Recently, laboratory-scale PCE for D−A polymers has reached well over 10% on optimized architectures on devices with small active areas.[10] However, these devices were prepared on rigid substrates, i.e., glass coated with indium tin oxide (ITO), that are not compatible with R2R manufacturing.[1] Moreover, rigid substrates mask the potential fragility of the D−A polymers and polymer:fullerene composites that could lead to mechanical failure in flexible modules.[2] The recent effort by Bundgaard et al. to screen 104 different combinations of D−A polymers has revealed that 13 out of 104 polymers outperformed P3HT on a merit factor that is weighted toward the suitability of the materials for R2R processing.[8] This merit factor accounted for not only the electrical performance but also the chemical stability and simplicity of the synthesis[8] but did not account for the predicted stability against thermomechanical degradation.

While most earlier work by us and others on the mechanical properties of organic semiconductors has focused on P3ATs,[2] a few studies have suggested some ways in which the molecular structures of the D−A polymers influence their mechanical properties. An earlier paper examined the mechanical properties of PDPP-2TTT (a D−A polymer whose repeating units comprise diketopyrrolopyrrole (DPP), thiophene (T), thieno-thiophene (TT), and thiophene in the backbone) and PDPP-4T (a close structural analog in which the fused thienothio-phene structure was substituted with bithiophene, which comprises two isolated thiophene rings).[11] The results of this work suggested (though not rigorously confirmed) that the polymer with the fused ring system produced a tensile modulus that was higher (0.99 GPa for PDPP-2TTT) than that of the polymer bearing the isolated rings (0.74 GPa for PDPP-4T).[11] In a separate study, we found that random incorporation of bithiophene units into the structure of PDPP-2FT (where F = furan) decreased the tensile modulus from 2.17 ± 0.35 to 0.93 ± 0.16 GPa.[12] The brittleness of polymers comprising rigid large fused rings in the backbone was also suggested by the results of Wu et al., who observed significant cracking in highly crystalline organic thin film transistors fabricated from a DPP-based polymer with four fused thiophene rings.[13] Additionally, Kim et al. also investigated the mechanical properties of D−A polymers, namely, that of PBDTTTPD (same structure as A9D2, however we did not have this material available for this study).[14] They found that the tensile modulus of the composite of PBDTTTPD and a nonfullerene electron acceptor (at 1:1 ratio) was 0.43 GPa, which is much lower than when combined with PCBM at 1.76 GPa (at 1:1.5 ratio), and were able to make a solar cell with good efficiency and high intrinsic deformability.[14] These experimental results have recently been complemented with computational tools designed to study the effects of molecular structures of conjugated polymers on mesoscale (∼10−100 nm) conformational structures and thus may also accelerate the understanding of the connection between molecular structure and mechanical properties.[15]

Despite the efforts noted above, mechanical data for D−A polymers is sparsely reported. We thus sought to lay the groundwork for a rigorous understanding of the structural determinants of the mechanical properties of D−A polymers by reporting the properties of a sufficiently large library comprising several popular donors and acceptors. We admit at the outset several limitations of this approach. First, the mechanical properties of polymers are determined not only by the molecular structure but also by the microstructure in the solid state. The microstructure/morphology is difficult to predict by computation[15] (though eventually it should be possible to do so), and moreover, the microstructure/morphology was not within our means to measure for the entire library. Second, the microstructure/morphology that forms is a strong function of the solvent, film-casting method, drying, and postprocessing steps,[9,16] which it was not practical to optimize for every material. Third, the molecular weight and dispersity (Đ) for step-growth polymerizations are notoriously difficult to control, though it is possible that the stiffness of D−A polymers precludes a highly entangled microstructure, even at high molecular weights.[17] Fourth, the mechanical properties of bulk heterojunction films are significantly affected by the electron-transporting phase.[2] For polythiophenes, we found that the tensile moduli of polythiophene:[60]PCBM blends was linearly correlated to the tensile moduli of the pure polymers,[18] though this behavior cannot be assumed for all polymers nor can it be assumed that methanofullerenes will be used in all organic solar cells in the future, and thus, we measured the properties of the pure polymers only. Despite these limitations, we found that several rules of thumb did emerge for increased deformability of D−A polymers. More-over, we expect that the mechanical characteristics of the library of polymers reported here will stimulate computational and microstructural studies designed to connect molecular structure not only to electronic performance but also to mechanical behavior.

■ EXPERIMENTAL DESIGN

Selection of Materials. We selected the combination of 8 different donor monomers and 13 different acceptor monomers in order to test a library of D−A polymers with diversity in chemical structures (Figure 1a and 1b). The library is a subset of that used in a recent paper by Bundgaard et al. on the viability of these materials for R2R fabrication.[8] The chemical structures were selected on the basis of polymers from the current literature that produced highly efficient solar cells, including polymers containing the subunits benzothiadiazole (BT), quinoxaline (as seen in TQ1), benzodithiophene (BDT), diketopyrrolopyrrole (DPP), carbozole, thiophene, and bithio-phene. Our initial hypothesis was that two prominent features of the chemical structures—(1) fused vs isolated rings and (2) branched vs linear side chains—would affect the mechanical properties of the films bearing them. The monomers containing fused rings are A6, A10, D1, D2, D3, D6, and D9. We made the distinction between structures with fused rings aligned along the backbone such as those found in diketopyrrolopyrrole (DPP) and fused rings not in the direction of the backbone such as benzothiadiazole (BT). The solubilizing side chains on the structures range from relatively short alkyl side chains of eight carbons (C_8H_{17}) to long alkyl side chains of 14 carbons ($C_{14}H_{29}$) as well as branching side chains of 2-ethylhexyl (EH) and 2-hexyldecyl (HD). We also examined the effects of molecular weight and dispersity on the mechanical properties of the polymers.

Measurement of Mechanical Properties. We measured the mechanical properties of the D−A polymers using two specific values: tensile modulus and the crack-onset strain. Both measurements are performed using the film-on-elastomer techniques. In particular, the tensile moduli were measured using the buckling instability as developed by Stafford et al.,[19] expanded to conjugated polymers by Tahk et al.,[20] and used extensively by us and others.[2,4,11,21] Low tensile modulus is regarded as "good" from the standpoint of mechanical stability,

because films that require a low energy density to elongate in the elastic regime will minimize interfacial stresses with other layers in the device stack that would otherwise lead to delamination.[2,22] For polythiophenes of comparable molecular weight, low tensile modulus is also highly correlated to high crack-onset strain. Crack-onset strains of films on elastomers are often interpreted as analogous to the elongation at fracture of bulk samples or free-standing films of the polymers, though these quantities are not exactly equivalent because poor adhesion of a film to a substrate—and unequal adhesion among different polymers—localizes strain to cracks and defects and causes premature cracking.[4,23] The polymer films were transferred to elastomeric substrates and stretched, and we recorded the crack onset strain by obtaining micrographs at each level of strain. We also took note of the qualitative nature of the cracks, i.e. either brittle cracks (which propagated the entire length of the film perpendicular to the stretched axis) or ductile cracks (whose propagation was limited). We note that previous studies by Stafford and co-workers[19,24,25] and O'Connor et al.[4] have shown that the tensile modulus of a thin film is a relatively weak function of its thickness when the film is above ~40 nm and below 500 nm. We judiciously prepared our thin films to be within this range. We also observed no significant deviation from the averaged value of the crack-onset strain for any polymer sample. Furthermore, we chose this range of film thicknesses to better correlate with the result from Bundgaard et al., in which the thicknesses of all devices were between 300 and 500 nm.[8]

■ RESULTS AND DISCUSSION

Tensile Moduli of Low-Band-Gap D–A Polymers. We began by measuring the tensile modulus of each D–A polymer using the buckling-based method. Figure 2a shows a comprehensive overview of all tensile moduli collected for the available polymers. The standard deviation of each value was calculated from the propagation of standard errors of the line fits (buckling wavelength vs film thickness) and the standard deviation of the tensile moduli of the PDMS substrates; the values are provided in Table 1. We discarded the values of the modulus from the samples in which the standard errors of the line fits were too high ($R^2 < 0.95$) or the characteristic buckling wavelengths could not be obtained. The reasons for the failure to obtain good linear fits or a consistent buckling wavelength arose from the difficulty in handling some thin films. In some cases, the films adhered too well to the glass substrates; strong adhesion to the glass substrate led to either partial transfer onto the PDMS substrate or damage to the films. For other cases, the strain induced by handling the transferred film on PDMS or the compressive strain induced to generate buckles resulted in delamination or cracking of the films or both. These defects in the films resulted in the misrepresentation of the buckling wavelengths because the compressive strain was accommodated by delamination and cracking, as opposed to by buckling.[26] Polymers with a high tendency to crack under the minute strains produced by transfer were treated as having effective crack-onset strains of 0%. Measurements of the crack-onset strain, described in the next section, were performed to further test the dependency of ductility on molecular structure.

The values of the tensile modulus occupied a range between 200 MPa and 4 GPa, which corresponded well with the range of the previously reported moduli for other D–A conjugated polymers using the same method of measurement.[2] The highest
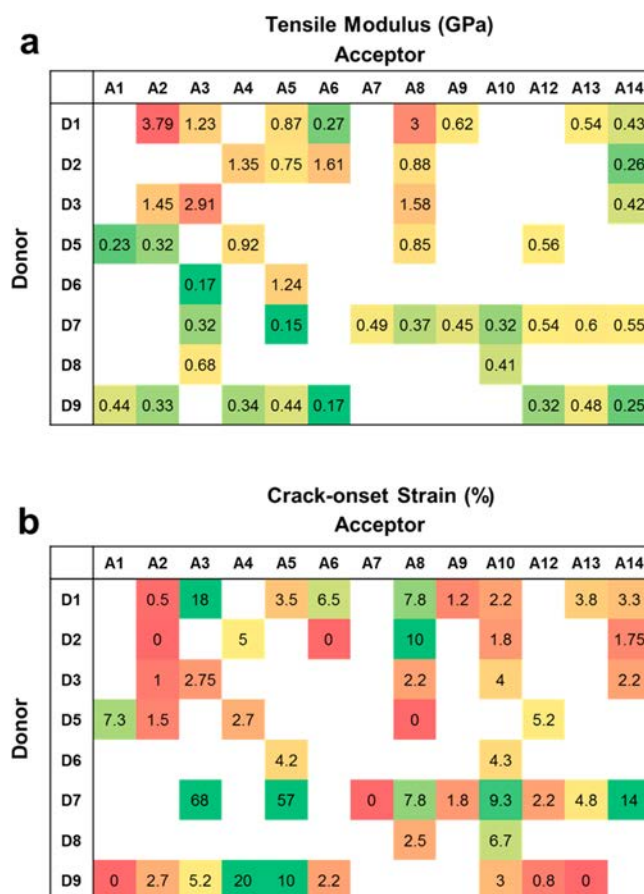
Figure 2. Summary of the mechanical properties measured in this paper. (a) Tensile moduli of the examined polymers in GPa. Indicated colors correspond to the ranking of the lowest value of the modulus (green) to the highest value of the modulus (red). (b) Crack-onset strain of the polymers. Colors correspond to the ranking from the highest value (green) to the lowest value (red). Standard deviations are omitted in this figure for the sake of clarity and provided in Table 1. No values were plotted for the polymers for which the measurements were not obtained.

value of tensile modulus measured was that of A2D1 at 3.79 ± 0.80 GPa. The first qualitative trend we observed was the relatively high stiffness (larger values of tensile moduli) of polymers comprising donor units with fused rings in the backbone. The polymers with donor units with fused rings (D1, D2, and D3) were found to have an average tensile modulus on the order of 1 GPa, while polymers with isolated rings such as D5, D7, and D8 had moduli on the order of 500 MPa. This qualitative trend agrees well with the previously reported increase in stiffness when the polymer backbone comprises fused rings rather than isolated rings.[11] We note here that D6 and D9 also comprise fused rings in their backbone; however, the resulting polymers from these two donor units were found to have much lower average modulus, which was similar to values obtained for polymers with isolated rings. We attributed this lower than expected moduli to the presence of long and branched solubilizing side chains found on both D6 and D9.

The effect of the length of the solubilizing side chains on the tensile modulus of P3AT was studied by us in a previous publication.[23] We found that an increase in the length of the alkyl side chain from 4 to 8 (P3BT to P3OT) dramatically reduced the tensile modulus by approximately an order of magnitude. This effect was attributed to the decrease in glass

Table 1. Tensile Moduli and Crack-Onset Strain of All Polymers Measured by the Film-on-Elastomer Technique in This Study[a]

polymer	M_n (Da)	Đ	tensile modulus (GPa)	crack-onset strain (%)	crack behavior
A1D5	9300	2.2	0.24 ± 0.08	7.3 ± 2	ductile
A1D9	6900	1.4	0.44 ± 0.18	0[c]	brittle
A2D1	9500	2.0	3.79 ± 0.80	0.5[d]	brittle
A2D2	12 400	11.4	NA[b]	0[c]	brittle
A2D3	90 000	4.5	1.45 ± 0.47	1[d]	brittle
A2D5	540 000	4.2	0.32 ± 0.02	1.5[d]	brittle
A2D9	9400	1.8	0.33 ± 0.12	2.7 ± 1.5	brittle
A3D1	50 000	10.8	1.23 ± 0.52	18 ± 5	ductile
A3D3	16 000	3.5	2.91 ± 1.30	2.75[d]	brittle
A3D6	3800	3.1	0.17 ± 0.02	NA[b]	NA
A3D7	24 000	2.7	0.32 ± 0.03	68 ± 14	ductile
A3D8	2200	3.1	0.68 ± 0.14	NA[b]	NA
A3D9	19 000	2.1	NA[b]	5.2 ± 2	ductile
A4D2	22 000	9.1	1.35 ± 0.76	5.0 ± 1.3	brittle
A4D5	29 000	9.2	0.92 ± 0.19	2.7 ± 0.6	brittle
A4D9	7000	1.5	0.34 ± 0.18	19.7 ± 1.5	ductile
A5D1	18 000	3.0	0.87 ± 0.11	3.5 ± 0.5	brittle
A5D2	100 700	3.1	0.75 ± 0.23	NA[b]	NA
A5D6	11 000	26.7	1.24 ± 0.29	4.2 ± 1.3	brittle
A5D7	34 000	3.4	0.15 ± 0.04	56.8 ± 9.9	ductile
A5D9	138 000	8.0	0.44 ± 0.15	10 ± 3.6	ductile
A6D1	9600	2.0	0.27 ± 0.02	6.5 ± 2.0	brittle
A6D2	11 000	2.2	1.61 ± 0.51	0[c]	brittle
A6D9	21 600	2.7	0.17 ± 0.05	2.2 ± 0.8	brittle
A7D7	1200	3.3	0.49 ± 0.18	0[c]	brittle
A8D1	16 000	2.0	3.00 ± 0.56	7.8 ± 0.8	brittle
A8D2	14 000	2.4	0.88 ± 0.40	10 ± 2	ductile
A8D3	14 000	2.2	1.58 ± 0.64	2.2 ± 0.8	brittle
A8D5	5000	1.4	0.85 ± 0.21	0[c]	brittle
A8D7	6100	2.6	0.37 ± 0.10	7.8 ± 1.6	ductile
A8D8	3700	2.2	NA[b]	2.5 ± 1.5	brittle
A9D1	9500	2.8	0.62 ± 0.20	1.2 ± 0.6	brittle
A9D7	7200	1.7	0.45 ± 0.17	1.8 ± 0.3	brittle
A10D1	21 000	2.5	NA[b]	2.2 ± 0.8	brittle
A10D2	103 000	3.3	NA[b]	1.8 ± 0.6	brittle
A10D3	68 000	3.3	NA[b]	4 ± 1	brittle
A10D6	6700	3.5	NA[b]	4.3 ± 1.3	brittle
A10D7	34 000	4.2	0.32 ± 0.06	9.3 ± 1.5	ductile
A10D8	1200	2.8	0.41 ± 0.22	6.7 ± 0.8	ductile
A10D9	2300	5.4	NA[b]	3 ± 1.7	brittle
A12D5	13 000	3.1	0.56 ± 0.25	5.2 ± 2.4	brittle
A12D7	5600	2.1	0.54 ± 0.24	2.2 ± 0.8	brittle
A12D9	37 000	2.3	0.32 ± 0.05	0.8 ± 0.6	brittle
A13D1	12 000	7.5	0.54 ± 0.25	3.8 ± 2.4	brittle
A13D7	10 000	2.1	0.60 ± 0.16	4.8 ± 0.3	brittle
A13D9	12 000	76.7	0.48 ± 0.13	0[c]	brittle
A14D1	9800	1.7	0.43 ± 0.26	3.3 ± 0.8	brittle
A14D2	4600	4.1	0.26 ± 0.05	1.75[d]	brittle
A14D3			0.42 ± 0.14	2.2 ± 1.0	brittle
A14D7	19 000	2.6	0.55 ± 0.09	13.7 ± 1.5	ductile
A14D9	1600	1.9	0.25 ± 0.12	NA[b]	NA

[a]The number averaged molecular weights and the values of dispersity are reproduced from ref 8. Polymers are separated by the designated number of the acceptor (Figure 1) for readability. [b]The values obtained from so-designated polymer samples were omitted or removed due to (1) insufficient material available, (2) failure to obtain smooth films, or (3) too large of propagated error. [c]The polymer samples cracked upon the start of the test under the strain of less than the minimum step of 0.5% strain. [d]The polymer samples exhibited inconsistent cracking behaviors, and the values of the crack-onset strains reported are the lowest measured crack-onset strains.
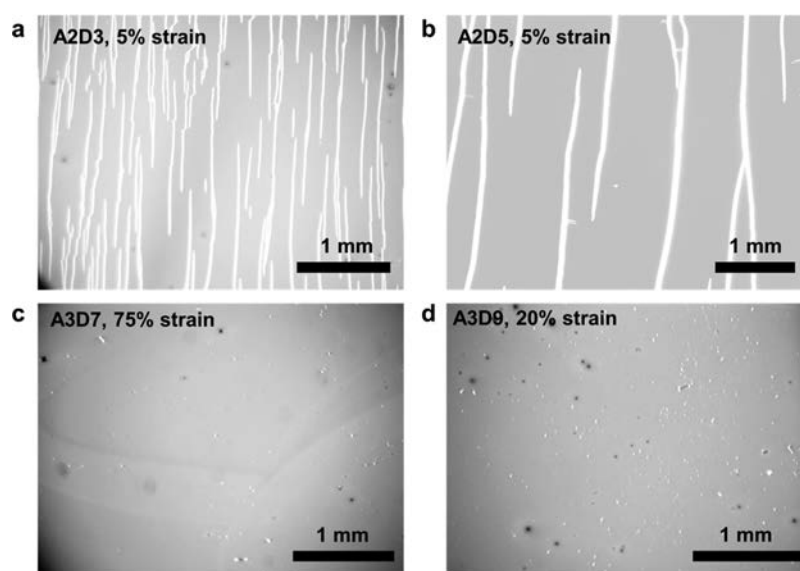
Figure 3. Optical micrographs of the two different natures of cracking behavior: brittle fracture (a, b) and ductile fracture (c, d).

transition temperature with longer side chains and the reduction of the volume fraction of the load-bearing main chain.[23] The presence of the long and branching side chains have been known to affect the microstructure and therefore electronic properties of the polymers in many aspects, for example, by increasing the separation between main chains.[16] This reduction in the intermolecular packing of the polymer

chains could explain the large reduction in tensile moduli found in polymers comprising D6 and D9.

Ductility of D−A Polymers. We measured the ductility of the D−A polymers as manifested in the crack-onset strain.[4,11,23] Figure 2b shows the average values of the crack-onset strains. The standard deviations, reported in Table 1, were taken from the statistics from measurements of different samples ($N > 3$). Six polymers cracked upon preparation of the film, transferring onto an elastomer substrate and mounting the film-on-elastomer onto the linear actuator, and their values are reported as 0% strains in Figure 2b and Table 1. However, it is important to note that despite the effort to minimize the applied strain during preparation of the samples, some finite tensile strains were induced during the preparation stages. We estimated this value to be lower than 0.5%.

We found that the majority of D−A polymers has relatively low crack-onset strains when compared to other conjugated polymers such as P3ATs. Most of the D−A polymer films experienced catastrophic cracking at tensile strains lower than 5% (Figure 2b). The cracking behavior of each film is also summarized in Table 1. We observed that the films with crack-onset strains below 5% cracked in a brittle mode. Specifically, the cracks that formed in these films tended to propagate rapidly along the entire axis perpendicular to the strained axis. In contrast, a few polymers comprising the combination of monomers A3, A8, D1, D5, D7, and D9 were found to have higher crack-onset strains (highlighted in green in Figure 2b). The increased crack-onset strains for these polymer films could potentially be explained by the nature of the ductile fracture found in these films. Cracks found in these polymer films, labeled "ductile" in Table 1, appeared as pinholes and exhibited less of a tendency to propagate with increased strain (qualitatively equivalent to greater fracture toughness). The example of the visual contrast between the two cracking behaviors is shown in Figure 3. While both brittle and ductile fractures are deleterious to the films and possibly to the performance of a fully fabricated OPV, the ductile films would have a lower tendency to propagate cracks and to cause failure, i.e., short circuits in devices with vertical charge transport (solar cells) and open circuits in devices requiring horizontal charge transport (thin-film transistors).

Previous studies on conjugated polymers have found a correlation between tensile modulus and the propensity of the polymer films to crack upon the applied tensile strains, i.e., films with higher moduli tend to crack at lower applied strains. However, these studies are usually performed on P3ATs.[21,23] The same correlation was not found when comparing the D−A polymers of vastly different structures. Figure 4 shows the crack-onset strain as a function of tensile modulus of 39 polymers (the subset of the library for which we were able to measure both tensile modulus and crack-onset strain). As described earlier, most of the samples with higher crack-onset strain exhibited ductile fractures (blue), and those with lower values exhibited brittle fractures (red). For many polymers, despite the low values of stiffness, the films did not appear to be ductile as previously predicted for P3ATs. From the 47 polymers in which the crack-onset strains were measured, only 16 polymers withstood at least 5% tensile strains before fracture. The brittleness of D−A polymers has also been reported in mixtures with either [60] PCBM or non-PCBM electron acceptor. Kim et al. measured the mechanical properties via the pseudo-free-standing tensile test for composite of PBDTTTPD (A9D2) and PCBM or P-
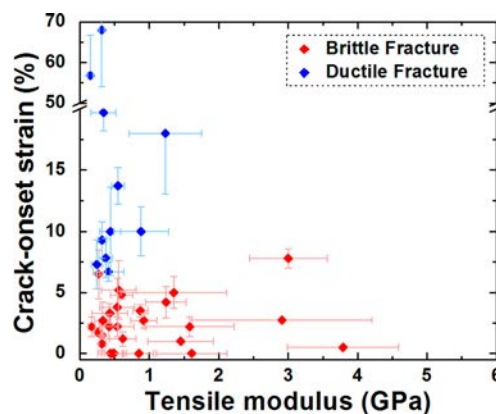

Figure 4. Plot of crack-onset strains vs tensile moduli of the polymers tested in this study. Data points are distinguished in color by the nature of the fracture: red (brittle) and blue (ductile).

(NDI2HD-T), a non-PCBM electron acceptor, by obtaining a pull test of the film supported on the surface of water.[14] The authors reported that the mixtures with PCBM cracked well before 0.30% strain, and the mixture with P(NDI2HD-T) cracked around 7% strain.[14] This apparent brittleness was further elucidated in the comparison between P3HT and PTDPPTFT4 (a DPP-based polymer with a ladder-like unit in the backbone comprising four fused thiophene rings) by Wu et al.;[13] P3HT films fabricated in the same manner as the D−A polymer could withstand over 100% tensile stains in contrast to <5% for the D−A polymer. Despite the lack of the inverse correlation between the stiffness and ductility of the D−A polymers, both quantities will be important for the implementation of a full working device designed for R2R fabrication.

Toward Rational Design for Mechanical Deformability. We sought to identify the molecular structural determinants that influence the mechanical properties of D−A polymers in an effort to co-optimize the mechanical and electrical performance and scalability, and found some general trends which could lead to qualitative design rules. However, exceptions to the rules were also identified. These exceptions could potentially arise from the indirect comparison between the combinations of donor and acceptor and the differences in molecular weight, dispersity, and possibly effects of certain combinations of donor and acceptor monomers that are otherwise difficult to predict. Critically, predictive trends in mechanical properties require understanding both the molecular structure and the solid-state microstructure or the way that the former produces the latter.[2] Solid-state packing structures[4] have been shown to greatly influence the mechanical properties, and certain combinations of monomers may lead to vastly different packing structures than those with similar donor or acceptor monomers.[12] For example, Mei et al. studied the effect of the addition of aliphatic conjugation-break spacers into the conjugated backbone of DPP-based polymers.[27] While the lamella spacing as measured from grazing incidence X-ray diffraction (GIXRD) decreased monotonically with higher concentration of the aliphatic conjugation-break spacers, the order of the crystalline domains, manifested as the lamella peak full width at half-maximum (fwhm), followed a nonlinear progression.[27] This result illustrated the competition between multiple effects of the molecular structures of the polymer: while the addition of conjugation-break spacers increased the
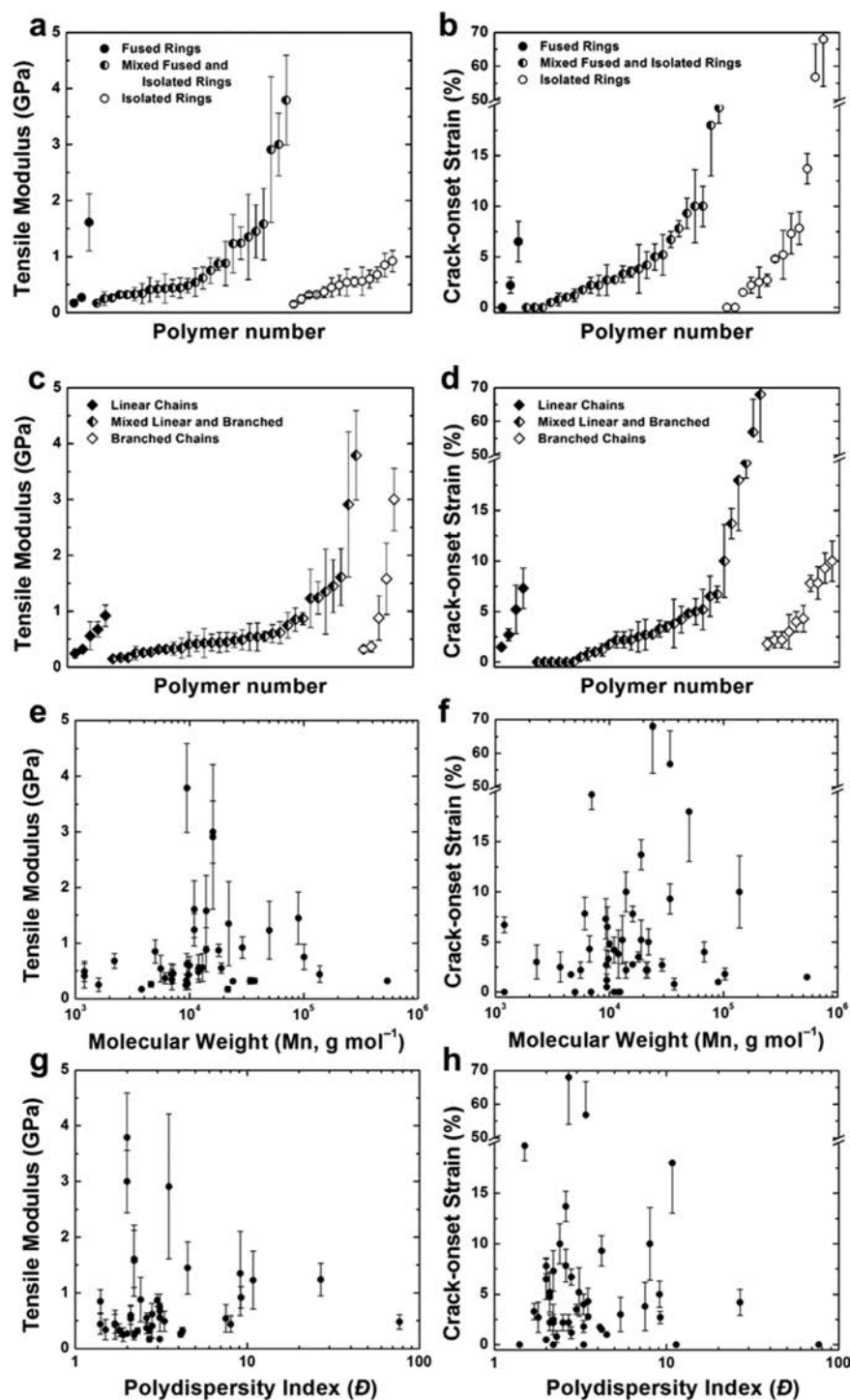
Figure 5. Illustration of the range of tensile modulus and crack-onset strains from all polymer samples. (a, b) Ranking of the polymer samples separated by the presence of fused rings in both donor and acceptor (filled circles), either fused ring in donor or acceptor (half-filled circles), and all isolated rings (open circles). (c, d) Plot in which the polymer samples are separated by the nature of the solubilizing side chains: all linear chains (filled diamonds), branched chain on either the donor or the acceptor monomers (half-filled diamonds), and all branched side chains (open diamonds). Plots of tensile moduli and crack-onset strains as a function of number-average molecular weight (e and f) and $Đ$ (g and h); values of M_n and $Đ$ are reproduced from ref 8.

flexibility of the backbone, it also increased the tendency of interdigitation of the alkyl side chains.[27] We outlined these trends in molecular structures below along with the identified exceptions.

1. Presence of Fused Rings in the Backbone. We found that the polymers with fused rings in the backbone structures (namely, the polymers with D1, D2, and D3) had average

tensile moduli on the order of 1 GPa. This value is of the same order as that of regioregular P3HT.[20,23] We attributed the increase in tensile moduli for these polymers to the fact that a fused ring reduces the flexibility while increasing the length of conjugation of the backbone. Polymers with donors comprising isolated rings (D5, D7, and D8) also showed an averaged tensile modulus of 0.58, 0.42, and 0.55 GPa with the highest

values coming from A4D5 (0.92 ± 0.19). There are, however, exceptions to this general trend, namely, the polymers comprising the donor unit D9 were found to have much lower tensile moduli, on the order of 500 MPa. This reduction in modulus for the D9 monomer was likely the effect of long and branching solubilizing side chains (2-hexyldecyl), which is further discussed in the next section. We found small effects on the tensile modulus from acceptors with fused-ring structures (A6 and A10). In addition, the polymer A6D1 that contained fused ring structures in both the donor and the acceptor monomers has a tensile modulus of only 0.27 ± 0.02 GPa.

The effects of fused rings on ductility were found to be less obvious. The values of the crack-onset strains of polymers containing D3 were found to be low (<5% crack-onset strain) and consistent with the trend, in which the fused ring in the backbone produced brittle polymer films. However, for polymers comprising D1 and D2, some combinations with certain acceptor monomers were found to produce ductile films, namely, A3D1 and A8D2 exhibited ductile fractures with crack-onset strain higher than 10%. Again, we believed the abnormality in the trend was the product of the side chains on the acceptors, which will also be discussed in the next section. The polymers containing the fused DPP monomer (A10) when combined with donor monomer with fused rings (D1, D2, D3, D6, and D9) also produced brittle films (i.e., low crack-onset strain). Interestingly, the combination of A10 and the nonfused donor monomers (D7 and D8) produced ductile films with higher values of crack-onset strain than the other combinations. We attributed this effect to a possible change in solid-state morphologies and packing when the DPP (A10) acceptors were combined with dialkoxybenzene (D7) and bithiophene (D8).

2. Influence of Long and Branching Solubilizing Side Chains. As mentioned in the previous section, the effects of long and branching solubilizing side chains can dominate the mechanical properties of a polymer film. The tensile moduli of the films containing donor units with branching side chains, 2-hexyldecyl (D6, D7, and D9), were found to be lower than donor units with linear side chains. We also observed an increase in ductility of the films with either 2-hexyldecyl or 2-ethylhexyl side chains, namely, 14 out of 16 polymers in which the crack-onset strain exceeded 5% were found to be in this category. Interestingly, three of the most ductile polymers found in this study comprised the donor D7: A3D7 (crack-onset strain of 68%), A5D7 (57%), and A14D7 (14%). Significant differences between the acceptors A2 and A3, whose similar structures comprise of benzothiadiazole with two flanking thiophenes, were attributed to the locations of the alkyl side chains. For A2, the alkyl side chains ($C_{12}H_{25}$) are located on the two flanking thiophenes, whereas for A3, the alkyl side chains ($C_{14}H_{29}$) are connected to the benzothiadiazole via ether linkages. With the exception of A3D3, whose stiffness and ductility are on the same order as polymers with A2 in the backbone structure, all polymers comprising A3 are less stiff and more ductile than the A2 counterparts. Notably, A3D1 and A3D7 were found to withstand large tensile strains (∼18% and ∼68%, respectively).

The correlation between the structures of the side chains and the mechanical properties of the polymers could be explained in part from the solid-state molecular packing.[28] While the mechanical properties and the molecular packing or crystalline quality are not necessarily related in a straightforward manner, we can draw some qualitative insights from the effects of the side chains. For example, Yiu et al. demonstrated that branched side chains on a DPP-based polymer led to more steric hindrance between neighboring polymer chains and lower crystalline coherence length when compared to linear side chains.[29] Segalman and co-workers have shown that replacing the hexyl side chains on P3HT to 2-ethylhexyl side chains (P3EHT) reduced the melting temperature and the crystallization kinetics of the polymer.[30] Furthermore, the backbone of the adjacent P3EHT chains have been shown to be significantly tilted, resulting in the larger spacing between the chains and the lower intermolecular coupling.[31] These results suggest that there is a reduction in packing efficiency and lower crystallinity when branched side chains are introduced; these effects could potentially lead to increased deformability.

3. Notes and Unresolved Questions. As mentioned in the previous section, the ability to predict the mechanical responses of the D−A polymers will require not only knowledge of the molecular parameters (fused-ring and side chains) but also the propensity to form crystallites,[4] degree of crystallinity, and rigidity (i.e., glassy behavior) of the amorphous domains.[12] We noticed this limitation of the predictive nature of focusing on one aspect of the molecular structures as depicted in Figure 5a−d. Figure 5a and 5b rank the D−A polymers by the tensile moduli and the crack-onset strains while separating them into three groups: (1) fused rings in both donor and acceptor, (2) fused rings in the donor or in the acceptor, and (3) all isolated rings. Figure 5c and 5d separate the polymers by the nature of the solubilizing side chains: (1) only linear chains, (2) branching chains in either the donor or the acceptor, and (3) all branching side chains. Our initial hypotheses would suggest that the polymers with all isolated rings and with all branching chains would be the least stiff and the most ductile. While the general trends we described hold relatively well, we observed that the polymers in each group sample occupied a large range of both values of the mechanical properties and substantial overlap. We note that further studies are required to fully isolate the complicated interplay between the nature of the polymer backbone and the nature of the side chains and their effects on the mechanical properties. For example, poly(3-dodecylthiophene) has linear alkyl side chains and has been reported by us to have high crack-onset strains.[23] However, for D−A polymers with relatively higher rigidity in the backbone, the linear side chains are less likely to lead to high crack-onset strains. Furthermore, some polymers comprising both isolated rings and branching side chains performed poorly mechanically. We attributed such outliers to the unknown stiffness of the chains and the solid-state packing structures of the polymers.

In addition, the dispersity and molecular weight of the D−A polymers must also be taken into account when predicting the mechanical properties. For P3ATs, the dependencies of the solid-state packing structure on molecular weight and regioregularity have been previously reported.[32−35] Furthermore, Kim et al. reported significant changes in mechanical and optoelectrical properties of P3HT as a function of regioregularity.[5] These rigorously controlled experiments in which the molecular weight, dispersity, and regioregularity were isolated required carefully controlled synthesis that is only possible for very few polymers, such as P3ATs, which are produced by a quasi-living process.[5,36] For most D−A polymers that require a Stille polycondensation reaction, the control over the molecular weight and the dispersity of the product is typically not high.[36,37] Moreover, the size-exclusion chromatography (SEC) system used to measure the values of Đ operates

at low temperatures and employs chloroform as the solvent. In these conditions, aggregation of some polymers could lead to unrealistic Đ values. Figure 5e−h plots the mechanical properties of the D−A polymers to the number-average molecular weight and Đ. We observed few correlations between the mechanical properties of the different D−A polymers and their molecular weight and Đ (though the usual caveats apply of obtaining molecular weight for conjugated polymers by size-exclusion chromatography when no similarly rigid standards are available). It is noteworthy to point out that while comparing the effect of molecular weight and Đ for a single polymer could potentially provide a meaningful trend, the molecular weight and dispersity of the polymer alone do not explain the measured differences in mechanical properties.

4. Introduction of an Electronic-Mechanical Merit Factor. We measured the mechanical properties of D−A polymers in the hope of identifying the design rules for optimizing the mechanical robustness and electrical properties for R2R fabrication. We observed that many of the D−A polymers tested exhibited brittle properties despite the low stiffness. This result suggests that it will be a significant challenge to incorporate some D−A polymers in applications demanding significant deformation as well as in R2R fabrication. However, we identified several promising candidates with favorable electronic and mechanical properties. We combined the power conversion efficiency as reported for the roll-fabricated solar cell reported in ref 8 and the tensile modulus and crack-onset strain into a new merit factor (ψ) defined as

$$\Psi = PCE \times \frac{1}{E_f} \times CoS \tag{1}$$

$$\Psi_{rel} = \Psi / \Psi_{P3HT} \tag{2}$$

where E_f is the tensile modulus and the CoS is the crack-onset strain. Figure 6 depicts the relative merit factor (Ψ_{rel}) of the polymers tested in this experiment when compared to the properties of P3HT. The blank cells represent the missing data (where at least one quantity was missing). Using this merit factor we identified nine promising polymers (highlighted in green), four of which comprise the donor D7. We note that the
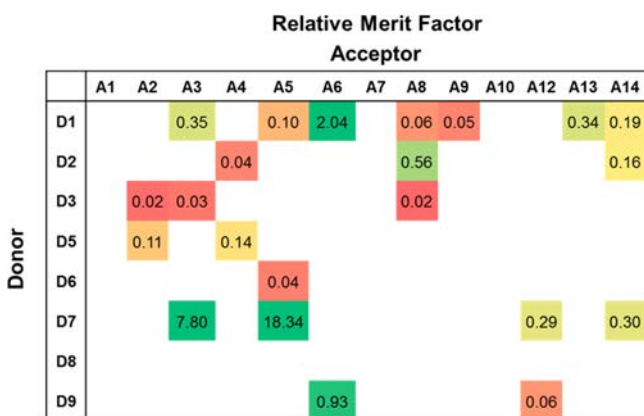
mechanical properties of the composites of the electron-donating polymer and an electron acceptor will be different than those of the pure polymers. The addition of fullerene-based electron acceptors (namely, [60] PCBM) has been reported by us and others to lower the mechanical robustness of the composites when compared to the pure polymers.[20,23] However, with the recent advancement in nonfullerene electron acceptors, this deleterious effect can potentially be avoided.[14] Furthermore, we admit to some shortcomings arising from the simplicity of the proposed figure of merit, namely, the equal contributions from power conversion efficiency, tensile modulus, and crack-onset strain. In order to characterize the electronic and mechanical properties fully, a more in-depth study of the effects of the addition of the electron acceptor, the film thickness, and the processing conditions on the electronic and mechanical properties of the whole modules will be required.

CONCLUSION

This paper described the mechanical properties of a library of D−A polymers with significant diversity in molecular structure. We identified some trends from the measured values of tensile modulus and crack-onset strain as well as plausible reasons for the exceptions. We found that the stiffness of most D−A polymers was on the same order of magnitude as P3HT or lower (occupying the range between 200 MPa to 1 GPa; however, most were brittle and tended to fracture at low strains, <5%). The polymers comprising the donors with fused rings tended to have higher stiffness and higher tendency to fracture. In addition, the polymers with branching solubilizing side chains were found to have high deformability. These trends are useful for general guidelines while designing highly mechanically robust materials for R2R fabrication. It is important to note the importance of co-optimization of electronic and mechanical properties for designing materials for both R2R fabrication and flexible or stretchable applications. From the library of D−A polymers, we identified potential candidates whose merit factors (weighted values comprising power conversion efficiency and mechanical properties) are better than those of P3HT. However, we also identified that the molecular structures of the D−A polymers do not completely govern the mechanical properties; further analysis of the solid-state packing structure from computation, microstructural analysis, and a complete theory thereof are required to fully understand the interplay between mechanical and electronic behaviors of this class of materials.

EXPERIMENTAL METHODS

Materials. Low-band-gap donor−acceptor polymers used for this work were described in a previous study by Bundgaard et al.[8] Briefly, 13 acceptor and 8 donor units (Figure 1a and 1b) were selected and all the combinations were synthesized, yielding 104 polymers. Several combinations were omitted in the mechanical studies due to difficulties in synthesis. After chemical and optoelectronic characterization of these materials, 75 polymers were initially available for mechanical characterizations. All of the polymers properties and synthesis procedures are reproduced from ref 8 in the Supporting Information. Polydimethylsiloxane (PDMS) (Sylgard 184) was purchased from Dow Corning. Chloroform and P3HT were purchased from Sigma-Aldrich and used as received.

Sample Preparation. The glass substrates (2.5 cm × 2.5 cm) were cleaned by bath sonication of Alconox solution, deionized water, acetone, and isopropanol for 10 min each and dried under compressed air before they were plasma treated for 3 min (30 W, 200 mTorr

Relative Merit Factor

	Acceptor													
Donor	A1	A2	A3	A4	A5	A6	A7	A8	A9	A10	A12	A13	A14
D1			0.35		0.10	2.04		0.06	0.05			0.34	0.19
D2				0.04				0.56					0.16
D3	0.02	0.03						0.02					
D5	0.11			0.14									
D6					0.04								
D7			7.80		18.34						0.29		0.30
D8													
D9						0.93			0.06				

Figure 6. Relative merit factor incorporating the power conversion efficiency (*PCE*) as reported for the R2R fabricated solar cells (from ref 8), the tensile modulus, and crack-onset strains in relationship to those of P3HT. Blank cells indicate missing information where at least one quantity was missing. The tensile modulus of P3HT and crack-onset strain, reproduced from ref 23, were 1.09 ± 0.15 GPa and (9 ± 1.2)% respectively.

ambient air). All polymer solutions were prepared by dissolution in chloroform at a 20 mg mL^{-1} concentration. The solution was then stirred on a hot plate using a magnetic stirrer at 50 °C for 2 h before cooling to room temperature and filtering through a 1 μm glass microfiber filter. For each polymer, three different thicknesses were prepared by spin coating the solution on top of the plasma-treated glass substrates at 500, 1000, and 2000 rpm for 2.5 min.

Tensile Moduli and Crack-Onset Strains. Polydimethylsiloxane (PDMS) substrates were prepared according to the manufacturer's instruction at a ratio of 10:1 (base:cross-linker) and cured at room temperature for 36−48 h. PDMS strips (1 cm × 8 cm × 0.3 cm) were then cut out using a razor blade and stretched to strains of 4% using a computer-controlled stage (Newmark model ET-100-11) and clipped onto a glass substrate with binder clips. To transfer the polymer film onto the PDMS strip the previously spin-coated polymer film was then pressed onto the prestretched PDMS strip. The sample was then dipped into DI water for a time ranging from 30 s up to 20 min depending of the polymer. The sample was removed from the water with tweezers, and the glass substrate bearing the polymer was stripped of the PDMS, leaving the polymer layer on top of the PDMS. The sample was dried in a desiccator under dynamic vacuum for 30 min. Finally, the prestrained PDMS was released to form buckles. The buckled polymer films were observed with an optical microscope. Optical micrographs of the buckles were acquired and analyzed via an in-house MATLAB code. The tensile modulus of the PDMS was measured for each batch with a conventional pull tester, and the thickness of the each polymer film was measured using a Veeco Dektak stylus profilometer. The tensile modulus of the polymers was calculated using eq 3.

$$E_f = 3E_s \left(\frac{1 - v_f^2}{1 - v_s^2} \right) \left(\frac{\lambda_b}{2\pi d_f} \right)^3 \tag{3}$$

Briefly, the buckling wavelength λ_b was plotted as a function of the film thickness d_f. The slope λ_b/d_f obtained by linear fit was then substituted in eq 3, where E_s is the PDMS substrate modulus and the Poisson ratios of the film (v_f) and the PDMS substrate (v_s) were assumed to be 0.35 and 0.5 respectively.[20] We prepared our films to be within the range from ~40 to 500 nm.[4,19,24,25] To minimize the change of experimental error, we also used the slope of the linear fit (λ_b/d_f) between the three data points. Ductility of the films as manifested in a form of the crack-onset strains were measured using the same film-on-elastomer method as described in previous work.[23] The polymer films transferred onto unstrained PDMS were then stretched using a computer-controlled linear actuator with a step size of 0.5% strain. Each step was imaged through an optical microscope to observe the generation of cracks. The crack-onset strain of each film was defined as the strain at which the first crack was observed.

ASSOCIATED CONTENT

Ⓢ Supporting Information

The Supporting Information is available free of charge on the ACS Publications website at DOI: 10.1021/acs.chemmater.6b00525.

Tables S1 and S2 and Figures S1 and S2, which relate spin-coating speed, film thickness, and mechanical properties (PDF)

AUTHOR INFORMATION

Corresponding Author

*E-mail: dlipomi@ucsd.edu.

Author Contributions

‡B.R. and S.S. contributed equally.

Notes

The authors declare no competing financial interest.

REFERENCES

(1) Krebs, F. C.; Espinosa, N.; Hösel, M.; Søndergaard, R. R.; Jørgensen, M. 25th Anniversary Article: Rise to Power − OPV-Based Solar Parks. *Adv. Mater.* **2014**, *26*, 29−39.

(2) Savagatrup, S.; Printz, A. D.; O'Connor, T. F.; Zaretski, A. V.; Rodriquez, D.; Sawyer, E. J.; Rajan, K. M.; Acosta, R. I.; Root, S. E.; Lipomi, D. J. Mechanical Degradation and Stability of Organic Solar Cells: Molecular and Microstructural Determinants. *Energy Environ. Sci.* **2015**, *8*, 55−80.

(3) Bruner, C.; Miller, N. C.; McGehee, M. D.; Dauskardt, R. H. Molecular Intercalation and Cohesion of Organic Bulk Heterojunction Photovoltaic Devices. *Adv. Funct. Mater.* **2013**, *23*, 2863−2871.

(4) O'Connor, B.; Chan, E. P.; Chan, C.; Conrad, B. R.; Richter, L. J.; Kline, R. J.; Heeney, M.; McCulloch, I.; Soles, C. L.; DeLongchamp, D. M. Correlations between Mechanical and Electrical Properties of Polythiophenes. *ACS Nano* **2010**, *4*, 7538−7544.

(5) Kim, J.-S.; Kim, J.-H.; Lee, W.; Yu, H.; Kim, H. J.; Song, I.; Shin, M.; Oh, J. H.; Jeong, U.; Kim, T.-S.; et al. Tuning Mechanical and Optoelectrical Properties of Poly(3-Hexylthiophene) through Systematic Regioregularity Control. *Macromolecules* **2015**, *48*, 4339−4346.

(6) Printz, A. D.; Zaretski, A. V.; Savagatrup, S.; Chiang, A. S.-C.; Lipomi, D. J. Yield Point of Semiconducting Polymer Films on Stretchable Substrates Determined by Onset of Buckling. *ACS Appl. Mater. Interfaces* **2015**, *7*, 23257−23264.

(7) Dang, M. T.; Hirsch, L.; Wantz, G. P3HT:PCBM, Best Seller in Polymer Photovoltaic Research. *Adv. Mater.* **2011**, *23*, 3597−3602.

(8) Bundgaard, E.; Livi, F.; Hagemann, O.; Carlé, J. E.; Helgesen, M.; Heckler, I. M.; Zawacka, N. K.; Angmo, D.; Larsen-Olsen, T. T.; dos Reis Benatto, G. a.; et al. Matrix Organization and Merit Factor Evaluation as a Method to Address the Challenge of Finding a Polymer Material for Roll Coated Polymer Solar Cells. *Adv. Energy Mater.* **2015**, *5*, 1402186.

(9) Guo, X.; Baumgarten, M.; Müllen, K. Designing π-Conjugated Polymers for Organic Electronics. *Prog. Polym. Sci.* **2013**, *38*, 1832−1908.

(10) Liu, Y.; Zhao, J.; Li, Z.; Mu, C.; Ma, W.; Hu, H.; Jiang, K.; Lin, H.; Ade, H.; Yan, H. Aggregation and Morphology Control Enables Multiple Cases of High-Efficiency Polymer Solar Cells. *Nat. Commun.* **2014**, *5*, 5293.

(11) Lipomi, D. J.; Chong, H.; Vosgueritchian, M.; Mei, J.; Bao, Z. Toward Mechanically Robust and Intrinsically Stretchable Organic Solar Cells: Evolution of Photovoltaic Properties with Tensile Strain. *Sol. Energy Mater. Sol. Cells* **2012**, *107*, 355−365.

(12) Printz, A.; Savagatrup, S.; Burke, D.; Purdy, T.; Lipomi, D. Increased Elasticity of a Low-Bandgap Conjugated Copolymer by Random Segmentation for Mechanically Robust Solar Cells. *RSC Adv.* **2014**, *4*, 13635−13643.

(13) Wu, H.-C.; Benight, S. J.; Chortos, A.; Lee, W.-Y.; Mei, J.; To, J. W. F.; Lu, C.; He, M.; Tok, J. B.-H.; Chen, W.-C.; et al. A Rapid and Facile Soft Contact Lamination Method: Evaluation of Polymer Semiconductors for Stretchable Transistors. *Chem. Mater.* **2014**, *26*, 4544−4551.

(14) Kim, T.; Kim, J.-H.; Kang, T. E.; Lee, C.; Kang, H.; Shin, M.; Wang, C.; Ma, B.; Jeong, U.; Kim, T.-S.; et al. Flexible, Highly Efficient All-Polymer Solar Cells. *Nat. Commun.* **2015**, *6*, 8547.

(15) Jackson, N. E.; Kohlstedt, K. L.; Savoie, B. M.; Olvera de la Cruz, M.; Schatz, G. C.; Chen, L. X.; Ratner, M. A. Conformational Order in Aggregates of Conjugated Polymers. *J. Am. Chem. Soc.* **2015**, *137*, 6254−6262.

(16) Duan, C.; Huang, F.; Cao, Y. Recent Development of Push−pull Conjugated Polymers for Bulk-Heterojunction Photovoltaics: Rational Design and Fine Tailoring of Molecular Structures. *J. Mater. Chem.* **2012**, *22*, 10416−10434.

(17) Takacs, C. J.; Brady, M. A.; Treat, N. D.; Kramer, E. J.; Chabinyc, M. L. Quadrites and Crossed-Chain Crystal Structures in Polymer Semiconductors. *Nano Lett.* **2014**, *14*, 3096−3101.

(18) Printz, A. D.; Savagatrup, S.; Rodriquez, D.; Lipomi, D. J. Role of Molecular Mixing on the Stiffness of Polymer:fullerene Bulk Heterojunction Films. *Sol. Energy Mater. Sol. Cells* **2015**, *134*, 64−72.

(19) Stafford, C. M.; Harrison, C.; Beers, K. L.; Karim, A.; Amis, E. J.; VanLandingham, M. R.; Kim, H.-C.; Volksen, W.; Miller, R. D.; Simonyi, E. E. A Buckling-Based Metrology for Measuring the Elastic Moduli of Polymeric Thin Films. *Nat. Mater.* **2004**, *3*, 545−550.

(20) Tahk, D.; Lee, H. H.; Khang, D.-Y. Elastic Moduli of Organic Electronic Materials by the Buckling Method. *Macromolecules* **2009**, *42*, 7079−7083.

(21) Awartani, O.; Lemanski, B. I.; Ro, H. W.; Richter, L. J.; DeLongchamp, D. M.; O'Connor, B. T. Correlating Stiffness, Ductility, and Morphology of Polymer:Fullerene Films for Solar Cell Applications. *Adv. Energy. Mater.* **2013**, *3*, 399−406.

(22) Dupont, S. R.; Oliver, M.; Krebs, F. C.; Dauskardt, R. H. Interlayer Adhesion in Roll-to-Roll Processed Flexible Inverted Polymer Solar Cells. *Sol. Energy Mater. Sol. Cells* **2012**, *97*, 171−175.

(23) Savagatrup, S.; Makaram, A. S.; Burke, D. J.; Lipomi, D. J. Mechanical Properties of Conjugated Polymers and Polymer-Fullerene Composites as a Function of Molecular Structure. *Adv. Funct. Mater.* **2014**, *24*, 1169−1181.

(24) Huang, H.; Chung, J. Y.; Nolte, A. J.; Stafford, C. M. Characterizing Polymer Brushes via Surface Wrinkling. *Chem. Mater.* **2007**, *19*, 6555−6560.

(25) Stafford, C. M.; Vogt, B. D.; Harrison, C.; Julthongpiput, D.; Huang, R. Elastic Moduli of Ultrathin Amorphous Polymer Films. *Macromolecules* **2006**, *39*, 5095−5099.

(26) Lee, J.-B.; Yoon, S.-S.; Khang, D.-Y. The Importance of Interfacial Adhesion in the Buckling-Based Mechanical Characterization of Materials. *RSC Adv.* **2013**, *3*, 17364−17372.

(27) Zhao, Y.; Zhao, X.; Zang, Y.; Di, C.; Diao, Y.; Mei, J. Conjugation-Break Spacers in Semiconducting Polymers: Impact on Polymer Processability and Charge Transport Properties. *Macromolecules* **2015**, *48*, 2048−2053.

(28) Mei, J.; Bao, Z. Side Chain Engineering in Solution-Processable Conjugated Polymers. *Chem. Mater.* **2014**, *26*, 604−615.

(29) Yiu, A. T.; Beaujuge, P. M.; Lee, O. P.; Woo, C. H.; Toney, M. F.; Fréchet, J. M. J. Side-Chain Tunability of Furan-Containing Low-Band-Gap Polymers Provides Control of Structural Order in Efficient Solar Cells. *J. Am. Chem. Soc.* **2012**, *134*, 2180−2185.

(30) Ho, V.; Boudouris, B. W.; Segalman, R. A. Tuning Polythiophene Crystallization through Systematic Side Chain Functionalization. *Macromolecules* **2010**, *43*, 7895−7899.

(31) Himmelberger, S.; Duong, D. T.; Northrup, J. E.; Rivnay, J.; Koch, F. P. V.; Beckingham, B. S.; Stingelin, N.; Segalman, R. a.; Mannsfeld, S. C. B.; Salleo, A. Role of Side-Chain Branching on Thin-Film Structure and Electronic Properties of Polythiophenes. *Adv. Funct. Mater.* **2015**, *25*, 2616−2624.

(32) Meille, S. V.; Romita, V.; Caronna, T.; Lovinger, A. J.; Catellani, M.; Belobrzeckaja, L. Influence of Molecular Weight and Regior-egularity on the Polymorphic Behavior of Poly (3-Decylthiophenes). *Macromolecules* **1997**, *30*, 7898−7905.

(33) Goh, C.; Kline, R. J.; McGehee, M. D.; Kadnikova, E. N.; Fréchet, J. M. J. Molecular-Weight-Dependent Mobilities in Regioregular poly(3-Hexyl-Thiophene) Diodes. *Appl. Phys. Lett.* **2005**, *86*, 122110.

(34) Wu, Z.; Petzold, A.; Henze, T.; Thurn-Albrecht, T.; Lohwasser, R. H.; Sommer, M.; Thelakkat, M. Temperature and Molecular Weight Dependent Hierarchical Equilibrium Structures in Semiconducting Poly(3-Hexylthiophene). *Macromolecules* **2010**, *43*, 4646−4653.

(35) Kline, R. J.; McGehee, M. D.; Kadnikova, E. N.; Liu, J.; Frechet, J. M. J.; Toney, M. F. Dependence of Regioregular Poly (3-Hexylthiophene) Film Morphology and Field-Effect Mobility on Molecular Weight. *Macromolecules* **2005**, *38*, 3312−3319.

(36) Burke, D. J.; Lipomi, D. J. Green Chemistry for Organic Solar Cells. *Energy Environ. Sci.* **2013**, *6*, 2053−2066.

(37) Brouwer, F.; Alma, J.; Valkenier, H.; Voortman, T. P.; Hillebrand, J.; Chiechi, R. C.; Hummelen, J. C. Using Bis(pinacolato)-diboron to Improve the Quality of Regioregular Conjugated Co-Polymers. *J. Mater. Chem.* **2011**, *21*, 1582−1592.

Freely available OPV—The fast way to progress

Frederik C. Krebs,*[a] Markus Hösel,[a] Michael Corazza,[a] Bérenger Roth,[a] Morten V. Madsen,[a] Suren A. Gevorgyan,[a] Roar R. Søndergaard,[a] Dieter Karg,[b] and Mikkel Jørgensen[a]

Abundance, fast manufacture, and low cost are what ideally epitomize organic and polymer photovoltaics. However, they have remained esoteric (in physical form) almost since their inception and though they have been extensively studied they cannot be said to be generally available to the public with the exception of a few samples. It is obvious that to qualify as a technology, polymer photovoltaics have to be generally available in significant quantities. We recently reported a fast, efficient combined printing and coating method[1] that enabled roll-to-roll processing of the polymer solar cell stack directly onto almost any flexible material, which ideally comprises a thin flexible barrier substrate.

Herein we describe the fabrication of 20 928 small modules (10.0 × 14.2 cm²) directly on barrier foil by employing a newly designed front electrode grid. This type of encapsulation results from efficient edge sealing by laser-cutting of the final modules. These "freeOPV" modules are, as the name suggests, made freely available to anyone who registers on our scientific website.[2] The general idea behind the establishment of such a program is that the power of analysis is closely linked to the amount of available data and we thus encourage feedback from any technical or scientific study regardless of its nature. The website will furthermore function as a platform through which new materials can be evaluated in the context of this new module.

The indium-tin oxide (ITO)-free solar cell modules were prepared by using previously described procedures,[1] although this current work was performed at higher speeds and with a module design specific to this purpose. A few distinct advances and differences are described in the following paragraphs. An illustration of the complete solar-cell stack is shown in Figure 1.

The front silver grid of the solar cell is processed by flexoprinting at high speed (20 m min⁻¹). We have previously reported the use of a hexagonal front grid made of silver in combination with highly conductive poly(3,4-ethylenedioxythiophene) poly(styrenesulfonate) (PEDOT:PSS) as a transparent electrode, but more-detailed studies have shown that the presence of small electrical shorts in the solar cell is much more pronounced in the areas where the silver front

[a] Prof. F. C. Krebs, M. Hösel, M. Corazza, B. Roth, Dr. M. V. Madsen, Dr. S. A. Gevorgyan, Dr. R. R. Søndergaard, Dr. M. Jørgensen
Department of Energy Conversion and Storage
Technical University of Denmark
Frederiksborgvej 399, DK-4000 Roskilde (Denmark)
E-mail: frkr@dtu.dk

[b] Dr. D. Karg
DCG Systems GmbH Institution
Am Weichselgarten 7, 91058 Erlangen (Germany)
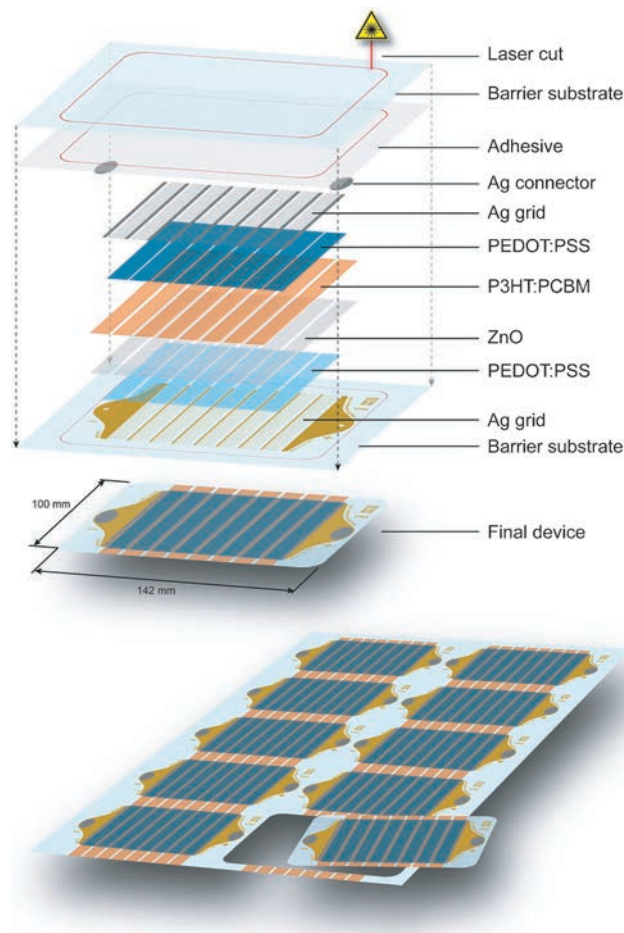
Figure 1. Outline of the multilayer structure of the general structure of the freeOPV sample (top) and an illustration of the a laser-cut freeOPV from the final roll-to-roll processed foil.

electrode grid and the silver back electrode grid overlap. Ideally a design should be developed for which no overlap occurs, but considering the current control of registration (horizontally and in the web direction) and the unpredictable thermal shrinkage and stretching (in the cross-web and in the web direction respectively) of the foil during the process, it is not currently possible to handle such precision at sufficiently high speeds. As an alternative approach, a comb structure with slants of ±5° for the respective grids has been chosen. In such a design there is only one region of overlap (or a maximum of two) thus minimizing the number of likely electrical shorts in the structure. Figure 2 a and b shows light-beam-induced current (LBIC) and dark lock-in thermography (DLIT) images of a module for which three of the eight cells are heavily shunted. In the thermographic image the

Figure 2. LBIC image (A) and DLIT image (B) of a freeOPV sample module showing severe shunting in 3 of the 8 serially connected cells. In frame C is a superimposed photograph and an IR image. The heat spot occurs exactly at the overlap of the two silver grids (one of the silver lines is blocked by the solar cell stack in the picture). The scale bars in A and B are 10 mm and in C it measures 100 μm.

shunted silver comb lines light up due to dissipation of heat at the short circuit located there. Careful analysis of the DLIT image using DLIT microscopy reveals just one 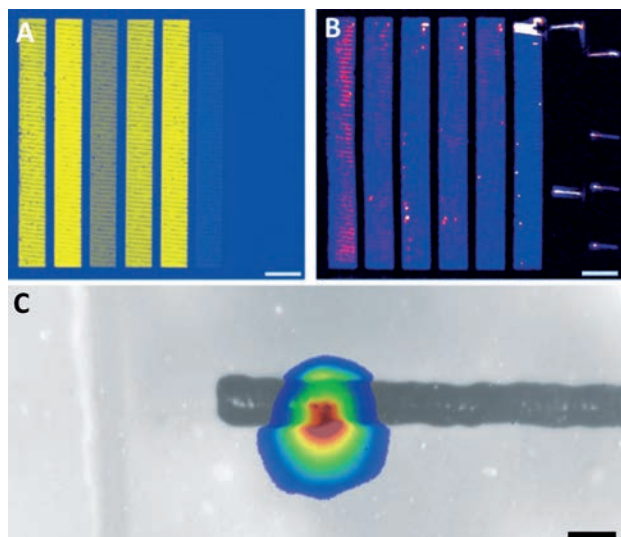point of contact. This technique (Figure 2c) enables extremely high resolution in the thermal image. The grid line is 100 μm wide and the pixel size in the infrared image is 3 μm. We found this new IR microscopy technique to be of exceptional value for the development of the grid electrode.

An extremely important factor in the operation of organic solar cells and modules is to ensure that the cells are properly encapsulated, while retaining the essential access to the electrodes. The previous method was to protect the organic solar cells by applying a barrier foil containing a pressure-sensitive adhesive over the active area while leaving the electrodes exposed for external access.[3] However, such sealing is very sensitive to the slow diffusion from the edges of the seal (a distance of a few millimeters). As an alternative, we present a method for encapsulating the solar cells by using a UV-curable adhesive (DELO Katiobond LP655). Access to the electrodes is subsequently achieved by piercing the finished solar cells through the area where a thick conductor is printed (we have employed both carbon and silver) with a metal push button (Figure 3).

The adhesive was applied to the encapsulation barrier foil by flexoprinting (30 $cm^3 m^{-2}$ anilox cylinder) and this foil was fed into a nip together with the solar cells where the combined foil was subsequently exposed to UV light from an array of twelve lamps. The lamination process was performed at a web speed of 2 $m min^{-1}$. The area containing the extra-thick silver layer ("Ag connector" in Figure 1) was used to make electrical contact after lamination by piercing a nickel-free metal connector through the foil.
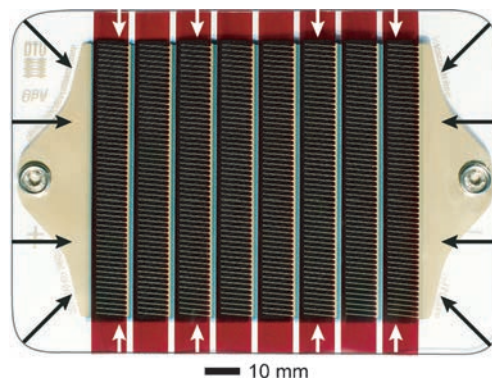
Figure 3. Illustration of the fully encapsulated solar cell. The black and white arrows show the diffusive pathway from the edges to the solar cell.

The finished solar cells were finally cut into individual units by laser cutting using a 90 W roll-to-roll CO_2 laser with a laser speed of 4.5 $m min^{-1}$. Besides the obvious issue of speed an additional advantage of laser cutting is that it minimizes the mechanical stress at the edges of the solar cell that would certainly be present if the cells were cut by conventional means using a knife. It is furthermore reasonable to assume that melting of the substrate at the edges actually seals the multilaminate further and avoids introducing a delamination defect/fracture that has a tendency to propagate. Figure 4 shows a photo of the laser-cutting process (a movie showing the process can be found in the Supporting Information).
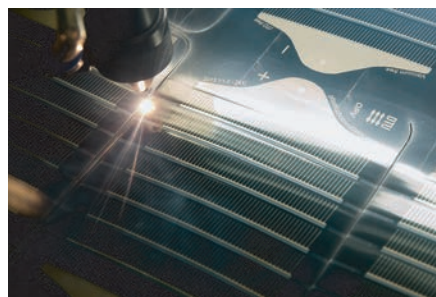
Figure 4. Photograph of the laser cutting process.

Despite the high speed of production the precision and accuracy in each step of coating, printing, encapsulating, and cutting provides high consistency in the device performance with a very low percentage of defective or malfunctioning devices. Figure 5a shows the distribution of the photovoltaic parameters for 80 samples randomly chosen from the roll. The I–V curve of a typical sample is shown in Figure 5b.

The results of short-term stability measurements in accordance with the International Summit on OPV Stability (ISOS-L and ISOS-D)[4] suggest that this new generation of samples is approximately as stable as its roll-to-roll processed predecessors, which have been shown to exceed 10 000 h lifetime under outdoor exposure conditions.[5] As a result of the aforementioned full encapsulation, the cells also exhibit an
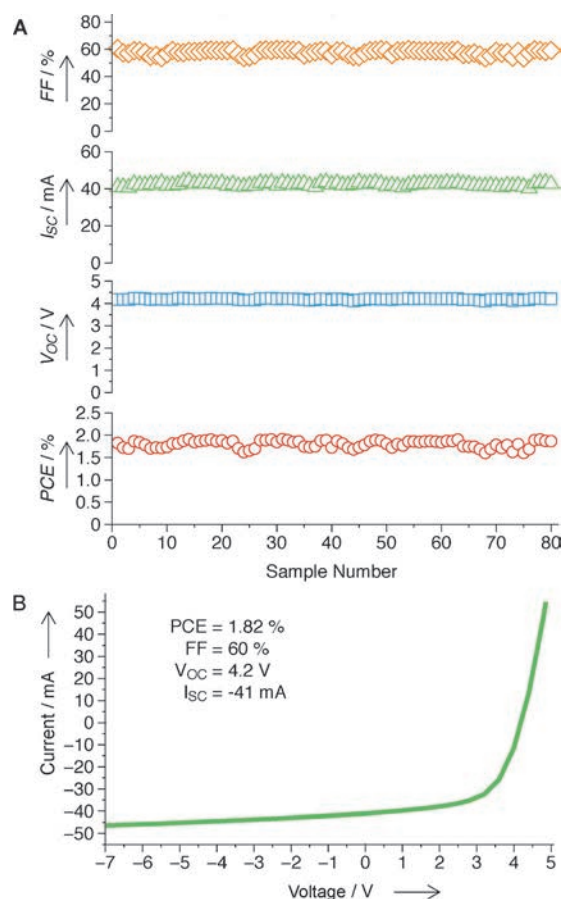
Figure 5. Distribution of the device performance for 80 modules (A) and the I-V curve of a typical module (B).

extremely long shelf life that allows for the samples to be shipped across long distances without degradation of the performance. However, due to their highly flexible nature the cells can be sensitive towards constant handling, excessive flexing, mechanical stresses, and heating, which may introduce flaws in the encapsulation and deteriorate the stability. Thus, the lifetime of such a sample is linked to its use, application, and handling during shipment. For the first experiment announced on the website, we aim to establish how the modules are affected by shipment without packaging (i.e., by sending them as a postcard). Initial results are promising and the interested reader can still participate in this study.

As mentioned above, the aim of distributing freeOPV samples is to generate a platform from which the roll-to-roll processing technology can be evaluated. Such evaluation is most efficiently performed with the technology freely available for everyone. Organic solar cell research has been conducted for more than 25 years now with the vision of mass-produced flexible roll-to-roll processed solar cells, but only a few researchers have actually had a flexible organic solar cell in their hands. It is our belief that the research progress is best evaluated by using comparisons among results with the same processing origin and this platform is intended to provide such an origin. For the same reasons the transparent ITO-free substrate Flextrode[2] is also freely available.

All freeOPV samples are equipped with a 2D barcode giving them a unique ID and full tracability. It will thus be possible to retrieve and reference all information on the processing and handling of a given cell and the platform will allow the receiver to give feedback on his/her specific cell through the website.[2] The purpose of this is to develop a methodology for processing, testing, and distributing an enormous amount of solar cells with minimal influence from a human operator while maintaining full traceability. The software we developed for this purpose can be experienced on the website. The 2D barcode can be scanned with any modern mobile device; for those without access to such a device there is also a code that can be typed in for extraction of the information. Again the purpose of the effort is to organize a fully automated platform for handling every aspect of the module along the value chain (preparation, distribution, service, and decommission).

The platform is furthermore thought of as a possible vector for testing of new materials in a roll-to-roll context. Very few research groups have access to roll-to-roll processing equipment for testing of their new materials and the platform will provide a means to do so. The module structure described here is sufficiently refined to enable development of new active materials and interface layers for this structure; pending success new results can be rapidly integrated in future freeOPV samples, again in a way that everyone can test and see for themselves. We have thus chosen an initial standard with this first freeOPV sample and a direct comparison can be performed by substituting just one or more of the components.

We have devised an efficient method to prepare small, flexible, ITO-free polymer solar-cell modules directly on barrier foil. The method is in principle generic and though we have exemplified the modules here with P3HT:PCBM as the commonly known active material, this methodology can also serve as a generic platform for the development of new and more-effective materials combinations, both with respect to performance and stability. The modules are true to the art in the sense that they are flexible, prepared using fast printing and coating methods, and of such a low cost that they can be made freely available to the public through a website. In fact the postage of the solar cell is significantly more expensive than the solar cell itself. All conceivable scientific or technical studies are encouraged and welcomed regardless of their nature.

Acknowledgements

[1] a) P. Sommer-Larsen, M. Jørgensen, R. R. Søndergaard, M. Hösel, F. C. Krebs, *Energy Technol.* **2013**, *1*, 15–19; b) D. Angmo, S. A. Gevorgyan, T. T. Larsen-Olsen, R. R. Søndergaard, M. Hösel, M. Jørgensen, R. Gupta, G. U. Kulkarni, F. C. Krebs, *Org. Electron.* **2013**, *14*, 984–994; c) M. Hösel, R. R. Søndergaard, M. Jørgensen, F. C. Krebs, *Energy Technol.* **2013**, *1*, 102–107.

[2] The Flextrode substrate and the freeOPV solar cell modules can be obtained free of charge by submitting a postal address and registering at the www.plasticphotovoltaics.org website.

[3] a) S. A. Gevorgyan, A. J. Medford, E. Bundgaard, S. B. Sapkota, H.-F. Schleiermacher, B. Zimmermann, U. Würfel, A. Chafiq, M. Lira-Cantu, T. Swonke, M. Wagner, C. J. Brabec, O. Haillant, E. Voroshazi, T. Aernouts, R. Steim, J. A. Hauch, A. Elschner, M. Pannone, M. Xiao, A. Langzettel, D. Laird, M. T. Lloyd, T. Rath, E. Maier, G. Trimmel, M. Hermenau, T. Menke, K. Leo, R. Rösch, M. Seeland, H. Hoppe, T. J. Nagle, K. B. Burke, C. J. Fell, D. Vak, T. B. Singh, S. E. Watkins, Y. Galagan, A. Manor, E. A. Katz, T. Kim, K. Kim, P. M. Sommeling, W. J. H. Verhees, S. C. Veenstra, M. Riede, M. G. Christoforo, T. Currier, V. Shrotriya, G. Schwartz, F. C. Krebs, *Sol. Energy Mater. Sol. Cells* **2011**, *95*, 1398–1416; b) F. C. Krebs, T. Tromholt, M. Jørgensen, *Nanoscale* **2010**, *2*, 873; c) F. C. Krebs, J. Fyenbo, D. M. Tanenbaum, S. A. Gevorgyan, R. Andriessen, B. van Remoortere, Y. Galagan, M. Jørgensen, *Energy Environ. Sci.* **2011**, *4*, 4116–4123.

[4] M. O. Reese, S. A. Gevorgyan, M. Jørgensen, E. Bundgaard, S. R. Kurtz, D. S. Ginley, D. C. Olson, M. T. Lloyd, P. Morvillo, E. A. Katz, A. Elschner, O. Haillant, T. R. Currier, V. Shrotriya, M. Hermenau, M. Riede, K. R. Kirov, G. Trimmel, T. Rath, O. Inganäs, F. Zhang, M. Andersson, K. Tvingstedt, M. Lira-Cantu, D. Laird, C. McGuiness, S. Gowrisanker, M. Pannone, M. Xiao, J. Hauch, R. Steim, D. M. De-Longchamp, R. Rösch, H. Hoppe, N. Espinosa, A. Urbina, G. Yaman-Uzunoglu, J. B. Bonekamp, A. J. J. M. van Breemen, C. Girotto, E. Voroshazi, F. C. Krebs, *Sol. Energy Mater. Sol. Cells* **2011**, *95*, 1253–1267.

[5] S. A. Gevorgyan, M. V. Madsen, H. F. Dam, M. Jørgensen, C. J. Fell, K. F. Anderson, B. C. Duck, A. Mescheloff, E. A. Katz, A. Elschner, R. Rösch, H. Hoppe, M. Hermenau, M. Riede, F. C. Krebs, *Sol. Energy Mater. Sol. Cells* **2013**, *116*, 187–196.

Carbon: The Ultimate Electrode Choice for Widely Distributed Polymer Solar Cells

Gisele A. dos Reis Benatto, Bérenger Roth, Morten V. Madsen, Markus Hösel, Roar R. Søndergaard, Mikkel Jørgensen, and Frederik C. Krebs*

As mass-produced, low-cost organic electronics enter our everyday lives, so does the waste from them. The challenges associated with end-of-life management must be addressed by careful design and carbon-based electrodes are central to these developments. Here, the reproducible production of vacuum-, indium tin oxide (ITO)-, and silver-free solar cells in a fully packaged form using only roll-to-roll processing is reported. Replacing silver with carbon as electrode material significantly lowers the manufacturing cost and makes the organic photovoltaic (OPV) modules environmentally safe while retaining their flexibility, active area efficiency, and stability. The substitution of silver with carbon does not affect the roll-to-roll manufacturing of the modules and allows for the same fast printing and coating. The use of carbon as electrode material is one step closer to the wide release of low-cost plastic solar cells and opens the door to new possible applications where silver recycling is not manageable.

1. Introduction

The vision of organic electronics being a very low-cost mass-produced commodity has several implications when it comes to the sustainability and environmental impact. When compared to alternative technologies, their fast and facile manufacture using little material and processes that use little energy does offer the possibility for a low environmental impact. However, some components used to manufacture polymer solar cells have been shown to impact the level of sustainability negatively unless special precautions are taken.[1–4] A process leading to a complex device such as a polymer solar cell module may be optimized with respect to the amounts of materials used, the speed of manufacture, and the energy used.[5,6] Interestingly the case for both polymer solar cells and organic electronics in general is exceptionally strong as it allows for optimization in all senses (low cost, flexibility, light weight, energy payback time for organic photovoltaics). Some of the ingredients however are mandatory in some device architectures and when such

ingredients have a negative environmental impact it becomes difficult to realize the potential of the technology unless the application grants an easy way of handling the potential environmental danger. A very good example is the use of silver metal electrodes in fully printed/coated polymer solar cells.[6] The high conductivity of silver has enabled devices that are as efficient as indium tin oxide (ITO) based semitransparent electrodes used in the past (see **Figure 1**) while fortuitously also enabling a much faster manufacture than is possible with ITO-based electrodes. In addition to imparting a high cost to the device silver also has a massive environmental impact, cannot be disposed of without special care, and cannot be distributed widely in nature without potentially doing more harm than good.[7,8] The use of silver in organic electronics is fortunately not unmanageable as was shown in a recent study where a silver-based polymer solar cell power plant could be operated and the silver efficiently recovered and recycled with several benefits (lower cost, shorter energy payback time, lower environmental impact).[8] The particular case, however, also presented the interesting boundary condition that the location of the polymer solar cells containing the silver is known at all times from manufacture, through installation to operation and decommissioning.[9] In such a case the use of silver was found to be fully justified and, in addition, making only reduced claims on the available silver resources if considered on a very large scale.[10] For consumer electronics based on very low-cost technology it is likely that the large scale implies that a huge number of discrete products will be characteristic of the application and as a consequence the distribution is likely to be vast. The environmental responsibility that the consumer feels when disposing of the product cannot be assumed to be sufficient. The environmentally responsible assumption is that the consumer will not always dispose the product correctly, which means that unwanted discharge into the environment will take place. The technology should therefore be developed in a form where environmental impact is eliminated or reduced to a level enabling full or partial recycling of the plastic materials, landfill, or incineration without harmful emission beyond CO_2.

Figure 1 shows the freeOPV platform that was conceived as a generic OPV module enabling development of processes, processing, testing of new materials and also importantly the

G. A. dos Reis Benatto, B. Roth, Dr. M. V. Madsen,
Dr. M. Hösel, Dr. R. R. Søndergaard,
Dr. M. Jørgensen, Prof. F. C. Krebs
Department of Energy Conversion and Storage
Technical University of Denmark
Frederiksborgvej 399, DK-4000 Roskilde, Denmark
E-mail: frkr@dtu.dk

RESEARCH NEWS
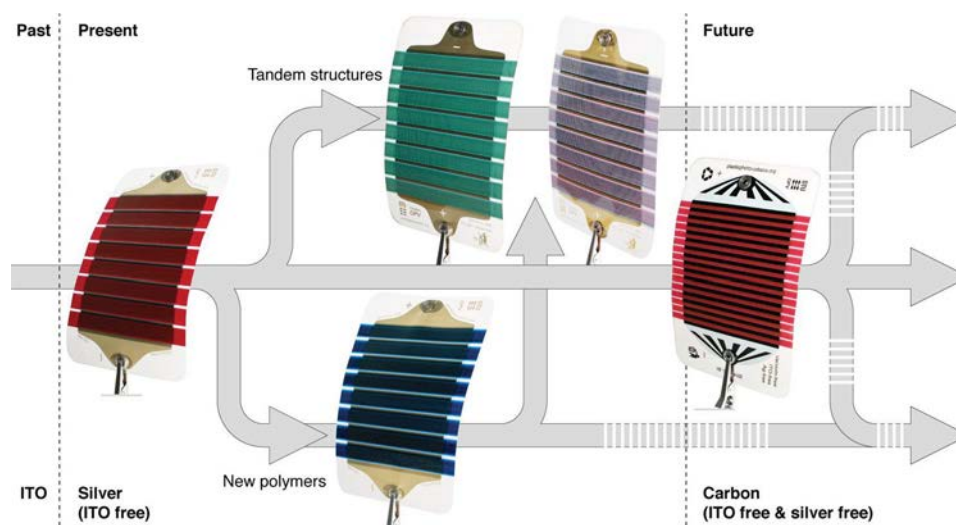
Figure 1. An illustration of the evolution of the freeOPV platform from its initial form based on slanted silver grids and poly(3-hexylthiophene):phenyl-C_{61}-butyric acid methyl ester (P3HT:PCBM) as the active materials to encompass novel polymer active materials and present complex multilayer architectures such as the tandem freeOPV. This work demonstrates printed carbon electrodes for consumer electronics with low environmental impact.

free distribution of OPVs to anybody with an interest.[11–13] The largest success of freeOPV has been its free distribution to school children and the majority of the distribution has been for teaching purposes especially in the recent context of the massive open online courses (MOOCs) where the freeOPV was used as part of the course material.[14] The massive demand on the freeOPV in its original silver-based form, tandem form and carbon-based form is shown in **Figure 2**. The demography of freeOPV is of some interest as it shows how a possible future organic electronics product is likely to distribute in the world and it is first of all clear that it presents a more or less global distribution to all continents and thus certainly demands management of its end-of-life through product design. Our motivation was thus to create a new version of freeOPV that can be disposed as regular plastic waste while at the same time maintaining the performance and functionality as a teaching tool and this is what we show in this report.

2. Results and Discussion

The silver-based freeOPV employs state-of-the-art printed grid electrode structures comprising a ±5° slant to minimize comb line cross-overs that often lead to a shunt.[6] The silver grid lines enable a low sheet resistivity of the silver poly(3,4-ethylenedioxythiophene):polystyrene sulfonate (PEDOT:PSS) composite electrode and enable cell dimensions in the direction of charge transport of 9–15 mm with current densities in the range of 6–12 mA cm^{-2}. In the case of a silver-free version relying on PEDOT:PSS alone the cell dimension is diminished somewhat and the optical transparency compromised.[7] Earlier demonstrations showed that cell dimensions of 1–2 mm were possible without loss using PEDOT:PSS[15] alone and these were also used in the case of the OE-A demonstrator in 2011[16] where carbon was also reported as a printed electrode.[7,17] However the packaging and operational stability proved to be
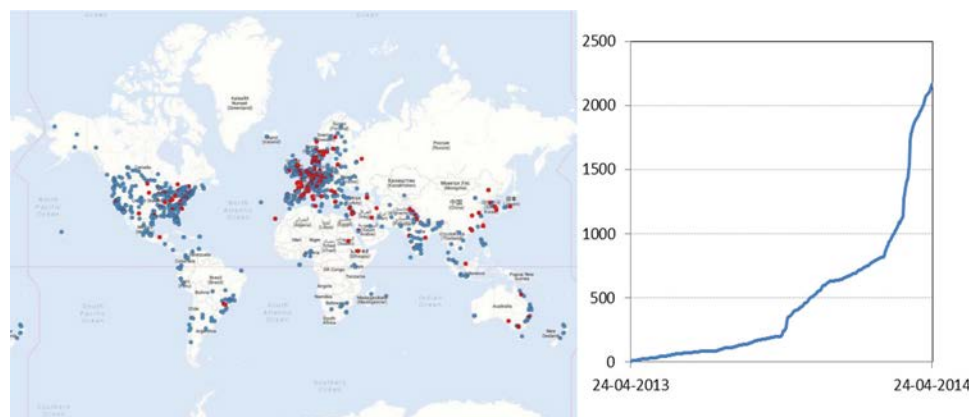
Figure 2. The world map showing the demography of single junction and tandem freeOPV modules with silver (red dots) and carbon (blue dots) based freeOPV (left). The graph shows the number of freeOPV shipped during the first year of the freeOPV initiative (right).
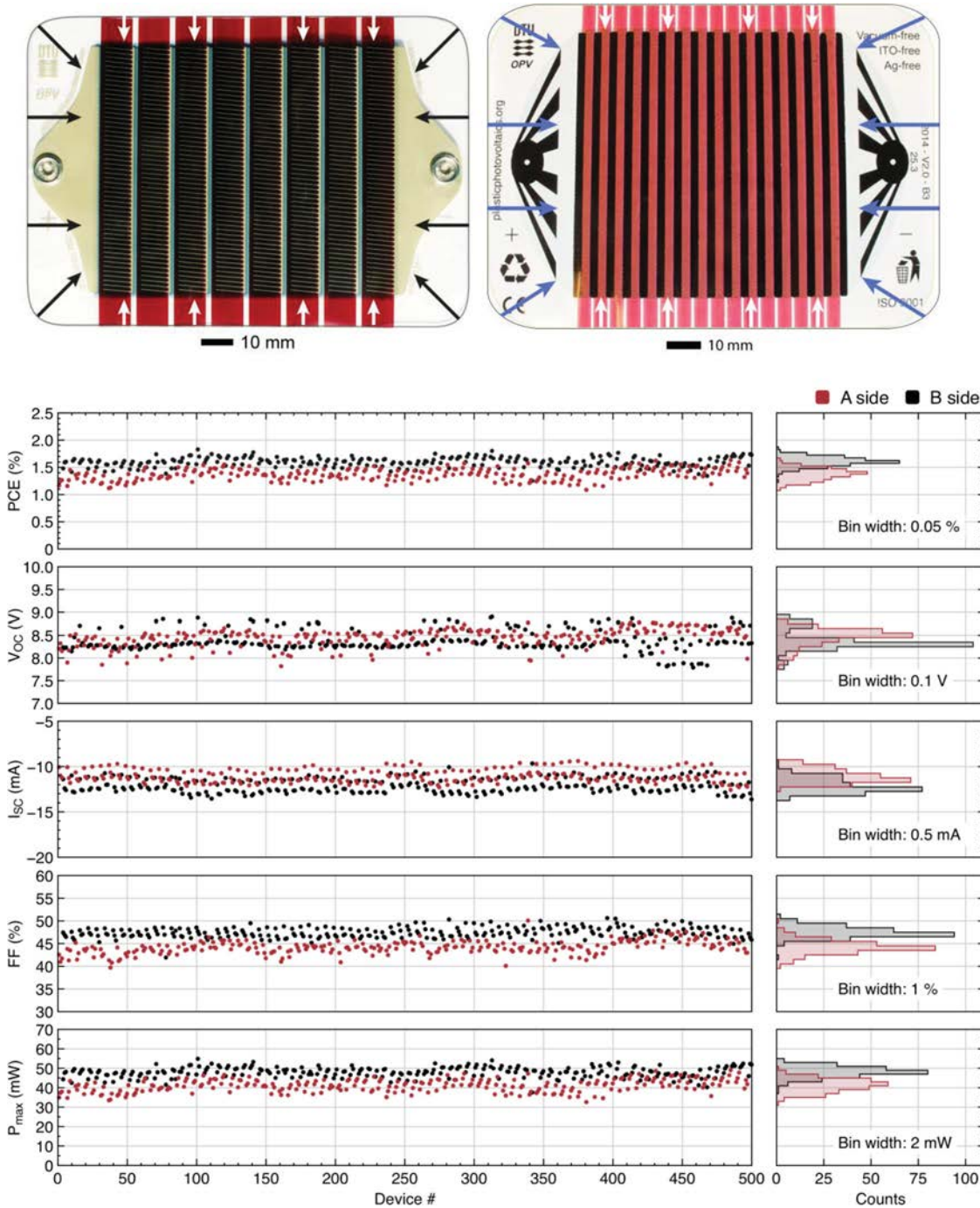
Figure 3. Top: Comparison of the diffusion path into the silver and carbon based freeOPV. The arrows show the diffusion pathways from the edges to the solar cell. Bottom: The reproducibility of 500 modules (250 A-side, 250 B-side) is shown with respect to the photovoltaic parameters and is also presented in a histogram (right) to highlight the distinct differences between the two sides of the web but also the relatively narrow distribution of performance.

challenging. In order to make an efficient edge seal and extract the current out of the cell based on a thin PEDOT:PSS layer alone, a new approach was sought. In the silver based freeOPV a thin (<250 nm) flexo-printed silver electrode is employed that enables a good edge seal.[12] Printed carbon does not enable this, as it provides a diffusion path into the device especially for oxygen. We thus employ a thin PEDOT:PSS layer as the bus-bar

and use this as the edge seal as seen in **Figure 3**. The printed carbon extraction lines do not extend all the way to the device area and enable similar performance to freeOPV with highly reproducible performance as shown for 500 modules (Figure 3) comprised in 83 printed motifs. The web width employed in the experiments was 305 mm and two modules were processed simultaneously (referred to as the A-side and the B-side). There
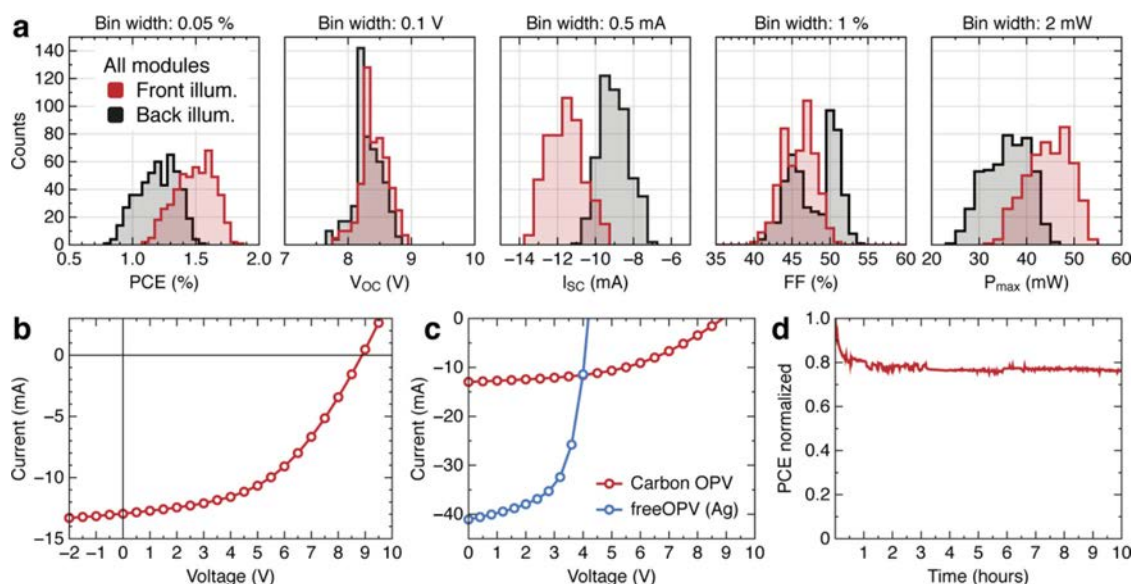
Figure 4. a) Front-versus-back illumination of 500 modules shown as histograms with the bin width quoted on top of each graph. b) A typical IV-curve of the carbon OPV module is shown along with a comparison of the original Ag-based freeOPV (c). d) Lifetime curve recorded under ISOS-L-2 conditions.[13]

are differences between the two sides in addition to experimental variation due to experiments with slightly different gap widths (evident as a clear repeating pattern for every three modules). We employed the same wet thickness for both the front and back PEDOT:PSS implying that the optical path from the front and back was similar and thus enabled bi-facial operation as shown in **Figure 4** and **Table 1**. The back PEDOT:PSS ink has a slightly higher solid content reducing the transparency somewhat leading to a slightly lower current and consequently a higher fill factor as expected. The general performance over the active area was very similar to freeOPV based on silver electrodes, but a sacrifice was of course made in the module power which for carbon based freeOPV was around 50 mW whereas the module power for silver based freeOPV typically is 100 mW. This is due to the poorer geometric fill factor which is a consequence of the larger number of cells (16 versus 8). In terms of sustainability and cost, the carbon-based free OPV is superior to silver-based freeOPV and the performance in terms of power

conversion efficiency on the active area and the operational stability is similar, as shown in Figure 4, with the only difference being that carbon-based OPV does not support exposure to liquid water near to the contacts.

3. Conclusions

We have accomplished the reproducible production of vacuum-, ITO-, and silver-free solar cells in a fully packaged form using only roll-to-roll processing. We showed that the replacement of silver with carbon as the electrode material significantly lowers the manufacturing cost and makes the OPV modules environmentally safe while retaining the flexibility, the active area efficiency, and the stability (except liquid water near contacts). Additionally, the substitution of silver with carbon does not affect the roll-to-roll manufacturing of the modules and allows for the same fast printing and coating. The use of carbon as the

Table 1. The photovoltaic parameters for 500 modules including the maximum values. Results from front and back side illumination and from the two different sides of the web are also quoted.

	PCE[a] [%] front	PCE [%] back	V_{OC}[b] [V] front	V_{OC} [V] back	I_{SC}[c] [mA] front	I_{SC} [mA] back	FF[d] [%] front	FF [%] back	P_{max}[e] [mW] front	P_{max} [mW] back
Average	1.49	1.20	8.41	8.31	11.57	9.01	45.86	47.85	44.67	35.90
Standard deviation	0.15	0.15	0.21	0.22	0.92	0.78	2.11	3.11	4.55	4.55
Maximum	1.83	1.54	8.91	8.80	13.6	10.81	50.67	53.74	54.96	46.19
	PCE [%] A side	PCE [%] B side	V_{OC} [V] A side	V_{OC} [V] B side	I_{SC} [mA] A side	I_{SC} [mA] B side	FF [%] A side	FF [%] B side	P_{max} [mW] A side	P_{max} [mW] B side
Average	1.37	1.60	8.45	8.37	11.02	12.11	44.22	47.51	41.20	48.14
Standard deviation	0.11	0.09	0.20	0.22	0.71	0.76	1.47	1.15	3.22	2.64
Maximum	1.64	1.83	8.78	8.91	12.55	13.6	50.13	50.67	49.15	54.96

[a] Power conversion efficiency; [b] open-circuit voltage; [c] short-circuit current; [d] fill factor; [e] maximum power.

electrode material is one step closer to the wide release of low-cost plastic solar cells and opens the door to new possible applications where silver recycling is not manageable. The freeOPV modules with carbon are about one third cheaper than the previous generation that contained silver and can be disposed of in the normal household waste for incineration or in the bin for plastic recycling, thus supporting further the philosophy of sustainable organic electronics. We encourage and welcome any inquiries, scientific or technical studies independent of their nature.[13]

Experimental Section

Materials and Inks: The front PEDOT:PSS was composed of PH1000 from Heraeus diluted with isopropanol (10:3 w/w) and the back PEDOT:PSS was composed of Agfa EL-P-5010 diluted with isopropanol (10:2 w/w). The ZnO ink was composed of nanoparticles dispersed in acetone with a concentration of 56 mg mL^{-1}. The active layer was composed of P3HT (Sepiolid P-200 from BASF) and [60]PCBM (from Merck). Both materials were dissolved at a concentration of 30 mg mL^{-1} in chlorobenzene. The carbon ink was Electrodag PF-407C (from Acheson) that was used as received. The adhesive used for encapsulation was VE110484 from DELO that was used as received. The flexible foil was a 42 micrometer thick barrier material from Amcor with a WVTR of 0.04 g m^{-2} day^{-1} and an OTR of 0.01 cm^3 m^{-2} day^{-1} that was used as both superstrate and back laminate during packaging.

Roll-to-Roll Processing: Four different roll-to-roll (R2R) processing machines were used. The solar cell stack was processed on an inline printing/coating machine with a web width of 305 mm, composed of an unwinder, edge guide, corona treater, flexo printer, slot-die coating unit #1, hot air oven #1 (2 m length), rotary screen printer active, slot-die unit #2, 3 × 1.5 kW IR driers, hot air oven #2 (2 m length), ink jet printer (for barcodes), barcode readers and rewinder. The first PEDOT:PSS layer (Heraeus) was rotary screen printed with a nominal wet thickness of 20 μm, a web speed of 10 m min^{-1}, infrared drying and a hot air oven temperature of 140 °C. A unique barcode was inkjet printed on each motif for later registration and indexing during this first printing step. The ZnO layer was slot die coated at 10 m min^{-1} a nominal wet thickness of 7 μm and dried using both ovens (90 °C and 140 °C). The active layer was coated at 2 m min^{-1} (to ensure thermal annealing of P3HT:PCBM) with a nominal wet thickness of 12 μm having both ovens at 140 °C. The back PEDOT:PSS layer (Agfa) was rotary screen printed at a speed of 4 m min^{-1} with a nominal wet thickness of 20 μm, infrared drying and the hot air oven set to 140 °C. The back carbon electrode was rotary screen printed in two steps. Firstly the text pattern and the extraction lines were printed with a nominal wet thickness of 10 μm at 10 m min^{-1}, IR drying and the hot air oven set to 140 °C. In a secondary printing step the interconnections between the cells were rotary screen printed with a nominal wet thickness of 40 μm at a web speed of 4 m min^{-1} using the same drying conditions. The devices were R2R tested before lamination that was carried out using a R2R UV-laminator operated at 2 m min^{-1} using hard UV lamp power of 2 kW (power rating) and a 350 W (optical output) light-emitting diode (LED) curing lamp. The adhesive was applied to the back barrier foil and the barrier foil carrying the printed solar cell stack was used as the laminate. The roll of fully laminated solar cells was then laser-cut into modules using a R2R laser cutter comprising unwinder, 90 W CO$_2$ laser cutter and rewinder, and the devices finally contacted using snap-button contacts.

Testing: R2R testing was carried out using a system composed of an unwinder, edge guide, bar code reader, test head and rewinder. Keithley 2400 SMUs were used for all current–voltage characterization. Solar simulation was carried out on a number of solar simulators. Results quoted are from a Steuernagel KHS1200 calibrated to 1000 W m^{-2}. ISOS-L-2[18] measurements were carried out at 85 °C. The active area was accurately measured for one module using ultrafast LBIC[19] whereas

the active areas in tables are nominal areas based on the nominal printing/coating overlaps defined by the pattern. Each printed motif has a total of six modules and each side (A and B side) has three slightly different device pattern with small variation in the gap between the cells to test. The periodic variation is clearly seen in Figure 3 where the B side presents the least spread in data. The active area of the device presenting the highest PCE in Table 1 was carefully determined using LBIC and the corresponding PCE corrected for the area was 1.85% as opposed to 1.83% based on the nominally printed area. The values quoted in Table 1 are based on the nominally printed active area and should therefore be viewed as quite accurate even though the exact active area was not established for every module.

[1] C. J. M. Emmott, A. Urbina, J. Nelson, *Sol. Energy Mater. Sol. Cells* **2012**, *97*, 14.

[2] B. Azzopardi, C. J. M. Emmott, A. Urbina, F. C. Krebs, J. Mutale, J. Nelson, *Energy Environ. Sci.* **2011**, *4*, 3741.

[3] N. Espinosa, R. García-Valverde, A. Urbina, F. C. Krebs, *Sol. Energy Mater. Sol. Cells* **2011**, *95*, 1293.

[4] N. Espinosa, F. C. Krebs, *Sol. Energy Mater. Sol. Cells* **2014**, *120*, 692.

[5] P. Sommer-Larsen, M. Jørgensen, R. R. Søndergaard, M. Hösel, F. C. Krebs, *Energy Technol.* **2013**, *1*, 15.

[6] F. C. Krebs, N. Espinosa, M. Hösel, R. R. Søndergaard, M. Jørgensen, *Adv. Mater.* **2014**, *26*, 29.

[7] N. Espinosa, F. O. Lenzmann, S. Ryley, D. Angmo, M. Hösel, R. R. Søndergaard, D. Huss, S. Dafinger, S. Gritsch, J. M. Kroon, M. Jørgensen, F. C. Krebs, *J. Mater. Chem. A* **2013**, *1*, 7037.

[8] R. R. Søndergaard, N. Espinosa, M. Jørgensen, F. C. Krebs, *Energy Environ. Sci.* **2014**, *7*, 1006.

[9] N. Espinosa, M. Hösel, M. Jørgensen, F. C. Krebs, *Energy Environ. Sci.* **2014**, *7*, 855.

[10] L. Grandell, A. Thorenz, *Renew. Energy* **2014**, *69*, 157.

[11] T. R. Andersen, H. F. Dam, M. Hösel, M. Helgesen, J. E. Carlé, T. T. Larsen-Olsen, S. A. Gevorgyan, J. W. Andreasen, J. Adams, N. Li, F. Machui, G. D Spyropoulos, T. Ameri, N. Lemaître, M. Legros, A. Scheel, D. Gaiser, K. Kreul, S. Berny, O. R. Lozman, S. Nordman, M. Välimäki, M. Vilkman, R. R. Søndergaard, M. Jørgensen, C. J. Brabec, F. C. Krebs, *Energy Environ. Sci.* **2014**, 10.1039/c4ee01223b.

[12] F. C. Krebs, M. Hösel, M. Corazza, B. Roth, M. V. Madsen, S. A. Gevorgyan, R. R. Søndergaard, D. Karg, M. Jørgensen, *Energy Technol.* **2013**, *1*, 378.

[13] FreeOPV samples can be obtained free of charge by submitting a postal address and registering at the www.plasticphotovoltaics.org website (accessed April 2014).

[14] The course is available for free enrolment on the Coursera website. https://www.coursera.org/course/opv (accessed April 2014).

[15] Y. Galagan, B. Zimmermann, E. W. C. Coenen, M. Jørgensen, D. M. Tanenbaum, F. C. Krebs, H. Gorter, S. Sabik, L. H. Slooff, S. C. Veenstra, J. M. Kroon, R. Andriessen, *Adv. Energy Mater.* **2012**, *2*, 103.

[16] F. C. Krebs, J. Fyenbo, D. M. Tanenbaum, S. A. Gevorgyan, R. Andriessen, B. van Remoortere, Y. Galagan, M. Jørgensen, *Energy Environ. Sci.* **2011**, *4*, 4116.

[17] T. T. Larsen-Olsen, R. R. Søndergaard, K. Norrman, M. Jørgensen, F. C. Krebs, *Energy Environ. Sci.* **2012**, *5*, 9467.

[18] M. O. Reese, S. A. Gevorgyan, M. Jørgensen, E. Bundgaard, S. R. Kurtz, D. S. Ginley, D. C. Olson, M. T. Lloyd, P. Morvillo, E. A. Katz, A. Elschner, O. Haillant, T. R. Currier, V. Shrotriya, M. Hermenau, M. Riede, K. R. Kirov, G. Trimmel, T. Rath, O. Inganäs, F. Zhang, M. Andersson, K. Tvingstedt, M. Lira-Cantu, D. Laird, C. McGuiness, S. Gowrisanker, M. Pannone, M. Xiao, J. Hauch, R. Steim, D. M. DeLongchamp, R. Rösch, H. Hoppe, N. Espinosa, A. Urbina, G. Yaman-Uzunoglu, J.-B. Bonekamp, A. J. J. M. van Breemen, C. Girotto, E. Voroshazi, F. C. Krebs, *Sol. Energy Mater. Sol. Cells* **2011**, *95*, 1253.

[19] F. C. Krebs, M. Jørgensen, *Adv. Opt. Mater.* **2014**, *2*, 765.

www.MaterialsViews.com

ADVANCED
ENERGY
MATERIALS
www.advenergymat.de

FULL PAPER

Matrix Organization and Merit Factor Evaluation as a Method to Address the Challenge of Finding a Polymer Material for Roll Coated Polymer Solar Cells

Eva Bundgaard,* Francesco Livi, Ole Hagemann, Jon E. Carlé, Martin Helgesen, Ilona M. Heckler, Natalia K. Zawacka, Dechan Angmo, Thue T. Larsen-Olsen, Gisele A. dos Reis Benatto, Bérenger Roth, Morten V. Madsen, Mats R. Andersson, Mikkel Jørgensen, Roar R. Søndergaard, and Frederik C. Krebs

The results presented demonstrate how the screening of 104 light-absorbing low band gap polymers for suitability in roll coated polymer solar cells can be accomplished through rational synthesis according to a matrix where 8 donor and 13 acceptor units are organized in rows and columns. Synthesis of all the polymers corresponding to all combinations of donor and acceptor units is followed by characterization of all the materials with respect to molecular weight, electrochemical energy levels, band gaps, photochemical stability, carrier mobility, and photovoltaic parameters. The photovoltaic evaluation is carried out with specific reference to scalable manufacture, which includes large area (1 cm^2), stable inverted device architecture, an indium-tin-oxide-free fully printed flexible front electrode with ZnO/PEDOT:PSS (poly(3,4-ethylenedioxythiophene):polystyrene sulfonate), and a printed silver comb back electrode structure. The matrix organization enables fast identification of active layer materials according to a weighted merit factor that includes more than simply the power conversion efficiency and is used as a method to identify the lead candidates. Based on several characteristics included in the merit factor, it is found that 13 out of the 104 synthesized polymers outperformed poly(3-hexylthiophene) under the chosen processing conditions and thus can be suitable for further development.

1. Introduction

Polymer solar cells (PSCs) are seen as an important solution to the estimated increase in global energy consumption of 1 GW per day due to the low energy payback time (EPBT), the potentially high energy return factor (ERF), the small or nonexisting ecotoxicity, and the fully scalable high speed manufacture. This is mainly ascribed to the reduced amount of energy used during production and the avoidance of scarce materials, which has already resulted in an EPBT of 90 days for system-integrated PSCs[1] with the potential of reaching an EPBT of only 1 day.[2] The potentially high ERF can be achieved through increased device lifetime, higher device efficiency, and lower energy production cost.

Research into PSCs has increased exponentially over the last decade, with more than 46 500 published papers.[3] This increase is partly attributable to the fact that the polymer composition in the active layer has varied due to the use of a large number of different types of conjugated polymers. The most common factor for comparison in the PSC research field is the power conversion efficiency (PCE). In the past decade, the main focus has been on increasing the PCE, and lately efficiencies of over 10% have been reported for small area devices (mm^2 scale).[4] Much of the increase in PSC efficiency arises from an optimization of the light-absorbing conjugated polymer applied in the active layer of the device. Low band gap polymers have been developed to absorb light at wavelengths longer than 650 nm and thus have a band gap below 2 eV.[5] This is done by a very common approach where two monomers, one electron donating and one electron accepting unit, are coupled to produce a low band gap polymer with a charge transfer band at longer wavelengths (lower energy) together with π–π transitions in order to cover a larger part of the solar spectrum. In theory this will give a higher photocurrent compared to, e.g.,

Dr. E. Bundgaard, F. Livi, O. Hagemann, Dr. J. E. Carlé,
Dr. M. Helgesen, I. M. Heckler, N. K. Zawacka,
Dr. D. Angmo, Dr. T. T. Larsen-Olsen,
G. A. dos Reis Benatto, B. Roth, Dr. M. V. Madsen,
Dr. M. Jørgensen, Dr. R. R. Søndergaard, Prof. F. C. Krebs
Department of Energy Conversion and Storage
Technical University of Denmark
Frederiksborgvej 399, 4000 Roskilde, Denmark
E-mail: evbu@dtu.dk
Prof. M. R. Andersson
Ian Wark Research Institute
University of South Australia
Mawson Lakes, South Australia 5059, Australia
Prof. M. R. Andersson
Department of Chemical and Biological Engineering/Polymer
Technology
Chalmers University of Technology
41296 Göteborg, Sweden

poly(3-hexylthiophene) (P3HT), which has a band gap of 2 eV, due to an absorption profile that is better matched with the solar spectrum. Thus, a potentially higher PCE of the PSC can be reached, given that the energy level alignment with the acceptor in the active layer is optimal.[5] For large-area PSC modules, the reported PCE values are significantly lower (2%–3%)[4] and studies by Jørgensen et al.[6] clearly demonstrate this. Thus, the 10% efficiency can be viewed as somewhat misleading for several reasons. First of all, interlaboratory measures of efficiency are not necessarily comparable, which has led to a practice of sending the hero devices to be certified at certain trusted laboratories. The same principle has been applied in so-called round robin studies,[7,8] where the same devices were tested at several laboratories with considerable variation as a result. Another important issue is that an overwhelming majority (95%) of the devices is made with glass substrates, often using indium-tin-oxide (ITO) as the transparent electrode and with a diminutive active area. Any real-world application would probably use flexible plastic substrates, no scarce materials (e.g., indium), roll-to-roll (R2R) fabrication, and considerably larger devices as convincingly demonstrated in the first polymer solar park.[1] However, less interest has been devoted to these types of devices, even though all indications show that the PCEs obtained in the former laboratory-scale devices cannot be transferred to larger R2R-fabricated devices.[9] The transfer of any successful PSC from small scale to large scale in a R2R setting requires ambient atmosphere, flexible substrates, freedom from indium and vacuum and, to complicate matters even further, potentially opens up for a myriad of film forming techniques and inks. Such a transfer, however, has been simplified by the development of the mini roll coater, which applies processing conditions similar to large-scale R2R, but in smaller scale (100×1 cm^2).[9] It is essential to note the vast number of choices which can influence the performance of a PSC based on a given active material, and to realize the impossibility of testing all factors for all active polymer materials. Instead, focus should be on settings that are realistic in the context of production and end application. For all the above reasons, the countless scientific studies obtained thus far will only offer a partial answer to the question of whether a given conjugated polymer is suitable for R2R-processed PSCs.

Our main interests lie in developing PSCs to the level of larger-scale fabrication, and we therefore needed a more rational approach. This was in part inspired by how pharmaceutical companies use screening studies to find lead compounds that can later be optimized both with respect to detailed structure and application. They start by building a large library of compounds, which is tested using fairly simple procedures. This gives insights into which chemical structures perform best and should be further elaborated. Even though several thousand different polymer materials have been applied as light-absorbing polymer material in the active layer, to our knowledge such a systematic screening has only been carried out in one instance in the field of PSC using ink jet printing. However, this screening was restricted to two different polymers and two different fullerenes.[10] Moreover, while many polymer materials have been compared in reviews,[11–13] one must keep in mind that laboratories using different methods (spin speed,

light source) will generate different PCE measurements of the same polymer as demonstrated in round robin studies.[7,8] This makes a review based on a comparison of different polymers measured at different laboratories less reliable. In the present study we have utilized a screening strategy comprising the selection of 8 donor and 13 acceptor monomers which give a total of 104 polymers after the combinatorial pairing. This constituted the library that formed the basis for the screening of the photovoltaic properties of roll-coated PSCs and other properties. Our work demonstrates the challenges associated with the design of polymer materials for scaled PSCs, which include a multitude of materials and processing parameters and progress significantly beyond simple criteria such as evaluation according to PCE alone. We conclude on the effort needed for identification of new lead candidates[14,15] and estimate that only a few percent of all newly reported polymers qualify for further development. We expect that only a small fraction of these will qualify for scaled manufacture of PSCs.

2. Results and Discussion

Table 1 offers a comprehensive overview of all the data collected for the 104 possible polymers based on 13 acceptor monomers (left column) and 8 donor monomers (top row). Each cell in the table represents a unique polymer and contains 8 entries: optical band gap (eV), highest occupied molecular orbital/lowest unoccupied molecular orbital (HOMO/LUMO) energies, hole mobility, average PCE and standard deviation together with the highest open circuit voltage (V_{OC}) obtained, PCE values from the literature, photochemical stability, and finally the number of synthetic steps.

2.1. Data Handling

Computer programs and databases were developed in order to handle the enormous amount of data which was produced upon characterization of the 104 polymer materials. For each polymer, 12 different PSC types were prepared (based on 2 different solvents in 2 different polymer/[60]PCBM (phenyl-C$_{61}$-butyric acid-methyl-ester) ratios coated with 3 different thicknesses). About 50 devices were made for each of these 12 combinations, for which at least 5 of the samples were measured to give the average PCE. This adds up to some 5340 $I–V$ curves measured in total. Each experiment had its own folder and the IV measurement program was set to save the data in the corresponding folder based on the solvent/ratio/thickness combination. On our internal webpage we added a data analysis program, which gave an overview of the data collected during the characterizations. This allowed us to keep track of the progress and gave a clear overview of which polymers performed best. The following measured data were also saved in the database: UV–vis (2 absorption curves for each polymer in solution and as film), square wave voltammetry (SWV; 4 curves for each polymer, i.e., 2 forward and 2 reverse), hole mobility (2 $I–V$ curves in the dark for 2 different active layer thickness), absorption curves used to determine photochemical stability (12 absorption curves are measured per hour, the total number

Table 1. Combination sheet for donors and acceptors in the screening. The dotted lines on the monomer unit indicate where the units are coupled together by a C–C bond. The values listed are: 1) The optical band gap in eV estimated from the absorption spectrum. 2) The value of the highest occupied molecular orbital (HOMO) measured by square wave voltammetry (SWV) and the lowest unoccupied molecular orbital (LUMO) estimated from the electrochemical HOMO and the optical band gap, both in eV. 3) Size exclusion chromatography (SEC) traces, which were calculated on the basis of polystyrene standards. The average number molecular weight, M_n (g mol^{-1}) and polydispersity (PD) are indicated. 4) The hole mobility measured on a pure polymer film (ITO/PEDOT:PSS/polymer/Al). For P3HT the hole mobility was found to be 1.26E-07 m^2 V^{-1} s (270 nm) and 8.02E-8 m^2 V^{-1} s (300 nm). The reported values are for an annealed film. An (x) indicates a value for a sample which has not been annealed. 5) The average and standard deviation (calculated from the 10 best performing devices) PCE from the PSC devices prepared by roll coating together with the V_{OC}. The value in () is the highest measured PCE. 6) Values of the reported PCE are listed for reference. Unless stated differently, here the devices were prepared by spin coating on a glass/ITO substrate, using thermal evaporation under vacuum for the back electrode with a normal device geometry and PC$_{60}$BM as acceptor. 7) The photochemical stability measured on the pure polymers. It is listed in the table as [% h^{-1}] ± standard deviation (absorption maximum). Notice that since the degradation rate is in % h^{-1}, lower values indicate more stable polymers. The degradation rate is 4% h^{-1} for P3HT and 1% h^{-1} for P3HT/[60]PCBM. 8) The number of synthetic steps for the polymer, indicated by #, starting from simple cheap and commercially available molecules, such as 3-bromothiophene or benzothiadiazole. For experimental details and all measured data, please use the links provided in the Supporting Information.

Continued

	D1	D2	D3	D5 R=C$_{12}$H$_{25}$	D6	D7	D8 R=C$_{12}$H$_{25}$	D9
1. E_g [eV]	1. 1.47	1. 1.35	NA	1. 1.79	NA	1. 1.73	1. 1.89	1. 1.69
2. HOMO/LUMO level [eV]	2. −5.00/−3.53	2. −5.06/−3.71		2. −5.50/−3.71		2. −5.07/−3.332	2. −5.39/−3.50	2. −5.43/−3.71
3. M_n [g mol^{-1}], PD	3. 96 000; 9.9	3. 2 370 000; 4.4		3. 9300; 2.2		3. 13 000; 2.1	3. 4700; 1.7	3. 6900; 1.4
4. Hole mobility [cm2 V^{-1} s]	4. 3.96E-07	4. 8.35E-09		4. 2.92E-08		4. 6.62E-07	4. NA	4. 1.93E-08
5. PCE% average ± std (highest); V_{oc} [V]	5. 1.30 ± 0.04 (1.37); 0.57	5. 0.37 ± 0.04 (0.45); 0.71		5. 5.02 ± 0 (0.02); 0.79		5. 2.0 ± 0.1 (2.21); 0.76	5. NA	5. 5.03 ± 0.07 (0.06); 0.57
6. PCE [in %] reported in literature [reference]	6. 5.6 (PC$_{70}$BM)[16,17]	6. 2.54 (D2 has 2 thiophenes)[18]	6. 1.71 (HD on D3)[19,20]	6. No PCE[21]	6. No reference	6. 2.2[22–24]	6. 1.23[21,25]	6. No reference
7. Photochemical stability [% h^{-1}]	7. 1.11 ± 0.10 (0.31)	7. 0.25 ± 0.03 (0.36)		7. 2.46 ± 0.15 (0.62)		7. 1.48 ± 0.16 (0.44)	7. 30.88 ± 2.61 (0.25)	7. 7.22 ± 0.3 (0.26)
8. #synthetic steps	8. #11	8. #9	8. #9	8. #5	8. #11	8. #6	8. #8	8. #8

A1

ADVANCED
ENERGY
MATERIALS
www.advenergymat.de

Materials Views
www.MaterialsViews.com

FULL PAPER

Table 1. Continued

A2

A3

Compound	1	2	3	4	5	6	7	8
A2 R=C$_{12}$H$_{25}$; D1 R=hexyl	1.52	−5.03/−3.51	9500; 2.0	4.28E-08	0.44 ± 0.03 (0.48); 0.54	2.95 (A2 R=H, PC71BM)	16.9 ± 0.5 (0.15)	#17
A2 R=C$_{12}$H$_{25}$	1.70	NA	50 000; 10.8	NA	0.21 ± 0.05 (0.32); 0.68	1.99[27]	12.0 ± 1.1 (0.13)	#14
A2 R=C$_{12}$H$_{25}$ (Gel)	1.70	−5.10/−3.49	2 300 000; 6.7			4.76[37]	0.54 ± 0.04 (0.24)	#15 / #12
A2 R=C$_{12}$H$_{25}$	1.61	−4.95/−3.30	12 400; 11.4	3.98E-08	1.02 ± 0.14 (1.3); 0.63			
A2 R=C$_{12}$H$_{25}$	1.69	−5.06/−3.37	90 000; 4.5	4.9.75E-10	0.5 ± 0.06 (0.61); 0.62	4.02 (PC71BM)[38]	1.17 ± 0.09 (0.26)	#12
A2 R=C$_{12}$H$_{25}$; D5 R=H	1.58	−4.92/−3.34	3 540 000; 4.2	9.87E-09	5.07 ± 0 (0.08); 0.50		0.45 ± 0.05 (0.44)	#8
D5 R=H	1.67	−4.98/−3.31	7300; 1.9	NA	0.49 ± 0.06 (0.59); 0.58	1.78[39]	NA	#11
A2 R=H	1.88	−5.51/−3.63	1860; 2.9	3.81E-09	NA	5.4 (A3 OC$_8$H$_{17}$, D6 N-C$_8$H$_{17}$, PC$_{71}$BM)[40,41]	8.51 ± 0.95 (0.27)	#14
A2 R=H	1.99	−5.41/−3.42	3800; 3.1	2.11E-07	0.19 ± 0.16 (0.21); 0.69		5.52 ± 0.34 (0.38)	#17
A2 R=C$_{12}$H$_{25}$	1.83	−5.15/−3.32	16 000; 3.5	1.99E-07	0.55 ± 0.07 (0.69); 0.68	No reference	1.55 ± 0.04 (0.64)	#15
A2 R=C$_{12}$H$_{25}$	1.65	−5.07/−3.42	7500; 3.2	1.48E-07	1.24 ± 0.1 (1.38); 0.65	No reference	0.83 ± 0.07 (0.60)	#9
A2 R=C$_{12}$H$_{25}$	1.83	−4.98/−3.15	3 24 000; 2.7	4.52E-07	0.35 ± 0.04 (0.43); 0.69	No reference	2.23 ± 0.02 (0.69)	#12
A2 and D8 R=C$_{12}$H$_{25}$	2.05	−5.17/−3.12	3 8600; 1.5	2.16E-08	NA		20.22 ± 3.05 (0.52)	#11
D8 R=C$_{12}$H$_{25}$	1.74	−4.92/−3.18	3 2200; 3.1	2.11E-07	0.22 ± 0.05 (0.32); 0.64	No reference	7.35 ± 0.59 (0.35)	#14
A2 R=C$_{12}$H$_{25}$	1.84	−5.30/−3.46	3 19 000; 2.1	5.58E-07	0.23 ± 0.04 (0.31); 0.71	No reference	5.08 ± 0.12 (0.49)	#14
A2 R=C$_{12}$H$_{25}$	1.64	−5.24/−3.62	9400; 1.8	4.1E-08	NA		5.67 ± 0.29 (0.21)	#11

Continued

Table 1. Continued

A4

	Col 1	Col 2	Col 3	D5 R=H	NA		D8 R=C$_{12}$H$_{25}$	
1.	1.70	1.66	1.82	1.73	NA	1.89	NA	1.96
2.	−5.16/−3.46	−5.25/−3.59	−5.19/−3.39	−5.28/−3.55		−5.24/−3.35		−5.50/−3.54
3.	15 000; 2.1	22 000; 9.1	8000; 6.1	29 000; 9.2		6400; 2.1		7000; 1.5
4.	2.07E-08	Unstable	Unstable	4.58E-10		1.66E-07		NA
5.	0.05 ± 0.01 (0.07); 0.66	0.17 ± 0.01 (0.2); 0.80	5.03 ± 3.34 (0.03); 0.59	0.49 ± 0.07 (0.68); 0.94		NA		NA
6.	No PCE[42]	No reference	No reference	6.0 (PC$_{71}$BM)[43]	No reference	2.82 (PC$_{71}$BM)[44]	No reference	No reference
7.	22.31 ± 0.72 (0.35)	3.10 ± 0.24 (0.66)	6.85 ± 0.20 (0.39)	1.51 ± 0.11 (0.25)		18.1 ± 0.45 (0.1)		5.81 ± 0.53 (0.17)
8.	#15	#13	#13	#9	#15	#10	#12	#12

A5

	Col 1	Col 2	Col 3	D5 R=C$_{12}$H$_{25}$			D8 R=C$_{12}$H$_{25}$	
1.	1.64	1.73	1.59	1.66	1.92	1.66	1.70	1.82
2.	−5.03/−3.39	−4.90/−3.17	−5.01/−3.47	−5.03/−3.37	−5.29/−3.37	−5.06/−3.34	−5.17/−3.32	−5.35/−3.53
3.	18000; 3.0	100700; 3.1	50 000; 1.3	119 000; 16.6	11 000; 26.7	34 000; 3.4	261 000; 7.6	138 000; 8.0
4.	NA	1.20E-08	Gel	6.24E-10	2.72E-09	2.40E-09	6.90E-07	2.00E-10
5.	0.29 ± 0 (0.29); 0.66	1.37 ± 0.07 (1.48); 0.65	1.09 ± 0.03 (1.13); 0.64	0.18 ± 0.3 (0.21); 0.62	0.1 ± 0 (0.1); 0.8	0.57 ± 0.06 (0.65); 0.65	0.06 ± 0.05 (0.1); 0.62	NA
6.	2.15 (A5, R in para, PC$_{71}$BM)[45]	No reference	1.68 (A5, R in para, PC$_{71}$BM)[45]	No reference	2.04 (inverted, PC$_{71}$BM)[34,46]	No reference	No reference	No reference
7.	8.84 ± 0.21 (0.23)	0.33 ± 0.01 (0.40)	5.71 ± 0.81 (0.10)	0.56 ± 0.06 (0.80)	1.85 ± 0.01 (0.83)	1.01 ± 0.08 (0.31)	3.09 ± 0.06 (0.25)	2.01 ± 0.08 (0.37)
8.	#15	#15	#15	#11	#17	#12	#14	#14

Continued

ADVANCED
ENERGY
MATERIALS

www.advenergymat.de

FULL PAPER

Materials Views
www.MaterialsViews.com
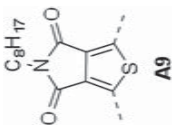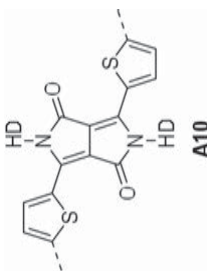
Table 1. Continued

A6							
1. 1.77	1. 1.95	1. 1.94	D5 R=H 1. 1.81	NA	1. 1.92	D8 R=C$_{12}$H$_{25}$ NA (not soluble)	1. 1.95
2. −5.13/−3.36	2. −5.23/−3.28	2. −5.21/−3.27	2. −5.15/−3.30	6. 2.04 (PC$_{71}$BM, A6 hexyl, inverted)[46]	2. −5.00/−3.08		2. −5.28/−3.34
3. 9600; 2.0	3. 11000; 2.2	3. 4600; 1.9	3. 1800; 1.4	8. #11	3. 15 000; 1.6	6. No reference	3. 21 600; 2.7
4. 1.40E-08	4. 3.28E-10	4. 4.15E-08	4. 3.20E-09		4. 7.60E-08	8. #8	4. Gel
5. 1.03 ± 0.1 (1.14); 0.7	5. 0.85 ± 0.1 (1.05); 0.77	5. 0.61 ± 0.07 (0.72); 0.66	5. NA		5. 0.30 ± 0.07 (0.45); 0.58		5. 0.71 ± 0.07 (0.87); 0.79
6. 5.59 (PC$_{71}$BM, A6 hexyl)[47]	6. 5.22 (A6 H, PC$_{71}$BM)[48]	6. 2.60 (PC$_{71}$BM)[49]	6. No reference		6. No reference		6. 3.0 (A6 hexyl)[50]
7. 10.8 ± 0.5 (0.17)	7. 1.03 ± 0.05 (0.61)	7. 0.81 ± 0.07 (0.82)	7. 1.85 ± 0.18 (0.57)		7. 3.58 ± 0.47 (0.32)		7. 2.32 ± 0.21 (0.49)
8. #11	8. #9	8. #9	8. #5		8. #6		8. #8

A6

A7							
1. 1.35	1. 1.61	1.1.59	D5 R=C$_{12}$H$_{25}$ 1. 1.81	NA	1. 1.55	D8 R=C$_{12}$H$_{25}$ NA	1. 1.87 (solution dewets on glass)
2. −5.23/−3.88	2. −5.31/−3.70	2. −5.33/−3.74	2. −5.62/−3.81	6. No reference	2. −5.26/−3.71	6. No reference	2. −5.75/−3.88
3. 2600; 1.6	3. 3200;3.5	3. 1200; 2.0	3. 1100; 1.6	8. #11	3. 1200; 3.3	8. #8	3. (225; 5.5)
4. 5.78E-08	4. 5.06E-10	4. 3.12 E-09	4. NA		4. 1.48E-09		4. NA
5. 0.02 ± 0.01 (0.03); 0.57	5. NA	5. NA	5. NA		5. 0.03 ± 0.93 (0.05); 0.47		5. NA
6. No reference	6. 1.96 (PC$_{71}$BM)[51]	6. No reference	6. No reference		6. No reference		6. No reference
7. 0.60 ± 0.04 (0.33)	7. 0.46 ± 0.04 (0.26)	7. 0.31 ± 0.07 (0.19)	7. NA		7. 1.30 ± 0.10 (0.28)		7. NA
8. #11	8. #9	8. #9	8. #5		8. #6		8. #8

A7

A8							
1. 1.36	1. 1.35	1. 1.36	D5 R=C$_{12}$H$_{25}$ 1. 1.27	NA	1. 1.56	D8 R=C$_{12}$H$_{25}$ 1. 1.57	1. 1.54
2. −5.01/−3.64	2. −5.21/−3.85	2. −5.09/−3.73	2. −5.11/−3.83	6. No reference	2. −5.04/−3.48	2. −5.06/−3.49	2. −5.46/−3.92
3. 16000; 2.0	3. 14000; 2.4	3. 14 000; 2.2	3. 5000; 1.4	8. #15	3. 6100; 2.6	3. 3700; 2.2	3. 1200; 4.8
4. 7.65E-07	4. 1.72E-08	4. 2.00E-08	4. 2.01E-07		4. 1.15E-07	4. 1.23E-08	4. 7.82E-09
5. 0.2 ± 0.03 (0.26); 0.51	5. 0.57 ± 0.06 (0.69); 0.69	5. 0.12 ± 0.02 (0.14); 0.57	5. 0.04 ± 0.02 (0.08); 0.82		5. 0.04 ± 0.02 (0.07); 0.63	5. 0.01 ± 0.01 (0.01); 0.56	5. 0.01 ± 0.01 (0.01); 0.56
6. 6.0 (PC$_{71}$BM, A8 C$_8$H$_{17}$)[52]	6. 9.0[53–55]	6. 7.4 (PC$_{71}$BM)[56]	6. No reference		6. No reference	5. NA	6. No reference
7. 0.62 ± 0.04 (1.06)	7. 1.27 ± 0.15 (0.48)	7. 0.8 ± 0.04 (0.34)	7. 7.62 ± 0.51 (0.18)		7. 5.17 ± 0.71 (0.33)	7. 3.67 ± 0.26 (0.24)	7. 12.4 ± 1.5 (0.18)
8. #15	8. #15	8. #13	8. #9		8. #10	8. #12	8. #12

A8

Continued

Table 1. Continued

			D5 R=H		NA	D8 R=C12H25	1. 2.06 (solution dewets on glass)
1. 1.73	1. 1.86	1. 1.86	1. 2.07 (solution dewets on glass)		1. 2.08 (solution dewets on glass)	1. 1.79	2. −5.76/−3.70
2. −5.37/−3.65	2. −5.43/−3.56	2. −5.35/−3.49	2. −5.53/−3.46	6. No PCE[64]	2. −5.41/−3.33	2. −5.28/−3.48	3. (425; 5.9)
3. 9500;2.8	3. 11000; 3.6	3. 41 000;14.5	3. 39 000;1.5	8. #12	3. 7200; 1.7	3. 3500; 1.3 (not all in solution)	4. NA
4. 5.53E-08	4. 7.42E-08	4. 3.40E-09	4. 3.90E-09		4. 7.20E-08	4. 1.80E-11	5. NA
5. NA	5. 0.67 ± 0.03 (0.74); 0.94	5. 0.47 ± 0.08 (0.64); 0.81	5. NA		5. NA	5. NA	6. No reference
6. 7.3 (PC71BM)[57]	6. 6.17[18,58,59]	6. 6.8[60–62]	6. 0.75 (A9 C12H25, D5 H)[63]		6. No reference	6. 5.1 (A9 C12H25)[65,66]	7. NA
7. 6.56 ± 0.79 (0.5)	7. 0.56±0.05 (0.37)	7. 0.54 ± 0.03 (0.64)	7. 0.63 ± 0.05 (0.26)		7. NA	7. 0.37 ± 0.02 (0.27)	8. #9
8. #12	8. #10	8. #10	8. #6		8. #7	8. #9	

A9

			D5 R=H			D8 R=C12H25	1. 1.52
1. 1.30	1. 1.35	1. 1.36	1. 1.30	1. 1.71	1. 1.38	1. 1.34	2. −5.34/−3.84
2. −5.13/−3.83	2. −5.24/−3.89	2. −5.26/−3.90	2. −5.15/−3.85	2. −5.27/−3.56	2. −5.07/−3.69	2. −5.06/−3.72	3. 2300; 5.4
3. 21000;2.5	3. 103000; 3.3	3. 68 000; 3.3	3. 233 000; 8.0	3. 6700; 3.5	3. 34 000; 4.2	3. 1200; 2.8	4. 1.80E-09
4. 7.60E-08	4. 5.20E-09	4. 5.80E-09	4. 2.08E-06	4. 9.70E-09	4. 1.73E-06	4. 1.68E-10	5. NA
5. NA	5. 0.04±0.47 (0.07); 0.58	5. NA	5. NA	5. NA	5. NA	5. NA	6. No PCE[74]
6. 2.10 (PC71BM)[67]	6. 6.60 (PC71BM)[59,68,69]	6. 2.83 (PC71BM)[67,69]	6. 4.7 (D5 R=H, PC71BM)[70]	6. 2.26 (D6 R=N–CH(C10H21)2)[71,72]	6. No reference	6. 3.2 (different side chains)[73]	7. 15.4 ± 0.4 (0.37)
7. 1.71 ± 0.03 (0.76)	7. 2.46 ± 0.05 (1.14)	7. 1.12 ± 0.04 (1.47)	7. 0.86 ± 0.08 (0.89)	7. 22.5 ± 0.94 (0.43)	7. 4.42 ± 0.18 (0.82)	7. 18.8 ± 0.6 (0.4)	8. #7
8. #10	8. #8	8. #8	8. #4	8. #10	8. #5	8. #7	

A10

Continued

Table 1. Continued

Legend for numbered entries in each cell: 1. optical/electronic gap; 2. HOMO/LUMO; 3. M_n; PDI; 4. mobility; 5. PCE data; 6. reference PCE; 7. value; 8. reference #.

A12
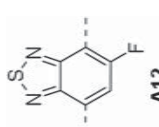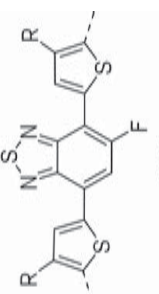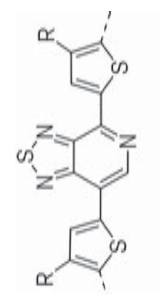
	C1	C2	C3	D5 R=$C_{12}H_{25}$	C5	C6	D8 R=$C_{12}H_{25}$	C8
1	1.50	1.69	NA	1.96	NA	1.71	2.09	1.67
2	−5.12/−3.62	−5.16/−3.47		−5.76/−3.80		−5.09/−3.38	−5.67/−3.57	−5.57/−3.90
3	6800; 1.9	313000; 10.8		13 000; 3.1		5600; 2.1	5300; 2.0	37000; 2.3
4	3.75E-07	3.13E-08		Unstable		1.77E-07	1.43E-08	9.25E-10
5	1.22 ± 0.03 (1.25); 0.67	0.16 ± 0.02 (0.19); 0.74		NA		0.85 ± 1.09 (0.89); 0.70	0.01 ± 0.01 (0.03); 0.40	0.25 ± 0.02 (0.28); 0.77
6	No reference	No reference	No reference	No reference	No reference	5.02 ($PC_{71}BM$)[36]	No reference	No reference
7	0.52 ± 0.02 (0.61)	0.13 ± 0.01 (0.27)		11.5 ± 0.5 (0.35)		0.63 ± 0.06 (0.37)	1.84 ± 0.24 (0.31)	32.3 ± 5.1 (0.15)
8	#11	#9	#9	#5	#11	#6	#8	#8

(Structure: A12)

A13

	A13 R=$C_{12}H_{25}$	A13 R=$C_{12}H_{25}$	A13 R=$C_{12}H_{25}$	A13 R=$C_{12}H_{25}$; D5 R=H	A13 R=$C_{12}H_{25}$	A13 R=$C_{12}H_{25}$	A13 R=$C_{12}H_{25}$; D8 R=HD	A13 R=$C_{12}H_{25}$
1	1.50	1.65	1.59	1.52	1.72	1.58	1.58	1.53
2	−5.08/−3.58	−5.09/−3.44	−5.09/−3.50	−4.95/−3.43	−5.37/−3.65	−4.91/−3.33	−5.18/−3.60	−5.23/−3.70
3	12000; 7.5	80000; 18.2	66 000; 9.0	512 000; 5.3	3200; 2.2	10 000; 2.1	2100; 1.9	12 000; 76.7
4	1.96E-08	2.12E-08	9.85E-07	NA	3.12E-08	6.80E-08	5.76E-08	3.71E-08
5	0.53 ± 0.11 (0.67); 0.65	NA	NA	NA	0.01 ± 0 (0.01); 0.50	NA	NA	NA
6	No reference	6.21 (A13 R=C_8H_{17}, D2 $C_{12}H_{25}$, $PC_{71}BM$)[75]	No reference	No reference	No reference	No reference	No reference	No reference
7	2.76 ± 0.12 (0.47)	0.42 ± 0.03 (0.23)	0.86 ± 0.09 (0.24)	NA	0.46 ± 0.04 (0.36)	0.92 ± 0.06 (0.35)	1.94 ± 0.08 (0.26)	2.27 ± 0.1 (0.19)
8	#14	#12	#12	#8	#14	#9	#11	#11

(Structure: A13)

A14

	A14 R=$C_{12}H_{25}$	A14 R=$C_{12}H_{25}$	A14 R=$C_{12}H_{25}$; D5 R=H	A14 R=$C_{12}H_{25}$	A14 R=$C_{12}H_{25}$	A14 R=$C_{12}H_{25}$	A14 R=$C_{12}H_{25}$; D8 R=$C_{12}H_{25}$	A14 R=$C_{12}H_{25}$
1	1.37	1.47	1.33	NA	NA	1.46	1.49	1.52
2	−5.14/−3.77	−5.05/−3.58	−4.92/−3.59			−5.04/−3.58	−5.31/−3.82	−5.33/−3.81
3	9800; 1.7	4600; 4.1	28 000; 11.1			19 000; 2.6	19 000; 2.5	1600; 1.9
4	6.07E-08	8.94E-08	Dewetting			1.43E-09	1.81E-08	5.03E-09 (x)
5	0.21 ± 0.06 (0.31); 0.59	0.35 ± 0.03 (0.40); 0.60	0.02 ± 0.01 (0.03); 0.41			0.19 ± 0.02 (0.21); 0.54	0.02 ± 0 (0.02); 0.70	0.06 ± 0 (0.06); 0.45
6	No reference	4.84 (inverted, A14 R=EH)[63,76]	No reference	1.34 (A14 R=hexyl)[35]	0.7 (A14 R=H)[35]	No reference	No reference	No reference
7	1.01 ± 0.02 (0.37)	0.20 ± 0.01 (0.46)	0.38 ± 0.09 (0.42)	NA	NA	1.9 ± 0.2 (0.33)	1.55 ± 0.07 (0.24)	2.76 ± 0.42 (0.25)
8	#14	#12	#8	#12	#14	#9	#11	#11

(Structure: A14)

Table 2. Manpower and materials consumption.

Manpower	Man months	Materials consumption (PSC)	Amount
Polymer synthesis	8	[60]PCBM	9.7 g
UV-vis, SEC, CV, mobility, stability	4	PEDOT:PSS	2 L
Program development	1	Silver ink	1 kg
Data analysis	6	Solvents	1.3 L
Paper writing	2	Foil	200 m^2
Sum	26		

depends on the lifetime of the polymer), and size exclusion chromatography (SEC; 1 curve per polymer).

2.2. Manpower and Consumption of Material

A large amount of resources, both in terms of manpower and materials, has been expended in the project as listed in **Table 2**.

2.3. Number of Synthetic Steps (Entry 8)

The embedded energy in a PSC is the amount of energy which has been put into the production of the final device, and here the light-absorbing polymer material is responsible for a large part of that energy, which scales with the number of synthetic steps.[78] Once a high-performing polymer material has been discovered, its application in large-scale R2R processes is the next step and thus large amounts are needed. In order to achieve a low embedded energy in the polymer, the number of synthetic steps has to be as low as possible and the synthetic procedure optimized to give a high yield. The purification (preferably by recrystallization and/or distillation procedures) should be facile and the starting materials have a low cost.[15] To exemplify this we show the synthetic routes for A8D2 (13 steps, best reported efficiency 9.0%[55]) and for P3HT (3 steps, best reported efficiency 6%)[79] in **Scheme 1**. A much higher embedded energy (and cost) for A8D2 compared to P3HT[80] is clearly indicated.

The polymers in Table 1 were synthesized by Stille or Suzuki cross coupling polymerizations. The number of synthetic steps from starting materials such as thiophene or benzothiadiazole is shown for each polymer.[15]

2.4. Synthesis and SEC (Entry 3)

The monomer units were chosen on the basis of high efficiencies reported in the literature and on the complexity of the synthetic route. For example, as A11 (see **Figure 1**) we chose an acceptor monomer, such as naphtha-dithiadiazole, which has been reported to give efficiencies up to 6%.[82–84] However, the synthesis is highly complicated using tetrasulfurtetranitride (S_4N_4), which is a shock-sensitive compound, and 1,5-dibromo-2,6-dihydroxynaphthalene as starting materials. Even though the latter was claimed to be commercially available, it was

not possible to purchase the final monomer compound. Consequently, in the end it was not chosen as one of the acceptors for the study. As another example, our choice for donor unit D4 (see Figure 1) was the benzo[2,1-b;3,4-b']dithiophene with 2-hexyl-decyl as side chains, which has shown PCEs of 4.5%.[67,85] However, the synthesis was insufficient in large scale and the subsequent purification too challenging to ensure a pure monomer. The side chains were chosen for each monomer to ensure a good solubility of all the resulting polymer materials, even though for some structures a shorter side chain, e.g., hexyl, would have been sufficient. All polymers were prepared by a Stille cross coupling polymerization of a di-stannyl and a di-bromo derivative of the donor and acceptor units, respectively, using a palladium catalyst. The exception was polymers based on D6, which were prepared by a Suzuki cross coupling.

Not all 104 polymers could be successfully synthesized due to low reactivity, or steric hindrance, which is indicated by a NA in the table. The polymers that were successfully synthesized were analysed by SEC (see the Supporting Information), and large variations in the molecular weight (M_n) were found. The low molecular weight polymers are mainly attributed to steric hindrance from side chains, (e.g., A4D8), to a low reactivity of the donor as in the case of D6, and to poor solubility leading to precipitation of oligomers. Finally, some monomers, such as D7, which cannot be purified by recrystallization, may contain minor impurities, which could complicate the polymerization reaction.

2.5. UV–Vis and Optical Band Gap (Entry 1)

The optical band gaps of the polymers were estimated from the onset of the UV–vis absorption spectra (see the Supporting Information) and were within the range of 2.09 to 1.27 eV with only four polymers having a band gap above 2 eV. This corresponds well with the aim of preparing low band gap polymers based on a donor/acceptor approach. The acceptors A8 and A10 produced the polymers with the lowest band gaps.

2.6. Electrochemical Measurements and Energy Levels (Entry 2)

The HOMO levels were estimated from the onset of the SWV curves using ferrocene as reference (see the Supporting Information) and calculated according to literature procedures.[86–88] The LUMO levels were calculated from the optical band gap and the HOMO level (see the Supporting Information). The HOMO level of P3HT was found to be −4.9 eV, which is somewhat higher compared to the literature value (−5.20 eV).[89] The LUMO level of [60]PCBM was found to be −3.85 eV, which is a little lower than the literature value (−3.75 eV).[90] The HOMO level of the polymer has an effect on the V_{OC}, since it is generally proportional to the difference between the HOMO of the donor polymer and the LUMO of the acceptor [60]PCBM. Thus, lowering the HOMO of the polymer will increase the maximum V_{OC}.[91] This should be considered in view of the fact that lowering the HOMO of the polymer will increase the band gap and thereby potentially also decrease the current. Several polymers, for instance A4D5, A8D5, and

ADVANCED
ENERGY
MATERIALS

www.advenergymat.de

Materials
Views

www.MaterialsViews.com
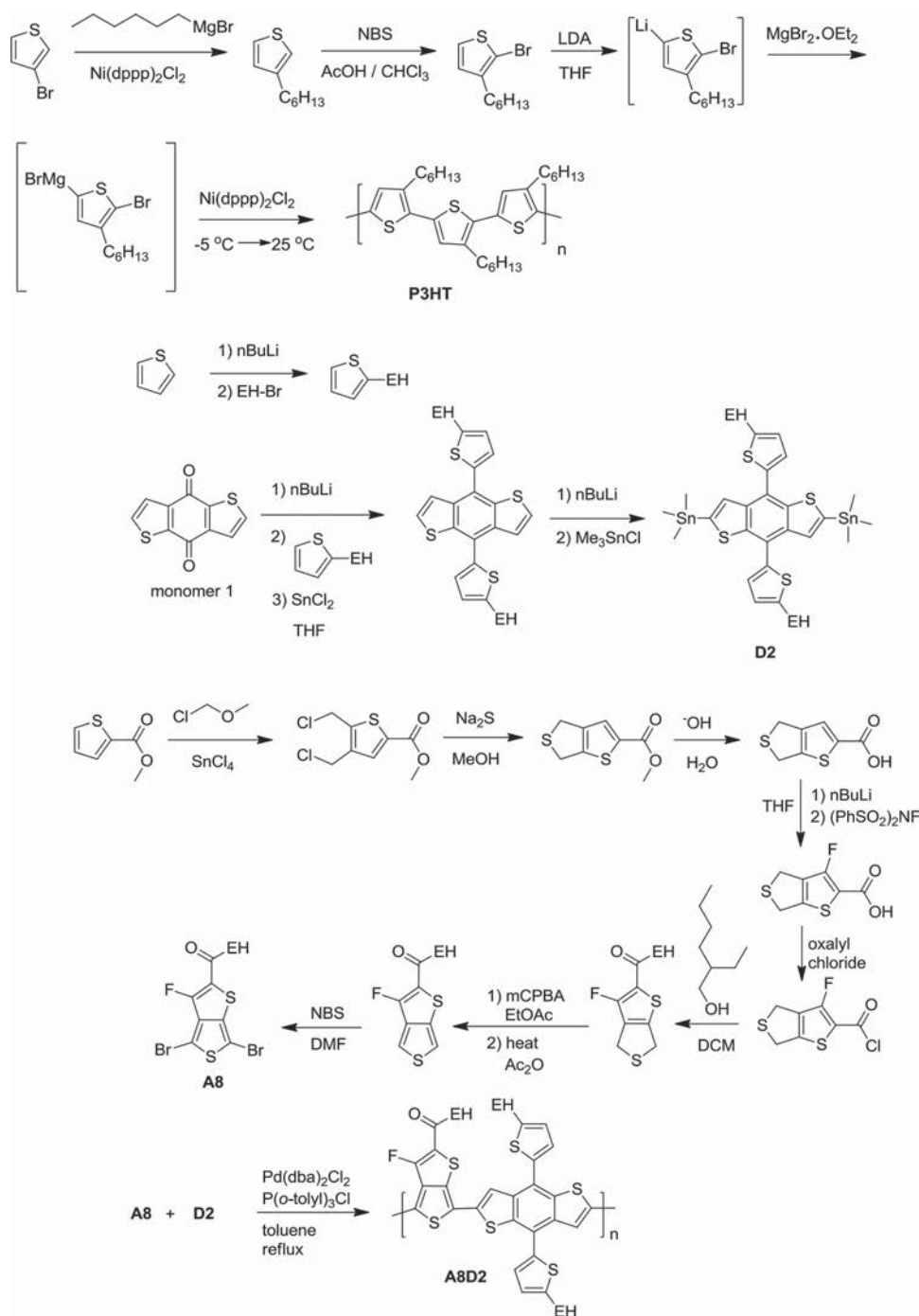
Scheme 1. Comparison of the synthetic routes of P3HT[81] (top) and the high performing polymer A8D2[55] (bottom). Monomer 1 is now commercially available in large quantities; it was, however, originally synthesized in two steps from 3-thiophenecarbonyl chloride.

A9D2, showed a very high V_{OC} compared to P3HT, which is a consequence of a low HOMO level. Unfortunately, the current density for these polymers in PSC devices was much lower than for P3HT, and the resulting PCE is therefore also lower (see **Table 3**). The current can be optimized for instance by varying the ratio between polymer and [60]PCBM. Thus, a high V_{OC} is especially important if one would like to use the polymer material in tandem solar cells.[92]

2.7. Hole Mobility (Entry 4)

The hole mobility was measured in the dark on a polymer film sandwiched between an ITO electrode, poly(3,4-ethylenedioxythiophene) polystyrene sulfonate (PEDOT:PSS), and an evaporated Al electrode (see the Supporting Information). The hole mobility is highly dependent on the solvent from which the analysed film is spin coated. The values
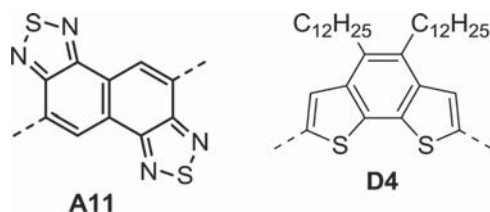
www.MaterialsViews.com

ADVANCED
ENERGY
MATERIALS
www.advenergymat.de

FULL PAPER

Figure 1. Structures of A11 and D4, which were eliminated from the matrix due to difficulties in the synthesis.

reported here were measured on films prepared from chlorobenzene and were found to be subject to some variation. The hole mobility of P3HT was measured at 1.26×10^{-3} cm^2 V^{-1} s^{-1} for a 270 nm thick film, which is in good agreement with the literature values (1×10^{-3}–6×10^{-3} cm^2 V^{-1} s^{-1}).[93] Several polymers, for instance A3D7, A5D8, and A8D1, showed a higher hole mobility than P3HT, but this did not result in a higher PCE (see Table 1), which could be due to poor morphology or insufficient thickness of the active layer film.

2.8. Photochemical Stability (Entry 7)

The photochemical stability of the polymer films was measured as described in the literature by means of an automatic set up that measured the absorption as a function of time at AM1.5 (1000 W m^{-2}).[94] The stability was found to be highest for polymers with the benzothiadiazole-like acceptor unit (A1, A2, A5, A7, A12, A13, and A14) and the donor unit thiophene (D5 and D8), dithienosilole (D1), and a combination of thiophene and benzene (D3 and D7). This is in good agreement with the literature, where the benzothiadiazole, dithienosilole, and thiophene units are reported to be among the most photochemically stable monomer units.[95]

2.9. Roll-Coated Polymer Solar Cells (Entry 5)

The polymers were employed in fully roll-coated and printed PSC devices using Flextrode substrate[96,97] on a mini roll

coater as described earlier.[9,98,99] Several parameters can be studied during such a screening, e.g., solvent, annealing, ratio between polymer and [60]PCBM, film thickness, and coating temperature. All these parameters influence the photovoltaic response of the PSC. However, evaluating all parameters would be impossible within a reasonable timescale, and it would certainly not be possible to do it in this study which included 104 polymers. Consequently, we chose to vary only a subset of the parameters during the screening. The parameters we chose to study included: (1) the ratio between the polymer and [60]PCBM (1:1 or 1:2), (2) the solvent from which the polymer/[60]PCBM mixture is coated (chloroform or o-dichlorobenzene), and (3) the thickness of the coated active layer (thin, medium, and thick, which corresponds to a wet thickness of around 10, 12, and 15 µm, and a dry thickness of around 315, 400, and 475 nm, respectively). The active layer was thick compared to spin coated films (100 nm) to avoid electrical shorts from the less smooth films.[100] The coating temperature was kept constant at 70 °C, which may have affected the morphology of the active layer. However, the choice of a high and low boiling solvent will also affect the different morphologies which can be obtained from a given polymer. The photovoltaic responses are presented as the average efficiency plus/minus the standard deviation together with the maximum recorded PCE and V_{OC}. Many of the polymers failed to generate working devices despite the variations tested. This was due to coating defects such as dewetting, insufficient solubility, destruction of the devices during switching,[97] and electrical shorts due to defects.

2.10. PCE Values from the Literature (Entry 6)

All monomers and some of the polymer materials have been reported in the literature. The values from these studies are listed for reference in Table 1. The PCE values are reported for small spin coated devices with a normal geometry, prepared with an ITO electrode and thermally evaporated electrodes under vacuum, rather than for roll coated devices with a larger area. Also, the devices made for this study were not optimized

Table 3. The maximum PCE for roll-coated devices relative to the PCE of P3HT/PCBM roll-coated devices. The colors indicate: bold: polymer performs better than P3HT, grey: roughly the same performance as P3HT, and plain text: poorer performance than P3HT. NA indicates a failure (please refer to Table S2, Supporting Information, for the specific type of failure).

	D1	D2	D3	D5	D6	D7	D8	D9
A1	0.9	0.3	NA	NA	NA	**1.4**	NA	NA
A2	0.3	0.8	0.4	0.3	NA	0.9	NA	NA
A3	0.2	NA	0.4	0.4	0.1	0.3	0.2	0.2
A4	NA	0.1	NA	0.4	NA	NA	NA	NA
A5	0,2	0.9	0.7	0.1	0.1	0.4	0.1	NA
A6	0.7	0.7	0.5	NA	NA	0.2	NA	0.6
A7	NA	NA	NA	NA	NA	NA	NA	NA
A8	0.2	0.4	0.1	0.1	NA	NA	NA	NA
A9	0.2	0.5	0.4	NA	NA	NA	NA	NA
A10	NA	NA	NA	NA	NA	NA	NA	NA
A12	0.8	0.1	NA	NA	NA	0.6	NA	0.2
A13	0.4	NA	NA	NA	NA	NA	NA	NA
A14	0.2	0.3	NA	NA	NA	0.1	NA	NA

FULL PAPER

for maximum performance, but rather prepared using the exact same procedures to make comparison possible.

2.11. Comparison of the Polymers

The PCE of the polymers relative to P3HT:PCBM (Table 3) shows that only one polymer (A1D7) generates devices with a better PCE. Only 8 polymers performed similarly to P3HT:PCBM and the rest much more poorly, which is indicated by the low value, or simply by NA in the table. Failure could have occurred for the following reasons: (1) problems in the synthesis, (2) insolubility, (3) dewetting of the active layer on the Flextrode substrate or dewetting of the PEDOT:PSS layer on top of the active layer, (4) no switching of the device, or (5) a shunted device, which is described in more details below. This result indicates the significant challenge in finding polymers that are suitable for R2R-fabricated PSC devices. As seen in Table 1, many of the polymers that failed have been shown to perform excellently in spin-coated devices, however, as described above it is not possible to compare these results with the results of this screening. The 9 polymers that performed on par or better than P3HT:PCBM, based on the PCE alone, are considered promising candidates for further optimization. These are based on the donors D1, D2, D7 and the acceptors A1, A2, A5, A6, and A12.

Although most reports in the literature focus on the PCE, other parameters are also important. We have combined all these factors in a merit factor (χ) defined as

$$\chi = \frac{\text{PCE} \times \text{stability} \times V_{OC} \times \text{band gap}}{\text{number of synthetic steps}} \quad (1)$$

$$\chi_{rel} = \chi / \chi_{\text{P3HT:PCBM}} \quad (2)$$

The photochemical stability of polymers used in PSCs varies greatly as shown in previous studies[95] and must be taken into consideration in the selection of an active material. In the merit factor, it is the degradation rate of the polymer normalized to the degradation rate of P3HT at equal absorption value (see the Supporting Information). It is desirable to have a high V_{OC}, and it is therefore incorporated into the merit factor. The band gap (in nm) of the polymer determines how much of the solar spectrum is utilized and gives a theoretical upper limit for the current output of the device. The voltage and band gap are included in order to indentify the polymers which could give high PCE, i.e., a high voltage and/or an absorption to longer wavelengths theorectically gives a higher PCE. Finally, we also consider the number of synthetic steps needed to prepare the polymer, since this obviously has a great impact on the embedded energy and therefore also on the cost. Instead of looking at the merit factor for each polymer we introduce the relative merit factor. The relative merit factor (χ_{rel}) of the polymers is a simplified measure of an overall score against the standard P3HT:PCBM active layer combination and is seen in **Table 4**. This ranks 13 out of the 104 polymers as better or equal to the standard, which makes them candidates for future development. This demonstrates that the success rate is quite low and that the requirements for roll and R2R fabrication seems to be much higher than for spin coating (which cannot be scaled to industrial applications).

Figure 2 provides an overview of the V_{OC}, the HOMO energy levels, and the optical band gap (E_g). It is clear that when preparing 104 different polymer materials, smooth and continuous variation in the different properties can be achieved. This highlights the strength of the synthetic organic chemistry approach to materials, since almost any number can be matched within a large range through the synthetic approach. We observed V_{OC} values within the range of 0.4 to 0.8 V, HOMO energy level within the range of −4.9 to −5.8 eV, and the band gap within the range of 2.1 to 1.3 eV. The relation between the HOMO and V_{OC} is known to be $V_{OC} = \text{HOMO}_{\text{polymer}} - \text{LUMO}_{\text{acceptor}} - 0.3\ \text{V}$[101] and we found that to some extend the polymers in this screening follow this trend though with a little higher loss in the device of 0.6 V (see Figure S1, the Supporting Information).

Table 4. The relative merit factor χ_{rel}. The colors indicate: bold: polymer performs better than P3HT, grey: roughly the same performance as P3HT, and plain text: poorer performance than P3HT. A minimum 70% yield for each step is assumed. Thus, the yield is not taken into account for the synthetic steps. NA indicates a failure (please refer to Table S2, Supporting Information, for the specific type of failure).

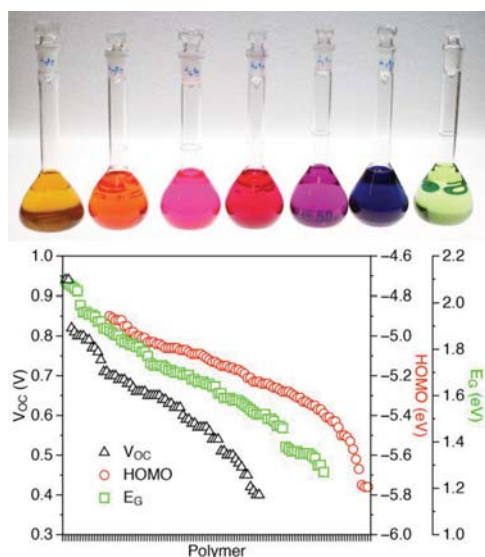|	D1	D2	D3	D5	D6	D7	D8	D9
A1	1.4	**3.0**	NA	NA	NA	**2.7**	NA	NA
A2	NA	**3.1**	0.6	1.0	NA	1.2	NA	NA
A3	NA	NA	0.2	NA	NA	0.1	NA	NA
A4	NA	NA	NA	1.0	NA	NA	NA	NA
A5	NA	**2.9**	0.4	0.2	NA	0.7	NA	NA
A6	0.2	0.8	0.5	NA	NA	0.1	NA	0.4
A7	0.1	NA	NA	NA	NA	0.1	NA	NA
A8	0.1	0.5	0.2	NA	NA	NA	NA	NA
A9	NA	1.9	0.9	NA	NA	NA	NA	NA
A10	NA	NA	NA	NA	NA	NA	NA	NA
A12	1.8	**2.6**	NA	NA	NA	**2.7**	NA	NA
A13	0.2	NA	NA	NA	NA	NA	NA	NA
A14	0.3	1.6	NA	0.1	NA	0.1	NA	NA

Figure 2. Top: Illustration of the different polymer solutions with the different color/absorbance achieved by coupling the different donor and acceptors in the screening. Bottom: Illustration of the accessible ranges for V_{OC}, E_g, and HOMO levels as a function of polymer number arranged according to the numerical data value (which is different for each property) to show the smooth variation that can be attained. For a complete list of polymers with numerical data, see Table S1, Supporting Information.

Figure 3. Illustration of the number of polymers that failed at a given step in the serieal value chain for the process that comprises steps: 1 = design, 2 = synthesis, 3 = characterization, 4 = ink, 5 = coating, 6 = device, 7 = performance (PCE), 8 = PCE better than P3HT.

The enormous spans of V_{OC}, HOMO, and band gap can be efficiently explored in final devices where overall performance for instance depends on band gaps being of a particular value (i.e., in tandem devices), or where energy levels need a certain value (i.e., with specific electrode materials).

3. Future and Outlook

It is clear from this study that a large research effort is required for the successful development of a material that meets all the requirements of roll coating/printing besides reaching the customary high efficiency target. The method presented here shows the magnitude of the task, but also how to rationally address the challenge and as such represent the first stage of the search. As we have demonstrated, there are a number of steps in the highly linear approach from synthesis through materials characterisation, processing and devices studies. As illustrated in **Figure 3**, the outcome for any of the materials may stop at any of these stations along the path. The entries in Figure 3 represent the following steps where failure may occur: 1) design, 2) synthesis, 3) characterization, 4) ink, 5) coating, 6) device, 7) PCE, and 8) PCE better than P3HT. As can be seen, failure at steps 1 to 4 account for 28 of the polymers. These failed mainly due to steric hindrance, low molecular weight, or insolubility. A solution could be to re-synthesize them with other side chains to enhance solubility, lower steric hindrance, and increase the molecular weight. Failure at step 5 accounts for 20 of the polymers. Failure mainly occurred due to dewetting of the active layer, which could be solved by using a different device structure, e.g., using a different substrate, or by
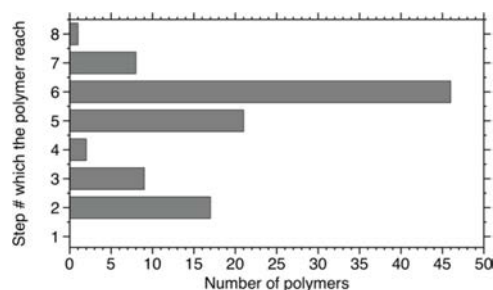
enhancing the adhesion of the polymer to the Flextrode substrate. Failure at step 6 accounts for almost half of the polymers. In some instances, it represents mechanisms, such as electronic shorts in the device during swithcing, which can be solved by increasing the thickness of the active layer, or insufficient switching, which can be solved by using a different device structure which does not need switching. However, in most cases (see Table 3), it represents a very low PCE. There are several possibilities to overcome this. For example, if the V_{OC} is low, another acceptor than [60]PCBM can be used. Similarly, if the I_{SC} is low, the ratio of the polymer and [60]PCBM can be optimized. For some materials, the hurdles may be overcome and the potential realized through suitable modification, but it is clear that the earlier in the process a material fails, the greater the effort needed to overcome the problem.

To progress from the results of this work, the most suitable candidates (see **Figure 4**) should be further explored through side chain engineering, processing optimisation, and device architecture studies. Of course, it is not impossible that this approach will miss the ultimate material for PSCs, but it is highly unlikely. The majority of materials that have been successful in the past already shows potential in an unrefined form, and this potential has been further explored in subsequent studies. This study should thus be seen as a mining effort for raw candidate materials that, when further refined, can be expected to deliver with respect to performance at all levels (efficiency, physical properties, operational stability, cost, and processability).

4. Conclusion

This screening of 104 light-absorbing polymers for PSCs has illustrated the massive challenge of discovering materials which can offer high efficiency, high stability, and compatibility with large-scale R2R processing. The challenge for the polymer materials has been shown to lie not only in the polymer backbone, but also in the side chains, more specifically where the side chains are attached, and in the size and nature of the side chain. The donor–acceptor approach has pointed out a number of units worthy of further study. A further study will include side chain variations, the morphology of the active layer, the stability of the device, new device structures like tandem architectures, where polymer materials with high
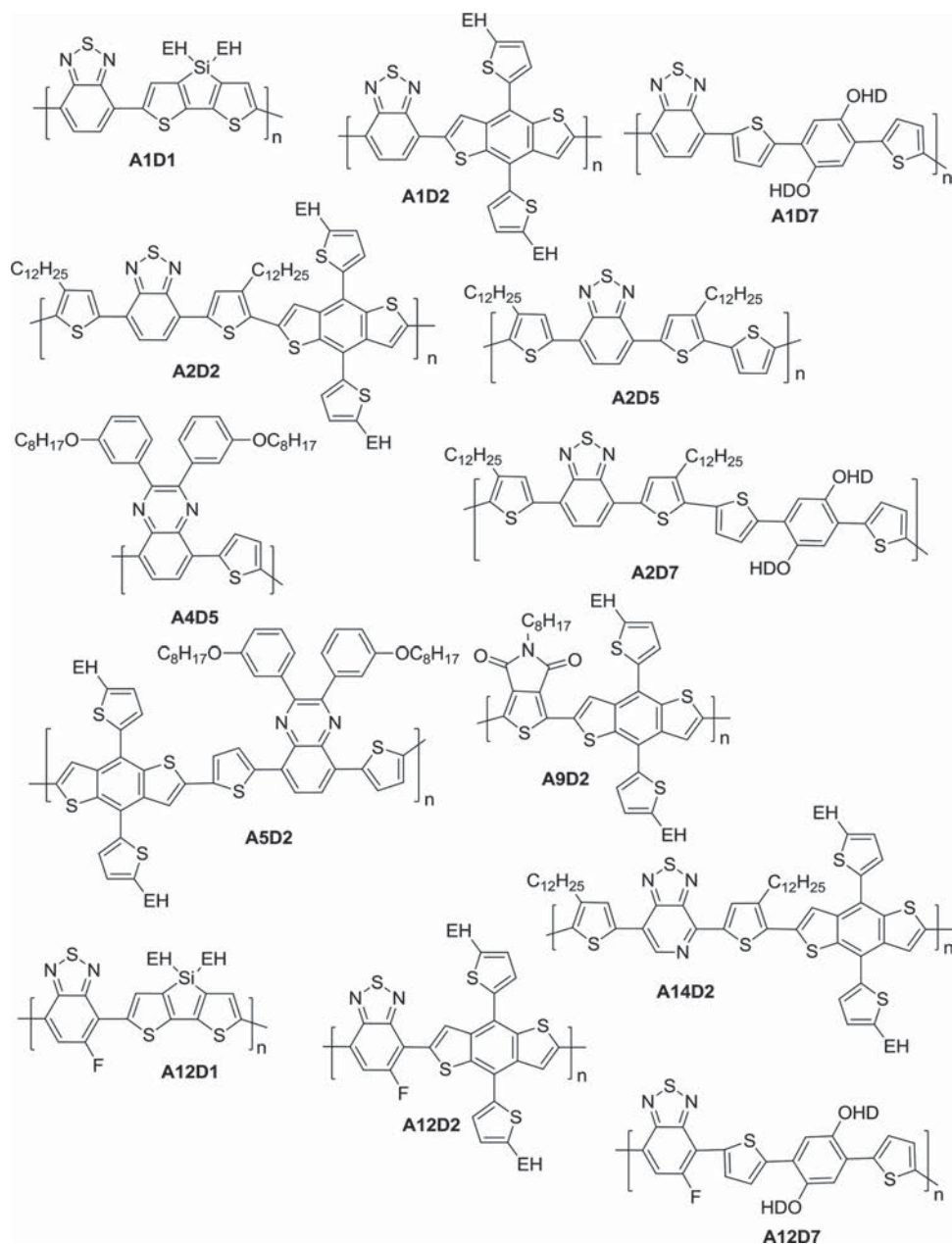
FULL PAPER

Figure 4. The 13 polymer backbones which were found to be suited for roll-coated PSCs in this screening. Side chains' length and position will be studied in future experiments.

V_{OC} are of great interest, and finally devices optimized through the use of other PEDOT:PSS types. The present study has shown that 13 polymers out of 104 (corresponding to 12.5% of the polymers) are performing better than the prototypical reference material P3HT and are therefore suitable for further development.

Supporting Information

Supporting Information is available from the Wiley Online Library or from the author.

Acknowledgements

[1] F. C. Krebs, N. Espinosa, M. Hösel, R. R. Søndergaard, M. Jørgensen, *Adv. Mater.* **2014**, *26*, 29.

[2] N. Espinosa, M. Hösel, D. Angmo, F. C. Krebs, *Energy Environ. Sci.* **2012**, *5*, 5117.

[3] Web of Science search: "polymer solar cells" "organic solar cells" "organic photovoltaics," **October 2014.**

[4] M. A. Green, K. Emery, Y. Hishikawa, W. Warta, E. D. Dunlop, *Prog. Photovoltaics Res. Appl.* **2014**, *22*, 1.

[5] E. Bundgaard, F. Krebs, *Sol. Energy Mater. Sol. Cells* **2007**, *91*, 954.

[6] M. Jørgensen, J. E. Carlé, R. R. Søndergaard, M. Lauritzen, N. A. Dagnæs-Hansen, S. L. Byskov, T. R. Andersen, T. T. Larsen-Olsen, A. P. L. Böttiger, B. Andreasen, L. Fu, L. Zuo, Y. Liu, E. Bundgaard, X. Zhan, H. Chen, F. C. Krebs, *Sol. Energy Mater. Sol. Cells* **2013**, *119*, 84.

[7] T. T. Larsen-Olsen, F. Machui, B. Lechene, S. Berny, D. Angmo, R. Søndergaard, N. Blouin, W. Mitchell, S. Tierney, T. Cull, P. Tiwana, F. Meyer, M. Carrasco-Orozco, A. Scheel, W. Lövenich, R. de Bettignies, C. J. Brabec, F. C. Krebs, *Adv. Energy Mater.* **2012**, *2*, 1091.

[8] S. A. Gevorgyan, O. Zubillaga, J. M. V. de Seoane, M. Machado, E. A. Parlak, N. Tore, E. Voroshazi, T. aernouts, H. Müllejans, G. Bardizza, N. Taylor, W. Verhees, J. M. Kroon, P. Morvillo, C. Minarini, F. Roca, F. A. Castro, S. Cros, B. Lechêne, J. F. Trigo, C. Guillén, J. Herrero, B. Zimmermann, S. B. Sapkota, C. Veit, U. Würfel, P. S. Tuladhar, J. R. Durrant, S. Winter, S. Rousu, M. Välimaki, V. Hinrichs, S. R. Cowan, D. C. Olson, P. Sommer-Larsen, F. C. Krebs, *Renew. Energy* **2014**, *63*, 376.

[9] J. E. Carlé, T. R. Andersen, M. Helgesen, E. Bundgaard, M. Jørgensen, F. C. Krebs, *Sol. Energy Mater. Sol. Cells* **2013**, *108*, 126.

[10] A. Teichler, R. Eckardt, S. Hoeppener, C. Friebe, J. Perelaer, A. Senes, M. Morana, C. J. Brabec, U. S. Schubert, *Adv. Energy Mater.* **2011**, *1*, 105.

[11] A. Facchetti, *Chem. Mater.* **2011**, *23*, 733.

[12] L. Bian, E. Zhu, J. Tang, W. Tang, F. Zhang, *Prog. Polym. Sci.* **2012**, *37*, 1292.

[13] H. Zhou, L. Yang, W. You, *Macromolecules* **2012**, *45*, 607.

[14] R. Po, M. Maggini, N. Camaioni, *J. Phys. Chem. C* **2010**, *114*, 695.

[15] G. Marzano, C. V. Ciasca, F. Babudri, G. Bianchi, A. Pellegrino, R. Po, G. M. Farinola, *Eur. J. Org. Chem.* **2014**, *2014*, 6583.

[16] J. Hou, H. Y. Chen, S. Zhang, G. Li, Y. Yang, *J. Am. Chem. Soc.* **2008**, *130*, 16144.

[17] H. Y. Chen, J. Hou, A. E. Hayden, H. Yang, K. N. Houk, Y. Yang, *Adv. Mater.* **2010**, *22*, 371.

[18] R. S. Kularatne, P. Sista, H. Q. Nguyen, M. P. Bhatt, M. C. Biewer, M. C. Stefan, *Macromolecules* **2012**, *45*, 7855.

[19] Y. Huang, F. Liu, X. Guo, W. Zhang, Y. Gu, J. Zhang, C. C. Han, T. P. Russell, J. Hou, *Adv. Energy Mater.* **2013**, *3*, 930.

[20] J. Hou, M.-H. Park, S. Zhang, Y. Yao, L. M. Chen, J.-H. Li, Y. Yang, *Macromolecules* **2008**, *41*, 6012.

[21] E. Bundgaard, F. C. Krebs, *Macromolecules* **2006**, *39*, 2823.

[22] J. E. Carlé, J. W. Andreasen, M. Jørgensen, F. C. Krebs, *Sol. Energy Mater. Sol. Cells* **2010**, *94*, 774.

[23] C. Liu, J. Tsai, W. Lee, W. Chen, S. A. Jenekhe, *Macromolecules* **2008**, *41*, 6952.

[24] T. L. Nguyen, H. Choi, S. J. Ko, M. A. Uddin, B. Walker, S. Yum, J. E. Jeong, M. H. Yun, T. Shin, S. Hwang, J. Y. Kim, H. Y. Woo, *Energy Environ. Sci.* **2014**, *7*, 3040.

[25] W. Yue, Y. Zhao, H. Tian, D. Song, Z. Xie, D. Yan, Y. Geng, F. Wang, *Macromolecules* **2009**, *42*, 6510.

[26] L. Huo, H.-Y. Chen, J. Hou, T. L. Chen, Y. Yang, *Chem. Commun.* **2009**, 5570.

[27] M. Helgesen, T. J. Sørensen, M. Manceau, F. C. Krebs, *Polym. Chem.* **2011**, *2*, 1355.

[28] L. Huo, J. Hou, S. Zhang, H. Y. Chen, Y. Yang, *Angew. Chem. Int. Ed.* **2010**, *49*, 1500.

[29] F. Wu, D. Zha, L. Chen, Y. Chen, *J. Polym. Sci. Part A Polym. Chem.* **2013**, *51*, 1506.

[30] X. Guo, M. Zhang, L. Huo, F. Xu, Y. Wu, J. Hou, *J. Mater. Chem.* **2012**, *22*, 21024.

[31] E. Zhou, J. Cong, K. Hashimoto, K. Tajima, *Macromolecules* **2013**, *46*, 763.

[32] B. Qu, H. Yang, D. Tian, H. Liu, Z. Cong, C. Gao, Z. Chen, L. Xiao, Z. Gao, W. Wei, Q. Gong, *Synth. Met.* **2012**, *162*, 2020.

[33] J. Hou, H. Y. Chen, S. Zhang, Y. Yang, *J. Phys. Chem. C* **2009**, *113*, 21202.

[34] N. Blouin, A. Michaud, D. Gendron, S. Wakim, E. Blair, R. Neagu-Plesu, M. Belletête, G. Durocher, Y. Tao, M. Leclerc, *J. Am. Chem. Soc.* **2008**, *130*, 732.

[35] A. Operamolla, S. Colella, R. Musio, A. Loiudice, O. H. Omar, G. Melcarne, G. Mazzeo, G. Gigli, G. M. Farinola, F. Babudri, *Sol. Energy Mater. Sol. Cells* **2011**, *95*, 3490.

[36] K. H. Ong, S. L. Lim, H. S. Tan, H. K. Wong, J. Li, Z. Ma, L. C. H. Moh, S. H. Lim, J. C. De Mello, Z. K. Chen, *Adv. Mater.* **2011**, *23*, 1409.

[37] B. Liu, X. Chen, Y. He, Y. Li, X. Xu, L. Xiao, L. Li, Y. Zou, *J. Mater. Chem. A* **2013**, *1*, 570.

[38] P. Ding, C. C. Chu, B. Liu, B. Peng, Y. Zou, Y. He, K. Zhou, C. S. Hsu, *Macromol. Chem. Phys.* **2010**, *211*, 2555.

[39] M. Helgesen, S. A. Gevorgyan, F. C. Krebs, R. A. J. Janssen, *Chem. Mater.* **2009**, *21*, 4669.

[40] R. Qin, W. Li, C. Li, C. Du, C. Veit, H. F. Schleiermacher, M. Andersson, Z. Bo, Z. Liu, O. Inganäs, U. Wuerfel, F. Zhang, *J. Am. Chem. Soc.* **2009**, *131*, 14612.

[41] A. A. B. Alghamdi, D. C. Watters, H. Yi, S. Al-Faifi, M. S. Almeataq, D. Coles, J. Kingsley, D. G. Lidzey, A. Iraqi, *J. Mater. Chem. A* **2013**, *1*, 5165.

[42] C. Gao, W. Wang, H. Wu, H. Liu, Y. Mi, Z. An, J. Liu, *CN102816305A* **2012**.

[43] E. Wang, L. Hou, Z. Wang, S. Hellström, F. Zhang, O. Inganäs, M. R. Andersson, *Adv. Mater.* **2010**, *22*, 5240.

[44] L. J. Lindgren, F. Zhang, M. Andersson, S. Barrau, S. Hellström, W. Mammo, E. Perzon, O. Inganäs, M. R. Andersson, *Chem. Mater.* **2009**, *21*, 3491.

[45] C. Bathula, C. E. Song, W. H. Lee, J. Lee, S. Badgujar, R. Koti, I. N. Kang, W. S. Shin, T. Ahn, J. C. Lee, S.-J. Moon, S. K. Lee, *Thin Solid Films* **2013**, *537*, 231.

[46] H. Il Kim, J. M. Cho, W. S. Shin, S. K. Lee, J. C. Lee, S. J. Moon, J. H. Kim, *J. Korean Phys. Soc.* **2012**, *60*, 2034.

[47] M. Zhang, X. Guo, Y. Li, *Adv. Energy Mater.* **2011**, *1*, 557.

[48] L. Huo, X. Guo, S. Zhang, Y. Li, J. Hou, *Macromolecules* **2011**, *44*, 4035.

[49] M. Yang, B. Peng, B. Liu, Y. Zou, K. Zhou, Y. He, C. Pan, Y. Li, *J. Phys. Chem. C* **2010**, *114*, 17989.

[50] J. E. Carlé, M. Helgesen, M. V. Madsen, E. Bundgaard, F. C. Krebs, *J. Mater. Chem. C* **2014**, *2*, 1290.

[51] H. R. Tseng, G. C. Bayan, L. Ying, B. B. Y. Hsu, W. Wen, *WO 2012/174561A2*, **2012**.

[52] S. Akiyama, M. Okabe, M. Furuya, *JP 2012233072 A* **2012**.

[53] S. Zhang, L. Ye, W. Zhao, D. Liu, H. Yao, J. Hou, *Macromolecules* **2014**, *47*, 4653.

[54] S.-H. Liao, H. J. Jhuo, Y. S. Cheng, S. A. Chen, *Adv. Mater.* **2013**, *25*, 4766.

[55] L. Yu, Y. Liang, F. He, *WO 2013/116643 A1* **2013**.

[56] Y. Liang, Z. Xu, J. Xia, S. T. Tsai, Y. Wu, G. Li, C. Ray, L. Yu, *Adv. Mater.* **2010**, *22*, E135.

[57] T. Chu, J. Lu, S. Beaupré, Y. Zhang, J. R. Pouliot, S. Wakim, J. Zhou, M. Leclerc, Z. Li, J. Ding, Y. Tao, *J. Am. Chem. Soc.* **2011**, *133*, 4250.

[58] J. Yuan, Z. Zhai, H. Dong, J. Li, Z. Jiang, Y. Li, W. Ma, *Adv. Funct. Mater.* **2013**, *23*, 885.

[59] T. E. Kang, H.-H. Cho, H. J. Kim, W. Lee, H. Kang, B. J. Kim, *Macromolecules* **2013**, *46*, 6806.

[60] C. Piliego, T. W. Holcombe, J. D. Douglas, C. H. Woo, P. M. Beaujuge, J. M. J. Fréchet, *J. Am. Chem. Soc.* **2010**, *132*, 7595.

[61] Y. Zou, A. Najari, P. Berrouard, S. Beaupré, R. B. Aïch, Y. Tao, M. Leclerc, *J. Am. Chem. Soc.* **2010**, *132*, 5330.

[62] Y. Zhang, S. K. Hau, H. L. Yip, Y. Sun, O. Acton, A. K. Y. Jen, *Chem. Mater.* **2010**, *22*, 2696.

[63] T. Umeyama, M. Oodoi, O. Yoshikawa, T. Sagawa, S. Yoshikawa, D. Evgenia, Y. Tezuka, K. Stranius, N. V. Tkachencko, H. Lemmetyinen, H. Imahori, *J. Mater. Chem.* **2011**, *21*, 12454.

[64] M. Leclerc, P. Berrouard, *WO 2013/056355 A1* **2013**.

[65] C. M. Liu, M. S. Su, J. M. Jiang, Y. W. Su, C. J. Su, C. Y. Chen, C. S. Tsao, K. H. Wei, *ACS Appl. Mater. Interfaces* **2013**, *5*, 5413.

[66] M. C. Yuan, M. Y. Chiu, S. P. Liu, C. M. Chen, K. H. Wei, *Macromolecules* **2010**, *43*, 6936.

[67] L. Huo, J. Hou, H. Y. Chen, S. Zhang, Y. Jiang, T. L. Chen, Y. Yang, *Macromolecules* **2009**, *42*, 6564.

[68] L. Dou, J. Gao, E. Richard, J. You, C. C. Chen, K. C. Cha, Y. He, G. Li, Y. Yang, *J. Am. Chem. Soc.* **2012**, *134*, 10071.

[69] S. Zhang, L. Ye, Q. Wang, Z. Li, X. Guo, L. Huo, H. Fan, J. Hou, *J. Phys. Chem. C* **2013**, *117*, 9550.

[70] J. C. Bijleveld, A. P. Zoombelt, S. G. J. Mathijssen, M. M. Wienk, M. Turbiez, D. M. de Leeuw, A. J. Janssen, *J. Am. Chem. Soc.* **2009**, *131*, 16616.

[71] E. Zhou, S. Yamakawa, K. Tajima, C. Yang, K. Hashimoto, *Chem. Mater.* **2009**, *21*, 4055.

[72] Z. Yingping, D. Gendron, R. B. Aïch, A. Najari, Y. Tao, M. Leclerc, *Macromolecules* **2009**, *42*, 2891.

[73] M. M. Wienk, M. Turbiez, J. Gilot, R. A. J. Janssen, *Adv. Mater.* **2008**, *20*, 2556.

[74] M. Düggeli, O. F. Aebischer, P. Hayoz, M. Rodona Turon, M. Turbiez, J.-C. Flores, H. J. Kirner, P. Murrer, N. Chebotareva, T. Schäfer, *WO 2010/136353A1* **2010**.

[75] Q. Peng, X. Liu, D. Su, G. Fu, J. Xu, L. Dai, *Adv. Mater.* **2011**, *23*, 4554.

[76] J. Yuan, X. Huang, H. Dong, J. Lu, T. Yang, Y. Li, A. Gallagher, W. Ma, *Org. Electron.* **2013**, *14*, 635.

[77] H. Kang, B. Zhao, Z. Cao, J. Zhong, H. Li, Y. Pei, P. Shen, S. Tan, *Eur. Polym. J.* **2013**, *49*, 2738.

[78] N. Espinosa, R. Garcia-Valverde, A. Urbina, F. Lenzmann, M. Manceau, D. Angmo, F. C. Krebs, *Sol. Energy Mater. Sol. Cells* **2012**, *97*, 3.

[79] G. Zhao, Y. He, Y. Li, *Adv. Mater.* **2010**, *22*, 4355.

[80] T. P. Osedach, T. L. Andrew, V. Bulović, *Energy Environ. Sci.* **2013**, *6*, 711.

[81] R. D. Mccullough, S. P. Williams, S. Tristram-Nagle, M. Jayaraman, *Synth. Met.* **1995**, *69*, 279.

[82] M. Wang, X. Hu, L. Liu, C. Duan, P. Liu, L. Ying, F. Huang, Y. Cao, *Macromolecules* **2013**, *46*, 3950.

[83] I. Osaka, M. Shimawaki, H. Mori, I. Doi, E. Miyazaki, T. Koganezawa, K. Takimiya, *J. Am. Chem. Soc.* **2012**, *134*, 3498.

[84] M. Wang, X. Hu, P. Liu, W. Li, X. Gong, F. Huang, Y. Cao, *J. Am. Chem. Soc.* **2011**, *133*, 9638.

[85] M. Yuan, A. H. Rice, C. K. Luscombe, *J. Pol. Sci. A: Pol. Chem.* **2011**, *49*, 701.

[86] A. J. Bard, L. R. Faulkner, *Electrochemical Methods: Fundamentals and Applications*, 2nd ed., Wiley, New York **2001**.

[87] C. M. Cardona, W. Li, A. E. Kaifer, D. Stockdale, G. C. Bazan, *Adv. Mater.* **2011**, *23*, 2367.

[88] V. V Pavlishchuk, A. W. Addison, *Inorganica Chim. Acta* **2000**, *298*, 97.

[89] M. Al-Ibrahim, *Sol. Energy Mater. Sol. Cells* **2004**, *85*, 13.

[90] C. J. Brabec, N. S. Sariciftci, J. C. Hummelen, *Adv. Funct. Mater.* **2001**, *11*, 15.

[91] M. C. Scharber, D. Wuhlbacher, M. Koppe, P. Denk, C. Waldauf, A. J. Heeger, C. L. Brabec, *Adv. Mater.* **2006**, *18*, 789.

[92] G. Dennler, M. C. Scharber, T. Ameri, P. Denk, K. Forberich, C. Waldauf, C. J. Brabec, *Adv. Mater.* **2008**, *20*, 579.

[93] D. M. DeLongchamp, B. M. Vogel, Y. Jung, M. C. Gurau, C. A. Richter, O. A. Kirillov, J. Obrzut, D. A. Fischer, S. Sambasivan, L. J. Richter, E. K. Lin, *Chem. Mater.* **2005**, *17*, 5610.

[94] T. Tromholt, M. V. Madsen, J. E. Carlé, M. Helgesen, F. C. Krebs, *J. Mater. Chem.* **2012**, *22*, 7592.

[95] M. Manceau, E. Bundgaard, J. E. Carlé, O. Hagemann, M. Helgesen, R. Søndergaard, M. Jørgensen, F. C. Krebs, *J. Mater. Chem.* **2011**, *21*, 4132.

[96] M. Hösel, R. R. Søndergaard, M. Jørgensen, F. C. Krebs, *Energy Technol.* **2013**, *1*, 102.

[97] T. T. Larsen-Olsen, R. R. Søndergaard, K. Norrman, M. Jørgensen, F. C. Krebs, *Energy Environ. Sci.* **2012**, *5*, 9467.

[98] T. R. Andersen, H. F. Dam, B. Andreasen, M. Hösel, M. V. Madsen, S. A. Gevorgyan, R. R. Søndergaard, M. Jørgensen, *Sol. Energy Mater. Sol. Cells* **2014**, *120*, 735.

[99] D. Angmo, H. F. Dam, T. R. Andersen, N. K. Zawacka, M. V. Madsen, J. Stubager, F. Livi, R. Gupta, M. Helgesen, J. E. Carlé, T. T. Larsen-Olsen, G. U. Kulkarni, E. Bundgaard, F. C. Krebs, *Energy Tech.* **2014**, *2*, 651.

[100] F. C. Krebs, *Sol. Energy Mater. Sol. Cells* **2009**, *93*, 394.

[101] M. C. Scharber, D. Mühlbacher, M. Koppe, P. Denk, C. Waldauf, A. J. Heeger, C. J. Brabec, *Adv. Mater.* **2006**, *18*, 789.

FULL PAPER

www.MaterialsViews.com

ADVANCED
ENERGY
MATERIALS

www.advenergymat.de

PROGRESS REPORT

Lifetime of Organic Photovoltaics: Status and Predictions

Suren A. Gevorgyan,* Morten V. Madsen, Bérenger Roth, Michael Corazza, Markus Hösel, Roar R. Søndergaard, Mikkel Jørgensen, and Frederik C. Krebs

The results of a meta-analysis conducted on organic photovoltaics (OPV) lifetime data reported in the literature is presented through the compilation of an extensive OPV lifetime database based on a large number of articles, followed by analysis of the large body of data. We fully reveal the progress of reported OPV lifetimes. Furthermore, a generic lifetime marker has been defined, which helps with gauging and comparing the performance of different architectures and materials from the perspective of device stability. Based on the analysis, conclusions are drawn on the bottlenecks for stability of device configurations and packaging techniques, as well as the current level of OPV lifetimes reported under different aging conditions. The work is summarized by discussing the development of a tool for OPV lifetime prediction and the development of more stable technologies. An online platform is introduced that will aid the process of generating statistical data on OPV lifetimes and further refinement of the lifetime prediction tool.

1. Introduction

In order to prove that organic photovoltaic (OPV) can take a prominent position in the competitive market of emerging photovoltaic technologies today, it is vital to demonstrate that OPV have reached a competitive level in all the three aspects of performance: cost, efficiency and stability.[1] While the potentially low cost, low resource claims, and infinite scalability are the vital characteristics of OPV,[2–6] efficiency and stability remain in question. OPV already outperform all known PV technologies with respect to processing speed and materials consumption and the key question may now be: can a lower performance in terms of efficiency and stability be outweighed by significant outperformance in terms of speed and material parsimony?

Recent calculations of the electricity cost generated by OPV based technologies predict competitiveness with fossil fuels, at the level of 5% efficiency and 5 years of lifetime.[4] Today, the record efficiency values on lab scale OPV are reportedly in the range of 10–12%.[7] However, the actual technological

performance level, especially when considering large-scale mass-produced modules, is predicted to be significantly lower.[8] Nevertheless, based on recent advances in the upscaling of OPV manufacture[9–12] it is reasonable to assume that the mass production of modules with an efficiency of more than 5% is an achievable target today. Durability of OPV is however yet to be proven and demonstrated.

Due to core architectural differences between OPV and inorganic technologies[13] the established testing standards of the latter are not applicable to the former.[1] Hence, for many years the stability testing of OPV has primarily been based on customized procedures that vary from one laboratory to another, generating incomparable data.[14] Moreover, due to the complexity of the OPV device architectures[15] and a multitude of aging mechanisms taking place at the same time[16] the aging curve of OPV often takes a complex shape, which is difficult to model,[14,17] thus making the identification of a practical operational lifetime difficult or impossible.[18] As a result, even with a multitude of reported review articles discussing OPV stability [16,19–24] at hand, it is still challenging to identify where the technology stands in terms of lifetime. To address this it is necessary to create a yardstick – a generic marker that allows accurate rating and comparison of the lifetime for OPV, and thus enabling the gauging of progress over time. An additional complication that has arisen due to the significant improvements in OPV stability and durability in recent years is that the determination of OPV lifetimes has become an impractically long process, and establishing markers for both accelerated and real operational test conditions (if successful) would allow developing a prediction tool that could speed up the stability testing process and tackle this issue.

The groundwork towards creating such a marker was laid in 2011 at the International Summit on OPV Stability (ISOS) where the ISOS testing guidelines were decided upon and described for OPV technologies.[18] These guidelines were primarily aimed at harmonizing testing procedures among different laboratories by offering a set of indoor and outdoor tests with controlled conditions. This has helped to reduce variations in the reported results, making the aging studies of different laboratories more comparable.[25] While the ISOS tests harmonized the test conditions, the questions of how to generically determine the lifetime from aging curves of diverse shapes, and how to build a technique for predicting the lifetime based on accelerated tests remained.

Dr. S. A. Gevorgyan, Dr. M. V. Madsen, B. Roth,
M. Corazza, Dr. M. Hösel, Dr. R. R. Søndergaard,
Dr. M. Jørgensen, Prof. F. C. Krebs
Characterization Laboratory for Organic
Photovoltaics (CLOP)
Department of Energy
Technical University of Denmark
Frederiksborgvej 399, 4000 Roskilde, Denmark
E-mail: surg@dtu.dk

ADVANCED
ENERGY
MATERIALS
www.advenergymat.de

PROGRESS REPORT

www.MaterialsViews.com

The work presented here introduces a method by which a generic lifetime marker is assigned to aging curves of any shape, allowing the efficient comparison of various samples reported in the literature. The work encompasses meta-analysis of the lifetime data of a large amount of OPV devices and reveals the main bottleneck associated with their stability. The current status of OPV lifetimes is discussed and recent progress is highlighted. The general aim of this study is to aid the process of developing a prediction tool for determining the operational lifetime of OPV based on a series of recorded laboratory data.

2. Methods

2.1. Literature Meta-Analysis

Using the ScienceDirect search engine, a search for OPV lifetime reports was conducted. The search criteria were defined by combining the following key expressions: polymer, plastic, organic, solar cells, photovoltaics, stability, and lifetime. The search was conducted in March 2013 and returned around 2500 articles. A few more reports of outstanding lifetime performance reported at a later stage were added to the list during the process of developing this work.

The articles were added to an online database where further filtering was conducted to remove articles from the list that did not contain actual stability data of organic solar cells. This involved eliminating unrelated results and studies related to hybrid technologies. The filtering retained 303 articles, from which accurate stability data, plus device specifications, could be extracted and added to a lifetime database. This data was then further analyzed using an online exploration tool that is discussed in the following sections.

We cannot exclude the possibility that some reports on OPV lifetime studies that do fulfill the requirements for accuracy in the data and device descriptions were overlooked in the searching and filtering process, but we contend that our database is representative of the field. Small molecule OPV devices that are included here also may have fewer occurrences among the analyzed articles, either because they simply appear at a lower frequency than polymer based devices, or because the reporting tradition falls outside the data requirements of our method.

2.2. Lifetime Marker

In the field of OPV it has become customary to use the term lifetime to describe the T_{80} value (time when the sample degrades by 20% from initial performance) independent of the testing conditions. The same will be practiced throughout this document. However, one has to bear in mind that the actual term lifetime refers mainly to the performance of a photovoltaic sample under intended (typically outdoor) real operational conditions.

In the literature, the degradation of OPV samples is typically reported via aging curves of photovoltaic parameters – in most cases as a plot of power conversion efficiency (PCE)

Suren A. Gevorgyan is a senior scientist at the Technical University of Denmark. He was born in Armenia in 1982 and received his PhD from the Technical University of Denmark in 2010. From the early years of his career Suren has worked in the field of organic photovoltaics and specialized in characterization and stability improvements of these devices. His main research interests include standard testing, electro-optical characterization and device engineering of organic solar cells.

Morten V. Madsen received his PhD degree in the stability and degradation of organic solar cells in 2012 from the Technical University of Denmark and currently works as a researcher. His interests include the stability and degradation of organic solar cells, product integration, data management, knowledge dissemination, and online teaching. Morten co-created the Coursera course Organic Solar Cells – Theory and Practice and he has been involved in the development of several additional e-learning initiatives.

Frederik C. Krebs received a PhD in 2000 and was appointed full professor in 2010 at the Technical University of Denmark. Since 2000, he has been working on polymer photovoltaics. His research interests are printed photovoltaics with low environmental impact, and the interplay between different disciplines that enable the use of polymer solar cells in energy systems. His academic work spans from materials procurement, manufacture, upscaling, life cycle analysis, and grid connection through use of novel electronics.

as a function of time. In rare cases spectral absorption and quantum efficiency are also utilized. The shapes of the reported aging curves often vary significantly and **Figure 1**a shows a few typical examples, with curve 1 presenting the most commonly observed "hockey stick" shape. The letter E stands for the aging indicator (for example PCE). As discussed in the introduction, the reason for such diversity is
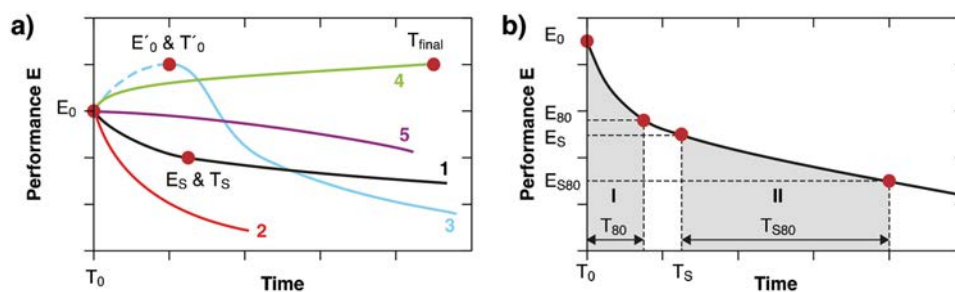
Figure 1. a) Examples of various shapes of aging curves taken from real data. b) Example of identifying the best pair describing the stability of the sample.

linked to the fact that several competing aging mechanisms often take place at the same time, resulting in variations in aging rate. Each of these mechanisms may be expressed to varying degrees, depending on the conditions of the test. As a result, the comparison of lifetimes based on such curves is rather challenging. A method was therefore developed where a generic lifetime marker was identified for each reported curve by means of a set of criteria. The method involved a number of steps described in **Table 1**.

The importance of having a pair of $[E_0;T_{80}]$ values representing the sample lifetime, rather than just the time parameter, comes from the fact that the already degraded device may show significantly slower degradation compared to the freshly prepared device, and a comparison of only the lifetime between the two can be misleading. It is important that the history of devices that are to be compared is known and is as similar as possible.

In the literature, extrapolation is often utilized to estimate the lifetime, if aging did not reach the T_{80} threshold during the course of the experiment.[26–28] Although such a procedure can give a hint towards the potential lifetime of the sample, extrapolation is often very inaccurate and cannot be used reliably in a scientific report, especially when it is extended to more than once or twice the duration of the actual measurements.[25] Moreover, there are often failure mechanisms that do not appear at the initial stage of OPV degradation, but cause a sudden acceleration of degradation at a later stage. An example is the gradual deterioration of the encapsulation of the samples, which does not affect the performance initially, but drastically accelerates the aging when delamination or cracking of the encapsulant takes place.[17] Thus, here, no data has been extrapolated for the determination of the lifetime, but rather the duration of the experiment was used as the maximum possible lifetime, denoted as T_{final}.

Table 1. The list of steps for determining the lifetime marker.

| Parameters	Method
Determination of starting point E_0 & T_0 E_0 – initial performance T_0 – initial time	T_0 & E_0 pair is either chosen at the first measurement point, or if the curve has an initial increase followed by a reduction (such as the curve 3 in Figure 1a) then T_0 & E_0 is set at the maximum point.
Determination of stabilized section E_S & T_S E_S – performance at the start of stabilized section T_S – starting time of stabilized section	If after a certain point the aging curve enters into a more stable phase (commonly observed during solar cell aging), then a second pair of starting values T_S & E_S is identified, typically chosen at a point from where the aging rate almost doesn't change anymore, as shown on curve 1 in Figure 1a.
Determination of T_{80} and T_{S80} T_{80} – time when performance reaches 80% of E_0 T_{S80} – time when performance reaches 80% of E_S	T_{80} (or if applicable T_{S80}) is determined by subtracting T_0 (or T_S) from the time when 80% of E_0 (or E_S) is reached. Figure 1b highlights the areas determined by T_{80} and T_{S80}
Lifetime marker $[E_0;T_{80}]$ or $[E_S;T_{S80}]$	The largest area among I and II in Figure 1b (part of the curve where the sample produces the largest amount of energy) will then determine the pair that will describe the lifetime. The simple geometrical calculations reveal that the ratio of the areas of the trapezoids I and II are proportional to the ratio of the areas of the rectangles defined by the products of $E_0 \times T_{80}$ and $E_S \times T_{S80}$. Thus the lifetime marker can be mathematically identified according to these rules: if $\dfrac{[E_0 * T_{80}]}{[E_S * T_{S80}]} \geq 1$ then the marker is $[E_0;T_{80}]$ if $\dfrac{[E_0 * T_{80}]}{[E_S * T_{S80}]} < 1$ then the marker is $[E_S;T_{S80}]$
Exceptions	Exceptions are made in the following cases: • If E_S is less than half of E_0, in which case the sample is considered to have degraded before stabilization (see curve 2 in Figure 1a, then $[E_0;T_{80}]$ is chosen by default to represent the lifetime. • If the measurements has been stopped prior to reaching the 80% threshold then "$T_{final} - T_0$" or "$T_{final} - T_S$", where T_{final} is the point of last measurement (see curve 4 in Figure 1a is chosen instead to represent the minimum possible lifetime.

ADVANCED
ENERGY
MATERIALS
www.advenergymat.de

www.MaterialsViews.com

PROGRESS REPORT
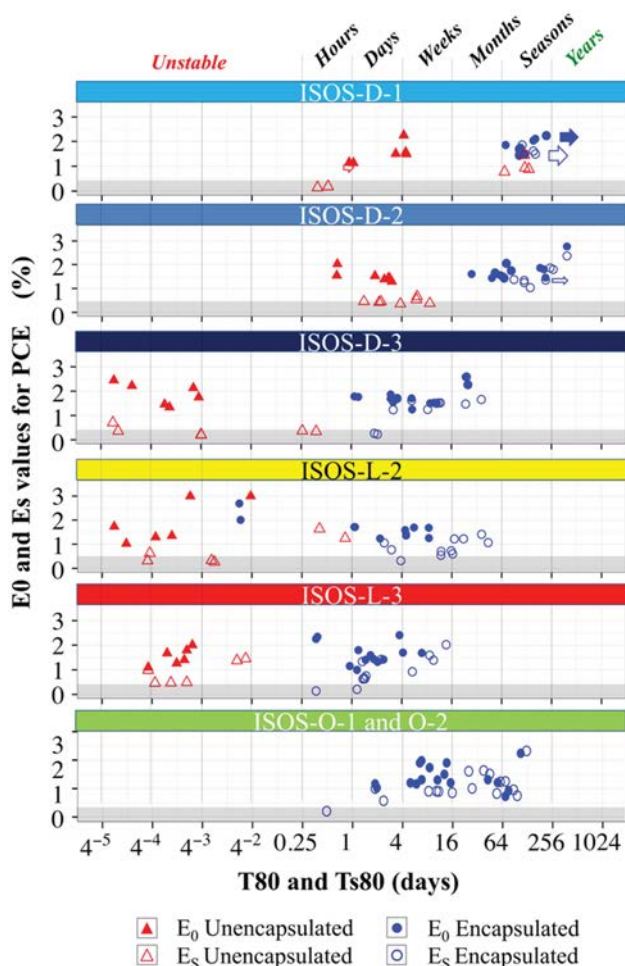
Figure 2. The o-diagram presenting [E_0;T_{80}] and [E_S;T_{S80}] values for all the tested samples under different ISOS test conditions. For the conditions of the tests see ref. [18]. The blue circles and the red triangles represent the devices with and without encapsulation, respectively. The arrow shows the data where T_{final} was used instead of T_{80}. Reproduced with permission.[30] Copyright 2015, Elsevier.

2.3. Comparing Lifetimes via the O-Diagram

After identifying all lifetime markers of all the reported aging curves according to the method described above, the values were inserted into a scatter plot, called the o-diagram, as described earlier (the '"o" stands for OPV).[25,29] The purpose of the diagram is to categorize the performance of the samples by means of simple time units, which makes the lifetime comparison straightforward. As an example, **Figure 2** shows the comparison of PCE for a number of differently processed OPV samples, tested under various ISOS test conditions, conducted in an earlier study.[29,30] The X-axis represents the time in logarithmic format with base 4, which allows its association with common time units as shown in the top part of the figure. The Y-axis represents the initial performance. In this plot, [E_0;T_{80}] and [E_S;T_{S80}] are shown via solid and open labels, respectively. The diagram allows the reported lifetime data to be gauged, and its progress to be followed based on the time units. Any data that exceeds the 'years' category, is considered to have durability on an industrial level.

In the earlier study a comparison of the performance of samples under different ISOS test conditions was made and it was concluded that, after encapsulation, the studied technologies could endure only weeks or months of accelerated indoor light exposure, but reached a shelf life of years. Meanwhile, in outdoor tests the samples showed intermediate performance.[30] Thus, the diagram allowed for the establishment of a link between the different tests. Although in the latter case the tests were limited to only a few OPV architectures and to outdoor tests in only one geographic location (Denmark), expanding the same concept to a large variety of samples and test conditions will eventually allow for the development of a generic empirical prediction tool. The o-diagram is also utilized in this study for comparing the literature data. The results are discussed in the following sections.

3. Status of OPV Lifetimes

3.1. All Data

Each scanned article contained stability data for around 3 samples on average, which sums to approximately 1000 data points from the 303 articles. **Figure 3** shows the o-diagram as PCE versus lifetime for all the data. The adjacent plots show the data distribution in terms of PCE and lifetime. The large majority of samples have a PCE distributed within 4%, due to the predominance of poly-3-hexylthiophene (P3HT) based devices (discussed in Section 3.4). In terms of stability, the lifetime of OPVs spans from unstable to years, with the largest portion of data falling in the range of months. Only a few reach the level of years. Note that the data is primarily based on literature reports up to March 2013 with a few additions of the best stability reports from 2014 and 2015. Additionally, it is important to note that some of the data are limited by the duration of the conducted experiment (T_{final}) rather than T_{80}. The lifetime data was also plotted against the publication year, as shown in **Figure 4**, which demonstrates the progress of OPV lifetimes in recent years. The plot contains samples tested both under light (green triangles) and in the dark (blue circles). The following sections further analyze the presented data in terms of device geometries, materials and testing conditions.

3.2. Device Geometry: Normal versus Inverted

The stack order of the organic solar cell layers is typically categorized into two groups: normal and inverted. In the former, the front transparent electrode is the anode and the back electrode is the cathode, while in the latter the electrodes are reversed. The differentiation among the two is, however, mostly rooted in the fact that the normal structure typically employs a low work function back electrode, such as aluminum (Al) and the inverted structure utilizes high work function metals, such as silver (Ag) or gold (Au). The vast majority of the lifetime data reported so far are based on samples that are sandwiched between a substrate (often glass) and an evaporated or printed top electrode, In such a nonsymmetrical geometry the bottom is protected by the substrate, while the top electrode is the first
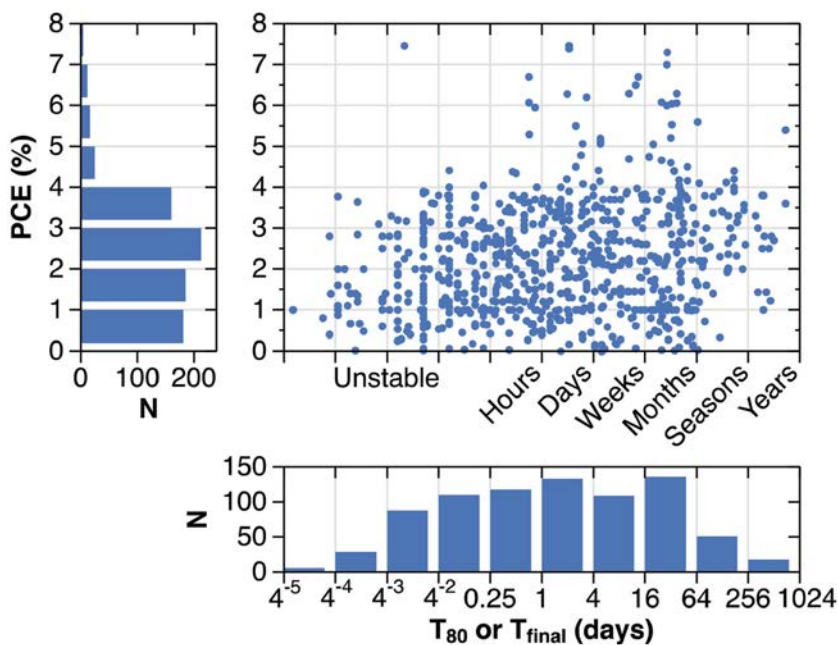
Figure 3. Total data collected from the literature presented in o-diagram. The left side histogram show the distribution of the data points in the efficiency bins, while the lower histogram shows the lifetime distribution of the data in the time bins.

to be exposed to the external environment and hence, is the first to play a dominant role in the aging of the device. For this reason the alterations in the geometry of the devices can result in significant differences in the stability of the samples.[31]

In the normal structure one of the most commonly reported failure mechanisms is the reactivity of Al when the latter is in contact with humid air. As a result, an oxide layer is developed at the inner interface, which resists the charge collection process in the device.[32–36] Especially in the case when there is no intermediate layer between the cathode and the photoactive layer (PAL), chemical modifications at the interface can further deteriorate the PAL and accelerate aging.[33–35] Conversely, Ag and Au are quite stable when exposed to the environment and appear to be less reactive towards organic materials. This
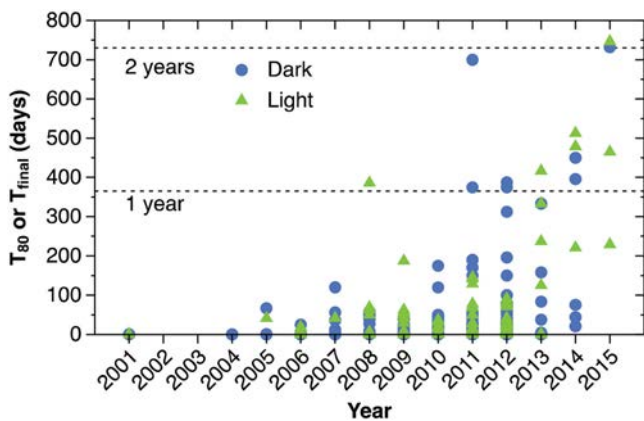
is why it is commonly believed that inverted structures are inherently more stable compared to normal structures.[32,34,37–39] However, it was shown that oxygen and water penetration through Al and Ag have different natures,[40–43] and that ultimately Al can be a more effective barrier against oxygen diffusion compared to Ag.[31] This has raised questions about which aging mechanisms dominate in the two structures, and which structure is intrinsically more stable under real operational conditions.

To inform this, the reported literature data were grouped according to the sample geometry and plotted in an o-diagram for comparison, as shown in **Figure 5**a–d. The plots on the left and right correspond to the data measured in the dark and under light respectively. For clarity, the data is separated into unencapsulated (a,b) and encapsulated (c, d) samples. For easier interpretation, each scatter plot is supported by an adjacent distribution curve. The red triangles and blue squares show the inverted and normal structures, respectively. The open squares show the cases where the cathode is directly applied onto the PAL. In accordance with expectations, the inverted structures (red squares) show significantly better stability for unencapsulated samples, and to some extent for encapsulated devices, for the tests conducted in dark (left plots in Figure 5). This however does not seem to be the case for the tests conducted under light (the plots of the tests conducted under illumination contain data for samples tested mainly under light sources with a full solar spectrum, that have appropriate amounts of UV light). Since the dark tests are typically conducted under ambient conditions with some humidity content, it is reasonable to assume that Al will react with the humidity and that this becomes the dominating degradation mechanism in the normal geometry device, as discussed above. Although oxygen diffusion is stronger in the inverted structures, oxygen alone does not seem to cause much damage to the device when in the dark, and since Ag and Au remain inert towards humidity, the inverted structures show exceptional stability in the absence of light. When illuminated, the heat of the solar simulator generates a dry environment around the sample. This drastically reduces the effect of humidity on the device performance. The presence of light and especially a UV-component, conversely, accelerate the reaction with oxygen,[44] which rapidly degrades the unprotected devices with inverted structures. Meanwhile, the normal structures are effectively protected from oxygen by the Al capping layer. Further proof of this argument can be found in the fact that when the devices are encapsulated, the oxygen diffusion becomes hindered in both geometries, resulting in equally stable performance (Figure 5d). It is important to note that the samples where the top Al electrode is directly applied onto the PAL show similar lifetimes under illumination independent of whether the device is encapsulated or not (Figure 5b,d). This suggests that, despite the elimination of oxygen and water, the Al/PAL interface remains detrimental to the performance of the device
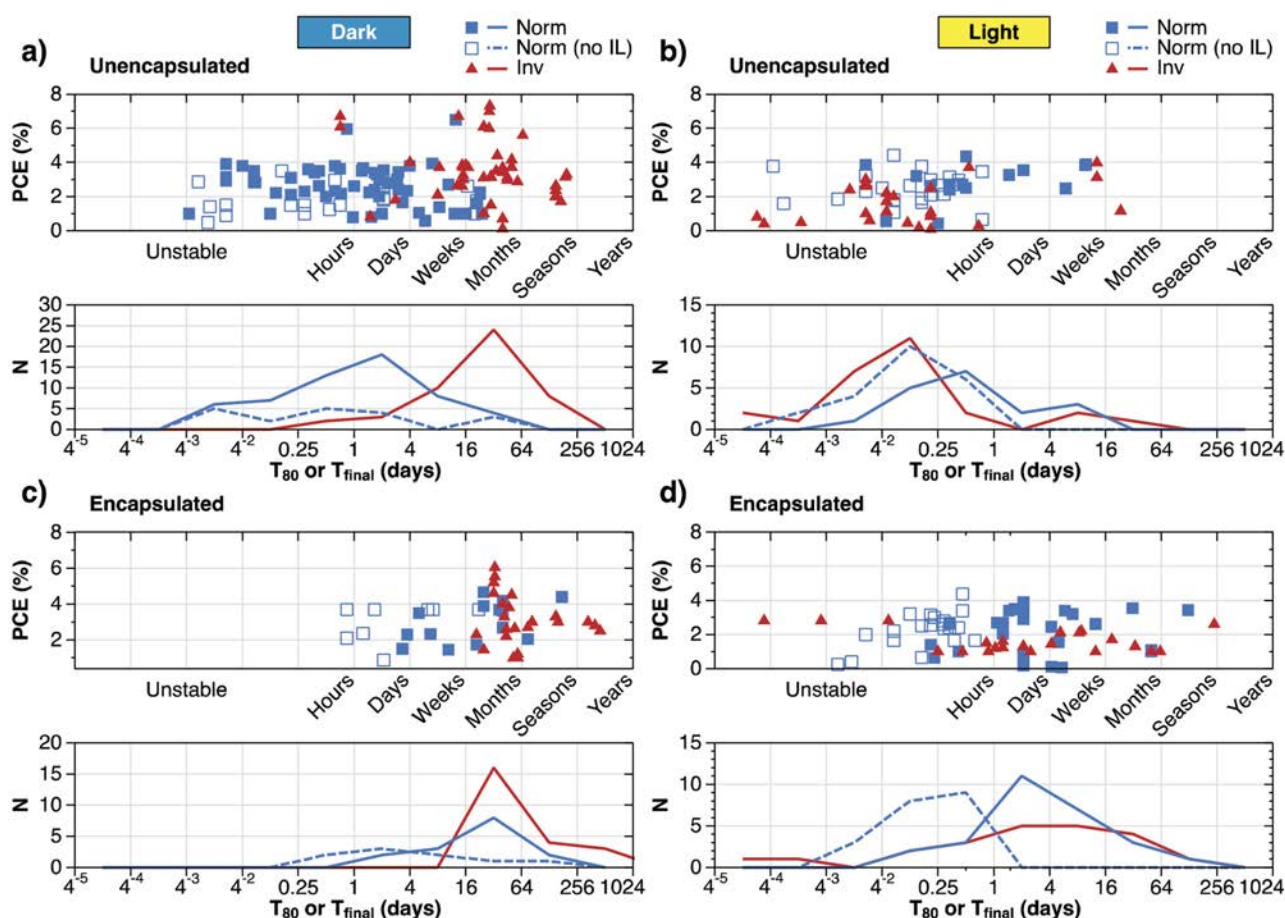

Figure 4. Scatter plot of reported lifetimes per year with the green triangles representing the samples tested under light and the blue circles representing the tests in darkness. The dashed lines correspond to the one and two year thresholds.

ADVANCED
ENERGY
MATERIALS
www.advenergymat.de

PROGRESS REPORT

www.MaterialsViews.com
Materials Views

Figure 5. Distribution of the lifetime for unencapsulated (a,b) and encapsulated (c,d) samples with normal (blue squares) and inverted (red triangles) structures tested under illumination (b,d) and in the dark (a,c). Each data point corresponds to one aged sample reported in the literature. The open blue squares correspond to normal geometry devices where the top electrode is directly applied onto the PAL. The bottom plots show the distribution of the data in a histogram format, where the y-axis represents the number of the reported data points.

and therefore protective intermediate layers are vital for optimal performance of the normal structures. However, special care must be taken when applying intermediate layers such as metal oxides or even Ag, as a recent study demonstrated that Al may still penetrate and react with intermediate layers resulting in device performance deterioration.[45]

The results of the device geometry analysis suggest that when considering real operational (outdoor) conditions in an environment with the presence of humidity, oxygen and light, both normal (Al) and inverted (Ag or Au) structures are prone to rapid degradation when unprotected, but can perform equally well when encapsulated.

It is important to stress that the final OPV products are envisioned to have a geometry compatible with roll-to-roll manufacturing[46,47] and economically viable symmetric packaging.[5,48] The latter does not include extra substrates or superstrates. Most of the reported devices analyzed have structures that do not meet these standards, so it is hard to predict what role the electrodes or the geometry will eventually play in a real OPV product. However, it is obvious that in a real product with symmetric encapsulation, the front transparent electrode will present equal or more important stability challenges compared

to the back electrode. Thus, it is important to harmonize the research with the true vision of OPV and address the stability issue of the devices from the perspectives of symmetric encapsulation and roll-to-roll compatible processes.

3.3. PEDOT:PSS Studies

A common debate in the field of OPV is the role of poly(3,4-ethylenedioxythiophene)-poly(styrenesulfonate) PEDOT:PSS in the aging of devices.[49] PEDOT:PSS is widely used due to its tunable intermediate work function, which allows appropriate alignment of the highest occupied molecular orbital (HOMO) of the donor material in the PAL with the work function of the electrode. Indium tin oxide (ITO)/PEDOT:PSS is the most commonly used combination typically utilized as an anode in the OPVs with normal geometry. In such a combination, apart from tuning the energy levels, PEDOT:PSS additionally smooths the rough surface of the ITO, eliminating possible shunts in the device, and improves wettability during the solution processing of the active layer.[21] In the devices with inverted geometry PEDOT:PSS is typically used to align the work function of the

top metal electrode (such as Ag or Au) and the active layer.[50] In addition, in the case of printed electrodes PEDOT:PSS protects the active layer from harmful solvents used, for example, in the silver paste.[51] In a recent report, PEDOT:PSS was reported in a cathode combination where it was used to smooth the Ag grid front cathode for further coating of the ZnO electron transport layer.[52] It has been well established that, despite the several benefits, PEDOT:PSS has a negative effect on OPV stability.[16,21,22] Although the aging mechanisms have not been completely understood, the hygroscopic nature of PEDOT:PSS is commonly linked to its aging.[43,53–55] In a humid environment this results in three distinct symptoms:

- PEDOT:PSS tends to lose conductivity due to water uptake[54]
- PEDOT:PSS accelerates the corrosion of the metal electrodes[56]
- The acidity arising from PSS is resulting in etching of ITO[43,53,57]

While the reaction between PEDOT:PSS and high work function electrodes such as Ag is much less pronounced, it is still believed that PEDOT:PSS is also a source of degradation in inverted device combinations.[35,37] Moreover, it was recently demonstrated that UV light is also detrimental for PEDOT:PSS conductivity.[58]

Nevertheless, despite the multitude of reported aging mechanisms of PEDOT:PSS, there have been instances where PEDOT:PSS was reported not to affect the aging rate of the devices,[32] or even to improve the stability when compared to metal oxides.[26] Thus, in order to understand this controversy, the literature data was analyzed with regard to the use of PEDOT:PSS in the devices, as shown in **Figure 6**. The data was separated into unprotected (a, b) and encapsulated (c, d) samples tested in dark conditions (left) or under illumination (right). The samples were further distinguished according to the positioning of PEDOT:PSS in the device structure in the following way:

- Normal geometry where PEDOT:PSS is between the transparent anode and the PAL (PEDOT-n)
- Inverted geometry where PEDOT:PSS is between the back electrode and the PAL (PEDOT-i)
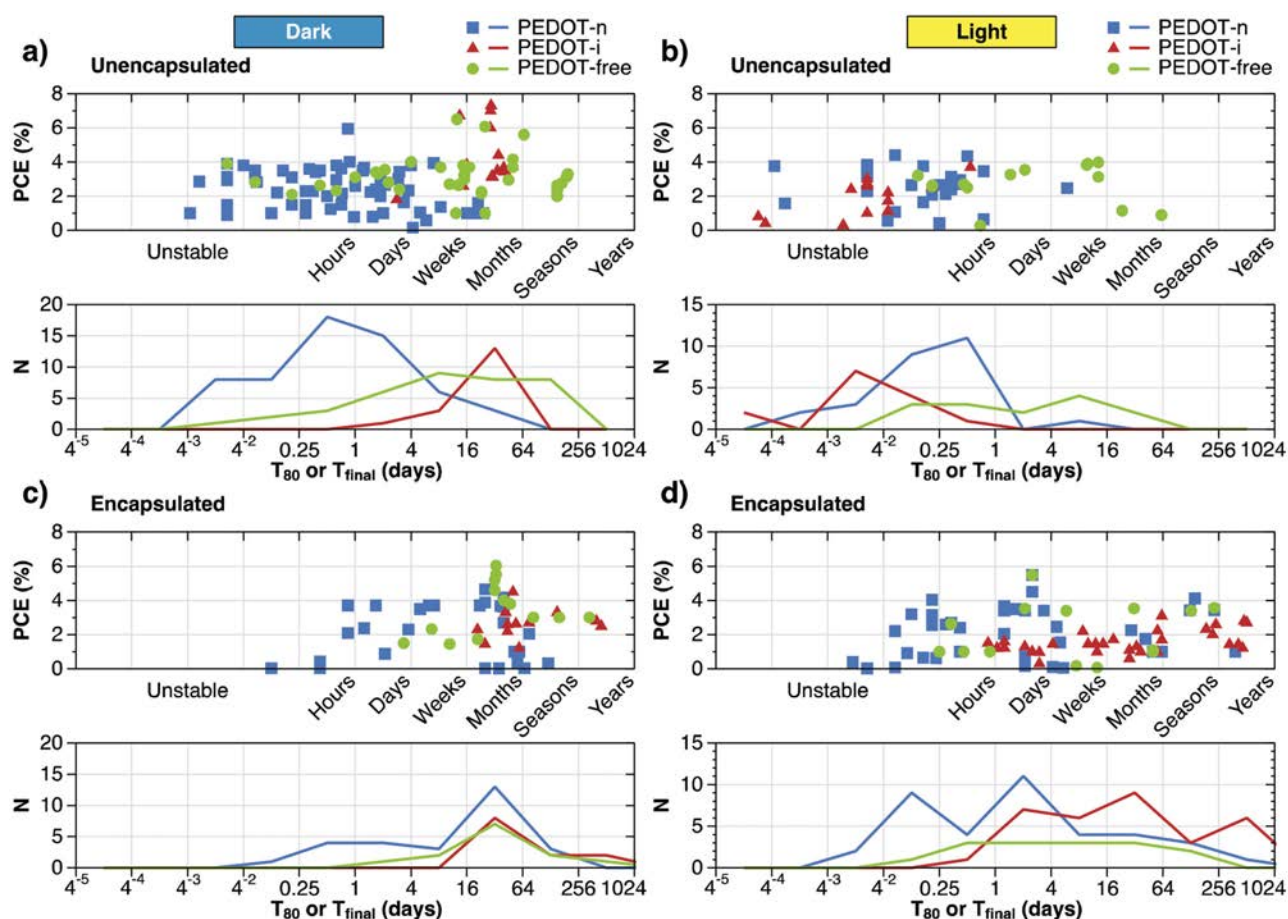- PEDOT:PSS free devices (PEDOT-free)

Figure 6. Distribution of lifetimes for unencapsulated (a,b) and encapsulated (c,d) samples grouped into three categories: samples with PEDOT:PSS between anode and the PAL in the normal architecture (blue squares), between the PAL and anode in the inverted architecture (red triangles) and PEDOT:PSS free samples (green circles). Plots are grouped according to dark (a,c) and illumination (b,d) tests. Each data point corresponds to one aged sample reported in the literature. The bottom plots show the distribution of the data in a histogram format, where the y-axis represents the number of the reported data points.

It is apparent that the unprotected devices with PEDOT:PSS as the first intermediate layer (normal geometry) have the shortest lifetime when stored in the dark. This is in accordance with the expectations that in a humid environment PEDOT:PSS will gradually absorb water, accelerate the aging of the cathode and react with ITO, as discussed above. Conversely, the samples with PEDOT:PSS integrated between the active mixture and the top electrode (inverted geometry) show a very good stability in the dark, which is in accordance with earlier studies claiming that PEDOT:PSS alone is quite stable under ambient dark conditions and becomes harmful only when in contact with ITO or Al.[56] In the illuminated tests of the unprotected samples, the inverted structures tend to be the least stable, which is partly ascribed to the low barrier properties of the top electrode towards the oxygen diffusion (as discussed above) and partly due to the aforementioned fact that PEDOT:PSS is vulnerable to UV light. The humidity in this case is significantly lower due to the heat generated by the illumination and thus, is less vital for the aging of the devices. The unencapsulated PEDOT:PSS free samples instead show relatively stable performance both in the dark and under illumination, independent of whether a normal or inverted geometry is utilized. This suggests that eliminating PEDOT:PSS from the stack is likely to improve the intrinsic stability of the devices. For the encapsulated samples, the lifetime difference between the three structures almost diminishes. This can perhaps be explained by the fact that the encapsulation significantly reduces the level of water and oxygen accessing the device structure. Additionally, typical encapsulation materials are either glass (with reduced transmission in the UV range) or plastic materials with a UV-filter, which to some extent protect the device layers from the UV-irradiation. Thus, in the encapsulated devices the aging mechanisms associated with PEDOT:PSS become negligible, resulting in similar performance of the samples with and without PEDOT:PSS on the given time scales. This explains the aforementioned controversial reports of stable PEDOT:PSS based devices, since the latter were encapsulated. Such a similar performance can however be deceptive since it is likely that aging processes associated with PEDOT:PSS will eventually appear over longer time scales, even in encapsulated samples, ultimately contributing to the device degradation. Thus, eliminating the PEDOT:PSS from the stack remains one of the primary areas of interest in the development of a stable device.

3.4. Role of the Photoactive Layer

The photoactive layer (PAL) plays an important role in the stability of the devices, as its deterioration will directly reflect on the light absorption and charge generating properties of the device. A typical PAL consists of a conjugated polymer acting as a donor and a fullerene based derivative acting as an acceptor. The polymer, the fullerene, and the morphology of their mixture are all susceptible to degradation.[16,21,22] Factors such as oxygen, water, light, or elevated temperature can both single-handedly, and especially when combined, rapidly deteriorate the PAL. Different materials in the PAL react differently to such external factors, which makes the study of the aging processes rather complex. Although many scenarios have been proposed

in literature, the key mechanisms of degradation in the PAL are not yet fully understood. Some of the commonly reported failure mechanisms of the PAL are as follows:

- Photochemical scission of the conjugated polymer chain,[44,59] typically initiated by oxygen and (UV-) light
- Oxygen doping of the PAL and generation of traps,[60,61] caused by oxygen and accelerated by light.
- Diffusion of the metal electrodes into the PAL and reactions with the polymer,[41,42,62] initiated by humidity, oxygen and light.
- Morphological reorganization of the polymer/fullerene mixture and deterioration of the interface,[63–65] initiated mostly by temperature and light, but also possibly by oxygen and humidity.

The degradation of the PAL depends greatly on the testing conditions. Typically, most of the PAL aging mechanisms are strongly accelerated when exposed to light.[66,67] For some polymers such as the polyphenylenevinylene (PPV) derivatives, rapid aging in the dark has also been reported.[68,69] Temperature is less detrimental since the typical device temperatures during operation in realistic test condition are below 100 °C. However, in some cases during the production process high temperature (above 100 °C) annealing steps are utilized, which can result in thermal aging of the polymer[63–65] and thus the thermal stability of the polymers becomes vital for the device lifetime.

The dominating aging mechanisms also greatly depend on the type of materials used in the PAL as mentioned earlier. PPV based polymers that were initially utilized for polymer solar cells were proven to be very unstable.[68–70] Those were succeeded by polythiophene based materials. Especially the polymer poly-3-hexylthiophene (P3HT) combined with the fullerene derivative phenyl-C61-butyric acid methyl ester (PCBM),[71] demonstrated significantly better lifetimes and have remained the primary choice in studies for many years This mixture still serves as an excellent reference. However, the efficiency of devices based on P3HT was typically limited to < 4%. Therefore the research for better materials continued, and recently many new polymers with higher efficiencies have emerged,[72] some of which (i.e., benzothiadiazole-based polymers, such as poly[N-9″-hepta-decanyl-2,7-carbazole-alt-5,5-(4′,7′-di-2-thienyl-2′,1′,3′-benzothiadiazole) (PCDTBT) or poly[(4,4-bis(2-ethylhexyl)-4H-cyclopenta[2,1-b;3,4-b]dithiophene-2,6-diyl-alt-2,1,3-benzothiadiazole-4,7-diyl] (PCPDTBT), see **Table 2**) were claimed to be intrinsically more stable than P3HT.[73,74]

In order to understand to what extent the PAL determines device stability, the literature stability data was plotted against the donor materials used in the PAL. **Figure 7** shows four plots corresponding to the tests conducted in the dark (left plots) and under illumination (right plots) for the unprotected samples (a,b) and encapsulated samples (c,d). The different PALs are highlighted in terms of:

- P3HT
- Small molecules
- High power conversion efficiency polymers denoted as h-PCE
- Others

Table 2. High efficiency polymers tested either in dark or light conditions. Among all the compounds PCDTBT is the most frequently reported polymer.

Name	Conditions	Description
PCDTBT[27,28,74–77]	Light, dark	poly[N-9″-hepta-decanyl-2,7-carbazole-alt-5,5-(4′,7′-di-2-thienyl-2′,1′,3′-benzothiadiazole)
PCPDTBT[73]	Light, dark	poly[(4,4-bis(2-ethylhexyl)-4H-cyclopenta[2,1-b;3,4-b]dithiophene-2,6-diyl-alt-2,1,3-benzothiadiazole-4,7-diyl]
BTI-BDT[78]	Light	bithiophene imide and benzodithiophene based copolymer
PDTSTPD[79]	Dark	poly(4,4-bis(2-ethylhexyl)-dithieno[3,2-b:2′,3′-d]-silole and N-octyl-thieno[3,4-c]pyrrole-4,6-dione)
PBDTTPD[80]	Dark	poly({4,8-di(2-ethylhexyloxy) benzo[1,2-b:4,5-b′] dithiophene – 2,6-diyl) – alt – ({5-octylthieno-[3,4-c] pyrrole – 4,6-dione-1,3-diyl)
PFDCTBT-C8[81]	Dark	poly(fluorenedicyclopentathiophene-alt-benzothiadiazole) with octyl side chains
a-PTPTBT[82]	Dark	Poly(thiophene-phenylene-thiophene – 2,1,3-benzothia-diazole)

Small molecule based devices typically comprise phthalocyanine-based materials (such as copper phthalocyanine (CuPc), zinc phthalocyanine (ZnPc), subphthalocyanine (SubPc), chloro aluminum phthalocyanine (ClAlPc) or Pentacene, each combined with either C60 or PCBM.[60] The materials representing the h-PCE devices are listed in Table 2. Among these PCDTBT was the most popular. h-PCE polymers were mainly used in mixtures with phenyl-C71-butyric acid ([70]PCBM) while P3HT polymers and most of the other polymers were mainly reported in blends with [60]PCBM (on rare occasions indene-C$_{60}$ bis-adduct ICBA was reported). A study of the effect of acceptors on lifetimes was not feasible in this case due to the dominance of [60]PCBM in the reported data.

From Figure 7 it is obvious that the P3HT:PCBM mixture is by far the most frequently studied blend. However, since current progress is being made mostly with h-PCE materials, this is likely to evolve in the years to come. Nevertheless, a distinct difference can be identified in the unprotected devices tested under illumination (Figure 7b), where the h-PCE polymers yield the most promising stability, while the small molecule devices show the shortest lifetimes. The differences become less pronounced for the dark tests, which points to the fact that light plays a vital role in the aging of the PAL. The difference almost completely disappears for the encapsulated devices. The reason is that the encapsulation significantly slows the diffusion of oxygen and water inside the device and, although the aging of the PAL still takes place, the difference becomes undetectable on the observed time scales.

It is important to note that some of the samples, although reported to present exceptional stabilities (beyond a year), often failed due to packaging and electrode deterioration rather than the PAL, while the post analysis showed that the PAL stayed almost intact after long-term tests.[17] Moreover, the wide distribution of the lifetimes of P3HT:PCBM based devices (Figure 7d), from minutes to years, is evidence that aging is not determined mainly by the PAL. The other parts of the device

(as discussed in previous paragraphs) can be more detrimental. This suggests that the current photoactive materials and especially the new h-PCE polymers may provide exceptional stability for several years or more and that the lifetime of OPVs is limited by failures in other parts of the device. Thus, in order to develop a stable technology it is of great importance to focus the research not only on the PAL, but to study all the parts of the OPV device and the encapsulation in order to identify the weakest links that most affect stability.

3.5. Best Structures

Figure 8 shows the structures of the unencapsulated samples with the best intrinsic stabilities reported in the dark (left hand image) and under illumination (right hand image). The top histograms shows the lifetime and the tables highlight the materials used in the structures, as well as the PCE values corresponding to the performance at the start of the stabilized part of the aging curves (E_S value). The arrows in the lifetime histograms distinguish the data that is limited by T_{final} (devices that did not reach T_{80}). The error bars show the performance distribution of a few devices with similar structures. From the plot on the right it is obvious that most of the stable devices tested under illumination do not contain a PEDOT:PSS layer and use Al as capping layer. It is worth mentioning, however, that the sample with the best lifetime tested under light (Figure 8 right hand side) suffered from a strong burn in with almost 50% loss of the performance prior to stabilization. This is possibly due to the diffusion of Al through the silver, as was reported recently in a different study.[45] In the dark tests, devices with PEDOT:PSS appear more frequently, yet they significantly underperform compared to the PEDOT:PSS-free samples. In addition, the majority of the dark tests have winning samples that utilize Ag or Au instead of Al. All these results corroborate well with the discussions of device geometry and PEDOT:PSS in sections 3.2 and 3.3.

3.6. Device Encapsulation

It has been estimated that the packaging has the largest share in the total material cost of the OPV modules, reaching as high as 60% of the cost.[5] Thus, cost reductions of the encapsulation can play a major role in the economy of OPV technologies and thorough studies of cheap materials and processing for encapsulation are of high importance. To contribute to such studies, analyzes were conducted of what has been reported in the literature with regards to the OPV device packaging and protection methods. The analysis revealed that many of the reports contained very limited information about the encapsulation procedures, describing in most cases only the type of the encapsulant, such as rigid glass or flexible polyethylene (PET), without specifying further details. Meanwhile, factors such as adhesive, encapsulation geometry (edge sealing), and the level of electrode protection that can play an important role in the device stability,[17,29,96–98] were often simply omitted. In some reports it was even not possible to identify whether the studied samples were encapsulated at all. This possibly comes from the
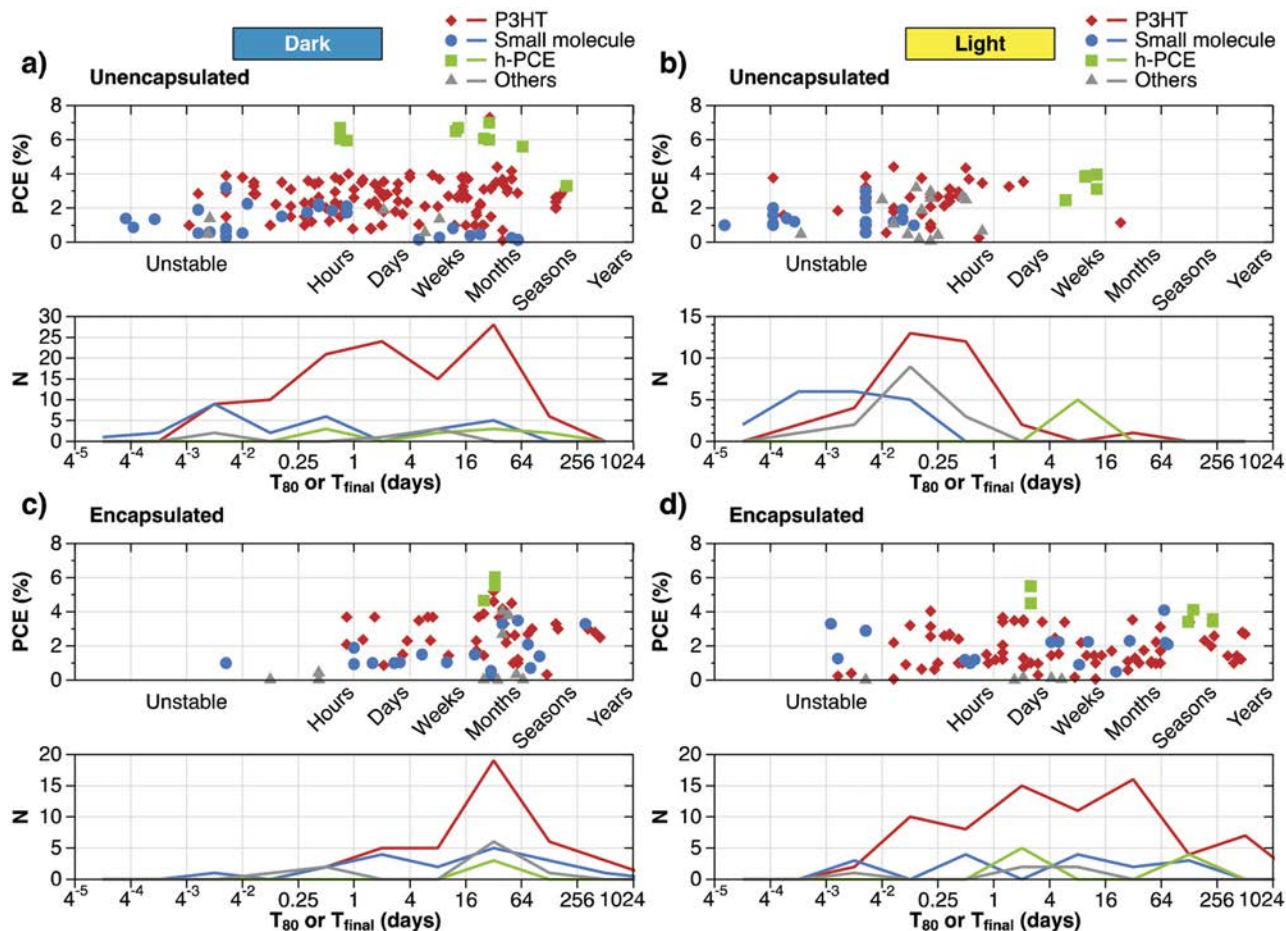
ADVANCED
ENERGY
MATERIALS

www.advenergymat.de

PROGRESS REPORT

www.MaterialsViews.com

Figure 7. Distribution of lifetime for samples grouped according to the photoactive layer categories: P3HT based (red diamonds), small molecule based (blue circles), high efficiency (green squares), others (grey triangles). a) Dark test of non-encapsulated samples, b) light tests of non-encapsulated samples, c) dark tests of encapsulated samples, and d) light tests of encapsulated samples. The data is presented via the scatter plot (o-diagram) and the corresponding histogram below each plot.
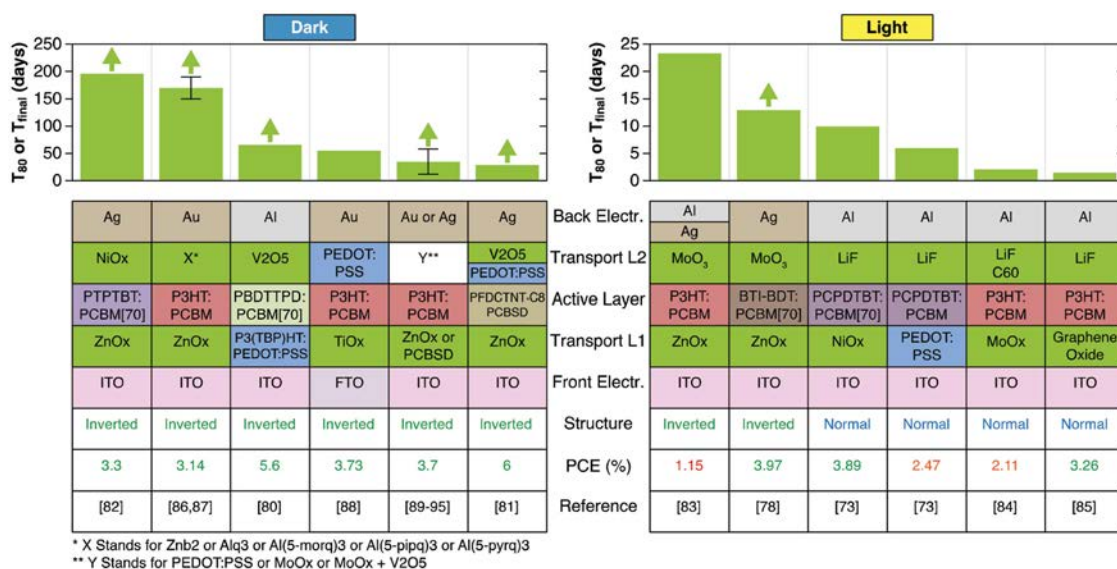

	Dark						Back Electr.	Light					
Back Electr.	Ag	Au	Al	Au	Au or Ag	Ag	Back Electr.	Al Ag	Ag	Al	Al	Al	Al
Transport L2	NiOx	X*	V2O5	PEDOT: PSS	Y**	V2O5 PEDOT:PSS	Transport L2	MoO₃	MoO₃	LiF	LiF	LiF C60	LiF
Active Layer	PTPTBT: PCBM[70]	P3HT: PCBM	PBDTTPD: PCBM[70]	P3HT: PCBM	P3HT: PCBM	PFDCTNT-C8 PCBSD	Active Layer	P3HT: PCBM	BTI-BDT: PCBM[70]	PCPDTBT: PCBM[70]	PCPDTBT: PCBM	P3HT: PCBM	P3HT: PCBM
Transport L1	ZnOx	ZnOx	P3(TBP)HT: PEDOT:PSS	TiOx	ZnOx or PCBSD	ZnOx	Transport L1	ZnOx	ZnOx	NiOx	PEDOT: PSS	MoOx	Graphene Oxide
Front Electr.	ITO	ITO	ITO	FTO	ITO	ITO	Front Electr.	ITO	ITO	ITO	ITO	ITO	ITO
Structure	Inverted	Inverted	Inverted	Inverted	Inverted	Inverted	Structure	Inverted	Inverted	Normal	Normal	Normal	Normal
PCE (%)	3.3	3.14	5.6	3.73	3.7	6	PCE (%)	1.15	3.97	3.89	2.47	2.11	3.26
Reference	[82]	[86,87]	[80]	[88]	[89-95]	[81]	Reference	[83]	[78]	[73]	[73]	[84]	[85]

* X Stands for Znb2 or Alq3 or Al(5-morq)3 or Al(5-pipq)3 or Al(5-pyrq)3
** Y Stands for PEDOT:PSS or MoOx or MoOx + V2O5

Figure 8. Device structures of unencapsulated samples showing the best lifetimes tested in dark (left)[80–82,86–95] and under light (right).[73,78,83–85] PCE represents the values at the point of stabilization of the aging curve (E_s value). The arrows in the histograms above distinguish the data that are based on T_{final} rather than T_{80} values. The error bars show the spread of the data for a few devices with similar structures.

www.MaterialsViews.com

ADVANCED
ENERGY
MATERIALS
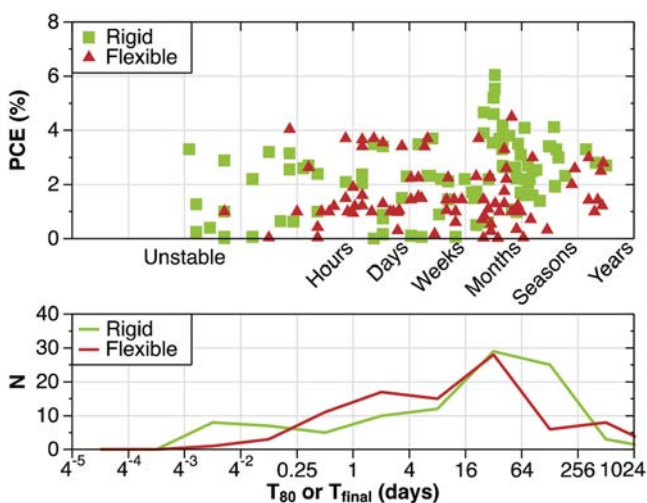www.advenergymat.de

PROGRESS REPORT

Figure 9. Distribution of the lifetime for samples grouped according to encapsulation type: rigid (green squares) and flexible (red triangles). The data is presented via the scatter plot (o-diagram) and the corresponding histogram below.

fact that for many years encapsulation was seen as a means for prolonging the lifetime of an experimental sample for further studies and for proving by all means that OPVs can last. Only in recent years has encapsulation and its economic aspects become an important element in OPV device production and attracted significant attention.[2,5,99]

Despite the lack of information, the reported data were filtered and plotted in the o-diagram according to whether rigid or flexible encapsulation methods were applied, as shown in **Figure 9**. Rigid encapsulation implied mainly full glass encapsulation (i.e., front and back) but in a few instances back metal plates were used, while flexible encapsulation typically involved the PET based commercial foils with integrated UV barriers. In either case pressure sensitive or UV curable epoxy based adhesives were often utilized.[97] Due to very limited available details on the reported encapsulation techniques it was hard to draw many conclusions on best practices. Nevertheless, from Figure 9 it is apparent that the overall distribution of the lifetimes for the samples encapsulated with the rigid and flexible materials was rather similar. Given the different levels of the water vapor transmission rates of the glass (zero) and

flexible barriers (varying from 10^{-1} to 10^{-6} gm^{-2} per day), the absence of differences on the given timescales suggests that the lifetimes of the samples were limited, not by the permeability of the packaging materials, but possibly by factors such as edge diffusion or unprotected electrode failure.[17,96,98] Thus, the results indicate that solving the problems associated with edges and electrodes are possibly the most important steps towards developing a technology with a level of durability appropriate for commercial applications.

This has been tested with a highly scaled installation with serially connected cells packaged in a continuous roll of foil at the solar park, established at the Technical University of Denmark. The solar park is based on fully R2R printed and coated solar foils in a high voltage serial configuration following the infinity concept.[100] **Figure 10**a shows one of the platforms of the park. The solar foils were rolled out and taped onto the wooden panels of the platform (inset of Figure 10a). The largest installation was made with 6 parallel connected solar foils. Each had a length of 100 m and 21 000 serially connected single cells, which generated a maximum output of >1.3 kW$_p$.[101] With the large module size (100 m × 0.305 m) the net length of the exposed edges was drastically reduced and limited the number of exposed electrode terminals (one at each end of the roll). The influence of the two major bottlenecks in the module stability was therefore efficiently addressed. Unfortunately, the system experienced previously unseen failure modes, associated with the very high operating voltages (>10 000 V) preventing the lifetime from reaching industrial levels.[102] Nonetheless, one packaging approach was fully operational for a period of two years, showing a lifetime (T_{80}) of around 400 days and retaining about 1% efficiency after 2 years of outdoor exposure (Figure 10b). This proves that solving the edge sealing and electrode protection challenges can drastically improve the durability of the technology.

3.7. Conditions of Testing

There are a number of reasons why it is important to carefully consider the test conditions when measuring the lifetime of photovoltaic devices. First, controlling the stress factors that affect device lifetime can significantly aid the investigation of the aging mechanisms.[103–106] Second, by accelerating the aging of the
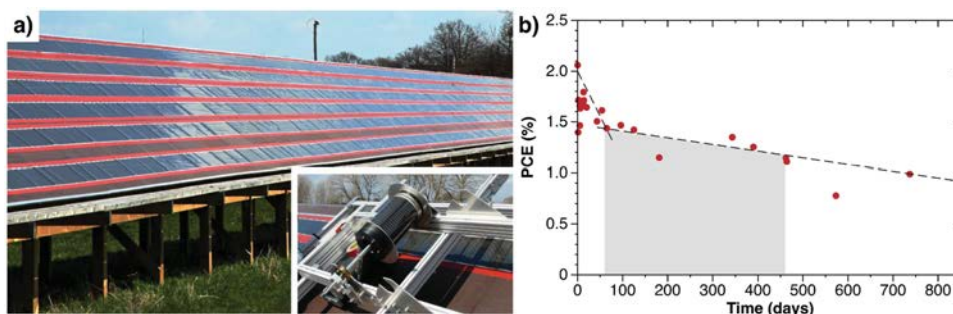

Figure 10. a) Photograph of R2R produced continuous OPV foils with a length of 100 m taped onto a wooden platform for outdoor exposure. Each foil contained up to 21 000 serially connected solar cells. The inset shows the process of unrolling the foils onto the platform. b) PCE values of one roll periodically measured at noon time under clear sky for a period of 2 years. The highlighted area marks the stabilized performance until the lifetime is reached after about 400 days.

PROGRESS REPORT

sample via increased stresses, one can predict the lifetime of the device under real test conditions within a shorter time period.[1,107] Moreover, accurate control of the test conditions improves the comparability of the results among different reports.[25] The lack of rigorous control of the test conditions has been a significant issue in the field of OPV for many years, and in most cases the reports from different laboratories varied to a large extent, making the comparison of the lifetime data difficult.[14] Only recently have the ISOS test guidelines addressed this issue.[18]

Nevertheless, in order to utilize all the lifetime data that was reported before the ISOS guidelines were established, we attempted to group and compare the data according to the following commonly reported testing categories:

1. Indoor white light soaking
2. Indoor low UV light soaking
3. Outdoor exposure
4. Dark (shelf life) test

This analysis also revealed a lack of details in the reported test conditions. In particular, in some circumstances it was not possible to identify whether the test was conducted under illumination or in the dark, under ambient conditions or under an inert atmosphere. The spectrum and intensity of the light source, which can have a major effect on the device lifetime,[14] were often not reported either. All the reports where the tests could not be classified according to the aforementioned categories were left out of the analysis.

Figure 11 shows the lifetime data for the encapsulated devices grouped according to the test conditions. According to the plot, white light indoor soaking is the most intensive test, producing the shortest lifetimes as expected. Meanwhile, the low UV light tests yield lifetimes in the same range as the dark tests. This basically confirms that the UV component is the main stress factor in the light spectrum[44] and that eliminating the UV reduces the test to the level of dark testing, putting into

question the usefulness of UV tests. One can argue that the low UV tests simulate the conditions when the tested sample has a UV filter integrated in the structure. In this case however, the UV filter will also gradually deteriorate under real test conditions, which cannot be accounted for by the low UV tests. Thus, the latter cannot truly reflect the real test conditions. The outdoor data shows rather good lifetime values, but with reduced initial efficiencies. This can be explained by the fact that the majority of the reported outdoor data were typically based on encapsulated large scale devices,[14,17,108–113] which were well adjusted for outdoor tests but typically had lower efficiencies.

Unfortunately, due to the lack of outdoor data and the large variations in the indoor soaking test conditions (temperature, humidity, light intensity, spectrum) it is not possible to establish a clear relationship between the lifetimes of indoor and outdoor tests, which could be useful for the development of a lifetime prediction tool. Therefore the field is still in urgent need of both accurately controlled indoor and outdoor measurements of different OPV technologies, conducted and reported systematically. It is important to ensure accuracy in such tests, which can be provided by carefully following the ISOS guidelines. Examples of such lifetime studies of various OPV technologies under both indoor and outdoor ISOS test conditions were reported recently[29,30] and are discussed in Section 2.3.

3.8. Lifetime Progress Diagram

For the presentation of the progress for the OPV lifetimes the literature data was filtered for the best reports and plotted similarly to the record cell efficiency diagram reported periodically by NREL.[7] **Figure 12** shows the record lifetimes of the OPVs reported through the development of the field. The reports are distributed according to the most commonly reported test conditions. The tests are shown in **Table 3**.

The dashed lines in Figure 12 are used as a guide to the eye. A few additional data points that are only slightly inferior to the record values have also been included in the plot. The data points that are defined by the final measurement time instead are highlighted with arrows. The table below the plot lists the PCEs, lifetimes and the references to the corresponding literature reports. The plot demonstrates the rapid improvements that have been made in these areas during the past few years. Such a fast development suggests that within a short period the technology will reach the desired level of durability. Despite the fact that the best current lifetime reports are in the vicinity of 1 to 2 years, it is strongly believed that OPVs today can last more than a few years. The demonstration of this, however, requires a longer period of testing and these results are possibly on their way. One also has to note that the plot presented here may not be comprehensive, as record stability reports made by industry that are not publicly available are not represented.
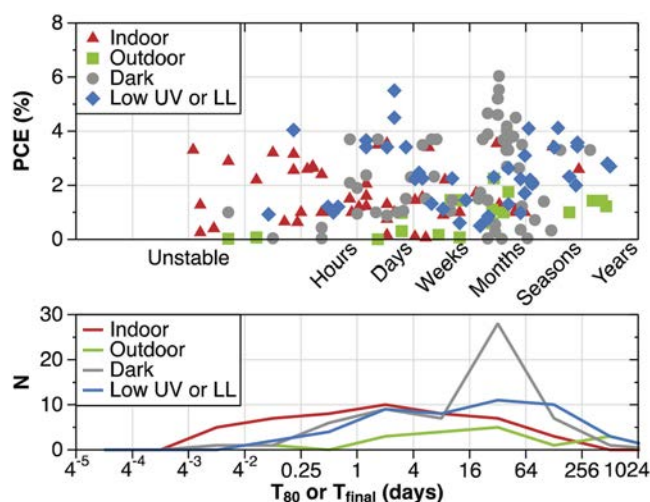

Figure 11. Distribution of the lifetime for samples grouped according to the test conditions: indoor white light soaking (red triangles), outdoor (green squares), dark tests (grey circles) and indoor low UV or low light soaking (blue diamonds). The data is presented via the scatter plot (o-diagram) and the corresponding histogram below.

4. Predicting Lifetime

The more stable the technology becomes the longer the required testing period is, which can hinder the progress of the research. It is therefore important to develop a methodology of
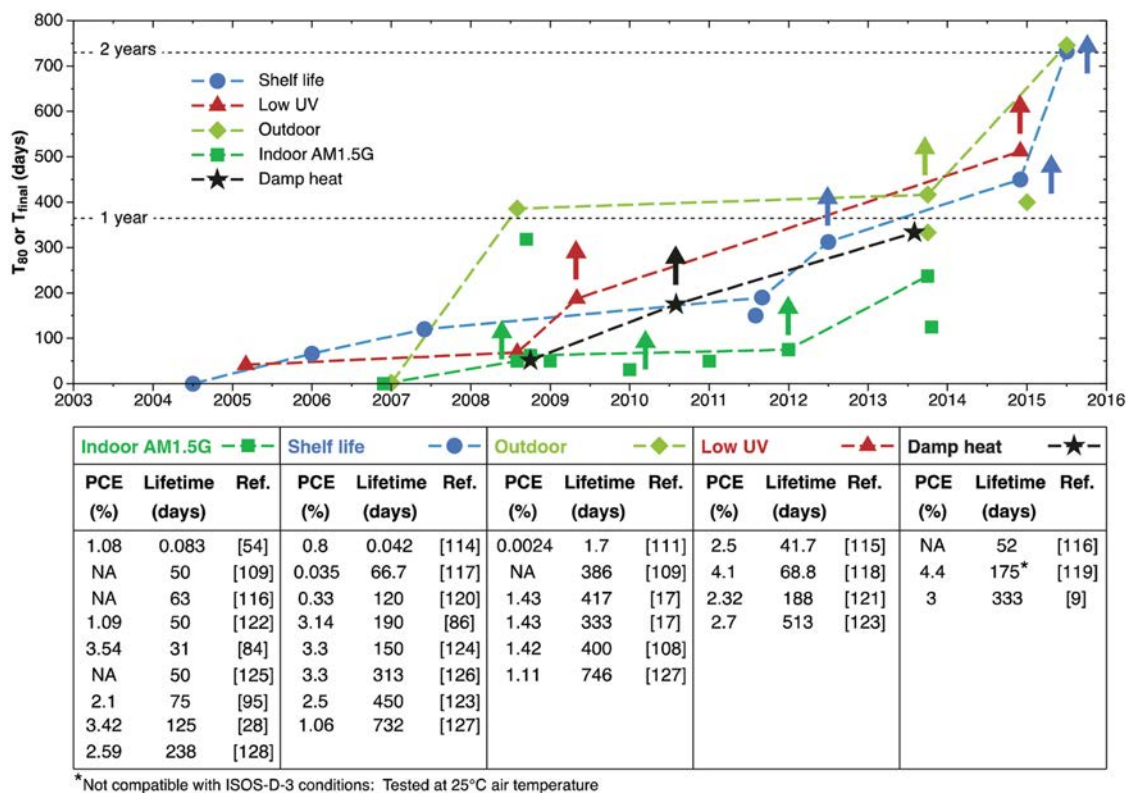
Indoor AM1.5G — ■ —			Shelf life — ● —			Outdoor — ◆ —			Low UV — ▲ —			Damp heat — ★ —		
PCE (%)	Lifetime (days)	Ref.	PCE (%)	Lifetime (days)	Ref.	PCE (%)	Lifetime (days)	Ref.	PCE (%)	Lifetime (days)	Ref.	PCE (%)	Lifetime (days)	Ref.
1.08	0.083	[54]	0.8	0.042	[114]	0.0024	1.7	[111]	2.5	41.7	[115]	NA	52	[116]
NA	50	[109]	0.035	66.7	[117]	NA	386	[109]	4.1	68.8	[118]	4.4	175*	[119]
NA	63	[116]	0.33	120	[120]	1.43	417	[17]	2.32	188	[121]	3	333	[9]
1.09	50	[122]	3.14	190	[86]	1.43	333	[17]	2.7	513	[123]			
3.54	31	[84]	3.3	150	[124]	1.42	400	[108]						
NA	50	[125]	3.3	313	[126]	1.11	746	[127]						
2.1	75	[95]	2.5	450	[123]									
3.42	125	[28]	1.06	732	[127]									
2.59	238	[128]												

*Not compatible with ISOS-D-3 conditions: Tested at 25°C air temperature

Figure 12. Diagram of the best OPV device lifetimes distributed according to the types of the test conditions. The arrows highlight the samples that are limited by measurement duration rather than the sample lifetime. The table below the plot outlines the references, PCE, and the lifetime of each data point.

accelerated tests where one can accurately predict or estimate the lifetime of a sample in a shorter period of time.[1] Due to the complexity of the degradation processes present in OPV devices it has been impractical to develop a theoretical model that would take into account all the aging mechanisms based on a set of simulated tests, and reliably predict the performance of a sample under real operational conditions. An alternative approach is the establishment of a lifetime database whereby the conduction of accurately controlled aging tests on a large

Table 3. The list of categories of lifetime tests commonly utilized in the field of OPVs and their compatibility with the ISOS guidelines.

General term	Compatible ISOS test	Description
Shelf life	ISOS-D-1	Storage in the dark under ambient conditions
Damp heat	ISOS-D-3 or similar	Storage in a damp heat chamber at elevated relative humidity and temperature levels
Outdoor testing	ISOS-O-1,2,3 or similar	Exposure to real sun irradiation under outdoor conditions
Indoor AM1.5G test	ISOS-L-1,2,3 or similar	Exposure to indoor light soaking under a solar simulator with a light spectrum close to AM1.5G
Low UV	Not compatible	Exposure to indoor light soaking under a solar simulator with a low UV component

number of OPV samples enables one to establish lifetime baselines and determine the statistical relationship between the accelerated and real condition tests.

The literature data presented in this work constitutes the core for the establishment of such a database. However, the analysis shows a significant lack of outdoor data and a great deal of variability in the indoor accelerated tests, making the literature data alone insufficient. This therefore puts the field in a position where testing under real operational (outdoor) conditions and under accurately controlled accelerated conditions is the most important step in the process of developing the lifetime prediction tool and accelerating the process of OPV industrialization.

To initiate such data generation and to aid the process of fully developing a lifetime predictor we have established an online platform at http://plasticphotovoltaics.org/lifetime-predictor that offers the following services:[131]

- The possibility of exploring and conducting in depth analysis on the literature data presented in this article.
- The possibility for uploading new lifetime data (requires login credentials, which can be obtained from the authors of this work) that then will be reviewed using the scanning method presented in this work and added to the general database. The new data can then be compared with the existing data.
- The diagram of the best OPV lifetimes is also uploaded and will be kept up to date to stimulate the competition for the record lifetime.

It is our hope that the platform will help the community in conducting lifetime studies and developing a database that can be exploited for the purpose of developing a lifetime prediction tool.

Based on the conducted analysis a set of simple steps are proposed that if followed can significantly improve the variability and reliability of the reported lifetime data:

- Follow the ISOS guidelines while conducting the experiments.
- Avoid conditions and instrumentation such as low UV light sources, inert atmosphere chambers etc., that are not in compliance with the ISOS guidelines.
- Conduct the tests using a large number of samples to statistically validate the data.
- When conducting indoor tests it is highly recommended to conduct an outdoor test in parallel and vice versa.
- When conducting aging tests it is highly recommended that the tested specimen resembles the end product in the closest possible way in terms of device geometry, architecture, electrodes, and packaging. It is also important to consider as many geographic locations as possible when conducting outdoor tests. In this regard interlaboratory or round robin studies can be advantageous.[14,15,17,129,130]

5. Conclusions

We have analyzed a large number of stability studies of OPVs reported in the literature and constructed a methodology in which the lifetimes of various OPV samples were identified and intercompared by means of a generic yardstick. The analysis revealed that while the early reports of OPV lifetime were at the level of minutes, today stable performance of up to years is reached. The analysis further helped in the identification of the bottlenecks related to the device geometry and materials used. In particular, it was confirmed that PEDOT:PSS presents a limitation to reachable intrinsic device stability. Furthermore, the data indicated that edge sealing and electrode protection are more critical to device lifetimes than the packaging material itself, and perhaps constitute the main challenges for OPV stability today. It was further revealed that most of the reported lifetime studies were conducted on OPV samples that did not meet the current vision of an industrial standard, which assumes cheap, symmetric and flexible packaging without extra substrates. More importantly, it was revealed that the field is in great deficit of outdoor lifetime studies and accurately controlled indoor accelerated tests conducted in a consistent and reproducible manner. This therefore challenges the process of developing a lifetime prediction tool. To address this, an online platform was developed that will serve as a database for collecting and comparing OPV lifetime reports based on indoor (accelerated) and outdoor tests conducted according to the ISOS guidelines. The general aim of the website is to become a platform for lifetime prediction and comparison.

[1] O. Haillant, *Sol. Energy Mater. Sol. Cells* **2011**, *95*, 1284.

[2] N. Espinosa, F. O. Lenzmann, S. Ryley, D. Angmo, M. Hösel, R. R. Søndergaard, D. Huss, S. Dafinger, S. Gritsch, J. M. Kroon, M. Jørgensen, F. C. Krebs, *J. Mater. Chem. A* **2013**, *1*, 7037.

[3] C. Powell, Y. Lawryshyn, T. Bender, *Sol. Energy Mater. Sol. Cells* **2012**, *107*, 236.

[4] C. J. Mulligan, C. Bilen, X. Zhou, W. J. Belcher, P. C. Dastoor, *Sol. Energy Mater. Sol. Cells* **2015**, *133*, 26.

[5] C. J. Mulligan, M. Wilson, G. Bryant, B. Vaughan, X. Zhou, W. J. Belcher, P. C. Dastoor, *Sol. Energy Mater. Sol. Cells* **2014**, *120*, 9.

[6] C. J. Brabec, *Sol. Energy Mater. Sol. Cells* **2004**, *83*, 273.

[7] National Renewable Energy Laboratory, Research Cell Efficiency Records, http://www.nrel.gov/ncpv (accessed: October 2015).

[8] M. Jørgensen, J. E. Carlé, R. R. Søndergaard, M. Lauritzen, N. A. Dagnæs-Hansen, S. L. Byskov, T. R. Andersen, T. T. Larsen-Olsen, A. P. L. Böttiger, B. Andreasen, L. Fu, L. Zuo, Y. Liu, E. Bundgaard, X. Zhan, H. Chen, F. C. Krebs, *Sol. Energy Mater. Sol. Cells* **2013**, *119*, 84.

[9] F. Yan, J. Noble, J. Peltola, S. Wicks, S. Balasubramanian, *Sol. Energy Mater. Sol. Cells* **2012**, *114*, 214.

[10] M. Helgesen, J. E. Carlé, G. A. dos Reis Benatto, R. R. Søndergaard, M. Jørgensen, E. Bundgaard, F. C. Krebs, *Adv. Energy Mater.* **2015**, *5*, 1401996.

[11] M. Vilkman, P. Apilo, M. Välimäki, M. Ylikunnari, A. Bernardi, R. Po, G. Corso, J. Hast, *Energy Technol.* **2015**, *3*, 407.

[12] Heliatek, Asia's largest Building Integrated Organic PV (BIOPV) First installation of HeliaFilm® completed in Singapore, http://www.heliatek.com/en/press/press-releases/details/asias-largest-building-integrated-organic-pv-biopv-first-installation-of-heliafilm-completed-in-singapore, (accessed: October 2015).

[13] H. Hoppe, N. S. Sariciftci, *J. Mater. Res.* **2004**, *19*, 1924.

[14] S. A. Gevorgyan, A. J. Medford, E. Bundgaard, S. B. Sapkota, H. F. Schleiermacher, B. Zimmermann, U. Würfel, A. Chafiq, M. Lira-Cantu, T. Swonke, M. Wagner, C. J. Brabec, O. Haillant, E. Voroshazi, T. Aernouts, R. Steim, J. A. Hauch, A. Elschner, M. Pannone, M. Xiao, A. Langzettel, D. Laird, M. T. Lloyd, T. Rath, E. Maier, G. Trimmel, M. Hermenau, T. Menke, K. Leo, R. Rösch, M. Seeland, H. Hoppe, T. J. Nagle, K. B. Burke, C. J. Fell, D. Vak, T. B. Singh, S. E. Watkins, Y. Galagan, A. Manor, E. A. Katz, T. Kim, K. Kim, P. M. Sommeling, W. J. H. Verhees, S. C. Veenstra, M. Riede, M. Greyson Christoforo, T. Currier, V. Shrotriya, G. Schwartz, F. C. Krebs, *Sol. Energy Mater. Sol. Cells* **2011**, *95*, 1398.

[15] D. Angmo, I. Gonzalez-Valls, S. Veenstra, W. Verhees, S. Sapkota, S. Schiefer, B. Zimmermann, Y. Galagan, J. Sweelssen, M. Lira-Cantu, R. Andriessen, J. M. Kroon, F. C. Krebs, *J. Appl. Polym. Sci.* **2013**, *130*, 944.

[16] M. Giannouli, V. M. Drakonakis, A. Savva, P. Eleftheriou, G. Florides, S. A. Choulis, *ChemPhysChem* **2015**, *16*, 1134.

[17] S. A. Gevorgyan, M. V. Madsen, H. F. Dam, M. Jørgensen, C. J. Fell, K. F. Anderson, B. C. Duck, A. Mescheloff, E. A. Katz, A. Elschner, R. Roesch, H. Hoppe, M. Hermenau, M. Riede, F. C. Krebs, *Sol. Energy Mater. Sol. Cells* **2013**, *116*, 187.

[18] M. O. Reese, S. A. Gevorgyan, M. Jørgensen, E. Bundgaard, S. R. Kurtz, D. S. Ginley, D. C. Olson, M. T. Lloyd, P. Morvillo, E. A. Katz, A. Elschner, O. Haillant, T. R. Currier, V. Shrotriya, M. Hermenau, M. Riede, K. R. Kirov, G. Trimmel, T. Rath, O. Inganäs, F. Zhang, M. Andersson, K. Tvingstedt, M. Lira-Cantu, D. Laird, C. McGuiness, S. Gowrisanker, M. Pannone, M. Xiao, J. Hauch, R. Steim, D. M. Delongchamp, R. Rösch, H. Hoppe, N. Espinosa, A. Urbina, G. Yaman-Uzunoglu, J. B. Bonekamp, A. J. J. M. Van Breemen, C. Girotto, E. Voroshazi, F. C. Krebs, *Sol. Energy Mater. Sol. Cells* **2011**, *95*, 1253.

[19] M. Jørgensen, K. Norrman, S. A. Gevorgyan, T. Tromholt, B. Andreasen, F. C. Krebs, *Adv. Mater.* **2012**, *24*, 580.

[20] H. Cao, W. He, Y. Mao, X. Lin, K. Ishikawa, J. H. Dickerson, W. P. Hess, *J. Power Sources* **2014**, *264*, 168.

[21] N. Grossiord, J. M. Kroon, R. Andriessen, P. W. M. Blom, *Org. Electron.* **2012**, *13*, 432.

[22] M. Jørgensen, K. Norrman, F. C. Krebs, *Sol. Energy Mater. Sol. Cells* **2008**, *92*, 686.

[23] J. U. Lee, J. W. Jung, J. W. Jo, W. H. Jo, *J. Mater. Chem.* **2012**, *22*, 24265.

[24] S. E. Shaheen, *IEEE 45th Ann. Int. Reliab. Phys. Symp.* **2007**, 248.

[25] S. A. Gevorgyan, M. Corazza, M. V. Madsen, G. Bardizza, A. Pozza, H. Müllejans, J. C. Blakesley, G. F. A. Dibb, F. A. Castro, J. F. Trigo, C. M. Guillén, J. R. Herrero, P. Morvillo, M. G. Maglione, C. Minarini, F. Roca, S. Cros, C. Seraine, C. H. Law, P. S. Tuladhar, J. R. Durrant, F. C. Krebs, *Polym. Degrad. Stab.* **2014**, *109*, 162.

[26] E. Bovill, N. Scarratt, J. Griffin, H. Yi, A. Iraqi, A. R. Buckley, J. W. Kingsley, D. G. Lidzey, *Appl. Phys. Lett.* **2015**, *106*, 073301.

[27] W. R. Mateker, I. T. Sachs-Quintana, G. F. Burkhard, R. Cheacharoen, M. D. McGehee, *Chem. Mater.* **2015**, *27*, 1.

[28] R. Roesch, K. R. Eberhardt, S. Engmann, G. Gobsch, H. Hoppe, *Sol. Energy Mater. Sol. Cells* **2013**, *117*, 59.

[29] M. Corazza, F. C. Krebs, S. A. Gevorgyan, *Sol. Energy Mater. Sol. Cells* **2014**, *130*, 99.

[30] M. Corazza, F. C. Krebs, S. A. Gevorgyan, *Sol. Energy Mater. Sol. Cells* **2015**, *143*, 467.

[31] F. C. Krebs, S. A. Gevorgyan, J. Alstrup, *J. Mater. Chem.* **2009**, *19*, 5442.

[32] M. T. Lloyd, D. C. Olson, P. Lu, E. Fang, D. L. Moore, M. S. White, M. O. Reese, D. S. Ginley, J. W. P. Hsu, *J. Mater. Chem.* **2009**, *19*, 7638.

[33] M. Wang, F. Xie, J. Du, Q. Tang, S. Zheng, Q. Miao, J. Chen, N. Zhao, J. B. Xu, *Sol. Energy Mater. Sol. Cells* **2011**, *95*, 3303.

[34] J. Wang, C. R. Friedman, W. Cabrera, K. Tan, Y.-J. Lee, Y. J. Chabal, J. W. P. Hsu, *J. Mater. Chem. A* **2014**, *2*, 15288.

[35] V. M. Drakonakis, A. Savva, M. Kokonou, S. A. Choulis, *Sol. Energy Mater. Sol. Cells* **2014**, *130*, 544.

[36] F. C. Krebs, J. E. Carlé, N. Cruys-Bagger, M. Andersen, M. R. Lilliedal, M. A. Hammond, S. Hvidt, *Sol. Energy Mater. Sol. Cells* **2005**, *86*, 499.

[37] M. T. Lloyd, C. H. Peters, A. Garcia, I. V. Kauvar, J. J. Berry, M. O. Reese, M. D. McGehee, D. S. Ginley, D. C. Olson, *Sol. Energy Mater. Sol. Cells* **2011**, *95*, 1382.

[38] F. J. Lim, K. Ananthanarayanan, J. Luther, G. W. Ho, *J. Mater. Chem.* **2012**, 25057.

[39] I. T. Sachs-Quintana, T. Heumüller, W. R. Mateker, D. E. Orozco, R. Cheacharoen, S. Sweetnam, C. J. Brabec, M. D. McGehee, *Adv. Funct. Mater.* **2014**, *24*, 3978.

[40] K. Norrman, S. A. Gevorgyan, F. C. Krebs, *ACS Appl. Mater. Interfaces* **2009**, *1*, 102.

[41] K. Norrman, F. C. Krebs, *Sol. Energy Mater. Sol. Cells* **2006**, *90*, 213.

[42] F. C. Krebs, K. Norrman, *Prog. Photovoltaics Res. Appl.* **2007**, *15*, 697.

[43] K. Norrman, M. V. Madsen, S. A. Gevorgyan, F. C. Krebs, *J. Am. Chem. Soc.* **2010**, *132*, 16883.

[44] H. Hintz, H.-J. Egelhaaf, L. Lüer, J. Hauch, H. Peisert, T. Chassé, *Chem. Mater.* **2011**, *23*, 145.

[45] E. Voroshazi, G. Uytterhoeven, K. Cnops, T. Conard, P. Favia, H. Bender, R. Muller, D. Cheyns, *ACS Appl. Mater. Interfaces* **2015**, *7*, 618.

[46] I. Burgués-Ceballos, M. Stella, P. Lacharmoise, E. Martinez-Ferrero, *J. Mater. Chem. A* **2014**, *2*, 17711.

[47] F. C. Krebs, *Sol. Energy Mater. Sol. Cells* **2009**, *93*, 394.

[48] N. Espinosa, R. García-Valverde, A. Urbina, F. C. Krebs, *Sol. Energy Mater. Sol. Cells* **2011**, *95*, 1293.

[49] L. Groenendaal, F. Jonas, D. Freitag, H. Pielartzik, J. R. Reynolds, *Adv. Mater.* **2000**, *12*, 481.

[50] F. Zhang, X. Xu, W. Tang, J. Zhang, Z. Zhuo, J. J. Wang, J. J. Wang, Z. Xu, Y. Wang, *Sol. Energy Mater. Sol. Cells* **2011**, *95*, 1785.

[51] F. C. Krebs, R. Søndergaard, M. Jørgensen, *Sol. Energy Mater. Sol. Cells* **2011**, *95*, 1348.

[52] J. E. Carlé, T. R. Andersen, M. Helgesen, E. Bundgaard, M. Jorgensen, F. C. Krebs, *Sol. Energy Mater. Sol. Cells* **2013**, *108*, 126.

[53] C. W. T. Bulle-Lieuwma, W. J. H. van Gennip, J. K. J. van Duren, P. Jonkheijm, R. A. J. Janssen, J. W. Niemantsverdriet, *Appl. Surf. Sci.* **2003**, *203–204*, 547.

[54] K. Kawano, R. Pacios, D. Poplavskyy, J. Nelson, D. D. C. Bradley, J. R. Durrant, *Sol. Energy Mater. Sol. Cells* **2006**, *90*, 3520.

[55] A. M. Nardes, M. Kemerink, M. M. de Kok, E. Vinken, K. Maturova, R. A. J. Janssen, *Org. Electron. Phys. Mater. Appl.* **2008**, *9*, 727.

[56] E. Voroshazi, B. Verreet, A. Buri, R. Müller, D. Di Nuzzo, P. Heremans, *Org. Electron. Phys. Mater. Appl.* **2011**, *12*, 736.

[57] M. P. de Jong, L. J. Van Ijzendoorn, M. J. A. de Voigt, *App. Phys. Lett.* **2000**, *77*, 2255.

[58] S. B. Sapkota, M. Fischer, B. Zimmermann, U. Würfel, *Sol. Energy Mater. Sol. Cells* **2014**, *121*, 43.

[59] M. Manceau, A. Rivaton, J. L. Gardette, S. Guillerez, N. Lemaître, *Polym. Degrad. Stab.* **2009**, *94*, 898.

[60] M. O. Reese, A. M. Nardes, B. L. Rupert, R. E. Larsen, D. C. Olson, M. T. Lloyd, S. E. Shaheen, D. S. Ginley, G. Rumbles, N. Kopidakis, *Adv. Funct. Mater.* **2010**, *20*, 3476.

[61] J. Schafferhans, A. Baumann, A. Wagenpfahl, C. Deibel, V. Dyakonov, *Org. Electron. Phys. Mater. Appl.* **2010**, *11*, 1693.

[62] M. Hermenau, M. Riede, K. Leo, S. A. Gevorgyan, F. C. Krebs, K. Norrman, *Sol. Energy Mater. Sol. Cells* **2011**, *95*, 1268.

[63] J. Zhao, A. Swinnen, G. Van Assche, J. Manca, D. Vanderzande, B. Van Mele, *J. Phys. Chem. B* **2009**, *113*, 1587.

[64] A. Rivaton, S. Chambon, M. Manceau, J. L. Gardette, N. Lemaître, S. Guillerez, *Polym. Degrad. Stab.* **2010**, *95*, 278.

[65] D. E. Motaung, G. F. Malgas, C. J. Arendse, *J. Mater. Sci.* **2011**, *46*, 4942.

[66] T. Tromholt, M. Manceau, M. Helgesen, J. E. Carlé, F. C. Krebs, *Sol. Energy Mater. Sol. Cells* **2011**, *95*, 1308.

[67] M. V. Madsen, T. Tromholt, K. Norrman, F. C. Krebs, *Adv. Energy Mater.* **2013**, *3*, 424.

[68] S. Bertho, I. Haeldermans, A. Swinnen, W. Moons, T. Martens, L. Lutsen, D. Vanderzande, J. Manca, A. Senes, A. Bonfiglio, *Sol. Energy Mater. Sol. Cells* **2007**, *91*, 385.

[69] F. Padinger, T. Fromherz, P. Denk, C. J. Brabec, J. Zettner, T. Hierl, N. S. Sariciftci, *Synth. Met.* **2001**, *121*, 1605.

[70] H. Neugebauer, C. J. Brabec, J. C. Hummelen, R. A. J. Janssen, N. S. Sariciftci, *Synth. Met.* **1999**, *102*, 1002.

[71] G. Dennler, M. C. Scharber, C. J. Brabec, S. Gowrisanker, J. J. M. Halls, D. Laird, S. Jia, S. P. Williams, *Adv. Mater.* **2009**, *22*, 3839.

PROGRESS REPORT

[72] L. Dou, J. You, Z. Hong, Z. Xu, G. Li, R. A. Street, Y. Yang, *Adv. Mater.* **2013**, *25*, 6642.

[73] J. Kettle, H. Waters, M. Horie, S.-W. Chang, *J. Phys. D. Appl. Phys.* **2012**, *45*, 125102.

[74] Y. Sun, J. H. Seo, C. J. Takacs, J. Seifter, A. J. Heeger, *Adv. Mater.* **2011**, *23*, 1679.

[75] Y. Sun, C. J. Takacs, S. R. Cowan, J. H. Seo, X. Gong, A. Roy, A. J. Heeger, *Adv. Mater.* **2011**, *23*, 2226.

[76] C. H. Peters, I. T. Sachs-Quintana, J. P. Kastrop, S. Beaupré, M. Leclerc, M. D. McGehee, *Adv. Energy Mater.* **2011**, *1*, 491.

[77] J. Sun, Y. Zhu, X. Xu, L. Lan, L. Zhang, P. Cai, J. Chen, J. Peng, Y. Cao, *J. Phys. Chem. C* **2012**, *116*, 14188.

[78] N. Zhou, X. Guo, R. P. Ortiz, S. Li, S. Zhang, R. P. H. Chang, A. Facchetti, T. J. Marks, *Adv. Mater.* **2012**, *24*, 2242.

[79] T. Y. Chu, S. W. Tsang, J. Zhou, P. G. Verly, J. Lu, S. Beaupré, M. Leclerc, Y. Tao, *Sol. Energy Mater. Sol. Cells* **2012**, *96*, 155.

[80] B. J. Worfolk, T. C. Hauger, K. D. Harris, D. A. Rider, J. a M. Fordyce, S. Beaupré, M. Leclerc, J. M. Buriak, *Adv. Energy Mater.* **2012**, *2*, 361.

[81] C. Y. Chang, Y. J. Cheng, S. H. Hung, J. S. Wu, W. S. Kao, C. H. Lee, C. S. Hsu, *Adv. Mater.* **2012**, *24*, 549.

[82] P. C. Yang, J. Y. Sun, S. Y. Ma, Y. M. Shen, Y. H. Lin, C. P. Chen, C. F. Lin, *Sol. Energy Mater. Sol. Cells* **2012**, *98*, 351.

[83] R. Rösch, D. M. Tanenbaum, M. Jørgensen, M. Seeland, M. Bärenklau, M. Hermenau, E. Voroshazi, M. T. Lloyd, Y. Galagan, B. Zimmermann, U. Würfel, M. Hösel, H. F. Dam, S. A. Gevorgyan, S. Kudret, W. Maes, L. Lutsen, D. Vanderzande, R. Andriessen, G. Teran-Escobar, M. Lira-Cantu, A. Rivaton, G. Y. Uzunoğlu, D. Germack, B. Andreasen, M. V. Madsen, K. Norrman, H. Hoppe, F. C. Krebs, *Energy Environ. Sci.* **2012**, *5*, 6521.

[84] D. Gao, M. G. Helander, Z. Bin Wang, D. P. Puzzo, M. T. Greiner, Z. H. Lu, *Adv. Mater.* **2010**, *22*, 5404.

[85] Y. J. Jeon, J. M. Yun, D. Y. Kim, S. I. Na, S. S. Kim, *Sol. Energy Mater. Sol. Cells* **2012**, *105*, 96.

[86] S. Dey, P. Vivo, A. Efimov, H. Lemmetyinen, *J. Mater. Chem.* **2011**, *21*, 15587.

[87] V. M. Manninen, W. A. E. Omar, J. P. Heiskanen, H. J. Lemmetyinen, O. E. O. Hormi, *J. Mater. Chem.* **2012**, *22*, 22971.

[88] J. Bandara, K. Shankar, C. A. Grimes, M. Thelakkat, *Thin Solid Films* **2011**, *520*, 582.

[89] S. Park, H. O. Seo, K. Kim, J. E. Lee, J. Kwon, Y. D. Kim, D. C. Lim, *Phys. Status Solidi RRL* **2012**, *6*, 196.

[90] Jing-Shun Huang, Chen-Yu Chou, Ching-Fuh Lin, *IEEE Electron Device Lett.* **2010**, *31*, 332.

[91] S. K. Hau, H.-L. Yip, N. S. Baek, J. Zou, K. O'Malley, A. K.-Y. Jen, *Appl. Phys. Lett.* **2008**, *92*, 253301.

[92] C. H. Hsieh, Y. J. Cheng, P. J. Li, C. H. Chen, M. Dubosc, R. M. Liang, C. S. Hsu, *J. Am. Chem. Soc.* **2010**, *132*, 4887.

[93] Y.-J. Kang, K. Lim, S. Jung, D.-G. Kim, J.-K. Kim, C.-S. Kim, S. H. Kim, J.-W. Kang, *Sol. Energy Mater. Sol. Cells* **2012**, *96*, 137.

[94] C. Y. Chang, C. E. Wu, S. Y. Chen, C. Cui, Y. J. Cheng, C. S. Hsu, Y. L. Wang, Y. Li, *Angew. Chem. Int. Ed.* **2011**, *50*, 9386.

[95] D. M. Tanenbaum, M. Hermenau, E. Voroshazi, M. T. Lloyd, Y. Galagan, B. Zimmermann, M. Hösel, H. F. Dam, M. Jørgensen, S. A. Gevorgyan, S. Kudret, W. Maes, L. Lutsen, D. Vanderzande, U. Würfel, R. Andriessen, R. Rösch, H. Hoppe, G. Teran-Escobar, M. Lira-Cantu, A. Rivaton, G. Y. Uzunoğlu, D. Germack, B. Andreasen, M. V. Madsen, K. Norrman, F. C. Krebs, *RSC Adv.* **2012**, *2*, 882.

[96] D. M. Tanenbaum, H. F. Dam, R. Rösch, M. Jørgensen, H. Hoppe, F. C. Krebs, *Sol. Energy Mater. Sol. Cells* **2012**, *97*, 157.

[97] M. Hösel, R. R. Søndergaard, M. Jørgensen, F. C. Krebs, *Adv. Eng. Mater.* **2013**, *15*, 1068.

[98] J. J. Michels, M. Peter, A. Salem, B. van Remoortere, J. van den Brand, *J. Mater. Chem. C* **2014**, *2*, 5759.

[99] N. Espinosa, F. C. Krebs, *Sol. Energy Mater. Sol. Cells* **2014**, *120*, 692.

[100] P. Sommer-Larsen, M. Jørgensen, R. R. Søndergaard, M. Hösel, F. C. Krebs, *Energy Technol.* **2013**, *1*, 15.

[101] F. C. Krebs, N. Espinosa, M. Hösel, R. R. Søndergaard, M. Jørgensen, *Adv. Mater.* **2014**, *26*, 29.

[102] M. Hösel, R. R. Søndergaard, M. Jørgensen, F. C. Krebs, *Adv. Energy Mater.* **2014**, *4*, 1.

[103] S. A. Gevorgyan, M. Jørgensen, F. C. Krebs, *Sol. Energy Mater. Sol. Cells* **2008**, *92*, 736.

[104] S. A. Gevorgyan, M. Jørgensen, F. C. Krebs, K. O. Sylvester-Hvid, *Sol. Energy Mater. Sol. Cells* **2011**, *95*, 1389.

[105] M. O. Reese, A. K. Sigdel, J. J. Berry, D. S. Ginley, S. E. Shaheen, *Sol. Energy Mater. Sol. Cells* **2010**, *94*, 1254.

[106] S. Karak, S. Pradhan, a Dhar, *Semicond. Sci. Technol.* **2011**, *26*, 095020.

[107] O. Haillant, D. Dumbleton, A. Zielnik, *Sol. Energy Mater. Sol. Cells* **2011**, *95*, 1889.

[108] B. Roth, G. A. dos Reis Benatto, M. Corazza, R. R. Søndergaard, S. A. Gevorgyan, M. Jørgensen, F. C. Krebs, *Adv. Energy Mater.* **2015**, *5*, 1401912.

[109] J. A. Hauch, P. Schilinsky, S. A. Choulis, R. Childers, M. Biele, C. J. Brabec, *Sol. Energy Mater. Sol. Cells* **2008**, *92*, 727.

[110] T.-N. Chen, D.-S. Wuu, C.-Y. Lin, C.-C. Wu, R.-H. Horng, *Thin Solid Films* **2009**, *517*, 4179.

[111] E. A. Katz, S. Gevorgyan, M. S. Orynbayev, F. C. Krebs, *Eur. Phys. J. Appl. Phys.* **2006**, *36*, 307.

[112] N. Espinosa, H. F. Dam, D. M. Tanenbaum, J. W. Andreasen, M. Jørgensen, F. C. Krebs, *Materials (Basel).* **2011**, *4*, 169.

[113] A. J. Medford, M. R. Lilliedal, M. Jørgensen, D. Aarø, H. Pakalski, J. Fyenbo, F. C. Krebs, *Opt. Express* **2010**, *18 Suppl 3*, A272.

[114] S. Heutz, P. Sullivan, B. M. Sanderson, S. M. Schultes, T. S. Jones, *Sol. Energy Mater. Sol. Cells* **2004**, *83*, 229.

[115] X. Yang, J. Loos, S. C. Veenstra, W. J. H. Verhees, M. M. Wienk, J. M. Kroon, M. a J. Michels, R. a J. Janssen, *Nano Lett.* **2005**, *5*, 579.

[116] J. A. Hauch, P. Schilinsky, S. A. Choulis, S. Rajoelson, C. J. Brabec, *Appl. Phys. Lett.* **2008**, *93*, 2008.

[117] G. Dennler, C. Lungenschmied, H. Neugebauer, N. S. Sariciftci, A. Labouret, *J. Mater. Res.* **2005**, *20*, 3224.

[118] R. Franke, B. Maennig, A. Petrich, M. Pfeiffer, *Sol. Energy Mater. Sol. Cells* **2008**, *92*, 732.

[119] J. H. Tsai, Y. C. Lai, T. Higashihara, C. J. Lin, M. Ueda, W. C. Chen, *Macromolecules* **2010**, *43*, 6085.

[120] C. Lungenschmied, G. Dennler, H. Neugebauer, S. N. Sariciftci, M. Glatthaar, T. Meyer, A. Meyer, *Sol. Energy Mater. Sol. Cells* **2007**, *91*, 379.

[121] B. Zimmermann, U. Würfel, M. Niggemann, *Sol. Energy Mater. Sol. Cells* **2009**, *93*, 491.

[122] R. Tipnis, J. Bernkopf, S. Jia, J. Krieg, S. Li, M. Storch, D. Laird, *Sol. Energy Mater. Sol. Cells* **2009**, *93*, 442.

[123] S. B. Sapkota, A. Spies, B. Zimmermann, I. Dürr, U. Würfel, *Sol. Energy Mater. Sol. Cells* **2014**, *130*, 144.

[124] C.-Y. Chang, F.-Y. Tsai, *J. Mater. Chem.* **2011**, *21*, 5710.

[125] S. Cros, R. De Bettignies, S. Berson, S. Bailly, P. Maisse, N. Lemaitre, S. Guillerez, *Sol. Energy Mater. Sol. Cells* **2011**, *95*, 65.

[126] N. Kim, W. J. Potscavage, A. Sundaramoothi, C. Henderson, B. Kippelen, S. Graham, *Sol. Energy Mater. Sol. Cells* **2012**, *101*, 140.

[127] D. Angmo, F. C. Krebs, *Energy Technol.* **2015**, *3*, 774.

[128] A. Karpinski, S. Berson, H. Terrisse, M. Mancini-Le Granvalet, S. Guillerez, L. Brohan, M. Richard-Plouet, *Sol. Energy Mater. Sol. Cells* **2013**, *116*, 27.

[129] M. V. Madsen, S. A. Gevorgyan, R. Pacios, J. Ajuria, I. Etxebarria, J. Kettle, N. D. Bristow, M. Neophytou, S. A. Choulis, L. Stolz Roman, T. Yohannes, A. Cester, P. Cheng, X. Zhan, J. Wu, Z. Xie, W. C. Tu, J. H. He, C. J. Fell, K. Anderson, M. Hermenau, D. Bartesaghi, L. Jan Anton Koster, F. Machui, I. González-Valls, M. Lira-Cantu, P. P. Khlyabich, B. C. Thompson, R. Gupta, K. Shanmugam, G. U. Kulkarni, Y. Galagan, A. Urbina, J. Abad, R. Roesch, H. Hoppe, P. Morvillo, E. Bobeico, E. Panaitescu, L. Menon, Q. Luo, Z. Wu, C. Ma, A. Hambarian, V. Melikyan, M. Hambsch, P. L. Burn, P. Meredith, T. Rath, S. Dunst, G. Trimmel, G. Bardizza, H. Müllejans, A. E. Goryachev, R. K. Misra, E. A. Katz, K. Takagi, S. Magaino, H. Saito, D. Aoki, P. M. Sommeling, J. M. Kroon, T. Vangerven, J. Manca, J. Kesters, W. Maes, O. D. Bobkova, V. A. Trukhanov, D. Y. Paraschuk, F. A. Castro, J. Blakesley, S. M. Tuladhar, J. Alexander Röhr, J. Nelson, J. Xia, E. A. Parlak, T. A. Tumay, H. J. Egelhaaf, D. M. Tanenbaum, G. Mae Ferguson, R. Carpenter, H. Chen, B. Zimmermann, L. Hirsch, G. Wantz, Z. Sun, P. Singh, C. Bapat, T. Offermans, F. C. Krebs, *Sol. Energy Mater. Sol. Cells* **2014**, *130*, 281.

[130] R. R. Søndergaard, T. Makris, P. Lianos, A. Manor, E. A. Katz, W. Gong, S. M. Tuladhar, J. Nelson, R. Tuomi, P. Sommeling, S. C. Veenstra, A. Rivaton, A. Dupuis, G. Teran-Escobar, M. Lira-Cantu, S. B. Sapkota, B. Zimmermann, U. Würfel, A. Matzarakis, F. C. Krebs, *Sol. Energy Mater. Sol. Cells* **2012**, *99*, 292.

[131] Lifetime database, http://plasticphotovoltaics.org/lifetime-predictor, (accessed: October 2015).

Roll-to-roll printed silver nanowires for increased stability of flexible ITO-free organic solar cell modules

Gisele A. dos Reis Benatto, Bérenger Roth, Michael Corazza, Roar R. Søndergaard, Suren A. Gevorgyan, Mikkel Jørgensen and Frederik C. Krebs*

We report the use of roll-to-roll printed silver nanowire networks as front electrodes for fully roll-to-roll processed flexible indium-tin-oxide (ITO) free OPV modules. We prepared devices with two types of back electrodes, a simple PEDOT:PSS back electrode and a PEDOT:PSS back electrode with a printed silver grid in order to simultaneously explore the influence of the back electrode structure on the operational stability of the modules that did not include any UV-protection. We subjected the devices to stability testing under a number of protocols recommended by the international summit on OPV stability (ISOS). We explored accelerated ISOS-D-2, ISOS-D-3, ISOS-L-2, ISOS-L-3, ISOS-O-1 and ISOS-O-2 testing protocols and compared the performance to previous reports employing the same testing protocols on devices with PEDOT:PSS instead of the silver nanowires in the front electrode. We find significantly increased operational stability across all ISOS testing protocols over the course of the study and conclude that replacement of PEDOT:PSS in the front electrode with silver nanowires increase operational stability by up to 1000%. The duration of the tests were in the range of 140–360 days. The comparison of front and back electrode stability in this study shows that the modules with silver nanowire front electrodes together with a composite back electrode comprising PEDOT:PSS and a silver grid present the best operational stability.

Introduction

Organic solar cells have been subject to intense studies with the general purpose of increasing the power output and stability in order to push the technology towards commercialization. Most of the research however has been focusing on laboratory scale devices that do not truly reflect the vision of a low cost solution processable technology with high throughput. To develop an economically viable OPV technology it is necessary to tackle a number of issues, such as eliminating the use of indium-tin-oxide (ITO) and developing fast roll-to-roll (R2R) processing methods with little or no loss of material. These issues have received more focus in recent years and several reports of ITO-free organic solar cells have been published with alternative transparent electrodes. Graphene,[1–3] highly conducting PEDOT:PSS,[4–6] highly conducting PEDOT:PSS in combination with silver grids[7–10] and silver nanowires (AgNWs)[11–13] have for example been used as transparent electrode substitutes for ITO demonstrating similar or even better performance in comparison. Comparison of transparent elec-

trodes includes a relationship between the conductivity of the electrode and the transmittance of light in the region of interest for the absorber of the solar cell. AgNW electrodes have in this context demonstrated extremely good conductivity/transmittance relationships which makes them a very interesting candidate for future use. The processability of AgNW by R2R has already been shown[14] and the fact that only very little silver is used in the process could justify the use of silver in the form of nanowires in spite of the relatively low abundance of silver in nature. This would require that the electrode is proven stable – something that could be questioned because of the very large surface-to-volume ratio of the nanowires which could result in faster failure than bulk silver based electrodes due to promotion of degradation mechanisms at the surface. An excellent report published recently by Mayousse *et al.* studied the stability of pristine AgNW without encapsulation over a period of more than 2 years upon stress by elevated temperatures and high humidity, exposure to light, exposure to elevated concentrations of hydrogen sulphide and under electrical stress.[15] The AgNWs were found to be very stable over time when left in ambient atmosphere in the dark and when exposed to high levels of humidity but showed decreasing conductivity over time when exposed to elevated temperatures due to breaking of some of the nanowires. The same

Department of Energy Conversion and Storage, Technical University of Denmark, Frederiksborgvej 399, DK-4000 Roskilde, Denmark. E-mail: frkr@dtu.dk

effect was observed if the nanowires were covered with a thin layer of PEDOT:PSS and stored in the dark in which case some of the nanowires seemed to slowly be etched away by the acidic components of PEDOT:PSS. When exposed to light the electrodes experience an increase in conductivity due to sintering of the nanowire network. The overall conclusion was that although the AgNW electrode in itself is generally very stable, further studies aimed directly at the intended use of the AgNW electrodes are necessary – something that to our knowledge has not yet been performed for organic solar cell modules. Additionally, from the environmental point of view, a printed front electrode comprising a hybrid AgNW/ZnO layer saves 2 printing steps and a substantial amount of energy in the flexible OPV manufacturing.

In this paper we describe a detailed stability study of fully R2R produced ITO-free organic solar cell modules using R2R printed AgNWs as front electrode, considering two different back electrodes (PEDOT:PSS with and without a printed Ag-grid) and investigating the influence on device stability. The modules were tested under ISOS-D-2, ISOS-D-3, ISOS-L-2, ISOS-L-3, ISOS-O-1, and ISOS-O-2 conditions and the results were compared with previously reported stability data for similarly sized modules that did not employ AgNWs. Our results demonstrate an increase in operational stability from a few days up to seasons under accelerated testing for polymer solar cell modules employing AgNWs.

Experimental procedures

Module processing

The modules were manufactured using previously described procedures.[9] The front silver contacts were processed by flexo-printing on flexible barrier foil (water vapour transmission rate 4×10^{-2} g m^{-2} day^{-1}, oxygen transmission rate 1×10^{-2} cm^3(STP) m^{-2} day^{-1}) without UV-filter. The previously reported 3 printing steps for the front electrode using a silver nanoparticle based Ag-grid in combination with highly conductive PEDOT:PSS and a nanoparticle ZnO layer was replaced by a rotary screen printed hybrid AgNW/ZnO electrode that was printed in a single printing step. The active layer of P3HT:PCBM was slot-die coated. Two types of modules were tested which differed only in the nature of the back electrode (Fig. 1). The modules with PEDOT:PSS/Ag-grid back electrode had the PEDOT:PSS as hole extraction layer and the Ag-grid as the back electrode, while the PEDOT:PSS back electrode modules do not have the printed Ag-grid. This means that one printing step and silver is saved in the latter case. The two device types had identical PEDOT:PSS thickness and were processed in the same manufacturing run where half of the modules were subjected to a final printing step where the silver grid/busbars were printed using rotary screen printing.

Measurements

2 to 5 modules of each of the two geometries were used per ISOS test. The exact number for each test was mainly depen-
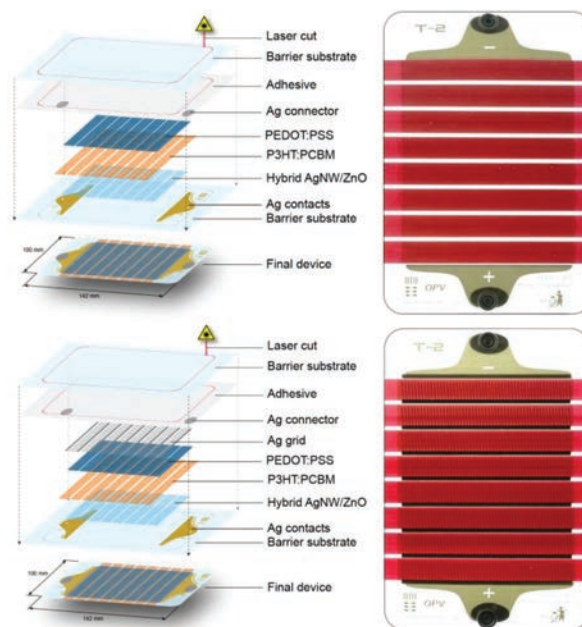

Fig. 1 Top: Architecture of the device with AgNW front electrode and PEDOT:PSS back electrode (left) and picture of the corresponding module (right). Bottom: Architecture of the device with AgNW front electrode and Ag-grid back electrode (left) and picture of the corresponding module (right). The dimensions of the modules are 14 × 10 cm.

dent on the space availability in the test setups for each test described in Table 1 and the number of available test channels. All the tests, including accurate *IV*-testing under calibrated light sources and outdoor measurement, were performed in the Characterization Laboratory for Organic Photovoltaics (CLOP) at the Department of Energy Conversion and Storage, DTU, Roskilde, Denmark. The outdoor experiments started on July 11th 2014 which is mid-summer in Denmark. For ISOS-D-2 the samples were kept in an oven at 65 °C; for ISOS-D-3 the samples were placed in a damp heat chamber (from Thermotron) set at 85% relative humidity (RH) and 65 °C air temperature. For ISOS-L-3 a xenon lamp based weathering chamber (from Q-Lab) was set to 65 °C air temperature, 85 °C device temperature (black panel), 50% RH and illumination of around 0.7 Sun. In ISOS-L-2 the experiment was carried out in the ambient at 65 °C under a solar simulator while in ISOS-O-1 and ISOS-O-2 the samples were left outside on a solar tracker. For both ISOS-L-2 and ISOS-O-2 the *IV*-curve tracing of the samples was performed using an automated acquisition setup with a Keithley 2400 SMU. In the other tests the samples were periodically removed from the ageing setup and tested under a calibrated solar simulator with AM1.5G spectrum and 1000 W m^{-2} of illumination. The recorded *IV*-curves were used to construct the degradation curves as recommended in the ISOS protocols.[16] A Microsoft excel based macro was used for raw data processing and analysis.[17] Images of the samples were taken using non-destructive light beam induced current (LBIC)[18] mapping on a desktop system (from infinityPV ApS) and an optical microscope.

Table 1 List of the main parameters used in the different ISOS protocols

	ISOS-D-2	ISOS-D-3	ISOS-L-2	ISOS-L-3	ISOS-O-1	ISOS-O-2
Light source	None	None	Simulator AM1.5G	Simulator AM1.5G	The sun, outdoor	The sun, outdoor
Temperature	65 °C (oven)	65 °C	65 °C	85 °C	Ambient outdoor	Ambient outdoor
Relative humidity	Ambient (low)	85% (environ. chamber)	Ambient (low)	Controlled (50%)	Ambient outdoor	Ambient outdoor
Characterization light source	Solar simulator	Solar simulator	Solar simulator	Solar simulator	Solar simulator	Sunlight

Results and discussion

Two different types of fully R2R processed solar cell modules with AgNW front electrode were tested in this study with the difference being in the nature of the back electrode. Fig. 1 shows the device architecture as well as a photograph of the devices. P3HT:PCBM was used as the active material and either a PEDOT:PSS layer or a PEDOT:PSS layer combined with a silver grid were used for the back electrode. The active area of the modules was determined by LBIC and was found to be approximately 57 cm^2 for all the tested modules. The modules were all tested according to ISOS-D-2, ISOS-D-3, ISOS-L-2, ISOS-L-3, ISOS-O-1, and ISOS-O-2 protocols. The main parameters of the different protocols are listed in Table 1. Not all the indoor tests were carried out for the same amount of time. Space issues, retrospective acknowledgement of the necessity of additional testing and device performances descending below the threshold where meaningful data could be extracted

were the reasons for the differences in time span. Generally, experiments were discontinued once the devices had descended below T_{50} (the time it takes to reach 50% of the initial efficiency) while still presenting rapid decline in performance. Fig. 2, 4 and 9 illustrate the normalized power conversion efficiencies (PCE), open circuit voltage (V_{OC}), short circuit current (I_{SC}), and fill factor (FF) over time for the different tests and Fig. 3, 5 and 10 show the *IV*-curves of the modules before, at the beginning, halfway and close to the end of the tests.

Dark tests

Fig. 2 it is obvious that in dry heat conditions (ISOS-D-2) the samples with Ag-grid back electrode show an increase in the current during the first 80 days of the test, while the samples with PEDOT:PSS exhibit rather stable performance. Nevertheless, when the humidity level is increased (ISOS-D-3), it results in a rapid degradation of all the samples after only a few days.
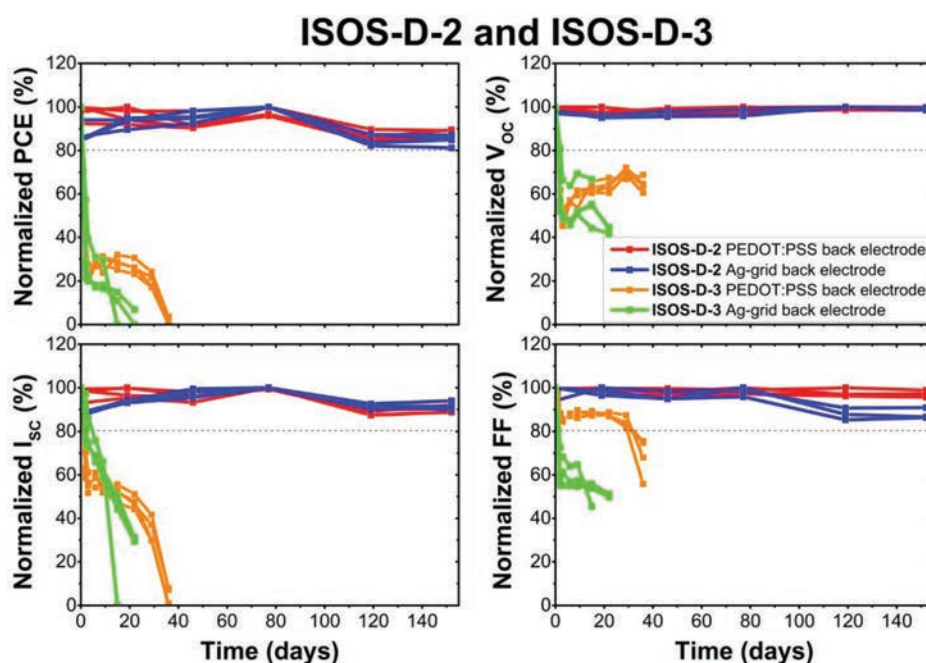

Fig. 2 Dry heat test (ISOS-D-2) and damp heat test (ISOS-D-3) on AgNW front electrode modules. Normalized stability curves of PCE, V_{OC}, I_{SC} and FF of samples with PEDOT:PSS back electrode and samples with Ag-grid back electrode.
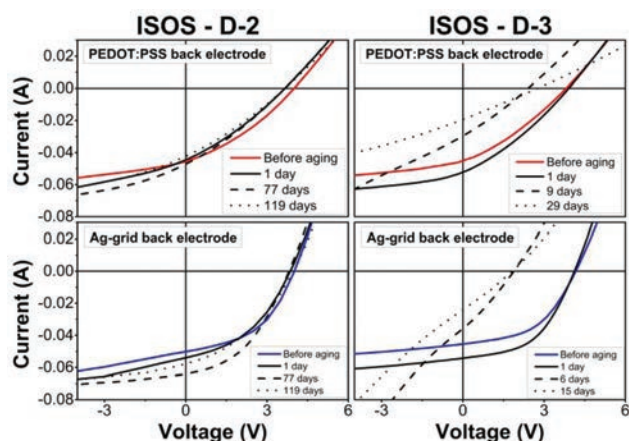
Fig. 3   *IV*-curves of ISOS-D-2 (left) and ISOS-D-3 (right) tests of beginning, halfway and close do the end of the test for AgNW front electrode modules. Sample with PEDOT:PSS back electrode (top) and sample with Ag-grid back electrode (bottom).

increase in performance until the 77th day and later a small decrease of current and fill factor. For the *IV*-curves of the ISOS-D-3 testing all samples exhibit a drastic decrease in the photovoltaic parameters. The PEDOT:PSS back electrode modules present a very slight S-shape after 9 days and for the Ag-grid back electrode it is evident indicating either de-doping of ZnO, water absorption by the PEDOT:PSS and/or further oxidation of the PEDOT:PSS/Ag interface.[19]

Indoor light tests

The tests under illumination further confirm the deteriorating effect of the humidity when comparing the results of the ISOS-L-2 dry test and ISOS-L-3 high humidity test (Fig. 4). In the test with only light and heat (ISOS-L-2) the Ag-grid back electrode samples show an increase in performance during the first 40 days and then start to degrade. This increase also matches the results of improved conductivity of the AgNW layer under light exposure as reported by Mayousse *et al.*[15] that demonstrated sintering of the silver nanowires at the crossing points leading to improved conductivity. Overall, the samples with Ag-grid back electrode show better stability under illumination compared to the PEDOT:PSS based samples. In the light, heat and humidity test (ISOS-L-3), the PEDOT:PSS back electrode samples show a linear decay while the Ag-grid back electrode samples stabilize at significantly lower efficiency after 40 days. The result is somewhat surprising, since such encapsulation was previously shown to result in similar rapid ageing of the samples under both ISOS-L-3 and ISOS-D-3 test conditions or even faster decay for the former.[17,20] This is a possible indication that PEDOT:PSS indeed loses the conduct-

The reason is ascribed to the diffusion of humidity through the edges of the module and the channels created at the device terminals (metal snaps), which has been demonstrated earlier for similar modules.[19] In damp heat both kinds of samples experience rapid decay across all the photovoltaic parameters. The *IV*-curve evolution of the samples during these ageing tests is demonstrated in Fig. 3, where for the samples under ISOS-D-2 the PEDOT:PSS back electrode devices present a slight variation of current and decrease in both FF and V_{OC}. The Ag-grid back electrode modules present an
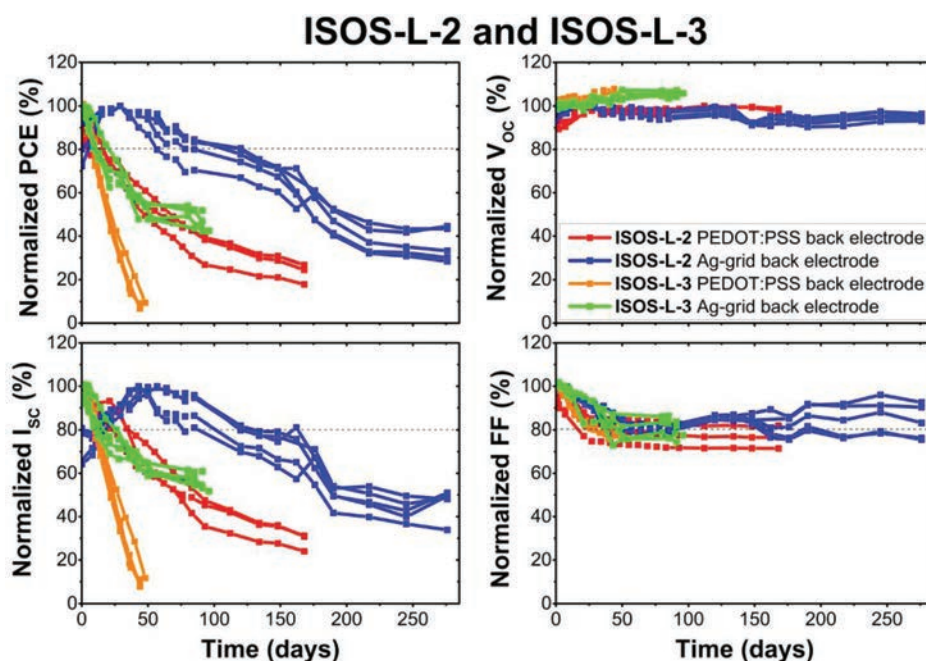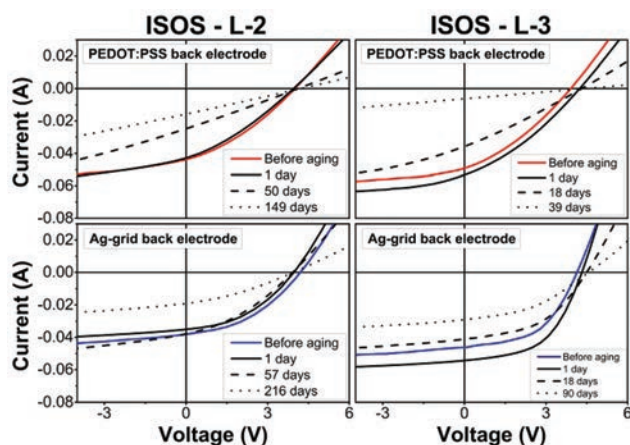

Fig. 4   Light dry heat test (ISOS-L-2) and light damp heat test (ISOS-L-3) on AgNW front electrode modules. Normalized stability curves of PCE, V_{OC}, I_{SC} and FF of samples with PEDOT:PSS back electrode and samples with Ag-grid back electrode.

Fig. 5 IV-curves of ISOS-L-2 (left) and ISOS-L-3 (right) tests of beginning, halfway and close do the end of the test on AgNW front electrode modules. Sample with PEDOT:PSS back electrode (top) and sample with Ag-grid back electrode (bottom).
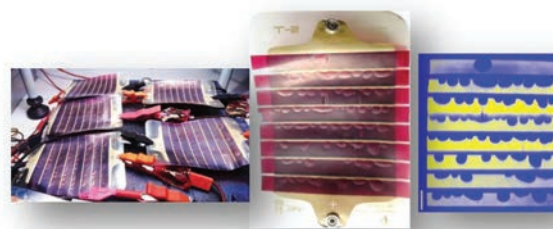

Fig. 6 Samples with AgNW front electrode and Ag-grid back electrode under ISOS-L-2 for 240 days (left). One of these samples (centre) and its corresponding LBIC image (right).

Fig. 7 Samples under ISOS-L-3 test with AgNW front electrode. Left: Samples after 2 weeks. Centre: Detail of the sample at the right bottom corner of the picture in the left. Right: Samples after finishing the test. Four samples on top are with PEDOT:PSS back electrode (no bubbles formed) and the four samples in the bottom with Ag-grid back electrode (extensive bubble formation).

ing properties when exposed to high levels of humidity and application of the Ag-grid is believed to compensate for this failure mechanism. The almost linear decrease in the current along with the drop in the fill factor further confirms the reduction of the conductivity of the PEDOT:PSS, which has also been reported in the literature.[21]

In relation to the IV-curves (Fig. 5), in the ISOS-L-2 tests we observe a clear decrease in I_{SC} and FF for both types of devices. The rectifying properties of the PEDOT:PSS back electrode samples are fully lost, however they are still present in the Ag-grid back electrode samples. In the ISOS-L-3 test it is also possible to observe an increase in the first day and then the strong decrease of the fill factor and current of the samples with PEDOT:PSS back electrode. The samples with a Ag-grid back electrode also present an increase followed shortly thereafter by a decrease in I_{SC} and FF, but they clearly retain their rectifying properties.

Bubble effect

During the ageing of the samples under illumination large bubble-like defects were gradually formed in the modules with Ag-grid back electrode. In the ISOS-L-2 test, nevertheless these defects were not observed in the first 120 days of testing. The area around the bubbles became inactive resulting in partial decrease of the photocurrent as it was possible to verify with LBIC imaging (see Fig. 6). Formation of bubble-like defects was also observed during the ISOS-L-3 test, again only in the samples with Ag-grid back electrodes (Fig. 7). The effect was in this case observed after only 15 days of testing. In Fig. 8 the microscope images of the areas with and without bubbles are compared and we can observe formation of cracks in the active layer and in the AgNW/ZnO layer in the vicinity of the areas where the bubbles formed. The cracks seem to emanate from the printed Ag-busbar. The back Ag-grid is the thickest printed layer in the OPV stack and it is highly porous with the Ag solid
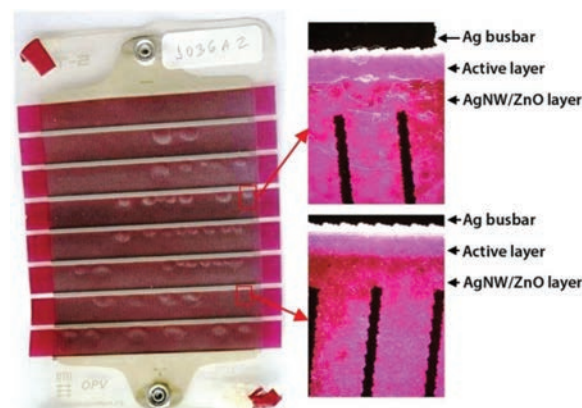

Fig. 8 Microscope images of a sample with AgNW front electrode and Ag-grid back electrode under ISOS-L-3 of a region with (right top) and without (right bottom) a bubble defect.

content corresponding to just 60% of the grid volume.[22] Solvents and/or gas trapped in the porosity of the printed Ag-grid could feasibly be the root cause of the bubble formation due to expansion/contraction of gasses in response to cyclic vari-

ation in temperature. However, further investigation is necessary to confirm the true nature of the effect. Even with such defects, the Ag-grid back electrode samples must be categorized as exhibiting stable behaviour until the end of the light tests although a catastrophic failure may be expected. Also, in the event that the bubble formation and subsequent delamination could be avoided, the performance over time would be much better as the decrease in short circuit current is mostly a result of active area loss due to delamination.

Outdoor tests

Fig. 9 shows the outdoor tests which were carried out for the entire duration of this study starting on July 11th 2014. The samples for ISOS-O-1 and ISOS-O-2 tests were placed on the same solar tracking platform. While the ISOS-O-1 samples were regularly dismounted from the platform to be measured indoors under a solar simulator and then remounted, the ISOS-O-2 samples stayed fixed on the platform connected to an automated acquisition setup. Results from these two tests are in good agreement with each other when taking all the factors that can affect the device performances into account (temperature, humidity, weather conditions, external contacts oxidation, *etc.*). For the ISOS-O-2 experiment the PCE and I_{SC} data were first normalized to 1000 W m^{-2} since the solar cells are measured under sunlight.

Most of the samples subjected to the outdoor tests start to show degradation after around 150 days of testing. For the Ag-grid back electrode samples under ISOS-O-1 the degradation seems to be evident even later after around 220 days. However these samples degrade severely after that, with a drop in both I_{SC} and V_{OC}, and in the end of the test they seem to

stabilise at a level underperforming the PEDOT:PSS back electrode samples and the samples under the ISOS-O-2 test.

For the PEDOT:PSS back electrode modules a slight decrease in I_{SC}, V_{OC} and FF is observed with none of the parameters being especially dominant for ISOS-O-1 but evidently being the main cause of decrease in current for the ISOS-O-2 tests.

Fig. 10 show the PEDOT:PSS back electrode modules losing their rectifying properties, while the Ag-grid back electrode modules still preserve them as observed in the ISOS-L-3 test.

Although the fluctuating curves do not allow making clear comparison, one obvious difference among the samples stands out in the ageing curves: the fill factor ageing is surprisingly faster for the Ag-grid back electrode devices. However, when looking at the *IV*-curves, it is obvious that the fill factor of the PEDOT:PSS based devices is already lower from the very start and thus the comparison is somewhat biased.

The complete ISOS-O-2 measurement can be seen in Fig. 11. The four samples show an increase in PCE during the first 20 days and a decrease during the autumn and winter time, which is due to the ageing, but also gradually decreasing irradiance and temperature.

When the frequency of sunny days and irradiance intensities increase at the beginning of the spring, there is a tendency for a further increase in PCE with illumination and temperature. However PCE decreases again after a short period of low irradiance (around day 260) with the final values at around 0.4% PCE for PEDOT:PSS back electrode and 0.5% PCE for Ag-grid back electrode devices.

Taking into consideration that many degradation mechanisms are linked to humidity, the AgNW modules demonstrate
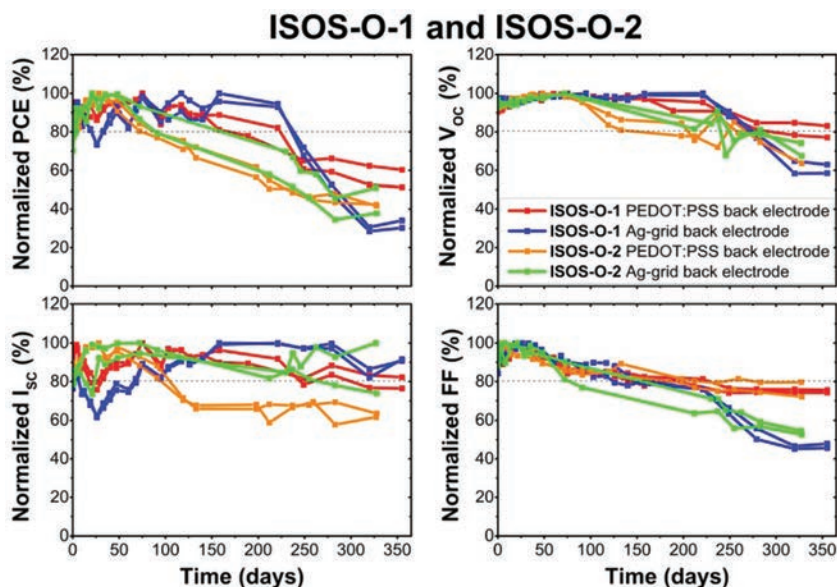

Fig. 9 Outdoor test (ISOS-O-1) and outdoor measured under sunlight test (ISOS-O-2) on AgNW front electrode modules. Normalized stability curves of PCE, V_{OC}, I_{SC} and FF of samples with PEDOT:PSS back electrode and samples with Ag-grid back electrode. Stability data measured under sunlight had PCE and I_{SC} normalized to 1 Sun (1000 W m^{-2}).
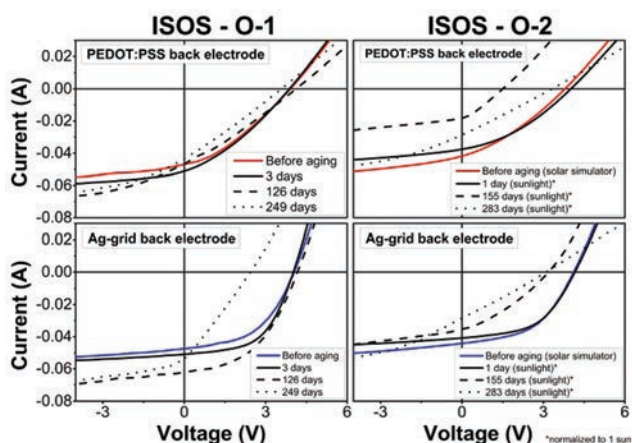
Fig. 10 *IV*-curves of ISOS-O-1 (left) and ISOS-O-2 (right) tests of beginning, halfway and close do the end of the test on AgNW front electrode modules. Sample with PEDOT:PSS back electrode (top) and sample with Ag-grid back electrode (bottom). *IV*-curves measured under sunlight had PCE and I_{SC} normalized to 1 Sun (1000 W m^{-2}).

considerable stability during one year of outdoor exposure. Since it is attributed to water diffusion through edges and electrodes with metal snaps, larger edges and new options for the contacts in these samples would make the devices last considerably longer.[19,23]

Comparison of devices with different front and back electrodes

The following paragraph compares the samples presented in this work with the previously reported stability of freeOPV modules.[17] These modules have the layer stack Ag-grid/PEDOT:PSS/ZnO/P3HT:PCBM/PEDOT:PSS/Ag-grid, therefore differing from the Ag-grid back electrode devices presented here only by the front electrode (no AgNW). The time that the device reaches 80% of its initial efficiency (T_{80}) gives very prac-

tical information for future application and highlights where developments are needed. Typical OPV devices often experience initial rapid ageing (burn in) followed by a more stabilized phase, however in the tests performed in this work many of the stability curves show no clear stabilization phase. We therefore considered the time it takes for the device to reach 50% of its initial efficiency (T_{50}) for better comparison. For the comparative presentation a diagram with logarithmic scale called the "o-diagram" with "o" referring to OPV is used (Fig. 12).[24] The time scale is chosen to be Log$_4$ (days) for the *X*-axis in order to associate the *X*-axis with the common time units shown in the upper part of the diagram. E_0 and E_{50} values are represented by the *Y*-axis. Combined in the o-diagram are the T_{80} (filled markers) and T_{50} (open markers) values *versus* the initial PCE (E_0) and 50% of initial PCE (E_{50}) respectively for the devices measured in this work and for the previously reported free OPV modules (no AgNW).

Under ISOS-D-2 test conditions, all samples are very stable and tend to last for years. For ISOS-D-3, similarly low T_{80} and T_{50} are obtained for all the devices, since the modules have identical packaging and thus experience the same edge diffusion failure mechanisms. ISOS-L-2 presents a remarkable increase in T_{80} for the AgNW devices, from one day (Ag-grid front and back electrode sample) to weeks for the PEDOT:PSS back electrode devices and to months for the Ag-grid back electrode devices with the best performing devices taking seasons to reach T_{80}. T_{50} also takes proportionally longer to be reached. For ISOS-L-3 a very important stability increase for the AgNW devices is also registered and even with the sensitivity of the whole device to humidity, the Ag-grid back electrode devices remain stable until the end of the test, although a catastrophic failure was expected due to the formation of bubbles previously mentioned. ISOS-O-1 show a much longer T_{80} from weeks for the front and back Ag-grid modules to seasons for the AgNW based devices. The modules with a PEDOT:PSS back electrode are generally less stable than the devices with Ag-grid, except in ISOS-O-1 although the variations between
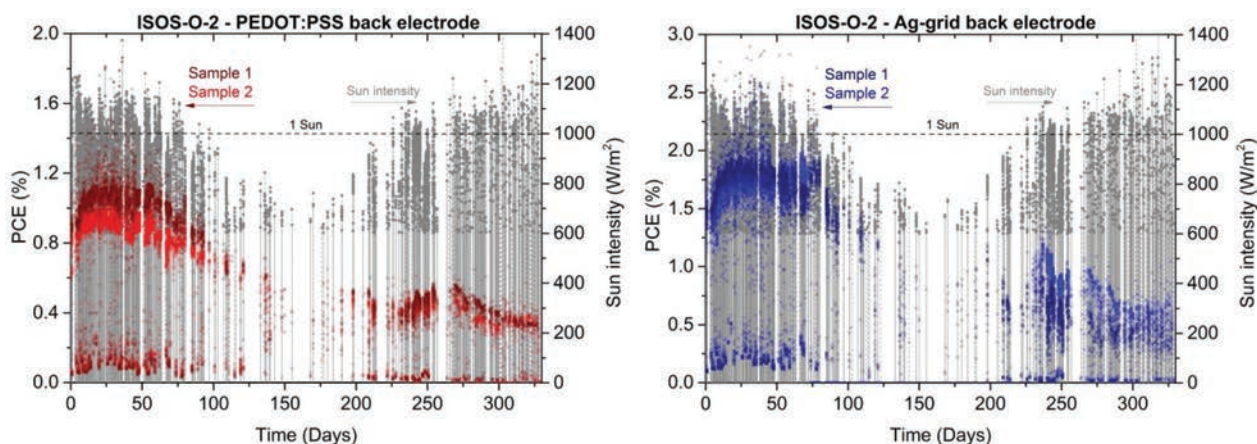

Fig. 11 ISOS-O-2 complete stability curves of two samples with PEDOT:PSS back electrode (left) and Ag-grid back electrode (right), all with AgNW front electrode. Sun intensity lower than 600 W m^{-2} were disregarded in order to consider the day light measurements only.
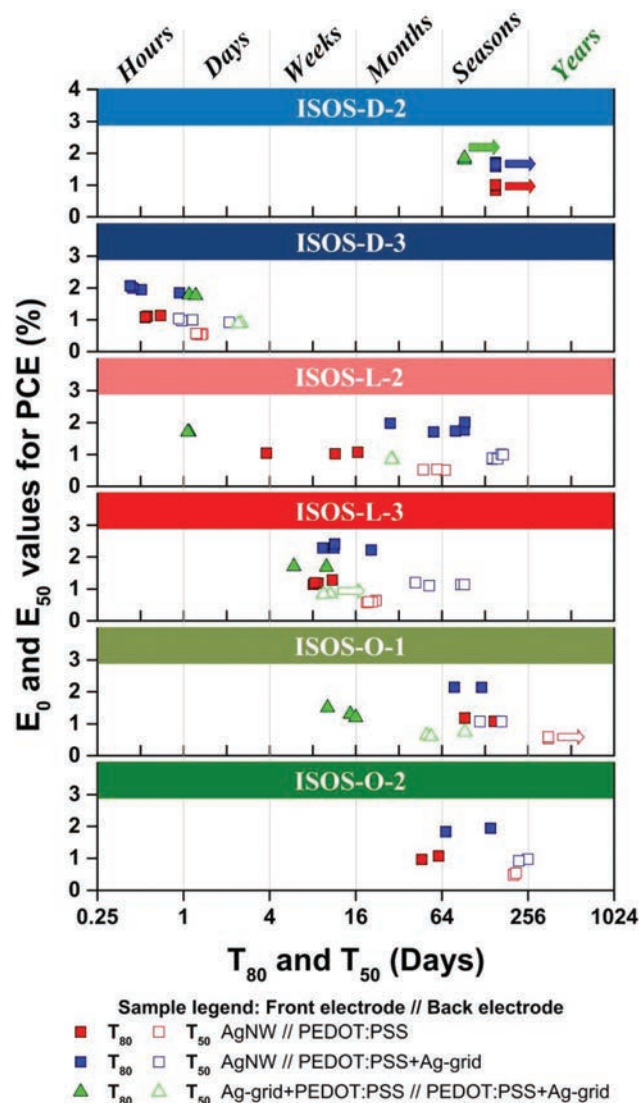
Fig. 12 The o-diagram presents the T_{80} (filled markers) and T_{50} (open markers) values of OPV modules with (square markers) and without (triangle markers) AgNW as the front electrode under different ISOS test conditions referred in Table 1.

ISOS-O-1 and ISOS-O-2 indicate that the T_{80} and T_{50} of both AgNW based modules are in the range of variation of outdoor tests.

As mentioned before, the degradation mechanisms leading to the loss of the rectifying properties of the OPV is linked to both oxygen and water that affects the conductivity of the ZnO and PEDOT:PSS layers leading to further oxidation of the Ag-grid. The characteristic S-shape of the *IV*-curve indicating these mechanisms is only observed in the ISOS-D-3 test during the stability study of the AgNW based devices, possibly representing the minimization of these mechanisms with the use of the AgNW/ZnO hybrid layer as front electrode instead of a ZnO layer as well as the use of PEDOT:PSS only in the back electrode. Even though the AgNW based devices are still sensitive to humidity due to the contacts and short edge seal, the

increase in T_{80} and T_{50} in the light and outdoor tests in comparison to modules with Ag-grid front and back electrodes present a substantial development in stability for large scale R2R produced OPV using AgNWs as the front electrode.

Conclusions

In the course of the stability tests and considering the overview provided by the o-diagram, we observed the following points:

(a) The stability curves and T_{80} and T_{50} parameters of ISOS-L-2 test for the samples with AgNW front electrode and Ag-grid back electrode indicate that the AgNW have a positive influence on the performance and stability of devices due to the sintering of the nanowire network under light exposure which corroborates the work of Mayousse *et al.*;

(b) Bubble formation in the samples with Ag-grid back electrode was observed and its cause associated to solvents and/or gas trapped in the porous volume of the printed Ag-grid that expands with exposure to light and high temperature cycling.

(c) The better performance and stability of the Ag-grid back electrode samples points to the importance of the Ag-grid in conjunction with PEDOT:PSS to maintain a high back electrode conductivity in the devices;

(d) Modules with AgNWs as the front electrode demonstrate an improved stability under ISOS-L-2, ISOS-L-3 and ISOS-O-1 conditions possibly due to the use of hygroscopic PEDOT:PSS in only one of the OPV electrodes and the printing of the ZnO in a hybrid layer together with the AgNW.

The use of AgNW as the front electrode in OPV saves 2 printing steps making the manufacture of the devices faster and more environmentally friendly and such improvements in the stability of the OPV devices bring them closer to commercialization. Further improvements are expected to be achievable by increasing the edge sealing and also by employing a UV-protective filter on the front face of the modules. Finally, development of new and less porous back electrode structures that avoid the bubble formation may provide OPV devices with longer lifetimes.

Acknowledgements

References

1 W. S. Koh, C. H. Gan, W. K. Phua, Y. A. Akimov and P. Bai, *J. Sel. Top. Quantum Electron.*, 2014, **20**, 1.
2 Z. C. Gomez, L. De Arco, Y. Zhang, C. W. Schlenker, K. Ryu and M. E. Thompson, *ACS Nano*, 2010, **4**, 2865.

3 K. Kim, S. H. Bae, C. T. Toh, H. Kim, J. H. Cho, D. Whang, T. W. Lee, B. Özyilmaz and J. H. Ahn, *ACS Appl. Mater. Interfaces*, 2014, **6**, 3299.

4 Y. Zhou, F. Zhang, K. Tvingstedt, S. Barrau, F. Li, W. Tian and O. Inganäs, *Appl. Phys. Lett.*, 2008, **92**, 1.

5 S. I. Na, S. S. Kim, J. Jo and D. Y. Kim, *Adv. Mater.*, 2008, **20**, 4061.

6 M. Kaltenbrunner, M. S. White, E. D. Głowacki, T. Sekitani, T. Someya, N. S. Sariciftci and S. Bauer, *Nat. Commun.*, 2012, **3**, 770.

7 D. Angmo, T. T. Larsen-Olsen, M. Jørgensen, R. R. Søndergaard and F. C. Krebs, *Adv. Energy Mater.*, 2013, **3**, 172.

8 F. C. Krebs, N. Espinosa, M. Hösel, R. R. Søndergaard and M. Jørgensen, *Adv. Mater.*, 2014, **26**, 29.

9 M. Hösel, R. R. Søndergaard, M. Jørgensen and F. C. Krebs, *Energy Technol.*, 2013, **1**, 102.

10 J.-S. Yu, I. Kim, J.-S. Kim, J. Jo, T. T. Larsen-Olsen, R. R. Søndergaard, M. Hösel, D. Angmo, M. Jørgensen and F. C. Krebs, *Nanoscale*, 2012, **4**, 6032.

11 S. Nam, M. Song, D.-H. Kim, B. Cho, H. M. Lee, J.-D. Kwon, S.-G. Park, K.-S. Nam, Y. Jeong, S.-H. Kwon, Y. C. Park, S.-H. Jin, J.-W. Kang, S. Jo and C. S. Kim, *Sci. Rep.*, 2014, **4**, 4788.

12 W. Gaynor, S. Hofmann, M. G. Christoforo, C. Sachse, S. Mehra, A. Salleo, M. D. McGehee, M. C. Gather, B. Lüssem, L. Müller-Meskamp, P. Peumans and K. Leo, *Adv. Mater.*, 2013, **25**, 4006.

13 J. H. Yim, S. Y. Joe, C. Pang, K. M. Lee, H. Jeong, J. Y. Park, Y. H. Ahn, J. C. De Mello and S. Lee, *ACS Nano*, 2014, **8**, 2857.

14 M. Hösel, D. Angmo, R. R. Søndergaard, G. A. dos Reis Benatto, J. E. Carlé, M. Jørgensen and F. C. Krebs, *Adv. Sci.*, 2014, 1.

15 C. Mayousse, C. Celle, A. Fraczkiewicz and J. Simonato, *Nanoscale*, 2015, 2107.

16 M. O. Reese, S. A. Gevorgyan, M. Jørgensen, E. Bundgaard, S. R. Kurtz, D. S. Ginley, D. C. Olson, M. T. Lloyd, P. Morvillo, E. a. Katz, A. Elschner, O. Haillant, T. R. Currier, V. Shrotriya, M. Hermenau, M. Riede, K. R. Kirov, G. Trimmel, T. Rath, O. Inganäs, F. Zhang, M. Andersson, K. Tvingstedt, M. Lira-Cantu, D. Laird, C. McGuiness, S. Gowrisanker, M. Pannone, M. Xiao, J. Hauch, R. Steim, D. M. DeLongchamp, R. Rösch, H. Hoppe, N. Espinosa, A. Urbina, G. Yaman-Uzunoglu, J.-B. Bonekamp, A. J. J. M. van Breemen, C. Girotto, E. Voroshazi and F. C. Krebs, *Sol. Energy Mater. Sol. Cells*, 2011, **95**, 1253.

17 M. Corazza, F. C. Krebs and S. A. Gevorgyan, *Sol. Energy Mater. Sol. Cells*, 2014, **130**, 99.

18 F. C. Krebs and M. Jørgensen, *Adv. Opt. Mater.*, 2014, **2**, 465.

19 S. A. Gevorgyan, M. V. Madsen, H. F. Dam, M. Jørgensen, C. J. Fell, K. F. Anderson, B. C. Duck, A. Mescheloff, E. a. Katz, A. Elschner, R. Roesch, H. Hoppe, M. Hermenau, M. Riede and F. C. Krebs, *Sol. Energy Mater. Sol. Cells*, 2013, **116**, 187.

20 F. Yan, J. Noble, J. Peltola, S. Wicks and S. Balasubramanian, *Sol. Energy Mater. Sol. Cells*, 2012, **114**, 214.

21 J. Liu, M. Agarwal, K. Varahramyan, E. S. Berney IV and W. D. Hodo, *Sensors Actuators, B*, 2008, **129**, 599.

22 H. F. Dam, T. R. Andersen, E. B. L. Pedersen, K. T. S. Thydén, M. Helgesen, J. E. Carlé, P. S. Jørgensen, J. Reinhardt, R. R. Søndergaard, M. Jørgensen, E. Bundgaard, F. C. Krebs and J. W. Andreasen, *Adv. Energy Mater.*, 2015, **5**, 1400736.

23 D. Angmo and F. C. Krebs, *Energy Technol.*, 2015, **3**, 774.

24 S. A. Gevorgyan, M. Corazza, M. V. Madsen, G. Bardizza, A. Pozza, H. Müllejans, J. C. Blakesley, G. F. a. Dibb, F. a. Castro, J. F. Trigo, C. M. Guillén, J. R. Herrero, P. Morvillo, M. G. Maglione, C. Minarini, F. Roca, S. Cros, C. Seraine, C. H. Law, P. S. Tuladhar, J. R. Durrant and F. C. Krebs, *Polym. Degrad. Stab.*, 2014, **109**, 162.

Round-Robin Studies on Roll-Processed ITO-free Organic Tandem Solar Cells Combined with Inter-Laboratory Stability Studies

Francesco Livi,[a] Roar R. Søndergaard,[a] Thomas R. Andersen,[a] Bérenger Roth,[a] Suren Gevorgyan,[a] Henrik F. Dam,[a] Jon E. Carlé,[a] Martin Helgesen,[a] George D. Spyropoulos,[b] Jens Adams,[c] Tayebeh Ameri,[b] Christoph J. Brabec,[b, c] Mathilde Legros,[d] Noëlla Lemaitre,[d] Stephane Berny,[e] Owen R. Lozman,[e] Stefan Schumann,[f] Arnulf Scheel,[f] Pälvi Apilo,[g] Marja Vilkman,[h] Eva Bundgaard,[a] and Frederik C. Krebs*[a]

Roll-processed, indium tin oxide (ITO)-free, flexible, organic tandem solar cells and modules have been realized and used in round-robin studies as well as in parallel inter-laboratory stability studies. The tandem cells/modules show no significant difference in comparison to their single-junction counterparts and the use of round-robin studies as a consensus tool for evaluation of organic solar cell parameters is judged just as viable for the tandem solar cells as for single-junction devices. The inter-laboratory stability studies were conducted according to testing protocols ISOS-D-2, ISOS-D-3, and ISOS-L-2, and in spite of a much more complicated architecture the organic tandem solar cells show no significant difference in stability in comparison to their single-junction counterparts.

Research on organic solar cells is thriving, but with the increasing number of publications comes the problem of consensus. The reported results come from a large variety of groups with different types of measuring equipment at their disposal, which can lead to ambiguous results. The organic solar cell community thus needs an approach to certify the obtained results in order to reach a common agreement on the status of the field. Very few laboratories have the capability to certify efficiency data for solar cells, and, although it is possible to acquire certification from them, this is not a viable approach as these laboratories would simply not have capacity to deal with such large volumes of certifica-

tion. In addition, certification is a rather costly affair for many groups. As alternatives to certification, round-robin studies (in which the same solar cell sample is characterized by independent participants) and inter-laboratory studies (in which the same type of cell is studied by independent participants) are powerful tools to reach a consensus, and both methods have been used successfully as evaluation tools on several occasions for inorganic solar cells[1] and polymer solar cells/modules.[2]

Organic tandem solar cells have recently received increased attention because of the prospects of harvesting a larger portion of the solar spectrum and which would bring about a corresponding increase in efficiency.[3] The tandem solar cell employs complementary polymers that absorb light in different wavelength regions to increase the total absorption band, and this is typically achieved by stacking the two junctions on top of each other with a recombination layer between the two to ensure effective charge flow through the device.

An important question to be answered with respect to the tandem cell is whether such a new cell design comprising a broader total absorption spectrum will impose larger (or lesser) discrepancies to the efficiency data between laboratories as compared to single-junction solar cells. The tandem cell contains a significantly increased number of processed layers in the solar cell stack (typically 10–14) compared to its single-junction counterparts, which of course renders the finished device more susceptible to defects. This is probably the

[a] F. Livi, Dr. R. R. Søndergaard, Dr. T. R. Andersen, B. Roth, Dr. S. Gevorgyan, Dr. H. F. Dam, Dr. J. E. Carlé, Dr. M. Helgesen, Dr. E. Bundgaard, Prof. F. C. Krebs
Dept. of Energy Conversion and Storage
Technical University of Denmark
Frederiksborgvej 399, DK-4000 Roskilde (Denmark)
E-mail: frkr@dtu.dk

[b] G. D. Spyropoulos, Dr. T. Ameri, Prof. C. J. Brabec
Institute of Materials for Electronics and Energy Technology (I-MEET)
Department of Materials Science and Engineering
Friedrich-Alexander University Erlangen-Nuremberg
Martensstraße 7, 91058 Erlangen (Germany)

[c] J. Adams, Prof. C. J. Brabec
Bavarian Center for Applied Energy Research (ZAE Bayern e.V.)
Renewable Energies
Haberstraße 2a, 91058 Erlangen (Germany)

[d] Dr. M. Legros, Dr. N. Lemaitre
CEA, LITEN, Department of Solar Technologies
F-73375 Le Bourget du Lac (France)

[e] Dr. S. Berny, Dr. O. R. Lozman
Merck Chemicals Ltd., Chilworth Technical Centre
University Parkway, Southampton SO16 7QD (UK)

[f] Dr. S. Schumann, Dr. A. Scheel
Heraeus Precious Metals GmbH & Co. KG
Electronic Materials Division
Chempark Leverkusen/Gebäude B 202, D-51368 Leverkusen (Germany)

[g] P. Apilo
VTT Technical Research Centre of Finland, Printed Functional Solutions
Kaitoväylä 1, FI-90571 Oulu (Finland)

[h] Dr. M. Vilkman
VTT Technical Research Centre of Finland, Printed Functional Solutions
Tietotie 3, FI-02150 Espoo (Finland)

Supporting information for this article is available on the WWW under http://dx.doi.org/10.1002/ente.201402095.

This manuscript is part of a Special Issue on printed energy technologies. A link to the issue's Table of Contents will appear here. This text will be updated once the Special Issue is assembled.
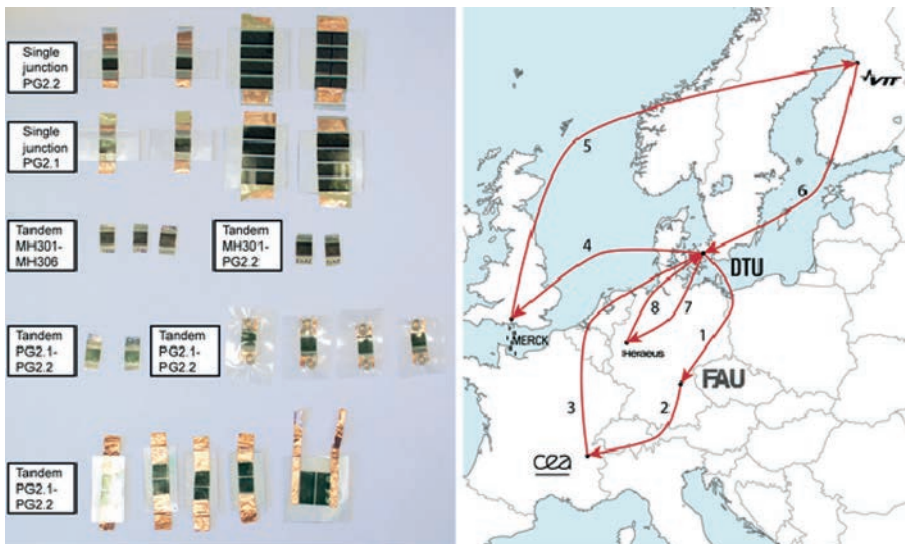
Figure 1. a) Photograph of all the cells and modules used in the round-robin experiments. b) Illustration of the travel routes performed by the operator/cells amongst the different participants in the round-robin analysis.

reason why very few results have been published to this point on flexible, polymer tandem solar cells[4,5] despite the fact that the original motivation behind the organic solar cell has always had its roots in roll-to-roll (R2R) solution processing on inexpensive flexible substrates. Testing of the tandem solar cell's device compatibility with flexible substrates and R2R-compatible coating and printing methods is thus very important to study along with the final device stability.

In this work we demonstrate a round-robin study of roll-processed, indium tin oxide (ITO)-
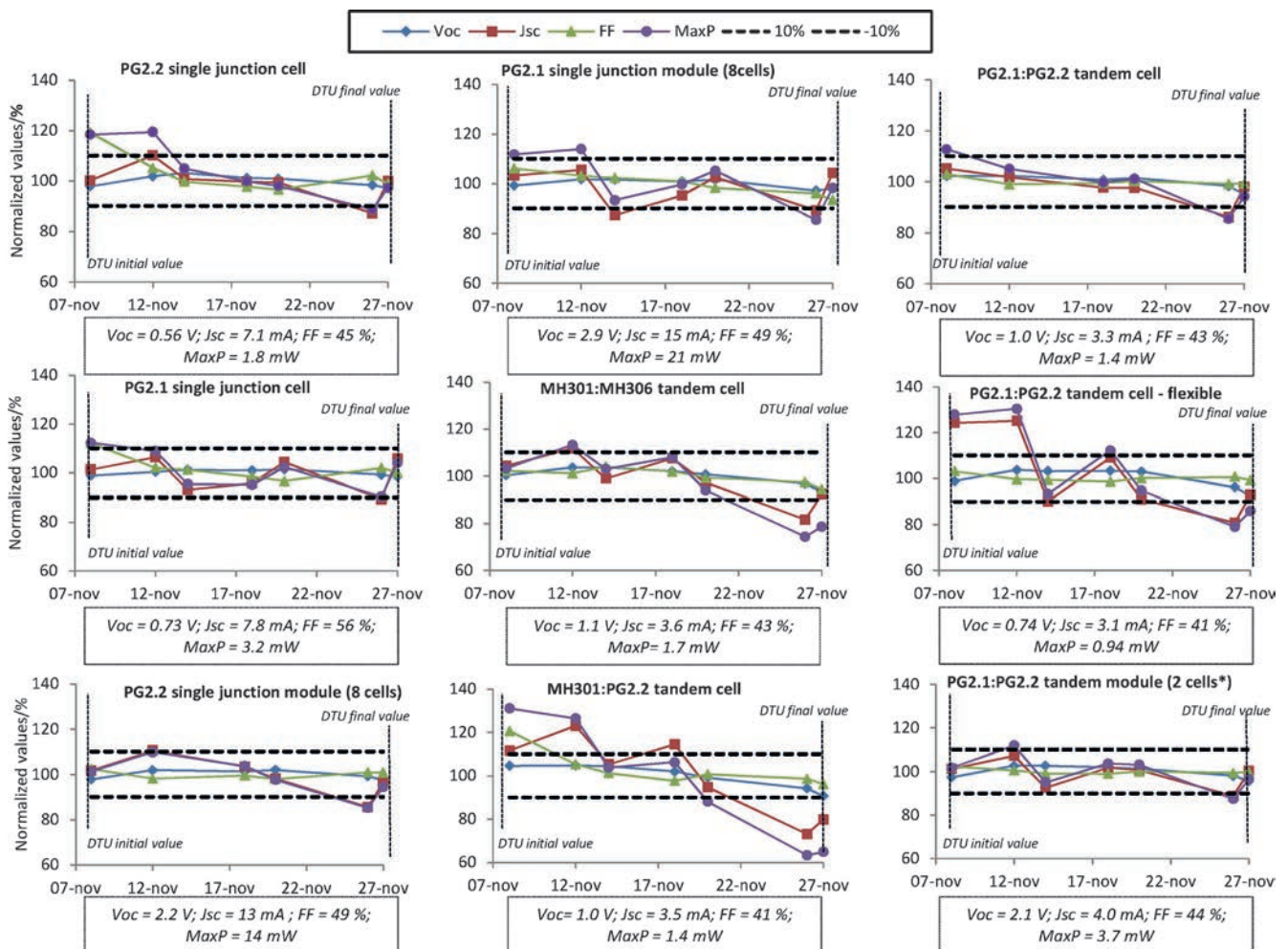
Figure 2. Round-robin experimental results. Graphical illustration for the normalized cell parameters for a typical cell of each type (the full data set can be found in the Supporting Information). The parameters are presented as a function of time and each data set for a particular date represents a new laboratory.
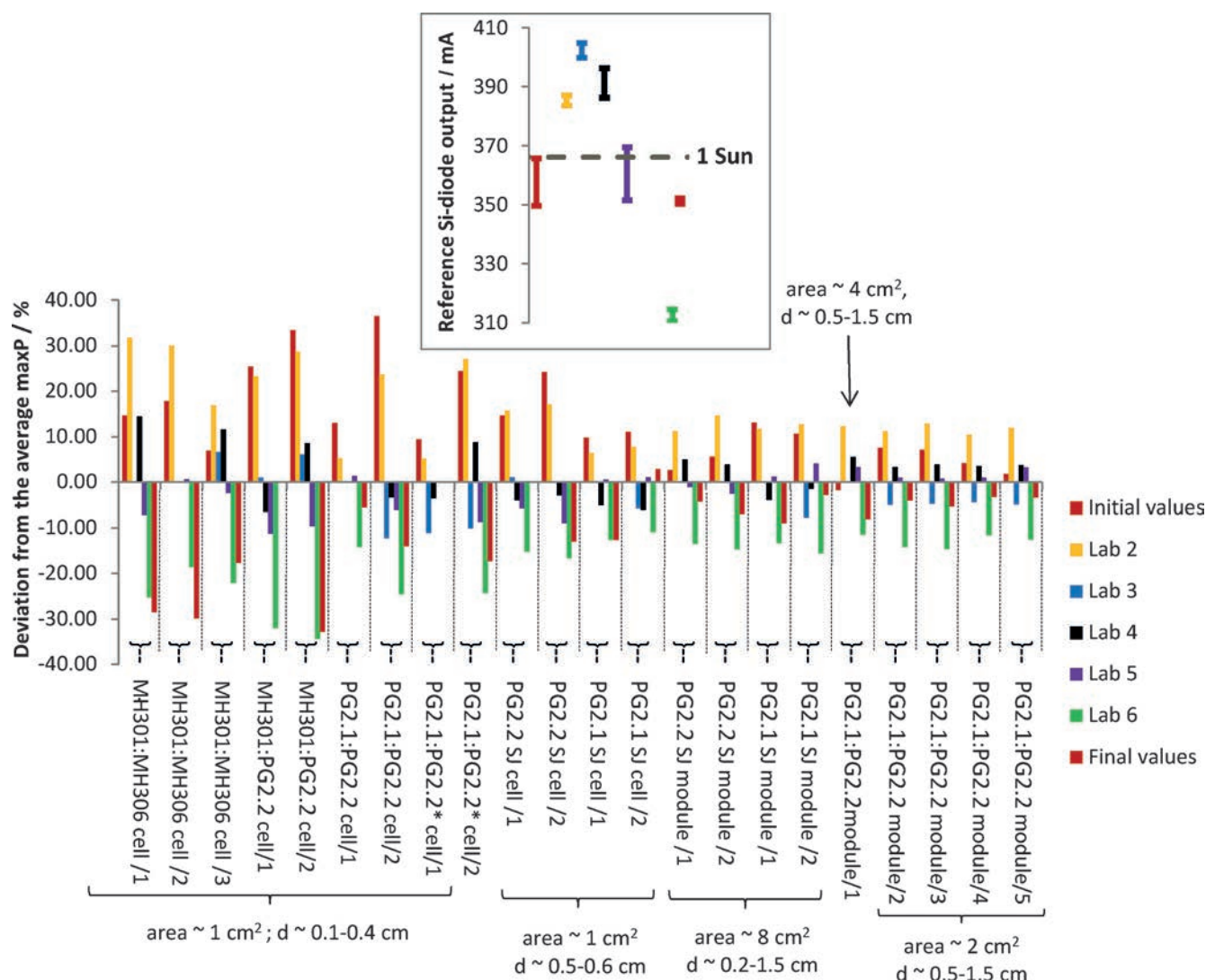
↖↖ These are not the final page numbers!

Figure 3. Relative deviation for each cell/module from the average values of the maximum power. The insert shows the measured light intensities for the calibrated system at each laboratory. The asterisk (*) indicates the cells that were encapsulated with a flexible barrier, and *d* represents the distance from the outer edge of the encapsulation glue to the edge of the solar cell.

free, organic tandem solar cells on flexible substrates. To minimize the influence of the operator, the same person has traveled along with the cells among the six involved participants and this same person has also performed all measurements at the different locations after calibration of the sun simulator by a local representative.

In parallel with the round-robin studies, an inter-laboratory stability study has been performed according to different International Summit on OPV Stability (ISOS) protocols[6] to examine the stability of the same types of cells.

Flexible organic tandem solar cells and modules as well as the corresponding single-junction counterparts were prepared by roll-coating/printing in mid-November 2013 at the Danish Technical University (DTU) in Denmark by using procedures previously described[4,7] followed by encapsulation with a glass or flexible barrier foil and a UV-curable adhesive. The cells were then characterized by a specified operator after which the same operator within the following two

weeks traveled amongst the other involved participants (CEA, France; FAU, Germany; VTT, Finland; Heraeus Clevios, Germany; and Merck, United Kingdom) carrying the same cells and characterizing them at each location (Figure 1b). After returning to DTU in Denmark the cells were characterized again to identify if any degradation had occurred during the study. Figure 1 shows a picture of the cells and modules used for the round-robin studies along with an illustration of the travel routes of the operator/cells. The cells were primarily prepared using two polymers from Merck [a high-band-gap polymer, Polymer Generation 2.1 (PG2.1), and a low-band-gap polymer, Polymer Generation 2.2 (PG2.2)], but as can be seen from Figure 1a, a few small tandem cells using different polymers (MH301 and MH306, see Supporting Information for chemical structures) were also included. A minimum of two cells of similar size and performance were studied for each cell/module type with the exception of the largest tandem module using PG2.1:PG2.2

These are not the final page numbers! ↗↗

for which only a single module was prepared. After completing the measurements, all values that deviated by more than 10% from the average value of the raw data were discarded. This allowed elimination of outliers that could infringe on the general average. A new normalized average value for each parameter (V_{OC}, I_{SC}, FF, and maximal power) was then calculated and used in the actual study. Representative graphs of the final results are shown in Figure 2, and the complete data set is included in the Supporting Information. The general observation is that there is no significant difference between the single-junction cell and the tandem cells. The data primarily lies within ±10% of the average values, which correlates well with what has been observed in previous round-robin studies. It is quite clear though, from the comparison of the initial and final power output, that some of the smaller cells have experienced degradation during the three weeks of the study whereas the larger modules were much less susceptible. This is further illustrated in Figure 3 showing the relative deviation of the maximum power (max$P$) for each specific cell type. Moreover there is a clear relationship between the distances from the outer edge of the encapsulation glue to the edge of the solar cell (noted as d in Figure 3) and the deviation in max$P$. Shorter distances result in larger deviations, which indicates that the decrease in performance is mainly due to edge-induced degradation. This is supported by the fact that the larger cells/modules appear less vulnerable as they have a lower edge/area ratio. Such degradation is of course not desirable in a round-robin study for which the physical parameters of a cell should be constant, but similar trends for the single-junction cells/modules were observed (compared with the tandem cells/modules), which suggests that there is no significant deviation between the single-junction and tandem cells in terms of round-robin certification. An internal silicon reference diode was used at all locations after calibration of the light sources according to the local calibration procedures. This was implemented as an extra measure to compare the light sources at each laboratory and to monitor any fluctuations in the light intensity over time. Comparisons of the results for the stable devices with the output from the reference silicon diode show close agreement (Figure 3) despite the difference in the spectral response between the organic samples and silicon diode. Laboratories with high light intensities (as determined by the reference diode) generally also showed higher power for the organic cells/modules. The complete data set as well as graphs adjusted to the 1 sun value of the photodiode can be found in the Supporting Information.

In parallel to the round-robin study, a stability study on the same type of cell was conducted at DTU and FAU to identify whether tandem cells show a significant stability difference in comparison to single-junction devices prepared with the same materials. The study was performed in agreement with the ISOS-D-2, ISOS-D-3, and ISOS-L-2 protocols.[6] Each laboratory performed two different experiments (DTU: ISOS-D-2 and ISOS-L-2; FAU: ISOS-D-2 and ISOS-D-3). Each experiment involved A) two tandem cells with polymer PG2.1 and PG2.2, B) two single-junction cells with

polymer PG2.1 and C) two single-junction cells with polymer PG2.2—a total of 24 cells were examined in the study and all were encapsulated in a similar way to the stable devices in the round-robin experiment. Figure 4 illustrates the outcome of the tests with respect to the normalized maximum power (for full I–V characteristics analysis see the Supporting Information). All three cell types behaved similarly during the tests. For the dark tests (D-2 and D-3), a slow continuous decrease in Max$P$ was observed, and a similar behavior was observed in the light-soaking experiment (L-2) after an initial burn-in.

The overall conclusion from the round-robin and stability studies performed on ITO-free, flexible, roll-processed organic tandem solar cells and their single-junction counterparts tested under dark and light conditions is that they show no significant differences. Round-robin certification is thus
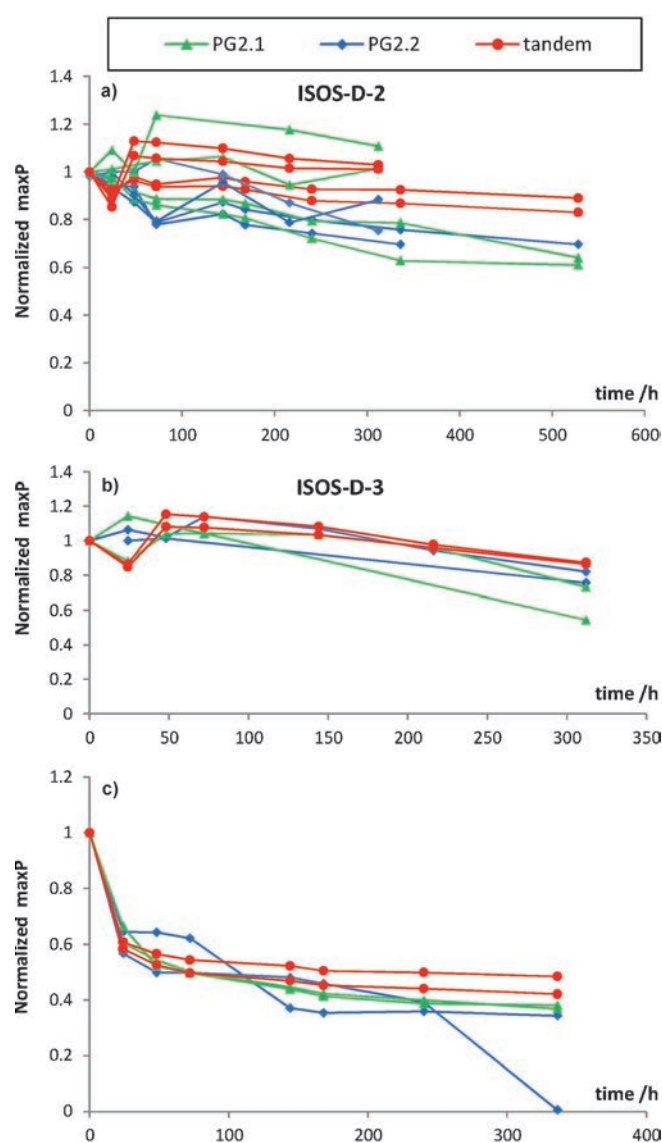

Figure 4. Stability tests performed under ISOS-D-2 (a), ISOS-D-3 (b), and ISOS-L-2 (c) conditions. The normalized maximum power is plotted against time.

�⫶ **These are not the final page numbers!**

found to be just as viable for application to tandem devices as for single-junction cells.

Experimental Section

All cells were prepared on ITO-free flexible Flextrode substrates[8] by roll coating as previously described.[4,7] The cells were encapsulated between two glass slides by using a UV-curable adhesive from DELO (LP655). In the cases utilizing flexible encapsulation, a three-ply barrier foil from AMCOR was used. A Hamamatsu photodiode (S5971) was used as the internal reference cell. For the devices that indicated a contact problem or other damage to the cell during evaluation, the data was excluded from the analysis.

Acknowledgements

[1] a) J. Metzdorf, T. Wittchen, K. Heidler, K. Dehne, R. Shimokawa, F. Nagamine, H. Ossenbrink, L. Fornarini, C. Goodbody, M. Davies, K. Emery, R. DeBlasio in *Photovoltaic Specialists Conf.*, *1990*, *Conf. Record of the 21st IEEE*, 21 May, **1990** Orlando, Florida; b) C. R. Osterwald in *Photovoltaic Specialists Conf.*, *1993*, *Conf. Record of the 23rd IEEE*, 10 May, **1993** Louisville, Kentucky; c) H. Ossenbrink, K. Krebs, R. V. Steenwinckel in *Conf. Record of the 18th IEEE Photovoltaic Specialists Conf.*, **1985** Las Vegas, Nevada; d) T. R. Betts, R. Gottschalg, D. G. Infield, W. Kolodenny, M. Prorok, T. Zdanowicz, N. van der Borg, H. de Moor, G. Friesen, A. Guerin de Montgareuil, W. Herrmann in *21st Eur. Photovoltaic Solar Energy Conf.*, **2006** Dresden, Germany; e) W. Herrmann, S. Mau, F. Fabero, T. Betts, N. van der Borg, K. Kiefer, G. Friesen, W. Zaaiman in *22nd Eur. Photovoltaic Solar Energy Conf.*, **2007** Milan, Italy.

[2] a) S. A. Gevorgyan, A. J. Medford, E. Bundgaard, S. B. Sapkota, H. F. Schleiermacher, B. Zimmermann, U. Würfel, A. Chafiq, M. Lira-Cantu, T. Swonke, M. Wagner, C. J. Brabec, O. O. Haillant, E. Voroshazi, T. Aernouts, R. Steim, J. A. Hauch, A. Elschner, M. Pannone, M. Xiao, A. Langzettel, D. Laird, M. T. Lloyd, T. Rath, E. Maier, G. Trimmel, M. Hermenau, T. Menke, K. Leo, R. Rösch, M. Seeland, H. Hoppe, T. J. Nagle, K. B. Burke, C. J. Fell, D. Vak, T. B. Singh, S. E. Watkins, Y. Galagan, A. Manor, E. A. Katz, T. Kim, K. Kim, P. M. Sommeling, W. J. H. Verhees, S. C. Veenstra, M. Riede, M. G. Christoforo, T. Currier, V. Shrotriya, G. Schwartz, F. C. Krebs, *Solar Energy Mater. Solar Cells* **2011**, *95*, 1398–1416; b) F. C. Krebs, S. A. Gevorgy-an, B. Gholamkhass, S. Holdcroft, C. Schlenker, M. E. Thompson, B. C. Thompson, D. Olson, D. S. Ginley, S. E. Shaheen, H. N. Alshareef, J. W. Murphy, W. J. Youngblood, N. C. Heston, J. R. Reynolds, S. J. Jia, D. Laird, S. M. Tuladhar, J. G. A. Dane, P. Atienzar, J. Nelson, J. M. Kroon, M. M. Wienk, R. A. J. Janssen, K. Tvingstedt, F. L. Zhang, M. Andersson, O. Inganäs, M. Lira-Cantu, R. de Bettignies, S. Guillerez, T. Aernouts, D. Cheyns, L. Lutsen, B. Zimmermann, U. Würfel, M. Niggemann, H. F. Schleiermacher, P. Liska, M. Grätzel, P. Lianos, E. A. Katz, W. Lohwasser, B. Jannon, *Solar Energy Mater. Solar Cells* **2009**, *93*, 1968–1977; c) T. T. Larsen-Olsen, F. Machui, B. Lechene, S. Berny, D. Angmo, R. Søndergaard, N. Blouin, W. Mitchell, S. Tierney, T. Cull, P. Tiwana, F. Meyer, M. Carrasco-Orozco, A. Scheel, W. Lövenich, R. de Bettignies, C. J. Brabec, F. C. Krebs, *Adv. Energy Mater.* **2012**, *2*, 1091–1094; d) T. T. Larsen-Olsen, S. A. Gevorgyan, R. R. Søndergaard, M. Hösel, Z. Gu, H. Chen, Y. Liu, P. Cheng, Y. Jing, H. Li, J. Wang, J. Hou, Y. Li, X. Zhan, J. Wu, J. Liu, Z. Xie, X. Du, L. Ding, C. Xie, R. Zeng, Y. Chen, W. Li, T. Xiao, N. Zhao, F. Chen, L. Chen, J. Peng, W. Ma, B. Xiao, H. Wu, X. Wan, Y. Chen, R. Chang, C. Li, Z. Bo, B. Ji, W. Tian, S. Chen, L. Hu, S. Dai, F. C. Krebs, *Solar Energy Mater. Solar Cells* **2013**, *117*, 382–389; e) R. Søndergaard, T. Makris, P. Lianos, A. Manor, E. A. Katz, W. Gong, S. M. Tuladhar, J. Nelson, P. Sommerling, S. C. Veenstra, A. Rivaton, A. Dupuis, G. Teran-Escobar, M. Lira-Cantu, S. B. Sabkota, B. Zimmermann, U. Würfel, F. C. Krebs, *Solar Energy Mater. Solar Cells* **2012**, *99*, 292–300; f) S. A. Gevorgyan, O. Zubillaga, J. M. V. de Seoane, M. Machado, E. A. Parlak, N. Tore, E. Voroshazi, T. Aernouts, H. Müllejans, G. Bardizza, N. Taylor, W. Verhees, J. M. Kroon, P. Morvillo, C. Minarini, F. Roca, F. A. Castro, S. Cros, B. Lechêne, J. F. Trigo, C. Guillén, J. Herrero, B. Zimmermann, S. B. Sapkota, C. Veit, U. Würfel, P. S. Tuladhar, J. R. Durrant, S. Winter, S. Rousu, M. Välimäki, V. Hinrichs, S. R. Cowan, D. C. Olson, P. Sommer-Larsen, F. C. Krebs, *Renewable Energy* **2014**, *63*, 376–387.

[3] a) N. Li, D. Baran, K. Forberich, F. Machui, T. Ameri, M. Turbiez, M. Carrasco-Orozco, M. Drees, A. Facchetti, F. C. Krebs, C. J. Brabec, *Energy Environ. Sci.* **2013**, *6*, 3407–3413; b) J. B. You, L. T. Dou, K. Yoshimura, T. Kato, K. Ohya, T. Moriarty, K. Emery, C. C. Chen, J. Gao, G. Li, Y. Yang, *Nat. Commun.* **2013**, *4*, 1446.

[4] T. R. Andersen, H. F. Dam, B. Andreasen, M. Hösel, M. V. Madsen, S. A. Gevorgyan, R. R. Søndergaard, M. Jørgensen, F. C. Krebs, *Solar Energy Mater. Solar Cells* **2014**, *120*, 735–743.

[5] T. T. Larsen-Olsen, T. R. Andersen, B. Andreasen, A. P. L. Böttiger, E. Bundgaard, K. Norrman, J. W. Andreasen, M. Jørgensen, F. C. Krebs, *Solar Energy Mater. Solar Cells* **2012**, *97*, 43–49.

[6] M. O. Reese, S. A. Gevorgyan, M. Jørgensen, E. Bundgaard, S. R. Kurtz, D. S. Ginley, D. C. Olson, M. T. Lloyd, P. Morvillo, E. A. Katz, A. Elschner, O. Haillant, T. R. Currier, V. Shrotriya, M. Hermenau, M. Riede, R. Kirov, G. Trimmel, T. Rath, O. Inganäs, F. Zhang, M. Andersson, K. Tvingstedt, M. Lira-Cantu, D. Laird, C. McGuiness, S. Gowrisanker, M. Pannone, M. Xiao, J. Hauch, R. Steim, D. M. DeLongchamp, R. Rösch, H. Hoppe, N. Espinosa, A. Urbina, G. Yaman-Uzunoglu, J. B. Bonekamp, A. J. J. M. van Breemen, C. Girotto, E. Voroshazi, F. C. Krebs, *Solar Energy Mater. Solar Cells* **2011**, *95*, 1253–1267.

[7] J. E. Carlé, M. Helgesen, M. V. Madsen, E. Bundgaard, F. C. Krebs, *J. Mater. Chem. C* **2014**, *2*, 1290–1297.

[8] M. Hösel, R. R. Søndergaard, M. Jørgensen, F. C. Krebs, *Energy Technol.* **2013**, *1*, 102–107.

Flexible ITO-free organic solar cells applying aqueous solution-processed V$_2$O$_5$ hole transport layer: An outdoor stability study

F. Anderson S. Lima,[1,2,3] Michail J. Beliatis,[4] Bérenger Roth,[4]
Thomas R. Andersen,[4] Andressa Bortoti,[2,3,5] Yegraf Reyna,[2,3] Eryza Castro,[5]
Igor F. Vasconcelos,[1] Suren A. Gevorgyan,[4] Frederik C. Krebs,[4]
and Mónica Lira-Cantu[2,3,6]

[1]*Departamento de Engenharia Metalúrgica e de Materiais, Universidade Federal do Ceará, Campus do Pici - Bloco 729, Fortaleza, CE 60440-554, Brazil*
[2]*Catalan Institute of Nanoscience and Nanotechnology (ICN2), Campus UAB, Bellaterra, 08193 Barcelona, Spain*
[3]*Barcelona Institute of Science and Technology (BIST), Campus UAB, Bellaterra, 08193 Barcelona, Spain*
[4]*Department of Energy Conversion and Storage, Technical University of Denmark, Frederiksborgvej 399, DK-4000 Roskilde, Denmark*
[5]*Departamento de Química, Universidade Estadual do Centro-Oeste – UNICENTRO, Campus CEDETEG, Guarapuava, PR, Brazil*
[6]*Consejo Superior de Investigaciones Científicas (CSIC), Campus UAB, Bellaterra, E-08193 Barcelona, Spain*

Solution processable semiconductor oxides have opened a new paradigm for the enhancement of the lifetime of thin film solar cells. Their fabrication by low-cost and environmentally friendly solution-processable methods makes them ideal barrier (hole and electron) transport layers. In this work, we fabricate flexible ITO-free organic solar cells (OPV) by printing methods applying an aqueous solution-processed V$_2$O$_5$ as the hole transport layer (HTL) and compared them to devices applying PEDOT:PSS. The transparent conducting electrode was PET/Ag/PEDOT/ZnO, and the OPV configuration was PET/Ag/PEDOT/ZnO/P3HT:PC$_{60}$BM/HTL/Ag. Outdoor stability analyses carried out for more than 900 h revealed higher stability for devices fabricated with the aqueous solution-processed V$_2$O$_5$. © *2016 Author(s). All article content, except where otherwise noted, is licensed under a Creative Commons Attribution (CC BY) license (http://creativecommons.org/licenses/by/4.0/).* [http://dx.doi.org/10.1063/1.4942638]

Over the last few years, the use of transition metal oxides (TMOs) with a large work function (WF) like NiO,[1] MoO$_3$,[2,3] WO$_3$,[4] or V$_2$O$_5$,[5] among others, has materialized as a viable option for their application as hole-transport layer in stable organic solar cells (OPV). The development of solution processing TMOs has also been successfully applied in perovskite solar cells.[6–8] The resulting oxide thin films have shown properties comparable to those grown by vacuum-processed resulting in devices with comparable or enhanced power conversion efficiencies (PCEs) and lifetime. Such is the case of NiO,[9] MoO$_3$,[10,11] CuO,[12] or V$_2$O$_5$.[13,14] For V$_2$O$_5$, one of its most widespread fabrication methods is the application of sol-gels made from vanadium (V) oxitriisopropoxide (V$_2$O$_5$–i)[14–18] or (NH$_4$)$_3$VO$_4$.[19,20,25] These precursors when used for the fabrication of flexible organic solar cells must be annealed at temperatures not exceeding 150 °C leaving behind organic residues that affect the OPV properties. In this work, we investigate the effect of aqueous solution-processed V$_2$O$_5$ (labelled V$_2$O$_5$–w) on the stability of polymer:fullerene bulk heterojunction solar cells and compare its performance with PEDOT:PSS. This water-based V$_2$O$_5$ oxide is highly compatible with the fabrication of thin film solar cells by large-area, low-cost, fast processing, and high-throughput printing fabrication.[14,17] Lab-scale OPVs on glass fabricated by spin
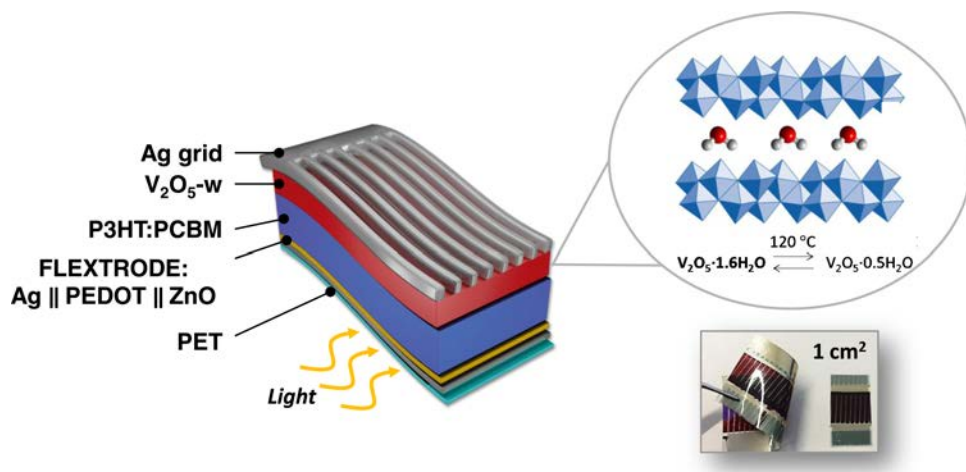
FIG. 1. Schematic representation of the organic solar cell configuration (left) and the structure of the water-based V_2O_5 hole transport layer (right).

coating applying the V_2O_5–w have already been fabricated in our group and demonstrated outdoor stability for more than 1000 h.[21] Here we demonstrate the fabrication of flexible ITO-free OPVs applying the V_2O_5–w fabricated by slot-die roll-coater. We will show the outdoor stability analyses of the flexible ITO-free OPVs for more than 900 h and demonstrate that the application of the oxide results in greater stability if compared to devices applying PEDOT:PSS.

We prepared inverted OPV devices with the configuration PET/Ag/PEDOT/ZnO/P3HT:PC_{60}BM/HTL/Ag (Fig. 1). The hole transport layer (HTL) was the V_2O_5–w and PEDOT:PSS, and the latter was used for comparison purposes. The water-based V_2O_5 was synthesised by the sol-gel method as reported.[21] The active layer for the single junction device was composed of P3HT (electronic grade from Rieke) and $PC_{60}BM$ (technical grade from Solenne BV). The PEDOT:PSS Clevios SV3 was brought from Heraeus. The V_2O_5 was diluted with isopropyl alcohol in the ratio 1:2 (w/w), and the PEDOT:PSS was diluted to a viscosity of 300 mPa s. A highly conductive PEDOT:PSS (Clevios PH1000 from Heraeus) was used to improve the contact between the HTL and the back electrode (Ag). This PEDOT:PSS was diluted with isopropyl alcohol in the ratio 10:3 (w/w), and its sheet resistivity was 60 Ω Square^{-1}. The back silver grid was printed using a screen printing silver past (PV410 from Dupont). Coating was performed on Flextrode that comprises a highly conducting metal grid, semi-transparent conductor, and hole blocking layer (PET/Ag/PEDOT/ZnO). The Flextrode was mounted on the roller using heat stable tape (3M) and the procedure began by first slot-die coating the active layer consisting of P3HT:PCBM (1:1, by weight) dissolved in chlorobenzene (40 mg/ml), with an addition of 10% of chloroform and 3% of chloronaphthalene. It was printed on the Flextrode electrode at 0.1 ml/min flow and 1.3 m/min for the web at 70 °C. The PEDOT:PSS layer was slot-die coated at 80 °C with a web speed 0.5 m/min. The V_2O_5 layer was slot-die coated at 90 °C with a web speed of 1.0 m/min. The flow of the solution was varied to give different thicknesses; the applied flows were 0.20 ml/min, 0.15 ml/min, and 0.10 ml/min. The theoretical, dry thickness for these layers is 80, 60, and 40 nm, respectively. The highly conductive PEDOT:PSS was slot-die coated on top of the HTL at 70 °C with a web speed of 0.4 m/min. The back silver electrode was applied by flexographic printing of heat curing silver paste PV410 (Dupont). The silver paste was added to the flexographic roll and further transferred to the substrate with a web speed of 1.2 m/min and roll temperature of 80 °C. The outdoor stability analyses were made following the ISOS-O-2 procedure[27] at the Catalan Institute of Nanoscience and Nanotechnology (ICN2-CSIC), located in Barcelona, Spain (41.30° N, 2.09° W), using a solar tracking positioning system. The system comprises a large dual axis-controlled platform with fully automated motors, which enables turning of the tracker hour angle up to 100° (which translates to nearly 7 h of perpendicular solar tracking) and turning of the tracker elevation angle from 15° to 90° (which enables full tracking of solar elevation). We developed in-house software to control

the photovoltaic response of sixteen solar cells at the same time and to continuously monitor light irradiation, temperature, and relative humidity over time. IV-curves were measured using a 2602 A dual-channel SMU multimeter and a 3700 series switch/multimeter (both from Keithley). PCE values were calculated using the maximum daily irradiance level. The light irradiation was measured with a Zipp & Konen CM-4 pyranometer. The temperature and relative humidity were monitored with a combined sensor (Theodor Friedrichs). Analyses were made in the summer of 2014, between the months of June and September.

V_2O_5 HTLs have been synthesised chiefly by multistep techniques.[21] As already mentioned, the applied fabrication methods are those obtained from sol–gels made from vanadium (V) oxytri-isopropoxide (ViPr) or $(NH_4)_3VO_4$, among others.[14–20] In these cases, the precursor materials are selected for the fabrication of flexible solar cells where the sintering temperatures cannot exceed 150 °C. Nevertheless, some organic residues from the precursors are not eliminated at those temperatures and are usually observed after thin film coating. In other cases, the precursors are not completely transformed into the oxide compound at low temperatures (see Fig. S1 in the supplementary material[28]). The V_2O_5 applied in this work is already an oxide at room temperature; it is in the form of a gel after synthesis and presents a layered crystalline structure where water molecules are intercalated between the oxide slabs (Fig. 1). There are no residues other than water after the V_2O_5–w is coated and heated at 120 °C, and the water molecules can be easily eliminated with soft heat. The latter makes this material very suitable for low temperature deposition by printing methods on flexible substrates (e.g., PET). The as-prepared thin film heated at 120 °C presents a nanostructured topology (Figs. 2(a) and 2(b)) and a preferential orientation of the layer structure as observed by gracing incidence X-ray diffraction analyses (Fig. 2(c)). While a powder sample will display crystalline peaks corresponding to the V_2O_5 oxide samples, a coated film shows the preferential orientation of the microcrystalline thin film at the C-axis, or perpendicular to the film plane. These peaks can be indexed as the $V_2O_5 \cdot H_2O$ monoclinic phase in well agreement with
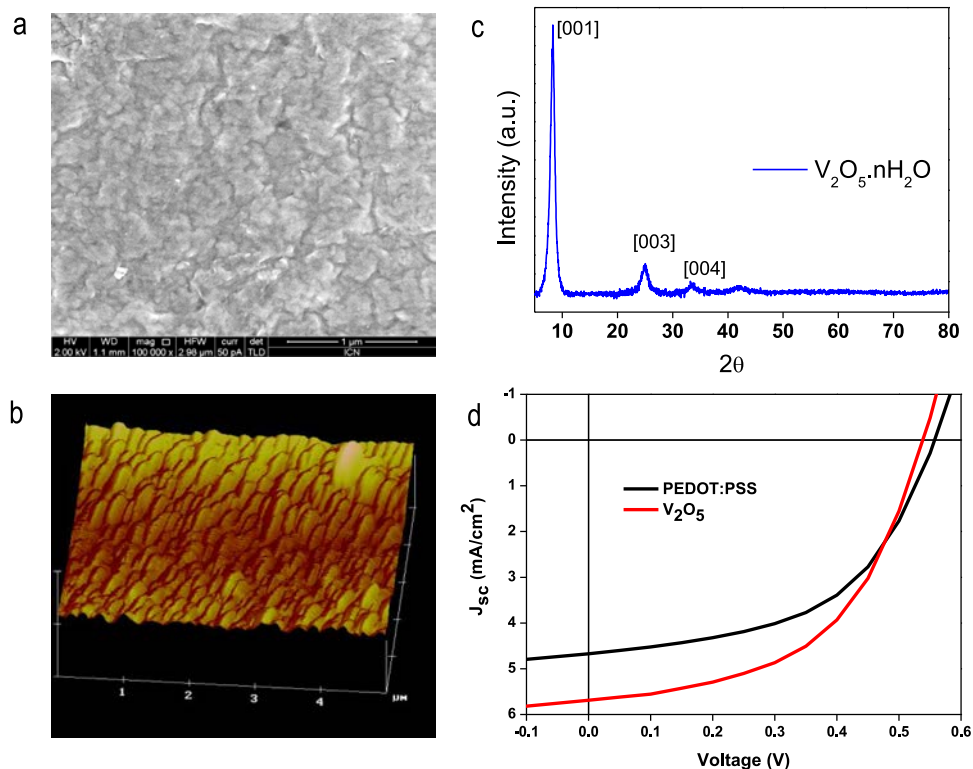

FIG. 2. Thin film of water based V_2O_5: (a) SEM top image, (b) AFM topography, (c) gracing incidence X-ray diffraction analysis, and (d) IV-curve of an inverted organic solar cell with the configuration PET/Ag/PEDOT/ZnO/P3HT:PC$_{60}$BM/HTL/Ag applying V_2O_5 and PEDOT:PSS as the HTL.

TABLE I. Average of five ITO-free OPVs with inverted configuration applying V_2O_5 and PEDOT:PSS as the HTLs. Data obtained under a sun simulator at 1000 mW/cm^2.

HTL	J_{SC} (mA cm^2)	V_{OC} (V)	FF/(%)	η (%)	η (max)/%
PEDOT:PSS	4.48 ± 0.22	0.56 ± 0.01	51.29 ± 0.66	1.27 ± 0.07	1.36
V_2O_5	5.18 ± 0.40	0.54 ± 0.00	53.29 ± 1.61	1.49 ± 0.07	1.59

pattern (JCPDS 21-1432).[26] The intensity of the (001) peak is assumed to be proportional to the fraction of quasi-ordered crystalline material in the sample, and usually, this peak is observed to increase as the annealing temperature increases. The interlayer spacing d in the $V_2O_5 \cdot n$ H_2O structure was calculated from the (001) diffraction peak at $2\theta = 8.24°$, resulting in a 10.76 Å. This value corresponds to one monolayer of water molecules intercalated within the V_2O_5 slabs, as expected.

We prepared inverted ITO-free OPV devices on PET, and the PCE of the device with V_2O_5 showed higher PCE than devices applying PEDOT:PSS hole transport layer (Table I, Figure 2(d)). The average of five devices analysed for each HTL with active area of 1 cm^2 is shown in Table I. The values of voltage (Voc) and fill factor (FF) are almost identical, 0.56 V and 0.54 V and 51% and 53% for PEDOT:PSS and V_2O_5, respectively. Major changes are observed for J_{sc}, which is larger for the OPV applying the water, based on V_2O_5.

The lifetime of OPVs is dependent on factors such as oxygen and moisture, especially when the PEDOT:PSS is applied due to its hygroscopic nature.[22,23] Due to the high relative humidity of the location of our outdoor testing facility (80% RH in Barcelona, Spain), the solar cells were encapsulated in glass for stability tests. Sealing our devices in glass permits to eliminate variables such as any defects from the encapsulation (any permeation issues, pinholes, or similar from the PET substrate) which is not the aim of our work. Fig. 3 shows the outcome of the outdoor stability test performed for the first 900 h to the OPVs applying the PEDOT:PSS (Fig. 3(a)) and the water-based V_2O_5 (Fig. 3(b), Table II). Values of irradiance (between 850 and 1000 mW/cm^2) and temperature (°C) are also included in each graph.
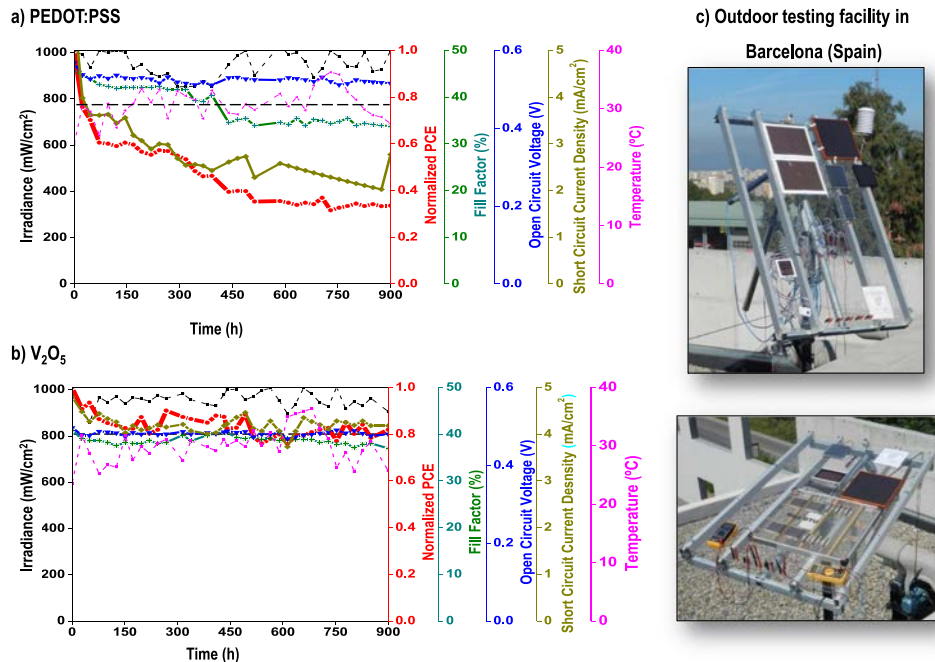

FIG. 3. Outdoor stability analyses (ISOS-O-2) of flexible OPV with an inverted configuration of the type PET/Ag/PEDOT/ZnO/P3HT:PC$_{60}$BM/HTL/Ag, where the HTL is PEDOT:PSS (a) or our water-based V_2O_5 (b). Active area is 1 cm^2. Outdoor analyses carried out at the outdoor testing facility of ICN2 in Barcelona, Spain (c). Data points correspond to sunlight irradiation between 850 and 1000 mW/cm^2 and temperature was measured to be below 35 °C.

TABLE II. Photovoltaic parameters evolution of the outdoor stability analysis of an inverted configuration OPV of the type PET/Ag/PEDOT/ZnO/P3HT:PC$_{60}$BM/HTL/Ag, where the HTL is our water-based V$_2$O$_5$ or PEDOT:PSS. Data obtained for the irradiation between 850 and 1000 mW/cm^2 in the outdoor sun tracker system in Barcelona, Spain.

PEDOT:PSS time (h)	J_{SC} (mA/cm^2)	V_{OC} (V)	FF/(%)	η (%)	X in T$_x$[a]
Initial	4.19	0.54	45.48	1.20	0
300 h	3.05	0.53	42.31	0.79	66
600 h	2.22	0.52	34.64	0.46	40
900 h	1.95	0.51	38.28	0.47	40
V$_2$O$_5$–wt time (h)	J_{SC} (mA/cm^2)	V_{OC} (V)	FF/(%)	η (%)	X in T$_x$
Initial	4.55	0.48	39.79	1.06	0
300 h	4.05	0.48	37.28	0.81	80
600 h	3.80	0.48	38.92	0.84	82
900 h	4.02	0.48	37.87	0.83	82

[a]x in Tx is defined as the point at which the efficiency of the device reaches X% of the initial efficiency.

The first interesting feature is that although the V$_2$O$_5$ layer has water molecules intercalated within its crystalline structure, the stability response of the device is steady and superior than the one observed for OPVs applying the PEDOT:PSS (Fig. 3). The observed T$_{80}$ lifetime (defined as the point at which the efficiency of the device reaches 80% of the initial efficiency, see Table II) was observed after only a few hours for PEDOT:PSS and after 400 h for the V$_2$O$_5$ (Fig. 3(b) and Table II). The period of time before reaching T$_{80}$ is a well-known event for OPVs related to the "burn-in" process that is characterized by an initial sudden drop in PCE followed by a stabilization of the solar cell response.[24] For devices applying the PEDOT:PSS OPV (Fig. 3(b) and Table II), the Voc and FF are maintained almost unchanged during the first 800 h, while Jsc and PCE show the aforementioned "burn-in" process and a drastic drop in efficiency until 400 h. In the case of devices with V$_2$O$_5$, the Voc and FF were kept almost unaffected for the whole stability analyses, and efficiency and Jsc were observed to drop only after 400 h. For the devices applying the PEDOT:PSS HTL, 40% of the initial PCE was maintained at the end of the test, after 900 h, while the OPV applying the V$_2$O$_5$ layer maintained the initial PCE at around 80% of the initial value after the same period of time.

The evolution of the IV curves throughout the stability tests for each of the OPVs is show in Fig. 4. In both types of OPVs, the V$_{oc}$ is kept almost identical after the degradation test, an indication that the interface between the active layer and the electrodes (HTL or ETL) is almost unaffected in both devices. The changes observed in FF are the result of different causes, among them is the reduced interfacial charge transfer efficiency between the different layers, the degradation of the active layer, or the increase of the recombination processes. These processes can be taking place in both OPVs but in the case of the devices applying the PEDOT:PSS, the drop in FF is stronger, especially at the end of the stability analysis. The strongest changes are observed on Jsc and, as a consequence, on the PCE. Changes in Jsc are due to many internal processes inside the OPV, like the increase of internal resistance due to the degradation of the electron transport layers, the electron donor, or due to the reduction of the transparency of any layer or interface, which could reduce the amount of light entering the cell. In general, all these degradation processes are taking place much faster and stronger for OPV devices applying the PEDOT:PSS HTL demonstrating the beneficial effect of applying the aqueous-processed V$_2$O$_5$–w HTL.

The beneficial effect on stability when our V$_2$O$_5$ oxide HTL is applied is clearly demonstrated with these results. Moreover, the feasibility to synthesise the gel in its oxide form at room temperature (Fig. 2) is also an advantage if compared to other oxides where the precursors are not completely transformed into the oxide at low temperatures. This is the case of the synthesis of V$_2$O$_5$ from precursors like powder V$_2$O$_5$ and (NH$_4$)$_3$VO$_4$.[12] Long *et al.* reported the fabrication of OPVs by employing this precursor for the preparation of the oxide layer as charge injection.[25] The authors demonstrated a similar power conversion efficiency of the OPV if compared with PEDOT:PSS but no stability test was carried out. Our X-ray diffraction analyses of a thin film made with this precursor showed that the (NH$_4$)$_3$VO$_4$ is transformed into the oxide until heating at 350 °C
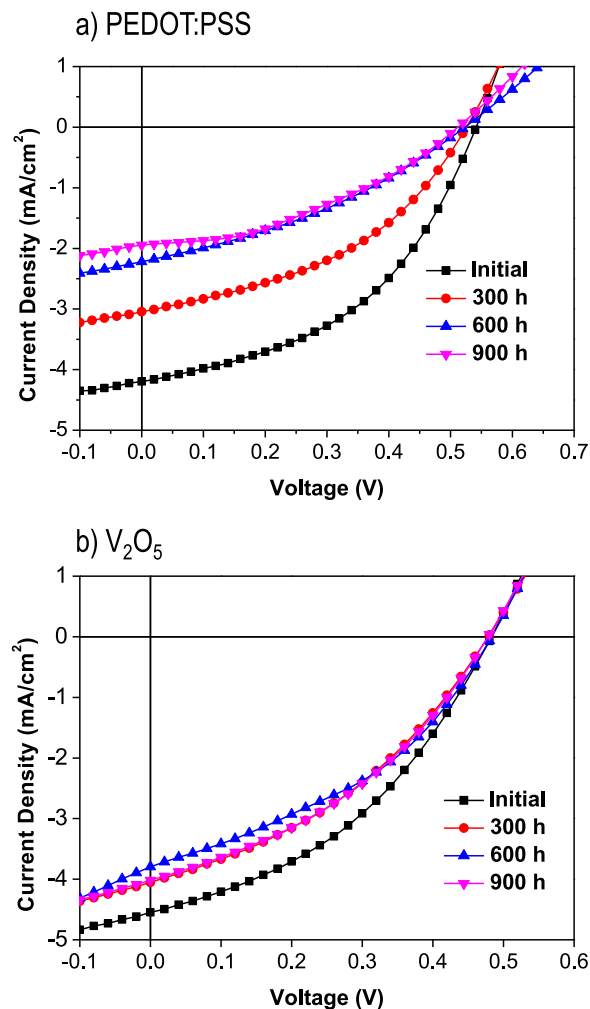
FIG. 4. Evolution of the IV curves throughout the outdoor stability analyses for 900 h (ISOS-O-2) of inverted configuration OPV of the type PET/Ag/PEDOT/ZnO/P3HT:PC$_{60}$BM/HTL/Ag, where the HTL is (a) PEDOT:PSS or (b) our water-based V$_2$O$_5$.

(Fig. S1).[28] Although the PCE of the device shows the same PCE (see Figure S2 and Table S1 in the supplementary material[28]), the stability of the solar cell is even worse than the one observed for OPVs applying PEDOT:PSS (Fig. S3).[28]

In summary, we have analysed the stability of flexible ITO-free organic solar cells fabricated by slot-die roll-to-roll methods applying a water-based V$_2$O$_5$ hole transport layer. The devices of 1 cm^2 active area were compared to OPVs applying PEDOT:PSS. Outdoor stability analysis (ISOS-O-2) revealed that, although the V$_2$O$_5$ contain water molecules within its structure, the device stability surpass greatly the stability of OPV devices fabricated with PEDOT:PSS.

[1] W. J. Yu, L. Shen, S. P. Ruan, F. X. Meng, J. L. Wang, E. R. Zhang, and W. Y. Chen, Sol. Energy Mater. Sol. Cells **98**, 212–215 (2012).

[2] J. Jung, D. Kim, W. S. Shin, S. J. Moon, C. Lee, and S. C. Yoon, Jpn. J. Appl. Phys., Part 1 **49**(5), 05EB05 (2010).

[3] A. K. K. Kyaw, X. W. Sun, C. Y. Jiang, G. Q. Lo, D. W. Zhao, and D. L. Kwong, Appl. Phys. Lett. **93**(22), 221107 (2008).

[4] S. Han, W. S. Shin, M. Seo, D. Gupta, S. J. Moon, and S. Yoo, Org. Electron. **10**(5), 791–797 (2009).

[5] K. Takanezawa, K. Tajima, and K. Hashimoto, Appl. Phys. Lett. **93**(6), 063308 (2008).

[6] J. Kim, G. Kim, T. K. Kim, S. Kwon, H. Back, J. Lee, S. Ho Lee, H. Kang, and K. Lee, J. Mater. Chem. A **2**, 17291–17296 (2014).

[7] C. Chueh, C. Li, and A. K.-Y. Jen, Energy Environ. Sci. **8**, 1160-1189 (2015).

[8] J. W. Jung, C. Chueh, and A. K.-Y. Jen, Adv. Mater. **5**, 1500486 (2015).

[9] Y. H. Lin, P. C. Yang, J. S. Huang, G. D. Huang, I. J. Wang, W. H. Wu, M. Y. Lin, W. F. Su, and C. F. Lin, Sol. Energy Mater. Sol. Cells **95**(8), 2511–2515 (2011).

[10] S. R. Hammond, J. Meyer, N. E. Widjonarko, P. F. Ndione, A. K. Sigdel, A. Garcia, A. Miedaner, M. T. Lloyd, A. Kahn, D. S. Ginley, J. J. Berry, and D. C. Olson, J. Mater. Chem. **22**(7), 3249–3254 (2012).

[11] K. Zilberberg, H. Gharbi, A. Behrendt, S. Trost, and T. Riedl, ACS Appl. Mater. Interfaces **4**(3), 1164–1168 (2012).

[12] M. Y. Lin, C. Y. Lee, S. C. Shiu, I. J. Wang, J. Y. Sun, W. H. Wu, Y. H. Lin, J. S. Huang, and C. F. Lin, Org. Electron. **11**(11), 1828–1834 (2010).

[13] Y. M. Chang and J. M. Ding, Thin Solid Films **520**(16), 5400–5404 (2012).

[14] K. Zilberberg, S. Trost, J. Meyer, A. Kahn, A. Behrendt, D. Lützenkirchen-Hecht, R. Frahm, and T. Riedl, Adv. Funct. Mater. **21**(24), 4776–4783 (2011).

[15] C. P. Chen, Y. D. Chen, and S. C. Chuang, Adv. Mater. **23**(33), 3859–3863 (2011).

[16] I. Hancox, L. A. Rochford, D. Clare, M. Walker, J. J. Mudd, P. Sullivan, S. Schumann, C. F. McConville, and T. S. Jones, J. Phys. Chem. C **117**(1), 49–57 (2013).

[17] T. T. Larsen-Olsen, T. R. Andersen, B. Andreasen, A. P. L. Böttiger, E. Bundgaard, K. Norrman, J. W. Andreasen, M. Jørgensen, and F. C. Krebs, Sol. Energy Mater. Sol. Cells **97**, 43-49 (2012).

[18] K. Zilberberg, S. Trost, H. Schmidt, and T. Riedl, Adv. Energy Mater. **1**(3), 377–381 (2011).

[19] J. Livage, Coord. Chem. Rev. **190-192**, 391–403 (1999).

[20] Q. Yue, H. Jiang, Y. Hu, G. Jia, and C. Li, Chem. Commun. **50**, 13362–13365 (2014).

[21] G. Terán-Escobar, J. Pampel, J. M. Caicedo, and M. Lira-Cantú, Energy Environ. Sci. **6**(10), 3088–3098 (2013).

[22] A. M. Nardes, M. Kemerink, M. M. de Kok, E. Vinken, K. Maturova, and R. A. J. Janssen, Org. Electron. **9**(5), 727–734 (2008).

[23] T. S. Glen, N. W. Scarratt, H. Yi, A. Iraqi, T. Wang, J. Kingsley, A. R. Buckley, D. G. Lidzey, and A. M. Donald, Sol. Energy Mater. Sol. Cells **140**, 25–32 (2015).

[24] R. Roesch, T. Faber, E. von Hauff, T. M. Brown, M. Lira-Cantu, and H. Hoppe, Adv. Energy Mater. **5**, 1501407 (2015).

[25] D. X. Long, Y. Xu, S. Kang, W. Park, E. Choi, C. Liu, and Y. Noh, Org. Electron. **17**, 66–76 (2015).

[26] V. Petkov, P. N. Trikalitis, E. S. Bozin, S. J. L. Billinge, T. Vogt, and M. G. Kanatzidis, J. Am. Chem. Soc. **124**(34), 10157–10162 (2002).

[27] M. O. Resee *et al.*, Sol. Energy Mater. Sol. Cells **95**(5), 1253–1267 (2011).

[28] See supplementary material at http://dx.doi.org/10.1063/1.4942638 for the photovoltaic response of OPVs applying a transparent V_2O_5 hole transport layer.